FOSSIL ENERGY

DOE/ID/13421-3
(OSTI ID: 790862)

EVALUATION OF RESERVOIR WETTABILITY AND ITS EFFECTS ON OIL RECOVERY

Final Report
October 2001

By:
Jill S. Buckley

Date Published: January 2002

Work Performed Under Contract No. DE-FC22-96ID13421

New Mexico Institute of Mining and Technology
Socorro, New Mexico

National Energy Technology Laboratory
National Petroleum Technology Office
U.S. DEPARTMENT OF ENERGY
Tulsa, Oklahoma

DOE/ID/13421-3
Distribution Category UC-122

Evaluation of Reservoir Wettability and Its Effect on Oil Recovery

By
Jill S. Buckley

January 2002

Work Performed Under DE-FC22-96ID13421

Prepared for
U.S. Department of Energy
Assistant Secretary for Fossil Energy

Purna Halder, Project Manager
National Petroleum Technology Office
P.O. Box 3628
Tulsa, OK 74101

Prepared by
Petroleum Recovery Research Center
New Mexico Institute of Mining and Technology
801 Leroy Place
Socorro, NM 87801

TABLE OF CONTENTS

LIST OF FIGURES

LIST OF TABLES

ABSTRACT

In this report, the final results of the project, "Evaluation of Reservoir Wettability and its Effect on Oil Recovery" are presented. The objectives of this five-year project are (1) to achieve improved understanding of the surface and interfacial properties of crude oils and their interactions with mineral surfaces, (2) to apply the results of surface studies to improve predictions of oil production from laboratory measurements, and (3) to use the results of this research to recommend ways to improve oil recovery by waterflooding.

In Part 1 of this project, we have focused on crude oil properties and crude oil/brine/rock (COBR) interactions. Properties of particular interest from the point of view of a crude oil's tendency to alter wetting include acidic and basic functionality and a measure of the stability of asphaltenes, as explained in an introduction to COBR interaction mechanisms. We have been highly successful in acquiring samples of crude oil for this study. Part I includes background studies on measurements of acid and base number and the results of tests with more than 140 oils. Significant emphasis has been placed on asphaltene characterization, an area where fundamental improvements in our understanding of asphaltene stability and how to characterize oils for their solvent properties with respect to their asphaltenes have been achieved.

Part 2 of this study is devoted to finding improved methods of wettability assessment. In smooth surface studies, mica has been established as a standard because of it's structural surface charge, molecular smoothness, and reproducibility. Improvements in the sequence of test conditions and in chemical detection of adsorbed organic material have been investigated. Mechanisms of interaction that are analogous to those previously established for glass surfaces have been demonstrated for mica and additional work has delineated the regime over which surface precipitation dominates COBR interactions. Square glass tubes of capillary dimensions

were studied as a simple model of porous media in which mixed-wet conditions can be established and studied. Glass micromdels were used to demonstrate the effects of surface precipitation on wettability and subsequent displacements. The effects of mixed wetting and the distribution of wetting were considered in a comparison of the most commonly used wettability tests, the USBM and Amott measurements. A significant volume of data—including relevant oil properties and wetting alteration tests—have been gathered into a relational database named CO-Wet

Improved oil recovery under conditions that are not strongly water-wet is the aim of Part 3. A study of oil recovery from Berea sandstone showed that after exposure to crude oil, flow-rate can affect displacements of oil by water in contrast to waterfloods in the same rocks under water-wet conditions. Although the effects are small in the cases studied, they are robust and reproducible, suggesting that assumptions about the uniqueness of relative permeability relationships in non-water-wet cores need more careful scrutiny. We also show that wettability should be considered a fixed reservoir property as is usually done in current reservoir models. The potential for wettability alteration exists during the productive life of a reservoir. Results of mechanistic studies are applied to demonstrate some conditions where changing wettability that could either improve or damage recovery should be expected.

EXECUTIVE SUMMARY

This report summarizes the five-year project, "Evaluation of Reservoir Wettability and its Effect on Oil Recovery." The objectives have been (1) to achieve improved understanding of the surface and interfacial properties of crude oils and their interactions with mineral surfaces, (2) to apply the results of surface studies to improve predictions of oil production from laboratory measurements, and (3) to use the results of this research to recommend ways to improve oil recovery by waterflooding.

Mixed-wetting can occur in oil reservoirs as a consequence of the initial fluid distribution. Water existing as thick films on flat surfaces and as wedges in corners can prevent contact of oil and mineral. Water-wet pathways are thus preserved. Depending on the balance of surface forces—which depend on oil, solid, and brine compositions—thick water films can be either stable or unstable. Water film stability has important implications for subsequent alteration of wetting in a reservoir. On surfaces exposed to oil, the components that are likely to adsorb and alter wetting can divided into two main groups: those containing polar heteroatoms, especially organic acids and bases; and the asphaltenes, large molecules that aggregate in solution and precipitate upon addition of n-pentane and similar agents. In order to understand how crude oils interact with mineral surfaces, we first gathered information about both these classes of compounds in a crude oil.

Part 1 of this project is focused on the mechanisms by which crude oils alter wetting and on characterizing crude oils in light of those mechanisms. Four distinct categories of interaction mechanisms can be demonstrated to occur when crude oils contact solid surfaces. In the absence of water, polar interactions can occur between the compounds in the oil that contain polar heteroatoms and mineral surfaces. Since water is always present in oil reservoirs, these are of less interest than interactions that occur in the presence of an aqueous phase. They are fairly

nonspecific, producing intermediately wetted surfaces. If an oil is a poor solvent for its asphaltenes, surface precipitation can occur. We expect that this mechanism is probably most influential just before the onset of precipitation, causing surfaces to become quite oil-wet, an hypothesis that has now been tested and verified for a number of oils. Attractive forces can be either enhanced or limited by the presence of water. Acid/base interactions account for pH-dependent adhesion and for electrophoretic mobilities of emulsified crude oil droplets. In the presence of divalent or multivalent ions, specific interactions, such as ion-binding, can occur. These can be very strong interactions, although they may require significant aging times to develop a strong bond to the surface. Specific instances when each of these mechanisms appeared to be dominant have been identified in tests using crude oils of different acid number, base number, and solvent quality.

To characterize crude oils with respect to acid/base interaction mechanisms, standard acid and base number non-aqueous potentiometric titration procedures were modified. Acid and base numbers are reported for more than 140 samples of crude oil and are shown not to be correlated with one another, making measurement of both an essential step in wettability characterization of crude oils.

A new approach has been developed to characterize the asphaltenes. Rather than focus on the amount of asphaltene that precipitates in standard ASTM tests or the amount of heptane or pentane that must be added to destabilize asphaltenes, we have concentrated on the solvent environment in each crude oil. We quantify solvent properties by refractive index (RI) measurements. Refractive index is related to the surface forces between asphaltene aggregates. It is linearly related to volume fractions of components in mixtures of crude oil, solvents, and precipitants and to solubility parameters of non-polar species. The RI at the onset of

precipitation provides a point of comparison among different asphaltene samples, and the difference between that point and the oil's RI is a measure of the stability of the asphaltenes in the stock tank oil. The onset of asphaltene precipitation with addition of n-heptane is reported at ambient conditions for 87 oil samples. Onset testing has been extended to conditions of higher temperatures and pressures. Trends established with heptane and paraffinic precipitants of higher molecular weight are shown to extend to propane and some initial experimental results using CO_2 are reported as well. The theoretical background for use of the refractive index to quantify the solvent quality of an oil for its asphaltenes has been developed. We apply this analysis to a wide range of crude oils and show how standard PVT analyses can be used to calculate refractive index during depressurization of an oil.

Of the mechanisms of wetting alteration, surface precipitation has been the least well documented. Experiments with five different crude oils showed that there can be a dramatic increase in the oil-wet character of mica surfaces contacted first with brine, then with crude oil to which heptane has been added to destabilize its asphaltenes.

Part 2 of this project is devoted to improved assessment of wetting. A baseline study of crude oil interactions with mica surfaces is reported. Mica is attractive for use as a solid substrate because it is easy to produce molecularly smooth surfaces by cleavage of mica plates, because its structure is well known, and because it is the subject of many other surface studies. Trends of wettability alteration are comparable to those reported previously for glass surfaces, but there are some significant differences as well, especially at elevated temperature.

We have used crude oil to alter the wetting of a very simple porous medium, i.e. square glass capillary tubes. Mixed-wet conditions can be produced if there is an initial water saturation

in the corners of the tube during exposure to oil. Direct visual observation of spontaneous imbibition into tubes with varying wettability is reported.

We demonstrate that improved wettability measurements can be made on smooth surfaces using a minor modification of our standard adsorption tests. Solids typically are treated first with brine, then with crude oil. Removal of the brine phase—by centrifuging the substrate under oil—led to more consistent contact angle measurements without changing previously reported wettability trends. There was less scatter in the water-advancing angles especially on surfaces that were fairly oil-wet, while the more water-wet conditions remained comparatively water-wet.

Chemical characterization of oil-treated surfaces was the aim of a study of a Fourier transform infrared spectroscopy (FTIR) technique known as attenuated total reflectance. The technique limits the depth of investigation and is often used to characterize surface properties. In the case of oil-treated mica, however, the depth is still too great, giving peaks for mica that obscure regions of the spectrum that would inform us about polar components adsorbed on the surface. Indications of adsorbed water are potentially the most useful application of the technique to wettability assessment.

Wettability assessment in porous media is the subject of Part 2.2. Toluene and heptane dilutions of a crude oil produced visibly different wetting conditions in two-dimensional glass micromodels. More oil-wet conditions in the model exposed to a mixture of Mars-Pink crude oil and heptane at the onset of asphaltene precipitation confirm comparable observations on flat mica surfaces. There is, however, no direct measure of wettability in porous media, but there are two widely used empirical tests: the Amott and USBM wettability tests. An exploration of the relationship between these two different but related indices was undertaken based on both

analytical and pore network model approaches. Analytical predictions for a uniform distribution of pores, neglecting the influence of connectivity, provided guidance in assessing the network predictions. The comparison showed that the two measures should give comparable estimates of wettability in fractionally-wet media where the mixture of water-wet and oil-wet surfaces within the pore space is randomly distributed. In mixed-wet media, the indices can differ both qualitatively and quantitatively depending on the details of distribution of surface wettability.

The third part of this project is aimed at finding ways to improve oil recovery. While the end-point relative permeability to water is constant under strongly water-wet conditions, careful tests show that its value can vary with flow rate when non-water-wet conditions prevail. Waterflooding strategies based on water-wet corefloods fail to account for inherent rate effects under more realistic wetting conditions. Weakly wetted conditions generated by treating Berea sandstone cores with crude oils have been used in a detailed examination of relative permeability to water. The results show that the end-point permeability to water measured in a core flood can significantly overestimate water permeability in the formation if unrealistically high flow rates are used. A fluid redistribution mechanism is suggested to explain the observed flow rate dependence.

Observations of different wetting conditions induced by the same crude oil as we alter the stability of its asphaltenes suggests that reservoir wettability may not be a constant property, but may change during production. Cases where regions of more oil-wet conditions might be expected to develop, either during pressure depletion or gas injection, are explored in the final section of this report.

ACKNOWLEDGMENTS

This work has been supported by the US Department of Energy under Cooperative Agreement DEFC22-96ID13421, by the State of New Mexico, and by industrial support from British Petroleum, Chevron, Mobil, Norsk Hydro, and Unocal.

Project contributors during this 5-year project have included:

Jill Buckley*	Senior Scientist, Head of Petrophysics and Surface Chemistry Group
Tianguang Fan*	Research Chemist
Jianxin Wang*	Senior Research Associate
Virginia Chang	Research Associate
Mary Downs Creech	Research Associate
Yu Liu	Research Associate
Rashid Al-Maamari	PhD student in Petroleum Engineering
Lisa Lauman	MS student, Chemistry
Ling Liu	MS student, Chemistry
Sue Von Drasek	MS student, Geochemistry
Shannon Bayes*	Undergraduate student (Chemical Engineering)
Matthew Chadwick	Undergraduate student (Chemical Engineering)
Mitch McBee*	Undergraduate student (Chemical Engineering)
Jeremy McCoy*	Undergraduate student (Chemical Engineering)
Joshua Narelsky*	Undergraduate student (Chemical Engineering)
Steen Christiansen	Visiting Scholar, Danish Technical
Stephanie Monsterleet	Visiting Scientist, France
Kristine Spildo	Visiting Scholar, University of Bergen, Norway
Rao Xiaotong	Visiting Scholar, Southwest Petroleum Institute, China
Xina Xie	Visiting Scientist, University of Wyoming
Kay Brower	Professor Emeritus, Chemistry Dept., NMIMT

*Current year

Collaborators from other institutions have included:

George Hirasaki & Baldev Gill	Chemical Eng., Rice University
Norman Morrow	Petroleum & Chemical Eng., Univ. of Wyoming
Ashok Dixit, Steven McDougall, & Ken Sorbie	Petroleum Eng., Heriot-Watt University
Simon Andersen	Chemical Eng., Danish Technical Univ.

INTRODUCTION

Objectives

The objectives of this five-year project are threefold:

- achieve improved understanding of the surface and interfacial properties of crude oils and their interactions with mineral surfaces,
- apply the results of surface studies in the laboratory to improve predictions of oil production, and
- use the results of this research to recommend ways to improve oil recovery by waterflooding.

Both existing methods of wettability assessment and new methods developed in the course of this research will be applied to advance our understanding of oil reservoir wettability and how wetting affects oil recovery.

Contents of this Report

This final report is broken into three main sections, each of which addresses one of the above objectives. In Part 1 we concentrate on the crude oil/brine/rock (COBR) interactions by which components of a crude oil can alter the wetting of mineral surfaces. Major subsections include background on the likely nature of these interactions, assessment of the acidic and basic character of more than 140 crude oil samples, assessment of asphaltene stability and of the ability of crude oils to serve as solvents for their asphaltenes. Both theoretical and experimental results are presented. Experiments have been conducted at ambient conditions and at elevated temperatures and pressures. An empirical correlation between refractive index (RI) at the onset of precipitation and the molar volume of the precipitating agent that may help predict onsets at

reservoir conditions is reported. A relational database has been assembled to collect oil properties and wettability alteration data.

Part 2 summarizes studies of wetting assessment on smooth surfaces, in square glass capillaries, and in porous media. Mica has been evaluated as a standard substrate and found to reproduce many of the earlier observations from contact angles measured on oil-treated glass surfaces. Because of it's molecular smoothness and reproducibility, Muscovite mica has been selected as the standard substrate mineral for the remainder of this project. Other improvements in the techniques used to produce oil-treated surfaces for wettability studies are also reported. An FTIR method was developed to study the chemistry of the material that remains on mica surfaces after exposure to crude oil.

Square glass capillaries are simple porous media, but the fact that they have corners means that they can retain water in the presence of oil. We have used them to test the generation of mixed wettability in this highly idealized porous media. Glass micromodels provide further visual evidence of wetting alteration that depends on crude oil composition. In porous media, the two main techniques used to assess wettability are Amott and USBM tests. The connection between them was investigated by analytical and pore network model techniques.

If wettability can change during production, improved recovery might result, as discussed in Part 3. Differences between strongly water-wet displacements and displacements in cores with altered wettability are reported, especially with respect to displacement rate. In water-wet media, capillary forces dominate and changing the rate of displacement has no effect beyond changing the extent of the well-known capillary end effects. Less well established are differences in relative permeabilities in weakly water-wet cores that depend on displacement

rate, as demonstrated in this study. Opportunities for alteration of wetting during the producing life of a reservoir are considered in the final section of this report.

Details of asphaltene onset observations and of experimental procedures in the onset tests at elevated temperatures and pressures are presented in Appendices.

PART 1. COBR INTERACTIONS

1.1 Mechanisms of COBR Interactions

This project began with the hypothesis that there are multiple mechanisms by which crude oil components can adsorb on mineral surfaces and alter their wetting properties. Using evidence from earlier studies of physisorption on amorphous silica surfaces and from the literature, several distinct interaction mechanisms were proposed. The extent to which these early observations apply, with due consideration to differences in surface charge and surface chemistry, to a variety of minerals, especially other oxides will be considered in subsequent sections of this report. It should be noted, however, that there are circumstances in which other mechanisms will dominate. One example is chemisorption of carboxylic acids on hematite surfaces (Peck *et al.*, 1966). Bearing in mind that exceptions will be encountered, it is still important to understand the more general mechanisms by which crude oils can alter the wetting of high energy oxide surfaces.

1.1.1 Summary of Proposed COBR Interactions

Four main categories of crude oil/brine/rock interactions have been identified, as illustrated in Fig. 1.1-1. They include:

- **polar interactions** that predominate in the absence of a water film between oil and solid,
- **surface precipitation**, dependent mainly on crude oil solvent properties with respect to the asphaltenes,
- **acid/base interactions** that control surface charge at oil/water and solid/water interfaces, and

- **ion binding** or specific interactions between charged sites and higher valency ions.

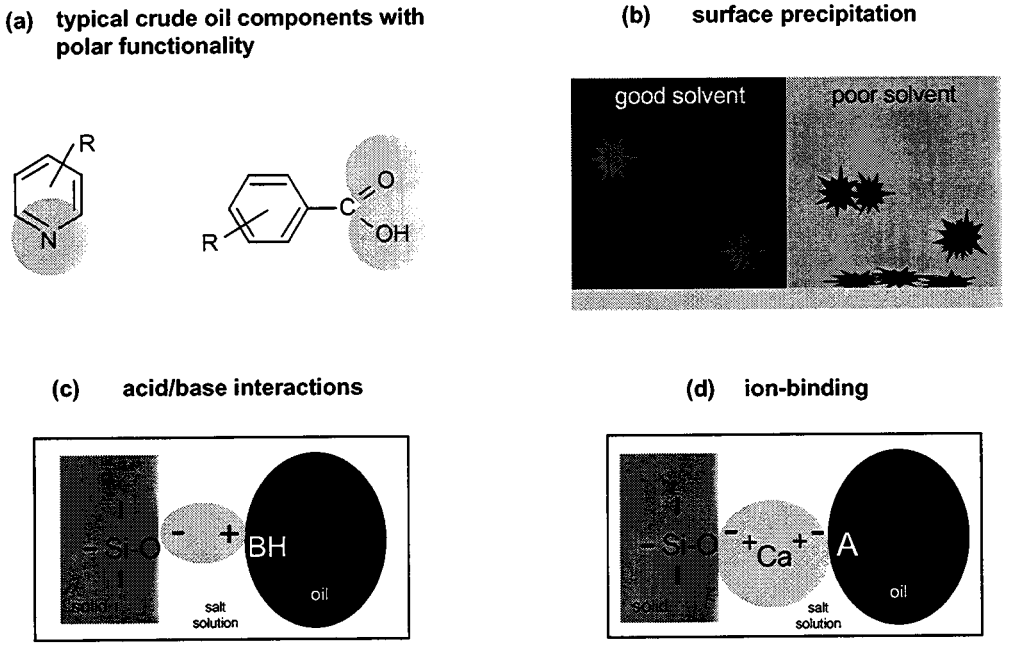

Figure 1.1-1. Mechanisms of interaction between crude oil components and solid surfaces.

1.1.1.1 Polar interactions

Adsorption of asphaltenes directly from oil onto mineral surfaces has often been reported. Some important variables that affect adsorption onto clay minerals in the absence of water include the type of clay and its exchangeable cations, nitrogen content of the oil, and the solvent in which the polar compounds are dissolved (Clementz, 1976, 1982; Czarnecka and Gillott, 1980). Monolayer adsorption was reported (Dubey and Waxman, 1991), except in nitrobenzene, a polar solvent. The thickness of the monolayer depended on the solvent from which it was adsorbed. Studies designed to separate out the effects of acidic and basic components (Denekas *et al.*, 1959) or various distillation

fractions (Cuiec, 1986) in different lithologies have mainly demonstrated the complexity of the interactions involved in these adsorption processes. The adsorbed material is enriched in nitrogen, oxygen, and sulfur and is higher in molecular weight than the oil from which it comes (Akhlaq, *et al.*, 1996). Two of the many types of functional groups that are likely to be involved in polar interactions are suggested in Fig. 1.1-1a. The variety of ways in which these species can interact with surfaces are grouped together here under the general heading of polar interactions to distinguish them from interactions between ionic species.

Direct measurements of surface forces between dry mica surfaces immersed in crude oil (Christenson and Israelachvili, 1987) showed slow adsorption of high molecular weight material. Water advancing contact angles on dry glass surfaces, after treatment with several different crude oils or with a solution of asphaltenes in toluene, have been reported to be in the range from 60 - 100 (Liu and Buckley, 1997; Buckley *et al.*, 1997; Wu, 1996).

1.1.1.2 Surface precipitation

As discussed in Section 1.2, crude oils vary widely in their ability to act as solvents for their asphaltenes. If the oil is a poor solvent for its asphaltenes, the tendency for wetting alteration is enhanced, as illustrated in Fig. 1.1-1b. Measurements of amounts of adsorbed material (Akhlaq *et al,* 1996), contact angles (Buckley *et al.*, 1997), and the rate of imbibition into Berea sandstone cores (Tang *et al.*, 1996) all indicate that more adsorption and less water-wet conditions are achieved as the oil becomes a poorer solvent for its asphaltenes.

1.1.1.3 Acid/base interactions

Water plays several important roles in mediating oil/solid interactions. In the presence of water, both the solid and oil interfaces become charged. Polar functional groups belonging to both the mineral and crude oil phases can behave as acids (giving up a proton and becoming negatively charged) and bases (gaining a proton and thus producing a positive charge) (Cuiec, 1975). There are two major ways in which the phenomenon of surface charge impacts interactions between crude oils, brine, and solid surfaces.

Net Charge Affects Water Film Stability: The influence of DLVO forces in stabilizing a thin film of water between mineral and oil is most significant when the brine phase salinity is low. For a given oil or solid surface, surface charge depends on the extent of acid/base dissociation reactions which, in turn, depend on pH at the surface. For some brine compositions, both oil/water and solid/water interfaces will have like charge. The resulting repulsion stabilizes the intervening water film. If the water film is stable, strongly water-wet conditions can be maintained. If not, the collapse of the water film allows wettability altering interactions to proceed.

Ionized Acidic and/or Basic Sites Influence Adsorption: Collapse of the water film is only the first step in wetting alteration. At this stage, crude oil components at the oil/brine interface can adsorb on the solid surface. Silica surfaces are negatively charged above pH 2; positively charged nitrogen bases can adsorb, as illustrated in Fig. 1.1-1c. Calcite surfaces are more complex, but may be positively charged below a pH of about 9.5, enhancing adsorption of acidic species.

1.1.1.4 Ion binding

When present, Ca^{2+} ions mask the purely acid/base interactions. Several interactions are possible:

oil—Ca—oil **mineral—Ca—mineral** **oil—Ca—mineral**

The first two can limit wettability alteration, while the last can promote it, as illustrated in Fig. 1.1-1d.

1.1.2 Interactions with Glass Surfaces

Polar Interactions: Figure 1.1-2 shows the results of contact angle measurements for water advancing against decane (θ_A) on glass surfaces. These measurements were made after the surfaces had been treated with one of four different crude oils. θ_A is shown for shorter (1 day) and longer (~20 days) aging times in oil and for two aging temperatures, 25°and 80°C. For all of these oils, aging in crude oil changes wetting from strongly water-wet to intermediate. Aging time and aging temperature have only small effects on the measured values of θ_A. Intermediate values of θ_A have also been reported for glass surfaces aged in varying concentrations of asphaltene dissolved in toluene (Buckley *et al.*, 1997).

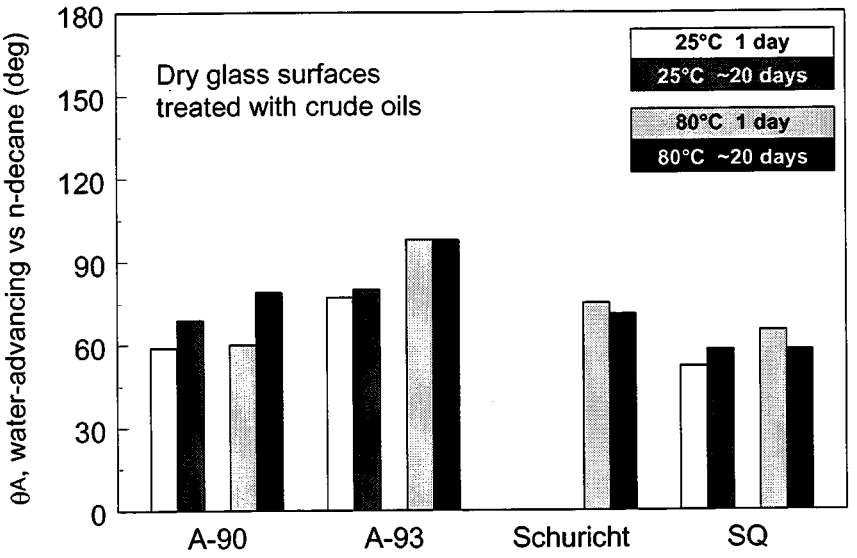

Figure 1.1-2. Glass surfaces, treated with crude oils in the absence of water. Polar interactions result in intermediate in wetting.

Surface Precipitation: If the oil is a poor asphaltene solvent, asphaltenes can precipitate. Even before precipitate can be detected in the oil, however, there can be an effect on wetting. Surfaces become increasingly oil-wet as the oil approaches the point of precipitation, as shown in Figs. 1.1-3a and b. Water/decane contact angles on surfaces treated with a synthetic reservoir brine, then aged in A-93 crude oil for three weeks at 80°C are shown. Washing with a precipitant (decane) produces an oil-wet surface with high advancing and receding angles. Rinsing with better solvents (toluene or cyclohexane) results in high advancing angles, but much lower receding angles (Fig. 1.1-3a). Similarly, aging in oil mixtures of 40% crude oil and 60% precipitant (isooctane) produced more oil-wet surfaces than aging in the oil alone or in oil to which similar amounts of solvents—toluene or α-methylnaphthalene (1-MN)—were added (Fig. 1.1-3b).

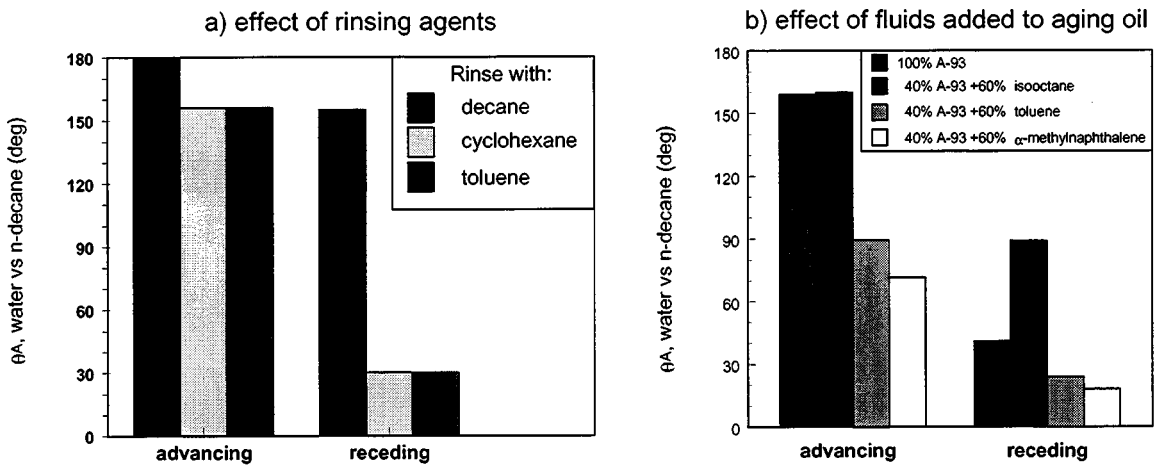

Figure 1.1-3. Contact angles (measured on glass surfaces treated with synthetic reservoir brine and A-93 crude oil) show that oil mixtures with poorer solvent quality have greater wettability altering tendency.

Acid/Base Interactions: Adhesion maps with NaCl brines show interactions between oil, brine, and solid as a function of brine composition. These tests highlight acid/base interactions. Fig. 1.1-4 shows the effects of adsorption during longer exposures of glass to oil. In these tests, too, the results depend strongly on brine composition. The water advancing angles can be quite water-wet or fairly oil-wet for the same oil and solid, aged under exactly the same conditions. The only difference is the pH and ionic strength of the brine. Note that the dependence on brine composition is expected to be different for every crude oil, since each oil has different acidic and basic components available for interfacial interactions.

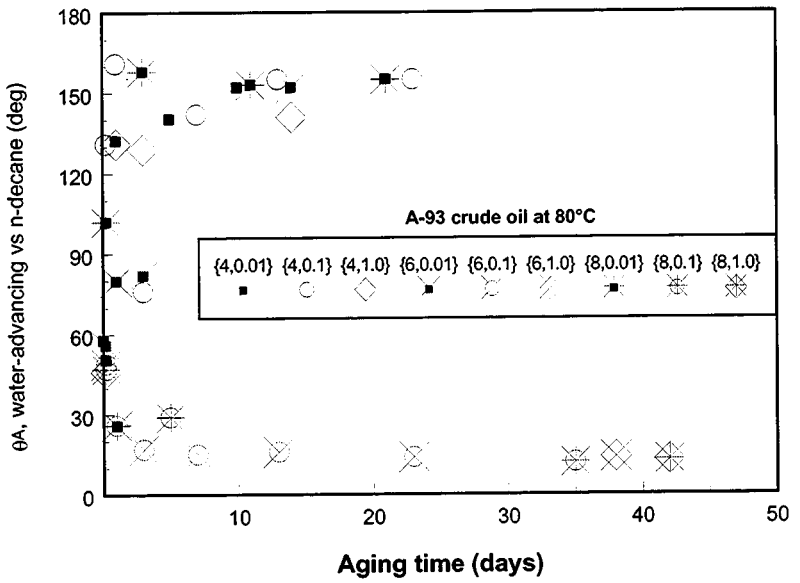

Figure 1.1-4. Brine composition can have a dominant effect on oil/solid interactions by the acid/base mechanism (after Liu and Buckley, 1997).

Ion Binding. When the brine phase contains dissolved salts of divalent or multivalent ions, the interactions become more complicated. pH is not directly a major determining factor in adhesion experiments (Buckley and Morrow, 1992), nor is adhesion a good indicator of adsorption interactions that occur with longer exposure times. The examples shown in Fig. 1.1-3 are for slides that were contacted with a synthetic reservoir brine that contains Ca^{2+} and Mg^{2+} in addition to Na^{+} and K^{+} cations before aging in crude oil. Interactions can be very dependent on temperature. High hysteresis, similar to that observed for acid/base interactions, has been observed. Interactions via ion binding appear to be somewhat more resistant to desorption than the acid/base interactions are for the same crude oil.

Summary. Some of the general characteristics identified for the four major categories of interaction are illustrated in Fig. 1.1-5. The arrows indicate typical rates at

which decane/water contact angles might increase on surfaces aged in oil. Solid lines indicate aging at elevated temperature and dotted lines are for room conditions. Similar diagrams have been drawn for each of the four mechanisms of interaction to summarize general features of many measurements of contact angles on brine and oil treated glass surfaces. These are collected in Table 1.1-1.

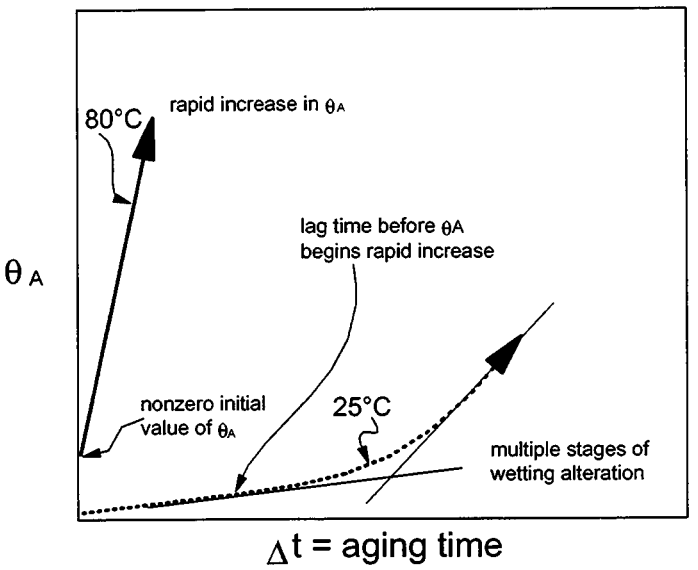

Figure 1.1-5. Illustration of the summary notation used in Table 1.1-1.

Table 1.1-1. Mechanisms of interaction between crude oils, brine, and solid surfaces

Type	Description	θ_A	Hysteresis (θ_A - θ_R)	Effects of Aging Conditions
Polar	If there is no water present, the strongest interactions are between polar atoms (N,S,O) and polar surface sites	~90	moderate	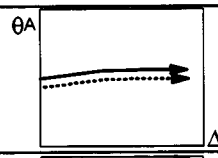
Surface precipi-tation	Occurs when oil is a poor solvent for its asphaltenes; changes in T, P, and in oil composition affect solvent properties	~180	low	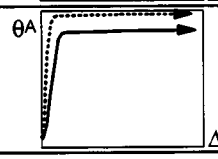
Acid/ base	Coulombic interactions between ionized acidic and basic sites; for **monovalent salt solutions at low concentration**, pH is the dominant variable	depends on oil & brine	high	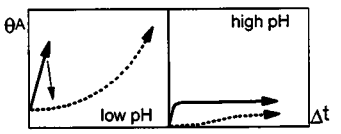
Ion binding	Coulombic interactions; divalent and multivalent ions can bind at both oil and solid/water interfaces and/or bridge between them	depends on oil & brine	high	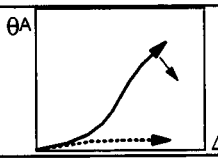

1.1.3 Interactions in Porous Media

Wetting in porous media can be inferred from observations of spontaneous imbibition. A standard method first described by Amott (1959) compares the amount of fluid that imbibes spontaneously with forced displacements. The results are Amott indices for water (I_w) and oil (I_o). Each index ranges from 0 (no spontaneous imbibition) to 1 (strongly wetted). The rate of spontaneous imbibition can also used to compare wetting in cores. Imbibition times can be scaled to account for differences in core length, porosity, permeability, fluid viscosities, and interfacial tension (Zhang *et al.*, 1995).

It is probable that more than one mechanism at a time contributes to crude oil/brine/rock interactions. Nevertheless, by comparing acidic and basic oils and oils of varying solvent quality, it is possible to see differences in wetting alteration that are consistent with the outlined mechanisms. Polar interactions that occur between oil and

dry surfaces are not likely to be important in most core studies since water is always the first fluid occupying the pore space.

Surface Precipitation: The best known example of wettability alteration by destabilizing the asphaltenes in a crude oil is the work of Salathiel (1973). In order to induce wettability alteration in cores, the crude oil was diluted with *n*-heptane. It is likely that surface precipitation contributed to the mixed-wet conditions observed.

Another example is the high gravity Lagrave crude oil. Lagrave readily alters wetting on silica and in sandstone cores (Gauchet, 1993; Morrow *et al.*, 1994) despite having only an intermediate acid number and low base number.

Acid/Base Interactions: The effect of aging Aerolith-10 (a synthetic porous medium that is composed primarily of silica) in A-93 crude oil has been shown to vary depending on brine pH (Buckley *et al.*, 1996). Low pH, favoring positive charge of basic functional groups, produced weakly water-wet conditions ($I_w = 0.5$), whereas at higher pH, with the same crude oil and aging conditions, strongly water-wet conditions ($I_w = 1$) were maintained.

Ion Binding—Three Crude Oils in Berea Sandstone: In natural sandstones, the interactions are more complex than in Aerolith. Acid/base interactions may still be important, but they cannot readily be isolated from the more complex contributions of the ion-binding mechanism. Ion binding provides an alternative mechanism for wetting alteration by which ions of the same sign as the solid surface can contribute. The details of this mechanism are undoubtedly complex and have yet to be worked out, but its consequences can be observed.

In Fig. 1.1-6, scaled imbibition rates show that wetting of Berea sandstone cores varies with oil composition for cores aged in three crude oils (Jadhunandan, 1990; Yildiz, 1995). The composition of the brine phase influences wetting alteration, especially for Moutray crude oil (Fig. 1.1-6a). The extent of wetting alteration does not correlate with the concentration of calcium ions in the brine nor with its total ionic strength (plotted as the gray bars in the legend).

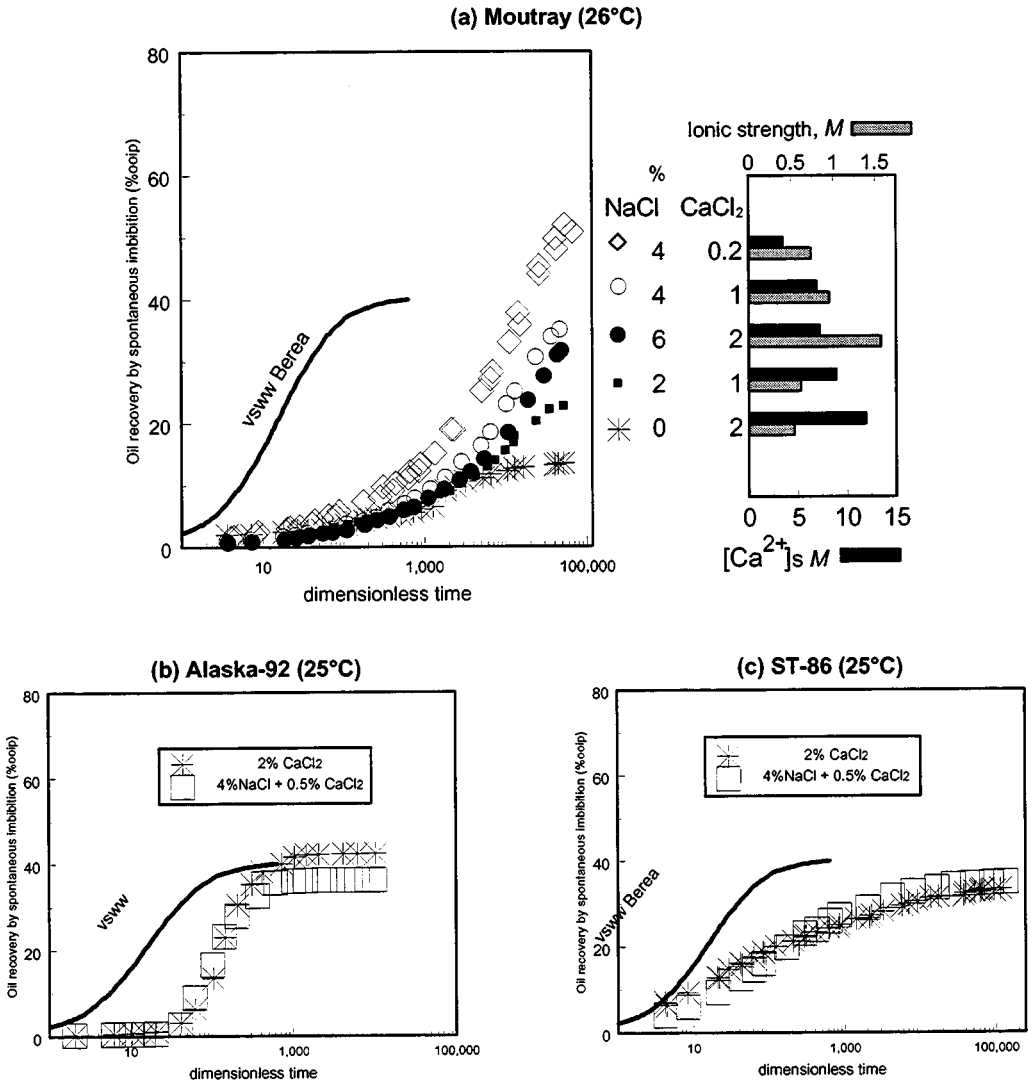

Figure 1.1-6. Rate of imbibition of brine into Berea sandstone cores after they were aged for 9-12 days with three different crude oil samples.

Counter ions (Na^+ and Ca^{2+}) are concentrated in the double layer near a negatively charged surface. Calculated values of calcium ion concentration near a negatively charged solid surface ($[Ca^{2+}]_s$) are shown in the bar graph in Fig. 1.1-6a. These values were calculated assuming a negative surface charge density of -0.2 C/m^2. The rate of imbibition decreases systematically with these calculated values of $[Ca^{2+}]_s$, suggesting that calcium ions are specifically involved in the interaction mechanism. Moutray, with a high acid number has many negatively charged interfacial sites and depends on the ion-binding mechanism for its wettability altering behavior.

Less acidic crude oils and those with different interfacial ratios of bases to acids respond differently than Moutray to changes in calcium ion concentration in the brine. For A-92, higher $[Ca^{2+}]_s$ *increases* the amount of oil produced by spontaneous imbibition (Fig. 1.1-6b) (Yildiz, 1995). Acid and base numbers are not available for A-92, but it is probably a fairly basic oil, judging by the other samples that have been tested from the same reservoir (A-90, A-93, and A-95). Wetting alteration by ST-86 (intermediate acid and base numbers) is almost completely insensitive to brine composition (Fig. 1.1-6c) (Jadhunandan, 1990).

The proposed ionic and surface precipitation mechanisms that are most relevant in oil reservoirs where both water and oil are present suggest that we need to characterize crude oils with respect to their polar components and the stability of their asphaltenes. Both of these areas are considered in the crude oil characterization program that follows.

1.2 Crude Oil Characterization

Crude oils consist of thousands of components and there are many ways to describe a given oil. Characterizations are constrained by technical limitations due to the complexity of the mixtures. The information that is most useful depends on the purpose for which it will be used. Since an important goal of this work is to relate oil composition to wetting alteration tendencies, chemical properties that relate to the identified interaction mechanisms have been the focus of characterization efforts in this work.

1.2.1 Measurements of Acid and Base Numbers

Acid numbers are routinely used to characterize the polar components of crude oils. Base numbers are less routinely measured, either because they are assumed to be correlated to acid numbers or because the values obtained have not been found useful. Base numbers measured by the standard method often underestimated the actual basic character of a crude oil. Since many of the interfacial properties of crude oils in contact with water appear to be traceable to acidic and basic functionality of interfacial species, it is of interest to measure both of these quantities by carefully standardized techniques for a wide range of crude oils.

1.2.1.1 Acid number measurements

Method ASTM-D664-89 was used for the determination of the acid number of crude oils. ASTM-D664-89 involves a potentiometric titration of a sample of crude oil (on average 2 to 5 g) dissolved in a mixture of toluene, isopropanol and water (50/49.5/0.5% by volume). The titration uses a 0.1N solution of KOH as titrant to determine the acid number. Contrary to the ASTM recommendation, the titration did not

completely exclude contact with air. The possibility of carbon dioxide contamination was addressed by purging the isopropanol with nitrogen before dissolving the KOH and by making a fresh solution of KOH every 2 weeks.

This method does not always give a sharp inflection point. Spiking the crude oil with a known amount of stearic acid in titration solvent (1ml of 0.1M) forces a clear inflection. The acid number can then be determined by difference, subtracting out the effect of the added stearic acid. This spiking procedure was verified via comparisons of spiked and unspiked titrations using oils which gave good inflections, as illustrated in Fig. 1.2-1.

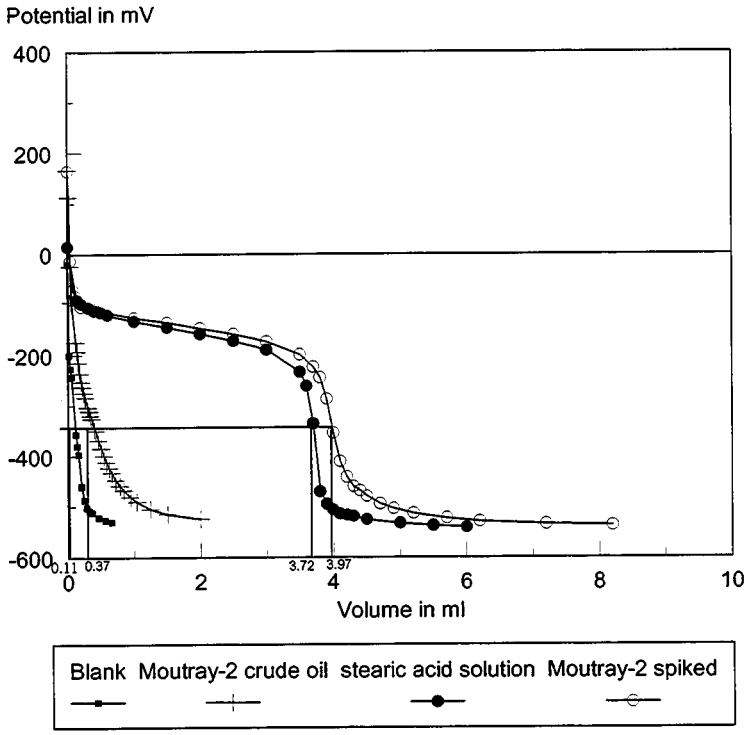

Figure 1.2-1. Comparison of Moutray-2 crude oil titrations with and without added stearic acid.

Ross half cells electrodes (the calomel electrode was filled with KCl electrolyte) were used, with an Orion pH/ISE meter model 520A. Titrant was added from a 25 ml burette, in increments of about 0.1 ml/min. The increment size was reduced to about 0.02

ml/min near the inflection point. For each sample, the solution was allowed to stabilize for 10 minutes before taking the first measurement. The end point was always observed between a potential of -300 and -400 mV. The end point was determined using the graphic method illustrated in Fig. 1.2-2.

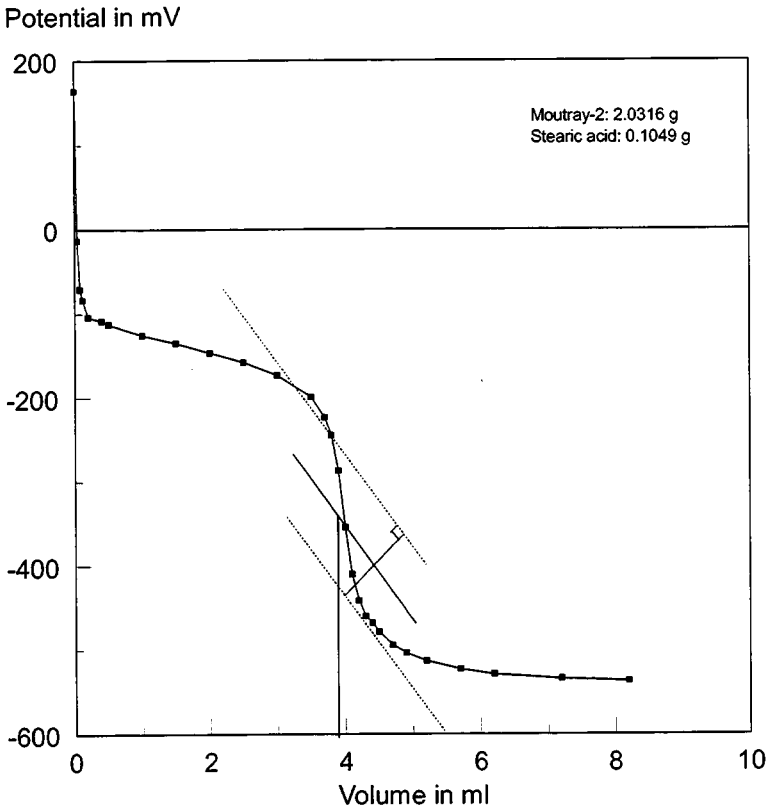

Figure 1.2-2. Titration of Moutray-2 crude oil spiked with stearic acid solution.

The acid number was calculated using the following equation:

$$AN, mgKOH/g = [(E-F) \times N_b \times 56.1] / S \qquad (1.2\text{-}1)$$

where E = equivalence point of the sample in ml,
F = equivalence point of the blank in ml,
N_b = normality of the KOH solution, and
S = sample size in grams.

1.2.1.2 Base number measurements

Method ASTM-D2896-88 was adapted for the determination of the base number of crude oils. ASTM-D2896-88 involves a potentiometric titration of a sample of crude oil (on average 1 to 3g) dissolved in 40 ml methyl isobutyl ketone. The titration uses perchloric acid at 0.025N as titrant to determine the base number.

The standard method does not give a sharp inflection point. To improve the analysis, the crude oil was spiked with a known amount of quinoline in decane (1ml of 0.08M) following the procedure of Dubey and Doe (1993). The presence of quinoline forced a good inflection. The base number was then determined by difference, subtracting out the effect of the added quinoline. The spiking procedure was verified by comparing spiked and unspiked titrations using oils which gave good inflections (see Fig. 1.2-3). The base numbers agreed within experimental error.

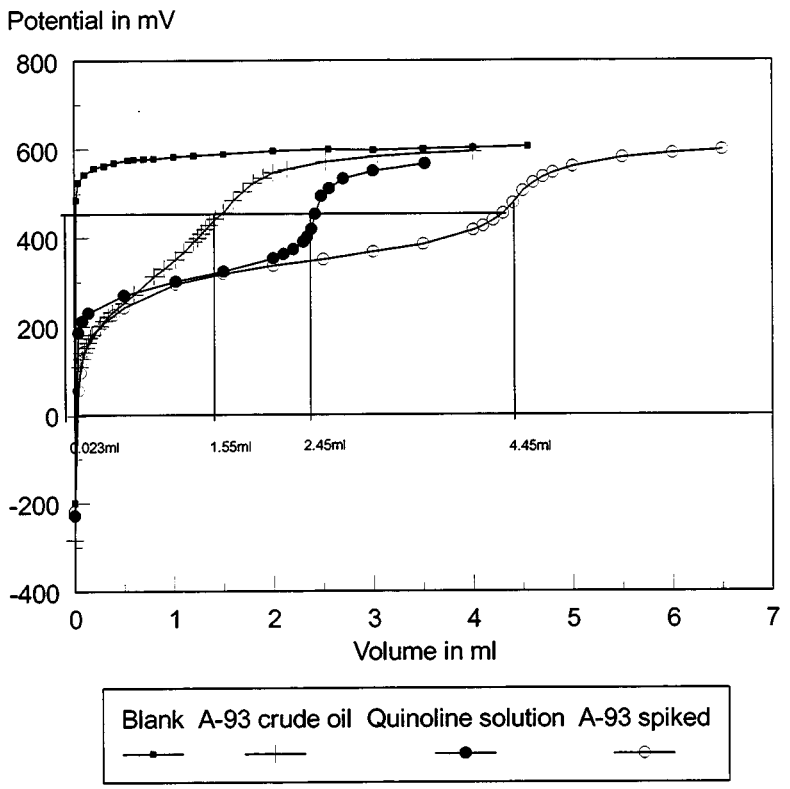

Figure 1.2-3. Comparison of A-93 crude oil potentiometric titrations with and without added quinoline.

For the potentiometric titration a combination pH electrode filled with a saturated solution of sodium perchlorate in isopropanol was used, with an Orion pH/ISE meter model 520A. Titrant was added from a 25 ml burette, in increments of about 0.1 ml/min. The increment size was reduced to about 0.02 ml/min near the inflection point. For each sample, the solution was left 10 minutes to stabilize before taking the first measurement. The end point was always observed between a potential of 400 and 500 mV. The end point was determined using a graphic method (illustrated in Fig. 1.2-4).

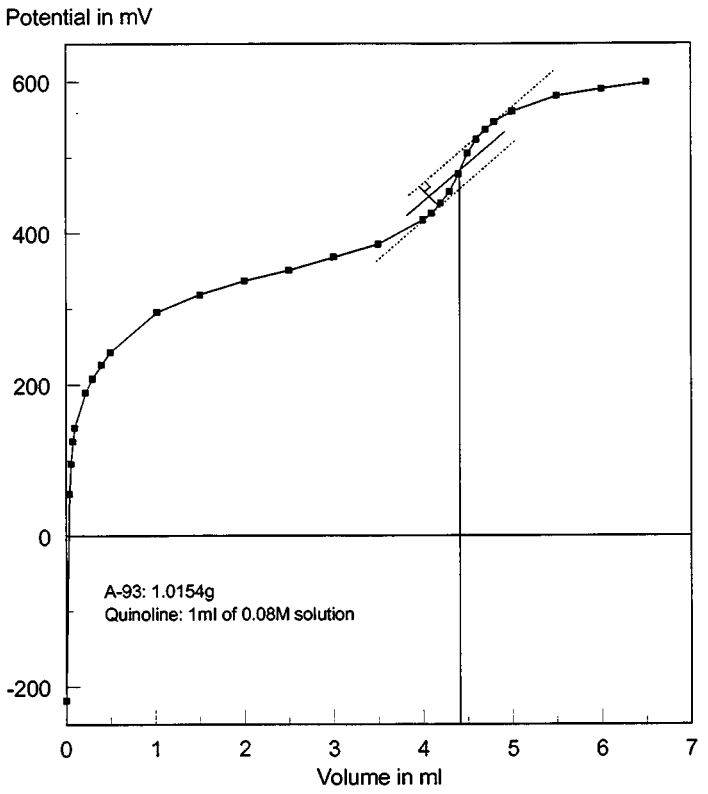

Figure 1.2-4. Graphical method for determination of the inflection point in a titration of A-93 crude oil plus quinoline.

The base number was calculated using the following equation:

$$BN, mgKOH/g = [(E-F) \times N_A \times 56.1] / S \qquad (1.2\text{-}2)$$

where E = equivalence point of the sample in ml,
F = equivalence point of the blank in ml,
N_A = the normality of the $HClO_4$ solution, and
S = the sample size in grams.

1.2.1.3 Results of acid and base number tests

Results of measurements of both acid and base number for 141 crude oil samples are summarized in Table 1.2-1. Acid numbers range from a low value of less than 0.01 mg KOH/g oil, which is the minimum detection limit, to a high value of 5.16 mg KOH/g oil. The average of all the acid numbers measured is 0.48. Base numbers range from a low of 0.11 to a high of 9.63, with an average value of 1.79 mg KOH/g oil.

Table 1.2-1. Acid and base numbers (in units of mg KOH/g oil)

Oil ID	Acid #	Base #
A-90	0.24	1.99
A-93	0.14	2.42
A-95	0.24	2.20
A-95-99	0.20	2.75
Arteza-22	0.12	1.28
Athel	0.02	0.20
B-1-00	0.04	0.85
Blindberry	0.07	0.72
Brookhaven	0.18	0.46
C-97	0.23	1.14
C-98	0.27	1.04
C-A1-00	0.34	3.44
C-A2-00	1.28	5.64
C-Ab-01	1.37	2.36
C-B-00	0.41	2.74
C-Br-01	0.08	0.11
C-BZ-01	0.68	2.66
C-GGC-00	1.49	0.94
C-HD-01	0.91	2.58
C-HL-01	<0.01	1.80
C-HM-01	0.08	4.31
C-K-01	0.99	5.21
C-L-01	0.35	2.29
C-LH-99	1.90	6.05
C-P-01	0.54	1.55
C-R-00	0.25	0.49
C-T1-00	0.10	3.60
C-T2-00	0.22	3.58
CA	0.39	5.19
CS	0.33	1.16
Cymric-12	5.16	9.63
Cymric-28	0.85	2.20
Dagang	0.66	4.67
DS-P-01	0.31	1.51
E-1XCO-01	0.18	1.93
E-1XD-00	1.56	2.98
E-1XFR-01	0.16	0.65
E-1XO-00	3.42	2.57
E-1XR-00	0.54	2.02
E-2XR-00	0.91	2.46
E-8XFR-01	1.03	0.74
E-BL-00	0.17	1.33
E-S1XCA-01	0.48	3.42
E-S1XG-01	0.14	1.57
E-S1XL-01	0.48	1.83
E-S3XR-01	0.23	2.03
Edop	0.29	1.27
EMSU	0.55	0.80
GOM(1)-00	0.35	1.75
GOM(1)-01	0.32	1.62
GOM(2)-00	2.02	1.79
Gullfaks-96	0.24	1.19
H3-97	0.17	1.67
JR-1	1.95	2.05
JR-2	0.56	1.92
JR-3	2.07	2.05
Lagrave	0.29	0.65
Lagrave-97	0.13	0.91
Maljamar	0.12	0.72
Mars-97	0.37	1.79
Mars-P	3.92	2.09
Mars-TC	0.49	1.88
Minnelusa	0.17	2.29
Moutray-1	0.55	0.81
Moutray-2	0.72	0.90
NBU-1	0.14	0.56
NE-224-55-A	0.10	1.07
NE-224-55-B	0.67	0.74
NE-224-55-C	0.66	0.33
NE-224-55-D	0.31	0.54
NE-224-55-E	0.04	2.95
NE-224-55-F	0.24	1.16
NE-224-55-G	0.29	0.11
NE-224-55-H	1.65	1.20
NE-224-55-I	0.20	0.58
NE-224-55-J	0.05	0.70
NE-224-55-K	0.21	0.67
NE-224-55-L	0.17	1.42
NE-224-55-M	0.25	0.76
NE-224-55-N	0.44	2.70
NE-224-55-O	0.60	1.63
NE-224-55-P	0.13	1.28
NE-224-55-Q	0.35	2.30
NE-224-55-R	0.15	1.76
NE-224-55-S	1.06	3.08
NH-01	0.22	1.06
NH-02	0.28	1.24
NH-03	0.20	1.58
NH-S4	0.17	1.54
OS034X	0.16	0.80
P-E-00	0.11	1.50
P-VE-00	0.05	1.54
Petroglyph	0.11	1.55
S-Ven-39	0.14	1.68
S-Ven-40	0.13	1.62
S-Ven-41	0.43	1.78
SA051X	0.25	0.80
Schuricht	0.28	2.09
Smackover	0.41	0.90
Smackover	0.24	1.99
Spraberry-1	0.32	2.83
Spraberry-3	0.09	2.65
SQ-94	0.45	0.24
SQ-95	0.16	0.62
ST-86	0.48	1.07
ST-87	0.29	1.17
ST-88	0.24	0.53
ST-89	0.10	0.92
Steen-NM-1	0.26	2.93
Steen-NM-2	<0.01	1.53
Steen-TR-000	0.69	2.06
Steen-TR-210	0.20	1.34
Steen-TR-253	<0.01	0.55
Tensleep	0.16	0.96
Tensleep-99	0.10	1.03
UBergen-1	0.09	1.79
W-Mi-01	<0.01	0.19
W-Mu*-01	0.02	0.20
W-Pe-01	0.66	4.76
W-PM-01	0.11	1.37
W-Po*-01	0.07	1.40
W-PT*-01	0.20	1.30
W-Tr*-01	0.50	0.64
W-TU*-01	0.44	0.97
W-Up-01	<0.01	0.67
W-Ur-01	0.20	1.45
W-Wy*-01	<0.01	0.27
Wasson	0.32	0.97

Figure 1.2-5 shows a log-log cross plot of acid and base numbers measured on identical samples. While there is a broad tendency for samples with higher acid numbers to have higher base numbers and vice versa, no clear correlation between the two numbers emerges. In general, base numbers are higher than acid numbers in the set of samples in our study.

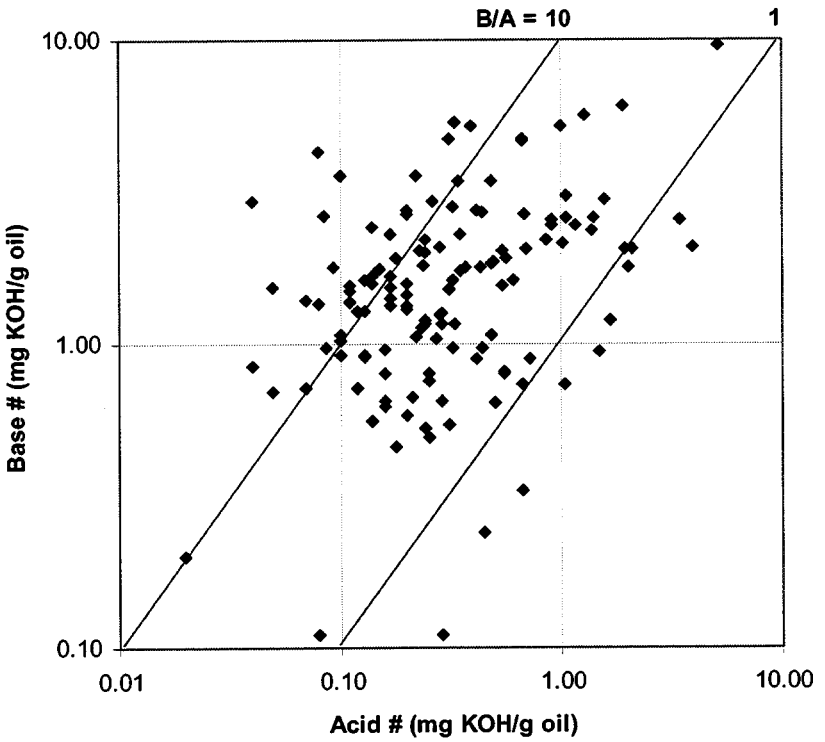

Figure 1.2-5. Log-log plot of base number vs. acid number where both were measured for the same crude oil sample. 141 samples are included in this comparison.

1.2.2 Onset of Asphaltene Precipitation at Ambient Conditions

The asphaltenes are implicated in wetting, but only recently has the connection between wetting alteration and the solvent environment of the asphaltenes begun to be established (Buckley *et al.*, 1997; Tang *et al.*, 1996). The *amount* of asphaltene in an oil is less important than the fact that it *is* present and in what solvent environment. The evidence suggests that as the oil becomes a poorer asphaltene solvent, its tendency to

make surfaces more oil-wet increases. Solubility parameters that have been used to characterize crude oils and onset conditions cannot be measured directly for the complex mixtures that constitute crude oils. A critical solubility parameter at the onset of asphaltene flocculation can be inferred from experiments at high dilution, but the relevance of such experiments is questionable. In order to account for the contribution of surface precipitation to wettability altering interactions, it is essential that a method be developed to characterize crude oils with respect to the stability of their asphaltene fraction. The development and application of such a method is described in the following sections.

1.2.2.1 Heptane onset at ambient conditions—RI_{oil} and P_{RI}

Refractive index can be used to quantify solvent quality (Buckley, 1996a). Refractive index (RI) measurements are used in tandem with observations of the onset of precipitation. The onset of asphaltene precipitation is readily observed microscopically at relatively low magnification (at least 45X). Asphaltene can usually be distinguished from other solids in the oil, especially paraffin, because it is amorphous. Crystalline wax appears as bright spots under polarized light, whereas asphaltenes are completely dark.

The use of RI to quantify the state of the asphaltenes can best be explained by a few simple illustrations. Figure 1.2-6 is a schematic outline of the procedure. In Fig. 1.2-7, RI is plotted as a function of the volume fraction of oil in a mixture of oil and precipitant. Small amounts of isooctane can be mixed with A-93 without causing precipitation. RI's of mixtures that remain free of asphaltene precipitate are indicated by open circles. In sufficiently high concentration, isooctane causes asphaltene to

precipitate from A-93 crude oil. Those mixtures containing precipitate are indicated by filled circles.

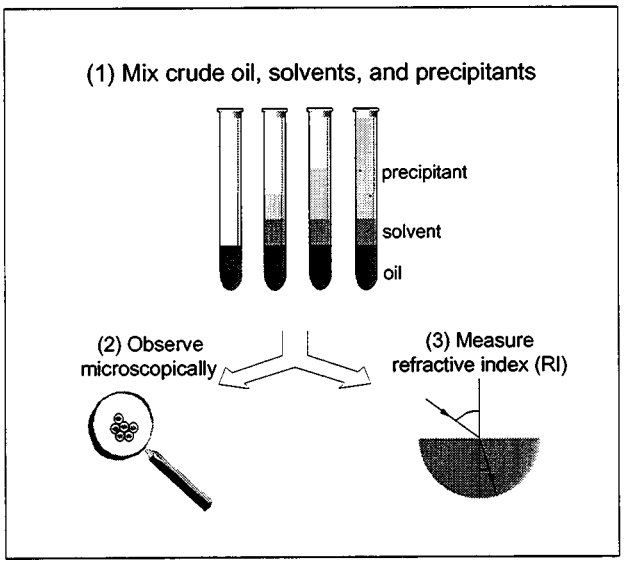

Figure 1.2-6. Schematic illustration of the onset of precipitation test procedure.

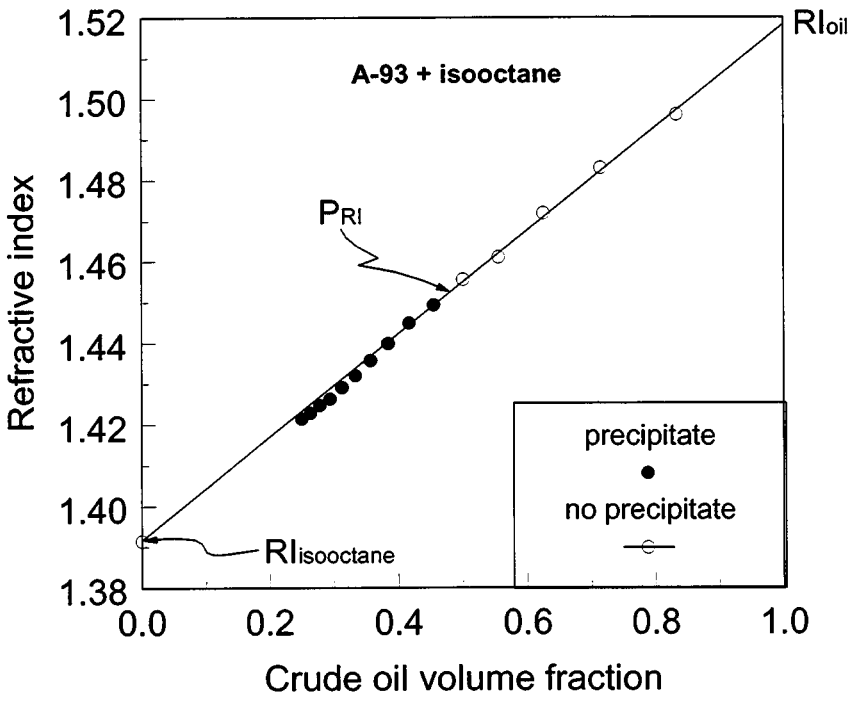

Figure 1.2-7. Refractive index of mixtures of a sample of crude oil from Prudhoe Bay with isooctane, plotted as a function of the volume fraction of the mixture that is crude oil. Open circles have no microscopically visible precipitate. Precipitate is observed in the mixtures indicated by the closed symbols.

The RI at the onset of precipitation, P_{RI}, is about 1.45 for A-93 and isooctane. RI of the stock-tank oil cannot be accurately measured if the oil is too opaque. It can, however, be estimated by linear extrapolation of the mixture RI's. Only the precipitate free mixtures and pure isooctane are used in this extrapolation. Once precipitation occurs, mixture RI's can deviate from the linear relationship. Figure 1.2-8 shows a case where RI can be measured directly, confirming that the relationship is linear and the estimate of RI_{oil} is accurate.

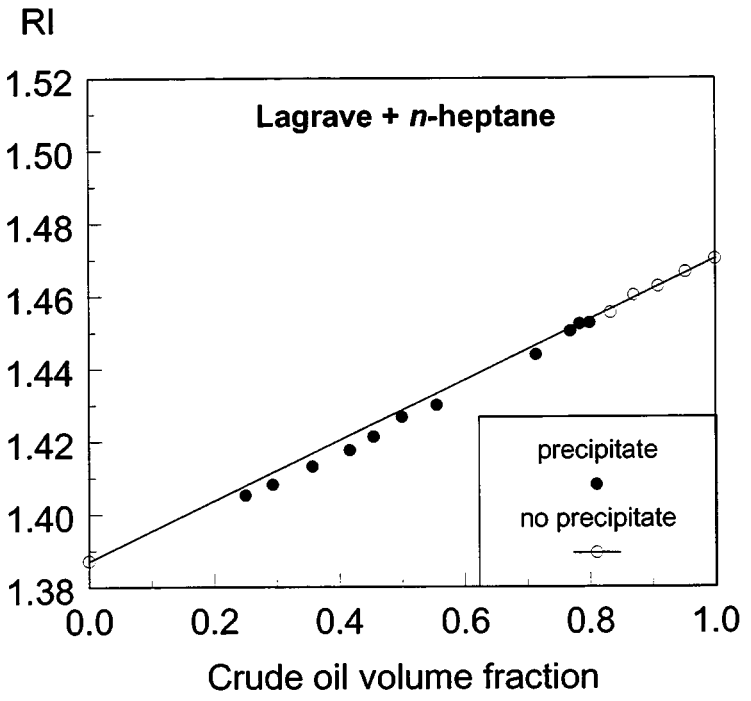

Figure 1.2-8. Accuracy of the linear extrapolation is demonstrated by mixtures of Lagrave crude oil and *n*-heptane.

The oil sample in Fig. 1.2-9 shows extreme deviation from linearity when precipitation has occurred. Separation of precipitate from the oil could also be observed in the bulk solution without the aid of a microscope. The range of precipitate-free solutions was limited, so RI_{oil} was confirmed by mixing oil and toluene.

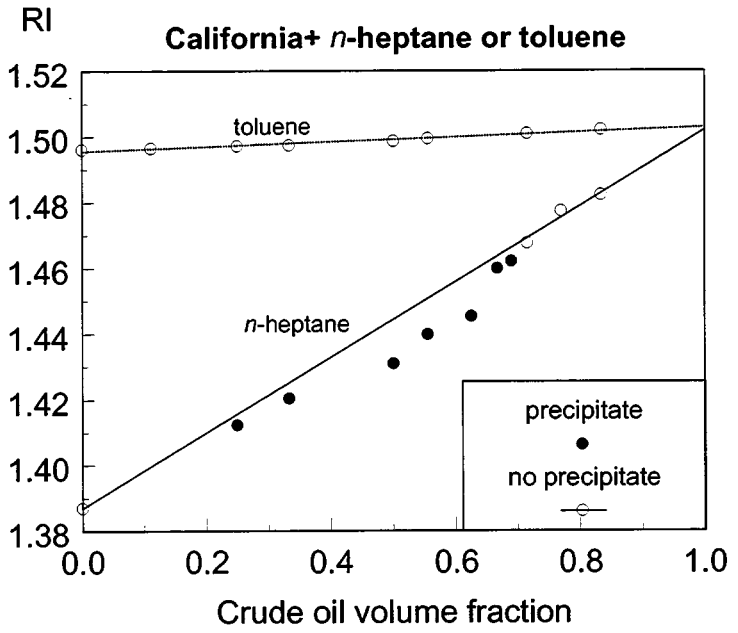

Figure 1.2-9. Deviation from linearity can be severe, as shown for a crude oil from the Ventura field. RI_{oil} was confirmed using mixtures of oil and toluene.

A detailed procedure for determining the onset of asphaltene flocculation is given in Appendix I. Onsets have successfully been determined from a wide variety of dead crude oil samples, including those that may have flocculated asphaltenes, precipitated wax crystals, and/or emulsified water droplets.

Two points, RI_{oil} and P_{RI}, are obtained for each oil. We can then define a measure of the stability of the asphaltenes:

$$\Delta_{RI} = RI_{oil} - P_{RI} \tag{1.2-3}$$

Values of RI_{oil}, P_{RI} and Δ_{RI} are summarized in Table 1.2-2. Stability of the asphaltenes in their crude oils can be judged from the Δ_{RI} values in the right column. The same comparison can be made visually as shown in Fig. 1.2-10.

Table 1.2-2. Summary of RI_{oil} and P_{RI} values

Oil ID	RI at 20°C	nC7 Pri	ΔRI
A-93	1.5170	1.4459	0.0711
A-95	1.5128	1.4513	0.0615
A-95-99	1.5139	1.4435	0.0703
B-1-00	1.4695	1.4339	0.0356
C-97	1.4858	1.4455	0.0403
CA	1.5024	1.4650	0.0373
C-A1-00	1.4816	1.4348	0.0468
C-A2-00	1.5146	1.4368	0.0778
C-B-00	1.4739	1.4234	0.0505
C-BZ-01	1.4910	1.4025	0.0885
C-GGC-00	1.4951	1.3943	0.1008
C-HD-01	1.5220	1.4329	0.0891
C-HL-01	1.4920	1.4421	0.0499
C-LH-99	1.5137	1.4231	0.0906
C-P-01	1.4845	1.4335	0.0510
C-R-00	1.4851	1.4444	0.0407
C-R-01	1.4846	1.4446	0.0400
C-T1-00	1.4868	1.4332	0.0536
C-T2-00	1.4887	1.4336	0.0551
Cymric-12	1.5512	1.4496	0.1016
Cymric-28	1.4998	1.4301	0.0697
E-1XCO-01	1.4795	1.4163	0.0632
E-1XD-00	1.5141	1.4336	0.0805
E-1XFR-01	1.4667	1.4039	0.0628
E-1XO-00	1.5142	1.4142	0.1000
E-1XR-00	1.4912	1.4071	0.0841
E-2XR-00	1.5040	1.4274	0.0766
E-8XFR-01	1.4676	1.4020	0.0656
E-BL-00	1.4896	1.4395	0.0501
EMSU	1.4830	1.4290	0.0540
E-S1XCA-01	1.5123	1.4626	0.0498
E-S1XG-01	1.4899	1.4681	0.0218
E-S1XL-01	1.4800	1.4088	0.0712
E-S3XR-01	1.4907	1.4238	0.0670
H3-97	1.4770	1.4380	0.0390
JR-1	1.5220	1.4330	0.0890
JR-2	1.5090	1.4320	0.0770
JR-3	1.5300	1.4230	0.1070
Lagrave	1.4659	1.4530	0.0129
Lagrave-97	1.4793	1.4613	0.0180
Mars-97	1.4952	1.4298	0.0655
Mars-P	1.5384	1.4288	0.1095
Mars-TC	1.5100	1.4508	0.0592
Minnelusa	1.5142	1.4768	0.0374
Moutray-1	1.4833	1.4346	0.0487
O-674-00	1.4768	1.4329	0.0439
O-677-00	1.4716	1.4116	0.0600
O-678-00	1.5291	1.4281	0.1010
O-680-00	1.4951	1.4288	0.0663
O-681-00	1.4936	1.4430	0.0506
O-682-00	1.4820	1.4449	0.0371
O-683-00	1.4964	1.4484	0.0480
O-685-00	1.5244	1.4215	0.1029
O-687-00	1.5126	1.4377	0.0749
O-688-00	1.5138	1.4424	0.0714
P-VE-00	1.4885	1.4388	0.0497
Schuricht	1.5130	1.4480	0.0650
SQ-95	1.4769	1.4223	0.0546
Steen-NM-1	1.5288	1.4683	0.0605
Steen-NM-2	1.4939	1.4620	0.0320
Steen-OLEOD	1.5331	1.4262	0.1069
Steen-TR-000	1.5644	1.4476	0.1168
Steen-TR-210	1.5205	1.4370	0.0835
Steen-TR-253	1.5033	1.4268	0.0764
S-Ven-39	1.4976	1.4465	0.0511
S-Ven-40	1.4922	1.4492	0.0430
S-Ven-41	1.4985	1.4504	0.0481
Tensleep	1.4877	1.4438	0.0439
Ventura-Rice	1.4900	1.4500	0.0400
W-Cl-01	1.5130	1.4117	0.1014
W-Fo-01	1.4740	1.4188	0.0552
W-Gu-01	1.4868	1.4142	0.0726
W-Mac-01	1.5160	1.4236	0.0924
W-Mau-01	1.5229	1.4432	0.0797
W-Mi-01	1.4747	1.4242	0.0505
W-Mu*-01	1.4648	1.4078	0.0570
W-Pe-01	1.5409	1.4445	0.0964
W-PM-01	1.5023	1.4436	0.0587
W-Po*-01	1.4836	1.4232	0.0604
W-PT*-01	1.4785	1.4158	0.0627
W-Tr*-01	1.4709	1.4182	0.0527
W-TU*-01	1.4769	1.4161	0.0607
W-Up-01	1.4909	1.4472	0.0438
W-Ur-01	1.4904	1.4202	0.0701
W-Wy*-01	1.4605	1.4033	0.0572

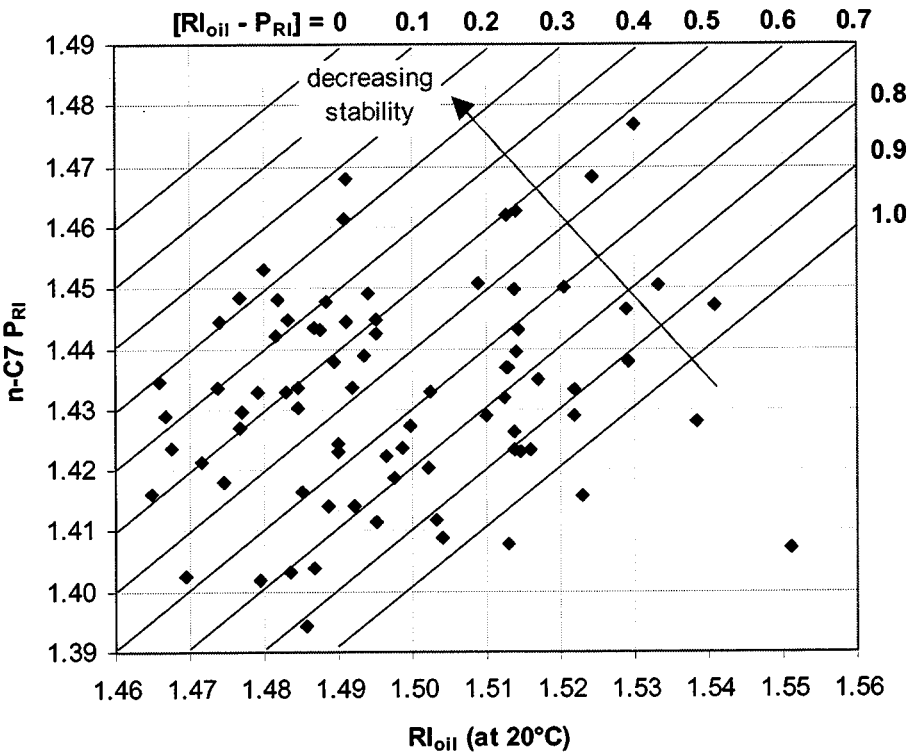

Figure 1.2-10. Asphaltene stability diagram compares RI_{oil} (a measure of the oil's solvent power) and P_{RI} (a measure of stability of the same oil's asphaltenes).

There are oils that do not produce any visible sign of asphaltene precipitation in tests with *n*-heptane. One such oil from the North Sea is shown in Fig. 1.2-11. Linearity is maintained over the whole range of mixtures. Some other oils in this category tested with the *n*-heptane procedure include NBU and Spraberry.

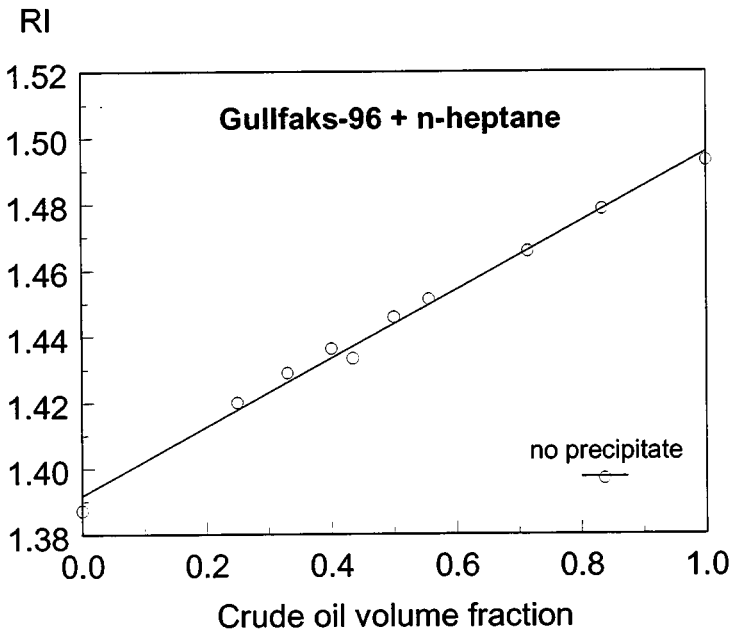

Figure 1.2-11. Mixtures of ST-86 and *n*-heptane are free of precipitate for all volume fractions of oil.

1.2.2.2 RI as a measure of solvent quality for asphaltene stability characterization—theoretical development

(in collaboration with G.J. Hirasaki and B.S. Gill, Department. of Chemical Engineering, Rice Univ.)

Thermodynamic models for predicting asphaltene precipitation traditionally have used the Hildebrand solubility parameter (Hildebrand and Scott, 1964) to estimate the heat of solution (Hirschberg *et al.*, 1984; Leontaritis and Mansoori, 1987; Burke *et al.*, 1990; MacMillan *et al.*,1995; Cimino *et al.*, 1995a, 1995b; Rassamdana *et al.*, 1996; Victorov and Firoozabadi, 1996; Pan and Firoozabadi, 1996). In these models, the heat of asphaltene-crude oil interaction, ΔH^M, is a function of the difference between the solubility parameter of the asphaltene (δ_a) and that of the remaining components of the crude oil (δ_s).

$$\Delta H^M \propto (\delta_a - \delta_s)^2 \tag{1.2-4}$$

where the subscript a denotes asphaltene and the subscript s denotes the remaining components of the oil or the "solvent."

The Flory-Huggins model describes the intermolecular interactions with a dimensionless interaction parameter, χ.

$$\chi = \frac{V_s}{RT}(\delta_a - \delta_s)^2 \tag{1.2-5}$$

This term represents the heat or excess energy of solute-solvent interactions. The models' predictions are limited by the accuracy of this term. The solubility parameter of the oil is estimated by approximating the cohesive energy density from the equation-of-state fit to live oil PVT data.

Assumption regarding London dispersion interactions

We assume that the dominant intermolecular interaction energy governing asphaltene precipitation is the London dispersion contribution to the van der Waals forces. London dispersion interactions occur between all molecules, including nonpolar ones; their occurrence is due to induced polarization. The London dispersion properties of a material can be characterized by the wavelength dependence of the refractive index (RI) or the "dispersion" of visible light. Polar interactions (dipole, ionic, charge transfer, hydrogen bonding, etc.), which are commonly used to describe asphaltene-resin interactions, are assumed to be of secondary importance. In the work that follows, the resin fraction of the crude oil will not receive special treatment. Resins will be considered to be components of the "solvent" fraction and the asphaltenes will be treated

as the "solute." Electronic polarizability, related to aromaticity, is an important resin property in this model.

In support of this assumption, we observe that nonpolar materials of similar molecular size and structure can be either solvents or precipitants for asphaltenes, depending on their degree of polarizability. Consider, for example, the 7-carbon compounds, *n*-heptane (RI=1.3878) and toluene (RI=1.4961). The former is a precipitant and the latter is a solvent for asphaltenes. Also consider liquid carbon dioxide, CO_2 (RI=1.195) and carbon disulfide, CS_2 (RI=1.6319). The former is a precipitant and the latter is a solvent for asphaltenes. Thus, the induced polarizability, as quantified by the RI, appears to be important in determining the ability of hydrocarbons to serve as a precipitant or as a solvent for asphaltenes.

Further support is provided by the solubility parameter mapping of Wiehe (1996) which shows that asphaltene insolubility is dominated by aromaticity and molecular weight, not by polar or hydrogen bonding interactions.

The assumption of dominance of London dispersion forces would certainly not be true if significant amounts of polar materials were added to the crude oil mixture. However, since polar components are relatively minor compared to the amount of hydrocarbon in crude oils, we will ignore the contribution of polar interactions in this analysis.

The interaction energy between asphaltene molecules in a solvent medium with only London dispersion interactions (assuming the adsorption frequency of the asphaltene and the solvent are the same) is as follows (Israelachvili, 1991, Eq. 6.35):

$$w(r) = -\frac{\sqrt{3}hv_e}{4}\frac{\left(n_a^2 - n_s^2\right)^2}{\left(n_a^2 + 2n_s^2\right)^{3/2}}\frac{a_a^6}{r^6} \tag{1.2-6}$$

$$= -\frac{C}{r^6}, \quad r > 2a_a$$

$$C = \frac{\sqrt{3}hv_e a_a^6}{4}\frac{\left(n_a^2 - n_s^2\right)^2}{\left(n_a^2 + 2n_s^2\right)^{3/2}} \tag{1.2-7}$$

where h is Planck's constant, v_e is the absorption frequency in the ultraviolet, n_a and n_s are the refractive indices of asphaltene and the solvent (extrapolated to zero frequency), a_a is the equivalent radius of the asphaltene molecule, r is distance between the centers of the molecules, and C is the coefficient of the distance dependence. The interaction energy is now expressed as a function of the differences between the squares of the refractive indices rather than the difference between the solubility parameters of asphaltene and solvent.

For a molecule of asphaltene interacting with the surface of a macroscopic body of asphaltene across a solvent medium, the energy is as follows (Israelachvili, 1991, Eq. 10.2):

$$w(D) = -\frac{\pi C \rho_a}{6D^3} \quad (\text{molecule} - \text{surface}) \tag{1.2-8}$$

where D is the distance of the molecule from the surface and ρ_a is the number density of asphaltene molecules in the macroscopic body. If the interaction is between two spherical aggregates of asphaltene or between a spherical aggregate and the surface of a macroscopic body of asphaltene, then the energy of interaction is as follows (Israelachvili, 1991, Eq. 10.5):

$$W(D) = -\frac{\pi^2 C \rho_a^2 R}{6D} \quad \text{(sphere – sphere or sphere – surface)} \qquad (1.2\text{-}9)$$

where R is the radius of the spherical particle. If the interaction is between two parallel surfaces of macroscopic bodies of asphaltene, the interaction energy per unit area is as follows (Israelachvili, 1991, Eq. 10.8):

$$W(D) = -\frac{\pi C \rho_a^2}{12D^2} \quad \text{(surface – surface, per unit area)} \qquad (1.2\text{-}10)$$

Hirasaki (1993) used a generalization of these concepts to predict the contact angles of non-polar materials on Teflon and the spreading of non-polar materials at the gas/water interface.

The solubility parameter will be approximated by the van Laar-Lorenz approach using the van der Waals equation of state (EOS) cohesion parameter (Hildebrand and Scott, 1964).

$$\delta \approx \frac{a^{1/2}}{V} \qquad (1.2\text{-}11)$$

where a is the van der Waals (vdW) EOS cohesion parameter and V is the molar volume. The vdW cohesion parameter can be expressed in terms of the parameters of the pair interaction energy (Israelachvili, 1991, Eq. 6.10):

$$a = \frac{2\pi N_o^2 C}{3\sigma^3} \qquad (1.2\text{-}12)$$

where σ is the hard sphere diameter. The pair interaction model, Eq. (1.2-6) & (1.2-7), will be used for the parameters in this equation. Let the "solvent" be vacuum (i.e., RI=1.0) and "asphaltene" be the species for which the solubility parameter is to be determined. The resulting expression for the solubility parameter is as follows:

$$\delta = \left(\frac{\sqrt{3}\pi}{384} \frac{h\nu_e}{\sigma^3} \right)^{1/2} \frac{\sigma^3}{V / N_o} \frac{n^2 - 1}{\left(n^2 + 2\right)^{3/4}} \tag{1.2-13}$$

This equation expresses the solubility parameter in terms of the refractive index.

The correlation between the solubility parameter and the RI at ambient conditions for a number of *n*-alkane and aromatic hydrocarbons (Weast, 1987; Barton, 1991) is illustrated in Fig. 1.2-12. The exponent of ¾ in Eq. 1.2-13 has been approximated by an exponent of unity. The comparison shown here is between a function of RI

$$F_{RI} = \frac{n^2 - 1}{n^2 + 2} \tag{1.2-14}$$

and the corresponding solubility parameters for paraffinic and aromatic hydrocarbons.

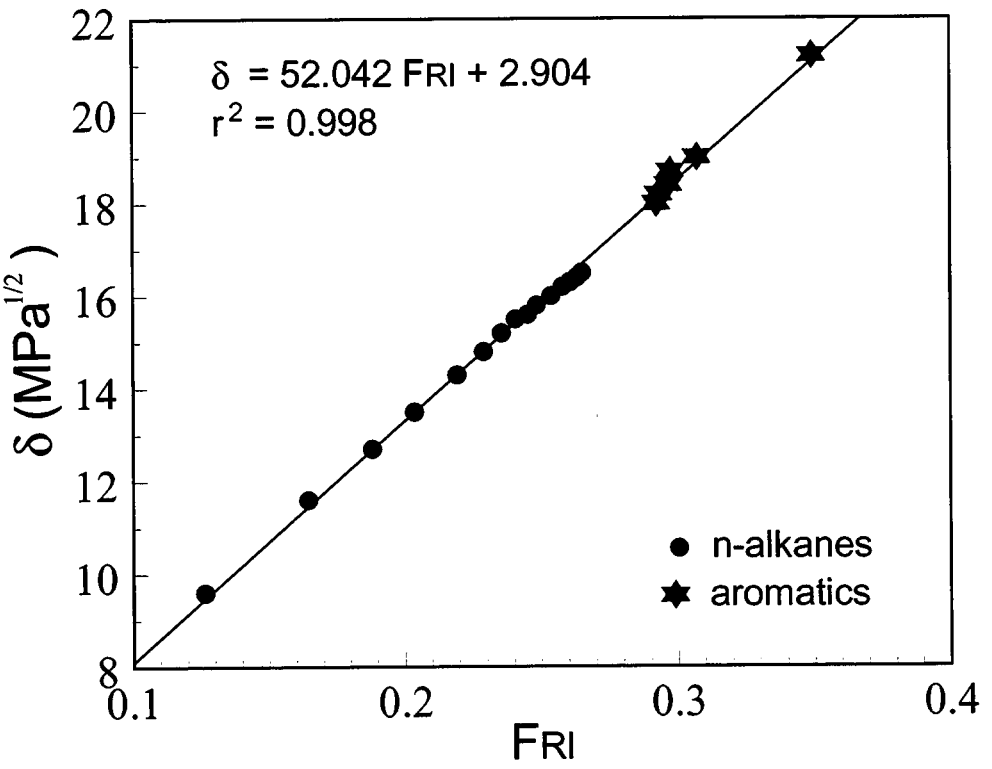

Figure. 1.2-12. Comparison of solubility parameter and F_{RI}.

Composition and density dependence of RI

The refractive index is expressed as a function of composition and density through the Clausius-Mossotti or Lorenz-Lorentz equation (Feynman, *et al.*, 1989; Vedam and Limsuwan, 1978).

$$\frac{3}{4\pi}\left(\frac{n^2-1}{n^2+2}\right)=\sum_i \frac{C_i \alpha_i}{4\pi \varepsilon_o N_o} \tag{1.2-15}$$

where C_i is the molar concentration of species i, α_i is the electronic polarizibility of species i, ε_o is the permittivity of free space, and N_o is Avogadro's number. This can be expressed in terms of the RI at some reference condition.

$$\left(\frac{n^2-1}{n^2+2}\right)=\sum_i \frac{C_i}{C_i^o}\left(\frac{n^2-1}{n^2+2}\right)_i^o \tag{1.2-16}$$

This expression describes the composition and density dependence of the RI. The coefficients of the C_i term are molar refractions. At ambient conditions and with ideal volume of mixing, the ratio, C_i / C_i^o is equal to the volume fraction of component i in the mixture. The molar refraction of a mixture can be expressed as a function of the mole fractions and molar refractions of its components by dividing Eq. 1.2-16 by the total molar concentration, C_Σ.

$$\begin{aligned}\frac{1}{C_\Sigma}\left(\frac{n^2-1}{n^2+2}\right)&=\sum_i \frac{X_i}{C_i^o}\left(\frac{n^2-1}{n^2+2}\right)_i^o \\ C_\Sigma &= \sum_i C_i \\ X_i &= \frac{C_i}{C_\Sigma}\end{aligned} \tag{1.2-17}$$

The validity of the Lorenz-Lorentz equation to describe the density dependence of RI was investigated by Vedam and Limsuwan (1978). For example, Fig. 1.2-13

compares the calculated and measured change in RI of *n*-octane with pressure. The observation that the calculated RI is greater than the measured RI implies that the electronic polarizability and molar refraction are not strictly independent of density.

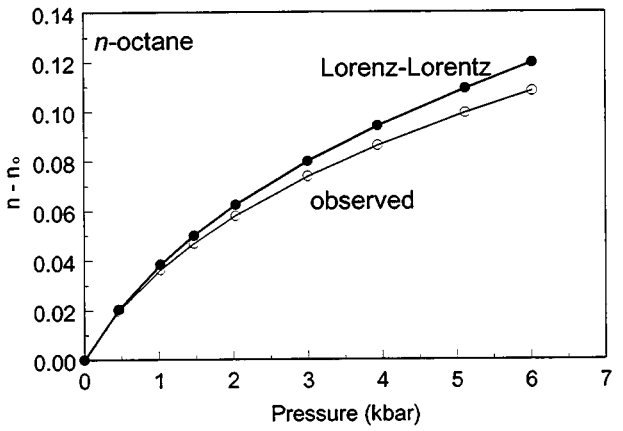

Figure. 1.2-13. Comparison of calculated and measured RI values for *n*-octane.

Live crude oil can be treated as a mixture of stock tank oil and separator gas. The RI of the live oil can be calculated from the formation volume factor, $B_o(P)$,(RB/STB), the solution gas/oil ratio, $R_s(P)$,(scf/STB), the RI of the stock tank oil, and the molar refraction of the separator gas.

$$\left(\frac{n^2-1}{n^2+2}\right)(P)=\frac{1}{B_o}\left(\frac{n^2-1}{n^2+2}\right)_{STO}+7.52\times10^{-6}\frac{R_s}{B_o}\frac{1}{C^o_{gas}}\left(\frac{n^2-1}{n^2+2}\right)^o_{gas} \quad (1.2\text{-}18)$$

The factor of 7.52×10^{-6} in the second term on the right-hand-side of Eq. 1.2-18 converts R_s from scf/bbl to moles/cm^3.

The molar refraction of the components of the separator gas can be calculated from group contributions (Weast, 1987).

$$\frac{1}{C^o_{gas}}\left(\frac{n^2-1}{n^2+2}\right)^o_{gas}=R_{gas}=\sum_i X_i R_i \quad (1.2\text{-}19)$$

where X_i is the mole fraction and R_i is the molar refraction of component *i*.

Refractive indices calculated from molar refractions and values reported from measurements (Weast, 1987) are compared for a number of *n*-alkanes and aromatic hydrocarbons in Fig. 1.2-14. The agreement is very good for all except styrene.

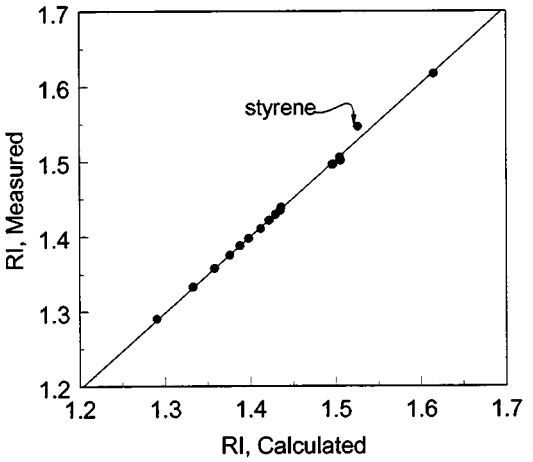

Figure 1.2-14. Comparison of calculated and measured RI.

Frequency dependence of RI

The expression for the intermolecular interactions in Eq. 1.2-6 has the RI, extrapolated to zero frequency, as a parameter. Often, the RI is available only at the frequency of the sodium-D line. Figure 1.2-15 is a Cauchy plot (Hough and White, 1980) of selected hydrocarbons. The slope is used to determine the absorption frequency, and the intercept gives the RI extrapolated to zero frequency. The value of RI at the sodium-D line is indicated. The curves are nearly parallel. Thus, since it is the difference between RI values that is related to the interaction energy, the values of RI measured at the frequency of the sodium-D line can be used to approximate the RI extrapolated to zero frequency.

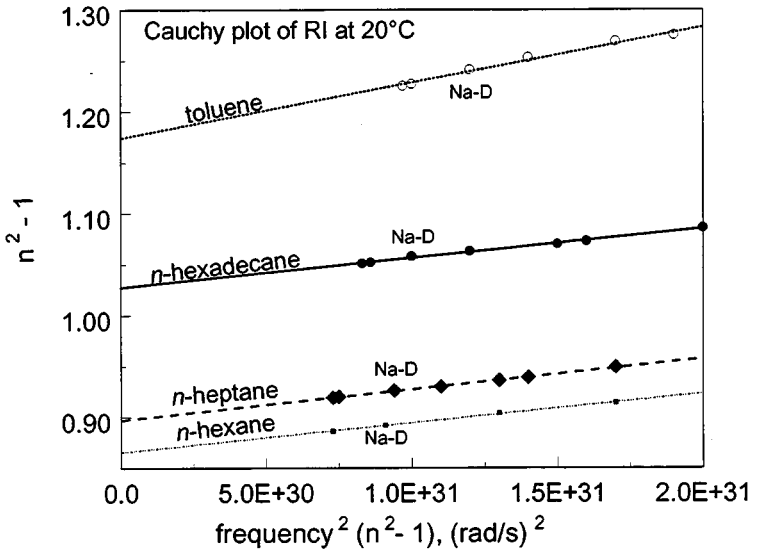

Figure 1.2-15. Dielectric polarizability is determined from RI as a function of frequency.

The frequency dependence of RI for asphaltenes probably does not parallel those for the transparent hydrocarbon shown in Fig. 1.2-15. Asphaltenes are black, indicating that they absorb in the range of visible wavelengths. Since they absorb at a lower frequency than the transparent hydrocarbons, they should have a larger Cauchy plot slope, contradicting the assumption implicit in Eq. 1.2-6 that asphaltene and solvent absorption frequencies are the same and that the Cauchy plots are parallel.

Precipitation of model systems

We have hypothesized that London dispersion interactions dominate asphaltene precipitation. Therefore, we have selected coronene as a model compound. Coronene is hexabenzobenzene, a flat molecule with six benzene rings surrounding a central benzene ring. It is a polyaromatic hydrocarbon with no polar functionality. We expect that coronene has an RI greater than 1.6, based on data for similar materials (see Tables 1.2-3 and 1.2-4 below).

Table 1.2-3. Density and RI of polyaromatic compounds (Weast, 1987)

Name	Formula	m.p., °C	Density	RI
naphthalene	$C_{10}H_8$	80.5	$0.962^{100/4}$ 1.0253	1.5898^{85} 1.4003^{24}
α-methylnaphthalene	α-$CH_3C_{10}H_7$	-22	$1.0202^{20/4}$	1.617^{20}
1,2,5 trimethylnaphthalene	1,2,5-$(CH_3)_3C_{10}H_5$	33.5	$1.0103^{22/4}$	1.6093^{22}
α-phenylnaphthalene	α-$C_6H_5C_{10}H_7$	45	$1.096^{20/4}$	1.6664^{20}
phenanthrene	$C_{14}H_{10}$	101	0.9800^{4}	1.5943
anthracene	$C_{14}H_{10}$	216	$1.283^{25/4}$	
1-methylanthracene	1-$CH_3C_{14}H_9$	85-6	$1.0471^{99/4}$	$1.680^{99/4}$
fluorathene	$C_{16}H_{10}$		$1.252^{0/4}$	
pyrene	$C_{16}H_{10}$	156	$1.271^{23/4}$	
coronene	$C_{24}H_{12}$	438-40	1.371	

Table 1.2-4. Solubility parameters (Barton, 1991)

Name	Solubility Parameter $MPa^{1/2}$	RI
naphthalene	20.3	1.5898^{85}
α-methylnaphthalene	21.2	1.617^{20}
phenanthrene	20.0	1.5943
anthracene	20.3	
average of above	20.4	1.60
carbon disulfide	20.5	1.6319^{20}

The solubility parameters of the model compounds above are close to the values of 19.5 and 20.5 $MPa^{1/2}$ estimated for asphaltenes by Hirschberg *et al.* (1984) and Burke *et al.* (1990), respectively. If these compounds are analogues for asphaltenes, then the estimated RI for asphaltene is about 1.6.

Approximately 3 mg/ml of coronene were dissolved in toluene (RI=1.496); *n*-heptane (RI=1.3878) was added as the precipitant. Precipitation occurred when the volume fraction of *n*-heptane was 0.61 and the mixture RI decreased below 1.4275. This

value of RI at the onset of precipitation is very similar to experimental observations with crude oils, shown in the next section. Unlike crude oils, however, the precipitation is sudden and crystalline material precipitates. Nevertheless, this experiment demonstrates that decreasing RI is sufficient to precipitate a polycyclic, aromatic hydrocarbon in a system with no polar interactions.

Refractive index of crude oils

The linear volumetric mixing rule, illustrated in Fig. 1.2-11 for Gullfaks-96 and n-heptane, is a special case of the more general relationship given in Eq. 1.2-16. Over the range of RI values of interest for crude oils, however, both mixture RI and F_{RI} are linearly related to the volume fractions of all of the components of the mixture, as shown in Fig. 1.2-16 for ST-87, another Gullfaks oil sample. Note that the crude oil can be considered as a single component as long as phase separation does not occur.

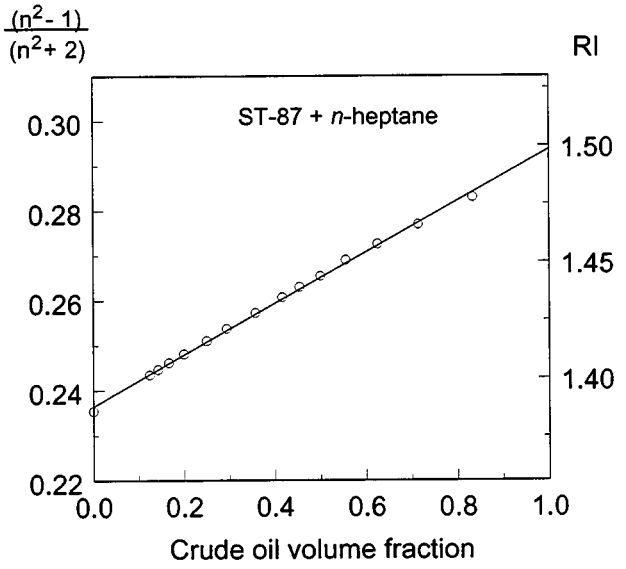

Figure 1.2-16. F_{RI} and RI of mixtures of ST-87 crude oil with *n*-heptane. No asphaltenes precipitated from any of these mixtures.

RI of asphaltene:

An estimate of the RI of the asphaltene fraction has been made by extrapolation from RI measurements for mixtures of asphaltenes that were first precipitated from A-93 crude oil with *n*-hexane, then redissolved in toluene (Fig. 1.2-17). Volume fractions were calculated based on a measured asphaltene density of 1.2 g/ml. The extrapolated value of RI is about 1.72, assuming no volume change on mixing.

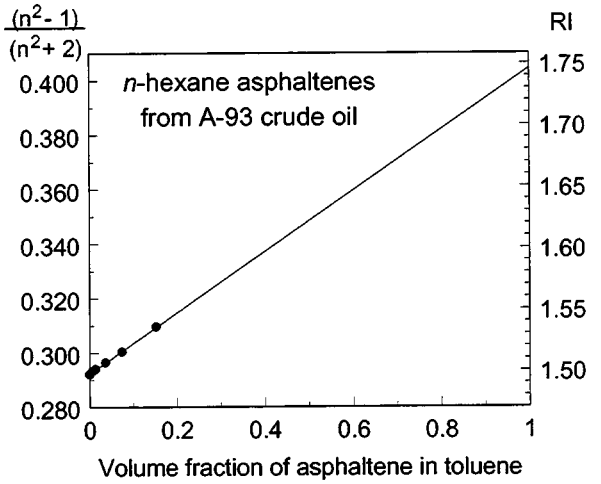

Figure 1.2-17. F_{RI} and RI of asphaltenes precipitated from A-93 crude oil by n-hexane.

This estimate is somewhat higher than the RI of material adsorbed from a crude oil of 1.67 reported by Christenson and Israelachvili (1987). RI can only be measured for fairly dilute solutions because the mixtures become opaque with increasing asphaltene concentration. A long extrapolation is required, reducing the certainty of the calculated value. The density was measured by displacement of water with asphaltene; that value also is uncertain. Different measurement methods give a range of density results for asphaltenes (Parkash *et al.*, 1979). If the density were 1.0 g/ml, the estimate of asphaltene RI would be reduced to 1.7.

As discussed in the section on the frequency dependence of RI above, the RI at the sodium-D line may not be appropriate for asphaltenes because of the slope of the

Cauchy plot and because the adsorption frequency of asphaltenes may be substantially different from other components of the crude oil. An alternative to measurements is to estimate RI of asphaltenes from analogous polyaromatic compounds (see Table 1.2-3).

Asphaltene/maltene/precipitant model of crude oil:

Thermodynamic models for the prediction of asphaltene precipitation will require the RI of the asphaltenes and of the remainder of the oil phase or solvent. This solvent pseudocomponent consists of (1) the deasphalted oil (resins, aromatics, and saturates), often known as maltenes, (2) precipitants such as methane, CO_2, or *n*-alkanes, and (3) added solvents such as toluene or AMN.

As an illustration, we can calculate the RI of the maltene fraction of a stock tank oil. The density and RI of asphaltene are assumed to be 1.26 g/cm^3 and 1.61, respectively for this calculation. The step is to convert asphaltene content from weight % , w_a, to volume fraction, $f_{V(asphaltene)}$.

$$f_{V(asphaltene)} = \frac{w_a \rho_o}{100 \rho_a} \tag{1.2-20}$$

The maltene RI is determined by extrapolation to zero volume fraction of asphaltene as shown in Fig. 1.2-18; determinations for three crude oils are illustrated in Table 1.2-5.

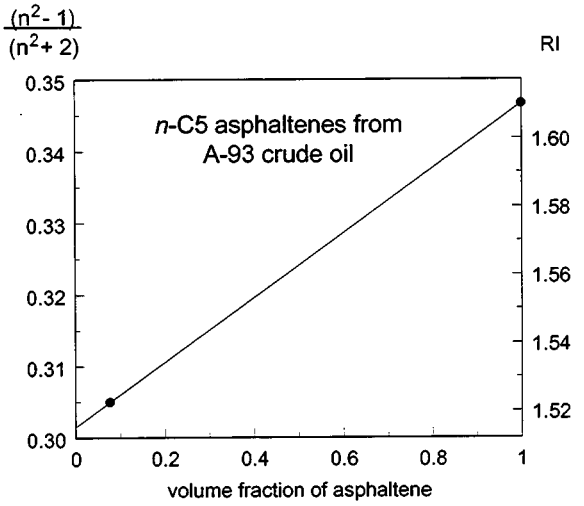

Figure 1.2-18. RI of maltenes calculated by extrapolation for A-93 crude oil.

Table 1.2-5. Estimation of maltene RI

Crude Oil	Asphaltene Fraction, wt %	Asphaltene Volume Fraction	RI of STO	RI of maltenes
Heavy CA	6.8%	0.050	1.550	1.547
Alaska-93	10.9%	0.077	1.522	1.515
Lagrave	3.8%	0.025	1.470	1.467

RI of live crude oil upon pressure depletion:

The RI of a 21.6°API gravity crude oil is modeled during pressure depletion as a binary mixture of stock tank oil (STO) and separator gas. Conventional "black oil" PVT data expresses the concentration of STO in the hydrocarbon liquid as the reciprocal of the formation volume factor, B_o (RB/STB). The dissolved gas is expressed as the solution gas/oil ratio, R_s (scf/STB). The concentration of separator gas in the hydrocarbon liquid is R_s/B_o. The PVT data is illustrated in Fig. 1.2-19.

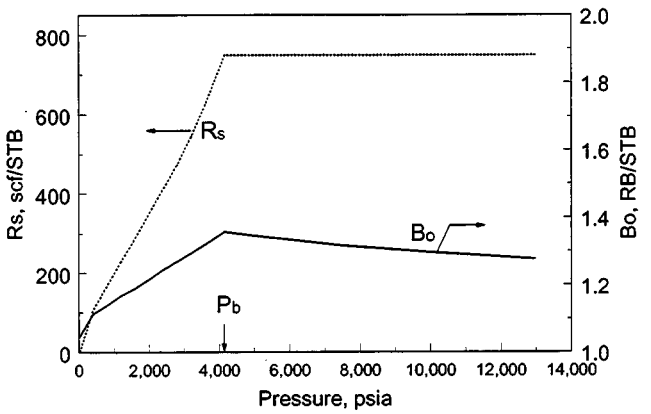

Figure 1.2-19. Black oil PVT data.

No STO was available, so RI could not be measured; it was estimated to be 1.53 from the correlation with API gravity. The separator gas was assumed to be methane with a molar refraction of 6.7 cm^3/mole. The calculated RI of the live oil at reservoir temperature during pressure depletion is shown in Fig. 1.2-20. For purpose of illustration, suppose that the precipitation RI, P_{RI}, is equal to 1.44, shown by the dashed line. This illustrates that asphaltene precipitation will occur slightly above the bubble point pressure as a result of density reduction and will continue below the bubble point until the RI is increased to a value above the P_{RI} as a result of loss of methane.

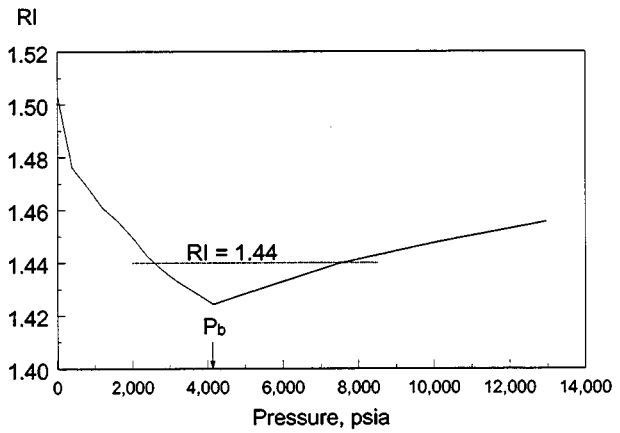

Figure 1.2-20. Calculated RI of crude oil during pressure depletion.

Remaining questions

We have assumed—first in Eq. 1.2-6 and again in substituting RI at the sodium-D line for RI extrapolated to zero frequency—that the asphaltenes have the same absorption frequency as the maltenes. This assumption is not strictly valid. A better approximation may be gained by determining RI of the asphaltenes as a function of wavelength and using the exact Lifshitz theory to calculate interaction energies.

Asphaltenes have been treated as a single component. In reality, the asphaltenes have a distribution of polarizability or RI and of molecular sizes. More realistic thermodynamic models of asphaltene solvation and precipitation will require treatment of the asphaltenes and resins as distributions of components. The aggregates they form must also be described as having distributions of size and composition.

Summary of theoretical developments

- The solubility parameters of several hydrocarbons have the dependence on RI as predicted for London dispersion interactions.
- The density dependence of the RI can be accurately estimated by the Clausius-Mossotti or Lorenz-Lorentz equations over the pressure range of interest in petroleum reservoirs.
- The difference between the RIs of hydrocarbons, extrapolated to zero frequency, can be estimated from the differences between the RIs measured at the sodium-D line if the hydrocarbons have similar absorption frequencies. This may not be valid for asphaltenes since they absorb in the frequencies of visible light.
- The F_{RI} of mixtures of a crude oil or its asphaltenes with hydrocarbon solvents and precipitants are a linear function of the volume fraction of the crude oil as predicted by the Clausius-Mossotti and Lorenz-Lorentz equations. This makes it possible to

estimate the RI of the crude oil or asphaltene when it is too opaque to measure directly.

- The RI of live crude oil during pressure depletion can be calculated from the RI of STO, molar refraction of the separator gas, the formation volume factor, B_o, and the solution gas/oil ratio, R_s.
- In a model system with the pure hydrocarbons, hexabenzobenzene and toluene, addition of *n*-heptane initiates precipitation when the RI drops below 1.4275. This value of P_{RI} is within the range of values observed for crude oil systems. Thus precipitation phenomena analogous to asphaltene precipitation occurs in a system with no polar interactions. This is evidence that polar interactions are not necessary for asphaltene precipitation.

1.2.2.3 Experimental measurements of P_{RI}

P_{RI} as a function of precipitant size

P_{RI} varies with the size of added precipitant, as shown by preliminary results for A-93 crude oil precipitated with *n*-alkanes from pentane to pentadecane (Fig. 1.2-21). For the lighter compounds (pentane and hexane especially), volatility of the precipitant necessitates measurements in a closed system. RI was estimated in these cases by linear interpolation between RI of the pure precipitant and that of the crude oil using the volume fractions at the onset of precipitation.

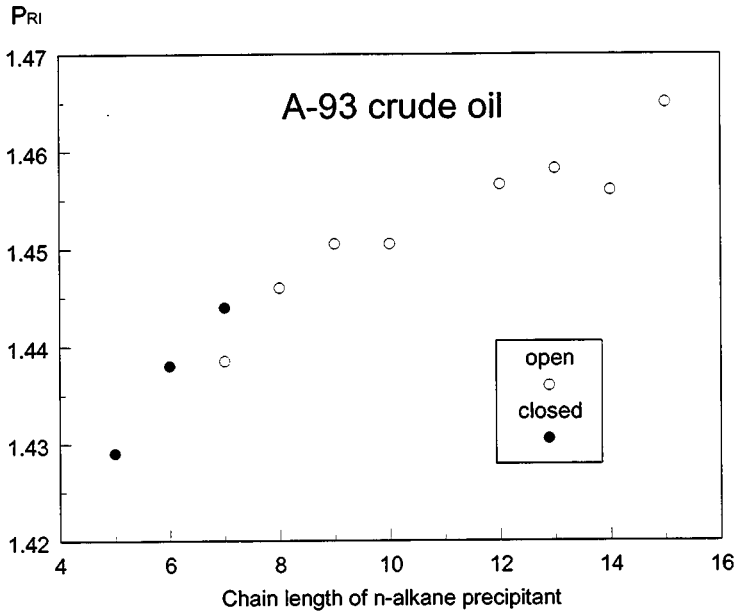

Figure 1.2-21. P_{RI} as a function of precipitant size.

This variation of P_{RI} with the size of the precipitant can be interpreted with the help of the expression for the Flory-Huggins parameter χ in Eq. 1.2-5. This dimensionless parameter is a function of both the solvent solubility parameter and the solvent molecular volume. The solvent in this case is the mixture of the crude oil and added precipitant. If the onset of precipitation occurs at a critical value of χ, then a solvent with a larger molecular volume must also have a larger solubility parameter at the onset of precipitation. Given the correlation demonstrated previously between solubility parameter and RI, precipitants with larger molecular volumes should initiate precipitation at higher RI, consistent with the results shown in Figs. 1.2-21.

This initial observation prompted a much more detailed experimental investigation of the relationship between the size of alkane precipitants and the corresponding onset conditions. Figure 1.2-22 summarizes P_{RI} measurements for six additional crude oils with precipitants from *n*-pentane to *n*-pentadecane. In all cases, P_{RI}

is a smoothly increasing function of the hydrocarbon chain length. While the magnitude of P_{RI} varies, the slope is remarkably consistent for all the crude oils tested.

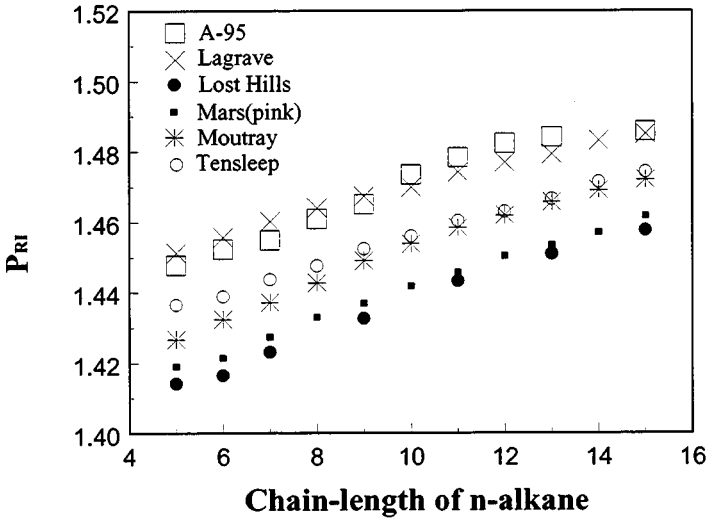

Figure 1.2-22. RI at the onset of asphaltene flocculation for six crude oils and *n*-alkane precipitants from pentane to pentadecane.

Empirical correlation

The regular increase in P_{RI} with carbon chain length suggested that it might be possible to correlate some physical property of the n-alkanes that increases with chain length with P_{RI}. Table 1.2-6 summarizes the values of the properties tested and the results are shown in Fig. 1.2-23. The most linear correlation is that with the molar volume of the alkane precipitant.

Table 1.2-6. Properties of normal alkane asphaltene precipitants

hydrocarbon	chemical formula	RI=n_D^{20}	δ $(MPa)^{1/2}$	ρ (g/ml)	v_p (ml/mol)
n-pentane	CH_3-$(CH_2)_3$-CH_3	1.3574	14.3	0.6262	116.1
n-hexane	CH_3-$(CH_2)_4$-CH_3	1.3751	14.8	0.6603	131.6
n-heptane	CH_3-$(CH_2)_5$-CH_3	1.3873	15.2	0.6843	147.5
n-octane	CH_3-$(CH_2)_6$-CH_3	1.3966	15.5	0.7025	163.5
n-nonane	CH_3-$(CH_2)_7$-CH_3	1.4050	15.6	0.7176	179.7
n-decane	CH_3-$(CH_2)_8$-CH_3	1.4112	15.8	0.7303	211.2
n-undecane	CH_3-$(CH_2)_9$-CH_3	1.4165	15.9	0.7405	228.6
n-dodecane	CH_3-$(CH_2)_{10}$-CH_3	1.4212	16.0	0.7487	243.7
n-tridecane	CH_3-$(CH_2)_{11}$-CH_3	1.4251	16.1	0.7564	261.3
n-tetradecane	CH_3-$(CH_2)_{12}$-CH_3	1.4290	16.2	0.7628	276.4
n-pentadecane	CH_3-$(CH_2)_{13}$-CH_3	1.4314	16.25	0.7686	294.1

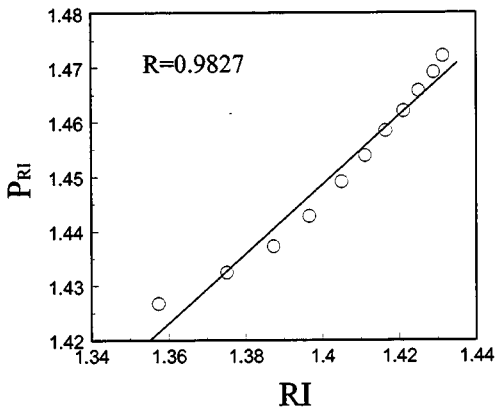

(a) P_{RI} as a function of precipitant RI

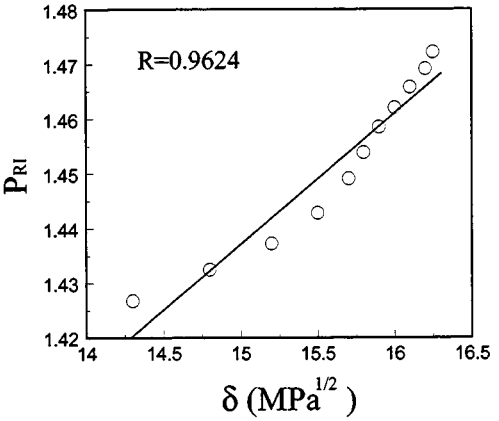

(b) P_{RI} as a function of precipitant solubility parameter

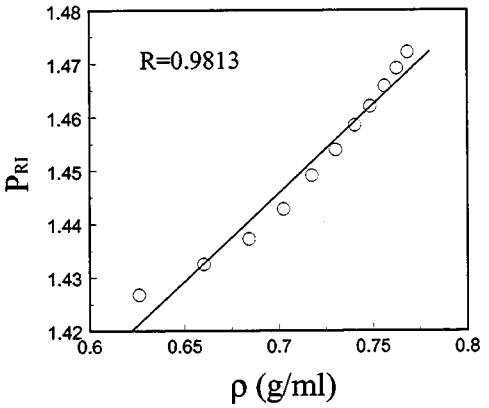

(c) P_{RI} as a function of precipitant density

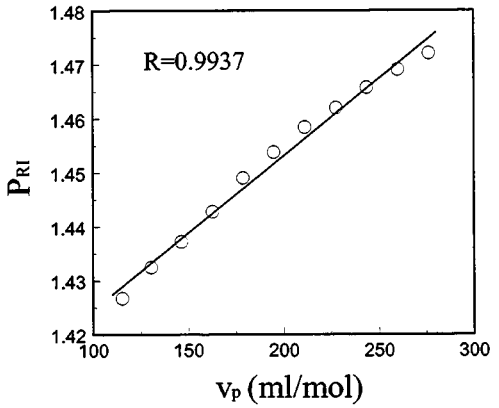

(d) P_{RI} as a function of precipitant molar volume

Figure 1.2-23. P_{RI} as a function of precipitant properties for Moutray crude oil: (a) refractive index at 20°C, (b) solubility parameter, δp (MPa$^{1/2}$), (c) density (g/ml), and (d) molar volume, vp (ml/mol).

Recalling that RI is linearly related to solubility parameter and that P_{RI} represents a critical value of RI, Eq. 1.2-5 suggests that the square root of the precipitant molar volume might give an even better linear correlation. This empirical correlation between P_{RI} and $v_p^{1/2}$ is shown in Fig. 1.2-24 for 7 crude oils. The linearity of the fits to the data for all these oils is confirmed by the high values of the correlation coefficients summarized in Table 1.2-7.

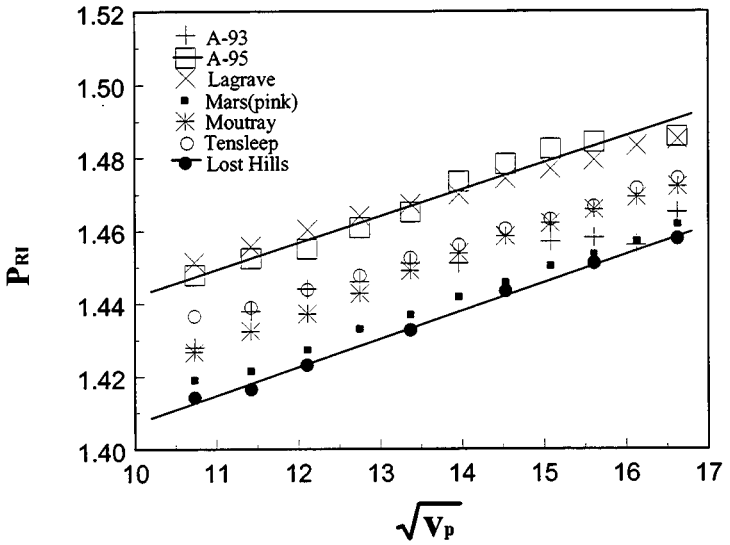

Figure 1.2-24. Linear relationship between P_{RI} and $(v_p)^{1/2}$ applies to all oils tested.

Table 1.2-7. Crude oil properties and least-squares linear relationships

Oil	Source	n_D^{20} *	$\phi_{\alpha\text{-MN}}$	nC_7 asph (wt%)*	mol wt (g/mol)*	intercept	slope	r^2
A-93	Prudhoe Bay	1.5220	0.0	6.86	256	1.3687	0.0073	0.967
A-95	Prudhoe Bay	1.5159	0.0	8.67	271	1.3798	0.0051	0.911
Lagrave	France	1.4832	0.3	6.69	188	1.3906	0.0057	0.998
Lost Hills	California	1.5137	0.0	2.78	265	1.3298	0.0077	0.996
Mars-Pink	Gulf of Mexico	1.5380	0.0	4.40	305	1.3386	0.0074	0.998
Moutray	West Texas	1.4827	0.2	1.29	242	1.3429	0.0079	0.996
Tensleep	Wyoming	1.4880	0.35	3.20	275	1.3644	0.0055	0.997

*measured before addition of α-methyl naphthalene (α-MN)

Mixed precipitants

In practice, asphaltene precipitation involves multi-component precipitants. How these various compounds combine to affect the onset of precipitation is something that must be understood in order to make successful predictions of the destabilization of asphaltene at reservoir conditions.

Two precipitants:

A mixed precipitant of n-C_9 and n-C_{15} was used to test how onset P_{RI} changes with the relative content of each precipitant. Volume fraction of n-C_{15} in the mixed precipitant ranged from 0 to 1. Three crude oil samples were chosen; they were Lagrave (with 30% 1-MN), Tensleep (with 35% 1-MN) and Moutray (with 20% 1-MN). For each combination of precipitants, the onset P_{RI} was evaluated. Results of P_{RI} measurements are summarized in Fig. 1.2-25 as a function of the volume fraction of n-C_{15} in the mixed precipitant.

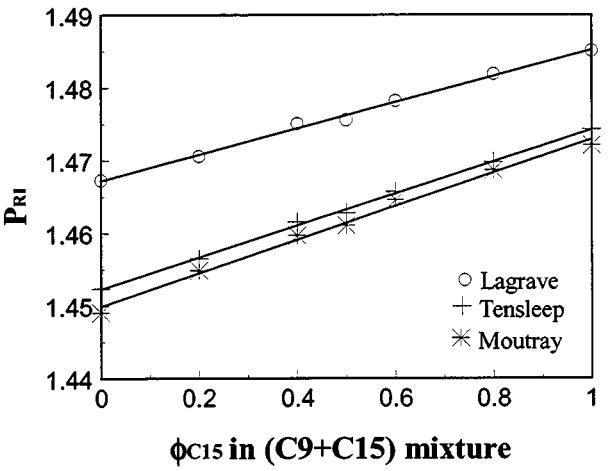

Figure 1.2-25. Aggregate onset induced by a mixture of n-C_9 and n-C_{15}. P_{RI} varies linearly with volume fraction of n-C_{15} in the mixed precipitant.

For all three oils, P_{RI} at various volume ratios of mixed precipitant falls on a straight line connecting P_{RI} for only n-C_9 as the precipitant and P_{RI} for only n-C_{15} as the precipitant. In other words, P_{RI} for the composite precipitant appears to be a linear combination of P_{RI} for each pure precipitant.

A much larger difference in precipitant molecular weights was tested with Mars-Pink and Lost Hills crude oils. Precipitant mixtures included n-C_7/n-C_{11}, n-C_7/n-C_{15}, and n-C_{11}/n-C_{15}. The Lost Hills crude oil was filtered through Millipore prefilters to remove

emulsified water before use. Similar to results shown in Fig. 1.2-25, the linear relationships between P_{RI} and volume fractions of mixed precipitant are observed for both Mars-Pink and Lost Hills crude oils with all three mixed precipitants (Fig. 1.2-26 to Fig. 1.2-28).

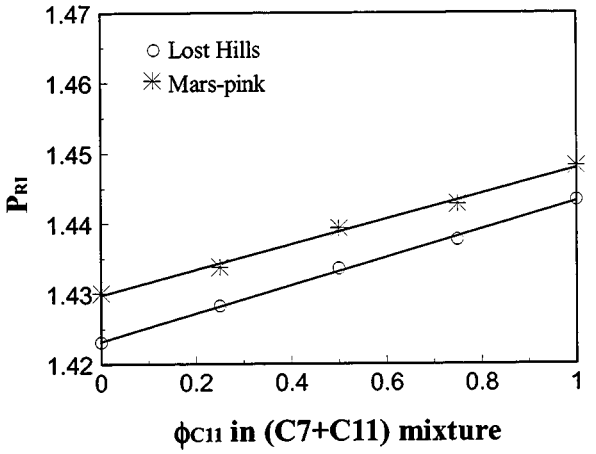

Figure 1.2-26. Aggregate onset P_{RI} for crude oils with n-C_7/n-C_{11} as the mixed precipitants.

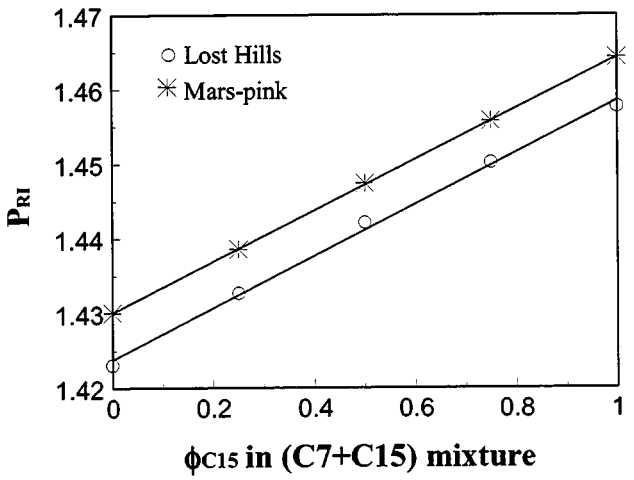

Figure 1.2-27. Aggregate onset P_{RI} for crude oils with n-C_7/n-C_{15} as the mixed precipitants.

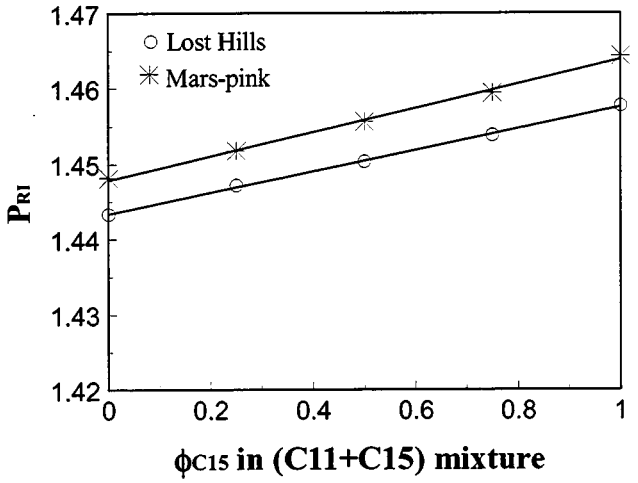

Figure 1.2-28. Aggregate onset P_{RI} for crude oils with n-C_{11}/n-C_{15} as the mixed precipitants.

Three precipitants:

A mixture of n-C_7, n-C_{11}, and n-C_{15} was employed to measure P_{RI} for Mars-Pink and Lost Hills crude oils. Measured P_{RI} are compared with values predicted from linear combinations of P_{RI} with n-C_7, n-C_{11} and n-C_{15} each as the precipitating agent, with volume fraction of each precipitant in the mixture as the weighting factor, i.e.,

$$P_{RI,cal} = \phi_{C7} P_{RI,C7} + \phi_{C11} P_{RI,C11} + \phi_{C15} P_{RI,C15} \qquad (1.2\text{-}21)$$

As shown in Table 1.2-8 and Table 1.2-9 and in Fig. 1.2-29, the predicted P_{RI} values are very close to measured ones. The deviation, ΔP_{RI}, for Lost Hills crude is 2%, while the deviation for Mars-Pink crude is only about 0.5% of the oil volume fraction.

All the five tested crude oils resulted in very similar trends, despite their differences in properties and the variety of precipitants tested. It is therefore quite reasonable to expect this trend to be applicable to other crude oils and precipitants.

Table 1.2-8. Onset P_{RI} for Lost Hills crude oil with n-C7/n-C11/n-C15 as mixed precipitant

ϕ_{C7}	ϕ_{C11}	ϕ_{C15}	$P_{RI,meas}$	$P_{RI,cal}$	ΔP_{RI}
0.25	0.25	0.50	1.4480	1.4454	0.0026
0.25	0.50	0.25	1.4433	1.4418	0.0015
0.50	0.25	0.25	1.4385	1.4368	0.0017

Table 1.2-9. Onset P_{RI} for Mars-Pink crude oil with n-C7/n-C11/n-C15 as mixed precipitant

ϕ_{C7}	ϕ_{C11}	ϕ_{C15}	$P_{RI,meas}$	$P_{RI,cal}$	ΔP_{RI}
0.25	0.25	0.50	1.4511	1.4517	-0.0006
0.25	0.50	0.25	1.4468	1.4477	-0.0009
0.50	0.25	0.25	1.4435	1.4432	0.0004

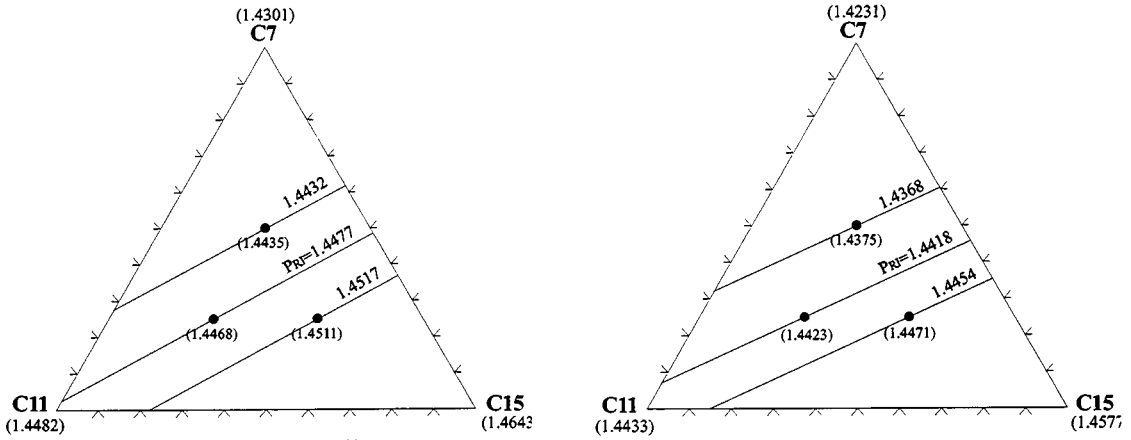

(a) Mars-Pink crude oil. (b) Lost Hills crude oil

Figure 1.2-29. Ternary diagrams of P_{RI} for Mars-Pink and Lost Hills crude oils as a function of content of each precipitant in the mixed precipitant. The constant P_{RI} lines are calculated based on linear combination. The values in the parentheses are measured P_{RI}.

Branched precipitants

Precipitants that exist in crude oil are, of course, not exclusively linear alkanes. Many branched paraffinic compounds are included in the saturate fraction. A few such compounds have been tested (Table 1.2-10). A comparison of the onset conditions for branched compounds with *n*-alkanes is shown in Fig. 1.2-30 for Mars-Pink crude oil. In

the C_6-C_8 range, asphaltenes appear to be slightly less stable to the branched compounds and somewhat more stable to precipitation induced by squalane, $C_{30}H_{62}$, although differences in the kinetics of flocculation that might influence these results have not yet been tested.

Table 1.2-10. Onset of flocculation with branched paraffins

Precipitant	v_p	P_{RI}		
	(ml/mol)	Lost Hills	Mars-Pink	Tensleep
iso-hexane	132.0	1.4248	1.4301	
2,2 dimethyl butane	132.8	1.4224	1.4348	
iso-octane	165.1	1.4348	1.4430	
squalane	522.0	1.4874	1.5018	1.5048

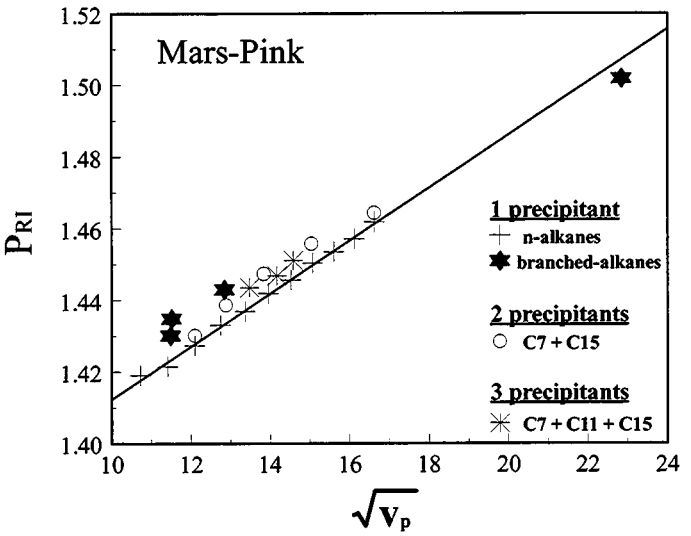

Figure 1.2-30. Branched alkanes follow a similar trend of P_{RI} vs. $v_p^{1/2}$ to that established with *n*-alkanes. Also shown are the results of precipitation tests with the mixtures of two and three precipitants.

Effects of dilution

Addition of aromatic solvents:

As reported previously (Buckley, 1996a), addition of aromatic or other hydrocarbon solvents has minimal effect on P_{RI}. The fractions of various components in the mixture, concentration of the asphaltene fraction, and ratio of precipitant to solvent all vary, but the RI at the onset of precipitation is constant.

Preliminary evidence of the effect of aromatic solvents, toluene and α-methylnaphthlene (1-MN), on the volume fraction of oil at the onset of precipitation is illustrated in Fig. 1.2-31. Compared to toluene, AMN has a higher RI and thus permits a greater dilution with the precipitant before precipitation occurs. Thus AMN is an analog of a resin in its solvating power for the asphaltenes even though AMN has no polar functionality.

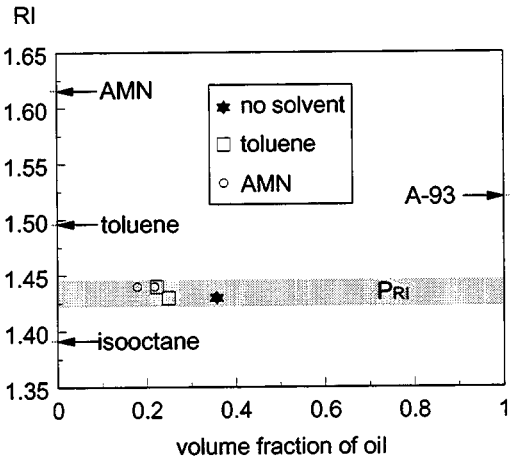

Figure 1.2-31. Onset of precipitation of asphaltenes induced by isooctane from A-93 crude oil and its mixtures with toluene and 1-MN (note AMN=1-MN) (data from Buckley, 1996a).

The accurate determination of onset of flocculation requires that the original crude oil contain no organic particles, especially no asphaltene aggregates. Some crude oils, especially those with high contents of paraffinic compounds and low RI value, may already have asphaltenes that flocculated during storage. These asphaltenes can be

removed by filtration through small pore size filter paper (e.g. 0.22 μm filter), or they can be dissolved by addition of an asphaltene solvent, such as 1-MN. The filtration is good for removing clays, sands and other organic particles rather than asphaltenes, but may potentially alter the crude oil composition if asphaltenes are removed. An example is given in Fig. 1.2-32, in which the Lagrave crude oil, which contained some asphaltene aggregates initially, was first filtered through a 0.22 μm filter, after which the onset of flocculation was measured. The onset P_{RI} values deviate from those results obtained from mixed Lagrave/1-MN, and are fairly constant for different n-alkane precipitants, quite different from the general trend observed for most crude oils (see Fig. 1.2-22).

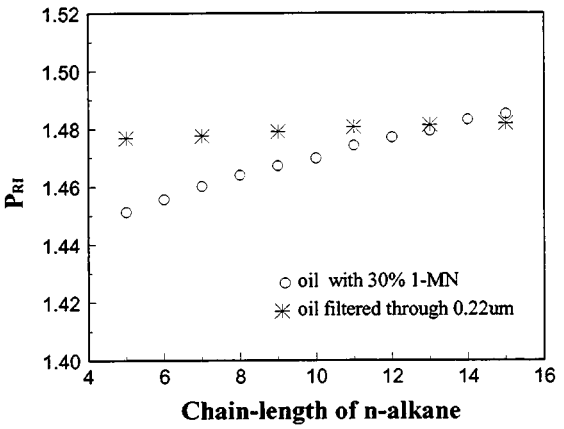

Figure 1.2-32. P_{RI} for Lagrave crude oil filtered through 0.22 μm differs from the Lagrave with 30% 1-MN.

A question may arise at this point as to how and to what extent the presence of 1-MN in crude oils might affect onset P_{RI}. To study this potential effect, two solvents, 1-MN and toluene, were mixed with Mars-Pink crude oil to various ratios. There were no particles in the original Mars-Pink crude oil. RI for these mixtures obeys quite well the rule of mixing, as shown in Fig. 1.2-33.

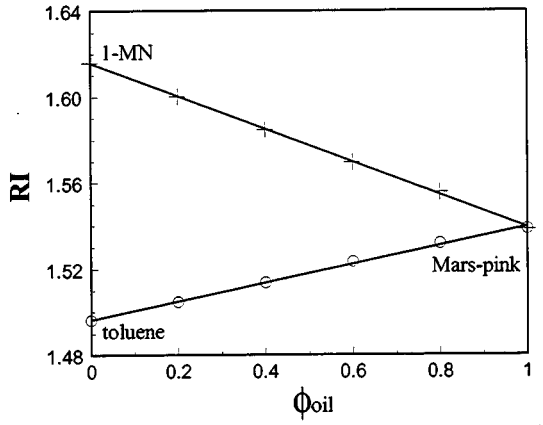

Figure 1.2-33. RI for mixtures of Mars-Pink crude oil with toluene and 1-MN, to various ratios.

Onset of precipitation was measured for all these mixtures with n-heptane as the precipitant. As shown in Fig. 1.2-34, P_{RI} decreases slightly with more 1-MN in the mixture. The difference between P_{RI} in pure crude oil and that mix with 35% 1-MN, which is the maximum ratio for all three oil/1-MN mixtures (Lagrave, Moutray, Tensleep), is about 0.001, within the error of the measurement. The mixture of Mars-Pink with toluene, on the other hand, gives a larger decrease in P_{RI}.

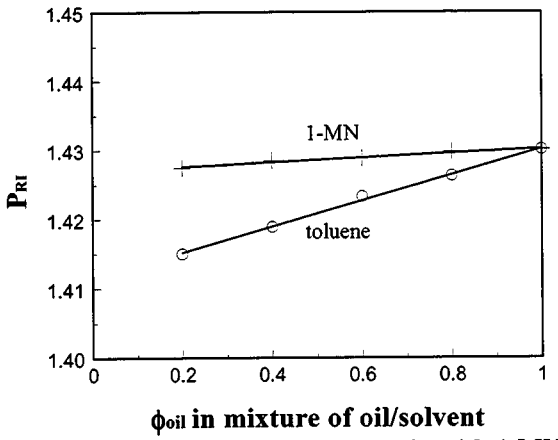

Figure 1.2-34. P_{RI} measured from mixtures of Mars-Pink crude with 1-MN and toluene with n-heptane as the precipitant.

Nevertheless, the deviations for P_{RI} are relatively insignificant as long as the concentrations of solvents in the mixture are low. As a comparison, the deviations of P_{RI}

from both A-93 and Mars-Pink crude oils at the same concentration of 1-MN and toluene in the mixture are listed in Table 1.2-11. Both oils give comparable magnitudes in P_{RI} deviation.

Table 1.2-11. Effect of solvents on P_{RI}

	P_{RI}			deviation
	crude oil	crude oil + 30% toluene	crude oil + 39% 1-MN	
A-93	1.440	1.438	1.443	-0.002 / +0.003
Mars-Pink	1.430	1.425	1.429	-0.005 / -0.001

P_{RI} —calculation from measurements at infinite dilution:

The values of both RI and P_{RI} vary from one crude oil to another. For a given set of crude oil and precipitant, however, P_{RI} is approximately constant (Buckley, 1996a). Addition of a hydrocarbon solvent, such as toluene, changes the volume fraction of precipitant required to initiate precipitation much more than the refractive index at which it occurs.

Destabilization at a constant ratio of solvent-to-precipitant has been reported by many observers (Heithaus, 1962; Bichard, 1969; Hotier and Robin, 1983; Reichert *et al.*, 1986; Dubey and Waxman, 1991; Cimino *et al.*, 1995b). Often, the volume of solvent greatly exceeds the amount of oil or bitumen in these tests. A constant solvent-to-precipitant ratio is observed since they are effectively working at infinite dilution. RI is determined by the ratio of solvent-to-precipitant. When the oil itself makes a significant contribution to mixture RI, the ratio can vary, but precipitation occurs at nearly the same value of RI for a particular combination of oil and precipitant.

Assuming infinite dilution, the ratios reported in the literature can be used to calculate a value of RI at the onset of precipitation, which we will call P_{RI}*. For a binary mixture of nonpolar molecules, RI can be calculated using Eq. 1.2-17 above.

Cimino *et al.* (1995b) precipitated asphaltenes with pentane from toluene and tetralin solutions. Table 1.2-12 shows the values used to calculate P_{RI}* from their published onset of precipitation data. These values of P_{RI}* are in the range expected from our experiments.

Table 1.2-12. P_{RI}* Calculated from onset of precipitation at infinite dilution. (Cimino *et al.*, 1995)

	***n*-pentane**	**toluene**	**tetralin**
M (g/mole)	72.15	92.14	132.21
ρ (g/cm^3)	0.6262	0.8669	.9702
RI	1.3579	1.4961	1.5413
precipitating mixture	201 g 240 g	296 g	 258 g
P_{RI}*		1.43	1.42

The results of similar calculations using the data of Hotier and Robin (1983) are shown in Fig. 1.2-35 as P_{RI}* as a function of number of carbon atoms in the precipitant. Many different solvents were used; the data for benzene, toluene, and xylene are shown here. P_{RI} is in the range of 1.42 - 1.43 for this oil (identified only as fuel oil K), when heptane is the precipitant.

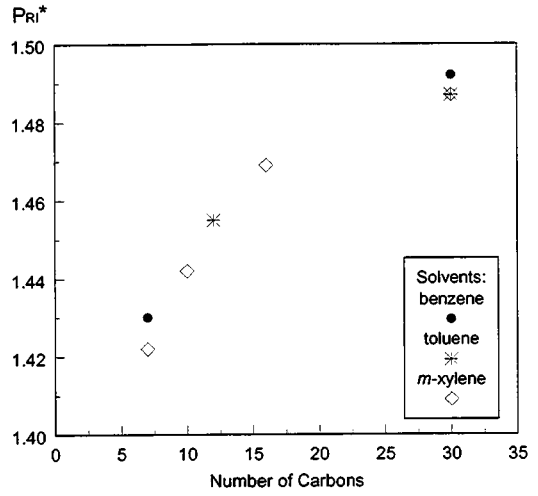

Figure 1.2-35. P_{RI}* as a function of precipitant chain length (from data of Hotier and Robin, 1983).

One set of direct comparisons between onsets determined with stock tank oil samples by the P_{RI} method and dilutions of the same oils by a continuous titration method. Solubility parameters were determined from the P_{RI} observations using the standard correlation; for the continuous titration, solubility parameters were calculated from the compositions of mixtures of toluene and heptane in which asphaltenes were first detected (Andersen, 2001).

In the automatic system, the onset of precipitation or incipient flocculation threshold was obtained through automatic titration of dilute toluene solutions of crude oil in a closed flow loop. The titration system consists of a Radiometer ABU93 autoburette, a Pharmacia P1 peristaltic pump, and a Beckmann spectrometer model B. The wavelength was 740 nm, and flow cuvettes were either 1 mm or 10 mm in pathlength depending on the opaqueness of the sample. Data acquisition and system control was performed using a PC. The titration rate was found to have a significant effect and in order to minimize over titration and local precipitation the rate was kept at 30 µl/30 sec based on experiments with asphaltene solutions. Solutions in the range of 0.5 to 1.5 g (to

the nearest 0.1 mg) oil in 5.00 ml toluene were analyzed. The critical solubility parameter for the asphaltene flocculation onset observed by this continuous technique was obtained from the known solubility parameters for toluene and heptane (Andersen, 1999).

Fig. 1.2-36 shows the onset determinations by the P_{RI} technique (in which microscopic observation is used to identify the appearance of asphaltenes) compared with continuous titration results. Both are expressed in terms of solubility parameters. All the comparisons fall below the equivalence line, but a parallel line (dashed line in Fig. 1.2-36) comes close to fitting most of the data points. The continuous titration consistently finds a lower value of the solubility parameter at the onset conditions than does the direct microscopic observation.

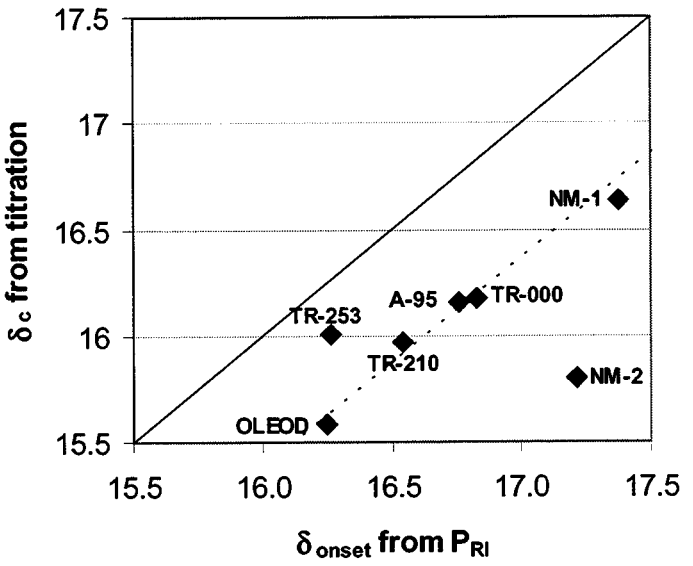

Figure 1.2-36. δ_c from automatic titration vs δ_{onset} calculated from batch determinations of P_{RI}.

The consistent difference between these two techniques may be primarily an effect of dilution with toluene, which is necessary in the continuous titration system to allow for light transmission. As shown in Fig. 1.2-34, addition of an excess of toluene can reduce the microscopically observed onset value by up to 0.02 RI units (or ~0.5

$MPa^{1/2}$ in solubility parameter terms), accounting for most of the difference between these two different measurement techniques. In addition, microscopic observations have shown that the very first appearance of microscopic particles cannot be detected by the automatic technique (Lauridsen, 1999). This may have been a problem particularly for NM-2, which had the smallest asphaltene fraction of the seven oils studied. Therefore this sample requires a larger offset from the real onset in order to generate sufficient quantities of particles such that light can be scattered.

Kinetics might also play a role in this comparison, since the microscopic observations are made one day after mixing whereas in the continuous titration, residence time is a function of titration and flow rates. Figure 1.2-37 shows how the P_{RI} determination for two crude oils changes slowly over a period of days or even weeks. This would also have the effect of shifting the data in Fig. 1.2-36 to the right.

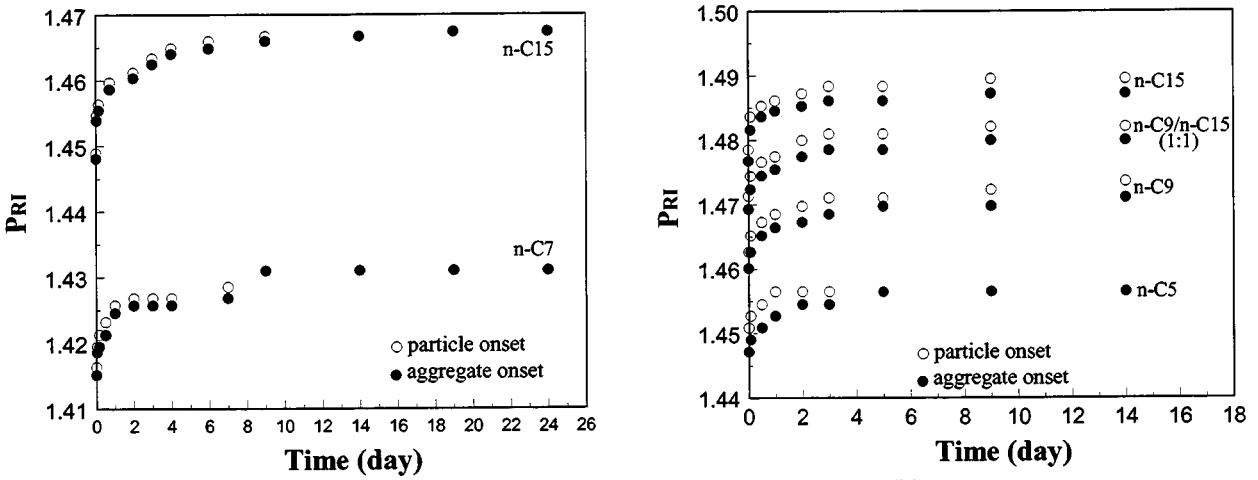

Figure 1.2-37. Onset P_{RI} shifts with aging time after mixing crude oils with precipitants.

Overall, the static, microscopic determination of P_{RI} gives the highest estimate of solubility parameter at the onset of asphaltene precipitation, with the continuous titration

giving a somewhat more optimistic evaluation. The high degree of correlation between the two measurements is quite encouraging, despite the offset in absolute values.

Reprecipitation of separated asphaltenes

Asphaltenes are often considered the main constituent of crude oil that alters wetting. Because of this perception, wettability studies often use asphaltenes that have been separated from a crude oil, then redissolved in a solvent such as toluene (e.g., Yan *et al.*, 1997). However, separated asphaltenes do not appear to give the same wetting changes as the original crude oil (Buckley *et al.*, 1997). In this section, we report on the stability of redissolved asphaltenes. Stability is expressed in terms of refractive index (RI) and, in particular, RI at the onset of flocculation (P_{RI}) as described above. The stability of isolated asphaltene fractions may differ significantly from the stability of the same fraction in the crude oil from which it was derived.

Asphaltenes were separated from six crude oils by mixing with n-heptane (1:40 by volume). After two days, the mixtures were filtered. Dried asphaltenes were re-dissolved in either toluene or 1-MN (1-MN) at concentrations from 0.5 to 1 gram asphaltene per 100 ml solvent. After one day, the onsets were measured with n-C5, n-C7, n-C9, n-C11, n-C13, and n-C15 as the precipitants. Properties of the six oil samples are repeated in Table 1.2-13.

Table 1.2-13. Selected crude oil properties

Oil	°API	RI	% nC_7 asphaltenes
A-93	25.5	1.5220	6.86
A-95	25.2	1.5159	8.67
Lagrave	37.1	1.4832	6.69
Mars-Pink	17.0	1.5380	4.40
Moutray	35.2	1.4827	1.29
Tensleep	31.2	1.4880	3.20

Figure 1.2-38 shows P_{RI} results for 1% wt/vol asphaltene solutions in toluene and 1-MN. Although similar increasing trends are apparent, variations between P_{RI} values for solutions of asphaltenes from different sources, whether in toluene or in 1-MN, is smaller than that for crude oil P_{RI}. In the crude oils, the differences come from the full range of asphaltenes and from the maltene compositions, while in these asphaltene solutions the differences are only from the properties of the fraction of asphaltenes that precipitated in n-heptane. For the same asphaltene, the onset P_{RI} for 1-MN solution is consistently higher than that for the toluene solution.

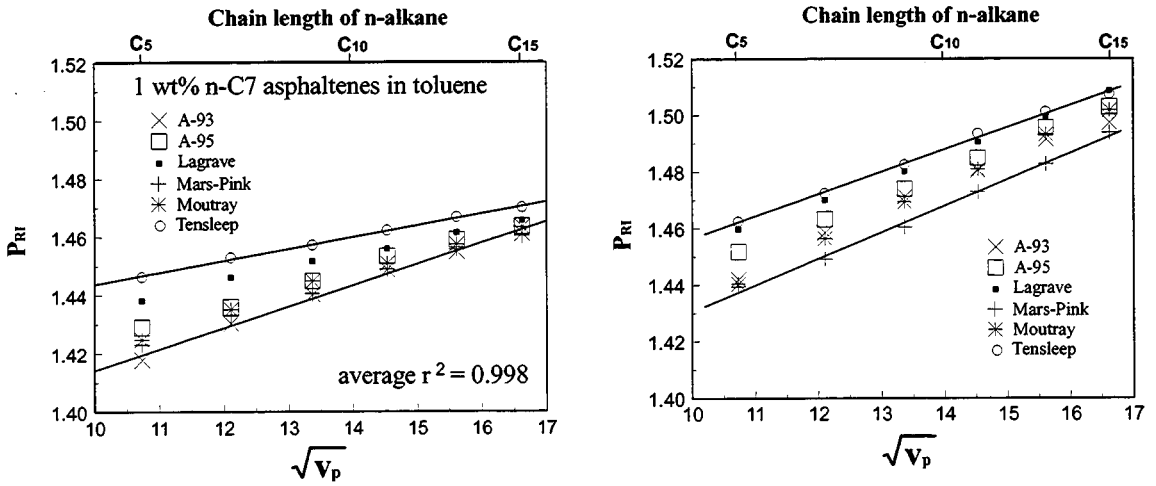

(a) toluene solutions (b) 1-MN solutions

Figure 1.2-38. Onset of asphaltene precipitation from solutions of n-C7 asphaltenes.

Table 1.2-14 shows the P_{RI} values measured for n-heptane-induced onsets for the original oil and 1% toluene and 1-MN asphaltene solutions. There are significant differences between the asphaltenes precipitating from their oil environments and from solution, but no clear trends. Judging by RI, toluene (RI=1.4961) is a better solvent than Lagrave, Moutray and Tensleep. A-93, A-95, and Mars-Pink should all be better solvents than toluene. If P_{RI} is higher in solvent than in crude oil (i.e., asphaltenes are less stable in the solvent), the value in Table 1.2-14 is positive. A negative difference indicates stability in solvent is greater than in the original oil. Among the high-RI, good-solvent oils, only Mars-Pink is a better solvent than toluene. Of the poor-solvent, low-RI oils, Tensleep appears to be a better solvent than toluene. If specific resin/asphaltene interactions, often invoked to explain the stability of asphaltene in oil, were important, we might expect that the oil would always be a more stable environment for its asphaltenes, but that is clearly not the case.

Table 1.2-14. Comparison of n-C_7 P_{RI} values for crude oils and their n-C_7 asphaltenes in 1% toluene and 1-MN solutions

Oil	n-C_7 P_{RI}			difference in δ ($MPa^{1/2}$)	
	oil	toluene soln.	1-MN soln.	toluene soln.	1-MN soln.
A-93	1.4516	1.4303	1.4585	-0.576	0.185
A-95	1.4546	1.4359	1.4621	-0.504	0.201
Lagrave	1.4602	1.4462	1.4700	-0.378	0.261
Mars-Pink	1.4274	1.4330	1.4490	0.155	0.586
Moutray	1.4372	1.4351	1.4564	-0.057	0.518
Tensleep	1.4438	1.4530	1.4723	0.248	0.762

Another possible explanation for differences between oil and solvent is that the concentrations of asphaltenes are different. Figure 1.2-39 shows comparisons of P_{RI} for

two different concentrations of n-C_7 asphaltenes for Lagrave and Mars-Pink. There is little, if any, effect of asphaltene concentration over this range of concentrations.

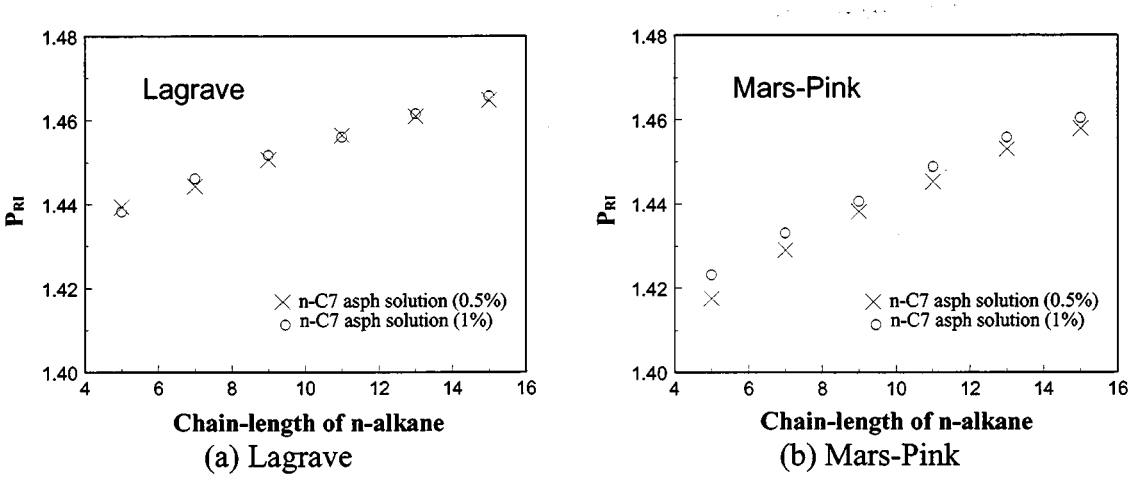

Figure 1.2-39. Effect of asphaltene concentration on onset of precipitation from Lagrave crude oil.

Looking at asphaltene concentration from a different perspective does show an interesting trend, however. If we compare the n-C_7 precipitation onsets for different oils on the basis of their original (as received) n-C_7 asphaltene content, two distinct trends emerge, one for the neat crude oil samples and another for the oils to which 1-MN was added (Fig. 1.2-40). Even if corrected to the concentrations of asphaltenes in the mixtures, the two trends remain distinctly separated. As shown in Fig. 1.2-34 for Mars-Pink oil, the addition of 1-MN to crude oil should have only a minor effect on the onset P_{RI}.

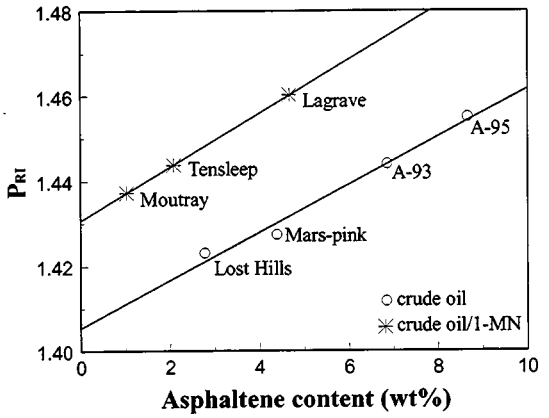

Figure 1.2-40. Correlations between original asphaltene concentration and onset.

Why do these samples separate into two distinct groups? In the first group, Moutray, Tensleep, and Lagrave all have lower RI values (about 1.48-1.49). The samples as received contained some asphaltene particles and aggregates, necessitating addition of 1-MN. In the second group, all four oils, A-93, A-95, Lost Hills, and Mars-pink, have higher RI values (>1.51) and no visible aggregates. The first group of oils likely contains less of the intermediate RI fractions, namely resins and aromatics, than the second group does since they have lower RI values with comparable amounts of asphaltene. Perhaps the low RI oils have lost a fraction of their original asphaltenes in production or in the reservoir. There are too few data to guarantee that these linear relationships are more than fortuitous, but it will be interesting to try to extend this observation to other oils in the future.

1.2.3 Onset of Asphaltene Precipitation at T & P

1.2.3.1 Onset detection at elevated T&P

In this section, a study is presented using a specially designed optical cell for observing precipitation onset and a commercially available PVT apparatus for controlling temperature, pressure, and fluid volumes. Volume fractions have been used to calculate

approximate RI's by linear interpolation. Details of the equipment, cell design, operational procedures, and RI calculation are given in Appendix II

Definitions

Some terms used to describe the asphaltenes in this study are defined as follows:

- fines: the smallest particles visible at 45X—usually relatively light in color;
- particles: a little larger than fines, deeper color (brown or black), with distinguishable edges;
- aggregates: groups of particles, usually with irregular shapes although chains and spheres were also observed;
- disappearance point: conditions of temperature, pressure, and composition at which precipitated asphaltenes completely redissolved.

Crude oils

Seven crude oil samples were tested: Sulimar Queen (from Southeastern NM), Alaska-93 (Prudhoe Bay), Gullfaks (North Sea), Spraberry (West TX), Lagrave (France), and the oils designated as CS and H3-97 for which geographic locations are unspecified. Table 1.2-15 summarizes the physical properties of the crude oil samples.

Table 1.2-15. Physical properties of crude oils

Oil	API gravity	% nC_5 asphaltenes	RI_{oil} at 25°C	Description of oil before addition of diluents		
				wax crystals?	other particles	opacity
A-93-1	25.5°	10.9	1.522	no	yes	very dark
CS	25°	0.8	1.507	melts at 59°C	yes	light
Gullfaks	27°	0.7	1.493	yes	no	light
H3-97	36°	2.6	1.477	melts < 60°C	yes	dark
Lagrave	41°	3.8	1.470	no	yes	light
Spraberry	36.5°	0.8	1.485	no	yes	light
Sulimar Queen	37°	2.9	1.476	yes	no	dark

Solvents and precipitants

Four pure substances—heptane, pentane, propane and CO_2—served as asphaltene precipitants. They all have low refractive indices. 1-MN was selected as a good asphaltene solvent because of its high RI value. Properties of solvents and precipitants are summarized in Table 1.2-16.

Table 1.2-16. Properties of diluents

Compound (purity)	RI*	d(RI)/dT	Effect on asphaltenes
propane (commercial)	1.2921		precipitant
pentane (99+%)	1.3578	-6.6×10^{-4}	precipitant
hexane (99.9%)	1.3759	-6.1×10^{-4}	precipitant
heptane (99.5%)	1.3880	-5.8×10^{-4}	precipitant
1-MN (97%)	1.6155	-6.6×10^{-4}	solvent

*at 1 atm and 20°C (except propane, P=250psi)

The bubble points for both propane and CO_2 mixed with crude oils were estimated by increasing pump cell volume at high pressure. Pressure declines steadily until the bubble point is reached. These measurements were intended to provide guidance regarding the pressures required to avoid formation of more than one fluid phase as a function of temperature and amount of added precipitant.

The estimated bubble points for propane as a function of temperature were found to be similar for different crude oils (average values are given in Table 1.2-17). When propane was used as the precipitant, the minimum pressure was maintained higher than bubble point, i.e., 200-250 psi for low temperature and 400-600 psi for high temperature.

Table 1.2-17. Average bubble points for propane and crude oils

	Temperature (°C)	Bubble point (psi)
Propane	20	140
	30	160
	90	330
	100	540

CO_2 was tested with two crude oils: Alaska-93 and Lagrave. The bubble points at which gas phase began to evolve depended on crude oil, CO_2 concentration, and temperature (Fig. 1.2-41). A minimum pressure of 1000 psi was applied in all precipitation tests with CO_2.

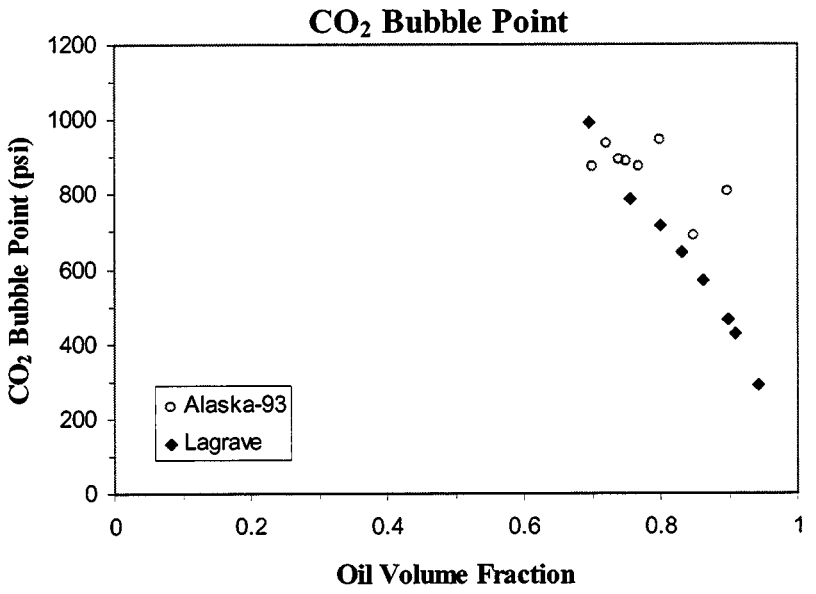

Figure 1.2-41. Approximate CO_2 bubble points when mixed with crude oils.

Preliminary test—comparison with standard procedure at ambient conditions

The initial results of this study confirmed that the onset of asphaltene precipitation can be quantified under controlled conditions of temperature and pressure by microscopic observation. Experimental measurements were made with one crude oil sample (A-93), three alkanes (*n*-pentane, *n*-hexane, and *n*-heptane), and temperatures varying from 10 to 60°C. The volume fractions at the onset of precipitation at ambient temperature and 100 psi are summarized in Table 1.2-18. Estimates of P_{RI} based on these volume fractions were shown above in Fig. 1.2-21 as the closed system results for pentane, hexane and

heptane where the comparison to standard microscopic observations and measured RI values is shown to be quite reasonable.

Table 1.2-18. Onset of precipitation from A-93 crude oil and paraffinic precipitants

precipitant	$f_{V,oil}$ at onset
n-pentane	0.439
n-hexane	0.435
n-heptane	0.428

Non-ideal mixing

Some uncertainty in calculation of mixture RI can be attributed to non-ideal mixing. Since most of the crude oil and all of the diluents are non-polar, this effect should only be important for molecules of widely divergent size. Of the substances used here, propane is the most likely to demonstrate non-ideal mixing. The extent of the problem is illustrated in Fig. 1.2-42. Equation-of-state density calculations were used as the basis for estimation of RI for mixtures of propane with pure hydrocarbons (*n*-pentadecane and 1-MN). If the deviation from ideal mixing is attributed exclusively to propane, an apparent RI of propane can be calculated. It is evident that significant deviation from ideal mixing can be expected.

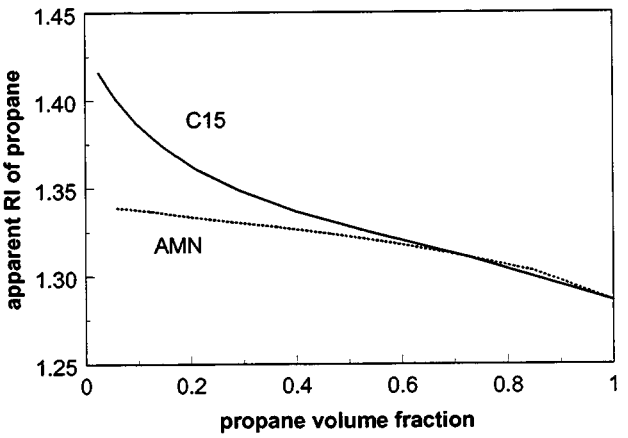

Figure 1.2-42. Effect of non-ideal mixing on RI of propane leads to varying estimates of propane contribution to mixture RI.

Onset with one precipitant.

Experimental results, summarized in Table 1.2-19 for the onset of asphaltene aggregation induced by addition of a single precipitant, show some interesting trends. As observed previously in tests at ambient conditions, P_{RI} decreases as the molecular weight of the precipitant decreases (e.g., A-93-1 and Sulimar Queen). Propane-induced aggregation could be observed in several oils for which no heptane-induced aggregates had been seen (CS, Gullfaks, and Spraberry). Precipitation of asphaltenes from Lagrave with propane stands out because it occurs at a much higher value of P_{RI} than that observed for any of the other oils; almost as high as reported previously for heptane (P_{RI} = 1.454).

Table 1.2-19. Best estimates of onset conditions for single precipitants

Oil	Precipitant	T°C	P(psi)	$f_{v,oil}$	P_{RI} (calc)	Comments
A-93	propane	29	250	0.580	1.416	aggregates observed at 70C, 400psi only after aging (and changes in T&P) ; disappear at 70°C, 5000 psi
	pentane	37	100	0.439	1.418	based on disappearance temperature
	hexane	31	100	0.435	1.433	based on disappearance temperature
	heptane	32	100	0.428	1.438	based on disappearance temperature
CS	propane	60	400	0.484	1.361	chain-like aggregates in all mixtures tested; coagulate at higher P; break up at higher T; aggregates in $f_{v,oil}$=0.454 persist at 100°C and 5000 psi.
Gullfaks	propane	32.5	400	0.344	1.350	large aggregates; a few remain even at T=98°C and P=5000psi
H3-97	propane	60	400	0.612	1.375	in $f_{v,oil}$=0.598 a few aggregates persist at T=90°C and 5000 psi.
Lagrave	propane	27	400	0.878	1.446	no change with P up to 5000 psi; aggregate size decreases as T increases up to 90°C
Spraberry	propane	31	400	0.454	1.370	many fines and a few small aggregates; disappear at 80°C and 4000 psi
Sulimar Queen	propane	31	250	0.608	1.395	no aggregates initially—lots of fines; aggregates appear in time, after lots of change in T&P
	pentane	32	100	0.410	1.399	Raised pressure (0.4095); 3000psi—aggregate size increasing;
	heptane	65	100	0.204	1.381	small aggregates; increased P—no change

In general, there is more scatter in these onset observations from one oil to another than observed previously in the experiments with heptane at ambient conditions. A better optical system would improve the ability to discern the onset conditions. Direct measurement of RI would also enhance the experimental accuracy. Nevertheless, these experiments illustrate the continuity of the onset phenomenon from the commonly used test precipitants (pentane and heptane) to the crude oil components that induce precipitation in the field, represented here by propane.

Onset with mixtures of precipitants.

Mixtures of propane, pentane, and heptane were tested for their effect on the onset of asphaltene aggregation from A-93 crude oil. The results are shown in Table 1.2-20. Why addition of larger volumes of pentane and heptane should depress the onset with propane is unclear and requires additional study.

Table 1.2-20. Estimate of onset conditions for A-93-1 precipitant mixtures

Oil + precipitants	final precipitant	T°C	P(psi)	$f_{v,oil}$	P_{RI} (calc)	Comments
A-93 + nC_5 + nC_7 0.8 + 0.1 + 0.1	propane	28	400	0.538	1.417	aged three hours at this composition (plus time at higher oil volume fractions)
A-93 + nC_5 + nC_7 0.6 + 0.2 + 0.2	propane	30	400	<0.428	<1.406	never saw aggregates; varied T (28,60°C), P (400, 5000 psi)

Effects of changing pressure.

Decreasing pressure decreases oil density and RI. However, if all components, including asphaltenes, have similar values of compressibility, the net effect on aggregation should be minimal. Only when there is a differential effect of pressure on various components in the crude oil mixture should decreasing pressure be expected to precipitate asphaltenes. Such a differential effect would be greatest when some of the

components in the mixture are near critical conditions, a regime not explored in this study.

In many cases, raising the pressure to values as high as 5000 psi left aggregates unchanged. In others the asphaltenes appeared to gather into larger aggregated clusters (CS + propane, Sulimar Queen + pentane). Disappearance of aggregates was noted in some cases, especially when both temperature and pressure were increased, although increase in the volume of the optical cell may have obscured observations at the highest pressures tested. Additional testing is needed to evaluate the effect of pressure.

P_{RI} for Lagrave and propane.

Previous tests at ambient conditions have shown that the onset of asphaltene aggregate formation occurs at a characteristic value of RI that is not affected by dilution of the oil with solvents. To test this observation under controlled conditions of T and P, Lagrave crude oil was first mixed with varying concentrations of 1-MN at 28°C and 400 psi, then propane was added until the onset conditions were found. The results are summarized in Table 1.2-21 and plotted on a ternary diagram in Fig. 1.2-43. In the left ternary, a value of 1.286 has been used for propane in calculations of mixture RI. Some lines of constant RI are indicated. Although the volume fractions at which aggregation was observed follow a linear trend, the calculated value of P_{RI} is not constant. However, if a slightly higher value of $RI_{propane}$ is assumed, the slopes of the iso-RI lines change and the revised estimate of P_{RI} does appear to be constant. Direct measurements of RI are needed to validate this observation.

Table 1.2-21. Onset in mixtures of Lagrave crude oil, 1-MN, and propane

$f_{v,oil}$	$f_{v,AMN}$	$f_{v,C3}$	P_{RI} if $RI_{propane}$=1.286	P_{RI} if $RI_{propane}$=1.355
0.878	0	0.122	1.446	1.455
0.702	0.078	0.220	1.438	1.455
0.564	0.141	0.295	1.433	1.455
0.448	0.192	0.360	1.428	1.455
0.273	0.273	0.454	1.421	1.455
0.142	0.331	0.528	1.415	1.455

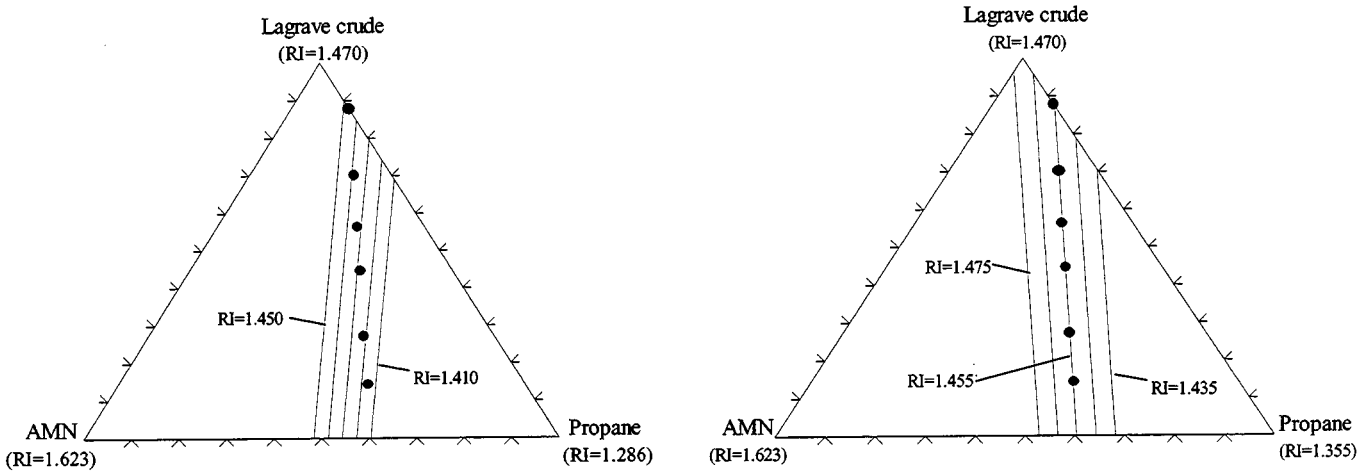

Figure 1.2-43. Calculation of constant refractive index for mixtures of Lagrave crude oil, 1-MN, and propane, plotted as volume fractions (not adjusted). In the left-hand ternary, ideal mixing is assumed with $RI_{propane}$ adjusted to T=28°C and P=400 psi. The value of P_{RI} appears to vary systematically from 1.41 to 1.44. In the right-hand ternary, assuming a more realistic value for $RI_{propane}$ shows that the onset occurs at a constant value of P_{RI} = 1.455.

Disappearance temperatures.

Once asphaltene aggregates have appeared, the process can be reversed—to some extent—by increasing temperature. As shown in Table 1.2-22, aggregates in mixtures of A-93 and various n-alkanes near the onset of precipitation disappeared with small increases in temperature. Experiments began with higher volume fractions of oil and lower temperatures. Precipitant was added gradually until onset conditions were reached. Then temperature was slowly increased until the asphaltene aggregates disappeared. Aggregates reappeared when the temperature was reduced. Increasing the volume of

precipitant increased the temperature at which the asphaltene aggregates disappeared, as shown in Fig. 1.2-44.

Table 1.2-22. Disappearance temperature—onset conditions change with T for A-93-1 crude oil

Precipitant	T (°C)	P (psia)	$f_{v,oil}$ at onset	$P_{RI,d}$	$P_{RI,d}$ at 25°C
C_3	28	250	0.580	1.419	1.420
	70	400	0.551	1.375	
n-C_5	37	100	0.439	1.418	1.428
	46	100	0.430	1.410	
	51	100	0.425	1.406	
	59	100	0.414	1.399	
n-C_6	31	100	0.435	1.433	1.438
	42	100	0.425	1.424	
	50	100	0.410	1.417	
n-C_7	32	100	0.428	1.438	1.444
	41	100	0.419	1.431	
	48	100	0.409	1.426	
	52	100	0.398	1.422	

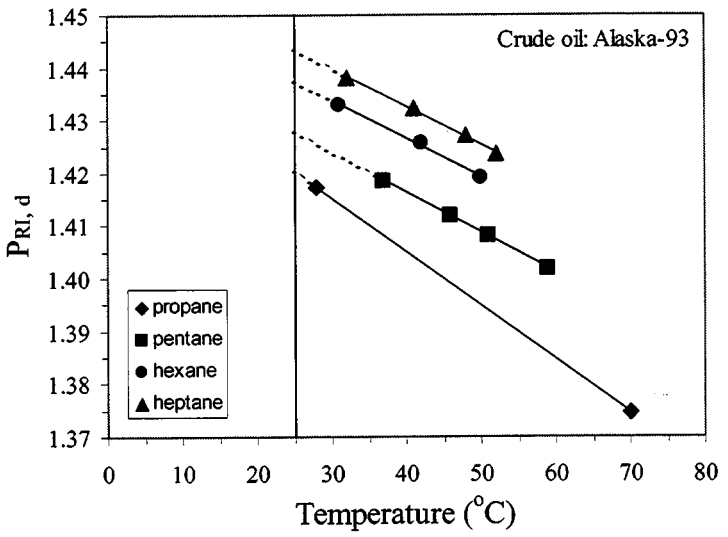

Figure 1.2-44. Refractive indices from the mixture of A-93 crude oil with different precipitants at asphaltene disappearance points ($P_{RI,d}$) decline with temperature.

While kinetic effects influencing both formation and dispersion of the asphaltenes are recognized, they were not systematically studied. Qualitative observations indicated that in mixtures well beyond the onset conditions, aggregation was less likely to be

reversed by increasing temperature. Aging of asphaltenes in the aggregated state may also have contributed to slower reversal of the aggregation process.

Some observations of asphaltenes in the presence of two fluid phases

In tests with CO_2 and A-93 and Lagrave crude oils, the objective of maintaining single-phase conditions was not consistently achieved. In the region where two fluid phases were present, reliable estimates of RI cannot be made from the information available. Nevertheless, some observations, summarized in Table 1.2-23, can be noted.

Table 1.2-23. Observations of crude oil mixtures with CO_2

Oil	$f_{v,oil}$	T°C	P psi	# fluid phases	Ppt*	comments
A-93	0.70	27-28	2000-3500	2	y	fines and sometimes aggregates
		28	4000	1	Y	"ash" where CO_2 bubble disappears
		40-75	2000	2	y	fines and "spheres"
		76-80	2000	1	n	very dark
	0.77	34	2000	2	y	fines
		34	4000	1	y	fines and some particles
	0.74	28	1000	2?	y	fines and some particles
		30.5	1000-1900	2	y	fines
		30.5	2000	1	y	"ash" spots
		30.5	5000	1	n	
	0.71	32	5000	1	y	aggregates
		32	3800	2	y	
Lagrave	0.91	31	1000	1	y	particles and a few small aggregates
	0.70	32	1000	1	Y	huge aggregates

*notation for presence of precipitation (ppt): n = no ppt, y = some ppt, Y = large amounts of ppt

Both fine particles and aggregates were observed when A-93 was mixed with CO_2, depending on composition, temperature, and pressure. Precipitate occurred in both single and two-fluid phase conditions, showing that the denser phase contained enough CO_2 to induce precipitation. Only at the highest temperatures and pressures tested did the precipitate disappear.

To some extent the interface between the CO_2-rich and oil-rich phases appeared dark because of the contrast in refractive indices. It appeared, however, that there was

also some positive attraction of fine particles to the CO_2-oil interfaces. Accumulated fine particles left a darker spot or "ash" at the positions where bubbles of the lighter phase disappeared as pressure was increased above the bubble point. Attraction of asphaltene to an oil-CO_2 interface is an interesting and unexpected observation that would require additional experimental and theoretical work to confirm and explain.

Summary of HTHP observations

- Visual observation can be used to identify the onset of asphaltene precipitation at elevated temperatures and pressures.
- Oils that have little or no asphaltene, as defined by standard tests with heptane, can form asphaltene aggregates in response to addition of propane.
- The characteristic onset RI established for higher molecular weight precipitants at ambient conditions has been extended to lower molecular weight oil components that are likely to be responsible for precipitation in the field.
- Reversal of the aggregation process in response to changing temperature and pressure has been demonstrated for near-onset conditions.

1.2.3.2 Application of the empirical correlation

A procedure has recently been proposed to predict the onset of asphaltene flocculation at reservoir conditions based on measurements at ambient conditions and PVT data of the crude oil (Wang and Buckley, 2001). The process can be summarized as follows:

(1) Estimate RI for live oil based on formation volume factor, gas/oil ratio, and gas compositions (Buckley *et al.*, 1998a).

(2) Measure onset P_{RI} induced by addition of varying n-alkanes at ambient conditions to establish trend of P_{RI} vs. $v_p^{1/2}$, where v_p is molar volume of precipitant.

(3) Adjust for effect of temperature on P_{RI} based on previous tests (Wang *et al.*, 2000).

(4) Extrapolate linear trend for P_{RI} vs. $v_p^{1/2}$ obtained in step 2 to lower molecular weight precipitants.

(5) Estimate the average molar volume of solution gas at reservoir conditions based on formation volume factor, gas/oil ratio, and pressure dependency of dead oil density (Wang and Buckley, 2001).

(6) Use the estimated molar volume of solution gas (precipitant) to estimate onset P_{RI} from the temperature-adjusted P_{RI}-$v_p^{1/2}$ correlation.

(7) Compare estimates of live oil RI and P_{RI} as a function of pressure. Over the range of pressures for which P_{RI} exceeds RI, asphaltenes are potentially unstable.

Using this process, ambient conditions onset data, and PVT data for C-GGC-00 live oil, the onset at reservoir conditions can be predicted. The ambient conditions onset data are summarized in Table 1.2-24. The oil required some pretreatment—to remove emulsified saline water and to disperse existing asphaltenes—before onset observations could be made. Two sets of onset determinations are reported in Table 1.2-24: one for a filtered sample and another for a mixture of oil and 1-MN that was washed with distilled water. Asphaltenes from the washed mixture were slightly more stable than those that remained in the filtered oil. The best estimate, provided by the washed mixture, is shown in Fig. 1.2-45 with the RI of the n-alkanes also shown for comparison. The asphaltenes from this oil are more stable than those from any oils previously tested. Even the intermediate n-alkanes (n-octane and above) are not precipitants for these asphaltenes.

Formation volume factor and gas/oil ratio for the live oil are shown in Fig. 1.2-46 and its composition is summarized in Table-1.2-25.

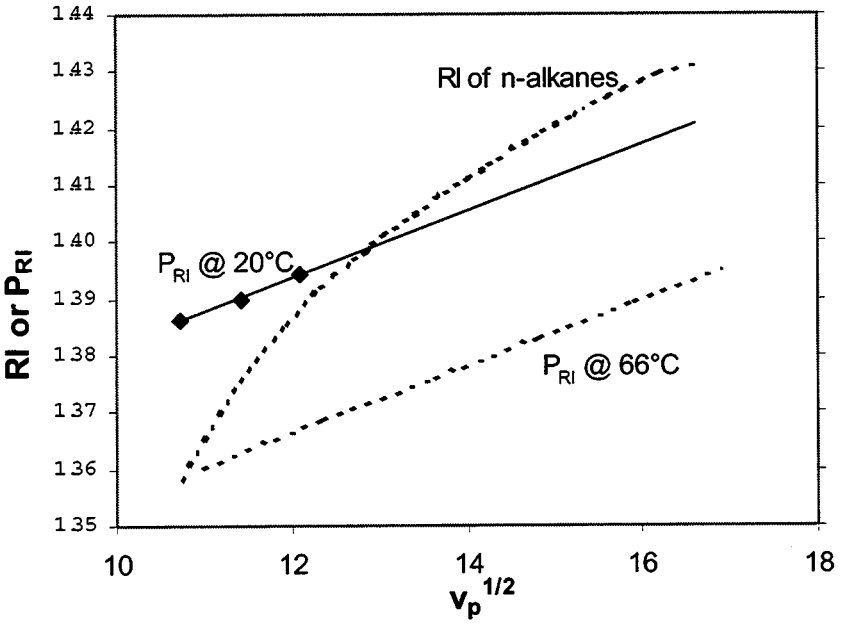

Figure 1.2-45. RI at onset of asphaltene flocculation (P_{RI}) for washed/centrifuged oil+1-MN mixture, measured at 20°C and calculated for 66°C. RI of n-alkanes is included for comparison.

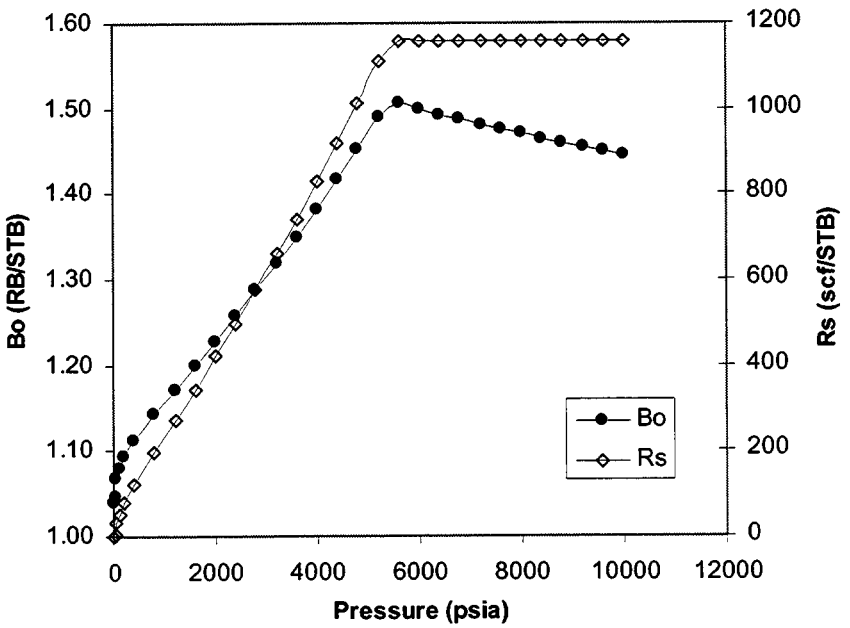

Figure 1.2-46. Formation volume factor and gas/oil ratio for live oil.

Table 1.2-24. C-GGC-00 crude oil and its asphaltenes at 20°C

Sample treatment	Appearance at 320X	RI_{oil}	Asphaltene content 40:1 dilution (%)		Onset (P_{RI})			
			nC5	nC7	nC5	nC6	nC7	nC8
Oil, as received (containing a saline water-in-oil emulsion; salt precipitates with asphaltenes)	Spherical, dark-colored droplets		4.90	4.20				
Oil, centrifuged at 3000 rpm for 1 hr.	Fine particles	1.4924						
Oil, centrifuged at 3000 rpm for 1 hr. then filtered (0.22 µm)	Clear	1.4916	0.98	0.06	1.3955	1.4002	1.4039	
1:1 mixture of oil and 1-MN, centrifuged at 3000 rpm for 1 hr.	Fine particles	1.4940[a]						
1:1 mixture of oil and 1-MN, washed with double distilled H_2O, then centrifuged at 2000 rpm for 4 hr.	Clear	1.4951[a]	1.08[b]	0.31[b]	1.3862	1.3899	1.3943	not detectable

[a] assuming RI of 1-MN (1-MN) = 1.61585

[b] grams of asphaltene per 100 ml of original crude oil sample

Table 1.2-25. Composition of C-GGC-00 crude oil

NAME	Mole Fraction	Molecular Weight(g/mol)
CO_2	2.86E-03	44.01
N_2	1.82E-03	28.013
METHANE	5.61E-01	16.043
ETHANE	5.67E-02	30.069
PROPANE	3.64E-02	44.096
I-C4	9.85E-03	58.123
N-C4	2.42E-02	58.123
I-C5	1.04E-02	72.15
N-C5	1.20E-02	72.15
N-C6	1.93E-02	86.177
N-C7	2.51E-02	100.203
C8	2.30E-02	107
C9	2.31E-02	121
C10	2.17E-02	134
C11	1.65E-02	147
C12	1.43E-02	161
C13	1.31E-02	175
C14	1.15E-02	190
C15	1.06E-02	206
C16	9.61E-03	222
C17	8.09E-03	237
C18	7.70E-03	251
C19	6.94E-03	263
C20	6.40E-03	275
C21	5.81E-03	291
C22	5.22E-03	305
C23	4.22E-03	318
C24	4.17E-03	331
C25	3.67E-03	345
C26	3.51E-03	359
C27	3.57E-03	374
C28	2.98E-03	388
C29	3.10E-03	402
C30+	3.20E-02	800

If we assume that the gas phase is composed only of the lightest components—methane, ethane, propane, N_2, and CO_2—low estimates of molar refraction for gas phase and of RI for the live oil will be obtained (Wang and Buckley, 2001)). We further assume that rate of decrease of P_{RI} with temperature is $dP_{RI}/dT = -4x10^{-4}/°C$, a value slightly less than that reported previously for A-93 crude oil (Wang *et al.*, 2000) and that the effect of pressure on dead oil density was

about $4x10^{-6}$ g/ml/psi. The resulting estimates of live oil RI and P_{RI} at reservoir temperature are shown in Fig. 1.2-47. Since the oil RI is never as low as the predicted value of P_{RI}, flocculation is not predicted at any pressure.

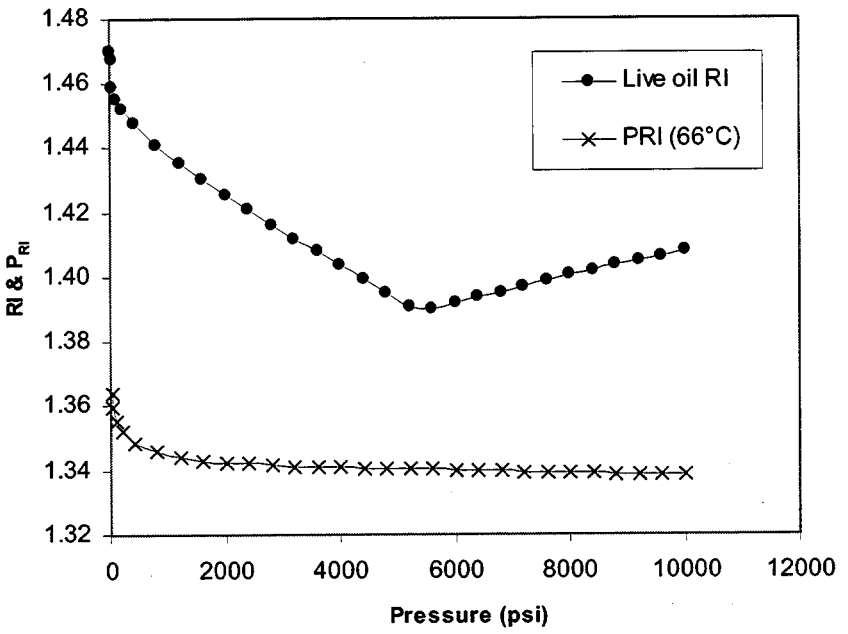

Figure 1.2-47. Comparison of live oil RI with the estimated onset condition shows that the asphaltenes in C-GGC-00 should be stable at all pressures encountered during production.

One question about these calculations is whether the temperature correction is reasonable. In this case, assuming no temperature correction raises the predicted onset P_{RI}, but the prediction remains the same for these unusually stable asphaltenes (Fig. 1.2-48a). The question of correcting onset conditions for changes in temperature will be important for other oils and requires additional study. The stability of asphaltenes from C-GGC-00 is unusual in our experience so far. It is possible that they are very slow to form. In our standard test, only one day elapses between mixing and observation. That may be insufficient in this case. Using the slightly less stable results for the filtered oil sample raises the predicted P_{RI}, but not enough to intersect the live oil RI (Fig. 1.2-48b).

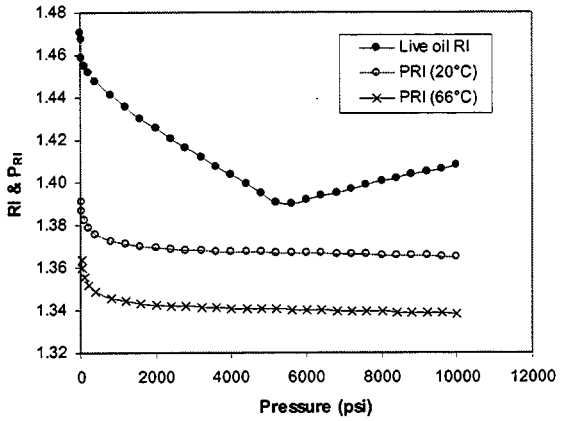

(a) comparison based on data from the washed mixture of C-GGC-00 and 1-MN.

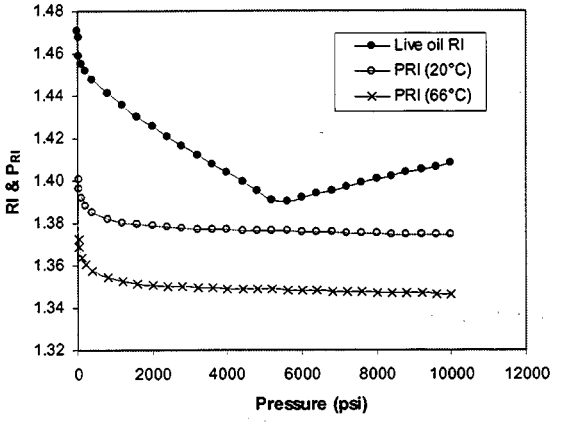

(b) comparison based on data from the filtered sample of C-GGC-00.

Figure 1.2-48. Comparisons of RI for live oil with the estimates of the onset P_{RI} for two temperatures.

Summary

Measurement of the amount of asphaltene and of the onset of asphaltene flocculation for C-GGC-00 crude oil was complicated by the presence of a persistent water-in-oil emulsion of very saline water. It was necessary to mix the oil with 1-MN to disperse the asphaltenes, after which the emulsion could be broken by washing with distilled water to reduce salinity. Finally, the oil was spun in a centrifuge to separate it from water. The oil sample produced contained no visible asphaltene particulates.

Because of the unusual stability of asphaltenes in C-GGC-00 crude oil at ambient conditions with liquid precipitants, even the most pessimistic predictions of the onset conditions at reservoir temperature show no pressures at which asphaltene flocculation should be expected. An overestimate of asphaltene stability might be made if the kinetics of flocculation were exceptionally slow for C-GGC-00 crude oil.

1.2.3 Moisture Analysis

Contact angle studies have consistently shown that in the presence of water, interactions between oil and solid can be quite different than when water is absent. On dry surfaces, polar

interactions with crude oil components are rapid, producing surfaces of neutral wetting (Buckley *et al.*, 1998b). The necessity of including the effects of brine complicates our experiments. In studies with probe fluids (usually decane and distilled water) on oil-treated surfaces, we often observe regions of zero contact angle, i.e. areas of the surface that remain strongly water-wet and perhaps water-covered, if the duration of aging in oil is less that 2-3 days. After longer aging times, the surfaces become more uniform. The water-removal process can be accelerated by centrifugation (Yang, 1998; see also section 2.1.2 of this report), but it is not necessary to rely on gravity drainage to remove bulk water. While thin films of water can be maintained indefinitely in cases where water films are stabilized by favorable electrostatic interactions, the initial presence of bulk water does not interfere in cases where water films are inherently unstable. In this report we consider what might be happening to that initial bulk water.

We have observed in previous work that the moisture content of crude oils can be substantially higher than the solubility limits of water in pure hydrocarbons would predict (Liu, 1993). The amount of moisture in a crude oil can change with the relative humidity of the environment in which it is stored. Thus, one possibility is that bulk water slowly dissolves in the crude oil. The rate and extent of dissolution would vary with temperature, interfacial area, and composition of the oil. Less polar oils would have lower solubility limits for water, similar to pure hydrocarbons, whereas more polar oils should be able to dissolve larger amounts of water.

As a first step toward quantifying the possible importance of water dissolution, we report on some preliminary measurements of moisture in crude oils.

Experimental Methods and Materials

Small amounts of moisture can be measured by Karl-Fischer titration, an accurate moisture measurement method based on the quantitative reaction of water with iodine:

$$I_2 + SO_2 + H_2O = 2HI + SO_3 \qquad (1.2\text{-}22)$$

In coulometric Karl-Fischer titration, the sample is added to a pyridine-methanol solution containing iodine ion and sulfur dioxide. The iodine, which is generated electrolytically at the anode, reacts with water as indicated in formula (1.2-22). Iodine is generated in direct proportion to the quantity of electricity according to Faraday's law.

$$2I^- - 2e = I_2 \qquad (1.2\text{-}23)$$

One mole of iodine reacts quantitatively with one mole of water. As a result, 1 mg of water is equivalent to 10.71 coulombs. Thus, the water content in the sample can be determined from the amount of electricity required for the electrolysis.

The moisture determination in petroleum products has traditionally been measured by distillation, a complicated and time-consuming process that is not accurate for amounts less than 0.1%. ASTM procedure D-1744 recommends Karl-Fischer titration for precise moisture determination in petroleum products and mineral oils. Metals, oxides, hydroxides, oxidants, and reducing agents are potential sources of interference. Below 50 ppm, large amounts of sample and solvent are required and measurement accuracy is decreased. To measure trace amounts of moisture in petroleum products, the combination of a moisture vaporizer and a Karl-Fischer moisture meter has been developed. Water molecules from an oil sample are transferred in the vapor phase to a Karl Fischer titration vessel, eliminating sources of interference and increasing accuracy to below 50 ppm.

In this study, a Mitsubishi moisture meter (Model CA-06) and a water vaporizer (Model VA-16) were used to determine the moisture contents of crude oil samples. The manufacturer's standard operating instructions were followed with one exception. Preliminary experiments showed that addition of mineral oil did not improve accuracy, so none was added to the crude oil

samples. Two parameters can be adjusted during the measurements: temperature or the vaporizer and the nitrogen carrier gas flow rate.

The procedure includes a baseline titration to establish background levels, followed by measurements of one to two gram aliquots of the crude oil samples. Water was driven to the titration vessel by dry nitrogen gas and the results were recorded from the electronic display at the end of each titration. Reagents used included Coulomat A anode solution, Coulomat C cathode solution, and Sicapent (with indicator), all from EM Science, and silica gel (with indicator) from Mitsubishi Kasei Co.

Calibration with water:

Distilled, deionized water was used to calibrate the instrument and test the vaporizer settings of temperature and carrier gas flow rate. When the vaporizing temperature was above 110°C and carrier gas flow rate above 300 ml/min, known amounts of water were correctly titrated (Fig. 1.2-49).

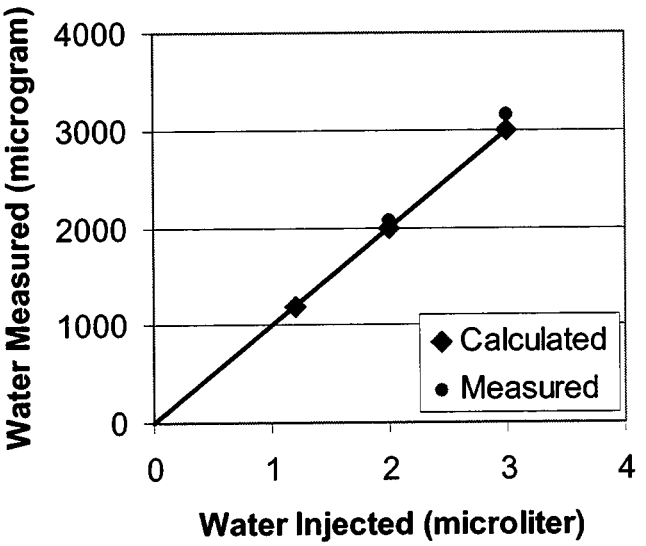

Figure 1.2-49. Test of moisture measurement accuracy using known amounts of distilled, deionized water.

Eleven crude oils were tested in this study. Their properties are summarized in Table 1.2-26.

Table 1.2-26. Crude oil properties

Oil ID	Density at 25°C (g/ml)	Viscosity at 25°C (cP)	RI (n_D^{20})	Acid # (mg KOH/g oil)	Base # (mg KOH/g oil)	Moisture (ppm)*	Emulsion?
A-93	0.8945	26.7	1.5196	0.14	2.61	201 ± 13	no
C-C-12	0.9732	5.2	1.5512	5.16	9.63	3263 ± 1100	yes
C-C-28	0.8859	0.9	1.4998	0.85	2.20	93 ± 13	no
C-LH-99	0.9074	70.0	1.4231	1.90	6.05	461 ± 35	no
Mars-97	0.8784	20.8	1.4950	0.37	1.79	150 ± 1	no
Mars-Pink	0.9458	341.6	1.5381	3.92	2.30	351 ± 173	yes
Minnelusa	0.8980	43.6	1.5142	0.17	2.29	3194 ± 538	yes
P-E-00	0.8267	7.5	1.4745	0.11	1.50	< 10	no
Schuricht	0.8964	46.0	1.5130	0.28	2.09	189 ± 14	no
SQ-95	0.8324	5.1	1.4769	0.17	0.62	178 ± 12	no
UWYO-CO_3	0.8212	4.0	1.4635	0.13	0.92	37 ± 7	no

* Measured with T=150°C and flow rate = 500 ml/min.

Moisture analysis results and discussion

Results of moisture measurements at a single set of conditions (T = 150°C and N_2 flow rate = 500 ml/min) are included in Table 1.2-26. Each value is the average of three measurements. For oils without microscopic emulsified water droplets, amounts of moisture varied over a wide range from undetectable (<10ppm) to 461 ppm. Higher values were measured for several oils, but it was clear that emulsified water dominated those measurements.

Experimental parameters (temperature and flow rate):

The results in Table 1.2-26 are for a consistent set of moisture-measuring conditions of temperature and nitrogen flow rate. Measurements for three oils at two different sets of conditions are compared in Table 1.2-27. In all three cases, the higher temperature and flow rate produced higher values of moisture. The reasons for these discrepancies are not entirely clear,

although condensation in the lines may contribute to lower values. In any case, the moisture results should be viewed as relative, rather than absolute, at this stage.

Table 1.2-27. Crude oil moisture measurements at different measuring conditions

Oil Sample	moisture (ppm)	
	T = 130°C N_2 flow rate = 300 ml/min	T = 150°C N_2 flow rate = 500 ml/min
A-93	84 ± 13	201 ± 13
Mars-97	40 ± 3	150 ± 1
Schuricht	85 ± 1	189 ± 14

Humidity and emulsion formation:

Some oil samples, as received, contain emulsified water droplets. Others have a separate aqueous phase at bottom of the sample container. Still others are free of either bulk or emulsified water. Some experiments were performed to show the effects that storage conditions might have on the amount of moisture in an oil sample.

SQ-95 was used to the test several different environments. Three sample vials, each containing about 30 grams of SQ-95 crude oil, were stored in contact with (1) ambient air (low humidity), (2) air at 100% humidity, and (3) a buffered brine (pH=6.0, [NaCl]=0.1*M*). After about 40 days, the amounts of moisture in each of these three samples were measured and compared to the moisture measured in the sample, as received (Table 1.2-28). The sample open to the air lost all of its original moisture. Those exposed to high humidity and brine formed emulsions, as suggested by the high moisture values plus high standard deviations and confirmed by microscopic inspection. Table 1.2-29 shows that, in some cases, centrifugation can be used to separate the emulsified water from oil, returning moisture levels to nearly their original values. The Mars-pink emulsion could not be broken by centrifugation, perhaps because of the oil's high viscosity.

Table 1.2-28. SQ-95 moisture measurements (T=150°C, N_2=500 ml/min)

Oil treatment	Moisture (ppm)	Emulsion
Original sample	178 ± 12	no
Open to low humidity air	< 10	no
Open to air at 100% humidity	377 ± 105	yes
Shaken with brine	2176 ± 1157	yes

Table 1.2-29. Crude oil moisture content after centrifugation (T=150°C, N_2=500 ml/min)

Crude Oil	Moisture (ppm)		
	original sample	shaken and aged with brine	centrifuged (hr, rpm)
Mars-97	150 ± 1	not measured	200 ± 13 (0.5, 1500)
Mars-pink	351 ± 173	not measure	2760 ± 1333 (6, 5000)
SQ-95	178 ± 12	2176 ± 1157	183 ± 17 (0.5, 1500)

Crude oil composition:

If we exclude from consideration all the samples known to have emulsified water droplets and use a single set of experimental parameters (T = 150°C, flow rate = 500 ml/min), we can compare the initial moisture levels in various oils with other physical properties. For example, we can consider whether oils tend to contain more water as their density increases (or their API gravity decreases). As shown in Fig. 1.2-50, the correlation between moisture and API gravity is weak, at best. The same is true of average molecular weight, viscosity, and refractive index, none of which are clearly related to an oil's polarity.

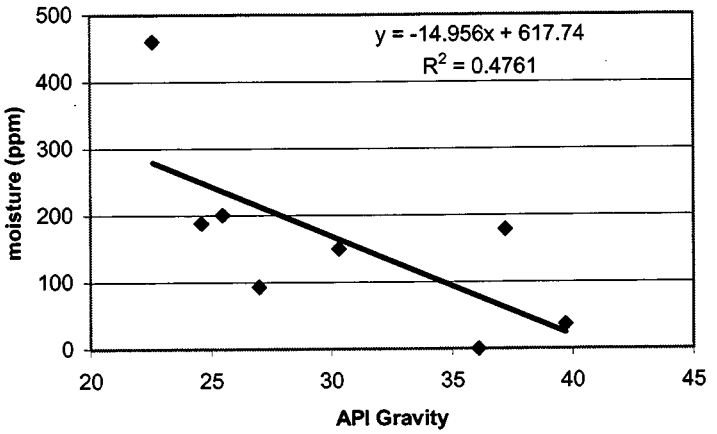

Figure 1.2-50. Correlation between moisture and API gravity is weak.

A better correlation can be obtained for moisture as a function of acid number ($R^2 = 0.62$) and still better relationships are found between moisture and base number or between moisture and acid number plus base number, as shown in Fig. 1.2-51. There is a great deal of scatter ($R^2 = 0.73$); much more data would be required to confirm this possible relationship, but it is reasonable that measures related to polarity such as acid and base numbers should correlate to the ability of an oil to dissolve water. Other measures of polar components, such as fractions of resins and asphaltenes, might also be expected to show positive correlation with moisture content.

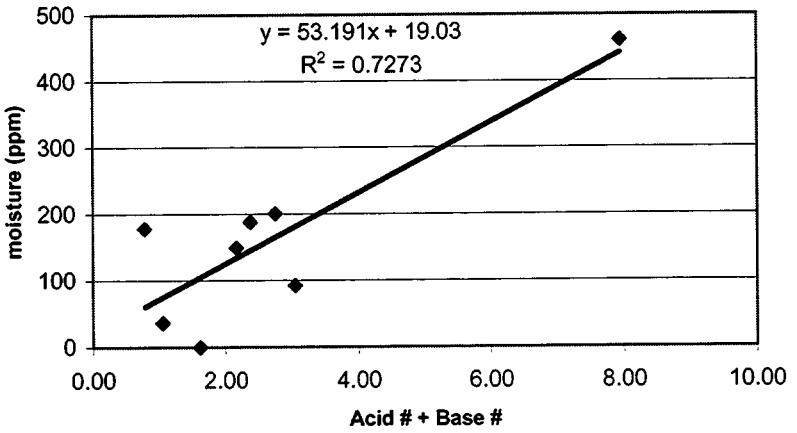

Figure 1.2-51. A better correlation exists between moisture and (Acid# + Base#).

Summary of moisture analysis results

It appears that there is some relationship between oil polarity—measured here by acid and base numbers—and the amount of moisture in crude oil samples. It is also clear that the amount of water in the oil can change. If a particular crude oil can dissolve or emulsify water, that may help to explain what happens to the bulk water on mineral surfaces immersed in crude oil. It would be difficult, however, to determine the extent to which water dissolution and/or emulsification contributes to wetting alteration, in view of the other important effects on wetting of polar components in an oil.

PART 2. WETTABILITY ASSESSMENT

2.1 Smooth Surface Measurements

2.1.1 Wettability Tests with Different Materials

2.1.1.1 Mica as a test substrate

In previous work, glass surfaces have been used for several systematic investigations of crude oil/brine/solid interactions. Microscope slides made of soft glass (Liu and Buckley, 1997) and plates of quartz glass (Xie, 1996) have both been used to observe adhesion and adsorption properties of crude oils.

Several mechanisms by which crude oil components can interact with silicate surfaces have been proposed (Buckley *et al.*, 1998b). However, mechanisms demonstrated on smooth glass surfaces are not necessarily predictive of wetting alteration in sandstone cores (Buckley *et al.*, 1996). Quartz is the major mineral component of sandstones and thus has traditionally been considered as a representative substrate for sandstone interactions with crude oils. However, pore surfaces, rather than bulk composition, are the important part of a rock, with respect to interactions with crude oil, and those surfaces may be dominated by minor components such as clays.

Muscovite mica is in many ways an ideal choice to replace glass in surface tests of the wettability altering potential of crude oils. Freshly cleaved surfaces are crystalline, molecularly smooth and readily reproduced. There is a wealth of data about the surface properties of mica. It is the main substrate used for measurements of surface forces (Israelachvili, 1991). Surface charge is determined by the ratio of substitution of Al^{3+} for Si^{4+} in the tetrahedral layers; the naturally occurring counter ion can be readily replaced by ion exchange. Muscovite has a surface structure similar to illite, a common clay mineral in sandstone reservoirs. Muscovite

itself is found in reservoir rocks (Hurst, 1985) and may be a more common reservoir mineral than is usually recognized because it can be mistaken for illite in x-ray diffraction studies (Herron *et al.*, 1997).

Mica, like quartz, is negatively charged except at very low pH. Thus, we might expect that the interactions with brine and oil should be similar for mica and quartz. There are differences, however, in surface structure, charging mechanisms, and roughness that may impact interactions. Given the difficulties inherent in studies of complex natural materials such as crude oil, it is necessary to document wetting alteration of mica with some well-studied oils, while samples are still available.

Experimental wettability test methods and materials for tests on mica

Mica:

Samples of mica were obtained from Ward's Natural Science Establishment. These included:

muscovite $\left(KAl_2(Si_3Al)O_{10}(OH,F)_2\right)$ and

biotite $\left(K(Mg,Fe^{2+})_3(Al,Fe^{3+})Si_3O_{10}(OH,F)_2\right)$

Both of these mica minerals exhibit perfect cleavage to produce molecularly smooth surfaces.

Aqueous solutions:

All solutions were prepared from deionized water, redistilled in glass and reagent grade salts. NaCl solutions with salinities up to 1*M* were weakly buffered using sodium acetate/acetic acid (pH 4) or sodium phosphate salts (pH 6 and 8). The pH values of the 2*M* NaCl solutions were adjusted with HCl or NaOH. For the NaCl solutions, pH and concentration are indicated within braces as {pH, [NaCl]}. The pH of $CaCl_2$ solutions was not adjusted; it ranged from 5.9 to 6.2.

Refined oils:

Toluene and decane were purified by passing the fluids through a column of silica gel and alumina.

Crude oils:

Two crude oils were used in these tests. Their properties are summarized in Table 2.1-1.

Table 2.1-1. Crude oil properties

	A-93 (Prudhoe Bay)	Moutray (W. Texas)
API Gravity (° API)	22.5	35.2
Acid Number (mg KOH/g oil)[1]	0.14	0.55
Base Number (mg KOH/g oil)[2]	2.42	0.81
n-C_5 asphaltenes (wt%)[3]	10.9	1.79
n-C_7 asphaltenes (wt%)	7.1	0.95
Elemental analysis[4]:		
H/C	1.671	1.803
N/C	0.003	0.002
S/C	0.004	0.002
O/C	0.004	0.006

[1] ASTM D664-89. [2] ASTM D2896-88; Dubey and Doe, 1993. [3] ASTM D2007-80. [4] Huffman Labs

Test protocols:

The tests used here have been described previously (Liu and Buckley, 1997). Additional details of the testing procedures with mica are also available (Liu, 1997). Briefly, they involve the following observations.

(1) *Adhesion* or non-adhesion of a drop of crude oil was observed as it was withdrawn from a clean, brine-covered surface after a short contact time between oil and solid. NaCl concentration, pH, and temperature have been identified as important variables in these tests.

(2) Water/decane contact angles were measured to assess the affect of *adsorption* on surfaces exposed first to brine and then to crude oil. Brine composition and oil exposure conditions (time and temperature) have been found to be the main variables

affecting adsorption for a given oil and surface. Crude oil was removed by washing with toluene prior to contact angle measurement.

Results of wettability tests on mica

Two oils that have been extensively tested on glass surfaces (Buckley and Morrow, 1990; Liu and Buckley, 1997; Xie *et al.*, 1997) and in Berea sandstone cores (Morrow *et al.*, 1986; Jadhunandan and Morrow, 1995; Zhou *et al.*, 1995, 1996; Yildiz, 1995; Buckley *et al.*, 1996; Tang and Morrow, 1997) are Moutray crude oil from West Texas and A-93 from Prudhoe Bay, Alaska. These crude oils were selected for a detailed comparison of wettability-altering interactions on mica to those previously reported on soft and quartz glass.

Wetting alteration—dry mica:

Previous studies on glass have demonstrated wetting changes that occur when dry surfaces are aged in crude oil. The resulting surfaces tend to have water-advancing angles (against decane) that are in the intermediate range ($60° < \theta_A < 120°$) and water-receding angles that are much lower ($\theta_R < 30°$) (Buckley *et al.*, 1998b). Figure 2.1-1 shows the results of comparable experiments on muscovite.

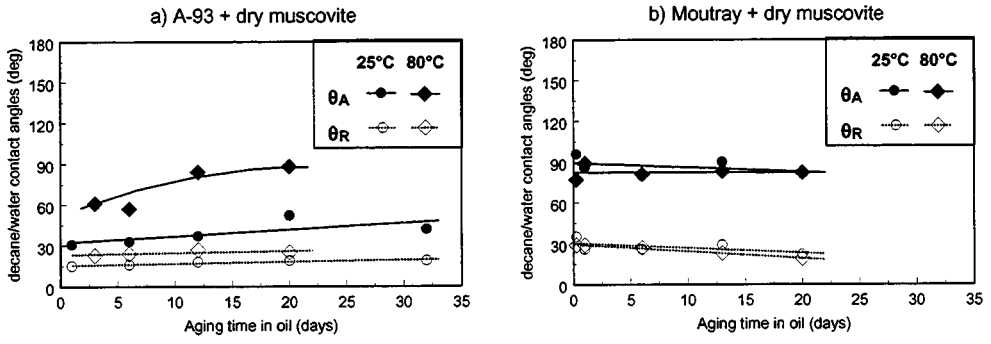

Figure 2.1-1. Contact angles on dry mica surfaces treated with A-93 and Moutray crude oils.

Interactions between dry mica and crude oils produce surfaces that are neither water-wet nor oil-wet. (Note that while the solid surfaces were dried before exposure to oil, water was not

rigorously excluded from any of these tests.) Differences between mica surfaces aged at room temperature and at 80°C are evident for A-93 oil, but not for Moutray. Changes with aging time are minimal in both cases. These observations are generally consistent with previously reported results with many different crude oils and glass surfaces where rapid alteration to intermediate conditions that vary little with temperature have been observed.

In the experiments summarized in Fig. 2.1-1, mica surfaces were rinsed with toluene to remove all but the adsorbed oil. Rinsing with a solvent other than toluene would likely produce different contact angles. More paraffinic solvents destabilize asphaltenes, whereas stronger solvents might remove some of the adsorbed material.

Wetting alteration of mica in the presence of water:

The presence of water complicates crude oil/solid interactions in several ways. Bulk water can shield solid surfaces from contact with high molecular weight compounds in the oil and limit their access to adsorption sites on the solid surface. Stable water films can also prevent adsorption, especially in low salinity, high pH regimes where electrostatic repulsive forces balance van der Waals attraction. If water films are unstable, alteration of wetting can be more pronounced than in the absence of water. The compositions of both oil and brine are key variables in determining the wetting alteration observed on a given surface.

Dependence of water film stability on brine pH and ionic strength indicates the contribution of acid/base interactions and is the basis of standard adhesion tests. Brine pH and NaCl concentrations for which adhesion was observed in two-minute tests with A-93 at 25°C and 80°C on mica are shown in Fig. 2.1-2. The adhesive areas are smaller than the corresponding areas on glass. Glass results are indicated in Fig. 2.1-2 by the dotted lines separating adhesion/transition observations from non-adhesion (Buckley *et al.*, 1997).

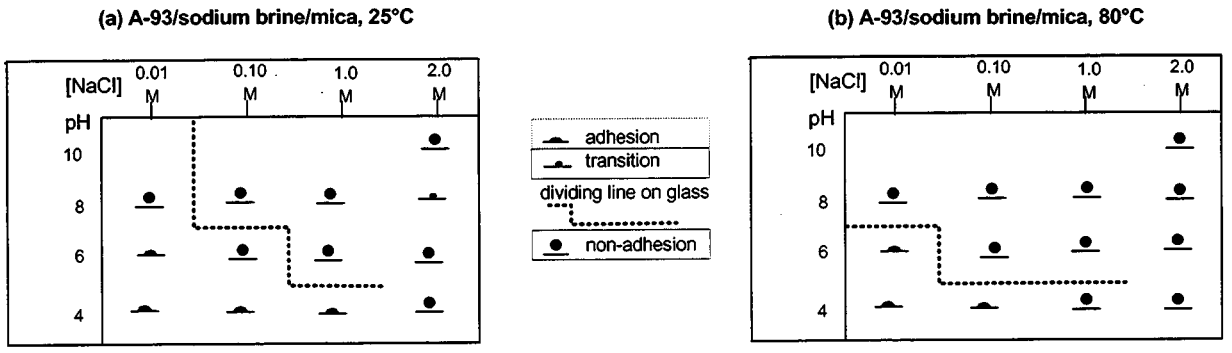

Figure 2.1-2. Adhesion maps for A-93 crude oil on muscovite and biotite mica.

The adhesion tests suggest a tentative outline of conditions where water films are stable (higher pH and higher ionic strength) and where they are unstable (lower pH and lower ionic strength), as illustrated in Fig. 2.1-3. Transitional conditions and those that change with temperature are included in the intermediate or conditionally stable region. That region is smaller for mica than for glass; regions that are clearly unstable are comparable.

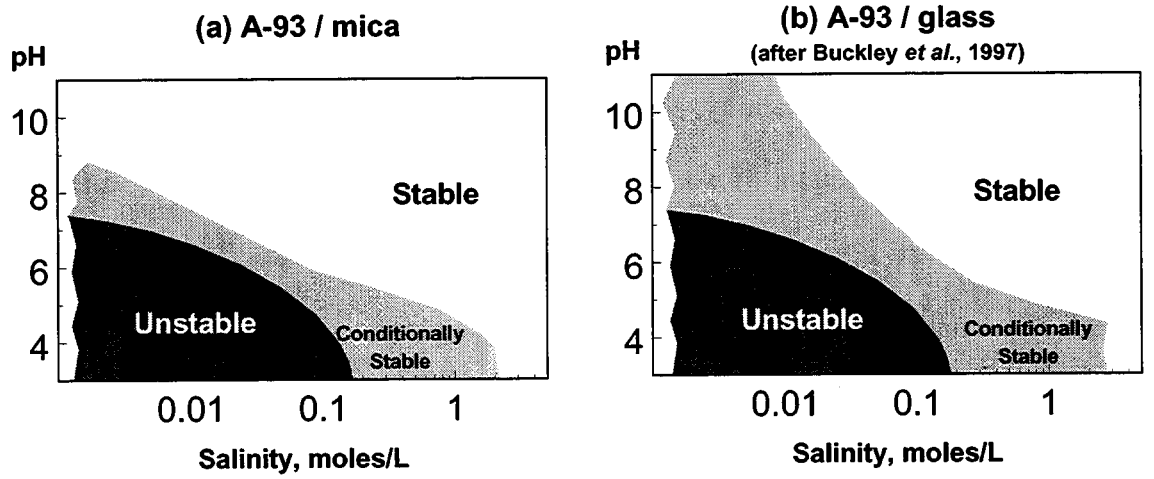

Figure 2.1-3. A-93 water film stability maps based on comparisons of adhesion at 25 and 80°C.

Comparison of different mica minerals:

Two different mica minerals have been tested. Muscovite is light in color and large areas appear to be smooth. Biotite, which has iron substituted in its inner layers, is darker in color and

the samples used in these tests often appeared to be macroscopically rough. Despite these differences, tests showed that wettability-altering interactions were similar for both types of mica. The examples shown in Fig. 2.1-4 illustrate that there are only small differences between muscovite and biotite after the first day of aging (Fig. 2.1-4a). Differences are more significant after samples have been aged for about three weeks (Fig. 2.1-4b). In most cases, the contact angles measured on biotite were somewhat higher than those on muscovite.

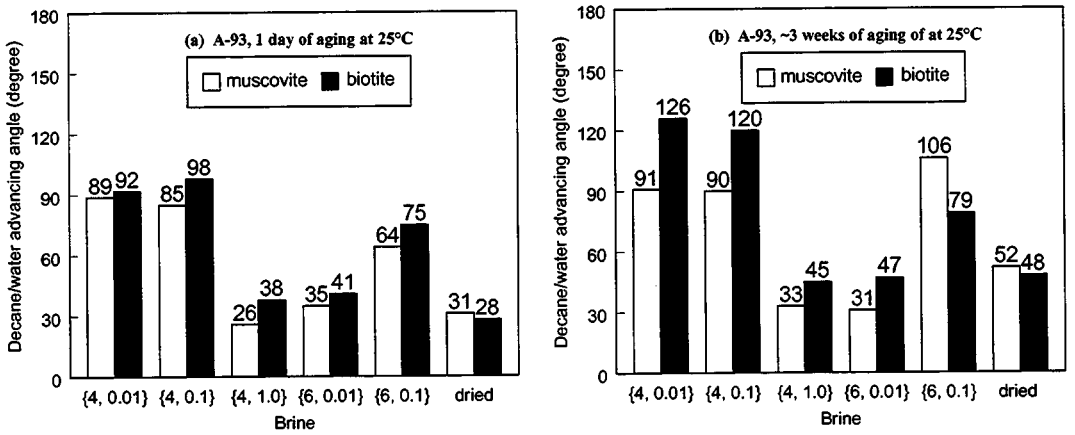

Figure 2.1-4. Muscovite vs. biotite.

Effect of roughness:

The effect of roughness was tested by selecting two sets of samples, specimens that appeared smooth and those that were obviously rough. As shown in Fig 2.1-5 for biotite, there were no systematic differences discernible in the contact angles on oil-treated surfaces that could be attributed to this macroscopic-scale roughness.

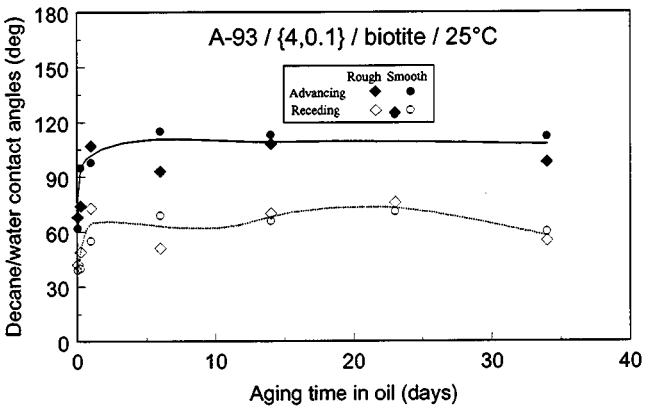

Figure 2.1-5. Comparison of macroscopically rough and smooth biotite samples.

Acid/base interactions with A-93, a high base number oil:

An oil with a high base number and low acid number should have ample positively charged interfacial sites to enable fairly strong interactions between oil components and the negatively charged mica surface, especially when pH is low. Unstable conditions permit contact of oil with surface and alteration of wettability by adsorption of positively charged crude oil components. As shown in Fig. 2.1-6, only the lowest pH and lowest ionic strength brine tested consistently produced contact angles above 90° (Fig. 2.1-6a). At the other extreme are the higher ionic strength brines ([NaCl] = 1*M*), all of which gave low water-advancing angles of about 40° or less (Fig. 2.1-6c). The pH 8 brine with [NaCl] = 0.1 *M* is also in this category. All the other brine compositions tested gave intermediate results that changed with aging temperature (Fig. 2.1-6b). The results in Fig. 2.1-6 lead to a somewhat revised picture of the water-film stability map, as shown in Fig. 2.1-7.

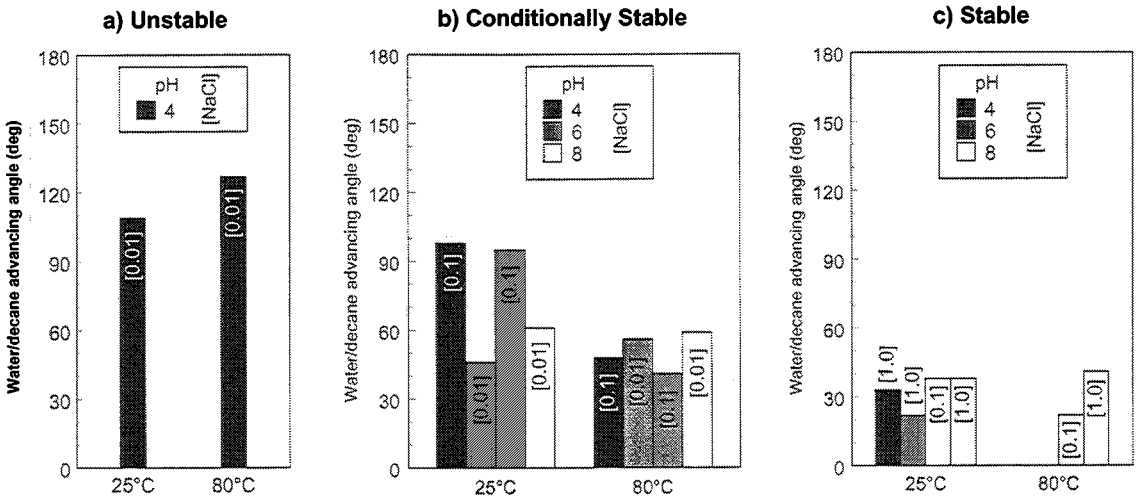

Figure 2.1-6. Alteration of wettability of muscovite aged in brine and A-93 crude oil.

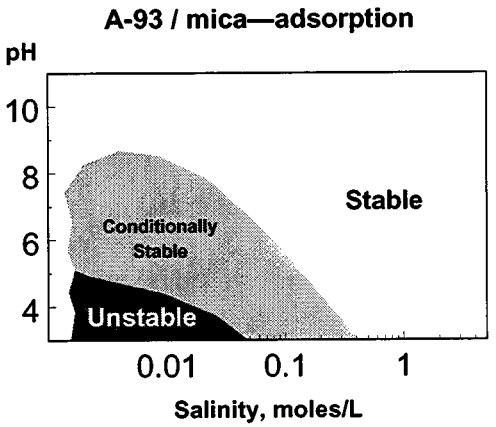

Figure 2.1-7. Water film stability map based on contact angles measured on mica surfaces aged in crude oil.

Comparisons of oil/brine/solid interactions on mica and glass have been reported previously by Basu and Sharma (1997). Using a method proposed by Ducker *et al.* (1994), they have applied atomic forces microscopy (AFM) to the measurement of force/distance relationships for water films between solid and oil. Their crude oil results are comparable to the observations based on adhesion and contact angle measurements. Water-film instability was

greater for glass than for mica. They attributed the difference primarily to asperities on the order or 20 to 30 nm on their glass surfaces.

The effect of temperature on interactions between oil, brine, and solid has yet to be clearly explained. Increasing temperature can release an adhering drop of oil. On the other hand, higher contact angles have been reported on glass surfaces aged at 80°C than on similarly treated surfaces aged in oil at room temperature (Liu and Buckley, 1998; Xie *et al.*, 1997). In cores, a similar dilemma exists. Berea sandstone cores aged in oil at elevated temperature often appear to be less water-wet than those aged in the same oil at room conditions (Jadhunandan and Morrow, 1991), but high temperature imbibition experiments produce more water-wet estimates of wetting than in similar cores tested at room temperature (Tang and Morrow, 1997). Factors that must be considered include asphaltene aggregation, rates of adsorption and desorption, and solubility of water in oil, all of which may vary with temperature.

One further factor is suggested by the observation that contact angles on mica can be lower at elevated aging temperature than at room temperature. This is the result that might be expected from the adhesion tests, especially for conditionally stable brine compositions. It is also consistent with more water-wet conditions in cores at high temperatures.

Why then are the opposite results observed on glass? The relative solubility of the two surfaces may provide some clues. Brady and House (1996) show solubility of crystalline quartz, SiO_2 glass, and muscovite at several temperatures in brines of varying pH. Approximate values at about pH 6 are summarized in Table 2.1-2. The rate for muscovite is cited at a higher temperature than that for the other materials. Nevertheless, it dissolves at a slower rate, especially near neutral pH. The soft glass of microscope slides probably dissolves at an even higher rate than SiO_2 glass cited here. Thus the contrast between dissolution rates of soft glass

and muscovite at the temperatures used in this study is probably at least three orders of magnitude. It is possible that long aging times at elevated temperatures are causing corrosion of the glass surface, enhancing the effect of crude oil/solid interactions with glass.

Table 2.1-2. Dissolution rates of mica, quartz, and SiO_2 glass at pH 6 (Brady and House, 1996)

Material	T°C	Rate of dissolution (mol cm^{-2} s^{-1})
SiO_2 glass	65	1×10^{-14}
Quartz	25	6×10^{-17}
Quartz	60	5×10^{-16}
Muscovite	70	3×10^{-17}

Ion-binding interactions with Moutray, a high acid number oil:

An oil with high acid number and low base number can—in the presence of divalent cations—alter wetting of a negatively charged surface by an ion-binding mechanism. These interactions often seem to require longer aging times and cannot be predicted from the results of two-minute adhesion tests. Moutray crude oil has a high acid number and low base number; it should be a better candidate for ion binding with mica treated mica surfaces than A-93. The contact angle results shown in Fig. 2.1-8 are consistent with this interpretation since, after aging in oil for about two weeks at 80°C, water-advancing angles on the Moutray-treated surfaces are much higher than those treated with varying concentrations of $CaCl_2$ brine and A-93 crude oil.

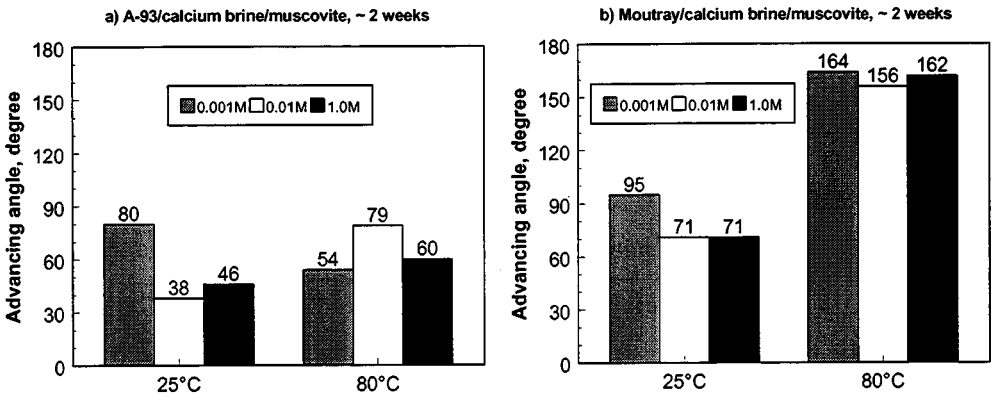

Figure 2.1-8. Alteration of wettability of muscovite aged in calcium brines and crude oils.

Summary of wettability observations on mica surfaces

- Muscovite mica, whose surface structure is analogous to illite clay, is a good choice for standard tests of crude oil/brine/solid interactions with negatively charged reservoir minerals. It has the advantages of being widely studied, molecularly smooth, and very reproducible.
- The wetting of mica surfaces can be altered by exposure to crude oils. Two oils, A-93 from Prudhoe Bay and Moutray from West Texas, have been tested to compare their wettability altering capabilities, previously studied on glass surfaces, with similar conditions and mica surfaces.
- In the absence of water, intermediately-wet conditions result from exposure of mica surfaces to either A-93 or Moutray.
- With NaCl brines, acid/base interactions influence water-film stability. Film stability on mica is similar to that demonstrated previously on glass.
- Ion-binding interactions with an acidic oil (Moutray) can produce fairly oil-wet surfaces.

- There are small differences in interactions with muscovite and biotite mica surfaces. Macroscopic surface roughness is not detected by contact angle measurements on oil-treated surfaces.
- Changes in dissolution rates with pH and temperature for different substrate materials may have an impact on wettability alteration.

2.1.1.2 Wetting alteration in square capillaries

Mixed wetting is increasingly accepted as a probable condition of oil reservoir rocks (Morrow, 1990; Cuiec, 1991; Buckley, 1996b). Although most clean mineral surfaces are strongly water-wet, components from the crude oil can adsorb and alter wetting. Mixed wetting can occur if pore-lining minerals differ in their surface energetics or if fluid distribution affects patterns of adsorption. The latter case, first suggested by Salathiel (1973), can lead to bicontinuous oil-wet and water-wet paths through a rock. To characterize rocks with respect to their wetting condition, the amount of water (or oil) that will spontaneously imbibe and the rate of imbibition are often observed (Amott, 1959; Denekas *et al.*, 1959; Anderson, 1986; Morrow and McCaffery, 1978; Morrow *et al.*, 1994), but many questions remain regarding interpretation of the results of imbibition tests, especially for mixed-wet conditions.

Alteration of the wetting of high-energy surfaces exposed to brine and crude oil has been studied on smooth, flat surfaces (Anderson, 1986; Buckley, 1996b), but relating contact angles to imbibition presents significant problems (Buckley *et al.*, 1996; Xie *et al.*, 1997). Capillary tubes of noncircular cross section provide a simple pore geometry for studies of mixed-wet conditions. For glass tubes, contact angles measured on flat glass surfaces can be used as a guide to the wetting alteration that should occur when tubes are exposed to brine and crude oils.

The purpose of this study is to assess the feasibility of generating mixed-wet conditions using brines and crude oils and of quantifying the results of wetting alteration in square glass tubes of capillary dimensions. This is a preliminary study in which a variety of procedures and measurements were examined including capillary rise of water against air and the rate, extent, and mechanisms of water imbibing into horizontal tubes containing oil.

Water film stability:

To create a range of wetting conditions, A-93 crude oil from Prudhoe Bay was used with brines of varying pH and NaCl concentration. Interactions between these fluids and glass surfaces have been studied extensively (Liu and Buckley, 1997; Basu and Sharma, 1996; Xie, 1996). Adhesion of crude oil to a solid surface is related to wettability alteration. Lack of adhesion may signify the presence of a water film, stabilized by double-layer repulsion between the crude oil and the solid surface. These forces are influenced by brine concentration and composition (Buckley *et al.,* 1989; Buckley and Morrow, 1990). In the absence of brine, polar interactions between oil components and solid can produce neutrally-wet surfaces. Other modes of interaction between oil and solid have been identified (Buckley *et al.*, 1997a). Because of the conditions selected for this study, the primarily interactions are likely to be (1) polar mechanisms that control interactions in the absence of water and (2) acid/base mechanisms that dominate when water is present, but lacks any divalent or multivalent ions.

Depending on the nature of the crude oil, different regimes of film stability are observed on a given solid surface. When water films are unstable, crude oil can contact the glass surface and adhesion and/or adsorption can occur. If the brine gives rise to stable water films, crude oil cannot contact the glass surface and adhesion does not occur. Between these two extremes is a region of brine compositions for which the films are conditionally stable. Whether or not the film breaks and crude oil contacts the surface can vary with experiment conditions.

Menisci in noncircular capillary tubes:

Noncircular capillary tubes have been the subject of many studies (*e.g.*, Lenormand *et al.*, 1983; Kovscek *et al.*, 1993). A meniscus in an angular tube can merge into liquid wedges in the corners. The MS-P method—so named by Mason and Morrow (1984) after the work of Mayer and Stowe (1965) and Princen (1969)—allows calculation of the shapes of wedging menisci.

Capillary systems can be divided into two groups. Nonwedging systems are those which have only a main terminal meniscus (MTM), bounded entirely by the solid perimeter, while wedging systems are those in which one or more arc menisci (AM) are formed and the MTM is bounded partly by solid and partly by liquid where it merges into the AMs (see Fig. 2.1-9).

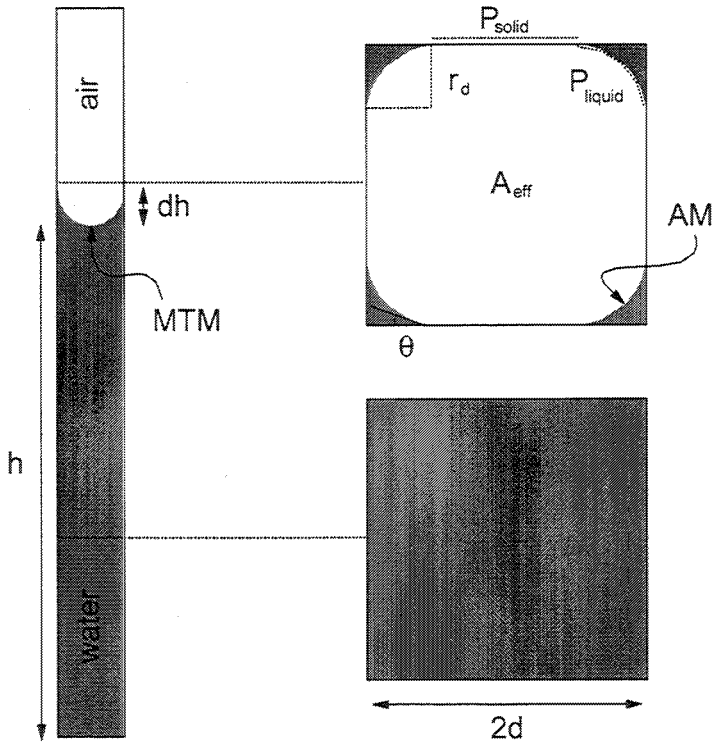

Figure 2.1-9. Main terminal meniscus (MTM), arc menisci (AM), radius of the AMs (r_d, contact angle (θ), effective area (A_{eff}), portions of liquid perimeter (P_{liquid}), and solid perimeter (P_{solid}) are illustrated for water rising against air in a square capillary.

At equilibrium, in the absence of gravitational forces, the curvature of the AMs must equal that of the MTM even though the shape of the MTM may be very complex. The simple geometry of the AM, with one radius of curvature equal to infinity, lends itself to analysis. The first experimental verification of the method was published by Mason *et al.* (1983). Since then, the method has been applied to a variety of pore geometries and wetting conditions (some examples include Mason and Morrow, 1984 and 1991; Walsh, 1989; and Ma *et al.,* 1996).

For a nonwedging system, the curvature of the main terminal meniscus equals the inverse of the hydraulic radius of the capillary. For a wedging system, the MS-P analysis can be applied to calculate curvatures. Consider the geometry defined in Fig. 2.1-9. The effective area of the cross-section shown above the MTM is not simply the cross-sectional area of the tube because the AMs occupy the corners, reducing the area available to the nonwetting phase. The presence of arc menisci also makes it necessary to consider the effective perimeter, P_{eff}, in parts: the solid perimeter, ΣP_{solid}, is all the perimeter that is not contacted by the liquid wedges and the liquid perimeter, ΣP_{liquid}, is the sum of the arc lengths.

As the works cited above explain in detail, the MS-P equation can be derived from an energy balance approach, considering a small displacement, dh, of the MTM as shown in Fig. 2.1-9. The virtual work balance gives:

$$p_c A_{eff} dh = (\sigma_{SV} - \sigma_{SL}) \Sigma P_{solid} dh + \sigma_{LV} \Sigma P_{liquid} dh \qquad (2.1\text{-}1)$$

Incorporation of Young's equation leads to the expression:

$$p_c A_{eff} = \sigma_{LV} \Sigma P_{solid} \cos\theta + \sigma_{LV} \Sigma P_{liquid} \qquad (2.1\text{-}2)$$

The capillary pressure, p_c, across a point in an interface is given by the Young-Laplace equation:

$$p_C = \sigma \cdot C \qquad (2.1\text{-}3)$$

Inserting this into Eq. 2.1-2 gives the following expression for the curvature:

$$C = \frac{\Sigma P_{solid} \cos\theta + \Sigma P_{liquid}}{A_{eff}} \tag{2.1-4}$$

If P_{eff} is defined as

$$P_{eff} = \Sigma P_{solid} \cos\theta + \Sigma P_{liquid} \tag{2.1-5}$$

Eq. 2.1-3 can be expressed as:

$$C = \frac{P_{eff}}{A_{eff}} \tag{2.1-6}$$

In a mathematical sense, the wedge will be infinitely long under constant curvature conditions. Thus, the arc menisci have radii of curvature of ∞ in the axial direction and r_d in the plane of cross-section, and thus:

$$C = \frac{1}{r_d} = \frac{P_{eff}}{A_{eff}} \tag{2.1-7}$$

A dimensionless expression for the curvature results if both sides of Eq. 2.1-7 are multiplied by some arbitrary characteristic tube dimension. For a square capillary the characteristic dimension is chosen to be half the width of the tube, d.

$$C_n = \frac{d}{r_d} = \frac{dP_{eff}}{A_{eff}} \tag{2.1-8}$$

Eq. 2.1-7 and 2.1-8 are both statements of the MS-P equation.

For the simple geometry of the $1mm^2$ tube under strongly water-wet conditions, the drainage radius r_d is 0.265 mm. The arc menisci held in the corners occupy 0.06 mm^2 or 6% of the cross-sectional area.

Square tube with nonzero contact angle and uniform wetting. Mason and Morrow (1984) applied MS-P theory to an n-sided tube with variable wetting. Appropriate expressions for A_{eff} and P_{eff} can be found from geometrical considerations. Substituting these into Eq. 2.1-8, with θ in radians, gives the following quadratic equation for (r_d/d):

$$\frac{1}{2}\left[\cos^2\theta - \cos\theta\ \sin\theta - \left(\frac{\pi}{4} - \theta\right)\right]\left(\frac{r_d}{d}\right)^2 - \cos\theta\left(\frac{r_d}{d}\right) + \frac{1}{2} = 0 \qquad (2.1\text{-}9)$$

Solving this equation for (r_d/d) gives two roots, only one of which is physically meaningful. When the $(r_d/d)^2$ coefficient becomes zero, which happens when $\theta = 45°$, there are no real roots. This represents the point where the wedge menisci disappear, so the condition for wedge menisci to occur in a square capillary is $\theta < 45°$. If the contact angle is less than 45° we have a wedging system, and the solution to the MS-P equation is:

$$C_n = \frac{d}{r_d} = \cos\theta + \sqrt{\frac{1}{2}\left[\sin 2\theta + \frac{\pi}{2} - 2\theta\right]} \qquad (2.1\text{-}10)$$

For contact angles in the interval $90° > \theta \geq 45°$, wedge menisci do not exist, and the curvature of the meniscus is equal to the curvature of a meniscus in a cylindrical capillary with radius d. If this curvature is converted to a dimensionless number, by multiplying by the characteristic dimension of the tube, the equation for meniscus curvature is:

$$C_n = \frac{d}{r_d} = 2\cos\theta \qquad (2.1\text{-}11)$$

Mixed-wet square tubes. The advantage of using noncircular tubes in this study is the opportunity they provide to produce and observe the effects of mixed-wet conditions. Adsorption of crude oil components is limited by the existence of water wedges; thus, after treatments with brine and crude oil, the corners remain more water-wet, while exposed portions of the glass surface may have high water-advancing contact angles.

The MS-P theory has been tested for mixed-wet conditions produced by using different materials to form different sides of pores (Walsh, 1989). Here an alteration of part of each pore wall to a less water-wet condition is envisioned, as illustrated in Fig. 2.1-10.

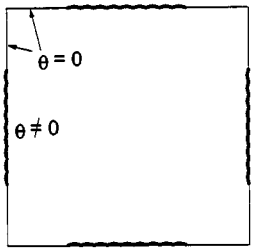

Figure 2.1-10. Square tube after exposure to brine and crude oil.

Curvatures calculated as a function of contact angle on the exposed surfaces in both uniform and mixed-wet tubes are shown in Fig. 2.1-11. For uniform wetting, curvatures were calculated using Eq. 2.1-10 for wedging systems and Eq. 2.1-11 for nonwedging systems. For the mixed-wet tubes, values are taken from the calculations of imbibition curvatures with hysteresis of Ma *et al.* (1996). Note that positive curvatures and spontaneous imbibition persist to contact angles greater than 90° for mixed-wet tubes.

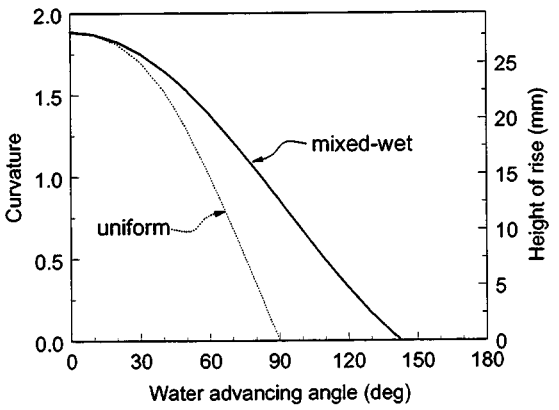

Figure 2.1-11. MS-P curvatures calculated for uniform and mixed-wet square capillaries.

Capillary rise:

Capillary rise is a commonly used measure of wettability (Anderson, 1986). Most of the previous studies of capillary rise and flow in capillaries have been conducted using cylindrical tubes. Noncircular capillaries can also be used with the MS-P method to relate height to curvature.

The change in capillary pressure with height above a free liquid surface is given by:

$$\Delta p_c = \Delta \rho g h \tag{2.1-12}$$

Considering rise of liquid in a capillary above a datum level, Eq. 2.2-12 can be combined with the Young-Laplace equation (Eq. 2.1-3), and multiplied by d, to give:

$$C_n = d\left(\frac{1}{r_1} + \frac{1}{r_2}\right) = d\left(\frac{gh\Delta\rho}{\sigma}\right) \tag{2.1-13}$$

where r_1 and r_2 are radii of curvature of the main terminal meniscus. Using Eq. 2.1-13, the curvature of the MTM can be calculated from capillary rise experiments if the density difference and the interfacial tension between the fluids are known.

In a capillary rise experiment, the curvature varies with the height of rise due to the influence of gravity, so the constant curvature condition is not strictly met. However, if the capillary forces are much greater than the gravitational forces, MS-P theory can still be applied. In a simple capillary rise experiment, the capillary forces will be governed by the relationship between the height of rise and the dimensions of the tube, and by wettability. For strongly wetting conditions, gravitational forces will be negligible if the height of rise is much larger than the characteristic dimensions of the tube (i.e. h/d>>1). However, Mason *et al.* (1983) demonstrated that the method provides a good approximation even outside this range. For other wetting conditions such a criterion is more difficult to establish.

Spontaneous imbibition:

The rate and amount of spontaneous imbibition are the basis of many commonly used measures of the wettability of core samples. The core is said to be strongly water-wet if large volumes of brine are rapidly imbibed, while lower rates and smaller volumes usually imply a more weakly water-wet core. If no water is imbibed the core is either oil-wet or neutrally wet (Anderson, 1996). Between these extremes are many wetting conditions of practical interest that might well be discerned from imbibition rate and extent, if we understood better how to interpret the data. While square quartz capillaries are not representative of many of the complexities of natural porous media, they have two important advantages as models in which to study imbibition. One is transparency, which allows us to see what is happening during imbibition, and the other is the existence of corners in which water can form wedges.

The rate of imbibition of a wetting fluid displacing air was given for cylindrical tubes by Washburn (1921). Flow of a wetting fluid in noncircular tubes was investigated by Ransohoff and Radke (1988). A dimensionless resistance factor was introduced to account for corner geometry and roundedness. Dong (1995) calculated and measured the rate of imbibition into square tubes, for both zero and nonzero contact angles in uniformly-wetted tubes. The effects on imbibition rate of a viscous nonwetting phase and of mixed-wet surface conditions remain to be investigated.

A dimensionless number, referred to as the spontaneous imbibition index (SI) is introduced. This number is defined as the ratio of the amount of oil produced by spontaneous imbibition in a given test to the amount of oil produced in the analogous strongly water-wet case. In most cases the SI index was not greatly different from the displacement efficiency, since the strongly water-wet tests were very efficient in these straight tubes.

Experimental materials and procedures for wetting alteration in square capillaries

Materials:

Fluids. Brines used for aging of the capillaries prior to treatment with A-93 crude oil were prepared according to the method described by Liu (1993). Brines ranged in pH from 4 to 8 and in ionic strength from 0.01 to 1 *M*. In this report, brine compositions are labeled using the shorthand notation {pH, I}. Properties of A-93 crude oil are summarized in Tables 2.1-3 and 2.1-4.

Table 2.1-3. Chemical and physical properties of the A-93 crude oil

Source	ρ at 25°C g/cm^3	μ at 25°C cP	Asphaltenes (wt%) precipitated by:		
			n-C_5	n-C_6	n-C_7
Prudhoe Bay	0.8945	26.7	11	7	4

Table 2.1-4. Gravity, acid and base numbers for the A-93 crude oil

°API	Acid number (mg KOH/g oil)[a]	Base number (mg KOH/g oil)b
25.5	0.14 ± 0.04	2.42 ± 0.33

[a]ASTM D664-89; [b]ASTM D2896-88

A 3 vol % solution of red food color in distilled water was the aqueous phase in the capillary rise experiments. The physical and interfacial properties of the dyed water are given in Tables 2.1-5 and 2.1-6.

Table 2.1-5. Viscosities and densities for the dyed water/decane system

Chemical	ρ g/cm^3	μ cP
distilled water	0.9982[c]	1.002[c]
dyed, distilled water	0.9989d	
{8,0.01} brine		0.94 ± 0.06
{8,1} brine		0.99 ± 0.06
decane	0.7300[c]	0.92[c]
dyed decane		0.92 ± 0.05

[c]CRC Handbook of Chemistry and Physics, 1st Student ed., 1988 (at 20°C); [d]measured at 20°C

Table 2.1-6. Interfacial tensions

Phases	IFT at 20°C mN/m
distilled water / air	74.0±0.4
dyed, distilled water/air	72.3±0.2
dyed decane / {8,0.01} brine	27.4
dyed decane / {8,1} brine	28.9
A-93 / {8,0.01} brine	26.5
A-93 / {8,1} brine	25.5

In water-oil experiments, an oil dye, Oil Red O from Sigma, was used to enhance the visibility of the decane phase. Excess dye was equilibrated with decane and the mixture was centrifuged to remove undissolved dye particles. Interfacial tensions and viscosities are given in Tables 2.1-5 and 2.1-6. Contact angles between {8,0.01} and {8,1} brines and dyed decane are in Table 2.1-7.

Table 2.1-7. Contact angles

Phases	θ_A (deg)	θ_R (deg)
{8,0.01} / dyed decane	22.1 ± 1.9	20.0 ± 1.25
{8,1} / dyed decane	20.1 ± 1.8	18.7 ± 0.8

Glass capillaries . The capillaries used in these experiments were obtained from Wilmad glass. The 10 cm long square capillaries had a nominal inner dimension of 1 mm^2 (V=0.1mL).

The inner dimensions of the square capillaries were measured to be 0.98±0.02 mm^2. Details of these measurements are given in Table 2.1-8. The 10 cm long rectangular tubes had nominal inner dimensions of 1 mm by 10 mm (V=1mL).

Table 2.1-8. Measurement of the tube inner dimensions

Test number	Length of tube (mm)	Volume of water contained (mL)	Estimated side length (mm)
1	99.5	0.1017	1.01
2	100.0	0.0922	0.96
3	110.0	0.1006	0.99
4	100.0	0.0947	0.97
5	110	0.0963	0.98
Average			0.98 ± 0.02

Prior to use, the capillaries were cleaned in an ultrasonic bath for at least 15 minutes in a solution composed of 9 parts hydrogen peroxide (30%) and 1 part ammonium hydroxide (20%). After cleaning, they were rinsed with copious amounts of distilled water and dried.

Exposure of capillaries to brine and oil:

Aging in either brine or A-93 crude oil was accomplished by submerging the completely filled capillaries in a closed container of brine or crude oil. Tubes were oriented vertically during aging periods. Two different treatment sequences were tested:

- Some tubes were completely filled with oil with no initial water saturation (S_{wia}=0, where S_{wia} is the initial water saturation during aging in oil).
- Others were aged in brine for 24 hours, drained to an S_{wi} of approximately 6%, then filled with oil ($S_{wia}\neq 0$).

For tests of capillary rise (water vs. air), tubes were washed, first with toluene, then with decane, to remove the crude oil. Finally, the tubes were dried. To test drainage, dried tubes were refilled with water.

Some of the spontaneous imbibition (water vs. oil) tests started with similarly washed and dried capillaries, after they had been refilled with oil. Imbibition thus began with no initial water saturation (S_{wii}=0, where S_{wii} denotes the initial water saturation at the start of imbibition). Other brine-treated tubes were drained, filled with crude oil, allowed to age in oil for a period of time t_a, then submerged directly in the imbibing brine, without the rinsing and refilling steps. The water saturation at the start of these imbibition tests was not zero, but the value to which the tubes were drained before aging in oil (S_{wii}=S_{wia}≠0).

Capillary rise:

The height of capillary rise was measured from the datum level to the bottom of the air/water meniscus (as shown in Fig. 2.1-12) using a ruler with 1 mm graduations. The accuracy of the measurement is ± 0.5 mm. The volume of the tubes, and of the water that rose during these experiments, was small compared to the total volume in the beaker, so no change in the datum level was observed during the experiments. More exacting experimental procedures (as described by Walsh, 1989) would be required for completely quantitative results. Several of the experiments were repeated to check reproducibility. For unexposed tubes, 10 measurements of capillary rise were performed. From these a mean value of 26±3 mm was calculated for the height of rise. Results are given in Table 2.1-9. Reproducibility is better in the square capillaries than in rectangular ones. The spontaneous influx of water began rapidly, but declined after approximately 30 seconds. Constant height of the water column was usually reached after 30-60 minutes. The height of the column was measured for as long as 24 hours, but no changes in height were observed after 1 hour.

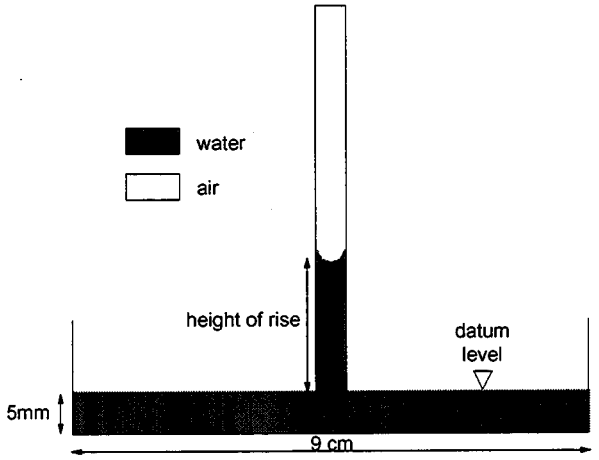

Figure 2.1-12. Schematic of the experimental setup for measuring capillary rise.

Table 2.1-9. Results for unexposed square capillaries

Experiment #	Capillary rise (mm)
1	25.0
2	28.0
3	24.5
4	24.0
5	24.0
6	31.0
7	26.0
8	28.5
9	21.0
10	23.0
average	25.5 ± 2.9

Spontaneous imbibition:

A syringe was used to fill treated capillaries with oil (either dyed decane or crude oil). Capillaries were secured in a holder—a small block of stainless steel into which a groove the size of the outer dimensions of the capillary tube was cut. Over the capillary, a piece of plexiglass was held in place with two screws. The whole assembly was submerged horizontally in the

invading brine. The weight of the stainless steel block kept the tube submerged and horizontal. A piece of heat-shrinkable Teflon tubing was used to connect the capillary to the syringe. The connection to the syringe was cut at the start of the imbibition experiment, leaving a piece of heat-shrinkable tubing around one end of the capillary. This end of the capillary was preferentially oil-wet, and water imbibed only from the other end, as illustrated in Fig. 2.1-13.

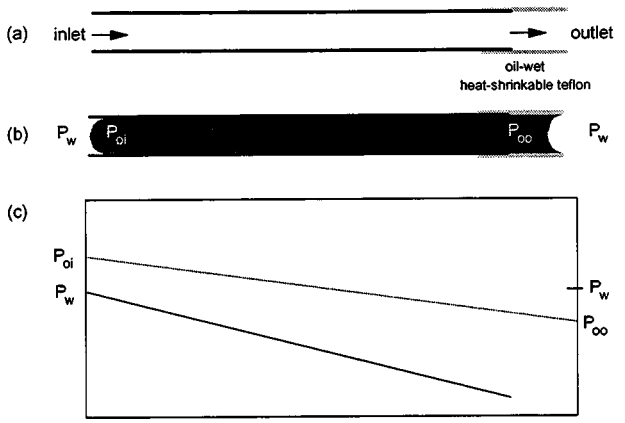

Figure 2.1-13. Inlet and outlet conditions for imbibition into glass capillary plus teflon.

Imbibition was monitored using a microscope and a video camera. Lengths of brine-invaded regions and lengths of oil droplets were measured with a scale in the microscope eyepiece lens. Altering the microscope focus produced a three-dimensional view of the tube and the fluids within it. It was therefore possible, to some extent, to see where remaining oil was situated (oil films on the walls, oil blobs extending from one wall of the capillary to the other, oil blobs sticking to one of the walls but not to the other, etc.), and thus to estimate the volume of oil produced. The estimated volume of oil produced is reported as a percentage of original oil in place (%OOIP). All procedures in the aging sequences and imbibition tests were conducted at ambient temperature.

Air/water capillary rise experiments

Observations:

Imbibition into clean tubes. The highest rise observed was for water in clean capillary tubes. Water rose to an average height of 25.5 mm (see Table 2.1-9), corresponding to C_n = 1.72±0.07, or to $\theta_A = 28.5°$. Contact angle measurements with dyed water and air on flat glass surfaces confirm that glass is strongly wetted by water ($\theta_A = 0°$) which would give $C_n = 1.886$ in a perfectly square tube. Quantitative application of this method will require that this difference between the expected and measured heights of rise be explained. Some possible factors include the effect of gravity, effects of temperature changes, a nonzero contact angle of dyed water in the cleaned tubes, variation in the actual dimensions of the tube, rounding of the corners, and accuracy of measured surface tension and density.

Meniscus height in brine and oil-treated square tubes. In all cases, treatment of capillaries with oil led to reduction of the meniscus height for water imbibing. The height of capillary rise decreased as the pH and salinity of the aging brine decreased and as the aging time in crude oil increased. The lowest meniscus heights were found for tubes aged in {4,0.01} brine followed by aging in A-93 crude oil. Drainage tests showed that hysteresis between θ_A and θ_R is significant. Details of these measurements are summarized in Table 2.1-10.

Table 2.1-10. Meniscus height, curvature, and contact angles in square capillaries (aging period in brine = 24 hrs; t_a is the aging time in A-93 crude oil)

Brine	pH	ta	Imbibition				Drainage			
pH/[NaCl]	measured	(hr)	h (mm)	Cn	θuniform	θmixed	h (mm)	Cn	θuniform	θmixed
4, 0.01	4.01	12	7.8	0.53	75	108				
4, 0.01	3.77	24	6.0	0.41	78	115	24.0	1.63	35	42
4, 0.01	4.01	48	5.0	0.34	80	119	26.0	1.76	25	29
4,0.01		528	3.0			128	24.5	1.66	32	39
4, 1	3.89	12	12.5	0.85	65	90				
4, 1	3.89	24	8.5	0.58	73	105	26	1.76	25	29
4, 1	3.82	46	6.5	0.44	77	113				
6, 0.01	6.06	12	16.0	1.08	57	78				
6, 0.01	6.06	24	7.5	0.51	75	109				
6, 0.01	6.06	24	7.5	0.51	75	109				
6, 0.01	6.06	46	7.5	0.51	75	109	27	1.83	18	19
6, 1	5.55	12	13.0	0.91	63	87				
6, 1	5.55	24	13.5	0.91	63	87				
6, 1	6.90	24	12.5	0.85	65	90				
6, 1	5.55	46	8.5	1.08	57	78				
8, 0.01	8.40	12	16.0	1.08	57	78				
8, 0.01	8.40	24	15.0	1.02	60	81				
8, 0.01	8.40	48	12.5	0.85	65	90				
8, 1	8.14	12	15.0	1.02	60	81				
8, 1	8.14	24	12.5	0.85	65	90				
8, 1	8.14	48	12.0	0.81	66	93				

Figure 2.1-14 shows the influence of aging time for all six brines. The effect of pH is shown in **Fig. 2.1-15** for tubes aged in crude oil for 48 hours.

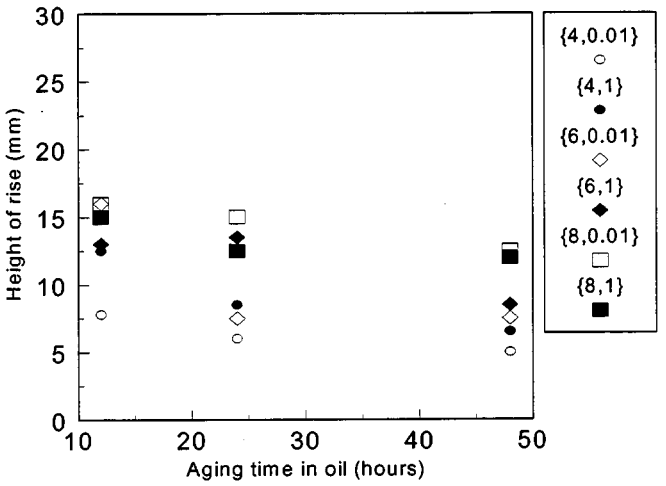

Figure 2.1-14. Meniscus height in square tubes aged in different brines as a function of aging time in crude oil.

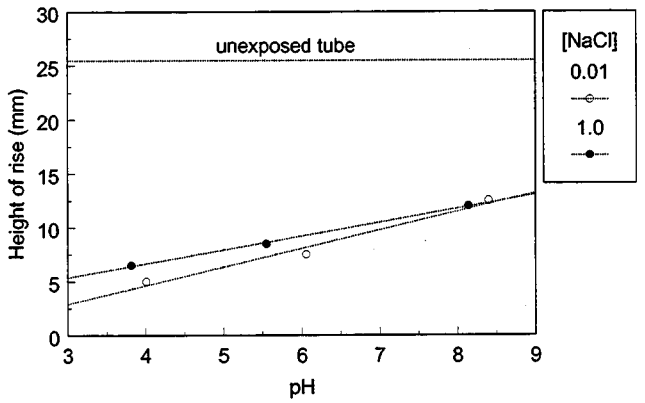

Figure 2.1-15. Capillary rise as a function of pH for tubes aged for 48 hours in A-93 crude oil.

According to Eq. 2.1-10, a uniformly wetted system is wedging only if the normalized meniscus curvature C_n, calculated from capillary rise experiments, is less than 1.414. In many cases, however, wedges could be seen above menisci with lower curvature, indicating that mixed wetting existed. The contact angles ($\theta_{uniform}$) calculated from Eq. 2.1-11 and those estimated from the hysteresis analysis of Ma *et al.* (1996) (θ_{mixed}) are included in Table 2.1-10, giving a lower and upper limit on estimates of both imbibition (water advancing) and drainage (water receding) angles.

Additional evidence for mixed wetting was obtained by rotating the tubes 90° from vertical to horizontal orientation and observing the rearrangement of water and air in the absence of gravity. Depending on wetting, results ranged from very little rearrangement to water advancing in the corners over the full tube length. Details of these observations are summarized in Table 2.1-11. The extent of water wedge formation in the pH 6- and 8-treated tubes indicates that the corners have remained water-wet.

Table 2.1-11. Fluid rearrangement in square capillaries turned from vertical to horizontal orientation after measurements of the height of rise

Brine {pH,[NaCl]}	Oil aging time (hrs)	Water and air rearrange?	Furthest extent of water into corners (mm)	Observation time	Other observations
{4,0.01}	48	y	9	< 1 hr	
{6,1}	12	y	80	>4.5 hrs	Wedges were visible before tube was turned. Wedges extended rapidly after turning the tube. Experiment terminated because water was evaporating.
{6,1}	24	y	80	1-2 hrs	Isolated water droplets form in corners when tube is turned. Droplets are reconnected by advancing water wedges.
{6,1}	48	y			Water wedge in one corner only.
{8,0.01}	12	y	100	< 5 min	Wedges are not of uniform thickness, develop very rapidly, and can break up.
{8,0.01}	24	y			Like {8,0.01} aged for 12 hrs.
{8,0.01}	48	y	100?		Wedges advance more slowly than in the other two {8,0.01} cases. Water reaches the outlet, but continuity is not always clearly observed.
{8,1}	12	y	100	1 - 2 min	Continuous films that vary in color depending on thickness.
{8,1}	24	y			Like {8,1} aged for 12 hrs.
{8,1}	48	y			Like {8,1} aged for 12 or 24 hrs.

Capillary rise in brine and oil-treated rectangular tubes. Detailed results from the measurements of capillary rise in rectangular tubes are given in Table 2.1-12. Interpretation of the results of capillary rise experiments in rectangular tubes is problematic. For each interface, a maximum value (measured near a corner) and a minimum height are reported. Higher rise near

the corners may illustrate mixed wetting, but variability of the tube dimensions is probably the limiting factor in these experiments.

Table 2.1-12. Rectangular capillary results (t_a(b) is the aging period in brine and t_a(co) is the aging time in crude oil. Max = highest point of capillary rise in the corners, min = lowest point on the water meniscus)

Brine	Measured pH	t_a (b)	t_a (co)	Capillary rise (mm)		Repeated measurements
				minimum	maximum	min - max
unexposed tube				18.0	21.3	
4, 0.01	4.16	24h	12h	9.5	10.5	
4, 0.01	4.16	24h	24h	9.0	9.5	
4, 1	4.04	24h	12h	9.0	11.0	
4, 1	4.04	24h	24h	8.5	10.5	Initially deformed, but flattens out
4, 1	4.04	24h	48h	9.0	10.0	8.5 - 11.5
6, 0.01	5.99	24h	12h	7.0	7.7	8.0 - 10.0
6, 0.01	5.99	24h	24h	10.0	18.0	10.5 - 18.5
6, 0.01	6.00	46h	24h	10.0	11.3	10.0 - 18.0
6, 0.01	5.99	24h	48h	7.0	10.5	
6, 1	5.55	24h	12h	10.0	11.0	
6, 1	5.55	24h	24h	9.5	12.7	
6, 1	5.55	24h	48h	10.5	12.0	
8, 0.01	8.40	24h	12h	9.0	12.5	
8, 0.01	8.40	24h	24h	9.0	12.5	
8, 0.01	8.40	24h	48h	7.5	17.5	
8, 1	8.14	24h	12h	11.0	13.0	
8, 1	8.14	24h	24h	10.5	12.5	
8, 1	8.14	24h	48h	8.5	14.0	

Discussion of capillary rise experiments:

When the wettability of a glass surface is altered by exposure to crude oil in the presence of water, a nonuniform or mixed wettability state can be generated. The average water saturation of tubes after drainage and before introduction of oil was estimated by a series of measurements

to be 6% ± 3%, in very good agreement with the amount predicted from a calculation of the MS-P drainage radius of perfectly wetted square tubes. Detail of these measurements are summarized in Table 2.1-13.

Table 2.1-13. Measurements of the S_{wi} before the tube was aged in crude oil

Test number	Measured length (mm)	Weight of water remaining (g)	S_{wi} (%)
1	100	0.0060	6.02
2	100	0.0057	5.71
3	104	0.0075	7.23
4	99	0.0043	4.36
5	110	0.0018	6.41
6	100	0.0078	7.82
7	109	0.0093	8.56
8	110	0.0021	1.91
9	100	0.0059	5.92
10	109	0.0064	5.87
11	100	0.0082	8.22
12	110	0.0058	5.29
average	104±5		6±3

Bulk water residing in the corners can maintain strongly water-wet surfaces. If the aging brine gives rise to stable water films, the flat walls of the capillary can also remain water-wet. Thus, situations ranging from protection of most of the capillary from crude oil adsorption to exposure of most of the tube can be generated by appropriate brine selection.

Contact angles resulting from crude oil treatments were more dependent on the pH and salinity of the aging brine than on the aging time in A-93 crude oil. None of the tubes became oil-wet at the aging temperature (25°C) and relatively short aging periods used in these experiments. Wettability of the originally strongly water-wet capillary was altered towards a less water-wet condition as the pH of the brine was decreased and the aging period in crude-oil

increased. Capillaries pretreated with {4,0.01}, {6,0.01}, or {4,1} brines produce higher contact angles, while those pretreated with {8,0.01}, {6,1}, or {8,1} brines produce lower contact angles. The observed trends are reasonable since {4,0.01} and {6,0.01} brines give rise to unstable water films, {4,1}, {8,0.01} and {6,1} brines form conditionally stable films and {8,1} brines produce stable films.

Mixed wetting has been demonstrated by the existence of wedges even when the curvature is low. High hysteresis and changes in wetting with aging time are all consistent with previous contact angle observations. The extent of alteration is somewhat surprising in view of the low temperatures used in all of these experiments. Greater differentiation between stable and unstable combinations of oil and brine might have been expected. It is likely that the procedure subsequent to oil exposure—i.e., rinsing with toluene and decane, followed by drying—does not entirely preserve strongly water-wet conditions in the corners.

Spontaneous imbibition of brine into oil-filled tubes

Visual observations of water displacing oil in horizontally oriented tubes were made to observe filling mechanisms, rate, and extent of the spontaneous invasion of water into capillaries containing only oil or both oil and water. Results are reported for dry tubes treated with crude oil and for capillaries that were aged first in brine (pH 4 to 8 and varying ionic strength), then in A-93 crude oil. Strongly water-wet conditions were tested using dyed decane.

Observations of filling mechanisms and rates:

Two classes of interface movement were observed, piston-like motion of the MTM and snap-off by water in the AMs. These two types of movement are illustrated in Fig. 2.1-16. When snap-off and bypassing occurred, the remaining oil took on a variety of shapes, as illustrated in Fig. 2.1-17. Volumes have been estimated based on lengths, but in the more irregular cases, these volumes are necessarily somewhat subjective.

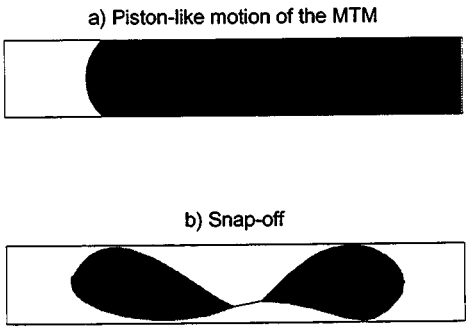

Figure 2.1-16. The two kinds of meniscus displacement observed during imbibition. a) Piston-like motion was generally observed for tubes with no initial water saturation. b) Snap-off was more commonly observed in tubes with an initial water saturation at the beginning of imbibition, and is the result of water advancing in the corners.

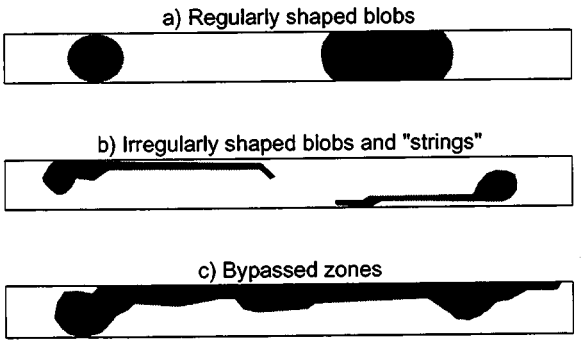

Figure 2.1-17. Different shapes of bypassed oil.

Strongly water-wet capillaries. Experiments with dyed decane as the oil phase were performed as the water-wet base cases for comparison to subsequent experiments with crude oil. The results of these experiments are summarized in Table 2.1-14; base case numbers are assigned for reference in later sections of this report. Figure 2.1-18 shows oil production as a function of imbibition time for the experiments where {8,1} was the imbibing brine. Snap-off occurred in all tubes containing initial water (i.e. $S_{wii} \neq 0$) in the corners at the onset of the imbibition experiment (Fig. 2.1-18b).

Table 2.1-14. Oil produced (%OOIP) from decane-filled tubes pretreated with different brines and with different initial conditions

Aging brine	S_{wia} (%)	S_{wii} (%)	Imbibing brine	Amount of oil produced (%OOIP)	Base case number
None	0	0	{8,0.01}	95	1
None	0	0	{8,1}	96	2
{4,1}	6	0	{8,0.01}	100	3
{8,1}	6	0	{8,0.01}	100	4
{4,1}	6	0	{8,1}	100	5
{8,0.01}	6	0	{8,1}	95	
{8,1}	6	0	{8,1}	100	6
Distilled water	6	6	{8,1}	99	
{4,1}	6	6	{8,1}	99	7
{8,0.01}	6	6	{8,1}	90	
{8,1}	6	6	{8,1}	84	8

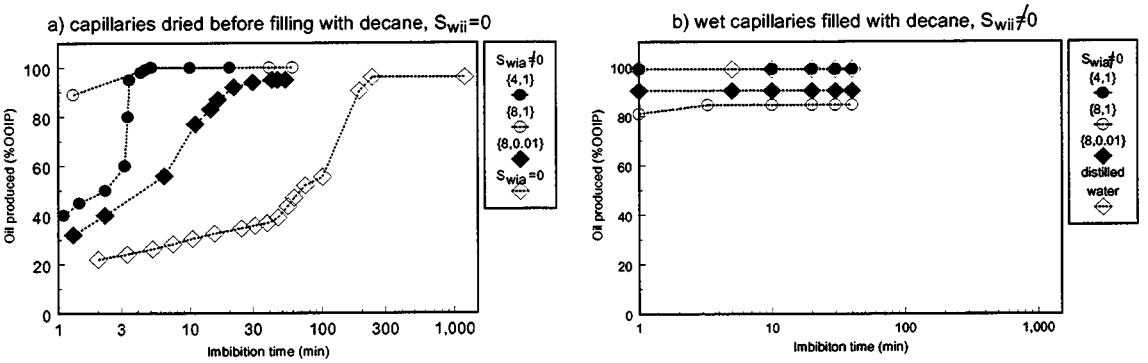

Figure 2.1-18. Decane produced as a function of imbibition time. {8,1} brine imbibing into (a) tubes dried before filling with decane (S_{wii}=0) and (b) tubes with an initial water saturation (S_{wii}≠0).

A-93 crude oil tests. In the following section, the results of treatment of square capillary tubes, either dry or wet, with crude oil are presented in terms of the rate of imbibition of two different brines. Preliminary experiments showed that almost no distilled water or pH 4 brine imbibed. However, if pH 8 brines were used, spontaneous imbibition was observed. Variables

included the brine compositions used to pretreat the tubes, the aging time (t_a) in A-93 crude oil, and the presence or absence of an initial water saturation at the start of imbibition.

Initially dry capillaries (S_{wia}=0)

No aging (t_a=0): Capillary tubes were submerged in brine immediately after filling with oil; aging time in oil was therefore only a matter of minutes (nominally t_a=0). Neither distilled water nor pH 4 and 6 brines imbibed. The {8,0.01} and {8,1} brines both imbibed. Some characteristic features of the imbibition process included:

(1) piston-like motion of the MTM (see Fig. 2.1-16a),

(2) an oil/water interface that appeared to be nearly flat during the displacement, and

(3) little or no movement of water in the corners ahead of the MTM.

For the first one or two hours, the moving interface left no oil behind. However, during the later stages of the imbibition process with {8,1} brine, oil began adhering to the walls of the capillary, leaving microscopic drops and oil films which became increasingly prevalent until finally the interface movement stopped. Results from the experiments are given in Table 2.1-15. In Fig. 2.1-19 the amount of oil produced (%OOIP) is plotted as a function of time.

Table 2.1-15. Amount of oil produced by spontaneous imbibition of brine (S_{wia}=S_{wii}=0, t_a=0)

Experiment	Imbibing brine {pH, [NaCl]}	Amount of oil produced (%OOIP)	Spontaneous imbibition index (SI)
Decane-filled (base case 1)	{8,.0.01}	95±1	1
1	{8,.0.01}	18±1	
2	{8,.0.01}	24±1	0.20±0.04
3	{8,.0.01}	16±1	
Decane-filled (base case 2)	{8,1}	96±1	1
1	{8,1}	23±1	
2	{8,1}	87±1	0.6±0.4
3	{8,1}	74±1	

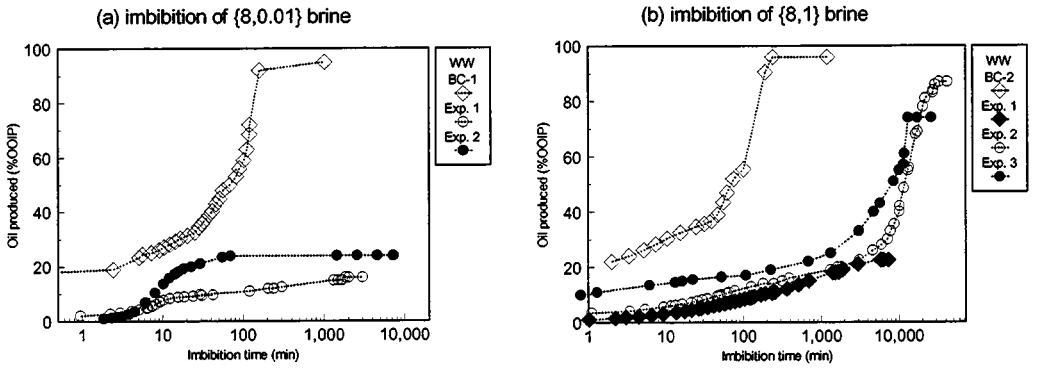

Figure 2.1-19. Crude oil produced by spontaneous imbibition of brine into capillaries with no initial water (S_{wia}=S_{wii}=0) or aging (t_a=0), plotted as a function of time for (a) {8,0.01} brine and (b) {8,1}.

Capillaries aged in crude oil (t_a≠0): If capillaries were allowed to age in oil before initiation of imbibition, the amount of water imbibed was significantly lower than for the t_a = 0 experiments, although the patterns of imbibition were similar. The results from the experiments are given in Table 2.1-16 and Fig. 2.1-20.

Table 2.1-16. Amount of oil produced by spontaneous imbibition of {8,1} brine ($S_{wia}=S_{wii}=0$, $t_a\neq0$)

Aging period in A-93 (hrs)	Imbibing brine {pH,[NaCl]}	Amount of oil produced (%OOIP)	Spontaneous imbibition index SI
Decane-filled (base case 2)	{8,1}	96±1	1
1	{8,1}	42±v1	0.44±0.02
2.5	{8,1}	7±1	0.07±0.02
4	{8,1}	8±1	0.08±0.02
6	{8,1}	21±1	0.22±0.02
16	{8,1}	5±1	0.05±0.02

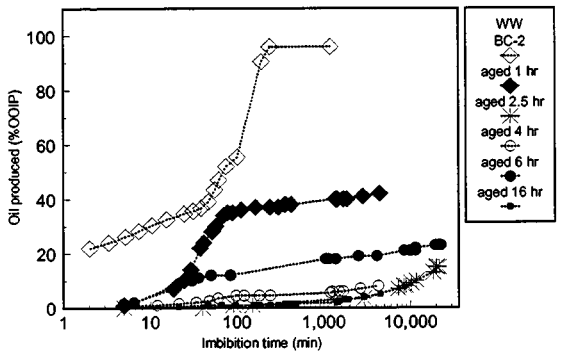

Figure 2.1-20. Oil produced by spontaneous imbibition of {8,1} brine into capillaries aged in crude oil but not in brine ($S_{wia}=S_{wii}=0$; $t_a\neq0$); plotted as a function of imbibition time.

Capillaries aged with connate water ($S_{wia}\neq0$)

Tubes cleaned and refilled with oil before imbibition ($S_{wii}=0$): Brine composition effects were investigated with tubes aged in {4,1}, {6,1}, {8,0.01}, and {8,1} brines. Little or no imbibition occurred in tubes pretreated with either {6,1} or {8,0.01} brine. However, tubes aged in either {4,1} or {8,1} brine imbibed either {8,0.01} or {8,1} brine for all aging times investigated.

In the tubes that imbibed, the interface shape initially appeared to be flat, similar to the shape of the oil/water interface during imbibition into dry tubes. Often this shape changed to a more rounded appearance after about 30 to 60 min, when water started advancing into the

corners. If water imbibed uniformly into all four corners, the meniscus shape was symmetric. If not, the distortion of the interface was greatest in the corner which had the highest water saturation. Further water movement in the corners led to snap-off (see Fig. 2.1-16b) by filling from the corners, followed by bypassing of oil. The bypassed oil either appeared as regularly shaped blobs or as irregularly shaped blobs, "strings" or "zones (see Fig. 2.1-17). Results from these experiments are given in Table 2.1-17. The general trend was towards a decrease in the amount of water imbibed as the aging period in crude oil increased. Plots showing the amount of oil produced as a function of time for tubes aged in {8,0.01} and {8,1} brine are given in Fig. 2.1-21.

Table 2.1-17. Amount of oil produced by spontaneous imbibition of brine ($S_{wia}\neq 0$, $S_{wii}=0$)

Aging period in A-93	Imbibing brine {pH,[NaCl]}	Amount of oil produced (%OOIP)	SI index
{4,1} as the aging brine			
Decane-filled (base case 3)	{8,0.01}	100±1	1
12	{8,0.01}	39±2	0.39±0.03
48	{8,0.01}	18±2	0.18±0.03
Decane-filled (base case 5)	{8,1}	100±1	1
12	{8,1}	16±1	0.24±0.06
37	{8,1}	0	0
{8,1} as the aging brine			
Decane-filled (base case 4)	{8,0.01}	100±1	1
12	{8,0.01}	66±2	0.66±0.03
24	{8,0.01}	55±1	0.55±0.03
48	{8,0.01}	30±1	0.30±0.03
50	{8,0.01}	26±1	0.26±0.03
Decane-filled (base case 6)	{8,1}	100±1	1
12	{8,1}	80±2	0.78±0.04
12	{8,1}	75±2	
24	{8,1}	41±1	
24*	{8,1}	55±1	0.47±0.07
24*	{8,1}	46±1	
50	{8,1}	24±1	0.24±0.06

*No initial MTM.

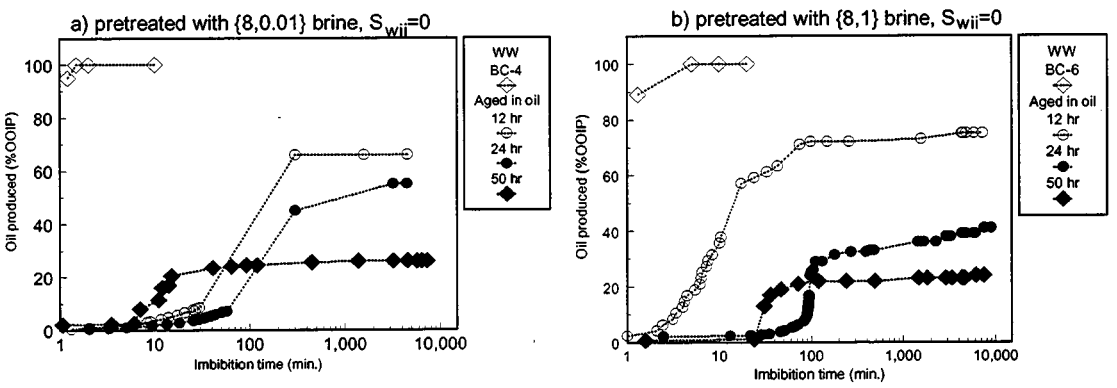

Figure 2.1-21. Oil produced by spontaneous imbibition of brine into capillaries aged in brine and crude oil (S_{wii} = 0), plotted as a function of imbibition time.

Cleaning step omitted (S_{wii}≠0): A more realistic situation with respect to imbibition into an oil reservoir is that an initial water saturation exists. In the remaining experiments, water was present in the corners at the start of imbibition. Tubes were pretreated with {4,0.01}, {4,1}, {6,0.01}, and {8,1} as the aging brines. Only capillaries aged in the {8,1} brine imbibed significantly. In these tubes, the imbibition mechanism was found to be significantly different from those with no initial water saturation at the beginning of imbibition. The most striking differences were (a) water advancement into the corners, leading to snap-off, usually started in the first few minutes after submersion of the capillary, (b) imbibition rates were much faster (see Fig. 2.1-22), (c) snap-off events were more frequent, and (d) all the bypassed oil appeared as regular-shaped blobs. Similarity to reported imbibition rate measurements in Berea sandstone cores treated with crude oil (*e.g.*, Zhou *et al.*, 1996; Tang and Morrow, 1996) can be noted and will be discussed later in this section.

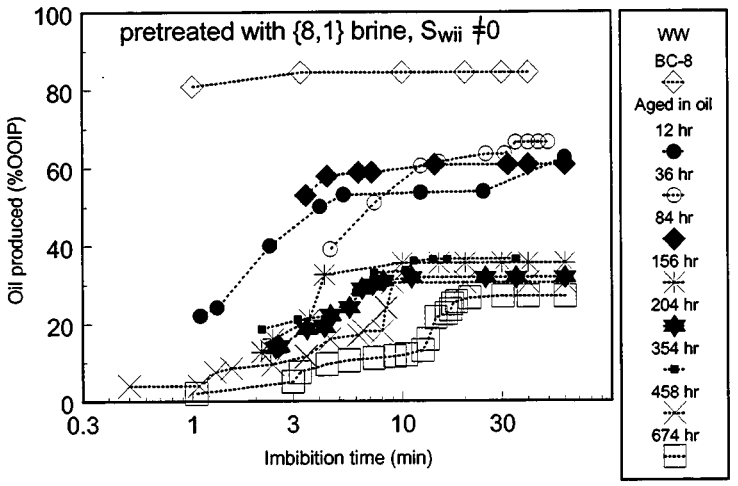

Figure 2.1-22. Oil produced by spontaneous imbibition of {8,1} brine into capillaries aged in brine and crude oil ($S_{wii} \neq 0$), plotted as a function of imbibition time.

Less water imbibed into capillaries aged in {4,1} brine prior to crude oil aging than into those aged in {8,1} brine and water advancement in the corners was less pronounced; no snap-off's were observed. The results from these experiments are summarized in Table 2.1-18.

Table 2.1-18. Amount of oil produced by spontaneous imbibition of {8,1} brine ($S_{wi}\neq 0$)

Aging period in A-93 (hrs)	Amount of oil produced (%OOIP)	Spontaneous imbibition index (SI)
{4,1} as the aging brine		
Decane-filled (base case 7)	100±1	1
12	10±1	0.10±0.04
37	3±1	0.03±0.03
{8,1} as the aging brine		
Decane-filled (base case 8)	84±1	1
12	63±1	0.75±0.04
36	66±1	0.78±0.04
60	39±1	0.46±0.04
84	61±1	0.73±0.04
90	45±1	0.54±0.04
156	36±1	0.43±0.04
204	32±1	0.38±0.04
235	34±1	0.40±0.04
354	36±1	0.43±0.04
384	41±1	0.49±0.04
458	30±1	0.36±0.04
674	27±1	0.32±0.04

Discussion of the spontaneous imbibition tests:

Reproducibility of imbibition measurements. The outcome of a particular spontaneous imbibition test is variable, even when tubes have been similarly treated. Some variability in tube dimensions is unavoidable. Another source of variability in many of the tests reported here is the amount and distribution of water remaining after tubes have been drained. The average of 6% for S_{wi} in a strongly water-wet drainage is in good agreement with the expected amount, but the standard deviation was 3% so there can be significant differences between replicate tests.

Vertical orientation of the tubes during aging means that gravity effects played a role in distribution of the fluids.

Variations in initial water saturation can affect the outcome of these tests in two distinct ways. First, the extent of wetting alteration depends on the amount, distribution, and composition of the brine in place during aging in crude oil, and second, the rate of imbibition and probability of snap-off events are both influenced by S_{wi}. These two different effects are recognized in the notation used here, with S_{wia} signifying the water saturation during crude-oil aging and S_{wii} indicating the water present in the tube at the onset of imbibition.

Whether or not there is an initial MTM influences the course of imbibition. In most cases, compression and expansion of the teflon tube as it was cut to separate the oil-filled capillary from the filling syringe caused a small amount of water to enter at the tube inlet and form an initial MTM. The only exceptions are two tests marked in Table 2.2-15.

Imbibition into water-wet square capillaries. When decane is used as the oil phase, the capillaries remained water-wet and water or brine always imbibed. The course of that imbibition varied, however, depending on whether or not there was an initial water saturation. Two experiments with no initial water saturation are compared in Fig. 2.1-23 (see also Table 2.1-14 and Fig. 2.1-18). As expected, brine composition makes no difference; the rates and amounts of water imbibed are almost identical. Decane was displaced by steady advancement of the MTM from inlet to outlet. No water was seen advancing in the corners ahead of the MTM.

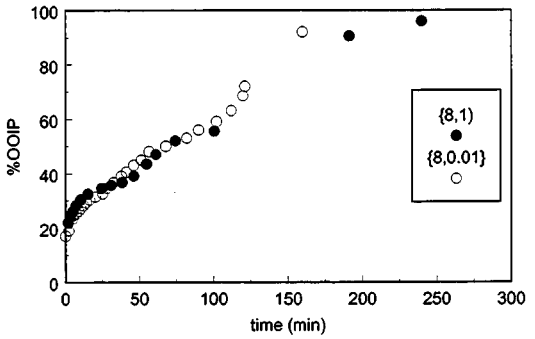

Figure 2.1-23. Imbibition of brine into decane-filled tubes.

Since θ_A for water and dyed-decane was only about 20°, wedges should be able to form, but they do not. The relative permeability to the water invading an oil-filled corner is very low and limits the rate at which water can fill the corner wedges. Evidently, for a contact angle on the order of 20°, filling of the corner wedges is slower than the rate at which the MTM moves to fill the tube with water. If $\theta_A = 0°$, the wedges should fill rapidly and trap some decane. That they do not is evidence that $\theta_A > 0°$, as confirmed by contact angle measurements.

If the capillaries were first filled with brine, flushed with decane to S_{wi}, then cleaned and dried before refilling with 100% decane, in the same sequence as was used for some of the tubes exposed to crude oil, imbibition rates were significantly faster (see Fig. 2.1-18a). There are two possible explanations: (1) salt dried in the corners of the tube helps to maintain more water-wet conditions ($\theta_A < 20°$), or (2) the salt dried in the corners might introduce an osmotic effect that assists in formation of corner wedges. Mennella *et al.* (1995) showed that a salt-coated glass plate had less tendency to adsorb crude oil components than a clean plate, but the contact angles reported were greater than 20°, so it is not obvious how this observation affects interpretation of the dyed-decane results. Additional work is needed to distinguishing between the contributions from these two possibilities.

The fastest imbibition times were for capillaries containing connate water. Again, there are two possible effects. The presence of water films may limit adsorption of dye on the capillary walls, maintaining more water-wet conditions and higher relative permeability to water in the water-filled corners permits more rapid imbibition. Imbibing water rapidly swelled the wedges. At some point, the swollen wedges reached the limiting curvature at which the AMs touch to form an unstable cylindrical interface. The imbibing liquid then spontaneously redistributed, snapping off segments of the nonwetting phase. Since the snap-off events reflect instabilities that can occur anywhere in the tube, the amount of oil produced varied in replicate experiments.

Capillaries contacted with crude oil. In capillaries that have been contacted with crude oil, the wetting conditions that develop are complex. For a given oil, the mechanisms of interaction can depend on brine composition and the history of exposure (including aging time, aging temperature, and water saturation).

Polar interactions in dry capillaries

When a clean, dry capillary tube was filled with crude oil, adsorption of polar material from the oil onto the glass surface began. Analogous tests on flat surfaces have been reported (Buckley *et al.*, 1997a). In those tests, water advanced over a decane-covered surface at 77° after only one day of aging in A-93 crude oil at 25°C. After 20 days of aging, the contact angle was essentially unchanged (θ_A=80°). Polar interactions between crude oil and solid typically occur quickly (on the order of a few hours) and make glass surfaces intermediately wet. Since there is no initial water in these tubes, wetting is altered uniformly. The effects of polar interactions are evident in Fig. 2.1-24. After 16 hours of aging in oil, very little water imbibes and the SI is less than 0.1, consistent with uniformly neutral wetting.

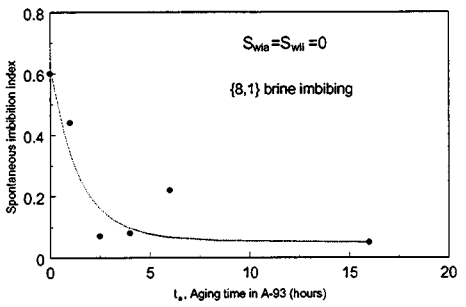

Figure 2.1-24. SI index as a function of aging time.

Acid/base interactions in wet capillaries

Interactions by the acid/base mechanism are dominant between a high base number, medium gravity oil—of which A-93 is a good example—and an acidic silicate surface (Buckley *et al.*, 1997a). In the presence of a brine phase, interactions between oil and solid are largely dependent on the composition of the brine. These interactions can continue to change surface wetting for days or even weeks.

In each experiment, there are two brine compositions: the brine in which the tube is aged and the imbibing brine. These two brines can be the same or they may be different. Aging brines tested included {4,1}, {6,1}, {8,0.01}, and {8,1}. Three of these are in the conditionally stable region. Only {8,1} produces stable water films with A-93 crude oil.

As shown in Table 2.1-19, aging brine plays an important role in determining whether or not a treated tube imbibes. For tubes aged in {6,1} or {8,0.01} brine and crude oil, no imbibition of water was observed. Those aged in {4,1} or {8,1} did imbibe.

Table 2.1-19. Brine combinations tested (S_{wii}=0)

Aging brine	Imbibing brines	Imbibed? (hours of aging)	Water moves in:	
			MTM	AMs
{4,1}	{8,0.01}	yes (12, 48)	X	X
{6,1}	{8,0.01}	no		
{8,0.01}	{8,0.01}	no		
{8,1}	{8,0.01}	yes (12, 24, 48, 50)	X	X
{4,1}	{8,1}	yes (12), no (37)	X	
{6,1}	{8,1}	no		
{8,0.01}	{8,1}	no		
{8,1}	{8,1}	yes (12, 24, 50)	X	X

The composition of the imbibing brine also influences the rate and amount of brine imbibed, as shown in Fig. 2.1-25. Imbibition of {8,0.01} and {8,1} brines are compared for tubes that were aged initially in {8,1} brine. Effects of both aging time and brine compositions on the amount of oil produced are shown in Fig. 2.1-26, where the variation in the SI index is plotted as a function of aging time in crude oil for tubes aged in {4,1} and {8,1} brines. Aging brine composition has the stronger influence, in agreement with the results of Tang and Morrow (1996).

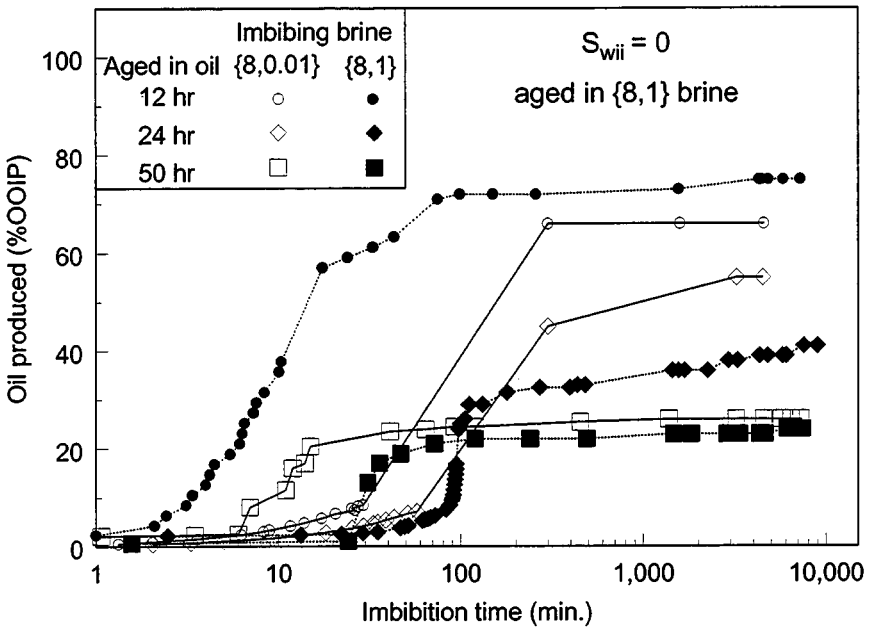

Figure 2.1-25. Influence of brine composition on imbibition rates.

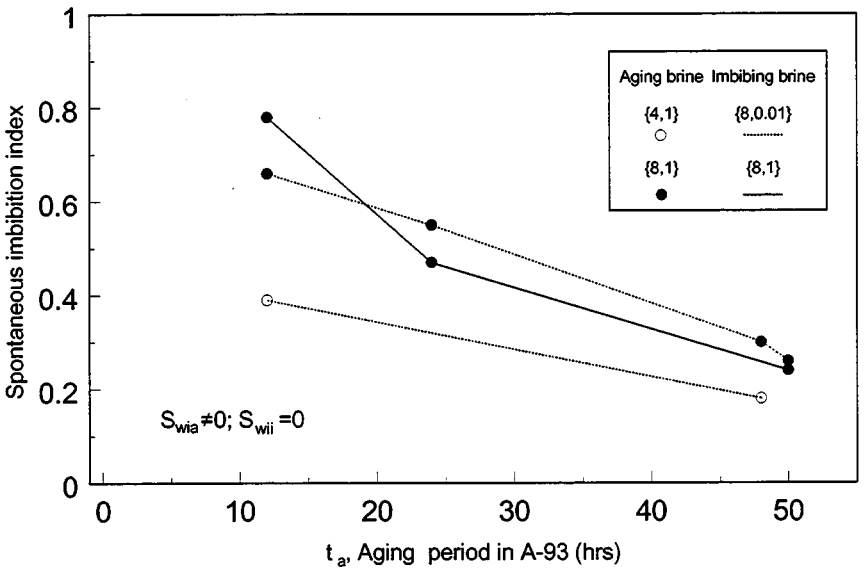

Figure 2.1-26. SI index as a function of aging time in A-93 crude oil.

Although these capillary tubes were cleaned and dried before filling with oil for the imbibition tests, the flow of water into these tubes was quite different from that into tubes which had never contained brine. Dry tubes that were treated with crude oil became uniformly altered in wetting and did not develop arc menisci. In the cleaned tubes that had first been treated with

brine, then with oil, water wedges were almost always noted. The corners remained more water-wet than other parts of the tube.

Several tests were performed with $S_{wii} \neq 0$. The brine that was present during aging in oil was not dried, nor was the oil replaced before beginning imbibition. Figure 2.1-27 shows the effect of aging time on the spontaneous imbibition index. Imbibition is much faster in these tubes with water already occupying the corners (*cf.*, Fig. 2.1-22). An MTM sweeps the tube until snap-off from AM growth occurs, trapping oil and creating new MTMs. Fluid movement ceased in an hour or less.

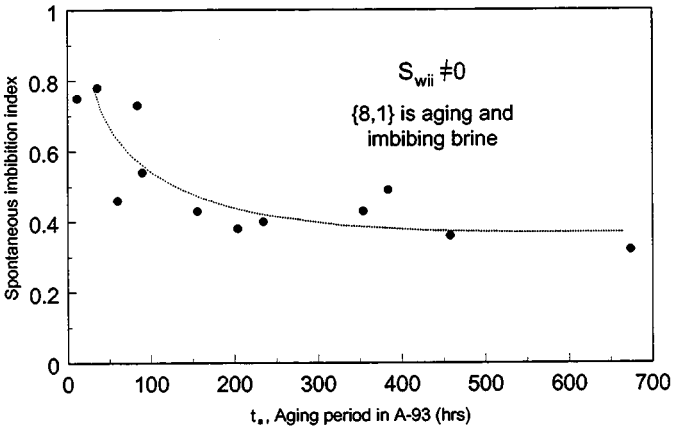

Figure 2.1-27. SI index as a function of aging time for capillaries with an initial water saturation at the start of imbibition.

These tests illustrate an effect of aging time, which is similar to that reported for aging Berea sandstone cores in A-93 crude oil (Zhou *et al.,* 1996, and references cited therein). Cores and tubes were most water-wet for short aging times, and imbibed less water as the aging time increased. Changes in the rate of imbibition continued over the 29 days of aging tested here. All of the tubes remain weakly water-wet.

Another feature found in imbibition rate curves for both square tubes and cores is the appearance of an induction time in the first stages of imbibition for weakly water-wet conditions

(Zhou *et al.*, 1996). In the square tubes, induction times are most marked for those systems that develop AMs, starting from $S_{wii} = 0$ (cf. Figs. 2.1-19, 20, and 21), although induction periods are also apparent in the more directly comparable case of aged tubes with $S_{wii} \neq 0$ (Fig. 2.1-22). In the square tubes, this induction period represents the time required to swell AMs before significant oil is swept out by movement of MTMs. It would be of interest to know to what extent this might also be true in cores.

Summary of wetting alteration in square tubes

Square tubes, exposed to brine and crude oil, become mixed wet. Water rising against air can form corner wedges even though the average contact angle, calculated from the height of rise, assuming uniform wetting, indicates that wedges should not form. A second set of contact angles, calculated from a mixed-wet model, are higher and show more differentiation between tubes treated with different aging brines. High hysteresis is observed, consistent with previous contact angle observations of glass surfaces contacted with brine and crude oil.

Oil displacement by a main terminal meniscus and the formation, extension, and swelling of arc menisci during spontaneous displacements of decane or crude oil by brine have been documented. A variety of conditions were tested. Variables included compositions of aging and imbibing brines, aging times in oil, and presence or absence of an initial water saturation.

The mechanism of displacement by imbibition depends on whether water wedges form in the corners. If the tube is preferentially water-wet, but water wedges are absent, oil recovery by movement of the main terminal meniscus can approach 100% in these straight capillaries. When water wedges are present, snap-off events exert a dominant, and sometimes unpredictable, influence over the amount of oil that is trapped.

Water wedges formed in all mixed-wet tubes. Only capillaries that were made uniformly neutral in wetting by aging in the absence of water failed to imbibe some water into the corners.

Imbibition rates were estimated by measuring lengths of brine and oil-filled sections of the capillary tube, with results that showed similarities to the rate of imbibition in much more complex porous media. An induction time during which water filled the corner wedges with little accompanying movement of oil was observed. Suppression of both the rate and amount of imbibition was reminiscent of results reported with this same crude oil in Berea sandstone cores.

The amounts of oil produced were compared using a spontaneous imbibition index. A consistent trend of decreased oil production with increased aging time emerged. Wetting alteration by polar and acid/base interactions was generally consistent with previous contact angle observations. Often the brine that produced the most stable water films with glass and A-93 crude oil was the only one that maintained sufficiently water-wet conditions to guarantee some imbibition of water.

In the future, baseline studies of very strongly water-wet conditions will help to distinguish between the possible effects of dye adsorption and the suggested contributions of salinity and osmotic effects. Other improvements in experimental techniques are needed; for example, better control over the initial water saturation. The focus will be on situations where S_{wia} and S_{wii} both are nonzero. Triangular tubes, which drain to give higher S_{wi}, might be more directly comparable to the angular pore spaces in most sandstones than the square tubes used in this study.

There are a wealth of unexplored combinations of brine and crude oils, including brines containing divalent ions and crude oils with different acidic and basic characteristics, that could be studied in noncircular capillaries. Coupling independent measurements of contact angles to

measurements of the rate, extent, and patterns of imbibition will help to elucidate imbibition mechanisms and their dependence on the details of wetting conditions in cores and in oil reservoirs.

2.1.2 Drainage of Initial Brine

A test for evaluating interactions between crude oils and solid surfaces—with or without brine—was first described by Buckley and Morrow (1992). Since then, the test protocol has evolved as experience has accumulated with a wide range of crude oils (Liu and Buckley, 1997; Buckley *et al.*, 1997; Buckley *et al.*, 1998b) and with different mineral surfaces (Liu and Buckley, 1998).

The adsorption test protocol was designed to capture key elements of crude oil interactions with mineral surfaces in an oil reservoir. Reservoir wetting is now considered to be the result of adsorption of materials from crude oil onto portions of the solid surface. The important roles played by connate brine—which can enhance some adsorption interactions while it shields other parts of the porous medium from contact with the oil—dictate that water, oil, and mineral must all three be considered as important variables in these tests.

There is as yet no one, irrefutable method for evaluating crude oil/brine/ rock (COBR) interactions. Instead, we have developed a consistent protocol that permits comparison of different oils, brines, and minerals under similar test conditions. The details of the procedure are somewhat arbitrary. Nevertheless, for comparative purposes it has been useful to have a standard evaluation procedure. The most important features of the standard protocol are outlined in Fig. 2.1-28.

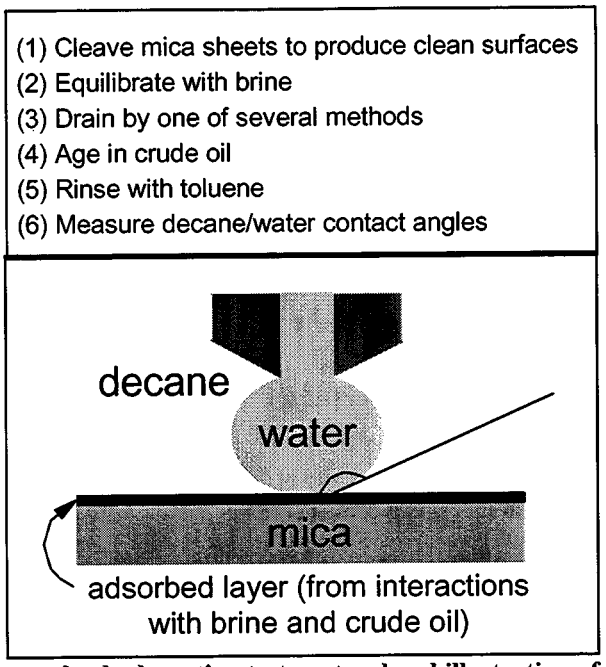

Figure 2.1-28. Outline of the standard adsorption test protocol and illustration of water-advancing contact angle measurement on brine and oil-treated surface.

The effects of variations in many of the steps in this protocol have been examined previously. Little difference was found between quartz glass and soft glass. Different minerals, with varying surface charge and surface chemistry, are important variables in COBR interactions. Differences between glass and mica have been shown (Liu and Buckley, 1998). The effects of pretreatment with brine, oil composition, and aging conditions of time and temperature are also variables that have been extensively studied (e.g. Buckley *et al.*, 1998b). Removal of bulk oil is a crucial step. Rinsing with a poor solvent that precipitates asphaltenes from the oil can make surfaces more oil-wet (Buckley *et al.*, 1997). Details of the contact angle measurements with probe fluids, after removal of bulk oil, show smaller effects of the order of measurement (water advancing or receding measured first) or measuring technique. Dynamic measurements using a Wilhelmy plate compare reasonably with static captive drop observations (Liu *et al.*, 1996).

One step that has not yet received sufficient attention is the treatment of the surface after equilibration in brine and before exposure to oil. In a recent paper, Yang *et al.* (1998) adopted a protocol similar to that described above, but with one potentially important difference. To accelerate drainage of brine from the surface, they imposed a centrifugal field. Whether variations in the extent of water drainage prior to exposure of a surface to crude oil affect the adsorption processes and thus the subsequently measured contact angles is explored in this report.

Experimental methods of wetting alteration

Materials:

Two crude oils were selected for comparison: Mars-97 crude oil, which produces fairly water-wet mica surfaces (Chang and Buckley, 1998), and C-98 crude oil, which can produce more oil-wet conditions. Table 2.1-20 lists physical properties of these two crude oils.

Table 2.1-20. Crude oil properties

Property	C-98	Mars-97
Density @ 25°C (g / mL)	0.8706	0.8811
API Gravity	29.9	30.3°
Acid # (mg KOH/g oil)		0.368
Base # (mg KOH/g oil)	1.00	1.79
RI @ 20°C	1.4952	1.4950
P_{RI} with n-C_7	1.442	1.432
Asphaltene ppt with n-C_5 (wt%)	2.37	3.25
Asphaltene ppt with n-C_7 (wt%)	2.00	1.86

Brine compositions based on seawater were used in these tests. The composition of synthetic seawater (SSW) is given in Table 2.1-21. A dilution to 10% of these concentrations was made by adding distilled water to the 100% brine. The pH values of the 100% and 10% SSW brines were 6.71 and 5.84 respectively.

Table 2.1-21. 100% Synthetic sea water (SSW) composition

Salt	Amount (g/L)
$NaHCO_3$	0.0382
Na_2SO_4	3.9163
$CaCl_2 \bullet 2H_2O$	1.4673
$MgCl_2 \bullet 6H_2O$	10.6395
NaCl	24.0047

HPLC grade toluene and *n*-decane were further purified chromatographically in a column of silica gel and alumina.

Procedures:

Muscovite mica samples were cut into 1"x 0.3" strips. Clean surfaces were obtained by cleaving the mica strips between two pieces of adhesive tape. The freshly cleaved mica strips were equilibrated with brine for 24 hours, drained, then transferred to a crude oil and aged for 24 hours (t_a=24 hrs) at an aging temperature of 25°C (T_a=25°C). After aging in oil, the mica samples were removed from the crude oil, rinsed with toluene, and immersed in decane. Contact angles were measured by the captive drop technique using a contact angle goniometer (Gaertner Scientific Corp.) to observe the water/oil contact line for water advancing and receding on mica.

Three methods of drainage were compared: (1) drainage of bulk water in air, (2) centrifuging in air, and (3) centrifuging in oil. The first method has been the standard procedure. After equilibration with brine, some bulk water is allowed to drain in air while the mica sample is held with forceps. Drops of water are removed by the wicking action of a clean laboratory paper towel. Using this procedure, an unknown amount of bulk water remains on the surface when it is immersed in oil. Some time is required for that water to redistribute in accordance with the surface properties of solid and oil. Remaining bulk water is indicated by portions of the surface on which a water drop spreads. After several days, the effects of the bulk water are usually less evident than they are initially (Liu, 1993).

Removing bulk water by centrifugation may provide a more uniform, thinner film of water as the initial condition of the surface when first exposed to oil. If water can redistribute, however, the results should eventually converge, regardless of the amount of water present initially, although less time might be required to redistribute water if some of it is removed by centrifugation. In the second series of tests, mica samples were centrifuged in air for approximately one minute at 1000 RPM, followed by immersion in crude oil. Finally, a third series of mica samples were removed from brine, immersed in crude oil and centrifuged in that oil for 15 minutes at 1000 RPM, after which they were allowed to age for the remainder of the 24-hour aging period.

Contact angles following different methods of initial water drainage

After 24 hours in oil, samples were removed, rinsed first with toluene, then with *n*-decane, and placed in a quartz optical cell containing purified *n*-decane. Contact angles were measured with distilled water and *n*-decane as probe fluids. The test conditions and average water-advancing angles on treated surfaces are summarized in Table 2.1-22.

Table 2.1-22. Summary of drainage tests (t_a=24hrs, T_a=25°C)

Crude Oil	Brine	Drainage Process	θ_A
Mars-97	100% SSW	(1) Drain in air*	34.0 ± 7.0
Mars-97	100% SSW	(2) Centrifuge in air	31.3 ± 6.1
Mars-97	100% SSW	(3) Centrifuge in oil	22.4 ± 4.7
C-98	10% SSW	(1) Drain in air	95.3 ± 23.8
C-98	10% SSW	(2) Centrifuge in air	129.6 ± 12.0
C-98	10% SSW	(3) Centrifuge in oil	121.5 ± 8.4

There is typically considerable scatter in the contact angles measured with water and decane on surfaces that have been exposed to crude oil. Scatter is particularly apparent when aging times are short (less than a few days at room temperature or a few hours at elevated

temperature). In the results reported in Table 2.1-23, standard deviations range from 7 to 25% of the average water advancing contact angles.

In Fig. 2.1-29, results from the standard drainage method are compared to samples from which 10% SSW was removed by centrifuging under C-98 oil. Two identically treated mica surfaces were tested using each drainage method. Six to eight drops were tested on as many different positions on each piece of treated mica and measurements were made on either side of the two-dimensional projection of each water drop. Figure 2.1-29a shows that significant scatter is associated with the standard drainage method. Discrepancies are smaller for sample 2 than for sample 1, but the average water-advancing contact angles on the two samples are comparable (93° and 98°, respectively). Centrifuging under oil produced more uniformly wetted surfaces and higher values of water-advancing contact angles, as shown in Fig. 2.1-29b (averages are 117° and 127°).

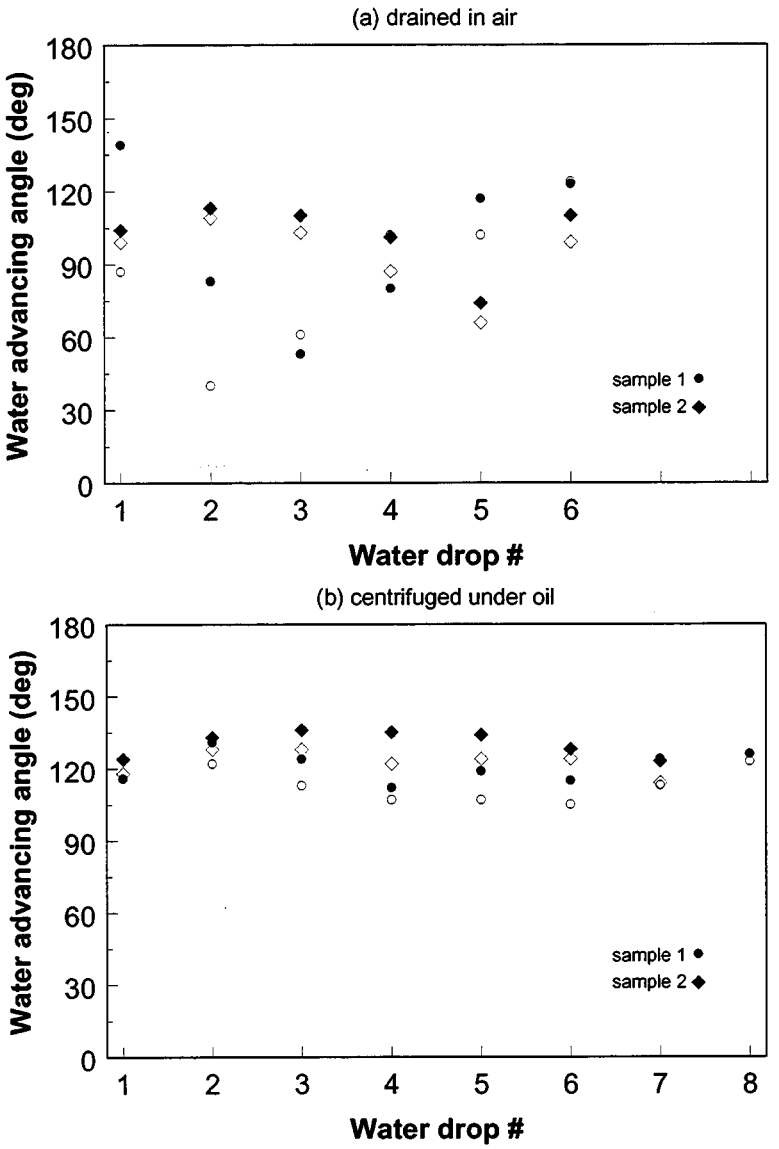

Figure 2.1-29. Contact angles measured on mica treated with 10% SSW and C-98 crude oil (t_a=24hrs; T_a=25°C). (a) Drained in air and (b) Drained under oil in centrifuge. Closed symbols are measured on the left side of the drop image, open symbols are from the right side.

A comparison of the average water-advancing angles for all the tests is shown in Fig. 2.1-30. All three methods lead to similar results for both the water-wet Mars-97-treated mica and the more oil-wet C-98-treated samples. In all cases, standard deviations are lowest for the samples centrifuged under oil (Table 2.1-22).

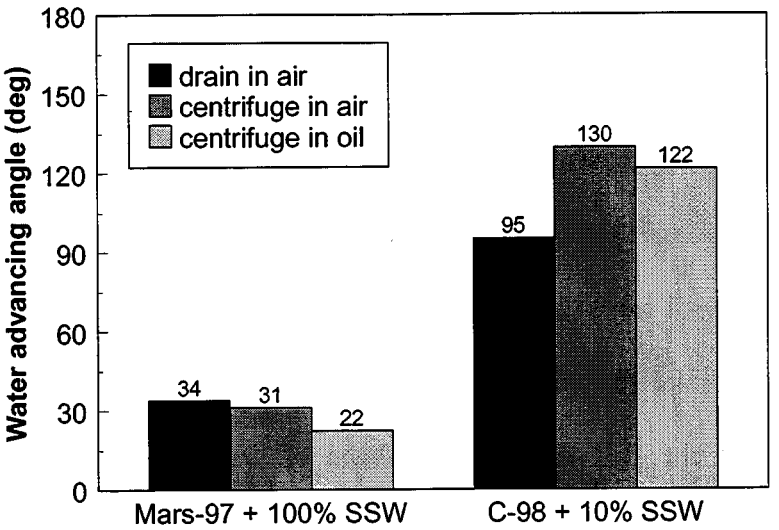

Figure 2.1-30. Comparison of average contact angles measured for two combinations of brine and oil using three different methods of draining the brine prior to oil exposure.

Previous experience suggests that with extended aging time in oil, wetting of samples prepared with the standard drainage method would become more uniform, but centrifuging under oil appears to accelerate the redistribution of water without biasing the results toward more oil-wet behavior. Centrifuging in air, included here for comparison, is not recommended because it provides an opportunity for evaporation that changes the brine composition and might even result in deposition of solid salt crystals on the surface.

2.1.3 Surface Precipitation

The effect of asphaltenes on wettability alteration has been the focus of much research. Despite these significant efforts toward understanding how asphaltenes might alter wetting conditions of mineral surfaces, many questions remain.

Some of these questions may arise because many of the previous studies used crude oil fractions (asphaltenes and/or resins) that had been separated from the remainder of the oil. Studies with known amounts of these fractions, dissolved in a solvent such as toluene, can give different wettability alteration than that obtained when the whole crude oil is used (Akhlaq *et al.*,

1996; Buckley *et al.*, 1997; Yan *et al.*, 1997). These results illustrate the importance of the composition of the whole crude with regard to its wettability-altering effects.

A second source of confusion is the complex role that water plays in mediating wettability alteration by crude oils. The presence of water in a rock can shield some surfaces from exposure to oil. Small pores that remain filled with water stay water-wet. What happens in larger pores is more complicated and depends on whether water films between rock and oil are stable or unstable. In the first case, the presence of water can actually promote wetting alteration. Studies that exclude water miss this important contribution to the process.

Based on studies carried out on glass surfaces, Buckley *et al.* (1998) suggested that the polar components of crude oils can adsorb by several distinct mechanisms, depending on factors that include brine composition and the ability of the oil to keep its asphaltenes dispersed. Ionic interactions appear to be dominant for oils with high values of either acid or base numbers while a colloidal mechanism dominates for oils that are poor solvents for their asphaltenes.

Refractive index (RI) provides a simple method for quantifying the properties of mixtures that determine whether or not the asphaltenes are stable (Buckley, 1998). As discussed in a previous section, P_{RI} is the refractive index at the onset of precipitation of asphaltenes. At this point, wetting alteration by surface precipitation should be favored, due to the interfacial aggregation of the colloidal asphaltenes, which may precede flocculation in bulk. As yet, only limited data exist to confirm the surface precipitation phenomenon. The study reported in this section represents a systematic approach to evaluation of the importance of surface precipitation for a range of crude oils of varying composition.

Contact angle is a measure of wettability. Contact angles are used to assess the partial wetting of crude oil and brine on a mineral surface. Although not directly applicable to oil

reservoir conditions because of differences in roughness, heterogeneity, geometry, and composition of solid surfaces (Anderson, 1986), they do provide an avenue to explore the tendency of a crude oil to change wetting under a wide variety of conditions.

In this section, excerpted from Al-Maamari (2000), we summarize the results of exposing initially water-wet mica surfaces to brine and one of five different crude oils to alter wetting (see also Al-Maamari and Buckley, 2000). Solvent properties of the crude oils were varied by adding *n*-heptane. Stability of asphaltenes was determined by microscopic inspection. The crude oil/heptane mixtures were characterized by RI and the difference between mixture RI and P_{RI}, the RI of mixtures in which solid asphaltenes first appear. Contact angles were used to assess the extent of wettability alteration on treated mica surfaces.

Experimental materials and methods for surface precipitation tests

Solid surfaces:

Muscovite mica ($KAl_2(Si_3Al)O_{10}(OH,F)_2$) was used as the solid surface. The advantages of using mica have been discussed in a previous section (see also Liu and Buckley, 1999).

Aqueous solutions:

A pH 4 buffer with ionic strength of 0.01M, denoted by the shorthand {pH4, 0.01M}, was used as the aqueous phase in this study. Other solutions ({pH 8, 1M} buffer and synthetic seawater) have been used with some crude oils. All solutions were prepared from deionized, double-distilled water. The chemicals used for buffer preparation are sodium acetate ($NaC_2H_3O_2$-$3H_2O$) and glacial acetic acid ($HC_2H_3O_2$) for pH4, sodium hydrogenphosphate (Na_2HPO_4-$7H_2O$) and sodium dihydrogenphosphate (NaH_2PO_4-H_2O) for pH8 solutions. Sodium chloride (NaCl) was used for salinity adjustment. Synthetic seawater composition is shown in Table 2.1-21 above.

Organic solvents:

HPLC grade toluene, heptane, decane, and cyclohexane were used. These solvents were purified by passing through dual-packed columns of activated silica gel and alumina.

Crude oils:

Five crude oils have been used in this study. Two of these oils (Lagrave and Tensleep) have some aggregates in the 100% oil sample. Some 1-MN was added to these oils to re-dissolve the asphaltenes. The mixture (AMN plus crude oil) at which the asphaltenes disappear was used as the starting "oil" (100 %). The properties of these five oils tested are listed in Table 2.1-23. For each oil, different compositions have been tested by mixing the crude oil with varying amount of *n*-heptane.

Table 2.1-23. Oil properties

Oil	ρ (g/cc) 25 °C	Asphaltenes wt.%(nC_7)*	RI_{oil}	P_{RI} (n-C_7)	Oil volume fraction at the onset
A-93	0.8891	4.00	1.51680	1.4436	0.431
Lagrave-97 + AMN (70:30)	0.8936	5.40	1.51931	1.4608	0.540
Mars-Pink	0.9474	6.50	1.53826	1.4291	0.270
Mars-Yellow	0.8783	1.86	1.49500	1.4316	0.417
Tensleep + AMN (65:35)	0.9175	2.46	1.53219	1.4469	0.390

* these values are for the original oil, without AMN mixture

Microscopic observations were used to determine the onset point for the crude oils. The onset point for Mars-Yellow and A-93 was determined after a short time of mixing the crude oil with the precipitant (heptane). For the rest of the crude oils, it was determined after at least one day. The onset point determined after one day for these oils was unchanged if the time was increased to one week.

Mica treatments:

Experiments were carried out using a standard sequence of exposure to brine and oil. The mica samples used were cleaned using a mixture of 9 parts of H_2O_2 and 1 part of NH_4OH in an ultrasonic bath for half an hour and then left in the mixture overnight. After that the mica samples were rinsed extensively with distilled and deionized double-distilled water. The mica was aged in brine for one day, then placed in a vial to which crude oil and heptane were added. After the mica was aged in crude oil it was rinsed with either toluene or cyclohexane, allowed to dry, and then immersed in decane.

Mixtures with varying amounts of oil and heptane were used to generate stable, unstable, and onset conditions. Other variations in mica treatment included aging time in the oil phase, aging temperature in oil, technique used to remove brine from the surface, and rinsing solvent. These variables are summarized in Table 2.1-24.

Table 2.1-24. Variables tested in the mica treatments with brine and crude oil

Variable	Range
preconditioning brine	{pH8, 1M}buffer {pH4, 0.01M} buffer synthetic sea water
crude oil	A-93 Lagrave + 1-MN Mars-Pink Mars-Yellow Tensleep + 1-MN
oil/heptane mixtures	100% oil asphaltenes stable onset of asphaltene precipitation asphaltenes unstable
aging time in oil	one day three weeks
aging temperature in oil	25°C 80°C
brine removal	mica allowed to drain, but not dry, or centrifuge at 2400 rpm (spin for ½ hr, wait 1 hr, spin ½ hr)

Table 2.1-25 shows a matrix of the conditions tested. Also noted in Table 2.1-24 is whether oil and heptane were premixed. If they were not premixed, wet mica samples were submerged in the oil, to which heptane was then added, followed by shaking of the sealed vial to ensure mixing of oil and heptane. Finally, Table 2.1-24 serves as a key to graphs of the contact angles measured on all these treated mica surfaces.

Table 2.1-25. Summary of conditions in mica treatments with brine and crude oil/heptane mixtures

Oil	Brine	Oil & heptane premixed	Centrifuged	Aging conditions in oil		Rinse	Composition ranges			Drop contact time (min)	Fig. #
				Aging temperature (°C)	Aging time (days)		Stable	Onset	Unstable		
A-93	{pH8, 1M}			25	1	toluene	X		X	2	2.1-31
				25	21	toluene	X		X		
				25	21	c-C_6	X	X		4	2.1-32
	{pH4, 0.01M}			25	1	toluene	X		X	2	2.1-33
				25	21	toluene	X		X		
				25	21	c-C_6	X	X	X	2	2.1-34
		X	X	25	24	c-C_6	X	X		4	2.1-35
		X	X	25	27	c-C_6	X	X			
		X		80	23	c-C_6	X	X		4	2.1-36
		X		80	26	c-C_6	X	X			
		X	X	80	21	c-C_6	X	X		4	2.1-37
		X	X	80	25	c-C_6	X	X			
Lagrave + AMN	{pH4, 0.01M}			25	23	c-C_6	X	X	X	4	2.1-38
				25	26	toluene	X	X		4	2.1-39
Mars-Pink	{pH8, 1M}			25	21	c-C_6	X	X		4	2.1-40
	{pH4, 0.01M}			25	22	c-C_6	X	X	X	4	2.1-41
				25	25	c-C_6	X	X			
Mars-Yellow	{pH4, 0.01M}			25	1	toluene	X	X	X	2	2.1-42
				25	21	toluene	X	X	X		
				25	21	c-C_6	X	X		2	2.1-43
		X	X	25	24	c-C_6	X	X		4	2.1-44
		X	X	25	28	c-C_6	X	X			
		X		80	23	c-C_6	X	X		4	2.1-45
		X		80	26	c-C_6	X	X			
		X	X	80	21	c-C_6	X	X		4	2.1-46
		X	X	80	25	c-C_6	X	X			
	synthetic sea water			25	1	toluene	X	X	X	2	2.1-47
				25	21	toluene	X	X	X		
Tensleep + AMN	{pH4, 0.01M}			25	21	c-C_6	X	X		4	2.1-48
				25	24	c-C_6	X	X			

Contact angle measurements:

The sessile drop method was used to measure the advancing and receding contact angles of a drop of water under decane, using a contact angle goniometer. The water advancing contact angle was measured after two to four minutes (the times used in each set of measurements are noted in Table 2.1-25). The water receding angle was measured by withdrawing the drop slowly from the surface back into the buret used to form the drop. All measurements were carried out at ambient conditions of pressure and temperature.

Results and discussion of surface precipitation experiments

Contact angle measurements:

The collected results of advancing and receding contact angle measurements are presented graphically in Figs. 2.1-31 to 2.1-48. The crude oil, brine, precipitant, rinsing solvent, and aging time and temperature in oil are noted on each figure. A vertical line marks the onset of precipitation—the dividing line between mixtures of oil plus heptane in which asphaltenes are stable and those in which asphaltenes precipitate. Refractive indices of the oil and heptane are plotted with respect to the right-hand axis, joined by a straight line.

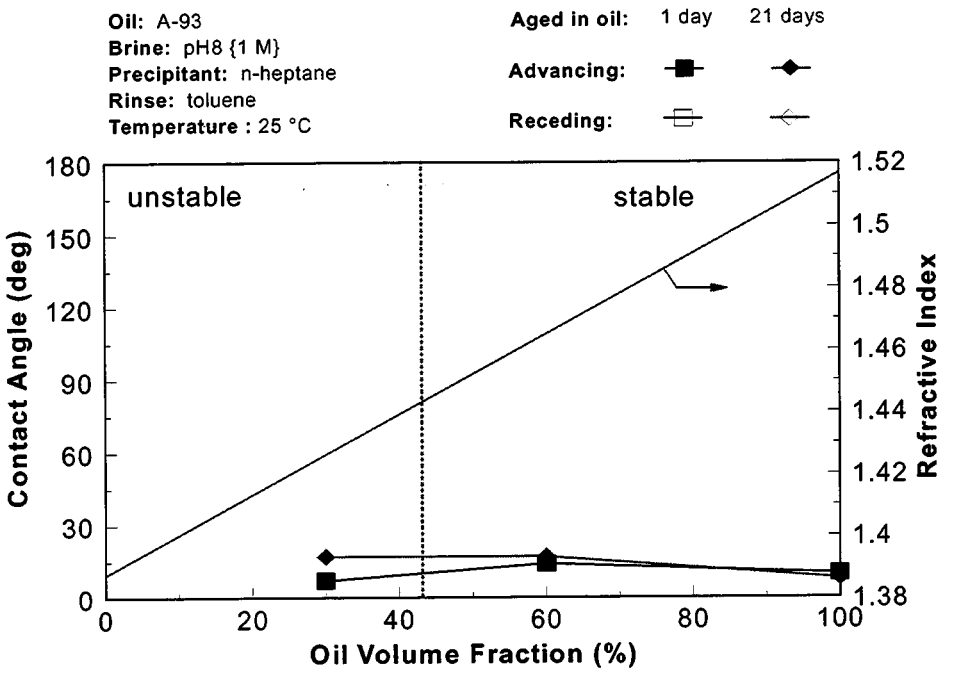

Figure 2.1-31. Contact angles for mica / {8, 1} / A-93 + heptane (25°C) / toluene treatments.

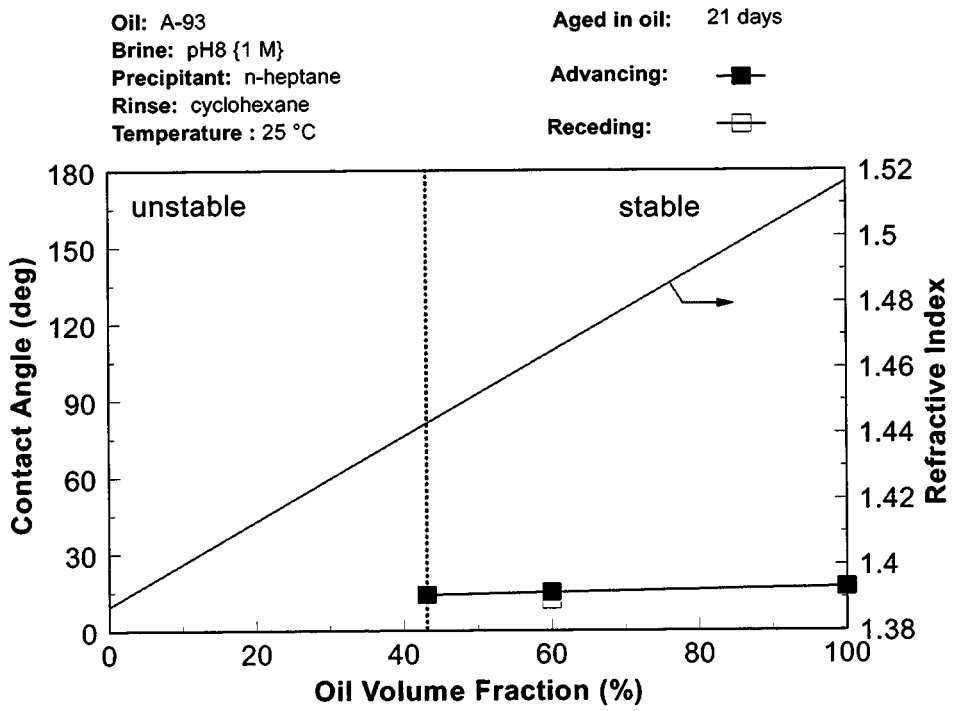

Figure 2.1-32. Contact angles for mica / {8, 1} / A-93 + heptane (25°C) / cyclohexane treatments.

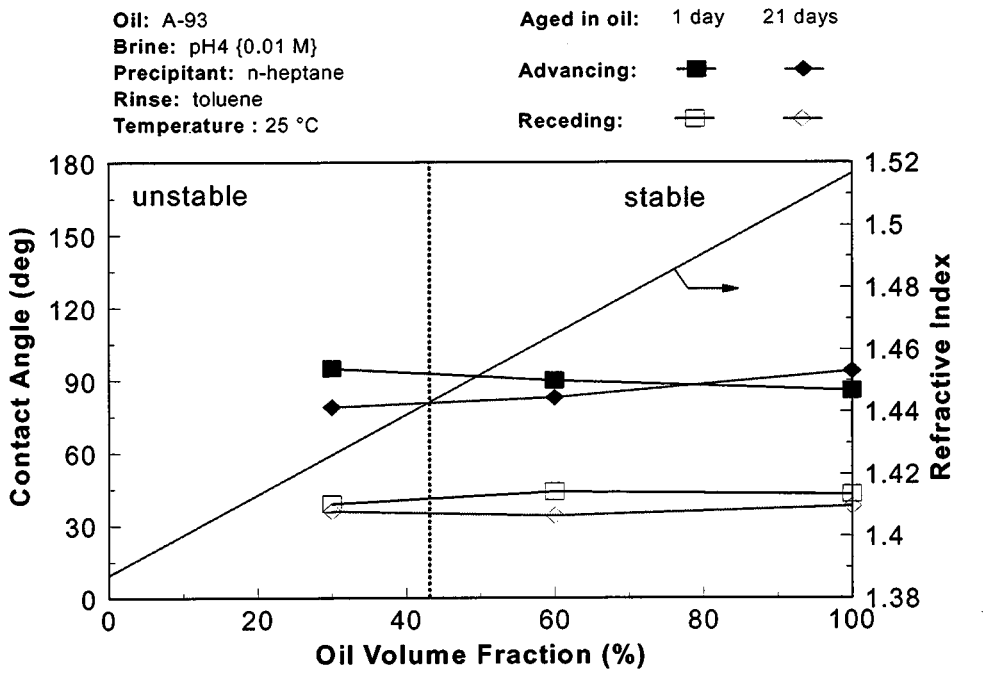

Figure 2.1-33. Contact angles for mica / {4, 0.01} / A-93 + heptane (25°C) / toluene treatments.

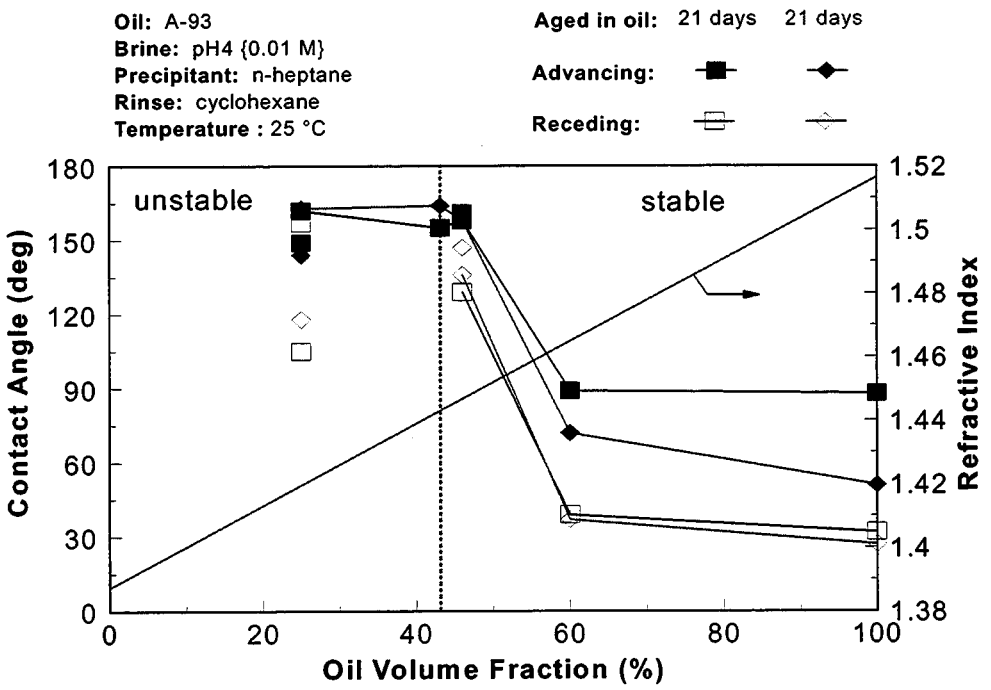

Figure 2.1-34. Contact angles for mica / {4, 0.01} / A-93 + heptane (25°C) / cyclohexane treatments.

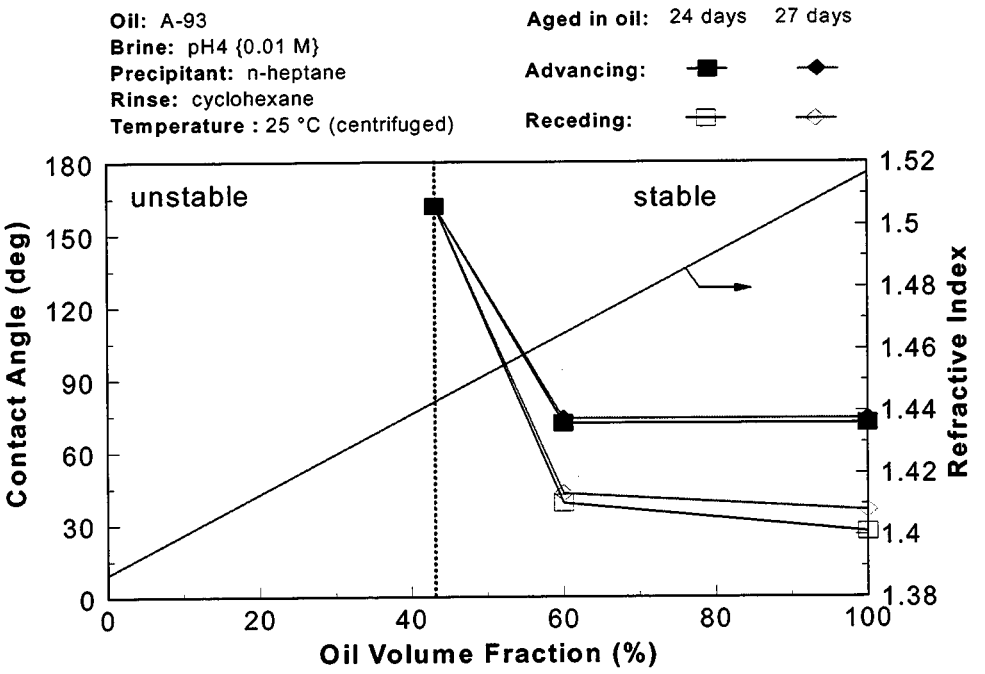

Figure 2.1-35. Contact angles for mica / {4, 0.01} centrifuged / A-93 + heptane (25°C) / cyclohexane treatments.

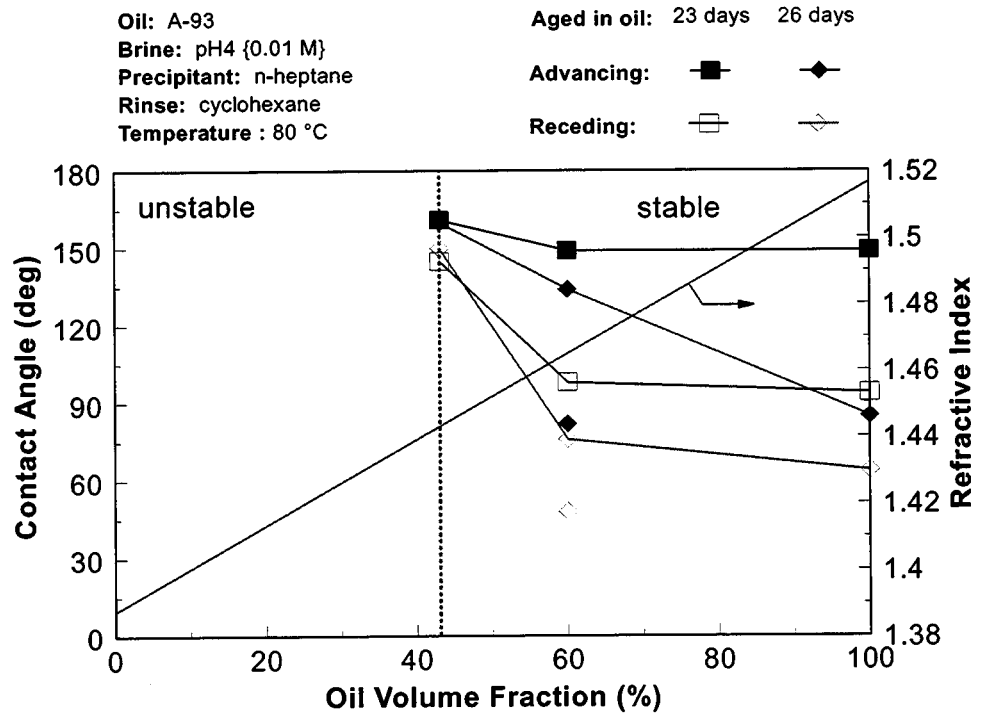

Figure 2.1-36. Contact angles for mica / {4, 0.01} / A-93 + heptane (80°C) / cyclohexane treatments.

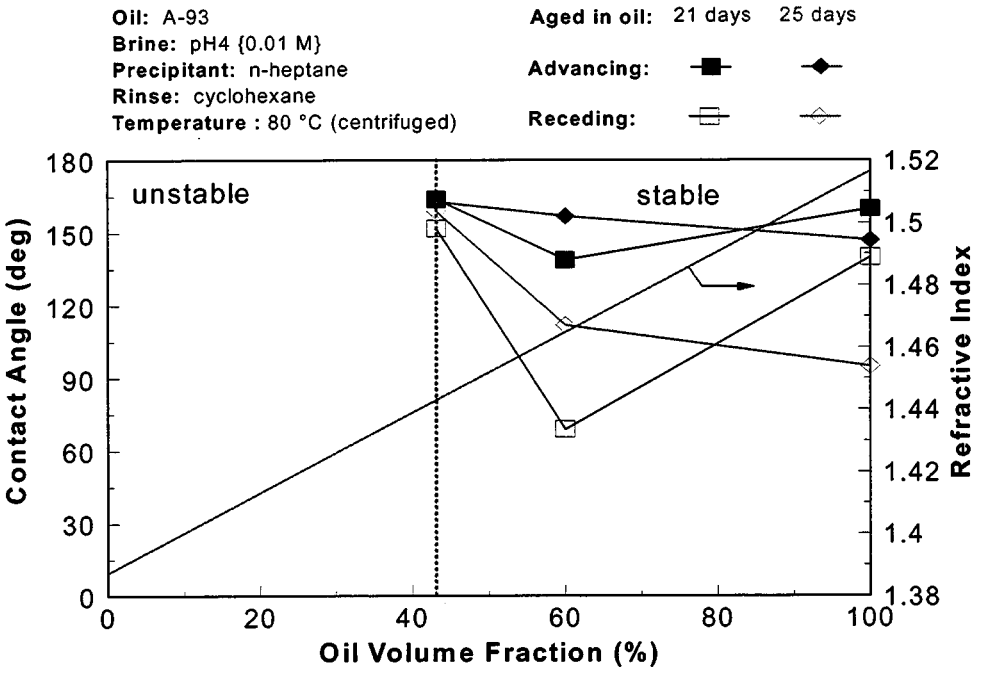

Figure 2.1-37. Contact angles for mica / {4, 0.01} centrifuged/ A-93 + heptane (80°C) / cyclohexane treatments.

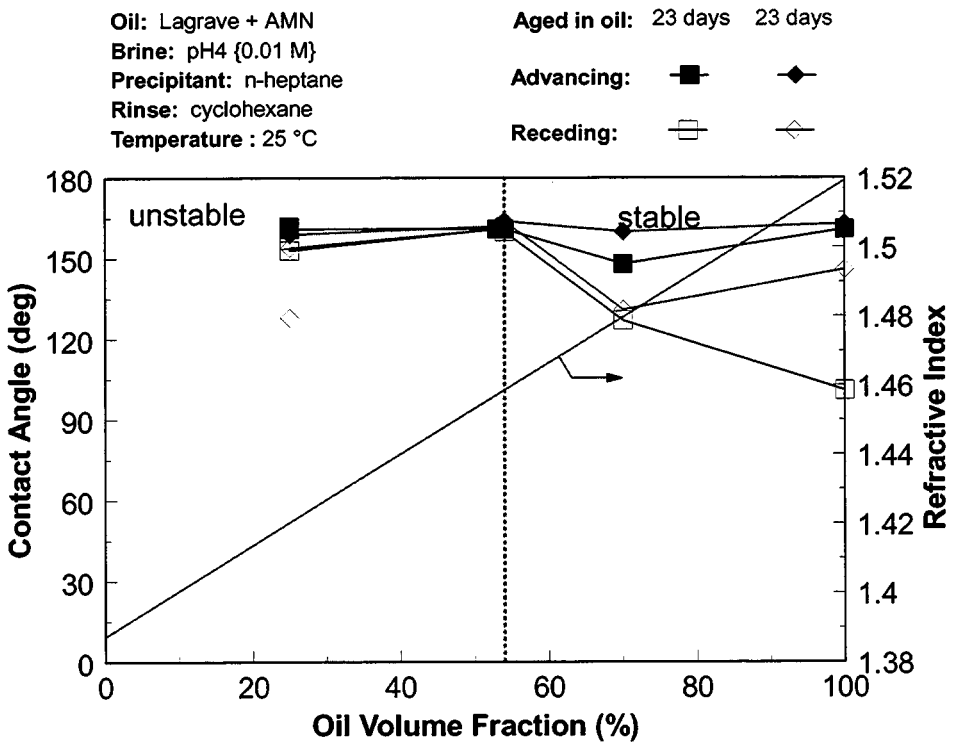

Figure 2.1-38. Contact angles for mica / {4, 0.01} / Lagrave + AMN + heptane (25°C) / cyclohexane treatments.

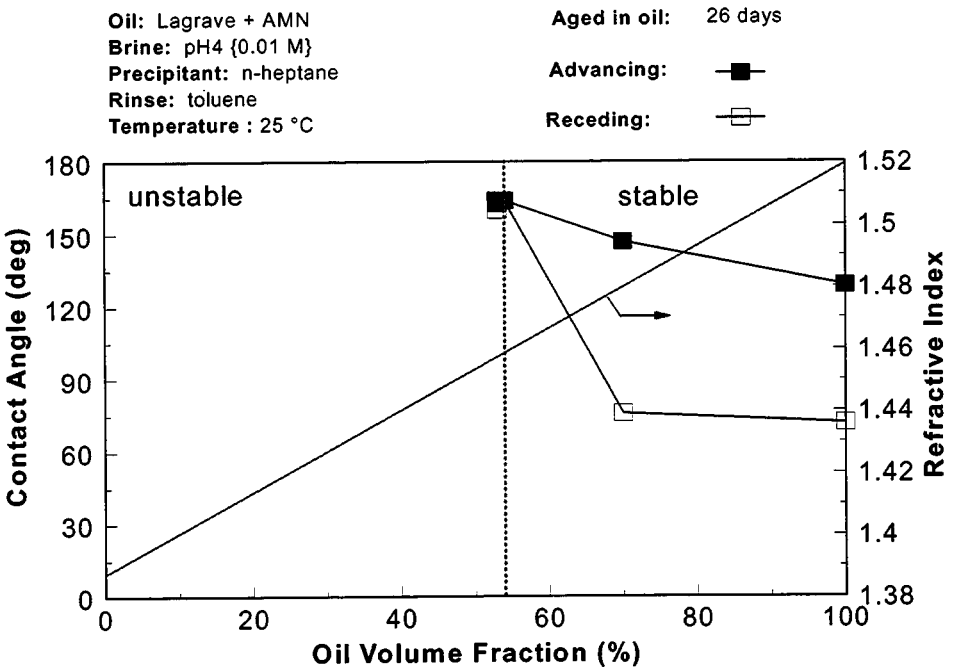

Figure 2.1-39. Contact angles for mica / {4, 0.01} / Lagrave + AMN + heptane (25°C) / toluene treatments.

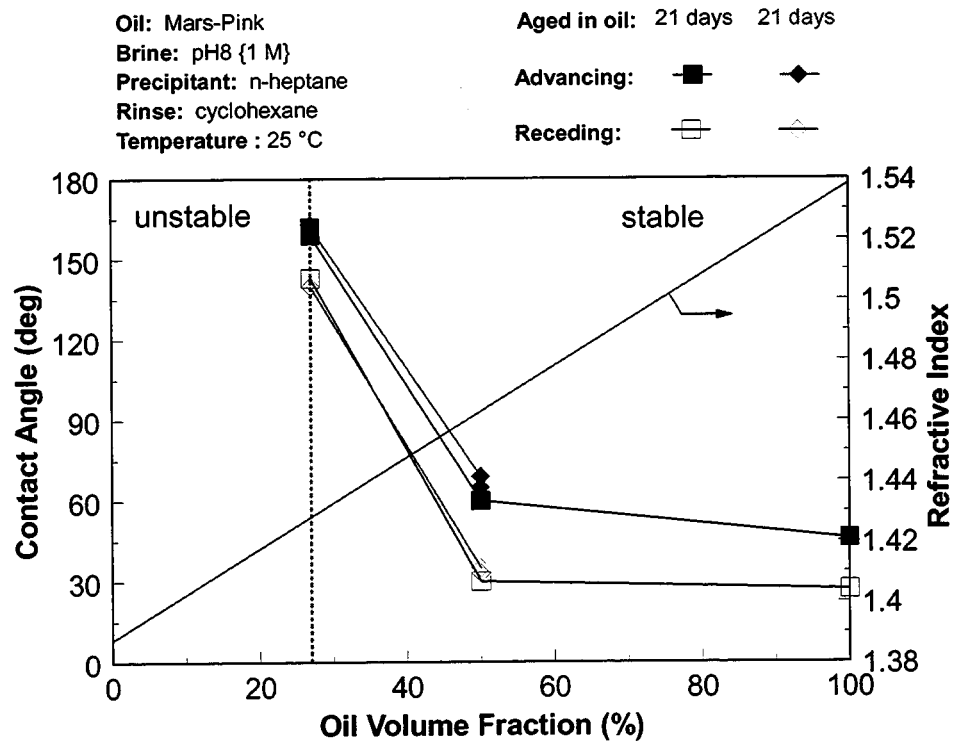

Figure 2.1-40. Contact angles for mica / {8, 1} / Mars-Pink + heptane (25°C) / cyclohexane treatments.

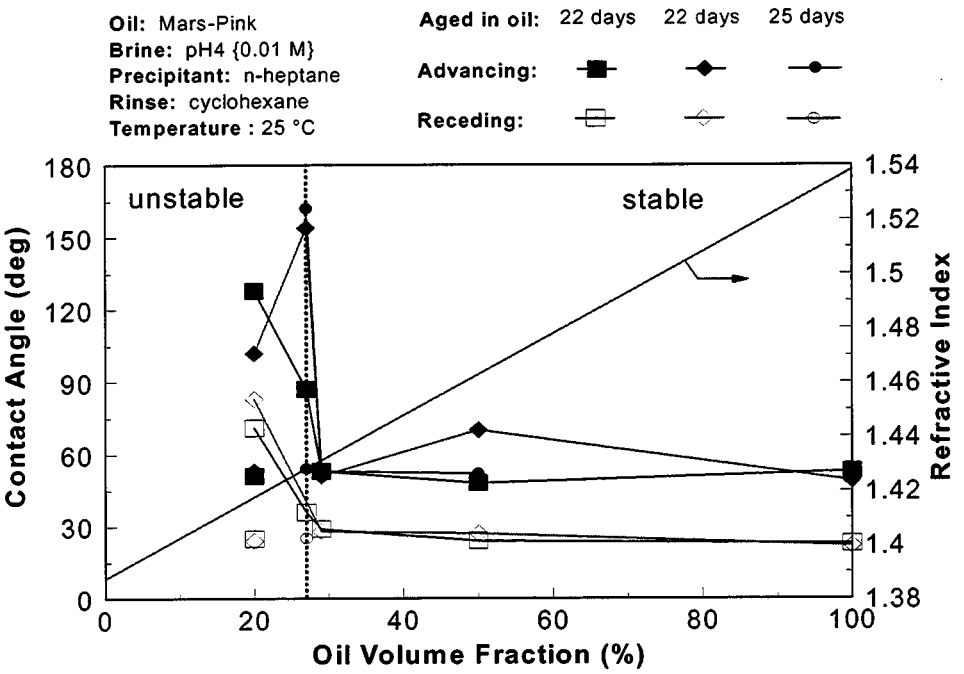

Figure 2.1-41. Contact angles for mica / {4, 0.01} / Mars-Pink + heptane (25°C) / cyclohexane treatments.

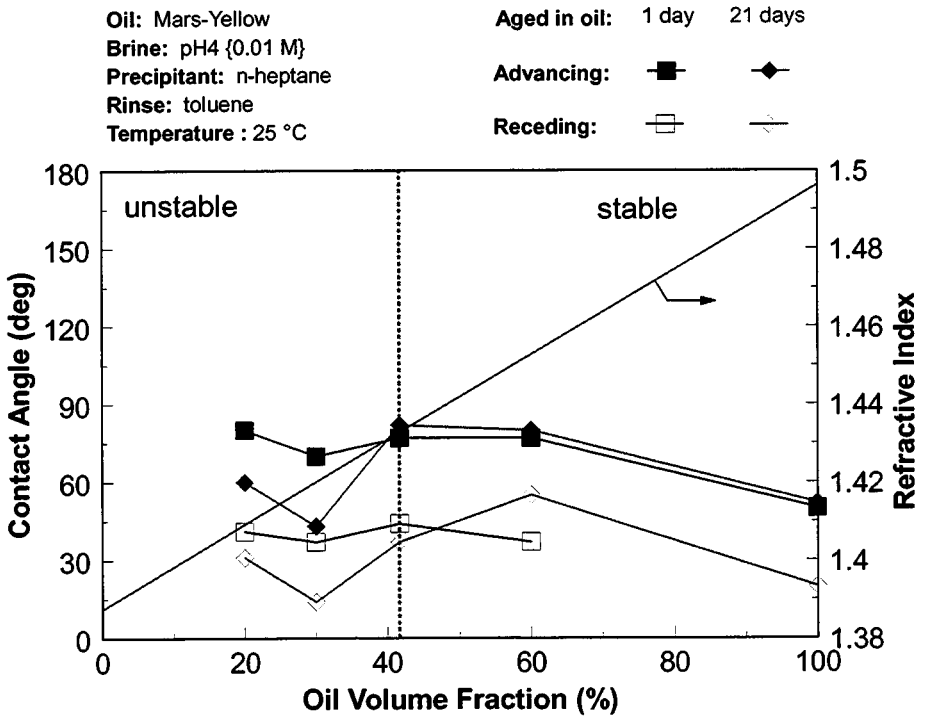

Figure 2.1-42. Contact angles for mica / {4, 0.01} / Mars-Yellow + heptane (25°C) / toluene treatments.

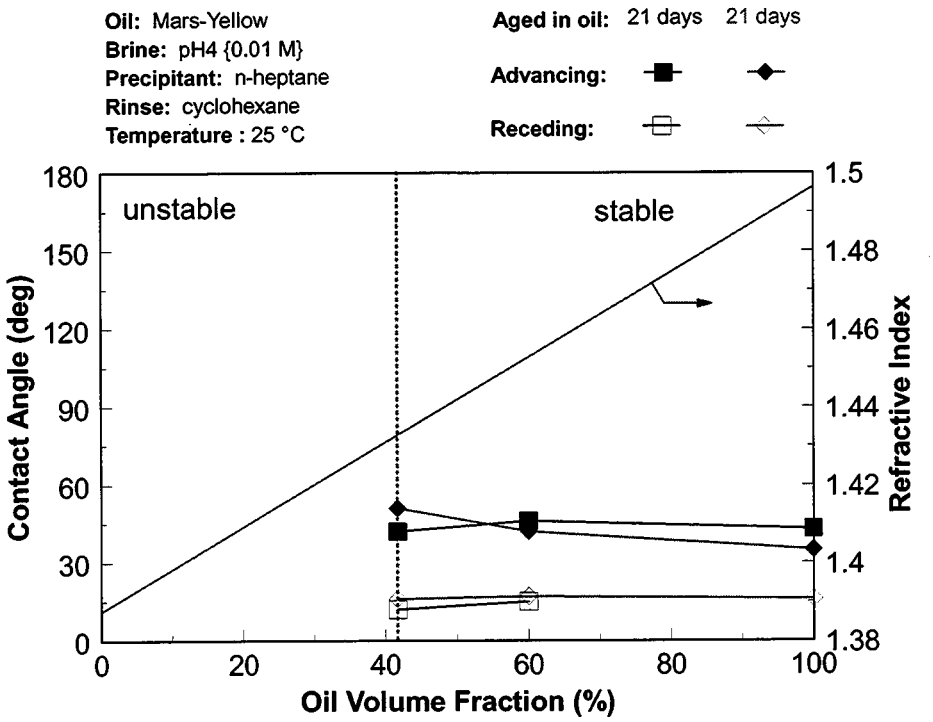

Figure 2.1-43. Contact angles for mica / {4, 0.01} / Mars-Yellow + heptane (25°C) / cyclohexane treatments.

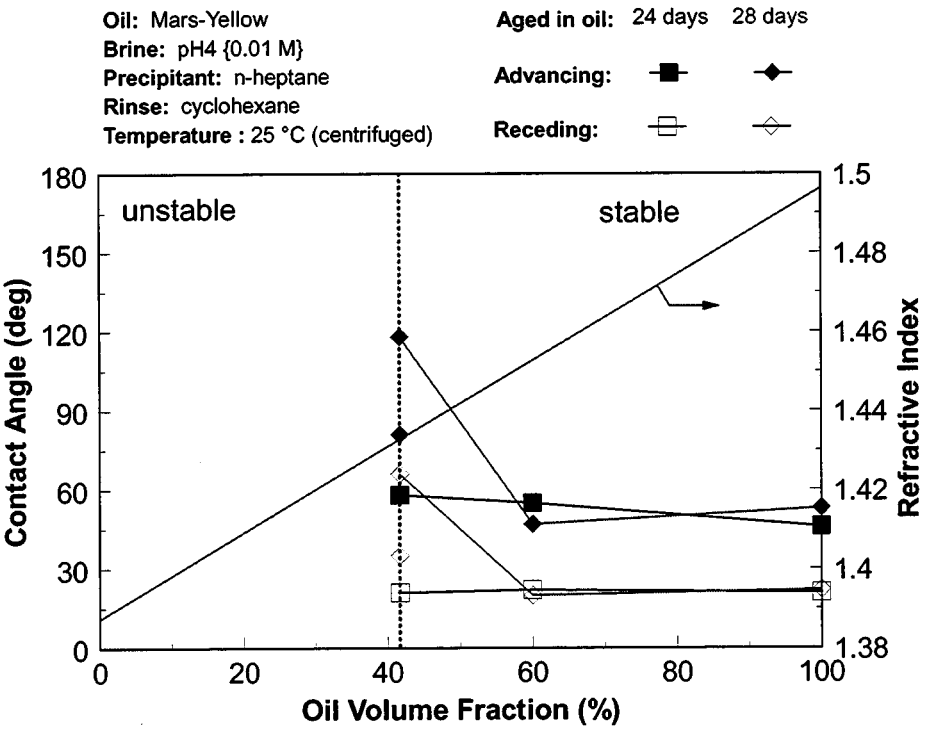

Figure 2.1-44. Contact angles for mica / {4, 0.01} centrifuged / Mars-Yellow + heptane (25°C) / cyclohexane treatments.

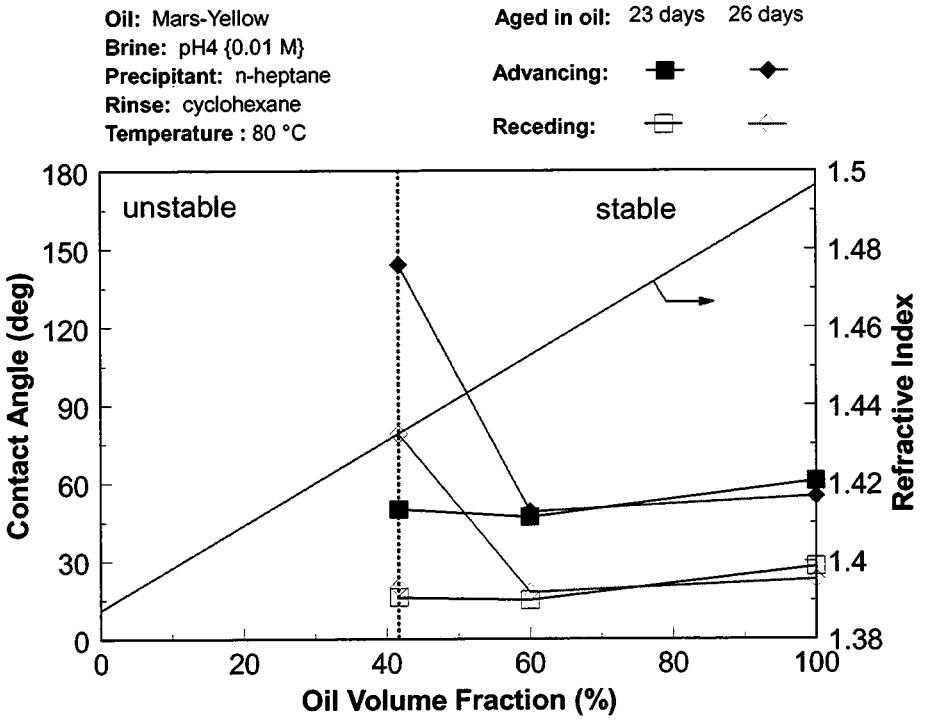

Figure 2.1-45. Contact angles for mica / {4, 0.01} / Mars-Yellow + heptane (80°C) / cyclohexane treatments.

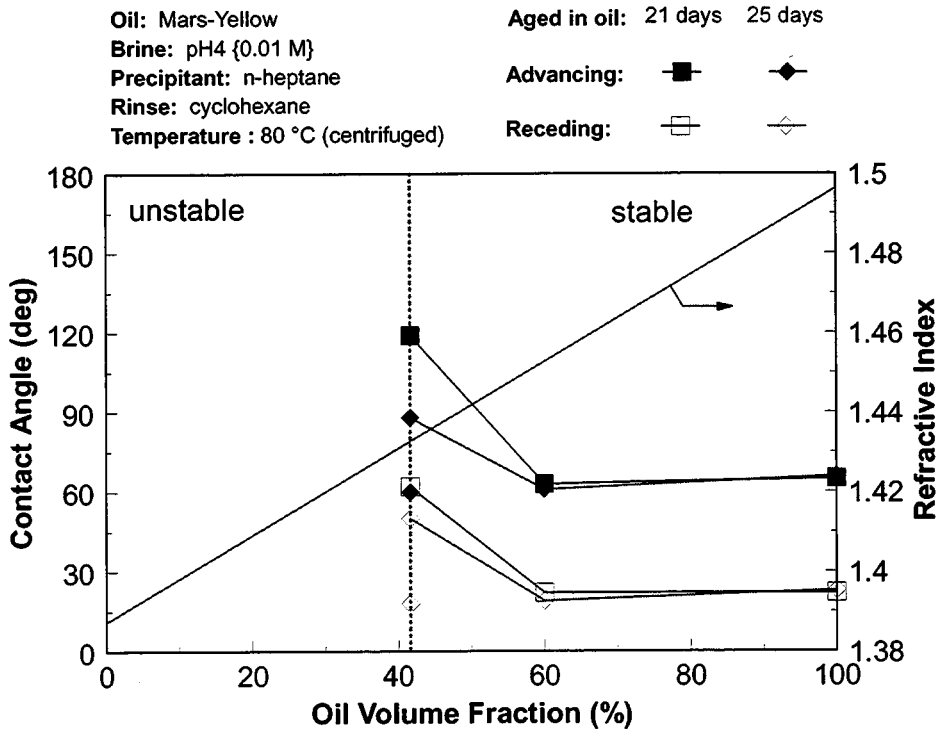

Figure 2.1-46. Contact angles for mica / {4, 0.01} centrifuged / Mars-Yellow + heptane (25°C) / toluene treatments.

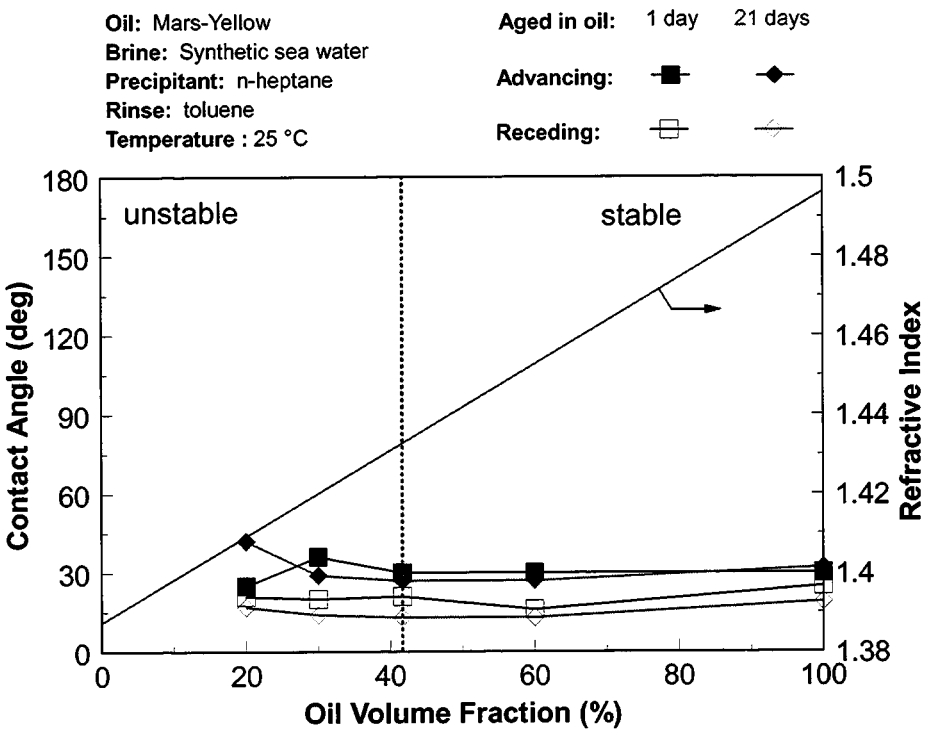

Figure 2.1-47. Contact angles for mica / SSW / Mars-Yellow + heptane (25°C) / toluene treatments.

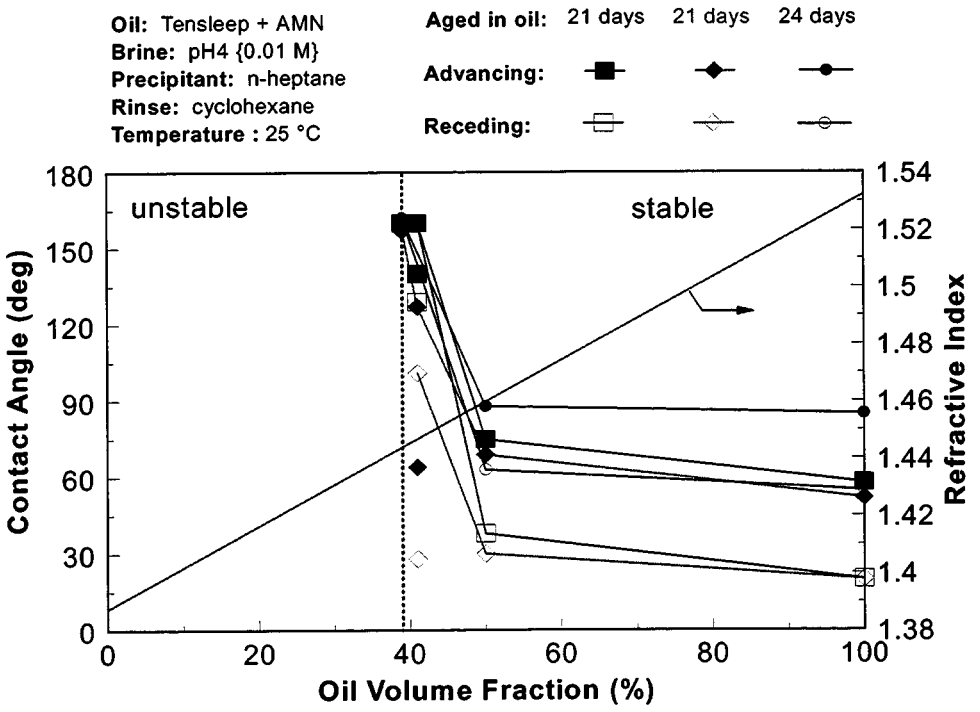

Figure 2.1-48. Contact angles for mica / {4, 0.01} / Tensleep + AMN + heptane (25°C) / cyclohexane treatments.

Reproducibility of the measurements:

In spite of every effort to reduce variability in these tests, some scatter in the results is unavoidable. The crude oil samples themselves are heterogeneous. To ensure that results are representative, measurements are repeated at numerous positions on each treated mica surface. In addition, duplicate samples are tested under identical conditions. One set of experimental data serves to illustrate both the normal reproducibility that can be attained in careful experiments and the extreme variability encountered with certain treatment conditions.

Table 2.1-26 shows details of the contact angle measurements on mica surfaces treated with {pH4, 0.01M} brine, then with Mars-Pink in mixtures with *n*-heptane. In all cases, surfaces were aged at room temperature for at least three weeks. During exposure to crude oil, the mica samples were contained in small sealed vials, resting at an angle so that only their ends contacted the walls of the container. After aging they were rinsed with cyclohexane and immersed in decane for measurements, first of water advancing, then water receding. The results can be divided into three main regions: mixtures (including 100% crude oil) in which the asphaltenes are stable, the onset condition, and mixtures with unstable asphaltenes.

Table 2.1-26. Reproducibility of contact angle measurements

Mica surfaces pretreated with {pH4, 0.01M} buffered brine, aged in mixtures of *n*-heptane and Mars-Pink oil for three weeks at 25°C, rinsed with cyclohexane.

Asphaltenes are:	$f_{v,oil}$	θ_A (°)	θ_R (°)	Notes
Stable	1.0	49 + 2.0	22 + 3.5	sample 1
		53 + 1.1	23 + 5.4	sample 2
	0.5	48 ± 3.9	24 ± 2.4	sample 1
		70 + 4.6	27 + 3.0	sample 2
		52 + 2.4	26 + 1.2	sample 3
	0.29	53 ± 1.1	26 ± 1.1	sample 1
		53 + 2.5	29 + 1.5	sample 2
		51 + 3.9	28 + 2.1	sample 3
Onset	0.27	87 ± 4.9	36 ± 4.3	sample 1
		154 + 4.3	~180	sample 2
		54 + 0.9	25 + 1.4	sample 3, side 1
		162 + 1.2	162 + 1.2	sample 3, side 2
Unstable	0.2	128 ± 16.7	71 ± 33	sample 1, side 1
		51 + 0.6	25 + 1.4	sample 1, side 2
		102 + 51.1	83 + 68.6	sample2, side 1
		53 + 3.7	24 + 1.9	sample 2, side 2

In the stable region, standard deviations in the advancing angle measured on any one mica sample ranged from 1-5°. For compositions with volume fractions of oil ranging from 0.29 to 1.00, the average advancing angle was almost constant at about 53° and the receding angle averaged about 26°.

The picture changes dramatically when surfaces are aged in mixtures at onset conditions. Although the standard deviations continued to be in the range of 1-5°, a significant difference emerged from one sample to another. The advancing angles measured on sample 1 were higher than those reported for mica aged under asphaltene-stable conditions, but were still in the neutral range. Sample 2 was oil-wet, with an average advancing angle of 154° and receding angles that were too high to measure reliably. Because of the discrepancy, additional samples were tested.

For sample 3 at onset conditions (Table 2.1-26), a difference in color was noted between one side of the oil-treated mica and the other, so measurements were made on both sides. The

discrepancy between the two sides was even larger than that between the first two samples. Side 1 was similar to the asphaltene-stable samples, whereas side 2 was oil-wet. The differences between the two sides might reflect the fragility of the deposited film, which is sometimes removed by washing. Alternatively, the difference might be caused by the slanting orientation of the sample. To test the latter hypothesis, additional samples were aligned either vertically or horizontally during exposure to oil plus heptane. The advancing angles measured on these and the tilted sample, already discussed, are compared in Fig. 2.1-49. Orientation does not appear to be the key to the discrepancies observed. Partial removal of some films during the washing step remains to be tested.

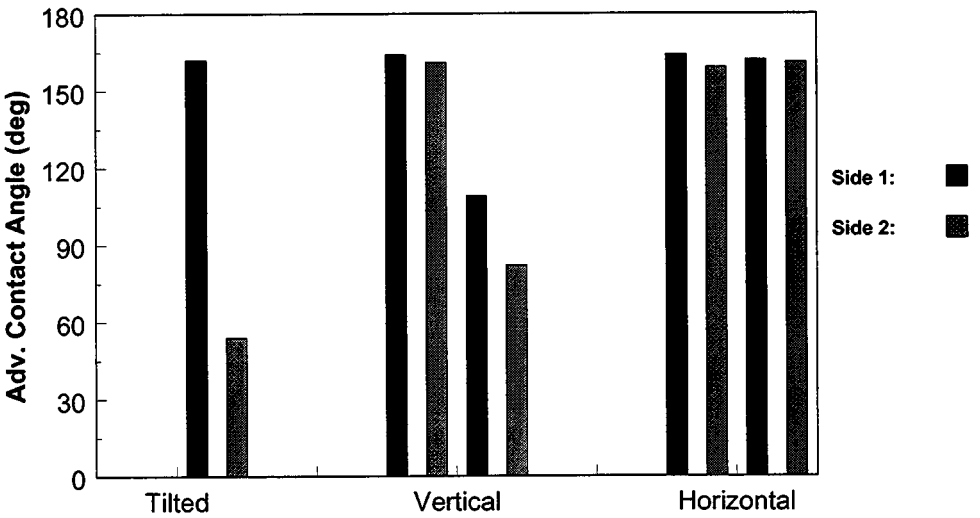

Figure 2.1-49. Water advancing angles on mica samples aged in oil with different orientations. Angles were measured on surfaces treated with {pH4, 0.01M} brine and then aged in the onset mixture of Mars-Pink and heptane for three weeks at 25°C, rinsed with cyclohexane.

Similar discrepancies were noted on opposite sides of mica samples treated under conditions where asphaltenes were precipitating. On the high-advancing-angle side, however, the deposited films were only poorly adhering to the mica surface. Part of the film was removed

during rinsing and handling, which resulted in a very heterogeneous surface, as evidenced by standard deviations of 17 and 51°, well above the normal level of scatter in these experiments.

Comparison of crude oils:

Scans of the asphaltene-stable and onset conditions for each of the five crude oils at a standard set of conditions is shown in Fig. 2.1-50. In each case, the brine was {pH4, 0.01M} buffer, samples were aged in oil for at least three weeks at 25°C, and oil was rinsed from the surface with cyclohexane. The average advancing angles are compared in Fig. 2.1-50 as a function of the volume fraction of oil in each oil/heptane mixture.

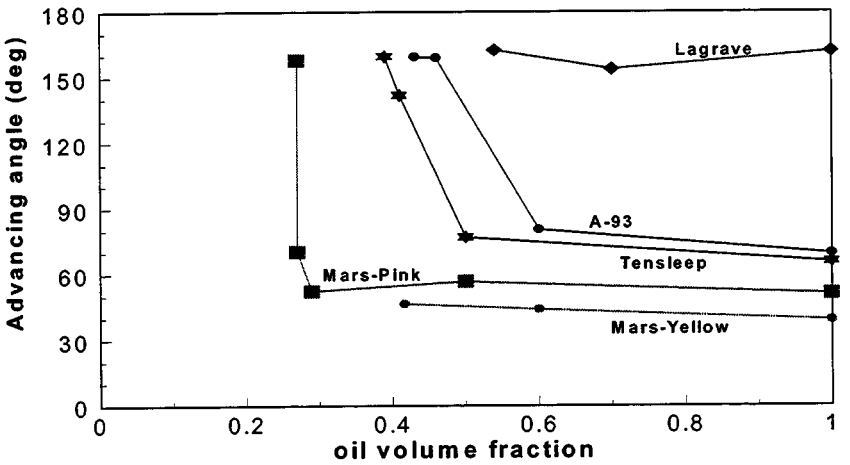

Figure 2.1-50. Water advancing angles on mica surfaces treated with {pH4, 0.01M} buffer, then aged in oil/heptane mixtures for three to four weeks at 25°C, rinsed with cyclohexane.

Water-wet:

Mars-Yellow. Advancing angles were all less than 50° on the mica surfaces treated with Mars-Yellow, representing fairly water-wet conditions. No evidence of any influence of the state of asphaltene aggregation is apparent, as angles on surfaces treated in stable oils and at onset conditions are nearly identical. Even more water-wet conditions were produced if synthetic sea-water was used as the brine, on surfaces aged either for one day or three weeks, then rinsed with toluene (Fig. 2.1-47).

Oil-wet:

Lagrave plus AMN. The other extreme in Fig. 2.1-50 is shown by Lagrave crude oil. Again, there is little evidence of change in wetting alteration with asphaltene stability, but in this case the reason is that all the surfaces produced are oil-wet. Some increase in the receding contact angles on surfaces treated at onset conditions was apparent (Fig. 2.1-38) as well as in both advancing and receding conditions on surfaces rinsed with toluene (Fig. 2.1-39). Presumably, there are ionic interactions that account for the wettability alteration in the stable region for this and other oils.

Transition at the onset of asphaltene precipitation:

The remaining three oils all showed a marked increase in advancing and receding angles from neutral or weakly water-wet conditions in stable mixtures to more oil-wet as the oil composition approached the onset of asphaltene precipitation. The correlation between wetting and oil composition is clarified if the data in Fig. 2.1-50 are replotted as a function of refractive indices. In Fig. 2.1-51, the oil volume fractions have been converted to refractive indices and are reported relative to P_{RI}, the refractive index of the onset conditions. The onset occurs at ($RI - P_{RI} = 0$); larger values of ($RI - P_{RI}$) represent mixtures in which the asphaltenes are increasingly stable.

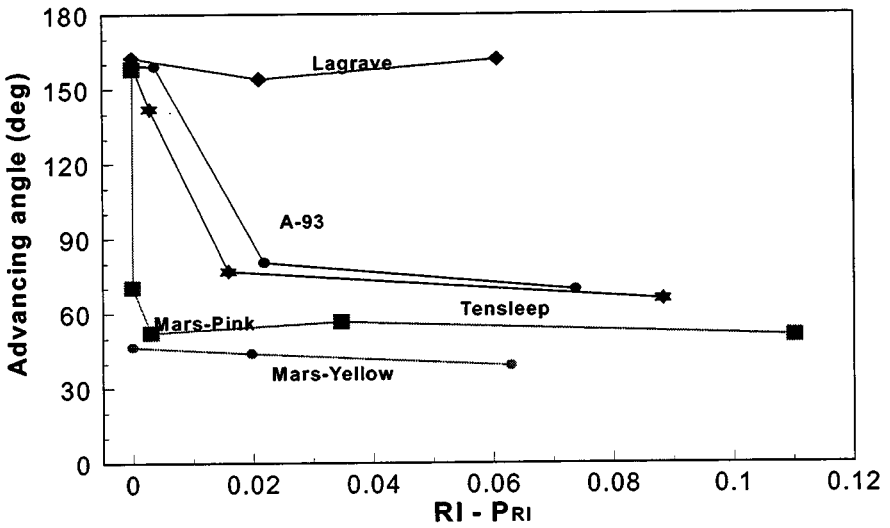

Figure 2.1-51. Water advancing angles on the mica surfaces shown in Fig. 2.1-50, as a function of refractive index of the mixture compared to RI at the onset (P_{RI}).

A-93. This is the only oil of the five in this study for which extensive previous work is available for comparison. Adhesion of A-93 on glass and mica have been reported, in addition to tests of oil-treated glass and mica surfaces similar to the present study (Liu and Buckley, 1997; Liu and Buckley, 1998). The brine composition of {pH4, 0.01M} was used in the majority of tests in this study because previous work had shown that water films are unstable with this brine and oil. The opposite extreme, again for A-93, is a higher pH and ionic strength {pH8, 1M} brine that produced stable water films and water-wet surfaces in previous tests. Table 2.1-27 compares the earlier measurements on mica with those obtained by various treatments in this study. Although there are some differences in treatment protocols, the results are similar. Preconditioning with the higher pH brine produced water-wet conditions in all tests. Neutrally-wet surfaces were produced by treatments with the lower pH brine at room temperature and increasingly oil-wet conditions at higher temperatures of aging in this oil.

Table 2.1-27. Comparison of advancing contact angles resulting from treatments with A-93

Brine	Aging T (°C)	Liu (1998) toluene rinse	rinse with toluene	rinse with c-C_6	centrifuged c-C_6-rinse
{pH4, 0.01M}	25	109°	90°	69.5°	73°
	80	127°		117°	153.5°
{pH8, 1M}	25	38°	9°	17°	
	80	41°			

What has not been investigated previously—even in the most extensive studies of interactions between A-93 and mineral surfaces with a wide variety of brines—is the role of a stable brine film that restricts interactions between oil and solid, vs. enhanced interaction by the surface precipitation mechanism at the onset of asphaltene precipitation. Scans of asphaltene-stable, onset, and unstable mixtures with pH8 buffer and A-93 crude oil show that a stable water film prevents interaction with the surface even at the onset of asphaltene precipitation (see Figs. 2.1-31 and 2.1-32).

In the unstable regime where precipitation is occurring, contact angles measured on one side of the mica sample were higher and the other side lower, as reported above for Mars-Pink crude oil (Fig. 2.1-41). With A-93, discrepancies from one side to the other were observed only for surfaces aged in unstable-asphaltene mixtures, not for those aged under onset conditions.

Tensleep plus AMN. Mica surfaces exposed to the Tensleep plus AMN mixture and washed with cyclohexane became weakly water-wet to neutrally wet in the stable regime. At the onset, a steep increase in advancing and receding angles indicated more strongly oil-wet conditions (Figs. 2.1-48, 2.1-50, and 2.1-51).

Mars-Pink. The characteristic behavior of weakly water-wet to neutral advancing angles in the stable regime, changing steeply to oil-wet conditions near the onset of asphaltene

precipitation, were observed with both {pH4, 0.01M}(Figs. 2.1-41, 2.1-50, and 2.1-51) and {pH8, 1M} (Fig. 2.1-40) buffers on mica surfaces exposed to Mars-Pink oil and rinsed with cyclohexane. Surfaces treated in a mixture with an RI that was only 0.003 greater than the onset condition had weakly water-wet characteristics very similar to others treated in more stable mixtures. An increase of 1% in the volume fraction of heptane made surfaces oil-wet, at least on one side.

Improving reproducibility:

Removal of bulk water. Yang and Hirasaki (1999) introduced a centrifuge technique for removing bulk water from mica samples. Spinning a wet mica sample under oil to remove bulk water was recently demonstrated to give results with improved internal consistency, without introducing bias toward either more oil-wet or more water-wet results (Creech and Buckley, 1999). Additional evidence that supports those preliminary findings is shown in tests conducted over a range of oil compositions in the asphaltene-stable and onset regimes with A-93 (Figs. 2.1-34 to 2.1-37, and 2.1-52) and Mars-Yellow (Figs. 2.1-43 to 2.1-46, and 2.1-53). The aqueous phase was {pH4, 0.1M} buffer, surfaces were rinsed with cyclohexane, and aging times were three to four weeks.

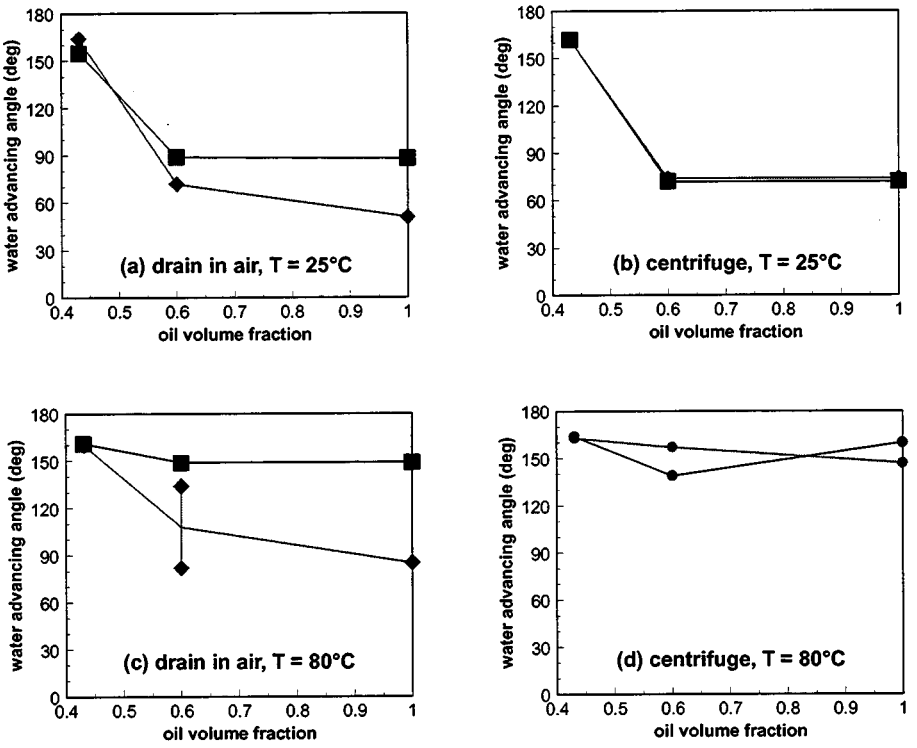

Figure 2.1-52. Water advancing angles measured on surfaces treated with {pH4, 0.01M} brine and mixtures of A-93 and heptane are more reproducible if the brine was removed by centrifuging under the oil. Poorer solvent and higher temperature produced more oil-wet conditions.

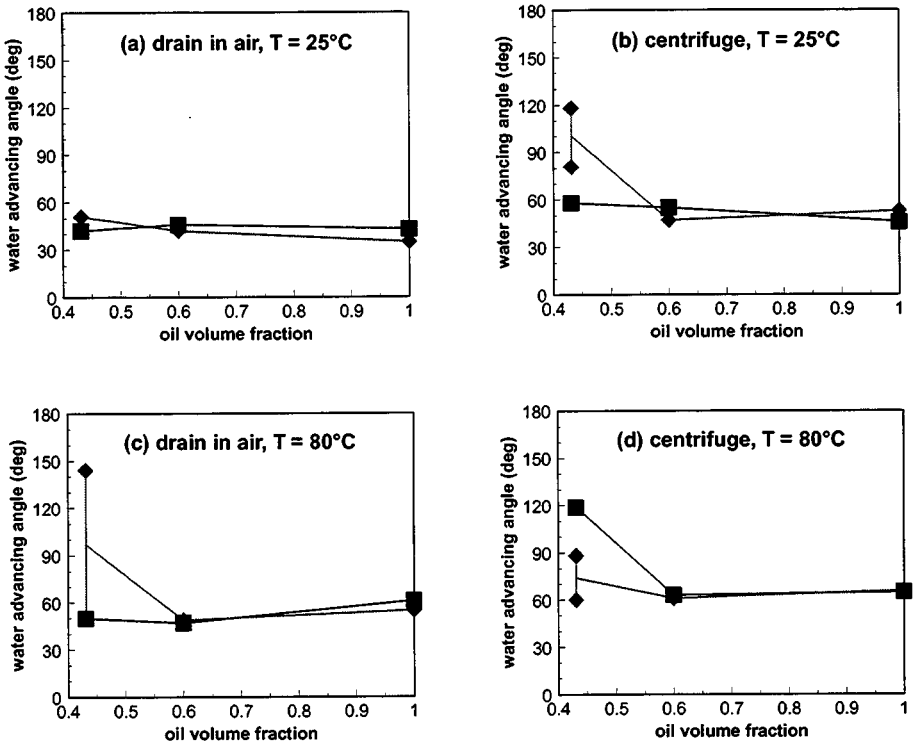

Figure 2.1-53. Water advancing angles measured on surfaces treated with {pH4, 0.01M} brine and mixtures of Mars-Yellow and heptane show transition to more oil-wet conditions only if the surfaces were centrifuged or aged at elevated temperature.

For A-93, centrifugal water removal gave better reproducibility at both low and high aging temperatures. The transition from neutral wetting in the asphaltene-stable region to oil-wet at the onset of asphaltene precipitation is confirmed for surfaces aged at 25°C. Aging at higher temperature created more oil-wet conditions.

A transition from weakly water-wet to neutral or more oil-wet conditions can be observed when mica surfaces are treated with Mars-Yellow at 80°C and if the samples are centrifuged at either temperature. Thus, transitional behavior that depends on the oil composition was observed for all five oils, although not for every sample. Discrepancies between one side and the other of oil-treated mica surfaces, as described previously, were commonly observed, as indicated by two symbols joined by a vertical line in Figs. 2.1-52 and 2.1-53.

Removal of bulk crude oil. Rinsing remains a significant problem. Direct comparisons, shown in Fig. 2.1-54, are inconclusive. Cyclohexane is on the borderline between solvents and precipitants. It may tend to tip the balance toward precipitation for some oils (e.g. Fig. 2.1-54a). Toluene is a better asphaltene solvent. In cases where adsorption is weak, toluene may have a greater tendency to clean asphaltic material off the surface (e.g. Fig. 2.1-54c). Often there is no difference between the two. Results such as those in Fig. 2.1-54d, where toluene rinsing results in higher water advancing angles, are difficult to explain. Comparisons of toluene and cyclohexane rinsing may help to differentiate between weakly and strongly adsorbed material.

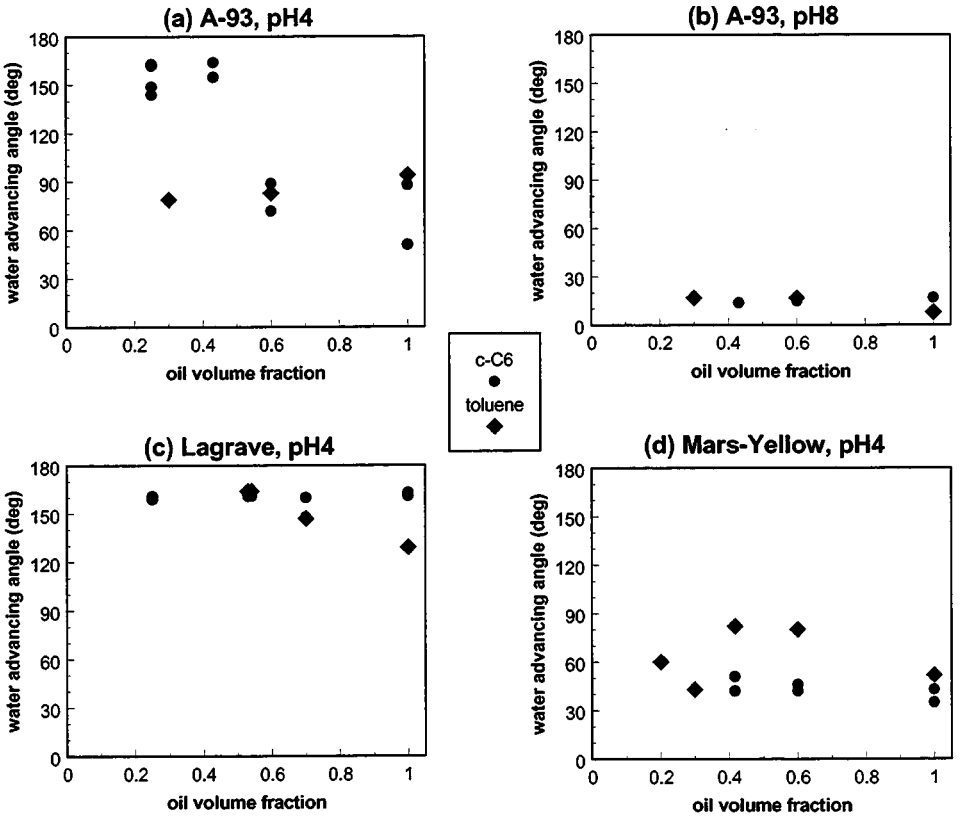

Figure 2.1-54. The effects of rinsing with either toluene or cyclohexane appear to be ambiguous. The samples compared were aged for 3-4 weeks at 25°C and none were centrifuged to remove brine.

Aging in unstable mixtures:

The region in which mixtures of heptane and oil are unstable is difficult to explore. In all the asphaltene-unstable cases tested in this study, mica was submerged in oil, after which heptane was added. Since asphaltenes can precipitate slowly, the composition of the mixture in contact with the solid surface changed with time. As asphaltenes settle out of the mixture, they may form weakly adsorbing layers of organic material that are at least partially removed even by gentle rinsing. The wettability effects of such precipitated material might be less a factor in oil reservoirs than their potential for plugging.

Aging without asphaltenes:

One way to observe the influence of asphaltenes is to remove them and test the effect of the remaining material, known as maltenes, on wettability of mica surfaces. Maltenes were prepared from Lagrave crude oil by adding 40 parts of *n*-pentane to 1 part of oil. The results of aging mica surfaces in Lagrave maltenes are shown in Fig. 2.1-55. Neutrally-wet conditions were obtained with the maltenes compared to oil-wet conditions for the whole crude oil, where the asphaltenes were present. In this case, material other than asphaltene is capable of altering wettability, although to a lesser extent than the asphaltenes. Addition of heptane (46%) to the Lagrave maltenes (54%) produced somewhat higher advancing angles. What might be responsible for this difference (e.g., aggregation of material in the maltenes, changes in oil surface charge, or even differences in viscosity) remains to be explored.

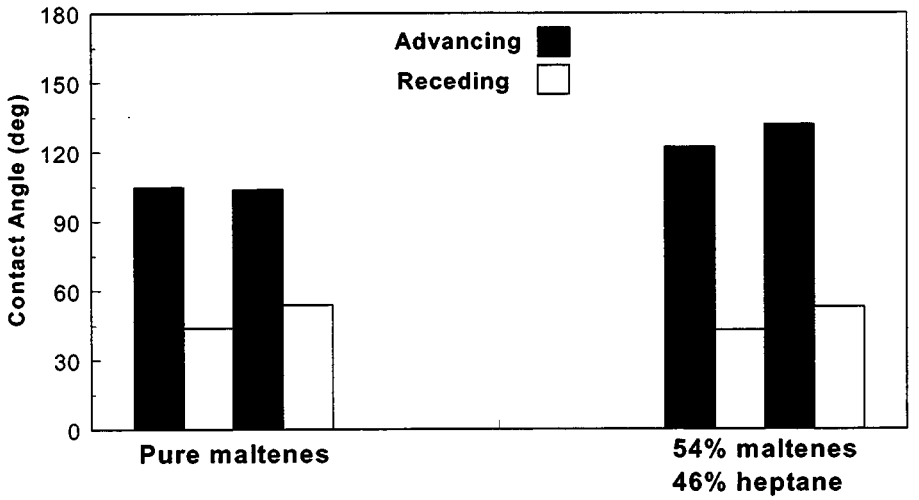

Figure 2.1-55. Water advancing and receding angles measured on surfaces treated with {pH4, 0.01M} brine and aged in Lagrave maltenes or their mixtures with heptane for three weeks at 25°C, rinsed with cyclohexane.

Summary of surface precipitation observations

This is the first systematic study of crude oil surface precipitation phenomena. It has demonstrated that an increased effect on wetting alteration to oil-wet conditions can occur as the onset of precipitation is approached. In the case of Mars-Pink, it was shown that even a 1% change in volume fractions can have a dramatic effect on the extent to which wetting is altered. For A-93, the transition is observed slightly above P_{RI}, showing that for some oils, the value of P_{RI} determined by microscopic identification of asphaltene aggregates may underestimate the conditions at which surface precipitation becomes important. If there are systems in which big wettability changes can be dissociated from the presence of particulate asphaltenes, such systems would be useful for separating the effects of wettability alteration and plugging by asphaltenes.

Previous observations about the mechanisms by which wetting is altered on surfaces exposed to crude oils have been broadly confirmed. Results of this study were consistent with those previously published for A-93 in situations where water films are either stable (water-wet) or unstable (more oil-wet).

Mixing heptane with crude oils in varying amounts produced mixtures in which asphaltenes were either stable or unstable. Between these two is a narrow band of onset conditions at which the most oil-wet conditions were often reported.

Near onset and asphaltene-unstable conditions, weakly adsorbed films sometimes produced very heterogeneous surfaces and large discrepancies between wetting conditions on opposite faces of the mica surface.

Changing crude oil composition by addition of a precipitant or a solvent will not only change the asphaltene stability, but it might change the properties of other components in the crude oil.

Reproducibility of the contact angle measurements was enhanced if bulk water was removed by centrifugation.

2.1.4 Chemical Investigation of Oil-Treated Surfaces by FTIR

This section describes an investigation of the adsorption of components from crude oil onto selected mineral surfaces. Adsorption of crude oil components within an oil reservoir influences wettability and thus the production of oil by waterflooding or other processes in which more than one immiscible phase is flowing. Surface interactions between crude oil, brine, and rock are involved in the adsorption processes that can alter a reservoir's wetting properties. The use of ATR-FTIR spectroscopy has been explored in an attempt to quantify these complex relationships.

Based on previous wettability studies, preferential adsorption of polar components of crude oils, including their acidic and basic fractions, was expected on mica and clay surfaces. ATR-FTIR, which focuses on the material at a sample surface and can in principle identify many of the functional groups of interest, was selected as the analytical tool to characterize material

adsorbing from different oils under varying conditions of brine chemistry on the basis of polar functional constituents. However, the amounts of material and their degree of enrichment in polar functional groups are both small, especially when compared to the contribution from the solid substrates, which also absorb in portions of the infrared, limiting the sensitivity of the measurements.

Some commonly used methods for physically characterizing surfaces include scanning electron microscope (SEM), environmental scanning electron microscope (ESEM), and atomic force microscopy (AFM). Methods used for studying the chemistry of surfaces and materials adsorbed on them include photoacoustics, X-ray photoelectron spectroscopy (XPS), nuclear magnetic resonance (NMR) spectroscopy, Raman spectroscopy, and Fourier Transform Infrared (FTIR) spectroscopy.

Physical characterization methods provide information about surfaces. SEM indirectly measures samples by scanning an electron probe across the sample surface producing an electronic image of morphology or topography. Sample preparation is a problem with SEM for non-conducting samples that must be coated with a thin layer of conductive material by sputter coating. Sputter coating is not needed with ESEM, thus allowing *in situ* observations. Recent studies have evaluated fluid/rock interactions at high magnification using ESEM (Gauchet *et al.*, 1993; Robin *et al.*, 1999).

AFM directly measures interactions between surfaces and a mechanical probe dragged or tapped along the surface of the sample. In a study by Sheth and Leckband, (1997), AFM detected submicroscopic characteristics of polymer films adsorbed onto mica. AFM images of A-93 and Alaskan crude oil (Buckley *et. al.*, 1997) showed adsorbed layers on mica that appeared to be 25-80 nm thick.

Used on their own, none of these physical methods would be able to provide chemical information about how the material adsorbs from a crude oil onto mineral surfaces, although they might provide insight about the distribution of material on a surface.

Chemical characterization methods are used to determine surface adsorption. Photoacoustic spectroscopy applies radiation to a sample and then modulates the energy at an acoustical frequency (Willard *et. al.*, 1988). However, the penetration depth for photoacoustics, at 30 microns, is too deep for use in observation of crude oil adsorption on mineral surfaces.

XPS, also known as electron spectroscopy for chemical analysis (ESCA), provides core-electron binding energies through the bombardment of molecules with high-energy X-rays. Only the outer electrons escape detection by XPS, revealing surface information to a penetration depth of 2 nm, which is in the range needed for crude oil adsorption detection (Willard *et. al.,* 1988). XPS analysis of oil-producing reservoir rocks has been reported to relate pore surface concentrations of organic carbon to rock wettability (Leon, *et. al.*, 1997). However, using XPS, Durand and Beccat (1997) reported that they were unable to separate carbon contamination in clays from organic carbon due to crude oil adsorption.

In Fourier Transform Infrared Spectroscopy (FTIR), infrared radiation is transmitted through a sample. As radiation is absorbed by molecules, chemical bonds vibrate with stretching and bending motions at characteristic frequencies, providing structural information about the molecules. Coupled with the use of a technique called Attenuated Total Reflection (ATR), which investigates surface interactions by attenuation of an evanescent wave with a penetration depth of one to ten microns (Harrick, 1967), FTIR provides an attractive alternative for probing the chemical properties of materials adsorbed from crude oil onto mineral surfaces.

Funk *et al.* (1995) used ATR-FTIR to analyze components of crude oil adsorbed on calcium carbonate. After subtraction of the initial spectrum from successive spectra, preferential adsorption of polar functional species, including OH, C=O, C-O, C-S, and S=O, could be identified.

The purpose of the study reported here, excerpted from a recent MS thesis (von Drasek, 1999), was to determine whether adsorbed material could be distinguished chemically from bulk oil using the ATR-FTIR technique. Assuming successful development of the technique, enrichment in specific polar functional species would be examined for correlation to the postulated mechanisms by which material adsorbs.

Experimental methods and materials

Attenuated total reflectance and Fourier transform infrared spectroscopy:

The main analytical technique used in this study was Fourier transform infrared spectroscopy (FTIR). In order to focus on surface properties, an attenuated total reflectance (ATR) device was selected: a ZnSe Prism Liquid Cell (Harrick) with a horizontal, single internal reflection cell as shown in Fig. 2.1-56.

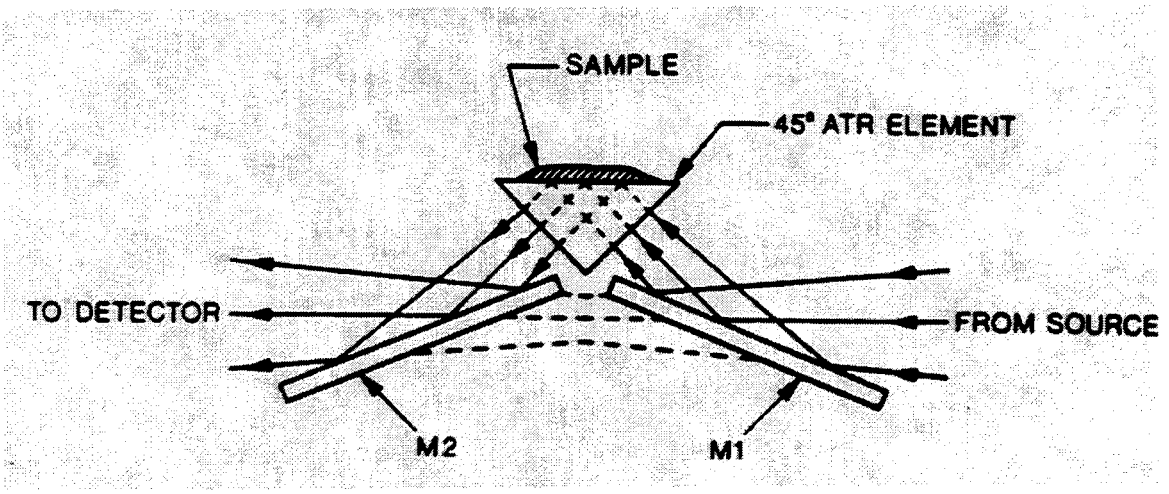

Figure 2.1-56. ZnSe 45° prism liquid cell (Harrick, 1996).

Thin pieces of mica were placed on the prism with a tweezers and a pressure plate was applied by the use of a clamp attached to a dowel pin. The clamping screw was hand-turned to secure the pressure plate as shown in Fig. 2.1-57.

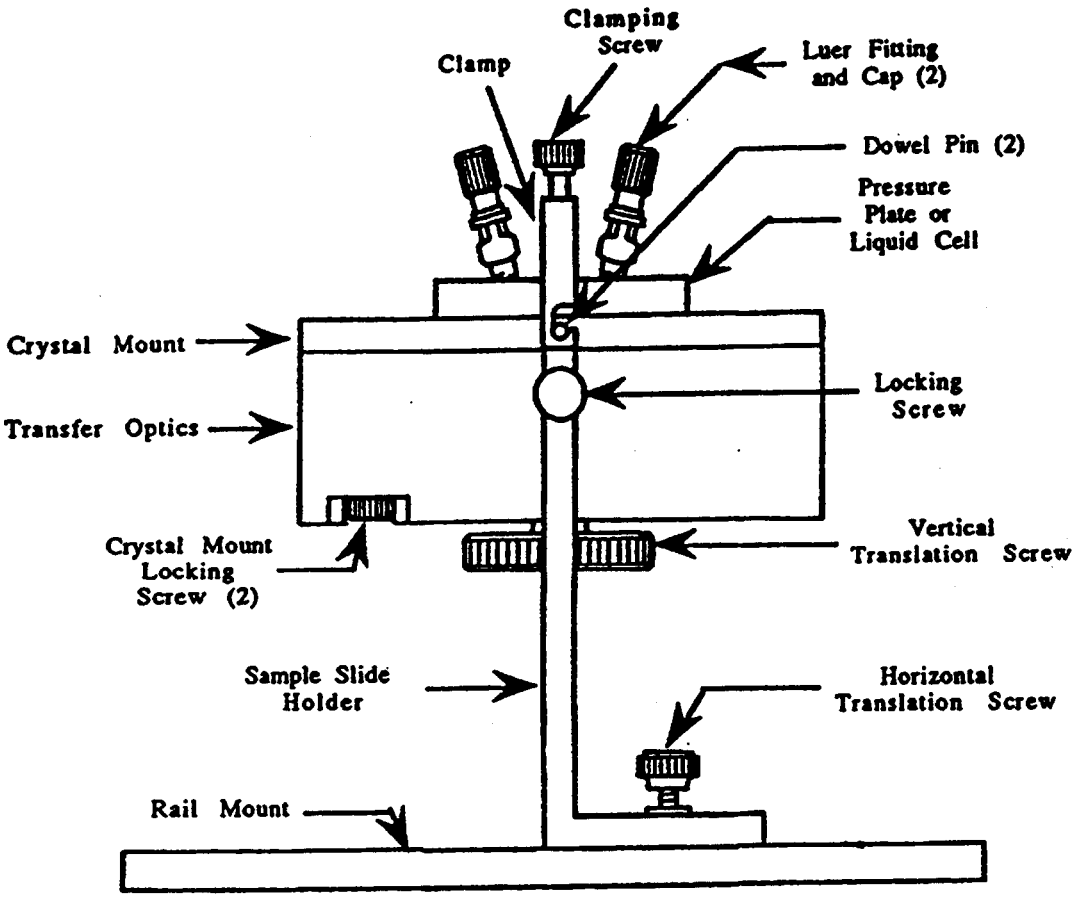

Figure 2.1-57. Single reflection prism cell (Harrick, 1996).

Spectra were recorded in the percent transmittance mode from 4000 cm^{-1} to 550 cm^{-1} with a Perkin Elmer 1710 FTIR. For liquid samples, including crude oil, 50 scans were acquired at a resolution of 4 cm^{-1}. Scans at a resolution of 1 cm^{-1} were acquired for the samples of mica (200 scans) and clay (100 scans) with adsorbed crude oil components. A background spectrum was run with the ATR prism before each run with the aged mica or clay.

Crude oils:

Six crude oils were used in this study; they include A-93, A-95, Moutray, Mars, SQ-95, and CS crude oils. Their composition and properties are shown in Table 2.1-28. Liquid crude oil was applied directly to the ATR prism and covered with a glass cover slip.

Table 2.1-28. Crude oil composition and physical properties

	A-93	A-95	Moutray	CS	Mars	SQ-95
Physical Properties						
Base number (mgKOH/g oil)	2.42	2.20	0.81	1.16	1.79	0.24
Acid number(mgKOH/g oil)	0.14	0.24	0.55	0.33	0.37	0.45
Base number/Acid number	17.3	9.17	1.47	3.5	4.9	0.53
Asphaltene ppt (wt%) n-C_5	10.9	5.00	1.79	1.38	3.25	2.90
Asphaltene ppt (wt%) n-C_7	7.10		0.95	0.48	1.86	
Atomic Ratios from Elemental Analysis *						SQ-94
H/C	1.671		1.803	1.742	1.635	1.813
O/C	0.004		0.006	0.004	0.003	0.009
N/C	0.003		0.002	0.004	0.002	0.001
S/C	0.004		0.002	0.002	0.009	0.004
wt % (O+N+S)	1.74		1.37	1.30	2.57	2.02

* Measured by Huffman Laboratories, Inc.

Brine:

All water was doubled distilled using a Mega-Pure water system and a Milli-Q water purification system. All brine used in this experiment was at concentration of 0.01M NaCl. HCl was added to the brine until reaching pH 4.

Adsorption on mica:

Dry muscovite mica, was cleaved and aged in brine of pH 4, 0.01 M NaCl from two to 24 hours. The brine-treated mica was aged in crude oil for three to 110 days. Bulk crude oil was removed by rinsing with toluene. Then the aged mica was placed directly on the ATR prism.

Adsorption on clay:

The clay was obtained from and characterized by George Austin of the New Mexico Bureau of Mines. XRD analysis of fractions of sizes less than two microns revealed 30% chlorite, 30% illite, 20% illite/smectite, 20% kaolinite, with a trace amount of smectite. XRD spectra are available elsewhere (Von Drasek, 1999). Non-clay particles included mostly dolomite, with some quartz and calcite, and only a small amount of feldspar.

The clay was ground with a mortar and pestle, then soaked in NaCl brine of pH 4 and concentration of 0.01M for two days. The clay/brine mixture was placed in vials, centrifuged for three minutes and aged in crude oil for 4-5 days. After aging, the clay mixture was centrifuged with cyclohexane to remove bulk crude oil. The process was repeated until the liquid was clear (approximately five to six times). Next the clay in the vials was spread on mica mounts and placed in covered glass jars for drying at room temperature. After drying, the clay side was placed directly on the ATR prism and clamped down with the pressure plate. The IR was purged with nitrogen gas to eliminate atmospheric carbon dioxide and water.

FTIR results

Crude oils:

Six crude oils were analyzed by the ATR method. A-93 and A-95 are Alaskan crude oils obtained from Prudhoe Bay. Moutray crude oil is from West Texas. Mars crude oil was obtained from the Gulf of Mexico region. SQ-95 is Sulimar Queen crude oil from Southeastern New Mexico. The geographic origin of CS crude oil is not available. Representative full spectra of the six crude oils are shown in Figs. 2.1-58 through 2.1-63. The main characteristic of all of the crude oil spectra is the dominance of intense CH stretching peaks found at 3000-2800 cm^{-1}. The next most prominent peaks included CH bending vibrations from aliphatic groups in the

crude oil found at 1459-1458 cm^{-1} and at 1378-1377 cm^{-1}. A doublet of aromatic and aliphatic bending motions was found at 745-742 cm^{-1} and 728-722 cm^{-1}, respectively. Similar features and assignments have been reported in many other FTIR examinations of crude oils and their derivatives (e.g., Funk *et. al.*, 1995; McLean and Kilpatrick, 1997).

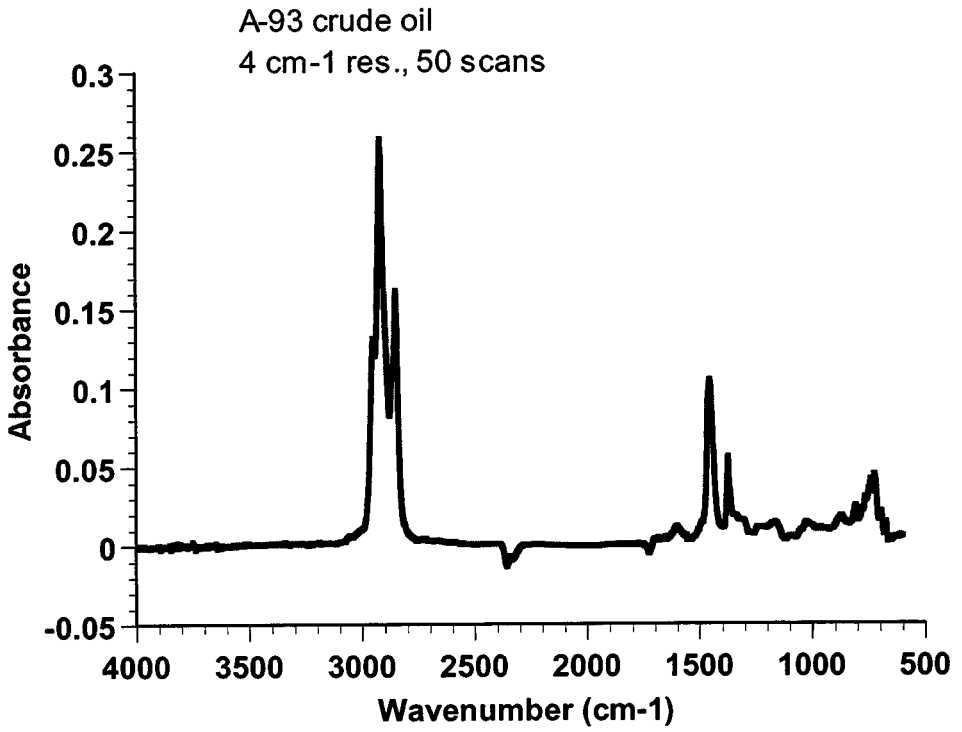

Figure 2.1-58. ATR spectrum of A-93 crude oil showing aliphatic CH stretching between 2953-2853 cm^{-1} with aliphatic CH bending at 1458 cm^{-1} and 1377 cm^{-1}.

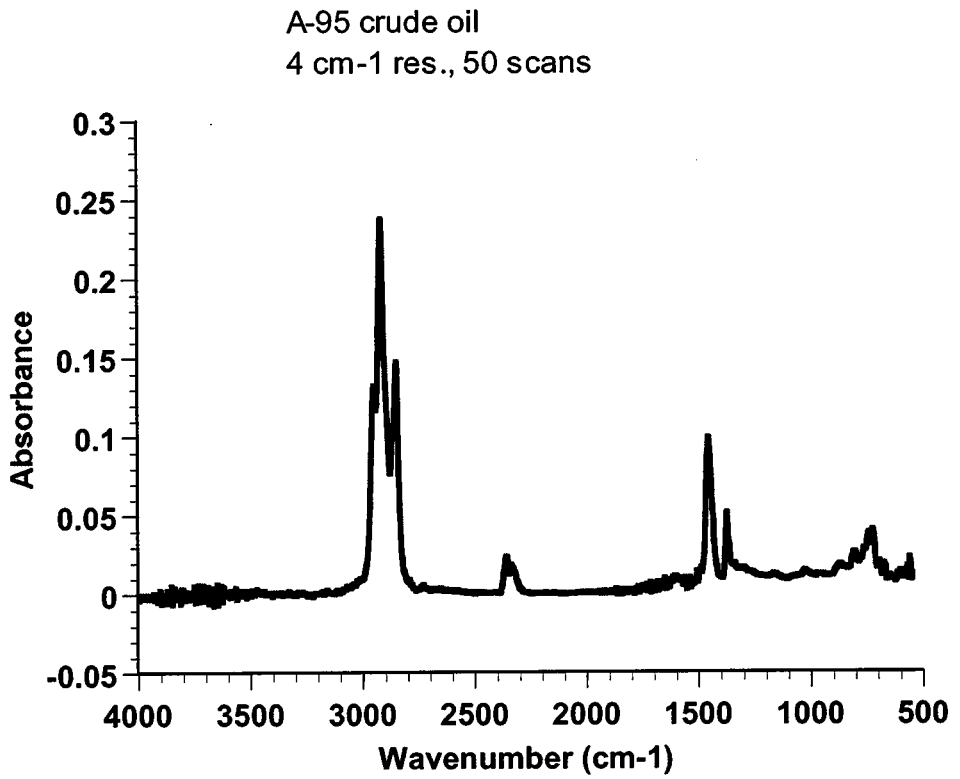

Figure 2.1-59. ATR spectrum of A-95 crude oil showing aliphatic CH stretching between2954-2853 cm^{-1} with aliphatic CH bending at 1459 cm^{-1} and 1377 cm^{-1}.

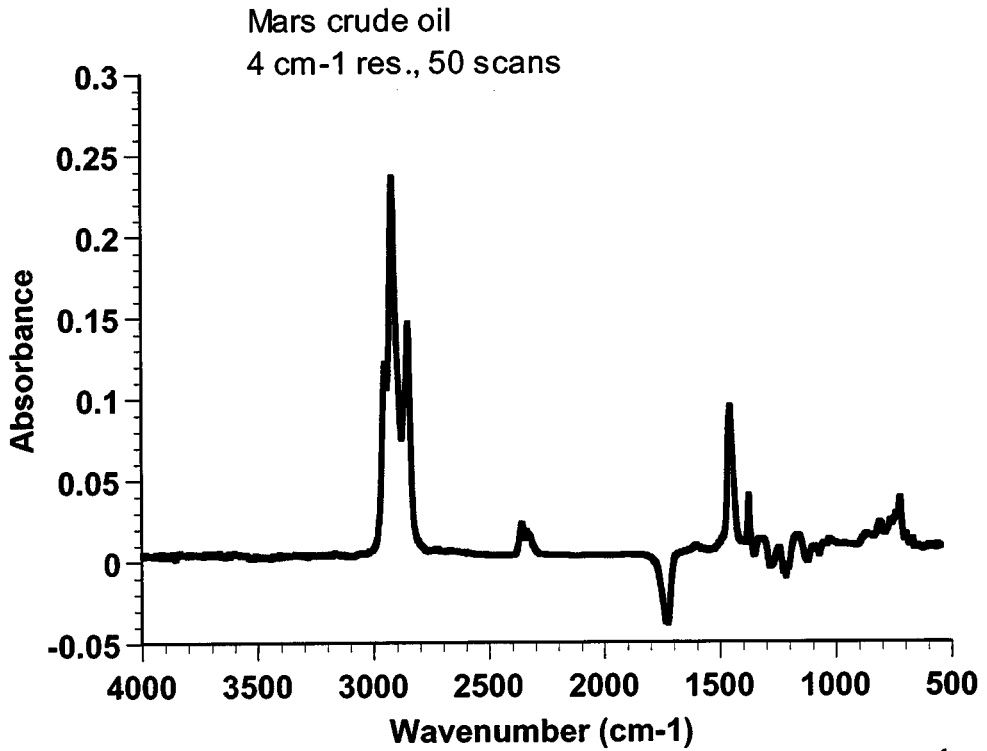

Figure 2.1-60. ATR spectrum of Mars crude oil showing CH stretching between 2953-2853 cm^{-1} with CH bending at 1458 cm^{-1} and at 1378 cm^{-1}.

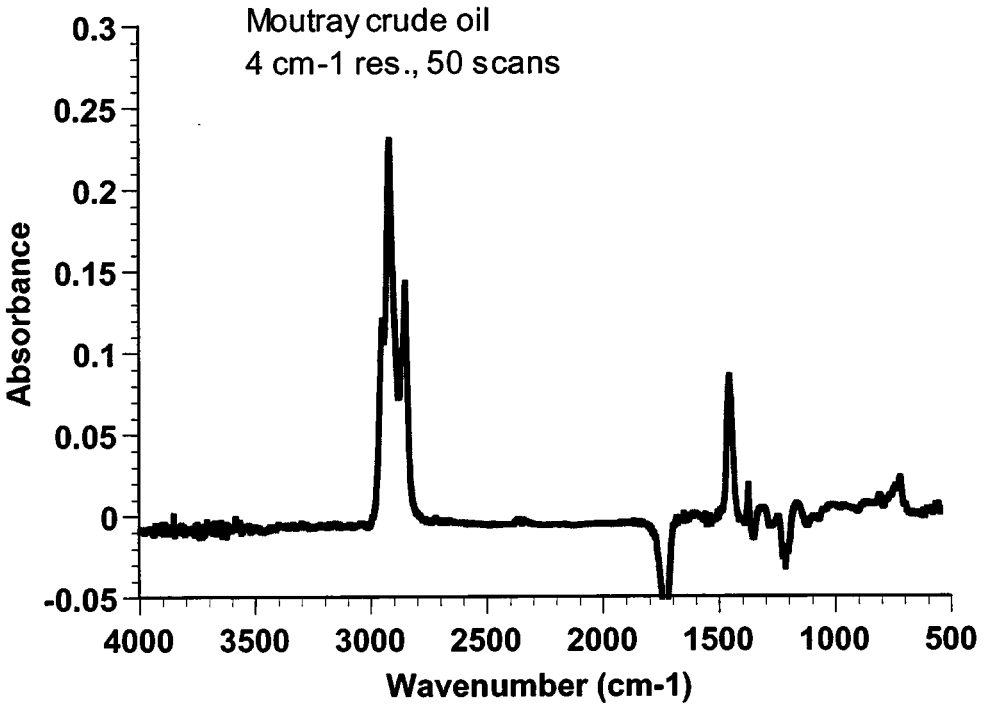

Figure 2.1-61. ATR spectrum of Moutray crude oil showing aliphatic CH stretching between 2953-2853 cm^{-1} with aliphatic CH bending at 1459 cm^{-1} and 1377 cm^{-1}.

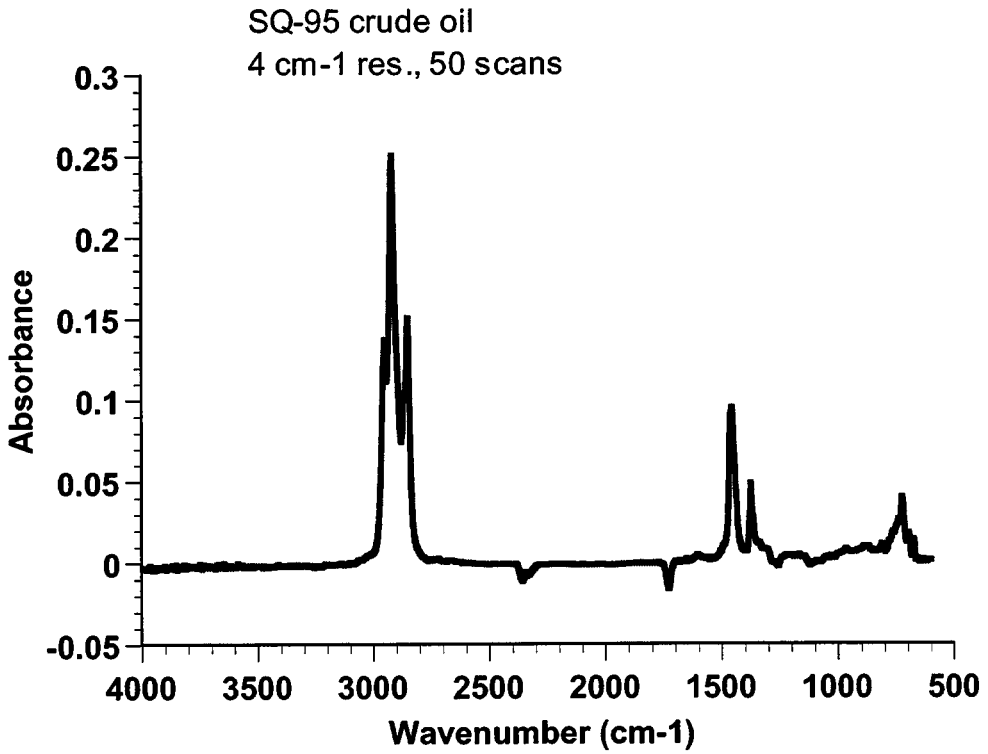

Figure 2.1-62. ATR spectrum of SQ-95 crude oil showing aliphatic CH stretching between 2955-2854 cm^{-1} with aliphatic CH bending at 1459 cm^{-1} and 1377 cm^{-1}.

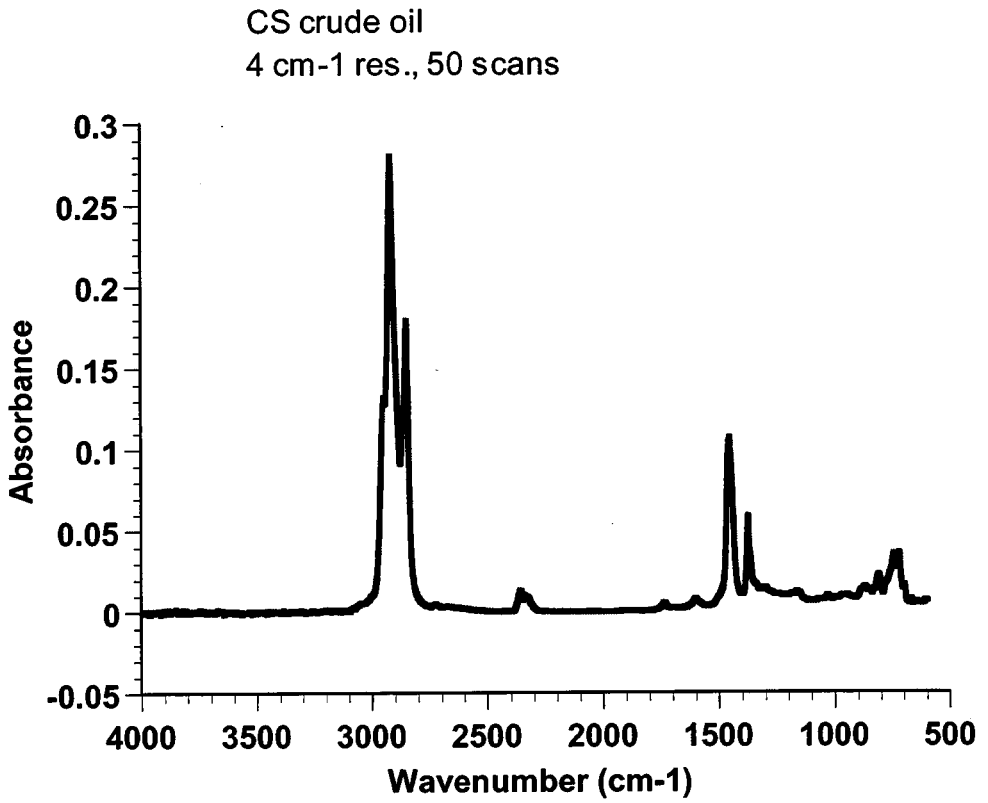

Figure 2.1-63. ATR spectrum of CS crude oil showing aliphatic CH stretching between 2952-2853 cm^{-1} with aliphatic CH bending at 1458 and at 1377 cm^{-1}.

Functional group assignments for crude oils. Functional group assignments for crude oils are shown in Fig. 2.1-64. Aromatic CH stretching is found at wavenumbers 3100-3000 cm^{-1}, while aromatic CH out-of-plane bending is from 900-600 cm^{-1} and aromatic C=C stretching is observed at 1600 cm^{-1}, as found in previous studies (Czarneka and Gillot, 1980; Funk *et. al.*, 1995; McLean and Kilpatrick, 1997). Aliphatic CH stretching is between 3000-2800 cm^{-1} and CH bending is between 1500-1350 cm^{-1}. OH stretching is above 3000 cm^{-1} (Moschopedis and Speight, 1976). Carbonyl C=O stretching is observed from 1900-1600 cm^{-1} (McKay *et. al.*, 1978). C-O and C-N stretching are located between 1300-900 cm^{-1}, with S=O stretching between 1100-1000 cm^{-1}; these peaks are coupled and their vibrations cannot be distinguished from one another.

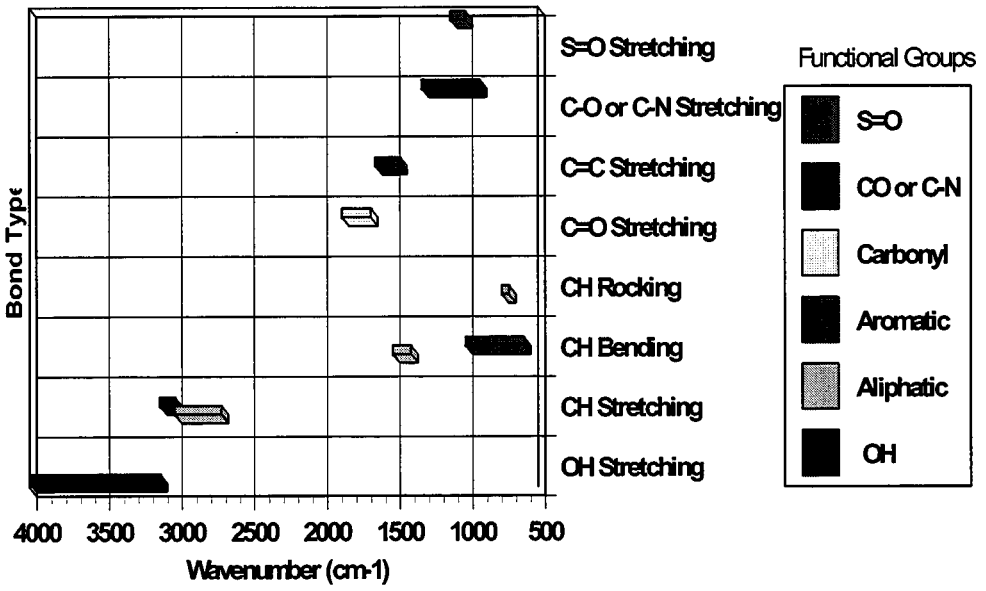

Figure 2.1-64. Functional group assignment of crude oils includes aromatic groups, which are designated by red bars. Aliphatic groups are green, OH stretching is blue, carbonyl C=O stretching is yellow, C-O and C-N are purple, and S=O is orange.

Reproducibility of the ATR-FTIR spectra. Crude oils are complex mixtures; samples taken from a single source can vary in composition. This could be a source of variability, especially in light of the very small volumes examined using the ATR technique. In order to establish the reproducibility both of sampling and the ATR-FTIR technique, five spectra of A-95 crude oil were compared. A summary of peak assignments is given in Table 2.1-29.

Only minor differences were observed among these five samples (Fig. 2.1-65). Differences in peak height between 2360-2340 cm^{-1} for CO_2 stretching reflect changes in atmospheric conditions. Other discrepancies include small peaks at 1736 cm^{-1} indicative of C=O stretching (observed in only one of the five samples) C-O-H bending at 1339 to 1341 cm^{-1} that appeared in two spectra, C-O or S=O bonds from 963-970 cm^{-1}, and 1030-1033 cm^{-1} denoting stretching. The latter were absent from one of the spectra. In all cases, the peaks involved were small. Other peaks matched well both in wavelength and absorbance.

Table 2.1-29. Peak assignment of A-95 crude oil (cm^{-1})

Assignment	Sample Number				
	Af2	Af3	Af4	Af5	Af6
CH_3 stretching, aliphatic	2954	2953	2954	2954	2953
CH_2 stretching (asymmetric), aliphatic	2922	2922	2922	2922	2922
CH_2 stretching (symmetric), aliphatic	2854	2853	2854	2853	2853
C=O stretching			1736		
C=C ring stretching, aromatic	1605	1605	1604	1606	1606
CH_3 bending (asymmetric), aliphatic	1459	1459	1459	1457	1458
CH_3 bending (symmetric), aliphatic	1377	1377	1377	1377	1377
C-O-H bending			1341	1339	
C-O stretching	1308	1309	1311	1306	1307
C-O stretching	1171	1170	1170	1169	1169
C-O or S=O stretching		1030	1032	1033	1032
C-O stretching		964	964	970	963
CH out of plane bending, aromatic	872	871	872	871	872
CH out of plane bending, aromatic	812	810	811	811	812
CH out of plane bending, aromatic	781	782	781	782	782
CH out of plane bending, aromatic	767	766	767	767	767
Doublet: CH out of plane bending, aromatic	743	743	743	742	743
Doublet: CH_2 rocking, aliphatic	728	728	725	728	728
CH out of plane bending, aromatic	698	698	697	698	698
CH out of plane bending, aromatic	676	676	676	675	676

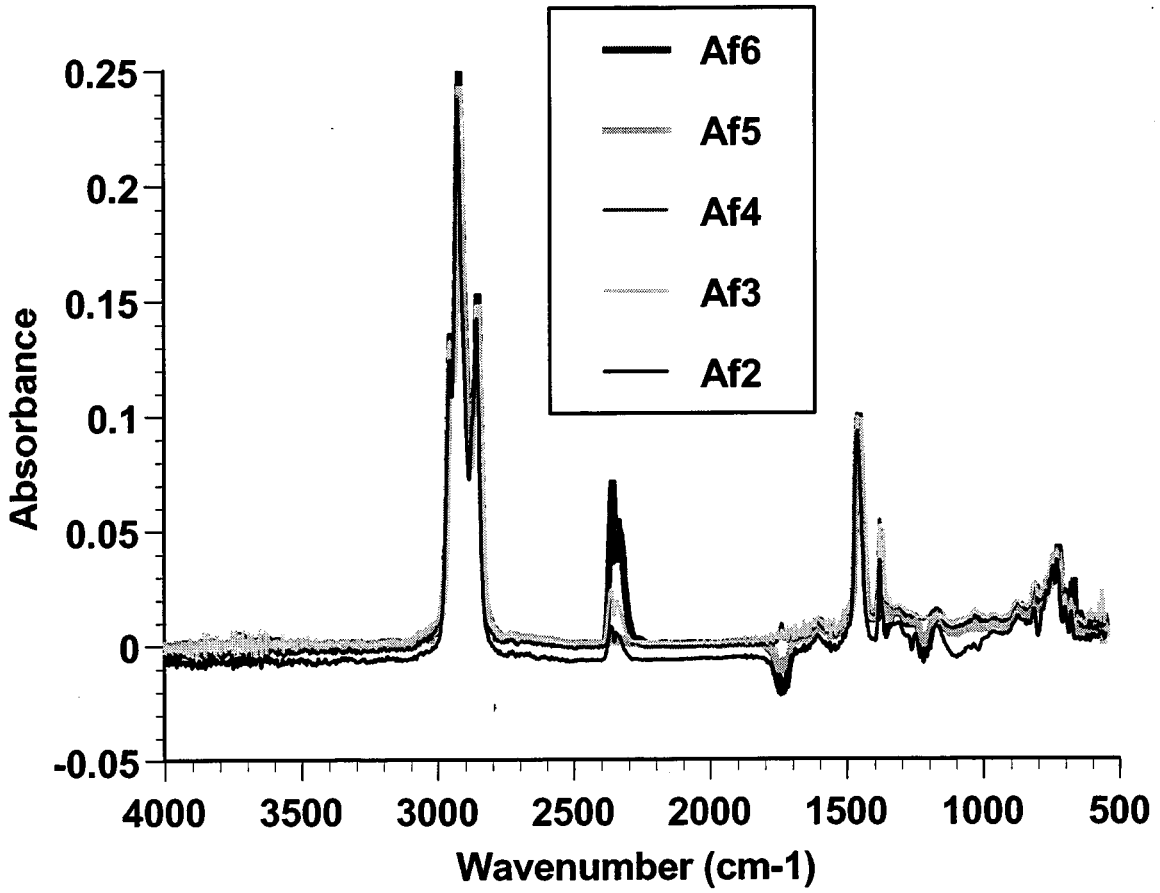

Figure 2.1-65. Five spectra of A-95 crude oil showing similar peak intensities and wavenumbers indicating crude oil reproducibility with the use of ATR-FTIR. Aliphatic CH stretching was between 2954-2853 cm^{-1} with aliphatic CH bending from 1459-1457 cm^{-1} and at 1377 cm^{-1}. (4cm^{-1} resolution, 50 scans)

Comparisons among different crude oils. Somewhat more diversity was found when the spectra of six different crude oils (A-93, A-95, Moutray, Mars, SQ-95, and CS) were compared, although assignments were generally similar. A summary of peak assignments is given in Table 2.1-30.

Table 2.1-30. Peak assignment of six crude oils (cm^{-1})

Figure	Assignment	A-93	A-95	Mars	Moutray	SQ	CS
2.1-66	CH_3 stretching, aliphatic	2953	2954	2953	2953	2955	2952
	CH_2 stretching (asymmetric), aliphatic	2922	2922	2922	2922	2922	2921
	CH_2 stretching (symmetric), aliphatic	2853	2853	2853	2853	2854	2853
2.1-67	C=O stretching	1736	1736				1737
	C=C ring stretching, aromatic	1605	1606	1608	1606	1606	1604
2.1-68	CH_3 bending (asymmetric), aliphatic	1458	1459	1458	1459	1459	1458
	CH_3 bending (symmetric), aliphatic	1377	1377	1378	1377	1377	1377
	C-O-H bending	1342	1340			1342	
	C-O, C-N stretching			1317	1311		1310
	C-O, C-N stretching	1305	1306		1303		1303
	C-O, C-N stretching	1169	1169	1170	1168	1170	1168
	C-O, C-N, or S=O stretching			1097			
	C-O, C-N, or S=O stretching			1088			
	C-O, C-N, or S=O stretching			1055			
	C-O or S=O stretching	1031	1032	1032	1032	1032	1033
	C-O, C-N stretching	965	965		967	966	
2.1-69	CH out of plane bending, aromatic	872	872	870	871	871	871
	CH out of plane bending, aromatic	811	811	813	813	813	813
	CH out of plane bending, aromatic	782	782		781	782	782
	CH out of plane bending, aromatic	767	767	767	766	767	
	Doublet: CH out of plane bending, aromatic	743	743	742	743	743	745
	Doublet: CH_2 rocking, aliphatic	728	727	724	723	727	722
	CH out of plane bending, aromatic	698	698	698	700	698	700
	CH out of plane bending, aromatic	676	676	676	675	675	
	CH out of plane bending, aromatic				669		669

More detailed comparisons can be seen in the following figures. The aliphatic CH stretching region between 3000-2800 cm^{-1} was very similar for all six crude oils, as shown in Fig. 2.1-66.

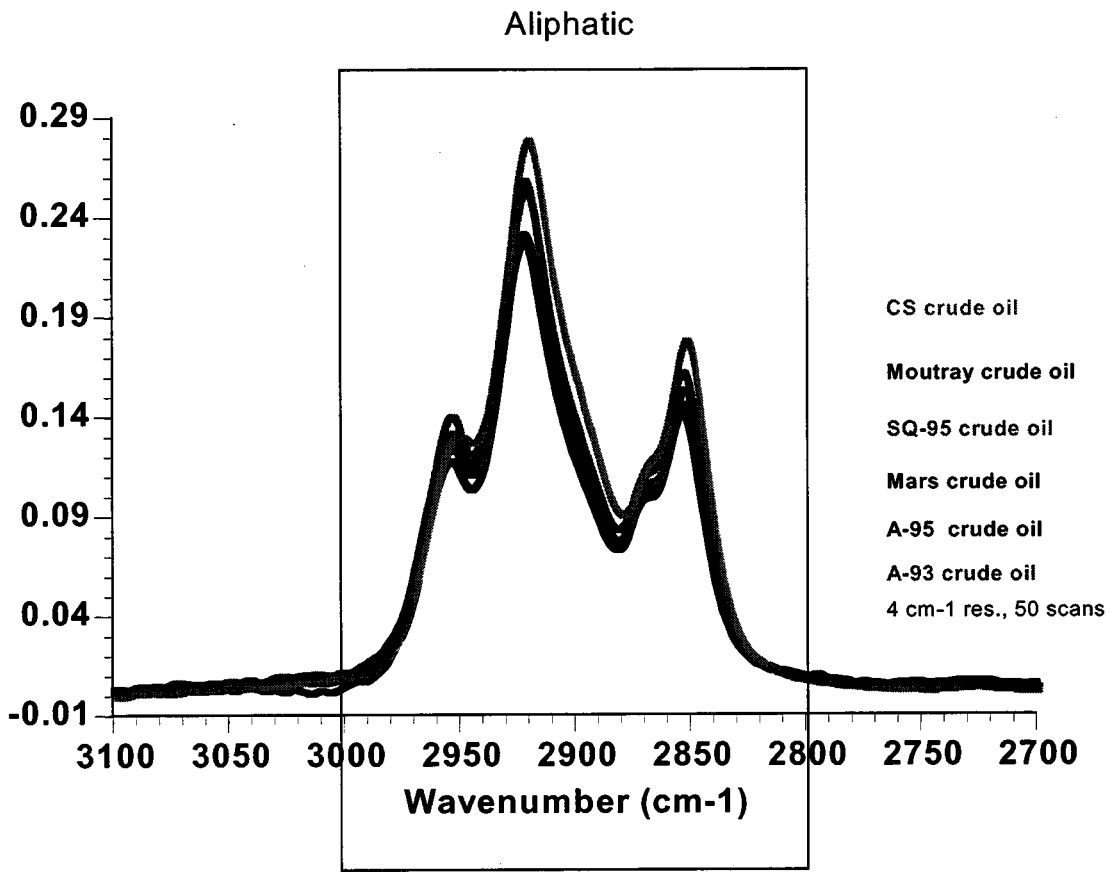

Figure 2.1-66. Crude oil similarities showing aliphatic CH_3 from 2955-2952 cm^{-1}, asymmetric aliphatic CH_2 stretching from 2922-2921 cm^{-1}, and symmetric aliphatic CH_2 from 2854-2853 cm^{-1}.

Carbonyl C=O stretching vibrations were found at 1736 cm^{-1} for A-93, A-95 (one of five samples), and CS crude oil (Fig. 2.1-67). Aromatic C=C ring stretching was evident at 1608-1604 cm^{-1} for all of the crude oils tested.

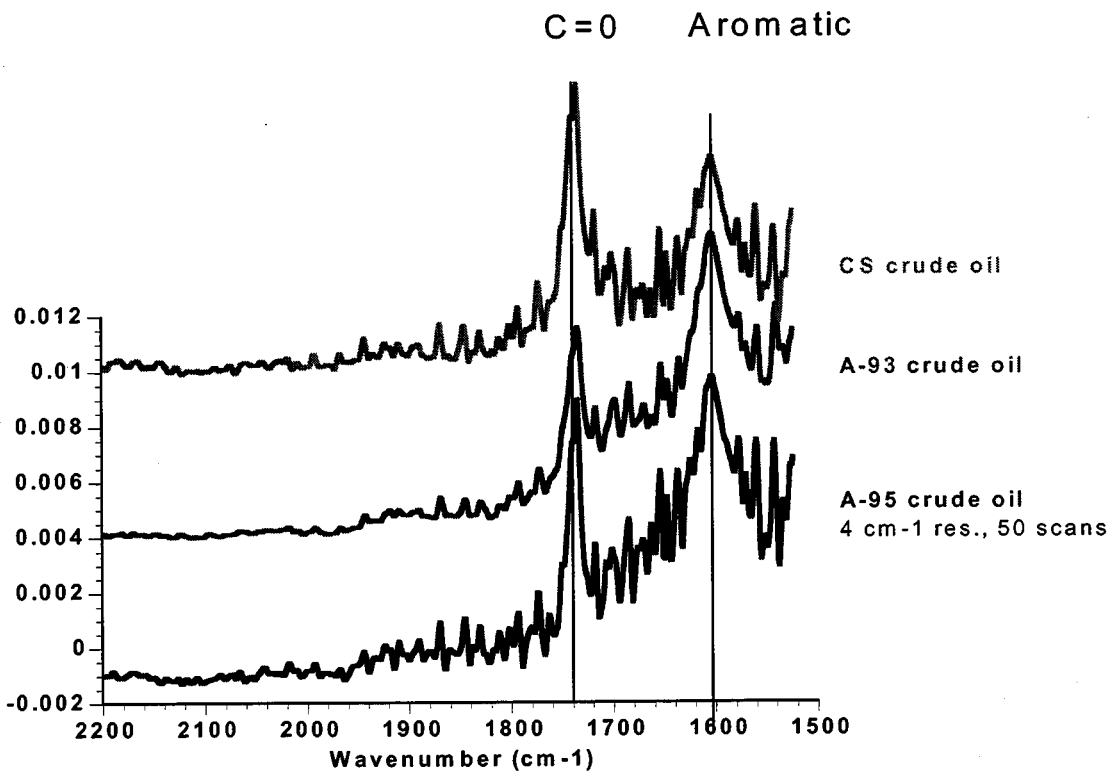

Figure 2.1-67. Carbonyl C=O stretching and aromatic C=C stretching for CS, A-93, and A-95 crude oils. The figure shows relative absorbance.

Band shapes between 1350-1000 cm^{-1} were distinctive, especially for Mars crude oil (Fig. 2.1-68). The region between 1300 and 900 cm^{-1} includes C-O or C-N and S=O stretching. There were C-O or S=O vibrations at 1034-1030 cm^{-1} for A-93, A-95, Mars, and CS crude oils. C-O stretching at 969-966 cm^{-1} was distinctive for Moutray and SQ-95 crude oils.

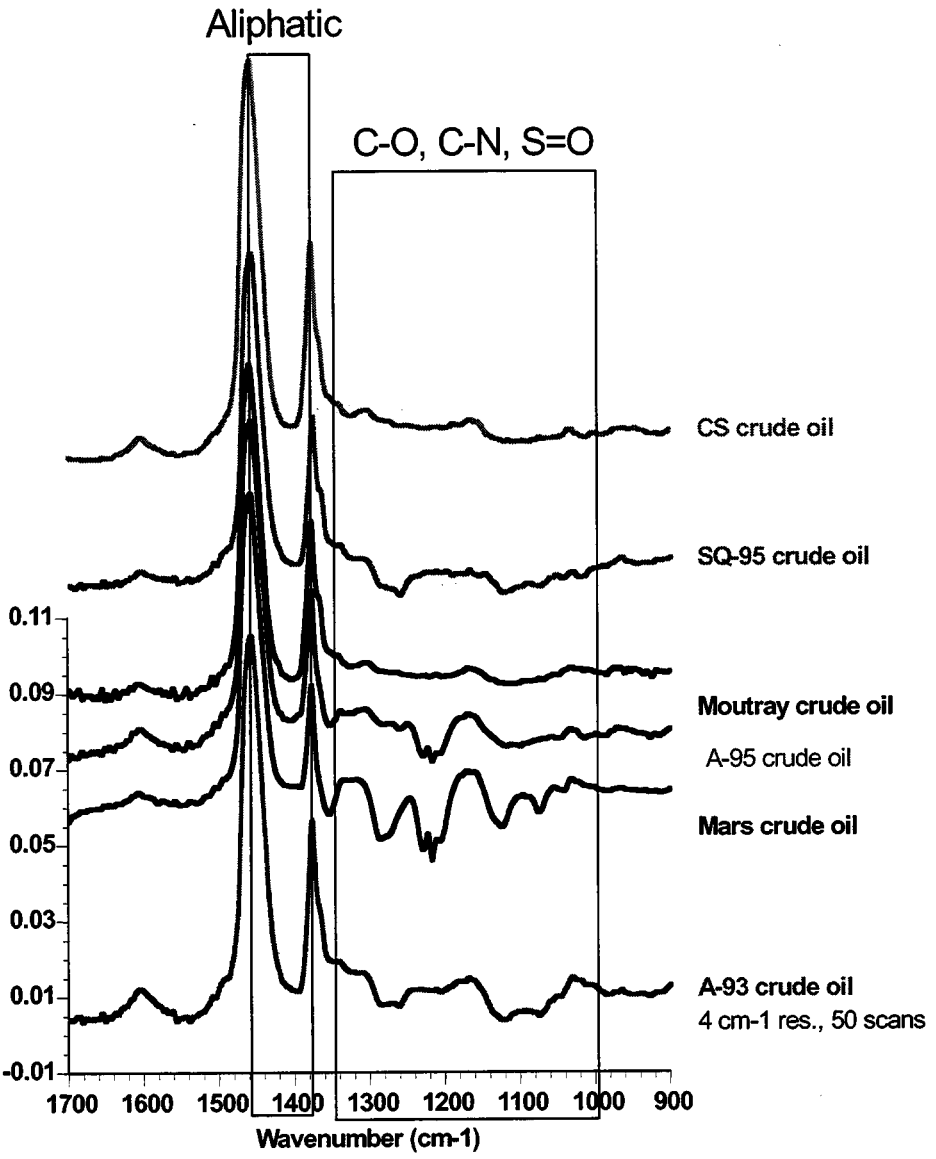

Figure 2.1-68. Aliphatic CH bending and C-O, C-N, and S=O stretching spectrum of CS, SQ-95, Moutray, A-93, A-95, and Mars Crude Oils. The figure shows relative absorbance.

Coupling of aromatic and aliphatic groups produce a doublet peak at 745-742 cm^{-1} and 728-722 cm^{-1}, respectively (Fig. 2.1-69). C-H out-of-plane bending vibrations were expected at 900-600 cm^{-1}, and there were definite peak vibrations found in the six crude oils tested at 872-870 cm^{-1}, 813-811 cm^{-1}, 782-781 cm^{-1}, 767-766 cm^{-1}, 700-698 cm^{-1}, and 676-675 cm^{-1}.

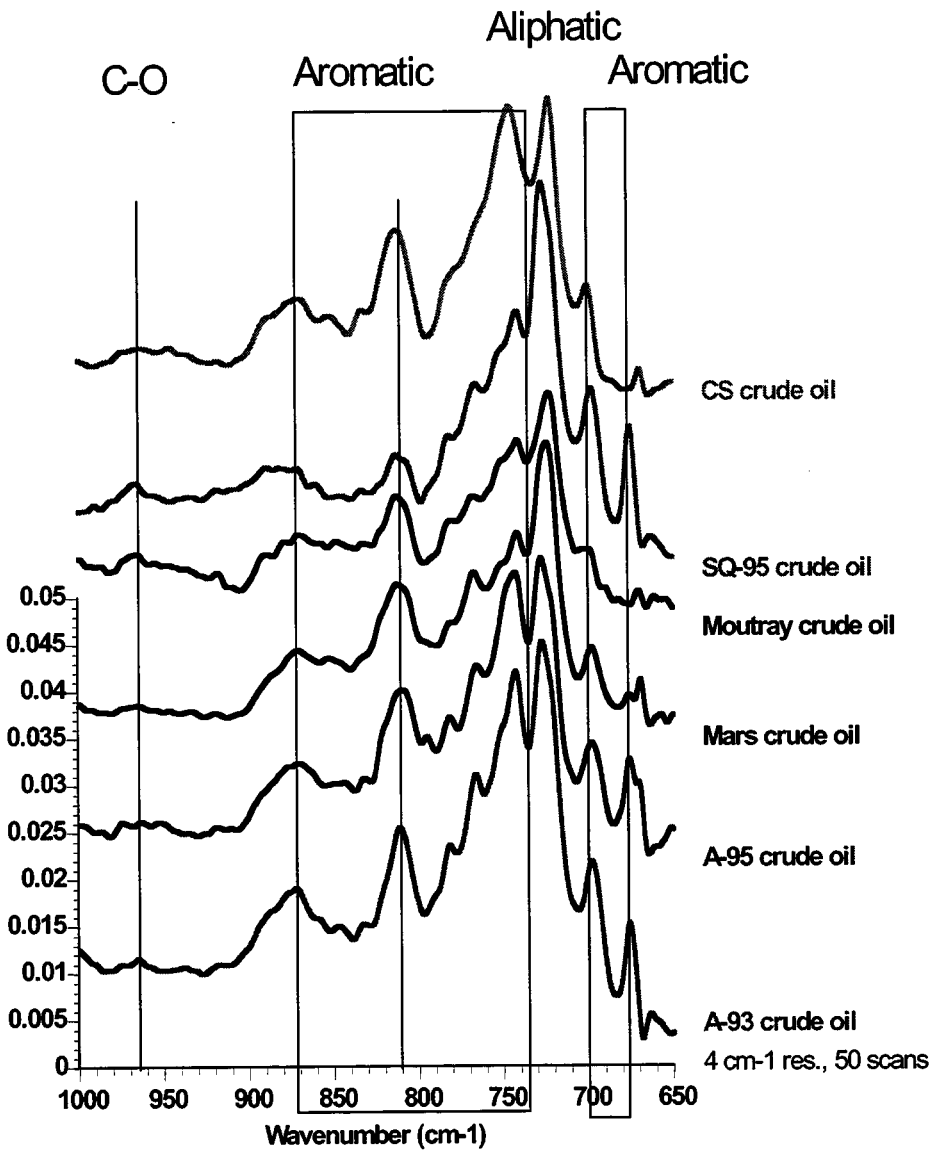

Figure 2.1-69. A doublet of aromatic and aliphatic bending motions were noted at 745-742 cm^{-1} and at 728-722 cm^{-1} respectively for CS, SQ-95, Moutray, Mars, A-93, and A-95 crude oils. Other aromatic bending vibrations observed from 900-600 cm^{-1} are also shown. Figure shows relative absorbance.

Mineral substrates:

Muscovite mica and clay powder were the minerals used as substrates in this study. XRD spectra of the clay powder are available (Von Drasek, 1999).

Mica. Si-OH stretching of muscovite mica was observed from 3700 to 3600 cm^{-1}. Si-O stretching occurs between 1100 and 600 cm^{-1}. Peak assignments are summarized in Table 2.1-31 for the spectrum shown in Fig. 2.1-70.

Table 2.1-31. Peak assignment of mica (cm^{-1})

Assignment	Wavenumbers (cm^{-1})
Si-OH stretching	3700-3600
Si-O stretching	1100-600

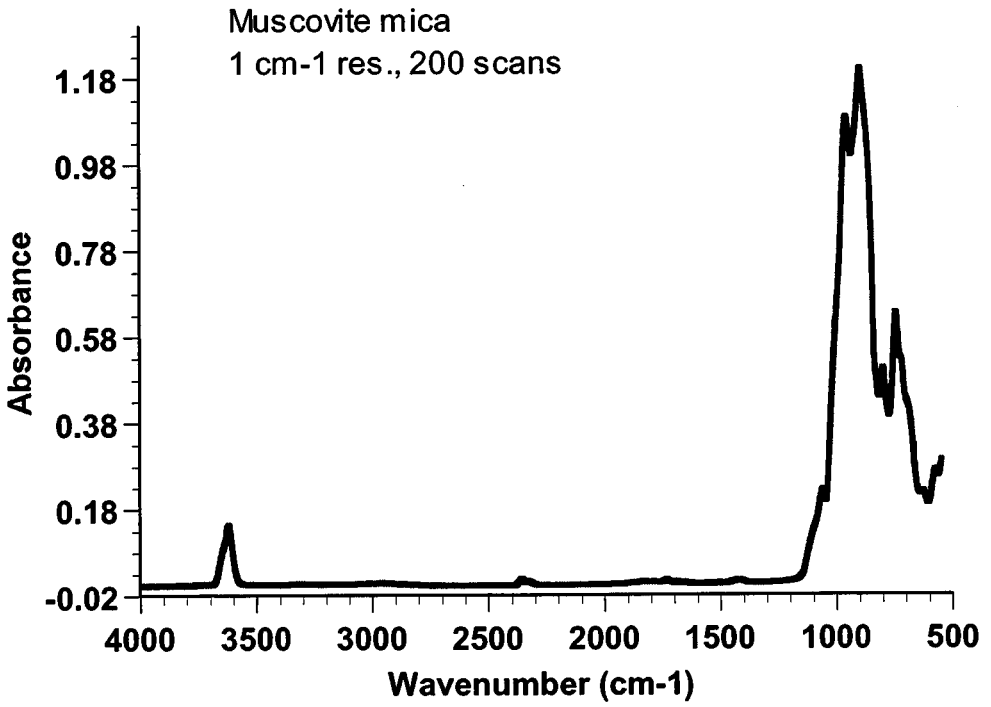

Figure 2.1-70. This ATR spectrum of mica shows intense vibrations between 1100 cm^{-1} and 600 cm^{-1}.

We attempted to subtract the mica spectrum from spectra of adsorbed material plus mica to enhance visibility of the adsorbed crude oil components. Significant error was introduced

with the subtraction process because of the degree of variability in the mica signal, which depended on the size, shape, and degree of contact of the mica with the ATR crystal. Without subtraction, the intensity and position of the mica Si-O stretching vibrations may have obscured polar adsorption peaks for crude oil between 1100 cm^{-1} and 600 cm^{-1}.

Clay. The spectrum of clay powder (Fig. 2.1-71) shows water adsorption (OH stretching between 3680-2950 cm^{-1}) and possible organic material in the clay (CH_3 bending at 1460 cm^{-1}). The clay powder showed intense vibrations of Si-O stretching at 1001 cm^{-1} and Si-OH bending at 874 cm^{-1}.

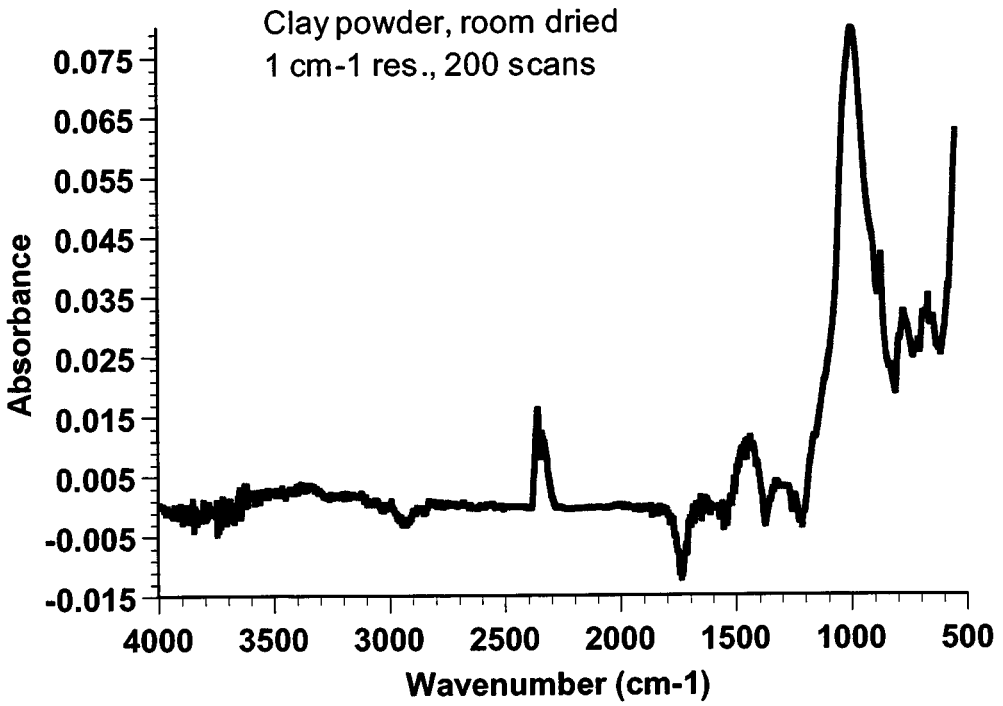

Figure 2.1-71. Untreated clay spectra showing possible organic contamination of hydrocarbons at 1460 cm^{-1}.

ATR-FTIR spectra of samples with adsorbed crude oil components:

Crude oil components adsorbed on both mica and clay were analyzed by the ATR-FTIR technique.

Adsorption on mica. Table 2.1-32 shows peak assignments for samples of mica that were treated first with NaCl solutions {pH4, 0.01M} and then with one of four crude oils (A-93, A-95, Moutray, and CS). Interference from Si-OH stretching between 3700 cm^{-1} and 3600 cm^{-1}, Si-O stretching between 1100 cm^{-1} and 600 cm^{-1}, and atmospheric CO_2 from 2400 cm^{-1} to 2300 cm^{-1} limited our interpretation in those regions. Peaks corresponding to adsorbed organic material are visible, but they are much weaker than the signal from the substrate. Fig. 2.1-72 for A-93 crude oil is typical.

Table 2.1-32. Peak assignment of crude oil adsorbed on brine-treated mica (cm^{-1})

Assignment	A-93	A-95	Moutray	CS
Si-OH stretching, mica	3620	3621	3628	3624
OH stretching, water			3590-2990	3590-2990
CH_3 stretching, aliphatic	2953		2952	2954
CH_2 stretching (asymmetric), aliphatic	2924	2922	2924	2923
CH_2 stretching (symmetric), aliphatic	2853	2851	2853	2851

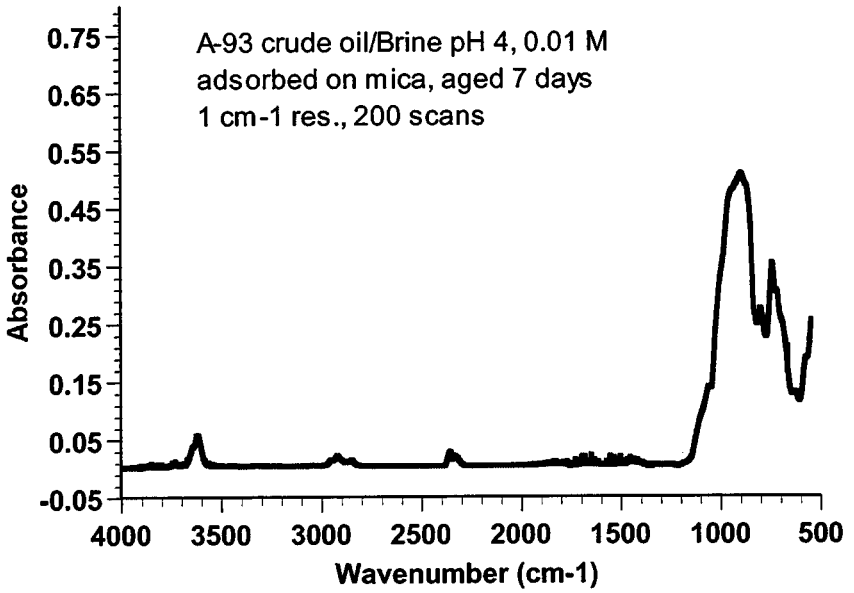

Figure 2.1-72. ATR-FTIR spectrum of A-93 crude oil adsorbed on mica.

Weak indications of adsorption of organic material (C-H stretching from 2960 cm^{-1} to 2850 cm^{-1}) are shown on an expanded scale in Fig. 2.1-73 for mica treated with A-93 crude oil and in Fig. 2.1-74 for A-95-treated mica. Similar expanded views of Moutray-treated mica (Fig. 2.1-75) and a CS-treated sample (Fig. 2.1-76) show a broad O-H stretch from 3590 cm^{-1} to 2990 cm^{-1}, indicating that some water remained on these surfaces, even after six days and three days aging in oil, respectively. Similar water signals were observed with samples aged in Moutray for 10 days and for 19 and 110-day aging periods in CS crude oil.

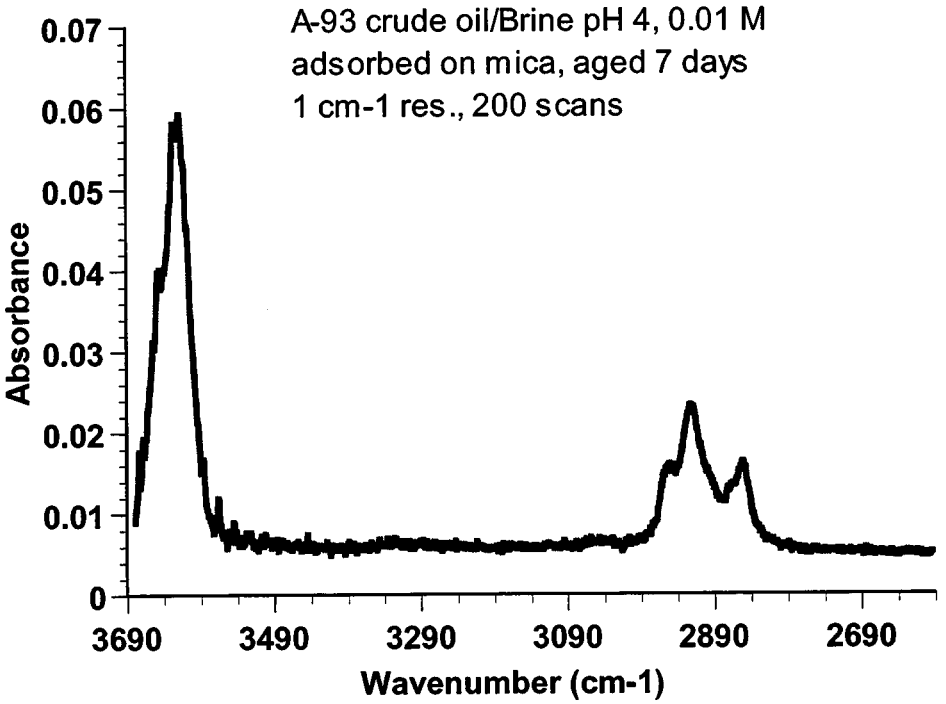

Figure 2.1-73. Expanded scale spectrum of material adsorbed from A-93 crude oil on mica.

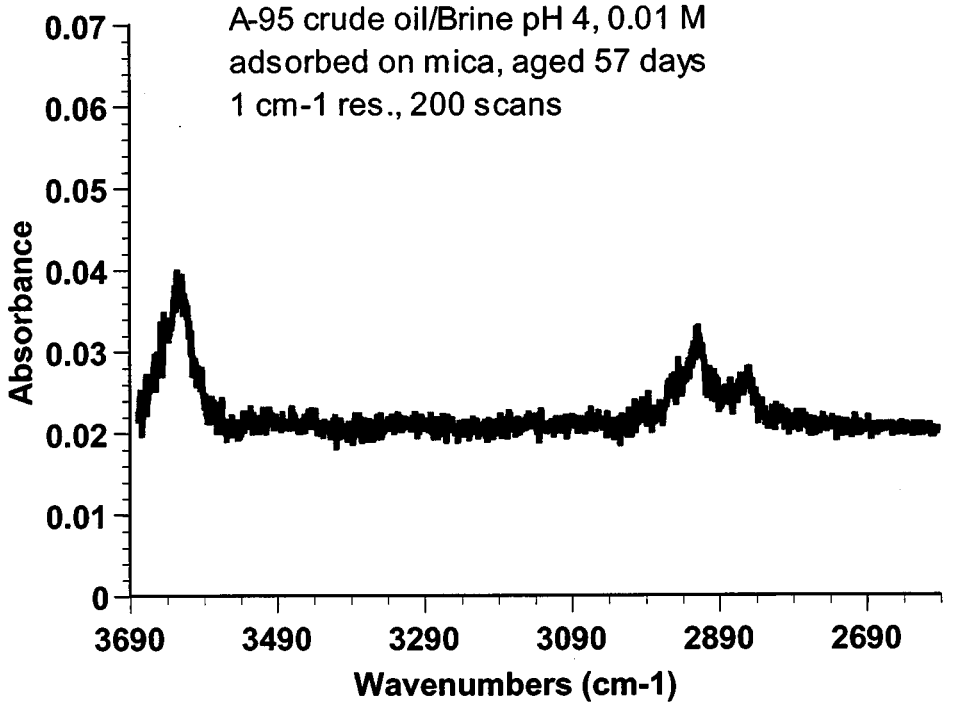

Figure 2.1-74. Expanded scale spectrum of material adsorbed from A-95 crude oil on mica.

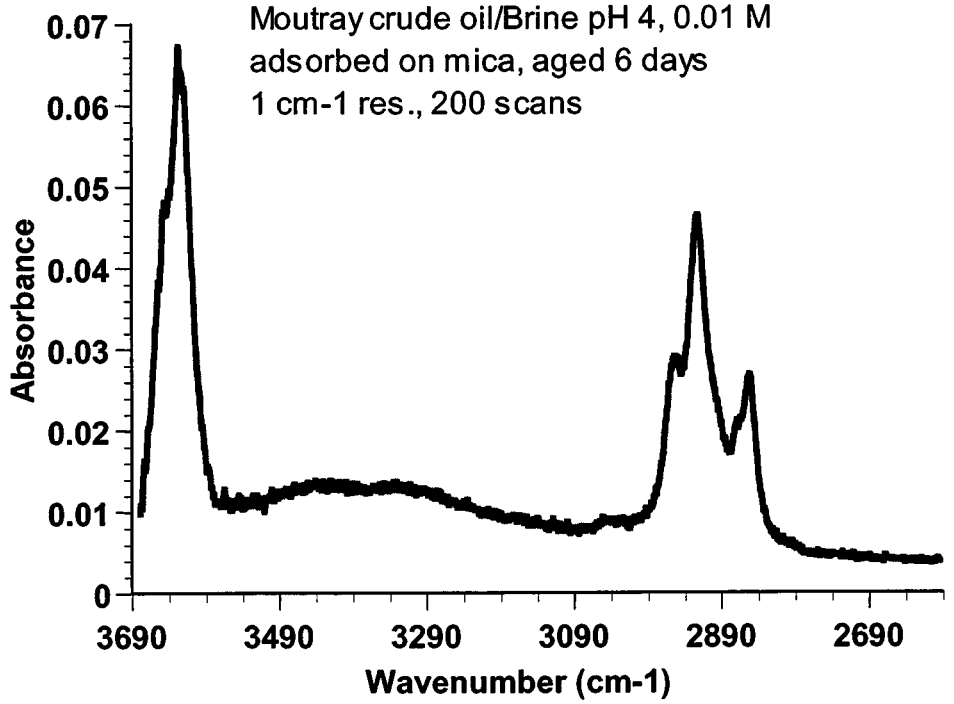

Figure 2.1-75. Expanded scale spectrum of material adsorbed from Moutray crude oil on mica.

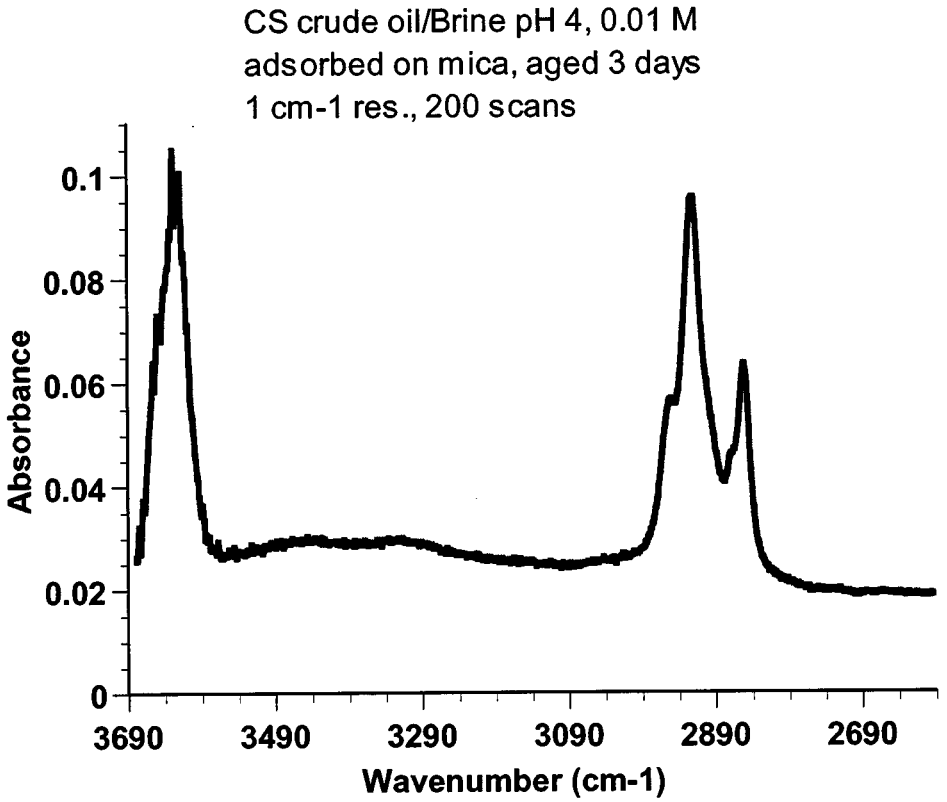

Figure 2.1-76. Expanded scale spectrum of material adsorbed from CS crude oil on mica.

Adsorption on clay. Clays provide increased surface area compared to mica. In order to enhance the signal of the adsorbed material over that of the substrate, brine-treated clay was exposed to A-95 crude oil. Fig. 2.1-77 shows a typical ATR-FTIR spectrum. Peak assignments are summarized in Table 2.1-33. A broad band of OH stretching between 3680-2950 cm^{-1} provides clear evidence of adsorbed water on the clay. The same sample, retested ten days later, showed no evidence of water.

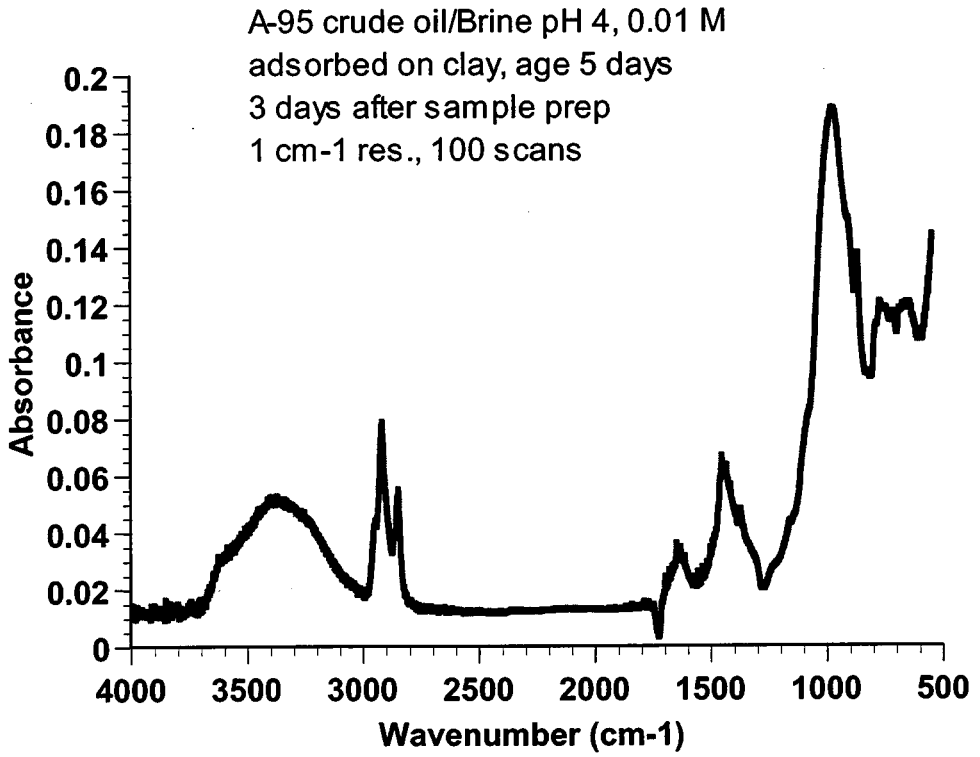

Figure 2.1-77. ATR-FTIR spectrum of material adsorbed from A-95 crude oil on clay. Peaks for water and organic material are clearly visible without expanding the scale.

Table 2.1-33. Peak assignment of crude oil adsorbed on brine-treated clay

Assignment	Clay	A-95
OH stretching, water		3680-2950
CH_3 stretching, aliphatic		2952-2950
CH_2 stretching (asymmetric), aliphatic		2924-2920
CH_2 stretching (symmetric), aliphatic		2852-2851
C=C ring stretching, aromatic		1636
CH_3 bending (asymmetric), aliphatic	1460	1457
Si-O stretching	1001	
Si-OH bending	874	

To summarize, crude oil spectra were dominated by CH stretching and bending vibrations from aliphatic groups. Mineral substrates had intense Si-O stretching vibrations between 1100 and 600 cm^{-1}. Adsorbed organic material on the mineral substrates gave a weak

signal due to interference from the strong substrate signal. CH stretching vibrations from aliphatic groups were identified adsorbing to both mica and clay. OH stretching from adsorbed water was also identified on both mica and clay.

Discussion of FTIR observations

The validity of the results obtained in this study can be demonstrated by comparison with published spectra and by checks of internal consistency. The lack of evidence for specific COBR interactions can be attributed mainly to weak IR signals and to difficulties with interpretation of important regions of the IR spectrum due to absorbance of the substrate and atmospheric contaminants. To the extent possible, the results are related to previous studies of COBR interactions with the same fluids and solid substrates. The presence of water on some surfaces and not others is an interesting feature of these results that may also be related to COBR interactions.

Validation of the ATR method:

To validate our use of the ATR method, spectra of known compounds were compared with published FTIR spectra. Figures 2.1-78 shows a published IR spectrum of toluene. The ATR spectrum in Fig. 2.1-79 compares well with respect to peak frequencies although the absorption is reduced.

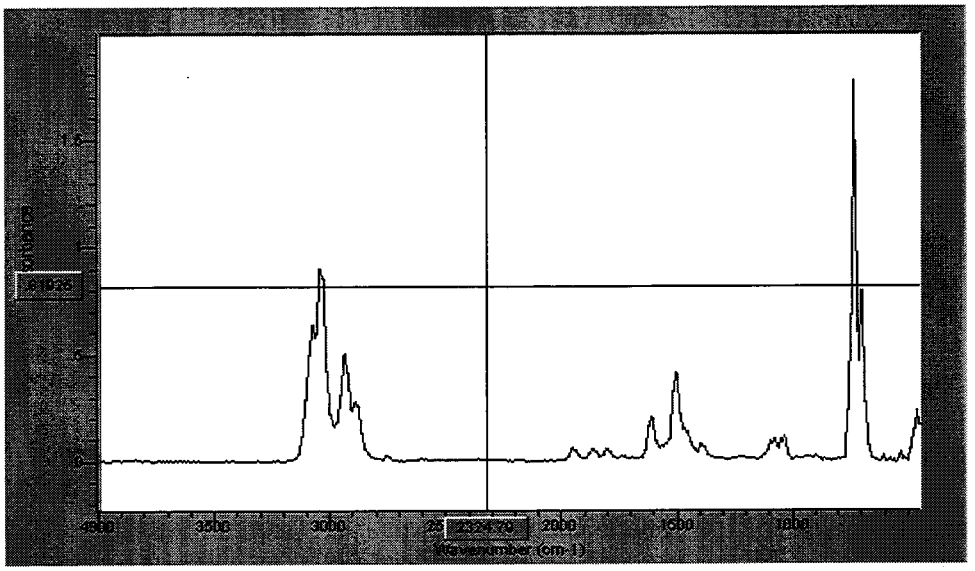

Figure 2.1-78. Published FTIR spectrum of toluene (Galactic Industries).

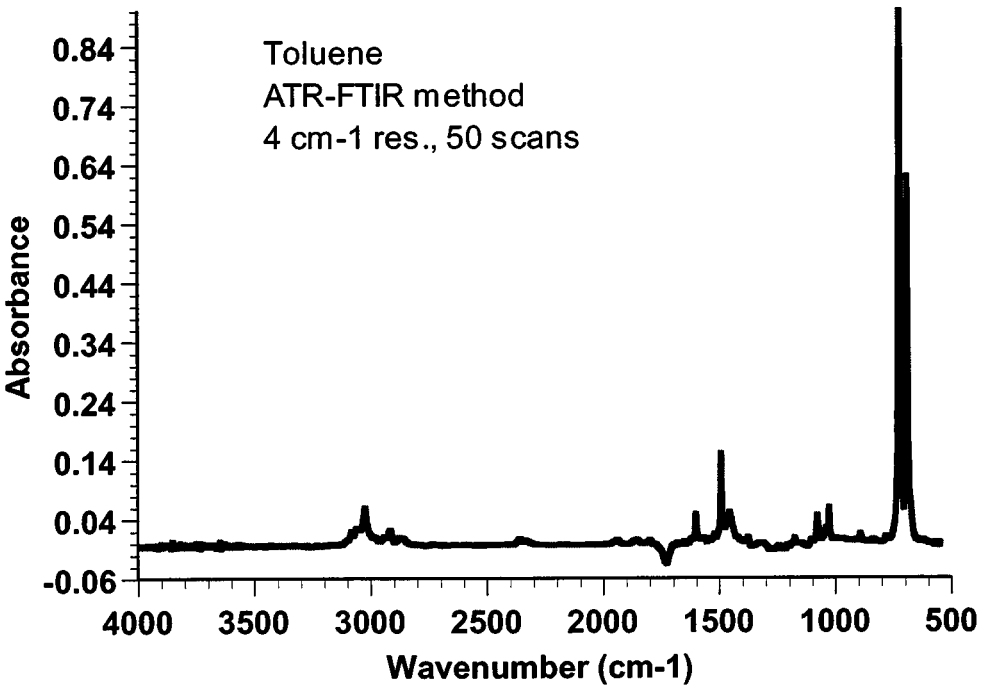

Figure 2.1-79. ATR spectrum of toluene.

A comparison between the FTIR spectra of A-95 crude oil produced using an NaCl plate and that obtained using the ZnSe ATR prism is shown in Fig. 2.1-80; details are highlighted in Fig. 2.1-81. Peak maxima were at nearly the same positions in the spectra from both techniques, as expected. Although the magnitude of absorbance obtained in the ATR spectra is reduced, there is nevertheless sufficient detail as shown at expanded scale in Figs. 2.1-80 and 2.1-81.

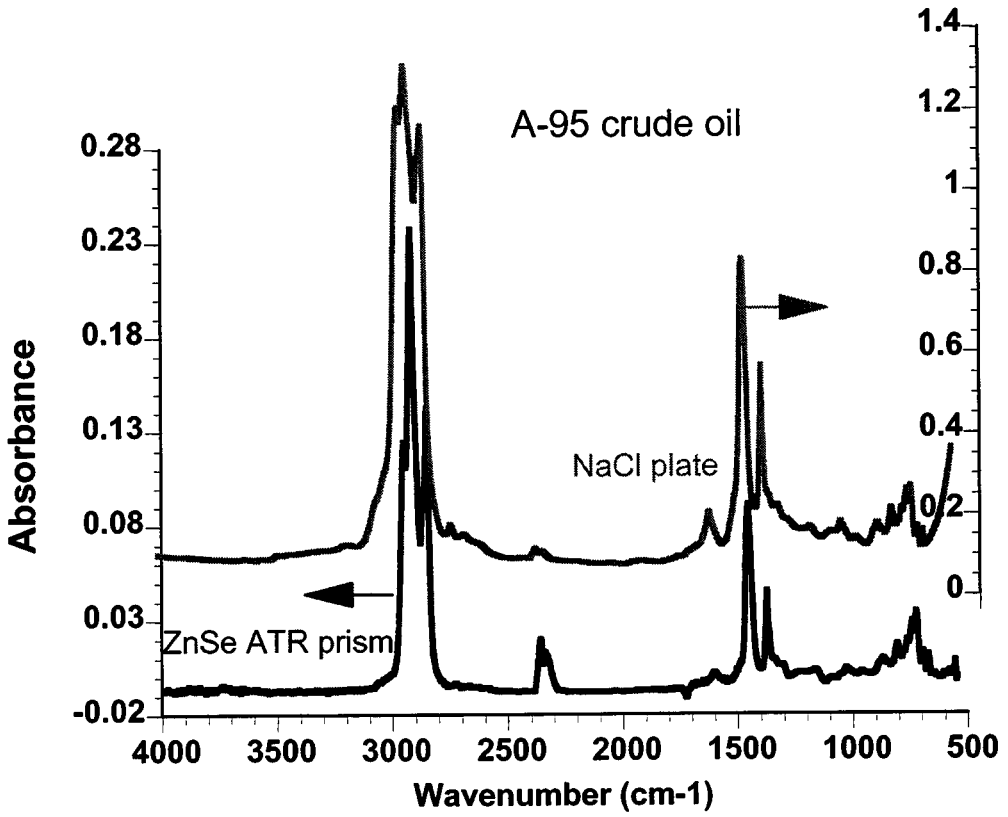

Figure 2.1-80. Comparison of spectra of A-95 crude oil produced by NaCl plate and ATR techniques.

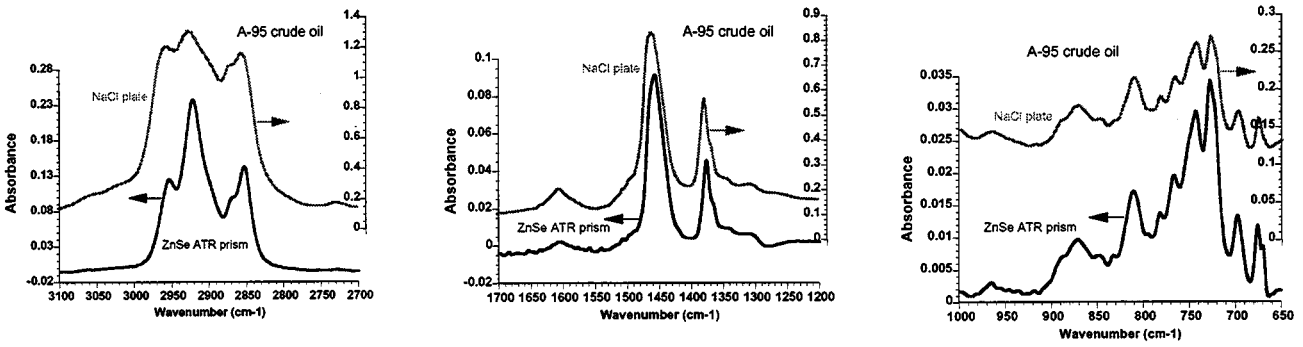

Figure 2.1-81. Three detailed comparisons of the A-95 crude oil spectra show excellent correspondence between peaks obtained by the ATR and NaCl plate techniques.

Adsorption of polar crude oil components:

Positively charged basic species can enhance adsorption of crude oil components to negatively charged mineral surfaces. The results of such interactions have been demonstrated for mica and A-93 crude oil (Liu and Buckley, 1999). Contact angles for water advancing over a mica surface treated under the same conditions as the sample used in this study averaged 127°, well into the oil-wet range. Recall that A-93 is distinguished by a high base number and low acid number (Table 2.1-28) and thus is expected to be a particularly good example of these acid/base interactions. As shown in Fig. 2.1-72, however, very little adsorbed material of any kind could be distinguished on an oil-treated mica surface. Even the strong absorbance of the aliphatic peaks (~2900 cm^{-1}) was barely detectable. More subtle features, including the signal from C-N bonds (in the range from 1300-900 cm^{-1}, refer to Table 2.1-30 and Fig. 2.1-68) that might be enhanced by preferential adsorption, were either below the level of detection or obscured by more prominent features. Similar results were obtained for mica surfaces treated with A-95 and Moutray crude oils.

Equally of interest are organic acids, which can also adsorb, although under different circumstances than the organic bases. In particular, we are looking for evidence of C=O

stretching, as shown in Fig. 2.1-67. Such a peak may be evident for CS on brine-treated mica in the region from 1800-1700 cm^{-1} (Figure 2.1-82), although atmospheric water was present making interpretation uncertain.

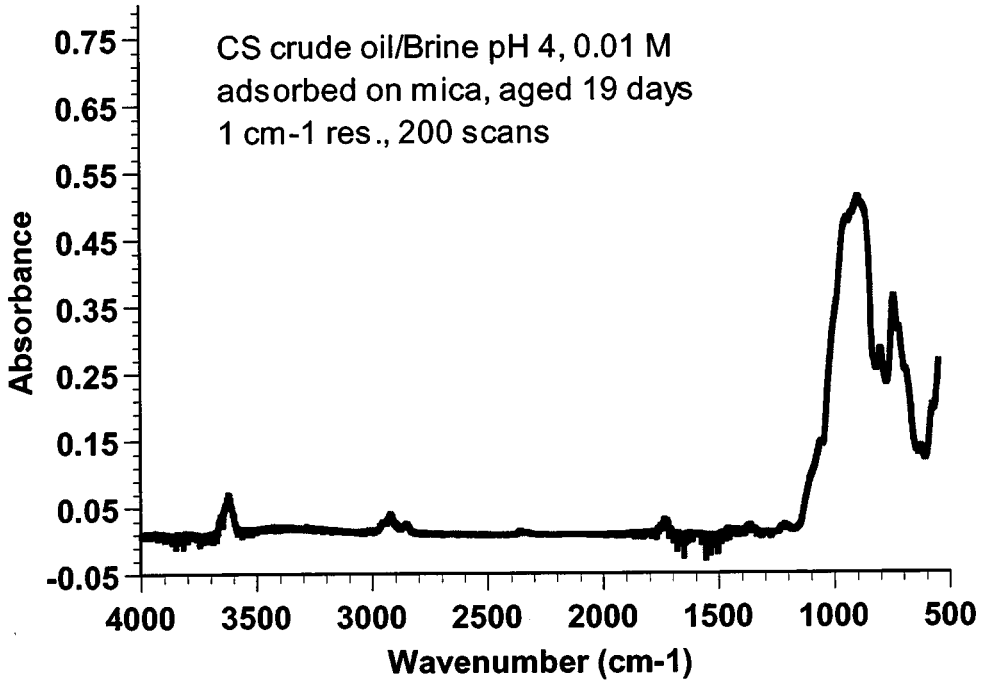

Figure 2.1-82. ATR spectrum of CS crude oil adsorbed on mica.

It is evident from this discussion that several factors combine to limit detection of the polar components of interest. First, there is a strong signal from the mica substrate beginning at about 1200 cm^{-1}, which obscures a region of particular interest. The second problem is that the organic signal is very weak, probably because the amount of adsorbed material is a monolayer or less. Absorbance of CO_2 (cm^{-1}) and atmospheric water (1900-1300 cm^{-1}) further obscure the picture.

Subtraction of inorganic signals. In order to circumvent the limitations due to the strong mica signal, a subtraction technique was investigated, as illustrated in Fig 2.1-83. A similar

approach was used successful by Funk *et al.* (1995). The mica signal was not as strong for mica plus adsorbed crude oil as it was for the mica alone, resulting in negative peaks. No significant enhancement of the signal due to the adsorbed material was observed.

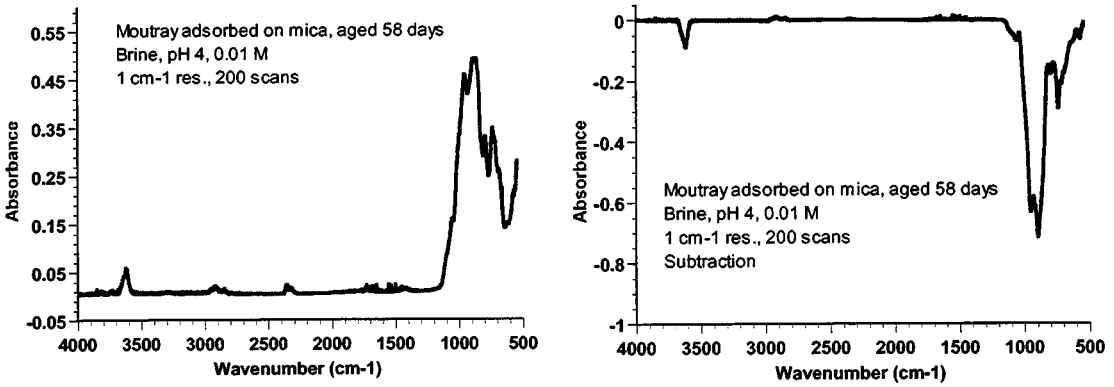

(a) adsorbed material + mica (b) adsorbed material only

Figure 2.1-83. Absorbance spectrum of Moutray crude oil adsorbed on mica.

Funk *et al* (1995) observed calcium carbonate and crude oil adsorption spectra over time. By subtracting the initial signal, they demonstrated adsorption of polar species, as indicated by peak heights that grew over a period of several days. Multiple reflections in their ATR cell enhanced the weak organic signal. The original signal from the undisturbed surface could be subtracted exactly to eliminate interference. The amount of adsorption may have been greater on the carbonate surface than on the silicates tested here. By focusing on interactions between polar components in the oil and dry surfaces, they further simplified the experiment, but might have been observing interactions other than those responsible for wetting in oil reservoirs, where water is always an important factor.

Enhancement of the adsorbed material signal by increasing surface area. Clay has a greater surface area than mica and thus should have associated with it a greater amount of adsorbed material. Moutray crude oil, adsorbed on brine-treated clay, is shown in Figure 2.1-77.

The organic signal is enhanced with respect to that from the inorganic substrate, although if polar species are present, their signal remains hidden. Differences between sample loadings of the clay in any two measurements would degrade the results of an attempt to subtract out the clay signal.

Atmospheric Water. Absorbance of atmospheric water was found between 1800 to 1300 cm^{-1}. Peak heights vary with atmospheric humidity. Since carbonyl C=O stretching is also found in this area of the spectrum, weak signals may be masked. Purging with nitrogen gas can eliminate this source of contamination (see, for example, Fig. 2.1-77).

Atmospheric Carbon Dioxide. Atmospheric carbon dioxide gives a signal between 2400 to 2300 cm^{-1}. When the FTIR system was purged with nitrogen gas, this peak was eliminated (see, for example, Figure 2.1-77).

Adsorbed water:

The ATR-FTIR technique, as applied to mineral surfaces treated first with brine, then with crude oil, was a surprisingly sensitive indicator of the presence of water remaining on the mineral surface.

Adsorbed water on mica. The presence of water on the surface (as opposed to the atmospheric water previously identified between 1800 and 1300 cm^{-1}) is shown by a broad band from about 3500 to 2900 cm^{-1}, between the Si-OH stretching (~3620 cm^{-1}) and the aliphatic signals (~2900 cm^{-1}). Figure 2.1-84 shows that water was absent from a surface aged for one week in A-93 crude oil, but water was still present on a similarly treated mica surface exposed to

Moutray crude oil. Note that all mica surfaces are wet with the brine phase when first exposed to oil. Similar results, i.e. no water on an A-95 treated surface and water on a surface aged in Moutray for 10 days, suggest that this observation is related to some property of the crude oil.

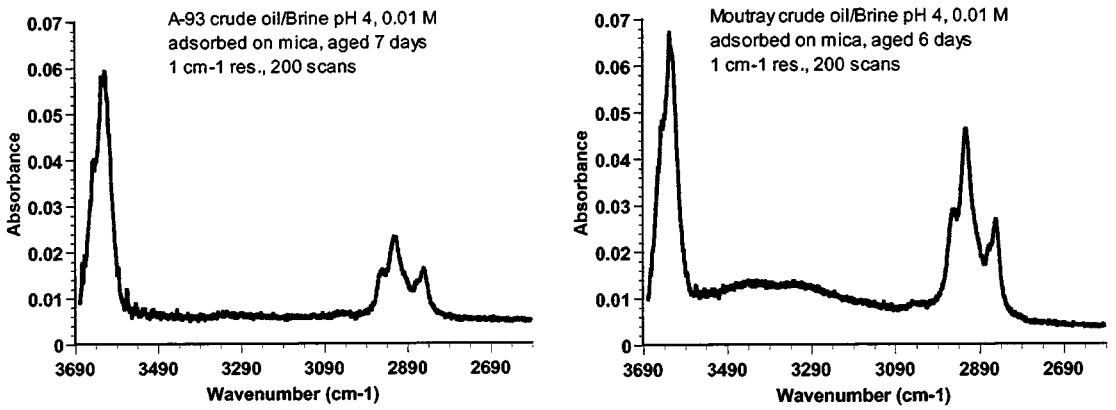

Figure 2.1-84. No water is evident on mica aged in A-93, whereas water is apparent from the spectrum of mica treated with Moutray.

Water remained adsorbed on brine-treated mica aged in CS crude oil even after 110 days of aging in the oil (Fig. 2.1-85). The amount of water appears to be decreasing slowly with aging time.

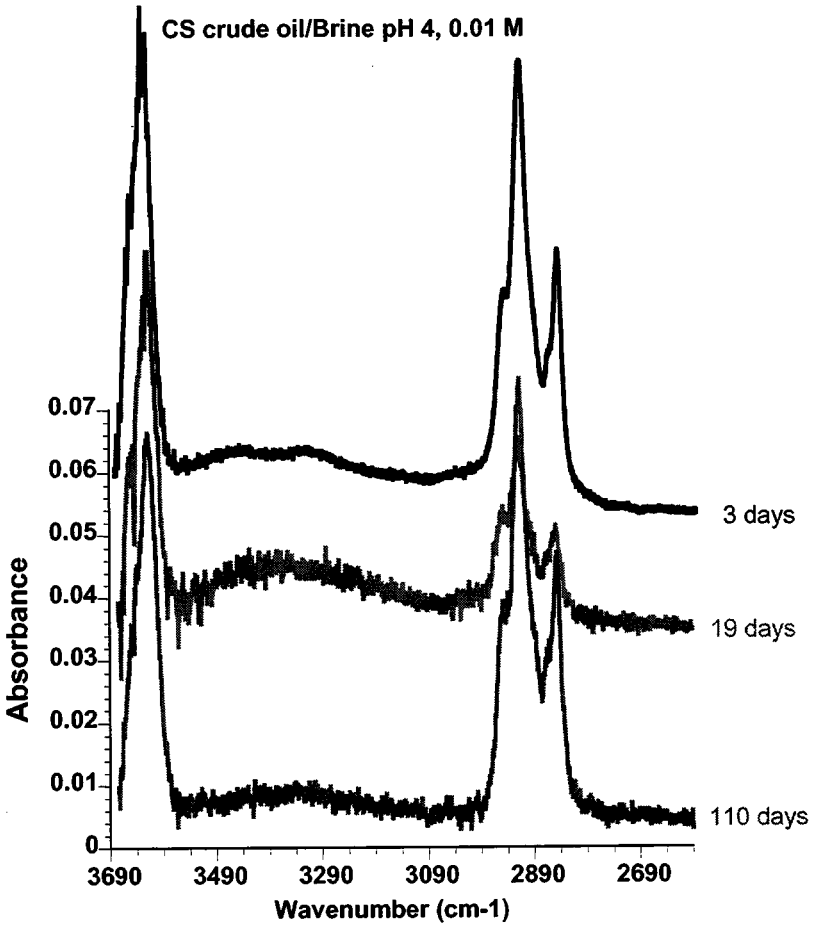

Figure 2.1-85. Amount of water remaining on mica treated with CS crude oil varies with aging time.

Identification of adsorbed water on clay. Water is even more evident in the spectra of brine and oil-treated clays. A broad, very strong band of OH stretching between 3680-2950 cm^{-1} provides clear evidence of adsorbed water on clay powder treated with brine and A-95 crude oil (Fig. 2.1-86a). The water peak is absent from a spectrum run on the same sample 10 days later (Fig. 2.1-86b), suggesting that interstitial water may have been the source of this peak. Recall that no water was found on mica surfaces aged in A-95 crude oil, suggesting that thin water films do not persist with this oil, in contrast to the CS samples for which water persisted even after 110 days in the oil.

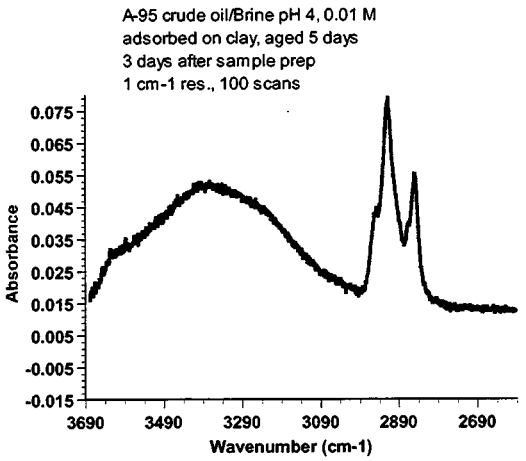

(a) Water remains in brine and oil-treated clay.

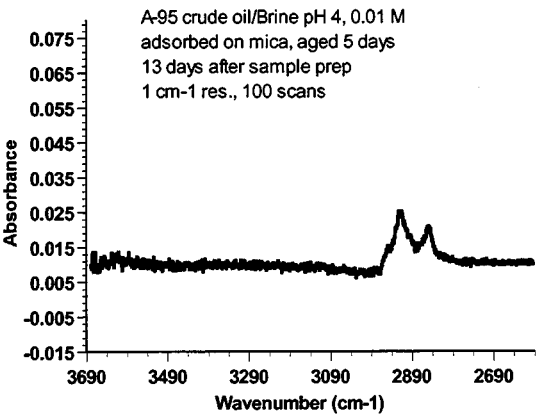

(b) After 10 days, the water peak is gone.

Figure 2.1-86. Water and A-95 crude oil adsorbed on clay.

Role of water. While it is tempting to blame the lack of success in finding polar components adsorbed to mica and clay in these tests on the initial presence of water, that is not consistent with other work on the alteration of wetting properties of minerals with these crude oils. Reduced adsorption of asphaltenic components from crude oils has been reported when water is present, compared to the amount of asphaltene that adsorbs on a dry surface (e.g., Collins and Melrose, 1983). However there are several issues that must be distinguished in order to make sense of the role of water.

Bulk water, present in the interstices of the porous medium, can limit access of the oil phase to the mineral surfaces. That may well have happened in the oil-treated clay samples, as suggested by the large water signal that disappears when evaporation is permitted to occur.

On the microscopic scale, however, thin films of water can either promote or inhibit interactions between oil components and mineral surfaces as it mediates the surface charge at the oil/brine and solid/brine interfaces. Much higher (more oil-wet) and much lower (more water-wet) contact angles have been demonstrated for many oils-surface combinations, depending on

the composition of the intervening aqueous phase. Examples using mica and some of the same crude oils as those used in this study were extensively studied by Liu (1997). Mica surfaces exposed to A-93 in the absence of water resulted in preferentially water-wet surfaces ($\theta_A = 31°$). Treating the mica first with an NaCl solution (pH 8 and I=0.01M) gave similar results ($\theta_A = 38°$), whereas treating with an acidic NaCl solution (pH 4 and I=0.01M), as was done in this study, gave more oil-wet conditions ($\theta_A = 127°$), even after the bulk crude oil was removed by washing with toluene.

It is intriguing to note that, in the case of the mica slides, no water was found with the two Prudhoe Bay oils (high base number, positively charged oil/water interface at pH 4) for which electrostatic attraction helps to destabilize the water film between oil and mica. The two acidic oil samples were the ones for which the water signal persisted, suggesting a stable water film. Whether this is really an indication of stability of the thin water film cannot be judged from these few results, but they do suggest a possible avenue for further research.

Summary of FTIR study

The ATR method compared well with conventional FTIR for known compounds and crude oil samples, although the absorbance signals obtained were consistently weaker. While this does not create a problem with peak identification for the liquids tested, and even gives better peak separation in some instances, it does contribute to the difficulties experienced in identifying small amounts of organic material adsorbed on mineral surfaces. Spectra of six crude oils were similar, with only minor differences mainly in the fingerprint region between 1000 and 650 cm^{-1}.

Several factors contributed to the inability of this method to distinguish significant chemical detail about the adsorbed organic material of interest. The signal obtained from the

ATR was weak, the small amount of material adsorbed on the mineral surface added to the challenge, a strong signal from the surface itself obscuring regions of particular interest, and interference from contaminants in the atmosphere all made it impossible to discern whether enrichment of polar functionality occurred. In fact, only the strongest aliphatic peaks indicated that there was organic adsorption.

The following main conclusions were obtained in this research.

1. Spectra of various crude oils showed more similarities than differences. While some polar groups were identified in some crude oils, they were present only as minor constituents and their occurrence was not well correlated with other measures of acidity or basicity of the oils.

2. Aromatic groups were easily identified in the crude oils studied, but they could not be quantified, due to coupling with aliphatic bending.

3. Attempts to subtract adsorbed organic material from mica were not successful.

4. Adsorption of organic components from the crude oils was indicated by very small aliphatic CH stretching peaks on both mica and clay. No other peaks associated with the adsorbed material could be identified.

5. Water remained on some mica and all clay samples. Whether water was associated with mica depended on which crude oil sample had been used to treat the mica and, to a lesser extent, how long the mica was aged in oil. The possibility that this water represents a stable water film remains to be investigated. On clay, the water appeared to be interstitial and was removed by evaporation.

Future work with the ATR-FTIR method would require that the problems that prevented identification of the chemical nature of the adsorbed material be solved. Atmospheric water and carbon dioxide can be readily eliminated by purging the atmosphere with dry nitrogen. Accurate

methods to enhance the signal and/or to subtract out the contribution from the substrate would be essential to successful application of the technique.

An alternative approach might be to adsorb crude oil components on a large quantity of high surface area material, such as the clay used in this study, then desorb and concentrate the material. This approach would alleviate the problems of too little material to give a sufficiently strong signal, but would introduce problems of its own since the most strongly adsorbed material might not be recovered.

Finally, it would be of interest to pursue the use of this technique to study the fate of the thin water films that are critical to the interactions between crude oil components and mineral surfaces.

2.2 Wetting Assessment in Porous Media

2.2.1 Visual Evidence in Micromodels

Micromodels that have been investigated in the literature include bead packs, single pore tubes, and network models. The materials used in construction of these models were also varied (e.g. glass, Lucite, Teflon, silicon, resins) (Buckley, 1991). Most models are two-dimensional networks. The geometry and topology of the two-dimensional models can be specified precisely compared to other idealized porous media such as packs of glass beads (McKellar and Wardlaw, 1982). Glass micromodels exhibit high surface energy and are initially water-wet. Like other two-dimensional network models, glass micromodels permit observation of fluid distributions and pore-level displacement mechanisms.

Roof (1970) showed that for water-wet pores, snap-off of oil does not occur until the oil/water interface has moved to a radius much larger than that of the throat of the constrictions. The snap-off is controlled by the relative size of throats and pores. The tendency to snap off is also reduced if the oil has a tendency to wet the pores; this effect favors the flow of oil as a continuous phase. Based on studies carried out in a glass micromodel consisting of a single pore-throat pair, Wardlaw (1982) found that the displacement efficiency and the amount of oil trapped is affected by the shape of the fluid interface. The shape of the interface is a function of the contact angle (i.e. wettability) and the geometry of the pore. Snap-off of the non-wetting phase was a function of pore-throat ratio and was high for strongly water-wet system. Large variations in interfacial tension (0.1-480 mN/m) have only small effect on the amount of non-wetting phase trapped. Formation of semi-rigid films at the interface between decane and phosphate solution inhibited snap-off non-wetting phase.

From visual observations of waterflood displacement in etched glass micromodels, Buckley (1995) reported that wetting alteration was caused primarily by the crude oil and that subsequent precipitation of asphaltic material from crude oil upon contact with low molecular weight paraffin does not necessarily alter the wetting of the porous media. This should be true especially if the original oil has a great tendency to change wetting.

In this report, from the PhD dissertation of Al-Maamari (2000), wetting changes are investigated with an oil that was shown in Section 1.2 to undergo a steep transition from more water-wet to more oil-wet contact angle behavior near the onset of asphaltene precipitation. One advantage of the glass micromodels is that plugging, if it occurred, would be obvious and could thus be differentiated from changes due to wettability alteration.

Materials for micromodel studies

Porous media:

Etched glass micromodels (McKellar and Wardlaw, 1982) made by Petrophysics Research Group (Royal School of Mines, Imperial College) were used. The models are made of fused glass plates. The dimensions and overall pattern of the models are shown in Figure 2.2-1 (note that the pattern is not to scale). Models were used as received; each model was used for one experiment only.

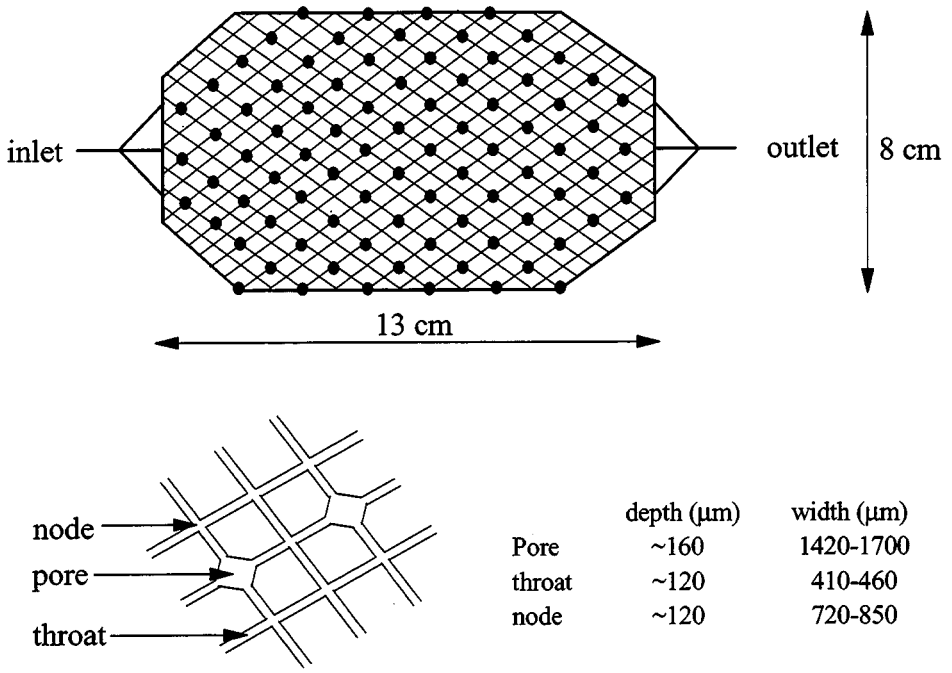

	depth (μm)	width (μm)
Pore	~160	1420-1700
throat	~120	410-460
node	~120	720-850

Figure 2.2-1. Dimensions and pattern of the glass micromodels used.

Aqueous phase:

An 0.01M solution of NaCl buffered at pH4, denoted by the short-hand designation {4,0.01}, was used as the aqueous phase in these experiments.

Oil phase:

Mars-Pink crude oil was used in the micromodel experiments. Toluene was added to the original oil to match the viscosity of the oil mixture at onset with *n*-heptane. Figure 2.2-2 shows the viscosity of Mars-Pink oil mixtures at different temperatures. The oil mixtures used were:

- Soltrol 130
- 21% Mars-Pink + 79% toluene
- 27% Mars-Pink + 73% *n*-heptane (onset mixture)

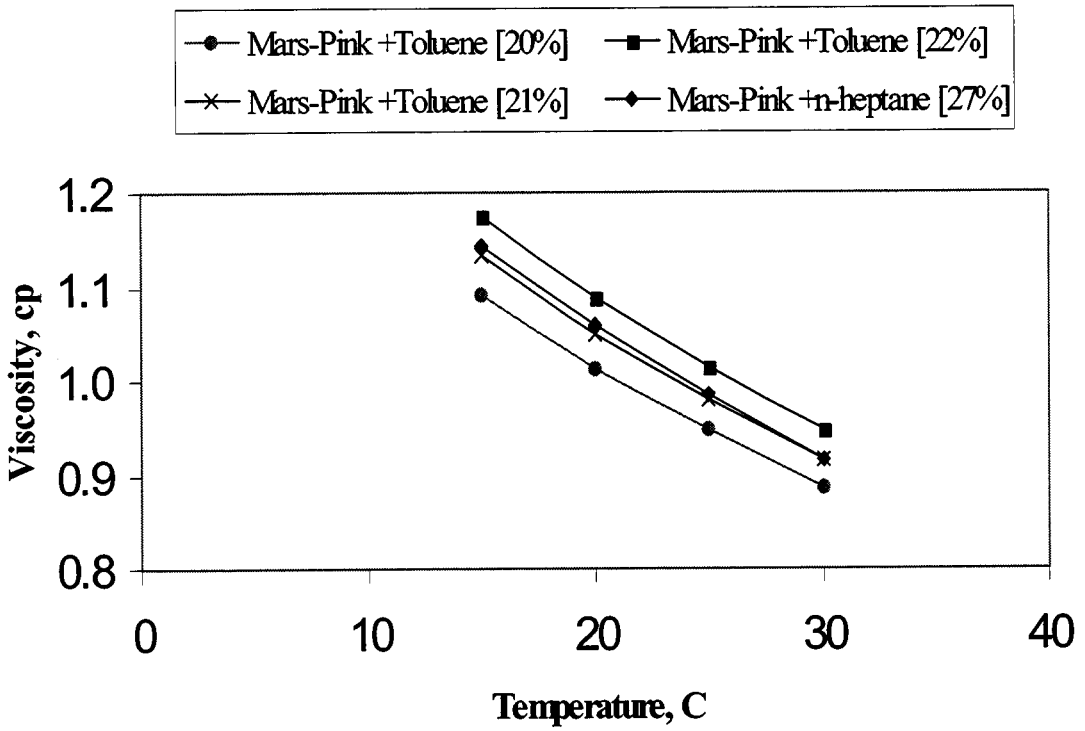

Figure 2.2-2. Viscosity of Mars-Pink oil mixtures as a function of temperature.

Experimental procedures

The models were first saturated with pH4 buffer and allowed to equilibrate for one day at ambient conditions. The buffer was then displaced by the oil at 10 ml/min to remove most of the water and the model was aged in oil for three weeks at ambient temperature.

The waterflood displacement was carried out at a rate of 2 ml/hr and recorded on videotape. When the flow of oil ceased, the rate was increased first to 10 ml/hr, then to 30 ml/hr to mobilize more oil. The wettability was assessed qualitatively from the shapes of the moving oil/water interface and the displacement mechanisms. The setup for the micromodel experiment is shown in Figure 2.2-3.

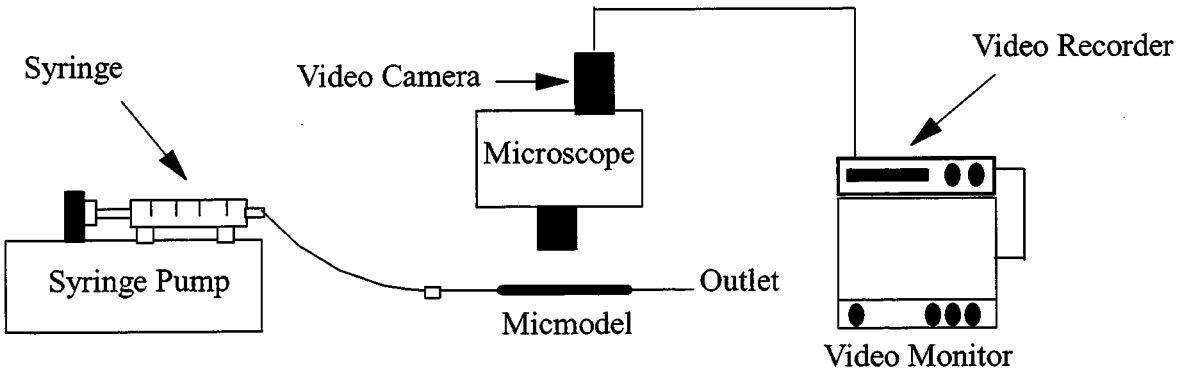

Figure 2.2-3. Apparatus for micromodel experiments.

Results

Figures 2.2-4 and 2.2-5 show sequences of displacement of the oil by brine for Mars-Pink plus toluene and Mars-Pink plus heptane, respectively. When the onset mixture of Mars-Pink and *n*-heptane was used, thin oil films at pore walls were clearly observed, as indicated by arrows on the photographs.

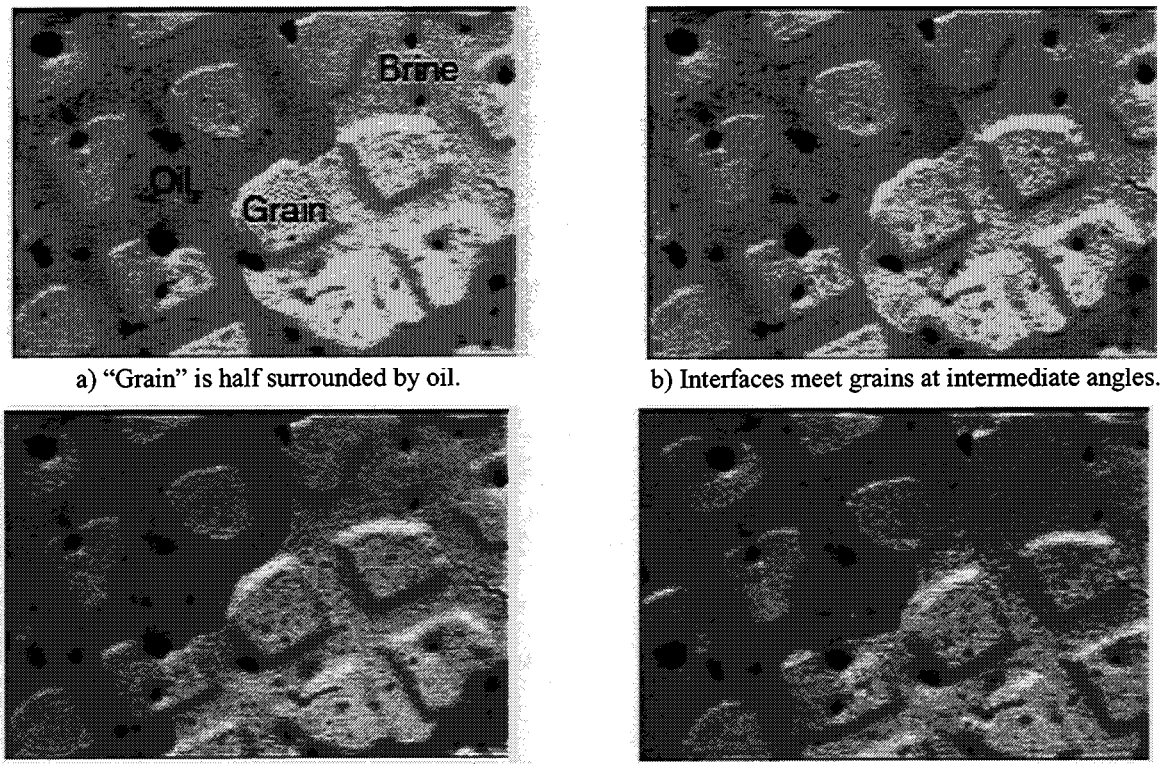

a) "Grain" is half surrounded by oil.

b) Interfaces meet grains at intermediate angles.

c) Water displaces oil from pore above "grain."

d) Oil almost completely cleared from marked "grain."

Figure 2.2-4. Successive photographs of the displacement of Mars-Pink mixture with toluene by {pH4, 0.01M} brine after aging in oil for three weeks.

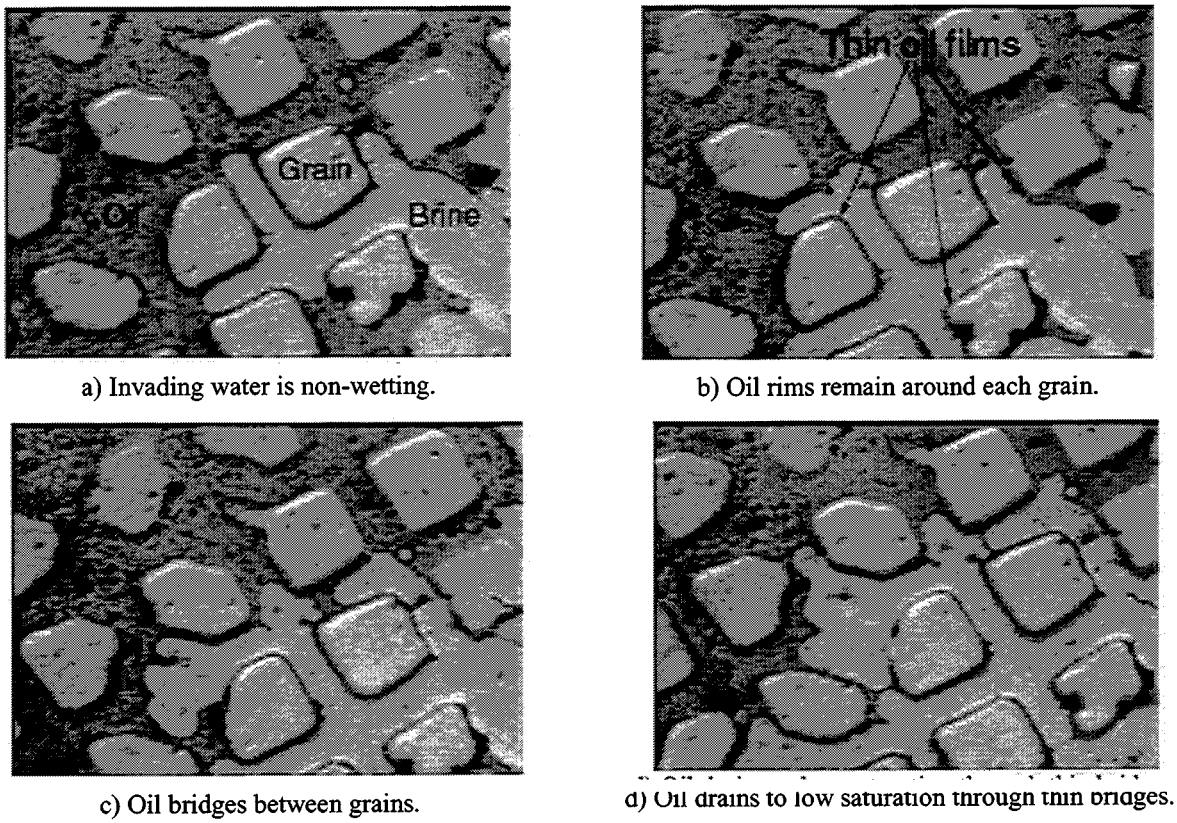

a) Invading water is non-wetting.

b) Oil rims remain around each grain.

c) Oil bridges between grains.

d) Oil drains to low saturation through thin bridges.

Figure 2.2-5. Successive photographs of the displacement of the onset mixture of Mars-Pink and *n*-heptane by pH4 {0.01M} brine after aging in oil for three weeks.

From the visual observation of the displacement of Mars-Pink plus toluene with brine, the system appears to be weakly water-wet. The oil is displaced smoothly from the pores and throats. On the other hand, when the onset mixture of Mars-Pink and heptane was used, the system appears to be oil-wet. Oil films surround the glass grains. These observations are in agreement with the results obtained on flat surfaces where more oil-wet conditions were obtained at the onset of asphaltene precipitation.

Snap-off of crude oil was not observed for either case. That might be attributed to the low aspect ratio between pores and throats. No evidence for pore plugging by asphaltenes was observed. The difference in the size of the asphaltene particles (~1μm) and the pores (~160 μm) minimizes the possibility of plugging. However, if oil mixtures with large asphaltene aggregates

are present, the effect of plugging should be considered, especially in cases where pore throat constrictions are small.

Summary of micromodel observations

Although the evidence provided by these micromodel experiments is qualitative, it is clear that wettability differs in the two experiments and that the onset mixture of oil and heptane produces a much more oil-wet condition than does the same concentration of oil diluted with toluene. This is exactly what we would predict from the contact angle

2.2.2 Comparison of Amott and USBM Wettability Indices

(in collaboration with A. Dixit, S. McDougall, and K. Sorbie, Department of Petroleum Engineering, Heriot-Watt University)

The wettability of a crude oil/brine/rock system is of central importance in determining the oil recovery efficiency of water displacement processes in oil reservoirs. Wettability of a rock sample has traditionally been measured using one of two experimental techniques: the United States Bureau of Mines and the Amott tests. The former gives the USBM index, I_{USBM}, and the latter yields the Amott-Harvey index, I_{AH}. As there is no well-established theoretical basis for either test, the relationship between the two, if any, is unclear.

Analytical relationships between I_{AH} and I_{USBM} for mixed-wet and fractionally-wet media have been derived assuming uniform pore size distribution and ignoring the effects of pore connectivity. This simple approach provides some guidelines regarding the influence of the distribution of oil-wet surfaces on I_{AH} and I_{USBM}. More detailed insight into the relationship between I_{AH} and I_{USBM} is provided by modelling the pore-scale displacement processes in a network of interconnected pores. The effects of pore size distribution, interconnectivity,

displacement mechanisms, distribution of volume and of oil-wet pores within the pore space have all been investigated by means of the network model.

The results of these analytical calculations and network simulations show, as expected, that I_{AH} and I_{USBM} need not be identical. The calculated indices and the relationship between them suggest explanations for some of the trends that appear in experimental data when both I_{USBM} and I_{AH} have been reported in the literature for tests with comparable fluids and solids. Such calculations should help with the design of more informative wettability tests in the future.

It is now well established that the wetting characteristics of a reservoir crude oil/brine/rock (COBR) system strongly influence water-oil displacement processes in petroleum reservoirs (Cuiec, 1991; Morrow, 1990; Jadhunandan and Morrow, 1995). Wettability is a surface phenomenon, classically defined using the concept of contact angle. No such direct test of wettability in porous media is available, however. The most widely used empirical wettability measurements for reservoir cores, including Amott (Amott, 1959; Boneau and Clampitt, 1977), USBM (Donaldson *et al.*, 1969) and combined Amott/USBM methods (Sharma and Wunderlich, 1985), are based on displacement studies.

I_{AH} and I_{USBM} are used almost interchangeably within the oil industry as indicators of rock wetting, although there are obvious differences. I_{AH}, by definition, must fall between –1 and +1, a restriction which does not apply to I_{USBM}; numerical discrepancies for strongly-wetted conditions are thus expected. Of more importance are comparisons over the wide range of weakly-wetted and intermediate conditions between these two extremes. Since I_{AH} reflects spontaneous imbibition, whereas I_{USBM} is derived from drainage capillary pressure curves, it is not immediately evident what the relationship between these two measures should be.

In cases where data for both measures are available, comparisons show significant scatter (Buckley, 1996b). At most only qualitative agreement between the two is observed, as shown in Figs. 2.2-6a and -6b, where I_{USBM} vs. I_{AH} is plotted for experimental data from many sources in the literature. In Fig. 2.2-6a, some of the scatter can probably be attributed to real differences between samples, since different pieces of core were used to measure I_{USBM} and I_{AH}. Figure 2.2-6b shows measurements made by the combined Amott/USBM technique (Sharma and Wunderlich, 1985) in which both indices are measured for the same piece of core in the course of a series of imbibition and drainage displacements. Consistency is better within any one set of data, but there are noticeable differences from one data set to another. Again, some of the discrepancies may represent real differences between the different sets of cores. In addition, however, while there is general agreement on the essentials of the Amott and USBM tests, important modifications have been introduced (e.g. Cuiec, 1975; Longeron *et al.*, 1994) and techniques can vary significantly from one laboratory to another.

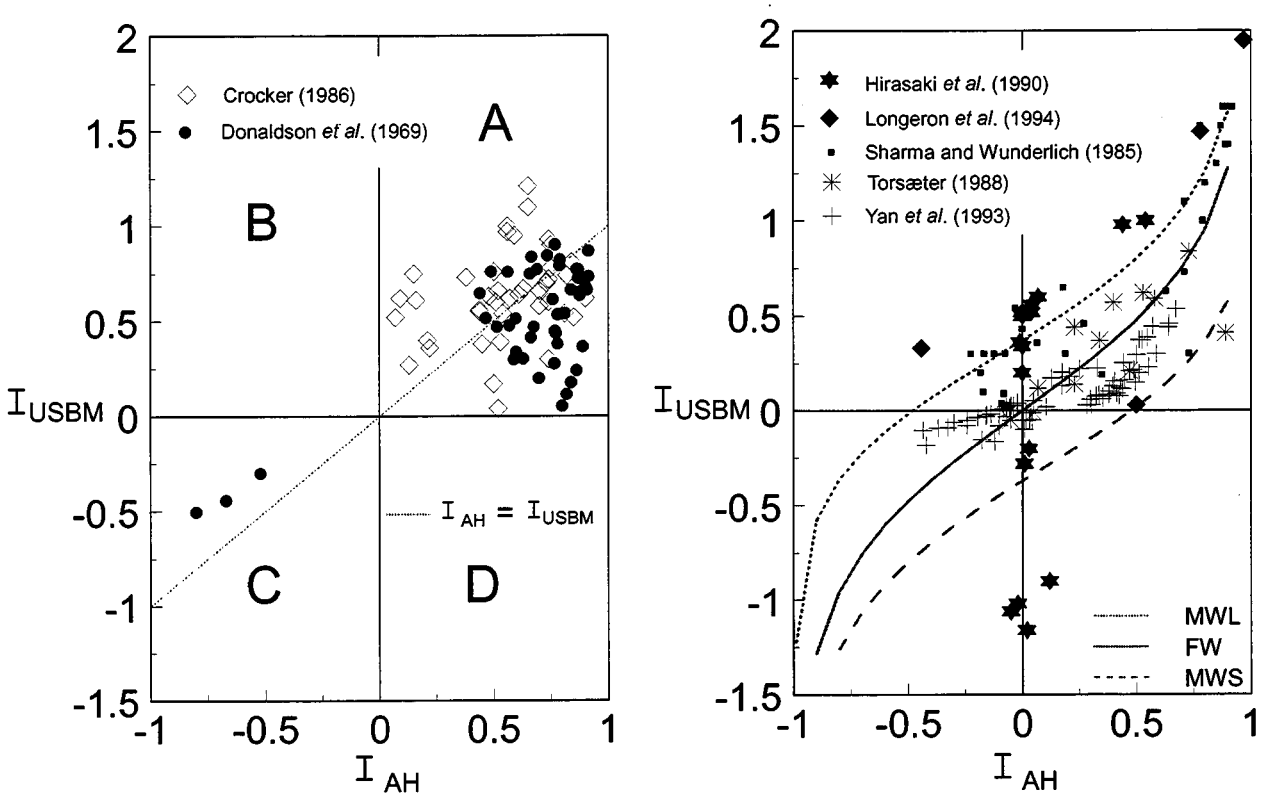

(a) separate measurements of I_{USBM} and I_{AH} (b) combined measurements of I_{USBM} and I_{AH}

Figure 2.2-6. Comparison of Amott-Harvey and USBM indices measured in (a) separate experiments with duplicate core plugs or (b) in a combined sequence of measurements with a single core plug (data from various literature sources, as indicated).

For future reference, the four quadrants in Fig. 2.2-6a are designated **A** ($I_{USBM} > 0$; $I_{AH} > 0$), **B** ($I_{USBM} > 0$; $I_{AH} < 0$), **C** ($I_{USBM} < 0$; $I_{AH} < 0$) and **D** ($I_{USBM} < 0$; $I_{AH} > 0$). Some trends can be observed immediately: (a) most points fall in quadrant A; (b) across the range from $I_{AH} = -1$ to $I_{AH} = +1$, there appears to be a systematic tendency for most points to lie *above* the $I_{USBM} = I_{AH}$ line; (c) there is an (almost) empty quarter, quadrant D, and (d) there are a fair number of points that fall in quadrant C where the USBM test indicates preferential wetting by water whereas the AH test suggests predominantly oil-wet behaviour.

In this section, our central objectives are (a) to explore the relationship between the AH and USBM wettability indices using analytical and pore-scale network modelling, and (b) to use

predicted correlations between I_{AH} and I_{USBM} to reexamine and interpret existing experimental data.

Analytical Results

It is shown elsewhere that, for a uniform pore size distribution (PSD), there are analytical relationships between I_{USBM} and I_{AH} for various wetting scenarios (Dixit *et al.*, 2000). In these calculations we distinguish *wettability types* that are based on the fraction of *oil-wet* pores, α, and their distribution within the pore space in the following ways:

- *fractionally-wet* where the oil-wet pores are uncorrelated to pore size (denoted FW);
- *mixed-wet* where the largest pores are oil-wet (denoted MWL); or
- *mixed-wet* where the smallest pores are oil-wet (denoted MWS).

Although not discussed in detail here, there are physical reasons why either the larger or smaller pores may become preferentially more *oil-wet* on ageing after primary drainage leading to the MWL and MWS cases. Simple pore filling sequences are assumed within the water-wet and oil-wet pore clusters and accessibility issues are neglected in these analytical calculations. The analytical relationships derived between I_{USBM} and I_{AH} for these three wettability types are given in equations 2.2-1 - 2.2-3.

Fractionally-wet (FW) case :

$$I_{USBM} = \log_{10}\left(\frac{1+I_{AH}}{1-I_{AH}}\right) \tag{2.2-1}$$

Mixed-wet case with *large* pores being oil-wet (MWL) :

$$I_{USBM} = \log_{10}\left(\frac{\left[\frac{I_{AH}(R_{max}^{v+1} - R_{min}^{v+1}) + (R_{max}^{v+1} + R_{min}^{v+1})}{2}\right]^{\frac{v}{v+1}} - R_{min}^{v}}{R_{max}^{v} - \left[\frac{I_{AH}(R_{max}^{v+1} - R_{min}^{v+1}) + (R_{max}^{v+1} + R_{min}^{v+1})}{2}\right]^{\frac{v}{v+1}}}\right) \tag{2.2-2}$$

Mixed-wet case with *small* pores being oil-wet (MWS) :

$$I_{USBM} = \log_{10}\left(\frac{R_{max}^{v} - \left[\frac{(R_{max}^{v+1} + R_{min}^{v+1}) - I_{AH}(R_{max}^{v+1} - R_{min}^{v+1})}{2}\right]^{\frac{v}{v+1}}}{\left[\frac{(R_{max}^{v+1} + R_{min}^{v+1}) - I_{AH}(R_{max}^{v+1} - R_{min}^{v+1})}{2}\right]^{\frac{v}{v+1}} - R_{min}^{v}}\right) \qquad (2.2\text{-}3)$$

where R_{min} and R_{max} are the uniform PSD limits and ν is the volume exponent (Dixit *et al.*, 1996). Fig. 2.2-7 shows the relationships between I_{AH} and I_{USBM} predicted by this simple analytical approach. The FW case is linear over the range $-0.5 < I_{AH} < 0.5$, following the $I_{USBM} = I_{AH}$ line. For a strictly FW system, there is a symmetric relationship between the wetting indices which is independent of the type or range of PSD or volume exponent, ν. Clearly, for either type of *mixed-wet* system—MWL or MWS—both the PSD limits (R_{min} and R_{max}) and ν do affect the relationship between the two indices.

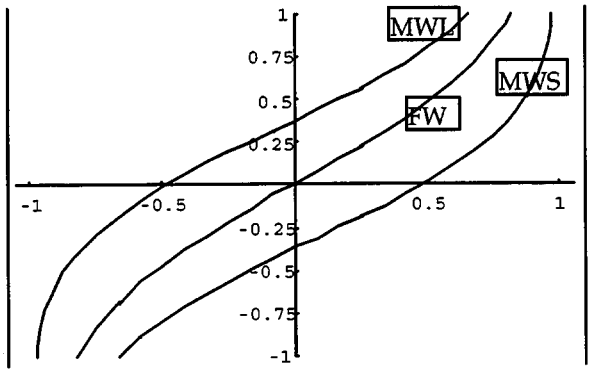

Figure 2.2-7. I_{USBM} vs. I_{AH} relationships for the simple analytical model with FW, MWL and MWS wettability types, uniform PSD, (1,50)μm pore size range, volume exponent ν=1.

The calculated I_{USBM} vs. I_{AH} relationships are clearly distinguished for mixed-wet conditions, with MWL systems predicted to lie *above* and the MWS systems predicted to lie *below* the $I_{AH} = I_{USBM}$ line in quadrant A. If current views of mixed-wet systems are broadly

correct (i.e. that wetting is altered in the *larger* pores), then most experimental data points should lie above the $I_{AH} = I_{USBM}$ line. In Fig. 2.2-6b, most of the data sets, with the exception of Yan *et al.* (1993), do indeed lie above the line. Wetting alteration in the experiments of Yan *et al.* was caused by exposure to oil-based drilling muds; perhaps in that case it is predominantly the *smaller* pores that become oil-wet.

Pore Scale Network Modelling Results

The analytical calculations above incorporated a number of simplifying assumptions:

- a uniform PSD was selected,
- accessibility functions were not considered (Heiba *et al.,* 1982, 1983; Stauffer and Aharony, 1994), and
- single contact angles (0° in the water-wet and 180° in the oil-wet pores) were assumed.

Recently network models have been developed which take into account a number of realistic pore-level flow phenomena, including wettability alterations after primary drainage (Dixit *et al.*, 1996; Blunt, 1997). The effects of wettability alterations on oil-water capillary pressure curves and the application of the *capillarity surface* concept to predict phase distributions have been discussed in McDougall *et al.* (1997). Using the same simulator, we have also studied waterflood recovery trends in fractionally-wet and mixed-wet systems and, based on these results, a *Regime*-based framework has been proposed for wettability classification (Dixit *et al.*, 1996). A typical Regime diagram is shown in Fig. 2.2-8. The three main Regimes (I, II and III) are defined by the value of α, the fraction of oil-wet pores in the pore network. An important boundary exists between Regimes I and II at $\alpha = \alpha_{crit}$ where α_{crit} is the critical fraction of pores that must be *oil-wet* in order to form an oil-wet spanning cluster

across the network. From percolation theory (Stauffer and Aharony, 1994) this quantity is given by, $\alpha_{crit} = D/[z \bullet (D-1)]$ for an uncorrelated network of dimension D and coordination number z. The network approach has also been used to explore hysteresis trends in water-wet and mixed-wet consolidated and unconsolidated media (Dixit *et al.*, 1997, 1998). Numerous, apparently conflicting, waterflood recovery results and relative permeability hysteresis trends have been interpreted with the help of the simulator.

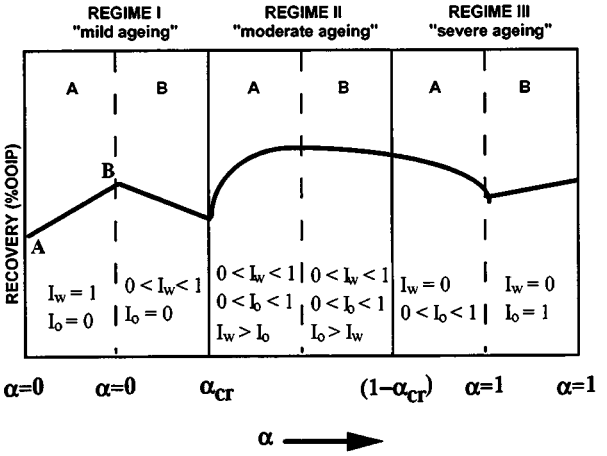

Figure 2.2-8. Schematic representation of *Regime*-based wettability framework relating wettability to waterflood recovery (from Dixit *et al.*, 1996).

Here the network simulator and Regime-based approach are applied in networks of 20x20x20 or 25x25x25 pores to evaluate the complex displacement processes that were not considered in the analytical approach above. The parameters tested for their impact on I_{USBM} and I_{AH} are summarized in Table 2.2-1. Complete results from this series of simulations are presented elsewhere (Dixit *et al.*, 2000). Here we present selected results for comparison with the analytical predictions and with existing experimental data.

Table 2.2-1. Parameters varied in network simulations

Parameters		Ranges tested
Topology	Pore size distribution (PSD)	Rayleigh (RAY), log uniform (LU), cubic (CU)
	R_{min} and R_{max}	(0.1,25)μm, (0.1,50)μm, and (0.1,100)μm,
	Coordination number (z)	4 and 6
	Volume exponent (ν)	1 - 3
Displacement mechanisms	Water-wet clusters	Snap-off (θ=0°), piston-like (θ=60-89°), & both (θ=0-89°)
	Oil-wet clusters	Piston-like only (θ=91-120°)
Wettability distribution	Fractional wetting (FW)	α = 0.187, 0.375, & 0.567
	Mixed with oil-wet large pores (MWL)	
	Mixed with oil-wet small pores (MWS)	

Effect of imbibition mechanism in the water-wet region:

The effect of the pore-scale imbibition mechanism in the water-wet region (i.e. snap-off or piston-like displacements) upon calculated wettability indices is shown in Fig. 2.2-9 for a fractionally wetted system. (For explanation of simulations involving different displacement mechanisms, see the discussion in Dixit *et al.*, 1997.) It is assumed that the displacements in the oil-wet region are mainly governed by piston-like displacements. The wettability Regime is varied by changing α over the range from 0.187 to 0.567 which shifts both I_{AH} and I_{USBM} from higher to lower values.

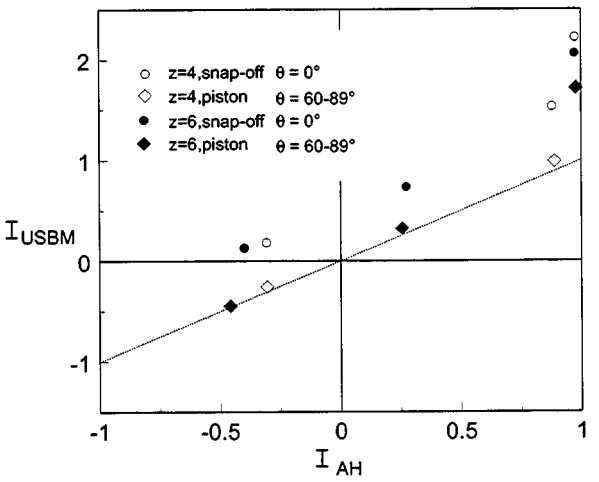

network size z=4	25x25x5	PSD	modivied RAY	**mechanism OW**	piston θ=91-120°
z=6	20x20x20		(0.1,50)μm; ν = 2	**WW**	as shown°
z	as shown	**α**	0.187, 0.375, 0.567	**wettability type**	FW

Figure 2.2-9. Effect of the pore-scale displacement mechanism in the water-wet region (assuming piston-like displacement in OW regions) on I_{USBM} and I_{AH} wettability indices.

When piston-like displacements are selected for water imbibition in the FW simulations, I_{USBM} almost equals I_{AH}, in agreement with the analytical prediction. With the change in imbibition mechanism from piston-like to snap-off in the water-wet pores, however, the USBM index increases significantly whereas the AH index remains practically unchanged. This trend is almost independent of the wettability Regime and overall coordination number of the network. Simulations in which both mechanisms were allowed resulted in I_{USBM} values that were almost as high as in the case with snap-off alone.

The effect of coordination number is small, except in the intermediate wetting cases (α=0.375) where changing z shifts the system from the borderline between Regimes I and II (z=4, α_{crit}=0.375) to Regime II (z=6, α_{crit}=0.25). Other simulations have shown that an increase in the volume exponent ν shifts both indices to lower values, preserving the differences between them. If snap-off is allowed, the USBM indices are consistently higher than the corresponding AH values, regardless of the value of ν.

Imbibition without snap-off:

In previous simulation studies, we have shown that the characteristic relative permeability hysteresis trends of poorly consolidated porous media could be reproduced by incorporating piston-like displacements in both wettability regions and by using a relatively high volume exponent and low conductivity exponent (Dixit *et al.*, 1997, 1998). Variations in I_{USBM} and I_{AH} with this combination of parameters—which is often associated with "poorly consolidated" porous media—are shown in Fig. 2.2-10.

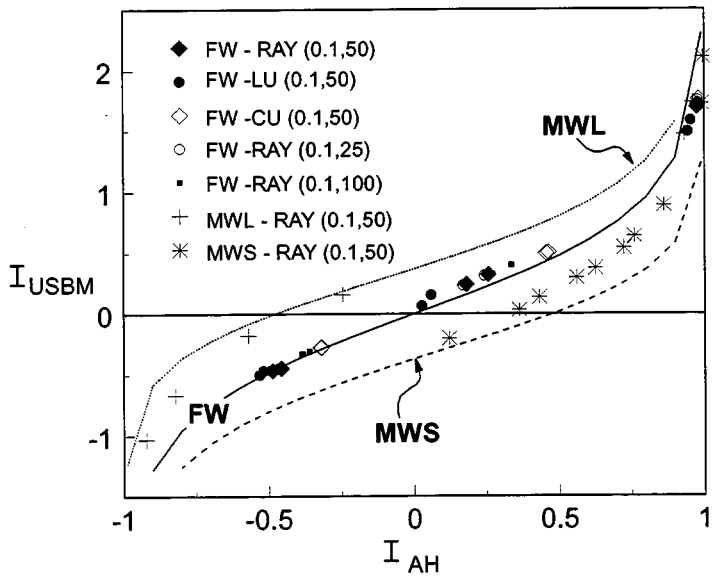

network size	20x20x20	**PSD**	as shown	**mechanism** **OW**	piston θ=91-120°
			ν = 3	**WW**	piston θ=60-89°
z	6	**α**	0.187, 0.375, 0.567	**wettability type**	as shown

Figure 2.2-10. Simulated I_{USBM} and I_{AH} wettability indices for "poorly consolidated" porous media.

For poorly consolidated, fractionally-wet systems, the correlation between the I_{AH} and I_{USBM} is excellent. This trend is quite insensitive to pore geometry and topological parameters, in agreement with the prediction of the simple analytical model. A similar result was shown in Fig. 2.2-9, for parameters more representative of consolidated porous media, when only piston-like displacement was allowed (as expected for weakly-wet conditions). The agreement between the full network model and the analytical prediction reflects the symmetry between the analytical assumptions and the full network calculation for a random distribution of wetting (FW) and piston-like displacement mechanisms regardless of wettability.

Asymmetry is introduced when we hypothesize that some of the large pores (MWL) or some of the small pores (MWS) become oil-wet, even if the mechanism continues to be restricted to piston-like displacement. As shown in Fig. 2.2-10, the MWL points lie above the $I_{USBM} = I_{AH}$ line and the MWS points lie below, as predicted by the analytical calculations. The MWS case is a particularly interesting result since this is the only one which gives points that lie

below the $I_{USBM} = I_{AH}$ line, suggesting that measurements in which $I_{USBM} < I_{AH}$ might represent porous media in which it is the small pores that are oil-wet.

Comparison of Predictions with Experimental Data

Figure 2.2-11 summarizes all of the simulations testing sensitivities to pore size distribution, pore size range, pore volume exponent, imbibition mechanism and coordination number.

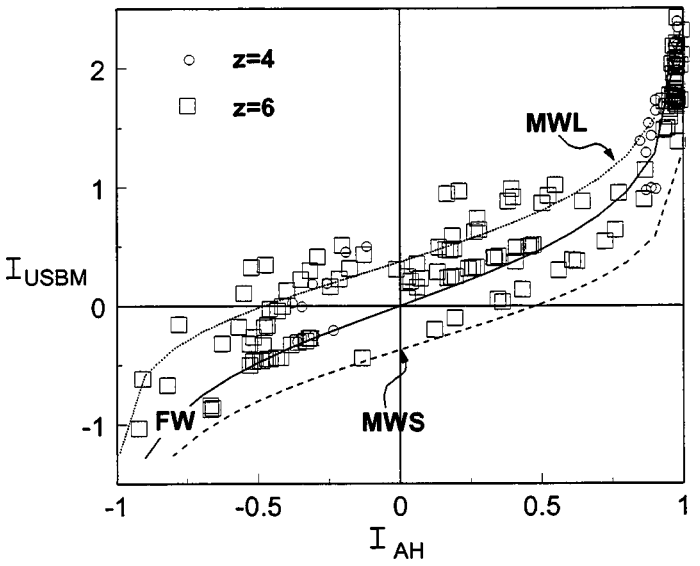

Figure 2.2-11. Simulated I_{USBM} vs I_{AH} trend for a wide range of sensitivities. See Table 2.2-1 for conditions tested.

Referring back to Fig. 2.2-6b, the sequential measurements of I_{USBM} and I_{AH} on a a single piece of core, some interesting comparisons emerge.

(a) There is a broad but scattered correlation between the USBM and AH indices for both the experimental results and the theoretical calculations.

(b) Most points in the I_{USBM} vs. I_{AH} correlation results fall in quadrant A in both the theoretical and experimental results. Clearly, in the theoretical calculations, this could be changed by simply taking more oil-wet network calculations. However, because of the

assumption that the water-filled pores at the end of the primary drainage remain water-wet, we tend to bias the system toward more water-wet conditions (as indeed occurs experimentally).

(c) Across the range from $I_{AH} = -1$ to $I_{AH} = +1$, there is a systematic tendency for the USBM test to indicate more water-wet behaviour than does the Amott test, with most points *above* the $I_{USBM} = I_{AH}$ line in both the theoretical calculations and the experimental results. This is particularly true in experimental results with $I_{AH} < 0$. This feature is captured by the numerical network simulations. The analytical result which predicts this behaviour suggests that this is due to the more common occurrence of the MWL wettability type (where larger pores tend to be oil-wet) in reservoir cores and to the influence of the snap-off mechanism in water-wet pores.

(d) Quadrant D is an almost empty quarter in both the simulations and in the experimental results. In the simulations, this may be partly a simple corollary of trend (b) above (since all points are moved upwards on the figure).

(e) A significant minority of points on the I_{USBM} vs. I_{AH} diagram lie in quadrant A but *below* the $I_{USBM} = I_{AH}$ line. Both the analytical results and the network simulations suggest that these points are due to small pores being oil-wet (the MWS wetting scenario) and piston-like displacement in both water-wet and oil-wet pore clusters.

Thus, encouraging agreement is seen between the experimental USBM and Amott wettability test results and the theoretical simulations. However, although most broad experimental trends are satisfactorily reproduced, further work is required to ensure that this is being done for the correct reasons in terms of the pore-scale physics. The analytical and network calculations provide some testable predictions, that—if confirmed experimentally—could extend the usefulness of the combination of AH and USBM indices in diagnosing the wetting conditions of porous media. For example, fractionally-wet media can be constructed by mixing grains of

different wetting. Our calculations predict that I_{AH} should equal I_{USBM} for such systems if they are weakly wetted or poorly consolidated (i.e., if snap-off is suppressed). The prediction that $I_{USBM} < I_{AH}$ occurs only if the smaller pores are the more oil-wet (again, with snap-off suppressed) might also be tested. It should be possible to determine, perhaps by tagging the imbibing fluids and examining their distribution after imbibition, to verify whether, in such a case, it really is the smallest pores that are oil-wet.

S*hould* $I_{AH} = I_{USBM}$?

Although these two empirical measures of wetting are clearly related, both the analytical study and network simulation suggest that only for weakly-wetted media with randomly distributed water-wet and oil-wet pores (the FW case) should the same numerical values be expected from the USBM and Amott-Harvey tests. For identical fractions of oil-wet pores, both indices are shifted by changing assumptions about the distribution and sizes of pores and the volume associated with each pore. If the larger pores are assumed to become oil-wet, the USBM index indicates more water-wet conditions than does the AH (i.e., $I_{USBM} > I_{AH}$). Snap-off in the water-wet pores also shifts USBM calculations to more water-wet values without affecting the Amott-Harvey results. Only if snap-off is suppressed and the smaller pores are the more oil-wet is the opposite trend, $I_{USBM} < I_{AH}$, predicted.

2.3 CO-Wet Database

2.3.1 Crude Oil Properties

It has long been recognized that components in crude oils can adsorb on mineral surfaces. Attention has focused on the asphaltene and resin fractions that contain most of the polar components of an oil, but attempts to correlate crude oil/brine/rock (COBR) interactions to specific crude oil properties have had only limited success. We now recognize that there are several—possibly competing—mechanisms by which COBR interactions can occur (Buckley *et al.*, 1998b).

Which mechanisms of interaction are dominant may depend on the nature of the mineral surface and ionic composition of the aqueous phase, as well as on the adsorbing species available in the oil. Additional complications arise because of the tendency of species in the asphaltene fraction to form aggregates of colloidal dimensions in response to changes in the oleic environment (Buckley, 1998).

In order to evaluate the wettability altering potential of an oil, something must be known about its acidic and basic properties. Some measure of the state of dispersion or aggregation of the asphaltene fraction is also required. Acid and base numbers, electrophoretic mobility, isoelectric point, and functional groups with heteroatomic species may be related to the acidic and basic nature of an oil. The ability of an oil to disperse its asphaltenes is related to bulk properties such as density, API gravity, refractive index (RI), and to the distribution of chemical species in the oil.

We have accumulated data characterizing a wide range of crude oils. In addition, we have experimental evaluations of COBR interactions with many oils, brines, and either glass or mica surfaces. The next step is to examine all this evidence for relationships between an oil's

properties and its tendency to alter wetting. A relational database is being developed to facilitate the search for what are undoubtedly complex relationships.

The relational database application selected for this task is Microsoft Access 97. Flexibility is an important consideration in the design of this database since research into COBR interactions is ongoing. It is essential, not only to capture all the information we have generated historically, but also to allow for the possibility that new tests will be added in the future as, with advances in our understanding, they almost certainly will.

The database is called "CO-Wet." Figure 2.3-1 shows a screen capture of the list of tables. "Crude Oils" is the table that identifies crude oil samples including such information as when they were received, how much, and from whom. Table names that begin with "Data" include measurements of the types indicated and experimental conditions. For example, the highlighted table contains refractive index data (sodium D line) measured as a function of temperature. Other tables contain information about the brines and buffers used in COBR tests, some basic information about pure hydrocarbons, and information about the laboratory technicians and students, in whose notebooks the raw data should be found.

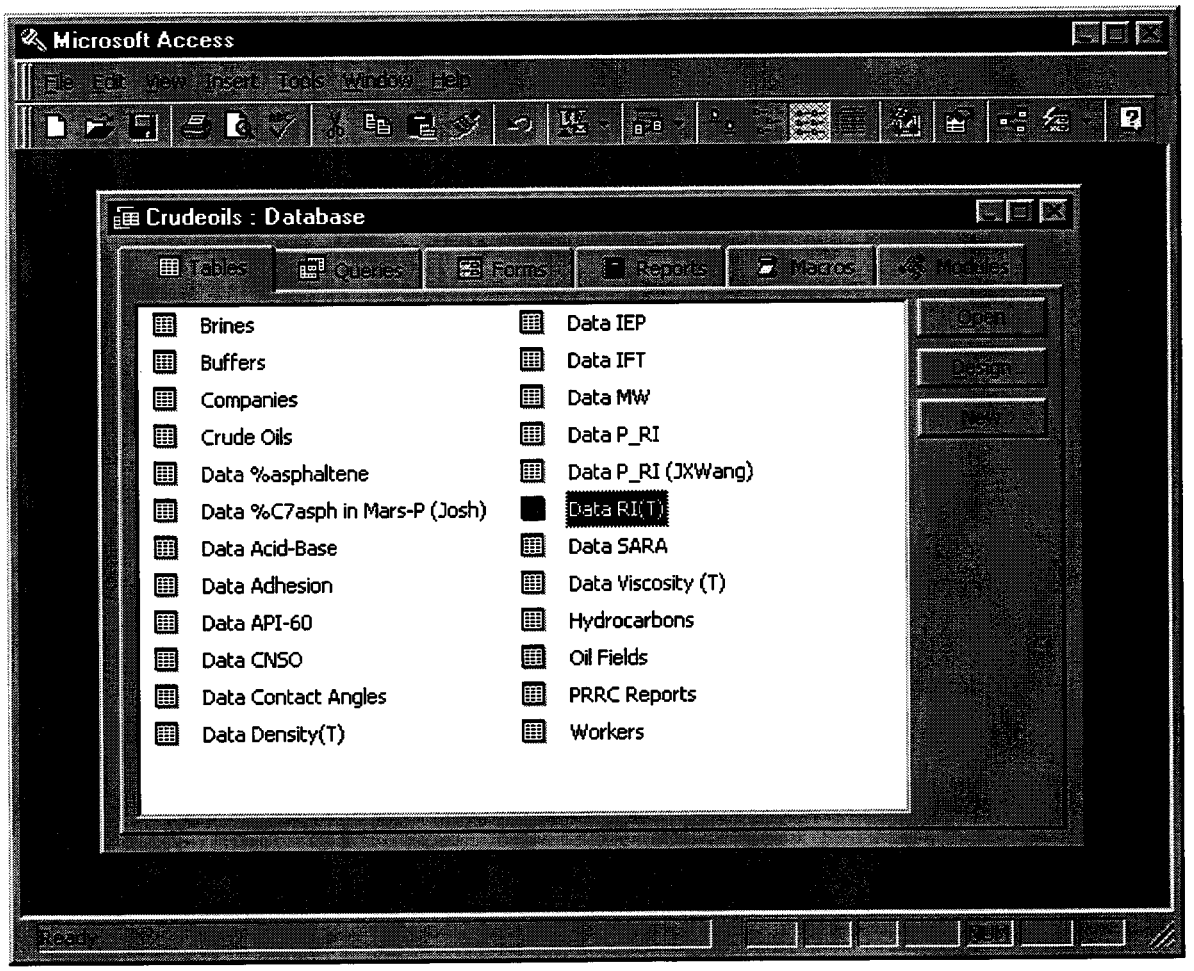

Figure 2.3-1. Main listing of tables in the "CO-Wet" database.

A sample of the information stored in the "Crude Oils" table is shown in Fig. 2.3-2. Each sample we receive is assigned a unique identifying name. (Note that because the cursor is placed in the OIL ID box, the appropriate prompt appears at the bottom of the outer frame.) That unique ID is used throughout the database to connect a variety of data types to a specific oil sample. Multiple samples from the same field are given different IDs because they can differ significantly from one another. The "active" check box can be used to identify samples for which measurements are in progress. A-92 is not active since there is very little sample left. There is room for comments on any other information we might have about a particular sample.

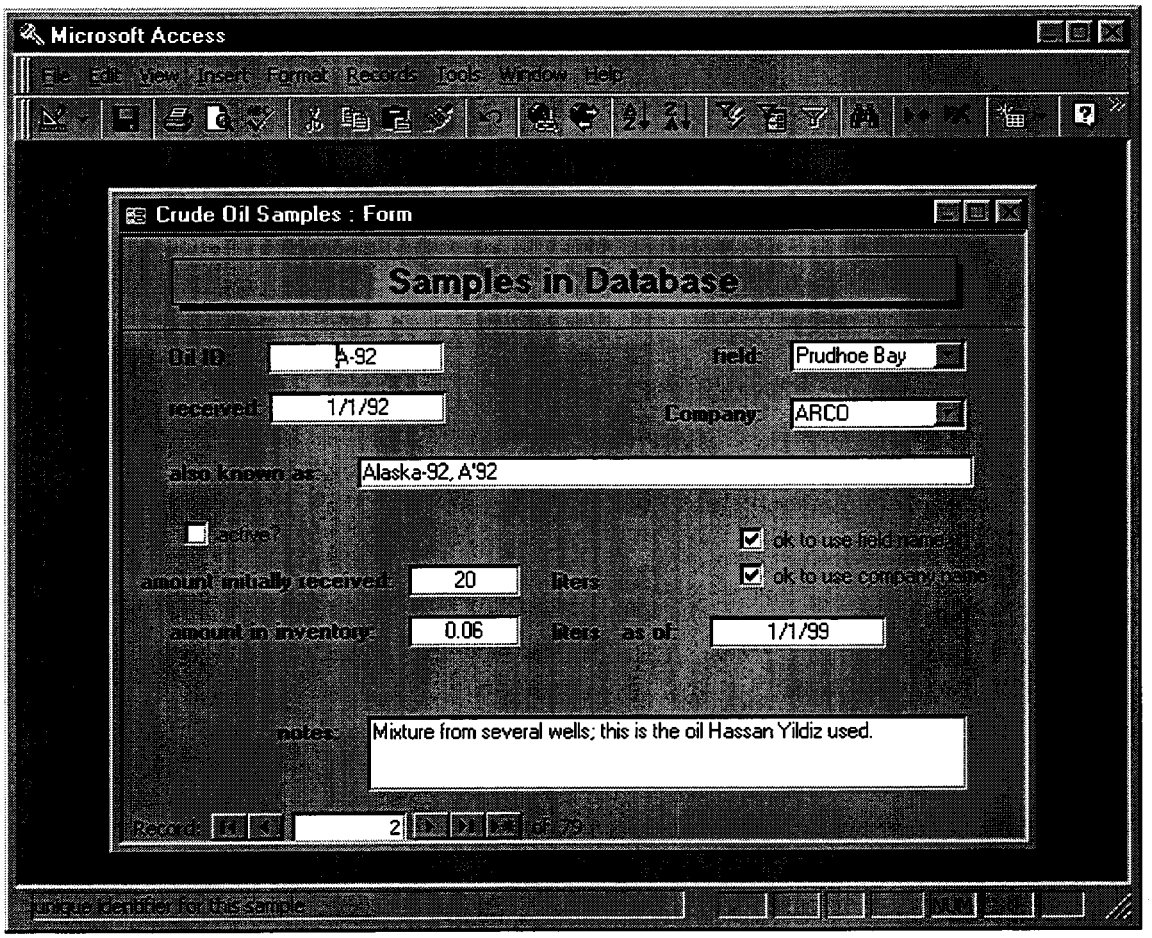

Figure 2.3-2. Form showing contents of a typical record in "Crude Oils" table.

Data tables have been populated both from our records of previous work and with newly measured data. For example, a record in the Data RI(T) table is shown in Fig. 2.3-3. Different tables are used to collect different types of data because the conditions that must be specified can vary. Breaking the data into tables of similar types of data minimizes the overall size of the database. Table 2.3-1 summarizes the oil properties that are being collected in the database.

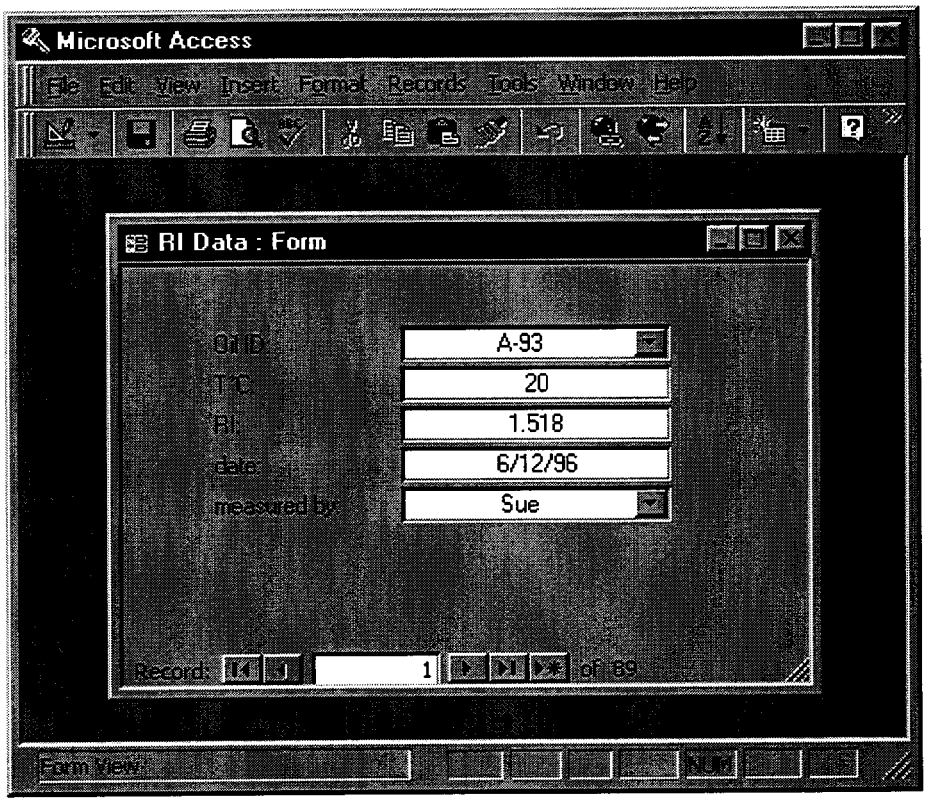

Figure 2.3-3. Entry in "Data RI(T)" table.

Table 2.3-1. Oil properties in "CO-Wet" database

Property	Units	Measurement conditions/techniques
acid number	mg KOH/g oil	ambient
API gravity	°API	60°F
asphaltenes	wt%	varying precipitants (including *n*-heptane)
base number	mg KOH/g oil	ambient
density	g/ml	range of temperatures (including 25°C)
elemental analysis	atom%	C, N, S,and O
isoelectric point	pH	microelectrophoresis
interfacial tension	dyn/cm	du Nuoy ring
average molecular weight	g/mol	freezing point depression
P_{RI} (RI at onset of precipitation)	RI units	varying precipitants (including *n*-heptane)
refractive index	RI units	range of temperatures (including 20°C)
SARA fractions	vol or wt%	chromatographic separation and Iatroscan
viscosity	cP	range of temperatures (including 25°C)

Not all properties are available for every oil. Many of the oil samples are no longer available; others we have only in very small quantities. The suite of measurements performed on any one oil depends on many factors, including:

- when was the oil sample supplied and what tests were we doing at that time,
- how much oil was originally available, and
- how certain are we that there are no oilfield chemicals contaminating the sample.

Selected measurements are summarized in Table 2.3-2 for a small subset of the oils currently in the database.

Table 2.3-2. Examples of crude oils and data

Oil ID	°API	RI@20°C	P_ri	nC7 ppt asph (wt%)	ρ@ 25°C (g/cm^3)	μ@25°C (cp)	Acid # (mg KOH/g oil)	Base # (mg KOH/g oil)
A-90	28.1				0.8797	15.1		
A-92	23.8				0.9033	38.2		
A-93	25.5	1.5187	1.4447	4.0	0.8945	26.7	0.14	2.61
A-95	25.2	1.5156	1.4498	5.8	0.8994	33.8	0.24	2.20
A-95-99	24.6	1.5138					0.20	2.75
Gullfaks-96	27.1	1.4930	no ppt	0.4	0.8856		0.24	1.19
ST-86	29.0		no ppt		0.8748	13.5	0.48	1.07
ST-87	27.8	1.4977			0.8814	23.2	0.29	1.17
Mars-97	30.3	1.4950	1.4340	1.9	0.8784	20.8	0.39	1.79
Mars-P	17.0	1.5383	1.4285	5.1	0.9458	342	3.92	2.30
Mars-TC	25.4	1.5100			0.8954	49.3	0.49	1.88

The data summarized in Table 2.3-2 show a relational application of the database since Table 2.3-2 was assembled by querying the database. Consider the samples with IDs beginning "A-", which are from the Prudhoe Bay field in Alaska. Numbers refer to the year that each sample was received. The oldest samples were used in core and surface tests before oil characterization work began. Although we cannot go back and measure acid numbers, base

numbers, and refractive indices for these samples, we can see from the later samples that the Prudhoe Bay oils appear to have consistent properties. All have low acid numbers and higher base numbers, and the dead oil samples are fairly good solvents for their asphaltenes (based on the RI values for the oil samples as compared to P_{RI} values at the onset of asphaltene precipitation). Similar characteristics may well have applied to the earlier samples from this field. Properties of oil samples from the Gullfaks field can also be seen to be fairly consistent over a long period of time. ST-86 and ST-87 were supplied from the Gullfaks reservoir more than 10 years ago; their properties are similar to Gullfaks-96, received much more recently. The three Mars samples, on the other hand, are clearly three different oils.

The accumulated data can be used to establish trends that facilitate estimates when measurements are unavailable. Figure 2.3-4 compares all the data currently in the database for measurements of both API gravity and refractive index on the same oil sample. There is a linear correlation ($r^2 = 0.94$) over a wide range of oil gravity values.

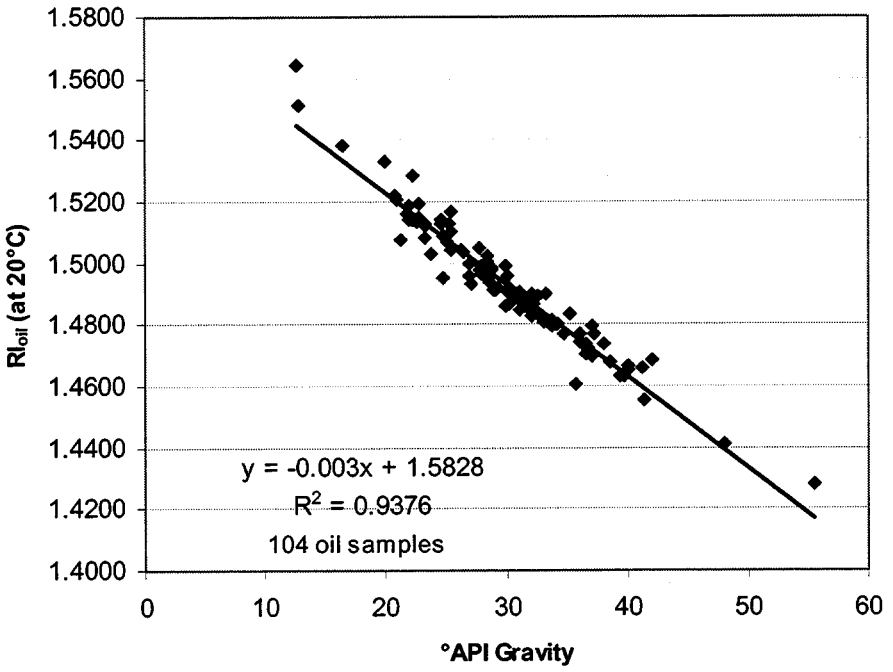

Figure 2.3-4. Correlation between API gravity and refractive index.

Correlation with API gravity has also been suggested for estimating acid and base number, but as shown in Fig. 2.3-5, such correlations are unlikely to provide sufficiently accurate results to be of practical use. It is also sometimes suggested that acid and base number should be related to one another. Figure 2.3-6 shows that there is even less correlation between these two important measures of polar components in oil than either of them has with API gravity. Two arbitrary lines of constant base number-to-acid number ratio (B/A=1 and B/A=10) are shown in Fig. 2.3-6. The database and library of oils can be used to test hypotheses that oils with an excess of bases over acids or those with an excess of acids over bases are most those most likely to be active in wettability alteration.

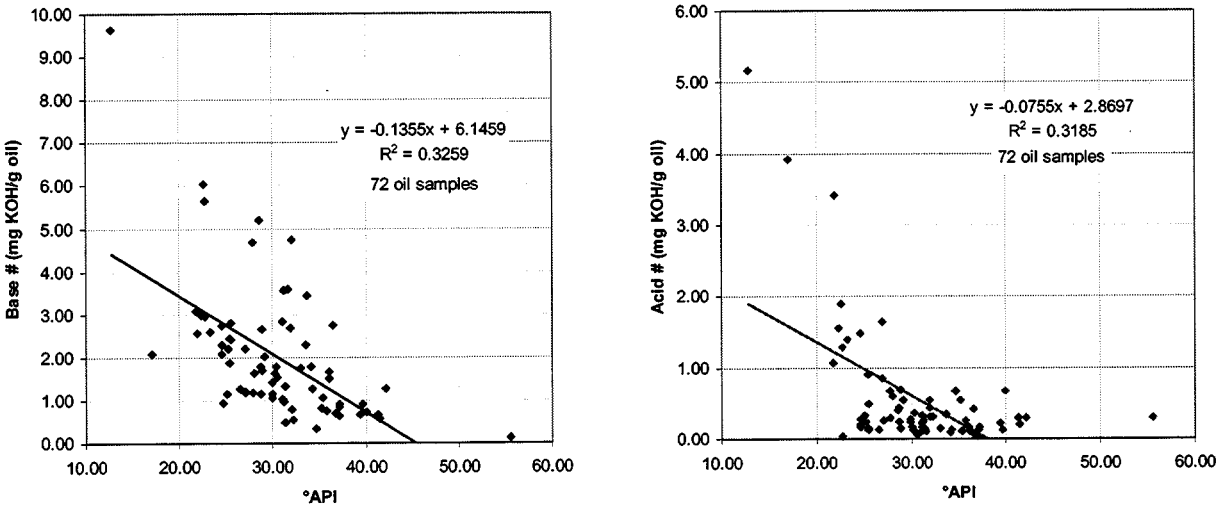

(a) base number vs API gravity

(b) acid number vs. API gravity

Figure 2.3-5. API gravity is only broadly correlated with either acid or base number.

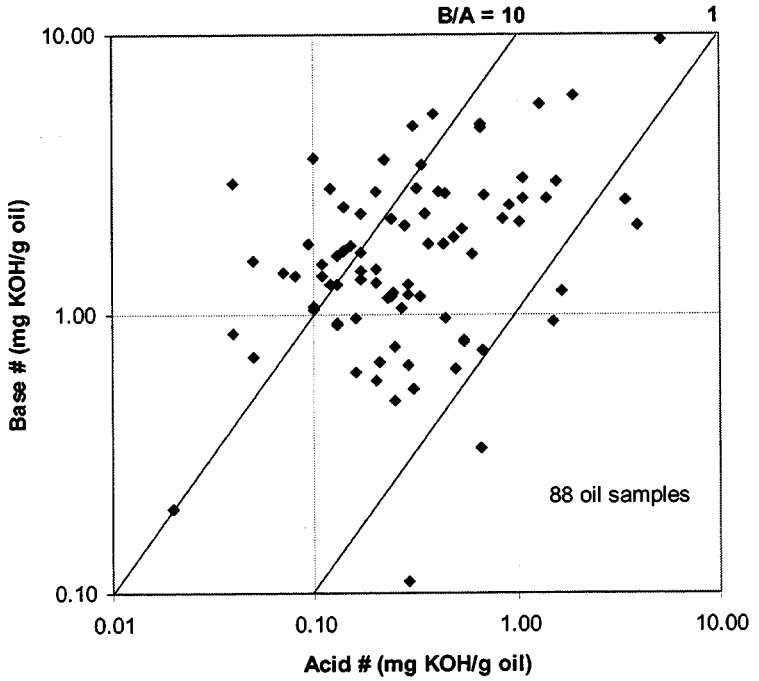

Figure. 2.3-6. The independence of acid and base number are illustrated with data for 88 oil samples. Lines of constant values of base number/acid number (B/A) are marked. On average, base numbers are greater in magnitude than acid numbers.

Figure 2.3-7 summarizes asphaltene stability data. The abscissa is the RI of an oil sample and is a measure of the solvent quality of that oil. Higher values represent better solvent quality.

The ordinate shows the RI at the onset of precipitation (P_{RI}) and is thus a measure of the tendency of asphaltenes in each oil to precipitate upon addition of n-heptane. Higher values indicate less stable asphaltenes. Together these parameters define the stability of asphaltenes in a particular oil sample. The closer P_{RI} is to RI_{oil}, the less stable is the overall mixture. Diagonal lines show constant values of RI_{oil} - P_{RI}, with stability decreasing toward the upper left-hand-side of the diagram. Oils in the least stable parts of the diagram are the most likely candidates for alteration of wetting by the surface precipitation mechanism.

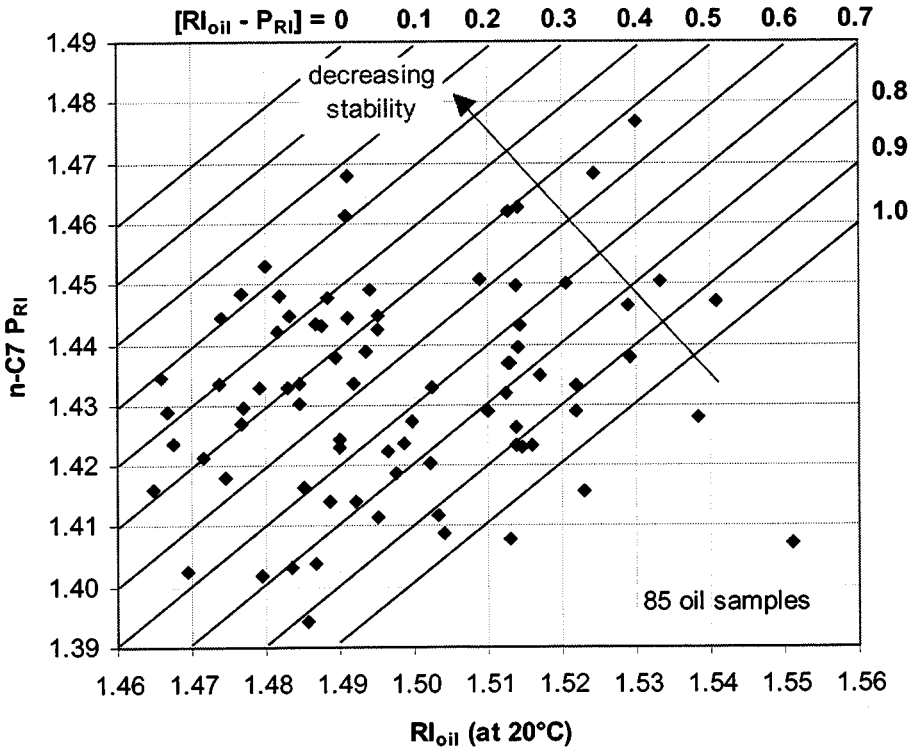

Figure 2.3-7. Asphaltene stability diagram. The abcissa is a measure of the oil's solvent quality—higher RI_{oil} corresponds to better asphaltene solvency. The ordinate is a measure of relative stability of different asphaltenes—higher numbers correspond to greater instability. Thus the least stable asphaltenes are those in oils that fall in the upper left-hand corner of the diagram, with stability increasing toward the lower right-hand corner.

2.3.2 COBR Interactions

In addition to crude oil properties, the database contains the results of our two standard tests of surface wetting properties of crude oils: (1) adhesion of a drop of crude oil under brine upon contact with a clean mineral surface and (2) probe fluid contact angle measurements on surfaces that have been exposed to brine and crude oil. An example of adhesion test results is illustrated in Fig. 2.3-8.

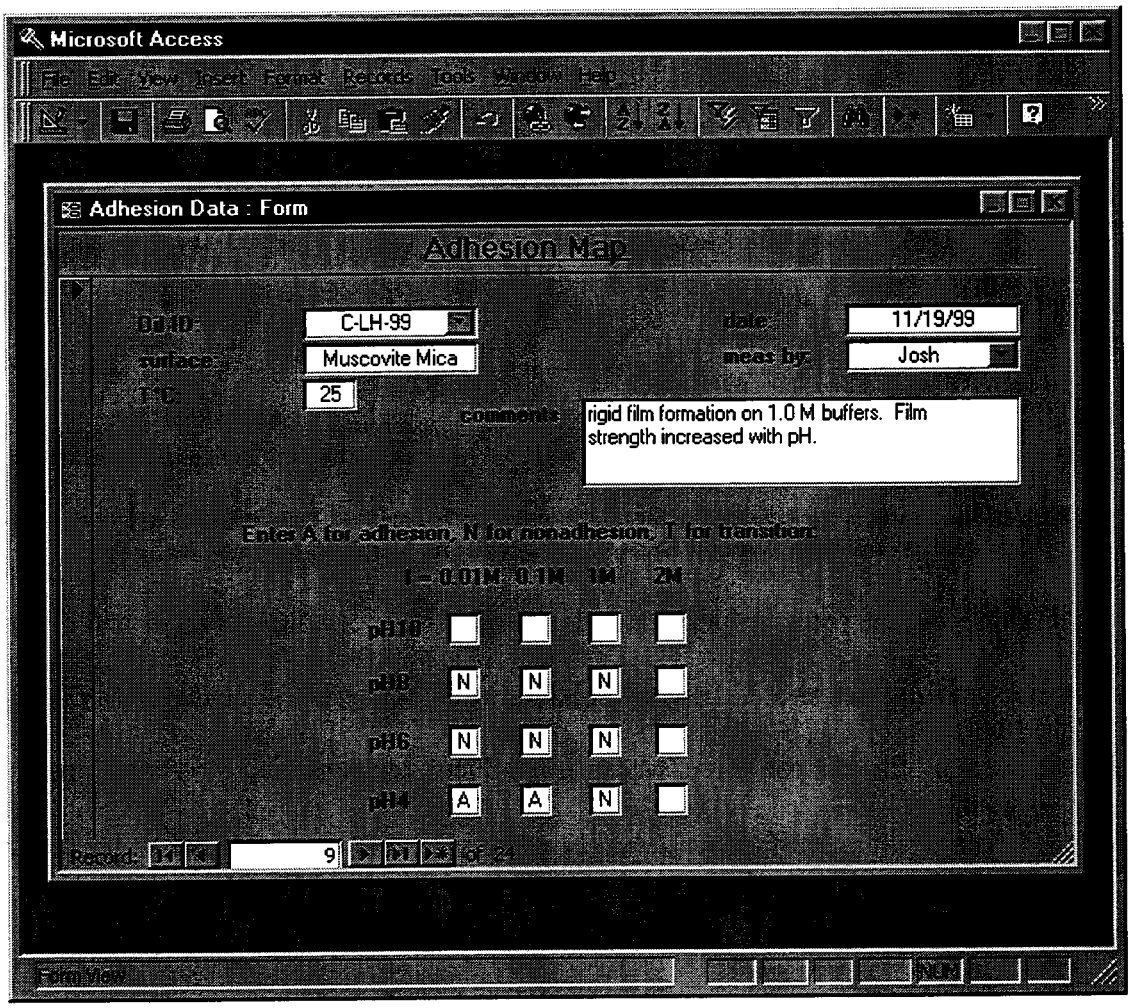

Figure 2.3-8. Results of adhesion tests are stored in a standard format that facilitates viewing of the results.

Examination of the adhesion data does not yet show any clear trends. Figure 2.3-9a shows adhesion indices for 17 different oil samples tested on mica; 12 oils tested on hematite are

shown in Fig.2.3-9b. The mica results are quite scattered. There may, however, be trends in the hematite data toward more adhesion with higher basicity of the oil (as indicated by B/A) and less stable asphaltenes (i.e., lower values of RI_{oil} - P_{RI}). There is more adhesion on hematite than mica overall. The trends observed with hematite may be fortuitous in that those oils tend to have an inverse correlation between B/A and RI_{oil} - P_{RI} whereas the oils tested on mica show no correlation between these two variables.

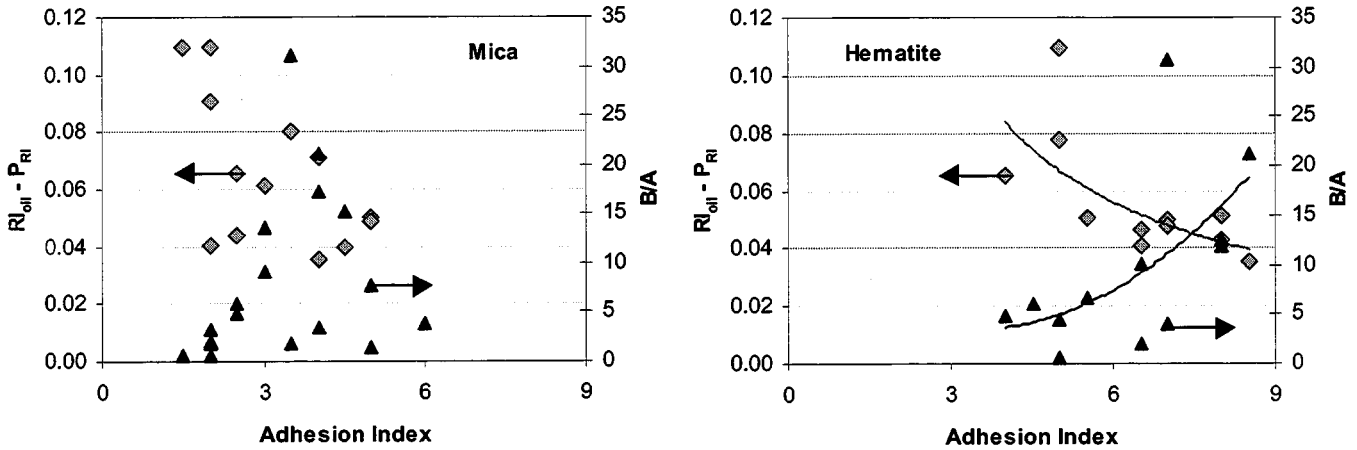

(a) Adhesion indices on mica surfaces

(b) Adhesion indices on hematite surfaces

Figure 2.3-9. Adhesion indices for crude oil adhesion to mica and hematite. Data on mica are very scattered, but weak trends with B/A and $RI_{oil} - P_{RI}$ may exist for adhesion on hematite.

In Fig. 2.3-10, the record of a contact angle test with probe fluids (water and decane) is shown. A mica surface was treated first with pH4 brine (0.01M NaCl), then with A-93 oil. The surface remained in the oil for three weeks at ambient temperature, then was rinsed with cyclohexane. The resulting surface was weakly water-wet with θ_A of 51° for water advancing over a decane-covered surface and 27° for a receding water drop.

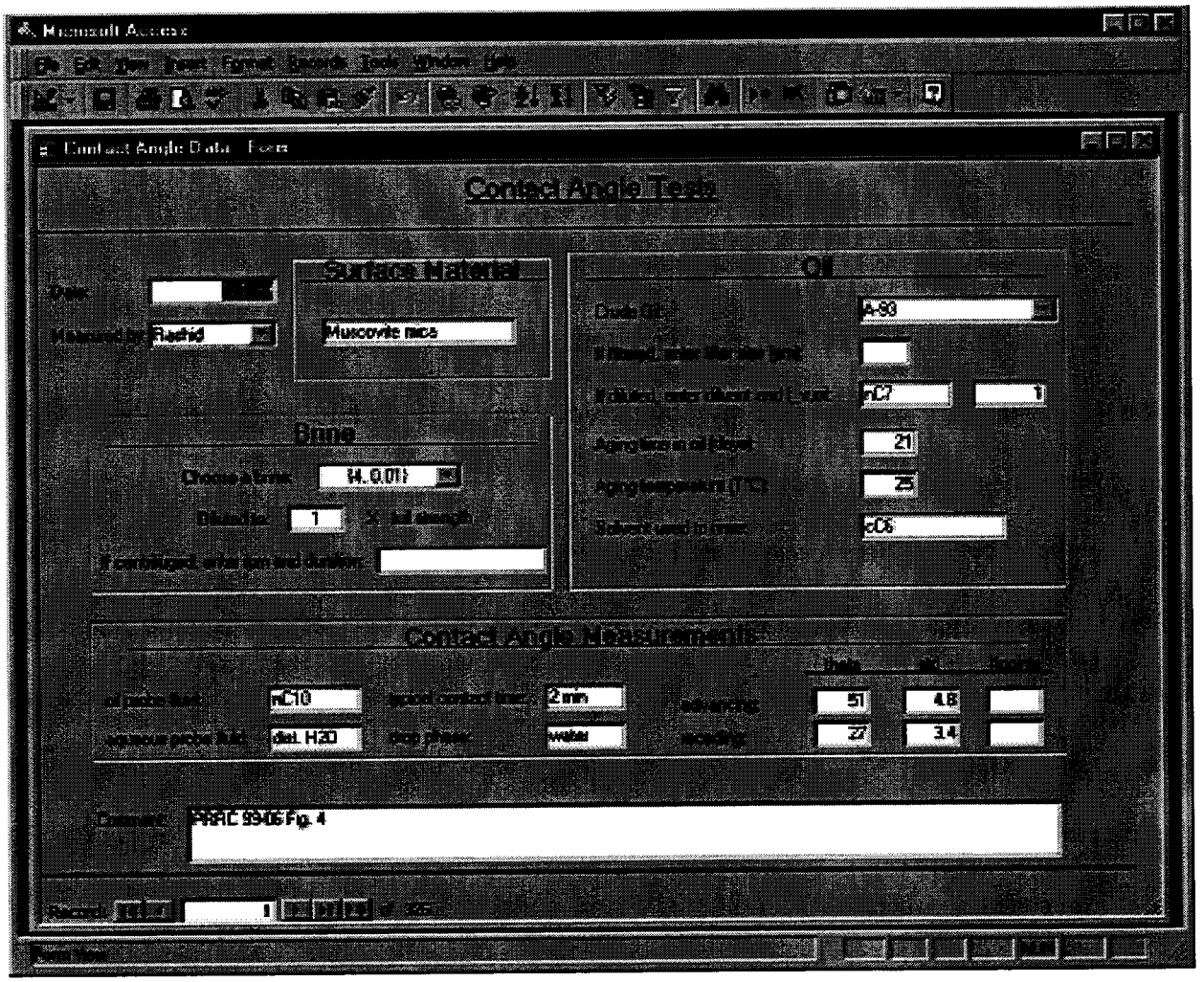

Figure 2.3-10. Records of contact angle tests document all the variables that may impact these results.

The database structure will allow us to manage additional information efficiently and to find relationships among the many variables that are important for the control of reservoir wetting.

PART 3. IMPROVED RECOVERY

3.1 Rate Effects in Non-Water-Wet Rocks

An investigation into the effects of flow rate on the relative permeability end points under different wetting conditions has been carried out. Results from extensive laboratory experiments on Berea sandstones indicated that rate dependence of relative permeability end points existed over a 400-fold range of flow rate variations (0.3ft/day to 120ft/day), and was influenced by wetting properties of porous media.

Wettability conditions established by exposing Berea sandstone cores to brine and crude oil were assessed by measurement of the imbibition rates. Initial rates of spontaneous imbibition were found to be a better indicator for wettability assessment than final oil recovery or residual oil saturation. Extensive waterflooding and/or aging core in brine at residual oil saturation may alter mixed-wet cores to more water-wet conditions.

For strongly water-wet conditions, water permeability at residual oil saturation was essentially independent of flow rate while residual oil saturation remained unchanged.

For mixed-wet conditions, however, increasing flow rate in a stepwise fashion could substantially increase water permeability end points, even after the mobilization of residual oil ceased. Hysteresis existed between rate-increasing and rate-decreasing processes. Water relative permeabilities at residual oil were generally lower if rates were increasing than those measured during experiments with rate decreasing. Moreover, pressure gradients were not proportional to flow rates during rate-increasing steps, whereas pressure gradients were linearly proportional to flow rate during rate-decreasing steps. These results demonstrated that apparent water permeability end points vary with flow rates when the rate is increasing, but are constant when the water flow rate is decreased.

Rate dependence of relative permeability end points could be ascribed to microscopic redistribution of the fluid phases within the pore space as flow rate varied. Outlet capillary end-effects were not distinguishable from other variables.

Caution should therefore be taken when conducting laboratory displacement tests at high flow rates for mixed-wet conditions. If fluid distributions within pore level are sensitive to flow rate even at fixed residual oil saturation, it is likely that different flowing patterns could occur between high flow-rate and low flow-rate waterfloods. Therefore, it is questionable whether relative permeability and displacement efficiency obtained from high flow-rate tests can be applied to the reservoir.

Some background on rate effects

The effects of the flooding rate on relative permeability as well as on the displacement efficiencies during waterflooding tests have long been a controversial subject in petroleum literature. This problem because a huge gap exists between the flow rate experienced by fluids in a reservoir—typically around several ft/day—and the flow rate conventionally employed in most laboratory displacement tests, which could be hundreds of times that in the reservoir. Both for convenience and to minimize artifacts introduced by capillary effects, high flow rates have been widely used in both steady-state and unsteady-state displacement tests. However, whether results from high and low flow rate tests are consistent or, if not, which result is more representative of transport properties in reservoir environments, remains an open question.

Effect of flow rate on relative permeability curves:

Previous experimental investigations reported in literature have led to divergent conclusions as to how the flow rate affects relative permeability.

No rate dependence: Leverett *et al.* (1939, 1941) attributed the influence of flow rate on relative permeability to an end effect, as previously described by Hassler *et al.* (1936). Leas *et al.*

(1950), Osoba *et al.* (1951), Richardson *et al.* (1952), Sandberg *et al.* (1958), and Pirson (1958) all found that drainage relative permeability is independent of the flow rate. Ehrlich and Crane (1969) concluded that both imbibition and drainage relative permeability measured by the steady-state method were independent of flow rate. Labastie *et al.* (1980) reported that, for both water-wet sandstone and fractional-wet carbonate cores, water relative permeability remained practically unchanged with velocity and only truncated to a different residual oil saturation when velocity was reduced, whereas oil relative permeability was a little different only when approaching residual oil saturation. In 1985, Odeh and Dotson asserted that rate dependence of drainage relative permeability for water-wet reservoir core samples was principally induced by an outlet end-effect and could be removed by an appropriate correction method.

Rate dependence (oil-water): Lefebvre du Prey (1973) concluded that relative permeability was a function of velocity (v) when the viscous forces predominate. Heaviside *et al.* (1987) found for intermediate-wet North Sea sandstone, water relative permeability, along with the end-point $K_{rw}(S_{or})$, was much lower for low rate floods than for high rate floods. They ascribed this rate sensitivity of relative permeability to the change of microscopic distributions of each phase in the pore space induced by varying flow rates, because no capillary end effects were observed.

Rate dependence (gas-liquid): Rate dependence is also found in gas-liquid systems. Wyckoff and Botset (1936) reported that relative permeabilities were rate sensitive when water and gas were flowing under the same pressure gradient. Morse *et al.* (1947), Henderson and Yuster (1948) found that relative permeability was rate dependent in all gas-liquid systems that were studied. Caudle *et al.* (1951) reported that relative permeability decreased with an increase in flow rate when one of the flowing phases was a gas.

Effect of flow rate on relative permeability end points:

Only a few studies have been reported in the literature that focus on the rate dependence phenomena of relative permeability at residual oil saturation.

Strongly water-wet Berea sandstones: In 1983, Morrow *et al.* investigated relative permeabilities at reduced residual oil saturations. For strongly water-wet Berea sandstone, they found that water relative permeabilities at the end of a normal waterflood were sometimes sensitive to pressure gradient. In one case, a highly permeable Berea core (K_a=860 md) showed a relative permeability decrease with increasing pressure gradient to about 141 psi/ft at the end of a low capillary number waterflood ($K_w\Delta P/L\sigma<10^{-6}$). This trend was observed to be reversible. In another case, however, a K_a=150 md core showed a slight increase in relative permeability end point with pressure gradient increasing to about 30 psi/ft. These results were generally erratic and not reversible. Once the critical pressure gradient was exceeded, oil began to move and a new reduced residual oil saturation was achieved. Consequently, a sharp increase of relative permeability was measured at each reduced oil saturation. However, rate sensitivity of relative permeability was no longer observed once oil was mobilized. This phenomenon was explained by the possible minor adjustments in both position and size of oil blobs in accordance with the applied pressure gradient changes. The residual oil blobs act as "leaky check valves" which might increase the blockage of pore throats and lead to increase in resistance to water flow.

Weakly water-wet Berea sandstone: Another experiment reported the influence of capillary number on relative permeability end point under weakly water-wet conditions (Morrow *et al.*, 1986). After aging in Moutray crude oil, Berea sandstone core plugs were waterflooded to residual oil under low capillary number ($K_w\Delta P/L\sigma\leq10^{-6}$). Pressure gradients were then increased in steps. Water relative permeability increased even before oil mobilization ($K_w\Delta P/L\sigma<8x10^{-5}$). This relative permeability variation was partly reversible. Observations from the water

displacement behavior in a 2D glass micromodel utilizing the same fluids revealed that most of recoverable oil was displaced from large pore bodies. A significant amount of retained oil was held in the pore throats that served to block water flow. This behavior is distinctly different from that under strongly water-wet conditions, in which most of residual oil was retained in large pore spaces. A "spotted" or "speckled" wettability was suggested to describe this kind of heterogeneous wetting. Increasing pressure could partially displace some residual oil from pore throats, even though it might not be produced, resulting in the reduction of resistance to water flow and increase of water permeability without a change in saturation. Oil could often regain its original position in the temporarily opened pore throats when the pressure gradient was decreased, leading to a restoration of low water permeability.

Intermediate-wet mudstones: Kamath *et al.* (1995) reported that both oil permeability at initial water saturation, $K_{ro}(S_{wi})$ and water permeability at residual oil saturation, $K_{rw}(S_{or})$, were sensitive to injection rates for short (L<2cm), low-permeability, intermediate-wet mudstone cores. $K_{ro}(S_{wi})$ increased smoothly with rate at low capillary number ($10^{-7}<v\mu/\sigma<2x10^{-6}$). $K_{rw}(S_{or})$ also increased with flow rate within similar capillary number range but showed the existence of critical points, $v\mu/\sigma\leq2x10^{-7}$, at which the increase of $K_{rw}(S_{or})$ was dramatic. Many PVs of injected fluid were required to reach equilibrium at a critical point. It was emphasized that under the conditions of very short cores and very low capillary numbers, end-effects predominated. Corrected $K_{rw}(S_{or})$ from a proposed technique showed that the true water permeabilities were underestimated about 63% for low rate and 31% for high rate. However, no details were given regarding how the water and oil saturations varied during rate-increasing floods. Therefore, it is impossible to evaluate how much contribution to permeability change comes from saturation variation rather than from change of flow rate.

Relative permeability:

Relative permeability is a measure of the ability of the porous system to conduct each fluid phase when more than one phase is present. For each phase, it is the ratio of effective permeability for that phase to the base permeability, which can be the air permeability, water permeability, or effective oil permeability at initial water saturation. Many parameters affect relative permeability, including pore geometry, wettability, fluid properties, fluid saturations, and saturation history.

Fundamental equations: It is commonly assumed that Darcy's law, an empirical equation for single phase flow, is valid to describe multiphase flow in porous media as well. For an immiscible, incompressible oil/water linear flow system, the combination of Darcy's law with mass conservation yields (Collins, 1961; Douglas *et al.*, 1958):

$$a(S_w)\frac{\partial S_w}{\partial \zeta}+\frac{\partial}{\partial \zeta}\left[b(S_w)\frac{\partial S_w}{\partial \zeta}\right]+c(S_w)\frac{\partial S_w}{\partial \zeta}=-\frac{\partial S_w}{\partial \tau} \tag{3.1-1}$$

where

$$\zeta=\frac{x}{L}, \qquad \tau=\frac{Qt}{\phi AL}=\frac{vt}{\phi L} \tag{3.1-2}$$

are dimensionless distance from flood front to core inlet end, and dimensionless displacement time, respectively. $a(S_w)$, $b(S_w)$, and $c(S_w)$ are defined as:

$$a(S_w)=\frac{d}{dS_w}\left[\frac{1}{1+\frac{k_{ro}\mu_w}{k_{rw}\mu_o}}\right] \tag{3.1-3}$$

$$b(S_w)=\frac{kk_{rw}\frac{dp_c}{dS_w}}{L\mu_w v\left[1+\frac{k_{rw}\mu_o}{k_{ro}\mu_w}\right]} \tag{3.1-4}$$

$$c(S_w) = -\frac{kg\sin\alpha}{Q}\frac{d}{dS_w}\left[\frac{\frac{k_{rw}}{\mu_w}\rho_w + \frac{k_{ro}}{\mu_o}\rho_o}{1+\frac{k_{ro}\mu_w}{k_{rw}\mu_o}}\right] \tag{3.1-5}$$

Equation (3.1-1) governs the water saturation profile during a water displacement process. It is a second-order, quasi-linear parabolic differential equation which can only be solved numerically (Douglas *et al.*, 1958, Chavent *et al.*, 1980). A 1-D finite element simulator based on the principle of equation (3.1-1) will be used to obtain water-oil relative permeabilities from experimental displacement results. Terms on the left side of equation (3.1-1) represent the contributions from viscous, capillary, and gravity forces, respectively. For a horizontal flow system (α=0), the third term vanishes. If $b(S_w)$ is small, the contribution from capillary force is also negligible compared to that from viscous force, allowing further simplification of equation (3.1-1) which gives (Collins, 1961)

$$\left(\frac{d\zeta}{d\tau}\right)_{S_w} = \frac{df_w}{dS_w} \tag{3.1-6}$$

where

$$f_w = \frac{1}{1+\frac{k_{ro}\mu_w}{k_{rw}\mu_o}} \tag{3.1-7}$$

is water fractional flow when both capillary and gravity are neglected. Equation (3.1-6) is the well-known Buckley-Leverett equation (Buckley and Leverett, 1942), which can be integrated to solve the two-phase flow problem directly from displacement data (Welge, 1952; Johnson *et al.*, 1959; Jones and Roszelle, 1978). The Buckley-Leverett approach gives a shock displacing front. The accuracy of this approximation strongly depends on the magnitude of $b(S_w)$.

Effects of capillary forces on displacement tests: Distribution and flow of immiscible phases in porous media are controlled by viscous, capillary, and gravity forces. Existence of capillary forces can cause diffusion of the displacement front and end-effects that are particularly influential in short cores.

Diffusion (or spreading) of the displacement front results if capillary forces are significant. For the strongly water-wet case, water can be spontaneously imbibed into the region ahead of the flooding front, causing a distortion to the shock front.

For strongly water-wet porous media, as soon as flooding water first contacts with the inlet surface, water spontaneously imbibes into the core at the point of contact, causing a simultaneous counterflow of oil out of the core. This establishes localized, low-resistance flowing paths to water. As the flood progresses, water tends to continue entering the core only in those low-resistance local areas, contributing to the establishment of regions of unstabilized, non-linear flow within the core. This inlet end effect is more serious with shorter core samples, high oil-water viscosity ratios, and high flooding velocities. It can result in early water breakthrough and reduction of oil recovery at water breakthrough.

When water first reaches the outlet face of a water-wet core, it will not leave the core but will accumulate inside a short region near the outlet, due to the abrupt change of capillary pressure (P_c=0). This results in an excess water saturation at the outlet face and retards the water breakthrough. The saturation distribution profile predicted by the Buckley-Leverett equation is distorted near the outlet end, and oil recovery at breakthrough is higher than expected.

Effects of flow rate on displacement tests: Neglecting gravity, increasing flow rate increases the viscous force and reduces the relative significance of capillary contributions.

Diffusion of the flooding front can be reduced if flow rate is increased, and the flow is more "stablized". However, one problem could be encountered when high flow rates are applied in strongly water-wet cores with high viscosity oils during an unsteady-state waterflood. The high viscosity oil will not have sufficient time to adjust to high rate at flooding front, thus injected water tends to finger through the large pores, causing channeling and early breakthrough and making the waterflood appear as if the core were oil-wet (Craig, 1971).

Flow rate has opposite impacts on inlet and outlet end effects. At the inlet face, low flow rate allows capillary forces to redistribute invading water over the whole cross-section, thereby reducing the severity of channeling. At the outlet face, high flow rate can minimize the zone of excess water accumulated and reduce the end effect. Generally the inlet end effect does not significantly affect the overall flooding behavior except for very short core samples, and is less important than outlet end-effect (Kyte and Rapoport, 1958). Therefore high-rate tests have often been recommended to maximize viscous forces and thus offset potential outlet end effects. However, tests at rates well above those typical in an oil reservoir can introduce other problems as we will see in this study, especially in cores that are not strongly water-wet.

When flow rate is extremely high, another problem, i.e., non-Darcy flow, can be encountered. As early as 1901, Forchheimer pointed out that high-velocity flow in porous media could result in a pressure gradient greater than that predicted by Darcy's law. Based on Forchheimer's proposal, Green and Duwez (1951) derived the following equation:

$$-\frac{dp}{dL} = \frac{\mu v}{k} + \beta \rho v^2 \qquad (3.1\text{-}8)$$

where ρ is fluid density, β is a rock characteristic parameter independent of the dimensions. Other parameters are as described in the nomenclature section. The first term on the right side of equation (3.1-8) represents the contribution from Darcian flow and the second term is the

contribution of high-velocity flow. At very high flow rates, higher order terms in velocity might also be required.

The mechanisms of non-Darcy flow are still not clearly known. Early descriptions (Fancher and Lewis, 1933; Cornell and Katz, 1953) attributed the nonlinearity to turbulent flow, but experiments showed that nonlinearity appeared much before the onset of turbulence (Green and Duwez, 1951; Ahmed and Sunada, 1969). Hassanizadeh and Gray (1987) stated that the increased microscopic viscous (drag) force on the pore walls is the source for the onset of nonlinearity. Barak (1987) ascribed the nonlinearity to microscopic inertial forces associated with formation of local vortices and development of tortuous streamlines within individual pores when Reynolds number increases. Temeng (1989) suggested that Darcy's law is adequate to describe the high-velocity flow if changes of fluid properties along the flowing path are taken into account. However, this opinion was later debated by Firoozabadi *et al.* (1995) through reexamining the experimental results reported.

Non-Darcy flow is encountered in many disciplines, including civil, chemical, hydrology and petroleum engineering. In petroleum, it is usually associated with gas flow near the wellbore, where gas velocity is very high. However, non-Darcy flow could theoretically occur for any fluid flow in porous media with sufficient high flow rate. The possible significance of non-Darcy flow at the flow rates employed in this study and its contribution to rate dependence of relative permeability end points will be examined.

Scaling coefficient: The extent of capillary influences on displacement in porous media, especially the outlet end effect, can be evaluated by the scaling coefficient $L\mu_w v$.

Rapoport and Leas (1953) found that for both oil-wet and neutral-wet alundum cores, oil breakthrough recovery was independent of length, velocity, and viscosity as long as $L\mu_w v$ was

higher than 1 cp·cm^2/min. Results from a variety of other porous materials also showed constant breakthrough recovery if $L\mu_w v$ was between 0.5 and 3 cp·cm^2/min. Under such conditions, the displacement was called "stabilized" and the influence of capillarity on flowing behavior, both end effects and diffusion of flood front, was assumed to be negligible. A critical scaling coefficient, $1<L\mu_w v<5$, has been widely accepted in the petroleum industry and is still commonly used as a criterion to minimize capillary effects in laboratory displacement tests.

Capillary number: The original application of "capillary number" or "critical displacement ratio" was to provide criteria for mobilizing residual oil. More than a dozen of different definitions of capillary number have been suggested (Taber, 1980), but they all represent the ratio of viscous to capillary forces. Most of those definitions can be cataloged into two major groups: $N_{cap} \propto \Delta P/L\sigma$ and $N_{cav} \propto v\mu_w/\sigma$, which are correlated by Darcy's law:

$$\frac{v\mu_w}{\sigma} = k_{rw}\frac{k_w \Delta P}{L\sigma} \tag{3.1-9}$$

where k_{rw} is water relative permeability with water permeability for water-saturated core as the base permeability.

Chatzis and Morrow (1984) found that for strongly water-wet Berea sandstone with Soltrol-130 as the oil phase and 2% C_aCl_2 as the brine phase, the capillary number $k_w\Delta P/L\sigma$ at onset of residual oil mobilization was around $2x10^{-5}$ over a wide range of permeability (148-1600md). Morrow *et al.* (1986) also reported an onset of residual oil mobilization to be around $8x10^{-5}$ for mixed-wet Berea sandstone.

It should be pointed out that the most successful applications of capillary number are in strongly water-wet porous media, mainly because the capillary force in a water-wet system ($\cos\theta=1$) can be simply described by the interfacial tension alone without explicitly accounting

for wettability (Heaviside *et al.*, 1987). For other wetting conditions, traditional capillary number becomes less meaningful because no simple description of capillary force is readily available.

In this study, N_{cap} and N_{cav} represent dimensionless pressure gradient and dimensionless flow rate, respectively. In commonly used units, these capillary numbers can be expressed as follows:

$$N_{cav} = \frac{1}{3.6\times10^{5}} \frac{Q\mu_w}{A\sigma} \left(\frac{\mu_w}{\mu_o}\right)^{0.4} \tag{3.1-10}$$

$$N_{cap} = 6.8044\times10^{-7} \frac{k_w \Delta P}{L\sigma} \tag{3.1-11}$$

where Q in ml/hr, A in cm^2, σ in dyn/cm, μ_w and μ_o in cp, k_w in md, ΔP in psi, and L in cm. An empirical factor $(\mu_w/\mu_o)^{0.4}$ is introduced in the capillary number N_{cav} to account for the influence of viscosity ratio (Abrams, 1975). At residual oil saturation, the ratio of N_{cav} to N_{cap} corresponds to $k_{rw}(S_{or})$:

$$k_{rw}(S_{or}) = \left(\frac{\mu_o}{\mu_w}\right)^{0.4} \frac{N_{cav}}{N_{cap}} \tag{3.1-12}$$

Wettability:

Wettability is the relative affinity of a solid surface for immiscible fluids. The importance of wettability lies in its influence on fluid distributions. It affects capillary pressure, relative permeability, waterflood displacement efficiency and electrical properties.

Wettability categories: In a crude oil/brine/rock (COBR) system, wettability can be divided into two major categories: uniform and nonuniform. Uniform wetting means that all surfaces have the same wetting preference, which could be a strongly water-wet, strongly oil-wet, weakly water-wet, weakly oil-wet, or intermediate-wet. Nonuniform wetting implies that

rock surfaces consist of both water-wet and oil-wet portions. This situation has been referred to by many terms: fractional, mixed, spotted, speckled, or Dalmatian wettability. A special type of mixed wetting was suggested by Salathiel (1973), in which oil-wet surfaces exist in large pores and form continuous paths throughout the core, whereas the smaller pores remain water-wet and contain no oil. This mixed-wet condition occurs if the oil deposits a layer of oil-wet organic material only on those rock surfaces that are in direct contact with the oil, but not on the brine-covered surfaces (Anderson, 1986a). This mixed-wet condition allows oil to have a finite permeability even at very low oil saturation, resulting in very efficient oil recovery. A reverse mixed-wet case was reported by Mohanty and Salter in 1983, in which the large pores have continuous water-wet surfaces, while the small pores are oil-wet. In some cases, mixed-wet cores may spontaneously imbibe both water and oil. Recent studies tend to suggest that mixed-wet conditions are likely to occur in many oil reservoirs.

Mechanism of wetting alteration: Most reservoir rocks are inherently water-wet, except for a few mineral surfaces (Anderson, 1986a). Wetting alteration occurs when polar components from crude oil adsorb onto mineral surfaces. Asphaltenes are generally assumed to have the greatest impact. Depending on the solvent quality of crude oil, asphaltenes can exist as either macromolecules (molecular weight: 1000-3000), colloids (molecular weight: hundreds of thousands), or states between these two extremes, leading to different mechanisms of wetting alteration.

As macromolecules, asphaltenes, as well as other crude oil components with polar functionality, can adsorb onto high energy mineral surfaces through polar interactions or ionic interactions. Polar interactions occur only when water is absent and thus have significance only in laboratory tests—but not in reservoirs where water is always a factor. Ionic interactions occur

when water is present. They are strongly dependent on the distribution of water, the compositions of oil and brine, and mineralogy of rock surfaces. The ability of crude oil to alter wetting through ionic interactions can be described by acid and base numbers of that oil. In general, oils with either high acid number or high base number, but not both, appear to be most active in altering wetting by ionic interactions.

The precipitation of colloidal asphaltenes onto mineral surfaces, which can precede the onset of flocculation of asphaltenes in bulk oil, provides another mechanism of wetting alteration. Extent of colloidal interactions is determined by stability of asphaltenes in a crude oil, which can be quantified by mixture refractive index. Colloidal interactions are most effective near the onset of asphaltene precipitation. The concentration of asphaltenes has less importance than the composition of the oil phase in which they are suspended.

Wettability measurements:

Many different methods, some quantitative and others more qualitative, have been proposed for characterizing the wettability of porous media (Anderson, 1986a). The three most commonly used quantitative methods are contact angle measurement, Amott method (Amott, 1959), and the USBM method (Donaldson *et al.*, 1969). Only the Amott method has been used in this study.

In the Amott method, spontaneous imbibition and forced displacement are combined to measure the average wettability of a core. The original procedure performed by Amott (1959) to measure core samples consisted of four steps: (1) spontaneous oil imbibition; (2) forced oil displacement; (3) spontaneous water imbibition; (4) forced water displacement, in which forced displacements were conducted with a centrifuge. Results were interpreted as wettability indices:

$$I_w = \frac{V_{osp}}{V_{osp} + V_{of}} \tag{3.1-13}$$

$$I_o = \frac{V_{wsp}}{V_{wsp} + V_{wf}} \tag{3.1-14}$$

where subscripts w and o stand for water and oil, respectively, sp for "spontaneous imbibition" and f for "forced displacement". I is Amott index, and V is volume. This method has been widely accepted, but with some modifications: (1) core was first oilflooded to irreducible water saturation, S_{wi}, then spontaneous water imbibition and forced water displacement were performed followed by oil imbibition and oil displacement; (2) forced displacements could be alternatively performed by core-flooding; (3) instead of 20 hours used by Amott, the imbibition time was extended to the point when imbibition was complete or when a time limit was reached (Anderson, 1986b).

Morrow *et al.* (1986) also proposed to measure the imbibition rates during spontaneous imbibition tests, which provides additional useful information in wetting assessment. To account for the effects of oil/water viscosity ratio and interfacial tension, rock porosity and permeability, sample shape, and boundary conditions on imbibition rates, a scaled imbibition time was proposed by Ma *et al.* (1995). For a cylindrical core sample without boundary restrictions, this dimensionless time, t_d, is

$$t_d = 0.6\sqrt{\frac{k_a}{1000\phi}}\frac{\sigma}{\sqrt{\mu_w \mu_o}}\left(\frac{4}{L^2} + \frac{8}{D^2}\right)t \tag{3.1-15}$$

where t_d = dimensionless imbibition time

k_a = air permeability, md

ϕ = porosity, fraction

σ = water-oil interfacial tension, dyn/cm

μ_w, μ_o = water and oil viscosities, cp

L = core length, cm

D = core diameter, cm

t = actual imbibition time, min

There are problems with the Amott method and its modifications. They are insensitive near neutral wetting conditions. They also are not able to distinguish between very strongly water-wet and slightly less water-wet conditions, a distinction that can have an important impact on displacement efficiency. Nevertheless, these methods provide a measure of rock wettability and are therefore frequently used.

Objectives of this study:

Considering that wettability is a major factor that controls distribution of fluids in porous media and consequently influences the displacement processes, an investigation of the impact of wettability on the rate dependence of relative permeability is necessary and will be helpful to clarify contradictory conclusions in literature. In this study, we investigate how flow rate influences water relative permeability at the end of a low-rate waterflood for different wetting conditions. Water relative permeability end points have been chosen as the focus of the study instead of the whole relative permeability curves because:

- Many factors, including displacement methods (unsteady-state or steady-state), pressure gradients, flow rates, fluid viscosity ratios, temperature, etc., might affect relative permeability curves. Thus the influence of wettability could be masked by other variables.
- For the unsteady-state method, relative permeability curves also depend on the methods used to interpret the displacement results, and thus might not be unique.
- At the residual oil saturation, only the water phase is flowing and distortion of saturation distribution induced by capillary end-effects become less serious or even negligible.

This could help to highlight the impact of wettability on the microscopic distributions of each phase and lead to a better understanding of rate-dependent mechanism.

• Finally, water relative permeability at residual oil saturation is an important parameter. Well-flooded areas, which would be the major targets for various EOR methods, and the areas around water injection wells are all at residual oil saturation. A better understanding of flow under residual oil conditions would be helpful for reservoir simulation, management and tertiary recovery processes.

Rate effects experiments

Materials:

Aqueous solutions: Three different brines were used. Sulimar Queen (SQ) synthetic brine had 75% of the concentration of ions reported in produced brine (Martin *et al.*, 1995). Spraberry (SP) synthetic brine was based on the ion compositions provided by Martin Water Laboratories, Inc. The third brine was 2% $CaCl_2$. All were prepared with distilled water and reagent grade salts, filtered through a 0.45 μm Millipore prefilter, and deaerated prior to use. Brine compositions and properties are listed in Table 3.1-1.

Table 3.1-1. Compositions and properties of synthetic brines

Brine	SQ brine	SP brine	2% $CaCl_2$
Compositions (mg/l)	$NaHCO_3$= 212 Na_2SO_4= 3227 $CaCl_2$= 4404 $MgCl_2$= 26188 NaCl= 196736	NaCl= 122,700 $CaCl_2$= 5,663	$CaCl_2$= 20,000
Total salinity(mg/l)	230,766	128,363	20,000
Ionic strength (M)	4.38	2.24	0.541
Density at 20°C (g/ml)	1.1548	1.0848	1.0147
Viscosity at 20°C (cp)	1.80	1.32	1.13
pH value	7.70	7.06	7.46

Oleic phases: Two crude oils, one from the Sulimar Queen oil field located in southeastern New Mexico and another from a Spraberry oil field in western Texas, were used in combination with their respective synthetic brines to generate mixed-wet conditions in Berea sandstone cores. A mixture of 80% Sulimar Queen crude oil with 20% heptane was also tested. Soltrol-130 (a refined oil) was used with 2% $CaCl_2$ brine for the strongly water-wet case. A more viscous refined oil, 180-190 Saybolt Viscosity Paraffin Oil, was employed to establish initial water saturations. Both Soltrol-130 and paraffin oil were used as received. Properties of each oil are listed in Table 3.1-2 (Buckley *et al.*, 1998b). The interfacial tensions, measured by the du Nuoy ring method, between each oil-brine combination are shown in Table 3.1-3.

Table 3.1-2. Properties of the oleic phases

Oil	SQ-95 crude	SQ-95 + heptane (8:2)	SP crude	Soltrol-130	Paraffin oil
Density at 20°C (g/ml)	0.8351	0.8107	0.8498	0.7565	0.8632
Viscosity at 20°C (cp)	5.84	3.41	9.93	1.59	84.81
Acid number*(mg KOH/g oil)	0.16	-	0.32	-	-
Base number*(mg KOH/g oil)	0.62	-	2.83	-	-
n-C_5 Asphaltenes (%)	3	-	0.8	-	-
Refractive Index, RI_{oil}	1.475	-	1.485	-	-
Refractive Index at onset of asphaltene precipitation with n-C_7, P_{RI}	1.402	-	-	-	-

Table 3.1-3. Interfacial tension (IFT) between each oil-brine pair

Oil --- Brine	IFT (dyn/cm)
SQ-95 crude oil --- SQ brine	11.7
SQ-95/heptane --- SQ brine	12.4
SP crude oil --- SP brine	21.2
Soltrol-130 --- 2% $CaCl_2$	34.5
Paraffin oil--- SQ brine	45.6

Porous media: All the core samples employed in this study were cut from a single block of Berea sandstone with an air permeability of about 800 md. The diameter and length of each core plug was in the range from 3.59 to 3.79 cm and 5.85 to 9.60 cm, respectively. Outcrop

Berea has traditionally been used as a standard porous medium for laboratory coreflood studies, probably because of its availability and homogeneity. Composed mostly of quartz, Berea sandstone also contains a fairly large amount of clay, with kaolinite, illite, mixed-layer clays, and chlorite as the most abundant clay minerals (Ma, 1988). Pore networks in Berea sandstone have high aspect ratios of pore-body size to pore-throat size (Chatzis *et al.*, 1983). Throats vary in size from 10 to 30 μm; pore body sizes vary from about 40 to 200 μm. This usually results in a high residual oil saturation with most of the oil blobs trapped in single pore bodies through the mechanism of snap-off under strongly water-wet conditions. Table 3.1-4 lists the physical properties of all the core samples used in this study.

Table 3.1-4. Physical properties of Berea sandstone core samples

Core ID	Length (cm)	Diameter (cm)	Permeability to N_2 (md)	Porosity (%)	Imbibition Tests	Waterflood (ml/hr)	Rate dependence Tests (ml/hr)	Oil/Water
B27	7.18	3.79	788	22.0	WI*			Soltrol-130 with 2% $CaCl_2$
B28	7.21	3.79	801	21.5	WI			
B29	7.13	3.79	844	22.0		8		
B30	9.60	3.79	770	22.0	WI	80	1-400-1	
B22	7.19	3.79	841	22.6	OI**→WI	8	1-400-1	SP crude with SP brine
B23	6.00	3.79	833	22.2	OI→WI			
B24	5.98	3.79	811	22.3	WI→OI			
B32	7.12	3.79	772	22.0	OI→WI	80	1-400-1	
B14	5.77	3.59	780	22.1	WI→OI			SQ crude with SQ brine
B15	5.73	3.59	786	22.2	OI→WI			
B19	7.28	3.79	814	22.4	OI→WI	8	1-400-1	
B35	7.21	3.79	803	22.1		80	1-400-1	
B25	5.8	3.79	793	22.1	OI→WI			SQ crude+heptane (8:2) with SQ brine
B26	5.98	3.79	780	22.0	WI→OI			
B31	7.52	3.79	823	22.4	OI→WI	8	1-400-1	

* WI --- Spontaneous water imbibition tests

** OI --- Spontaneous oil imbibition tests

Procedures:

Core sample preparation: After being drilled from the sandstone block, cylindrical cores were polished on both ends to ensure smooth surfaces perpendicular to the longitudinal axis. The polished areas were cleaned with a brush to remove debris that might damage permeability. The core samples were then dried in a mechanical convection oven at 80°C. Usually two to three days were required before constant core weights were achieved (Δweight < 0.003% core weight, over a period of four hours). After cooling to room temperature in a vacuum chamber, the dimensions of cores were measured with a vernier caliper to an accuracy of 10^{-2}cm, and the dry weights were measured with an electronic balance to an accuracy of 10^{-4}g. Permeability to nitrogen was measured with an apparatus and method similar to that described by Ma (1988).

Establishment of initial water saturation: Dried core plugs were first saturated with degassed brine under a vacuum, weighed for porosity calculations, then soaked in brine for one week at ambient conditions to permit equilibration. After soaking, about 10 PV of fresh brine were flushed through the cores and water permeabilities were measured at low flow-rates (<20 ml/hr). Samples selected for the rate-dependence tests were also tested at high rates (up to the maximum rate to be used in subsequent experiments).

Cores were flushed with paraffin oil at a pressure gradient of about 20 psi/ft until water production ceased. This usually resulted in a water saturation of about 25% PV after only two to three PV of oil injection. The pressure gradient was then increased to about 120 psi/ft. Another 5% PV additional water was displaced as a series of small, discontinuous droplets during 10-15 PV of oil injection. Flowing direction was then reversed followed by another five PV of injection at 120 psi/ft to ensure a uniform distribution of water. Water was usually not produced during this stage. Then paraffin oil was miscibly displaced by at least 20 PV of the target crude

or refined oil. Viscosity of effluent oil was measured periodically to check whether the displacement was completed or not. Again, no additional water was produced.

A possible problem might be encountered during miscibly displacing paraffin oil by crude oils: if paraffin is not completely compatible with crude oils, precipitation might occur in pore spaces resulting in a reduction of permeability. This was checked by the following procedure:

- mix paraffin with crude oil in various ratios (crude oil % = 5, 10, 20, 40, 60, 80 % mixture volume);
- centrifuge the mixed fluid.

No solid precipitates were found from any tested crude oil (SP, SQ, SQ-H) at any ratios, indicating a good compatibility of paraffin with crude oils used.

After this series of preparative steps, all the core samples had an initial water saturation of around 20% PV. Permeability to oil at S_{wi} was measured at constant flow rate. Rate dependence of oil permeability was also tested in selected samples.

Establishment of wettability: To establish the wettability, cores were immersed in crude oil in a pressurized, high-temperature aging cell (Fig. 3.1-1). The cell was filled with crude oil and sealed. The whole assemble was put in a mechanical convection oven at 80°C to age for two weeks. After cooling to room temperature, cores were taken out and flushed with 10 PV of fresh crude oil to displace the aged oil. Permeabilities to oil at varying rates were remeasured.

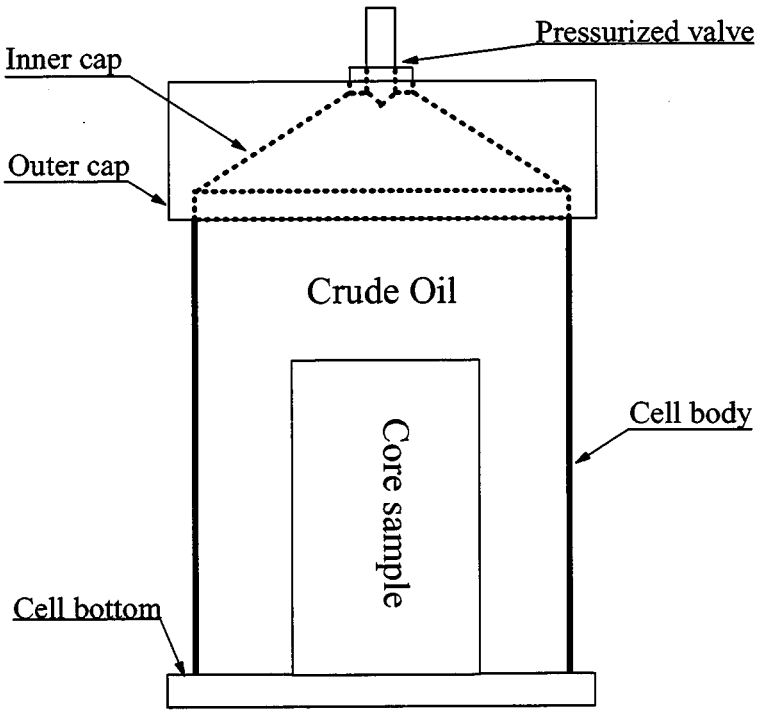

Figure 3.1-1. Pressurized high temperature aging cell.

Spontaneous imbibition: The Amott method (Amott, 1959) was employed in this study to assess the wettability of cores exposed to crude oil. During spontaneous imbibition, the displaced volumes were measured either by gravimetric or volumetric methods. Figure3.1-2 schematically shows the gravimetric method while the volumetric method is shown in Fig. 3.1-3.

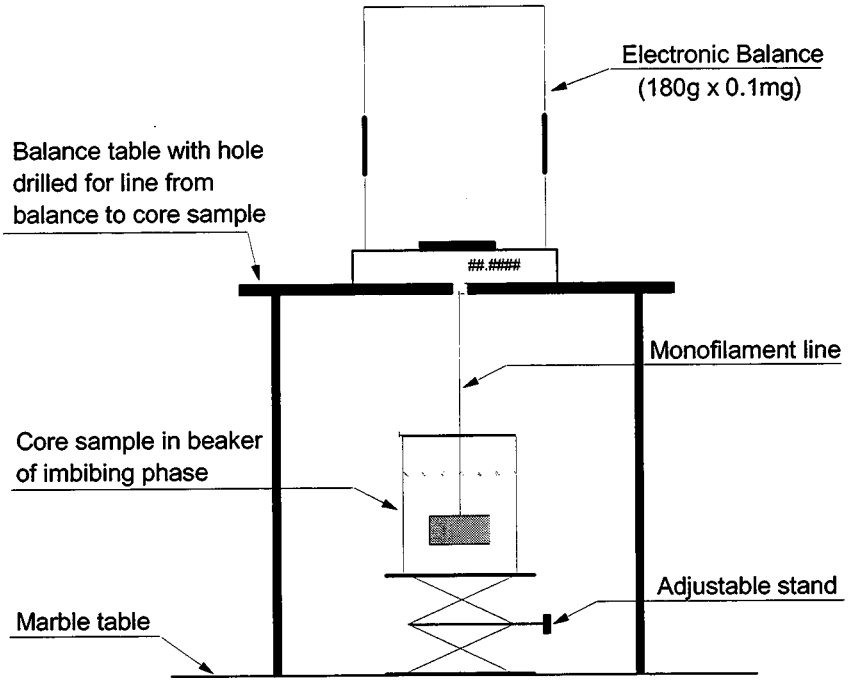

Figure 3.1-2. Gravimetric imbibition set-up.

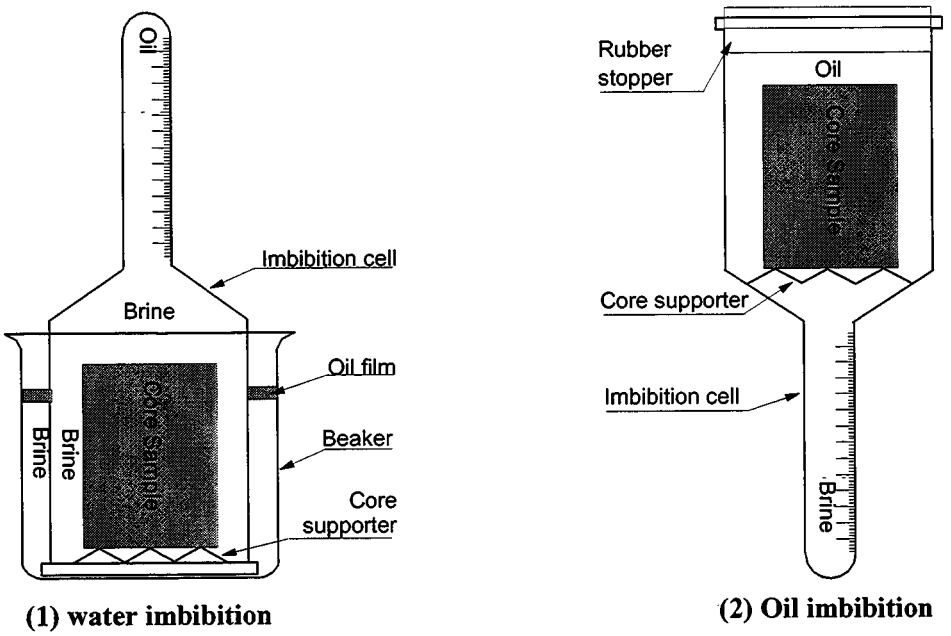

Figure 3.1-3. Volumetric imbibition set-up.

There are advantages and disadvantages to both methods. For the volumetric method, the volume of fluid displaced from a core can be measured directly from its accumulation in a graduated tube. However, some oil droplets might stick to the core surface or to the surface of the funnel-shaped portion of the imbibition cell, resulting in delayed recording of recovery. The total recovery can be corrected at the end of the imbibition test by detaching those droplets. The extent of the delay depends on the wetting properties and the total amount of fluids displaced.

The gravimetric method measures the weight of core immersed in the displacing phase at the time when all the attached droplets on the core surface are removed by a syringe. This procedure avoids the delay problem encountered in the volumetric method. Based on material balance, the volume of displaced phase remaining in the core can be readily derived as:

$$V_b = \frac{W_{total} - \left[W_{dry} - (V_{bulk} - V_{pore})\rho_a\right]}{\rho_b - \rho_a} \qquad (3.1\text{-}16)$$

where subscripts a and b represent displacing phase and displaced phase, respectively, W_{total} is the weight of core immersed in displacing phase, ρ is fluid density, and other parameters are as defined in the nomenclature. The total volume displaced is the difference between V_b and the volume of phase b in the core at the start of imbibition. Variations of the densities of the fluid phases occur with changes in temperature. These were taken into account by recording the temperature at the time of measurement and interpolating the density from density-temperature curve for each fluid.

For water imbibition, the bulk volume of water in a beaker is covered with a thin oil layer to prevent evaporation. For oil imbibition, however, oil evaporation is difficult to avoid, even if the beaker is sealed with plastic film or aluminum foil immediately after each weighing. This causes two related problems: loss of crude oil light ends and change of oil density. The density, which is crucial to accurate calculation of displaced volumes, can be corrected by periodic re-

measuring, but changes in composition could influence wetting during the imbibition processes. On balance, the volumetric method has proved more appropriate for oil imbibition tests than the gravimetric method.

For each crude oil-brine combination, two matched cores were treated so that spontaneous imbibition tests could proceed simultaneously. The core for water imbibition testing started at initial water saturation after aging in crude oil. Another core was waterflooded to residual oil saturation and oil imbibition was tested.

Coreflooding: A schematic diagram of the coreflood setup used for waterflood and end-point tests is shown in Fig. 3.1-4. Two Isco-314 high-pressure metering pumps, each with a capacity of 375 ml and maximum flow rate of 200 ml/hr, were combined to provide a displacing source with maximum capacity of 750 ml and maximum flow rate of 400 ml/hr for either waterflooding or oilflooding tests. Two glass columns, each with a 650 ml of capacity, were arranged to serve as brine reservoirs while four other columns were designated as oil reservoirs. Isco pump(s) injected the working fluid (decane) into the column assembly at a constant flow rate, displacing water or oil. Both water and oil were filtered through 0.45μm prefilters before entering the core sample. Upstream pressure was measured with a 25 psi SENSOTEC pressure transducer while the downstream pressure was atmospheric. A graduated manometer was connected upstream to measure the lowest pressures (<1 psi) as well as to serve for pressure transducer calibration within the low pressure region. The hydraulic head in the manometer is converted to pressure by the following equation:

$$\Delta p = 1.42282 \times 10^{-2} \times \rho \times \Delta h \qquad (3.1\text{-}17)$$

where Δp is pressure in psi, ρ is fluid density in g/ml and Δh is relative elevation (in cm) of fluid in the manometer compared to the reference level (i.e., the level of the transducer).

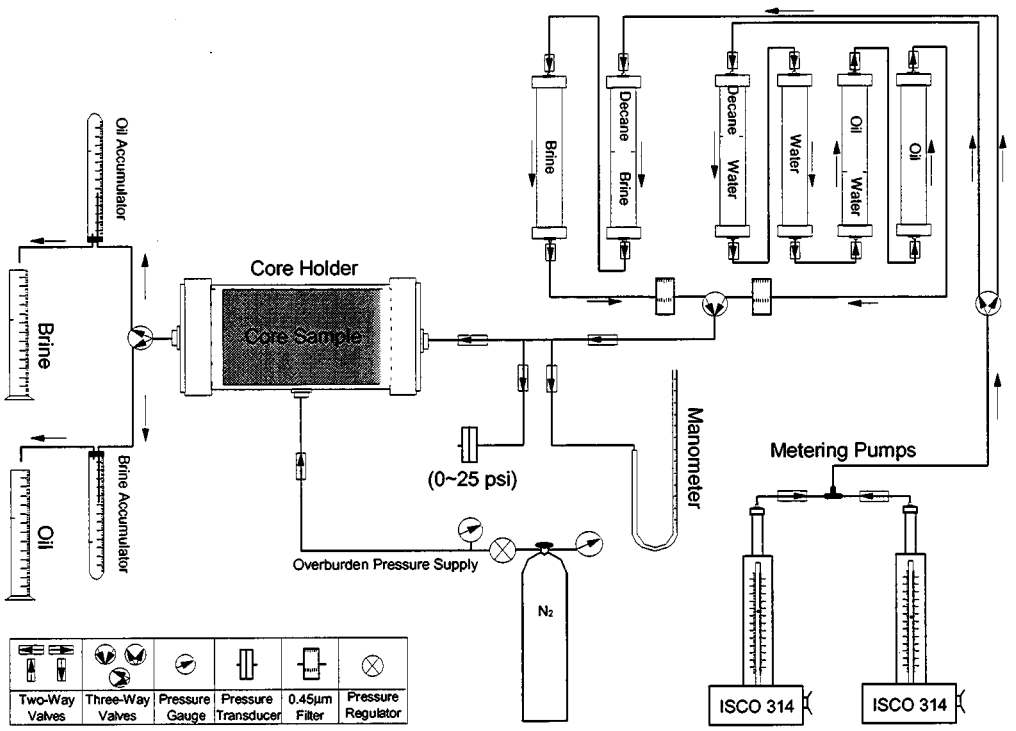

Figure 3.1-4. Coreflooding set-up.

A nitrogen cylinder provided an overburden pressure of 200 psi to the Hassler coreholder. At 200 psi sleeves sealed well for these low pressure flooding experiments so problems with sleeve rupture that were encountered in preliminary tests at 300 psi overburden pressure were avoided. Graduated tubes (15ml x 0.1ml) were positioned downstream to separate and accumulate oil or water. The total fluid produced was accumulated and measured with another graduated tube at the effluent end with an accuracy of 0.1ml. Each flow rate was then calculated from the volume produced, ΔV, within a time interval, Δt, which was indicated by a stopwatch (error=0.01s for Δt<30min), through

$$Q = \frac{\Delta V}{\Delta t} \times 3600 \tag{3.1-18}$$

where Q is total flowrate in ml/hr, ΔV in ml and Δt in sec.

During waterflooding experiments, pressure drop across the core, oil produced, and total fluid injected were recorded in each time interval. A Windows-based finite element 1-D simulator, with the capability of considering capillarity, inlet and outlet end-effects, and gravity effects, was used to estimate relative permeability curves from the waterflood data.

During rate-sensitivity tests, flow rate was varied in steps. At each flow rate, injection was continued until the pressure drop across the core reached a stable value. This generally required at least 1 PV injection for flow rates higher than 20 ml/hr. At least two to four ml more of fluid was then accumulated in the graduated tube, assuring a relative error for volume measurement of less than 2.5%. The error from time measurement was typically around 0.1%. The pressure transducer gave an accuracy to 0.01 psi, corresponding to an error of 1% for 1 psi pressure drop.

From Darcy's law, for a single phase flow,

$$K = \frac{Q \times \mu \times L}{0.24822 \times \Delta p \times A} \tag{3.1-19}$$

where K is permeability to the flowing phase in md, Q is flow rate in ml/hr, μ is viscosity in cp, L and A are length and cross section of core sample in cm and cm^2, respectively, and Δp is pressure drop in psi. Since L, A and μ are fixed during each experiment, the error in permeability, K, caused by inaccuracy of measurements of flow rate, Q, and pressure drop, Δp, can then be written as

$$\frac{\delta K}{K} = \frac{\delta Q}{Q} + \frac{\delta(\Delta p)}{(\Delta p)} = \frac{\delta V}{V} + \frac{\delta t}{t} + \frac{\delta(\Delta p)}{(\Delta p)} \tag{3.1-20}$$

where each term refers to the relative error for that parameter. A 2.5% error of volume measurement, 0.1% error of time measurement and 1% error of pressure drop will combine to yield a maximum 3.6% error in the permeability calculation.

It should be emphasized that during all these rate tests, produced brine was re-injected into the core sample to avoid any possibility of reduction of oil saturation inside the core due to minor solubility of oil in brine.

Calibration of the pressure transducer: A graduated manometer with an inner diameter of 1.1 cm and height divisions of 0.1 cm was used to calibrate the pressure transducer for the low pressure region ($p<2$ psi). Capillary pressure across the meniscus inside the manometer is negligible (<0.004 psi). The accuracy of the hydraulic head is about 0.0014 psi (see equation (3-2)). At $p>2$ psi, a 15 psi pressure gauge with accuracy 0.02 psi was used instead of the manometer as the standard pressure indicator. Figure 3.1-5 shows the corresponding transducer's reading, P_r, at each pressure measured, P_m, from manometer or pressure gauge. The correlation can be divided into three segments:

for 0.01 psi $< P_r <$ 0.07 psi: $P_m = 7.643\text{x}10^{-1}P_r + 1.129\text{x}10^{-2}$, $R = 0.998$

for 0.07 psi $\leq P_r <$ 2 psi: $P_m = 9.945\text{x}10^{-1}P_r - 3.892\text{x}10^{-3}$, $R = 0.999$

for 2 psi $\leq P_r \leq$ 15 psi: $P_m = 9.739\text{x}10^{-1}P_r + 4.616\text{x}10^{-2}$, $R = 0.999$

where R is the correlation coefficient. Pressure drops in most of the tests fell within these ranges. The segment for 2psi $\leq P_r \leq$ 15psi was extrapolated to account for a few pressure points which were a little higher than this range.

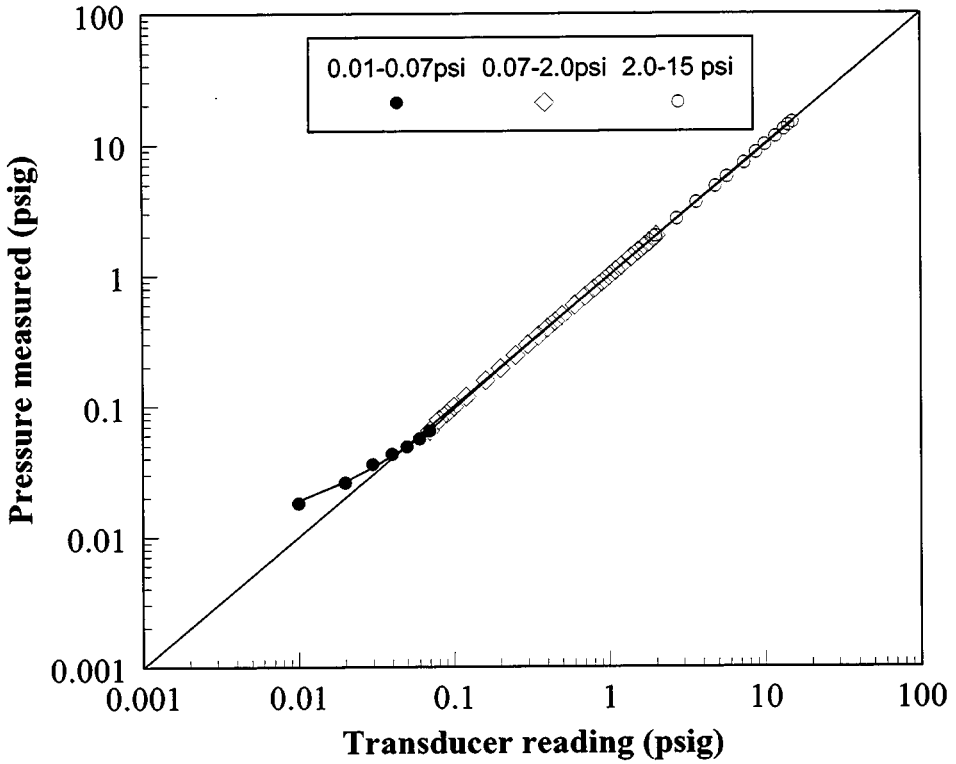

Figure 3.1-5. Calibration of pressure transducer.

Results

In this study, all the Berea core samples had nearly identical rock characteristics and very similar initial water saturations (~20% PV, except core B28 with S_{wi}=0% PV). Wetting conditions were varied using different combinations of brines and oils. Properties and the test sequences for each core sample are listed in Table 3.1-4. Results from tests of spontaneous imbibition, waterflooding, and rate sensitivity of water relative permeability at residual oil will be presented in this chapter for a sequence of case studies.

Case 1—Strongly water-wet:

Oil	*Brine*	*Cores*
Soltrol-130	2% $CaCl_2$	Berea sandstone B27, B28, B29, B30

Refined oil (Soltrol-130) and 2% $CaCl_2$ brine were used to study four cores, B27, B28, B29, and B30, under naturally water-wet conditions. The test sequences and main results are listed in Table 3.1-5.

Table 3.1-5. Experiments with water-wet cores

Core	Treatment	Test	S_{wi} (%)	S_{wf} (%)	R_{oil} (% OIP)	R_{water} (% WIP)	I_w	I_o
B27	none	1) WI	19.3	46.2	33.7			
		2) WF, 10 PV, to get end point	46.2	46.2	0		1	
B28	none	1) WI	0	53.1	46.9			
		2) WF, 10 PV, to get end point	53.1	53.1	0		1	
B29	none	1) WF, constant Q=8 ml/hr	20.4	57.6	46.8			
		2) Rate test, Q=1-400 ml/hr	57.6	57.6	0			
B30	none	1st cycle:						
		1) WF, constant Q=80 ml/hr	19.8	60.1	50.3			
		2) Rate test, Q=1-400 ml/hr	60.1	60.1	0			
		3) OF, to establish S_{wi}	60.1	17.0		71.7		
		4) WI	17.0	55.9	46.8			
		5) WF, 10 PV, to get end point	55.9	55.9	0		1	
	clean with IPA	2nd cycle (after cleaning):						
		1) WF, constant Q=8 ml/hr	20.2	51.3	39.0			
		2) OF, to establish S_{wi}	51.3	19.5		62.0		
		3) WI, 1st	19.5	47.1	34.0			
		4) WF, 10 PV, to get end point	47.1	47.1	0		1	
		2) OF, to re-establish S_{wi}	47.1	31.8		32.5		
		3) WI, 2nd	31.8	49.6	26.1			
		4) WF, 10 PV, to get end point	49.6	49.6	0		1	

WI = spontaneous water imbibition
WF = waterflood
R_{oil} = oil recovery, % OIP
S_{wi} = initial water saturation, % PV

OI = spontaneous oil imbibition
OF = oilflood
R_{water} = water recovery, % WIP
S_{wf} = final water saturation, % PV

Imbibition tests: Oil displaced during spontaneous water imbibition is plotted in Fig. 3.1-6. Dimensionless time, t_d, is employed here to account for the effects of fluid properties, core dimensions, and boundary conditions on the rate of spontaneous imbibition. Note that B30 was oilflooded to a new initial water saturation, S_{wi}=31.8% PV, after the first imbibition test (WI1), and imbibition was repeated (WI2).

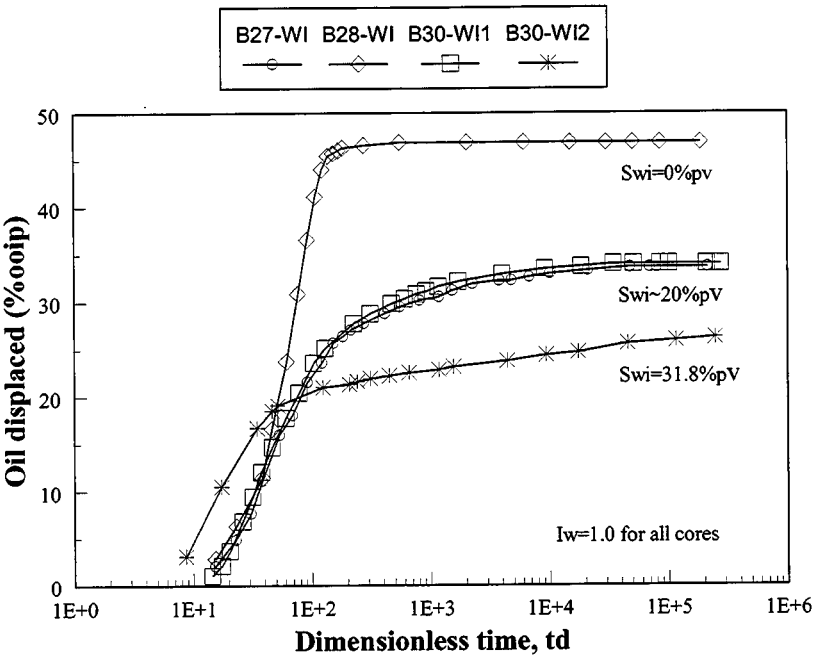

Figure 3.1-6. Oil displacement during spontaneous water imbibition (strongly water-wet).

Fluids: Soltrol-130 and 2% $CaCl_2$ brine

After spontaneous imbibition, about 10 PV of brine were injected into each core at steadily increasing rates up to 400 ml/hr. No additional oil was produced in any of these four imbibition tests, indicating an Amott indix to water, I_w, equal to 1.0 (**strongly water-wet**).

Waterflooding tests: Core samples B29 and B30 were waterflooded at constant flow-rates of 8 ml/hr and 80 ml/hr, respectively, immediately after establishment of initial water saturation. Results shown in Fig.3.1-7 indicate that both waterfloods gave a clean breakthrough, consistent with typical water-wet behavior. The final oil recovery from the low rate (8 ml/hr) flood (46.8% OOIP) is lower than that from high rate flood (50.3% OOIP). No additional oil was produced from either B29 or B30 during rate-dependence tests which followed, to a maximum flow-rate of 400 ml/hr. A second cycle of waterflooding at 8 ml/hr was performed on B30 after it was cleaned with 20 PV throughput of isopropanol. Even less oil was recovered by low flow-rate (8 ml/hr) waterflooding the cleaned core (R=39.0% OOIP).

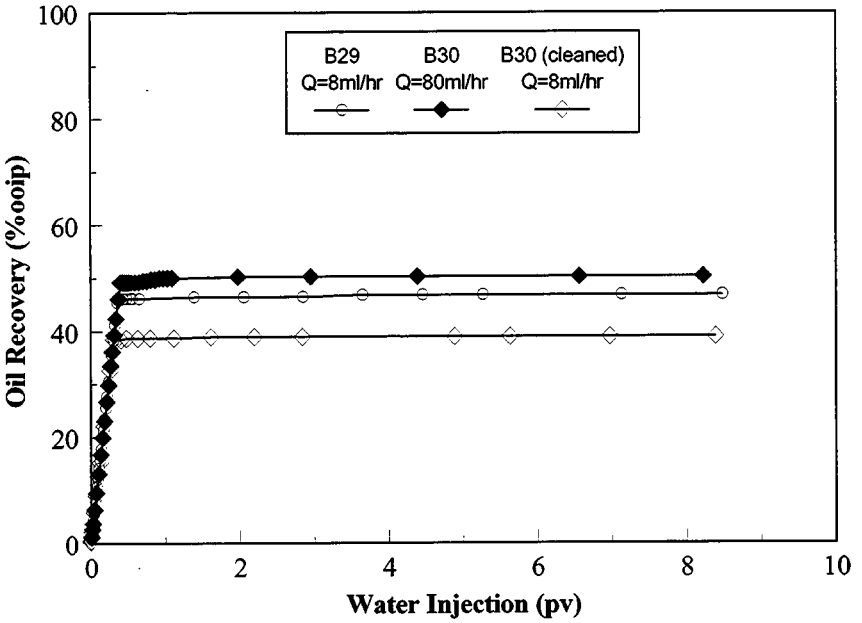

Figure 3.1-7. Oil displacement during waterflood (strongly water-wet).

Fluids: Soltrol-130 and 2% $CaCl_2$ brine
B29: S_{wi}=20.4%, S_{or} =42.4%, Q=8 ml/hr, R=46.8% OOIP, $K_{rw}(S_{or})$=0.081
B30: S_{wi} =19.8%, S_{or} =39.9%, Q=80 ml/hr, R=50.3% OOIP, $K_{rw}(S_{or})$=0.11

Rate-dependence tests for k_{rw} at S_{or}: At the end of waterflooding, both B29 and B30 were subjected to a series of rate-sensitivity tests to determine the possible influence of flow-rates on $k_{rw}(S_{or})$. To complete a test loop, flow-rate was first reduced to 1 ml/hr, then increased steadily to the maximum flow-rate desired for each loop, then decreased steadily back to 1 ml/hr. Injection continued at each flow rate until pressure drop became constant. Both flow rate and pressure drop were then recorded.

Figure 3.1-8 shows the relationship for core B29 between pressure drop and flow rates, as well as their corresponding dimensionless capillary numbers N_{cap} and N_{cav}. No hysteresis exists between rate-increasing and rate-decreasing processes. Both processes gave a linear relationship between N_{cav} and N_{cap} over a range of 400 ml/hr, corresponding to a constant $k_{rw}(S_{or})$ of about 0.082.

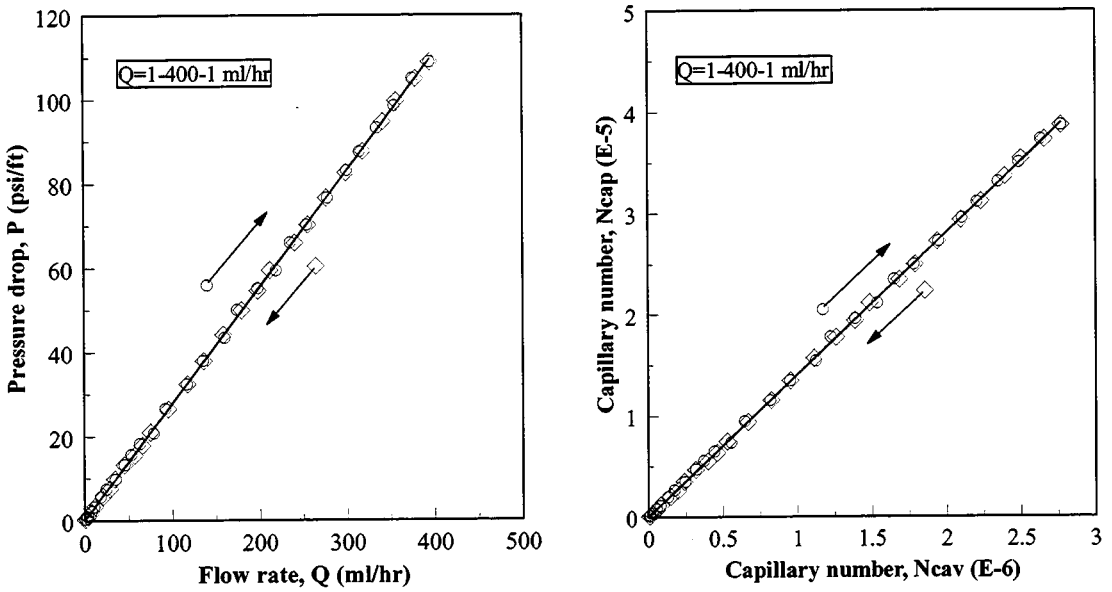

(a) pressure drop vs. flow rate (b) N_{cap} vs. N_{cav}

Figure 3.1-8. No rate dependence after low-rate (8 ml/hr) waterflood (strongly water-wet).

Fluids: Soltrol-130 & 2% $CaCl_2$ brine
B29: S_{wi}=20.4%, S_{or}=42.4%, $K_{rw}(S_{or})$=0.082

Similarly to B29, results from B30 also show no hysteresis, linear relationship between N_{cav} and N_{cap} over four different test loops (1-40-1 ml/hr, 1-80-1 ml/hr, 1-200-1 ml/hr, and 1-400-1 ml/hr), corresponding to an average $k_{rw}(S_{or})$ of about 0.106. Note that B30 had a lower S_{or} and higher $k_{rw}(S_{or})$ than did B29. Figure 3.1-9 shows the result from the 1-400-1 ml/hr test loop for B30.

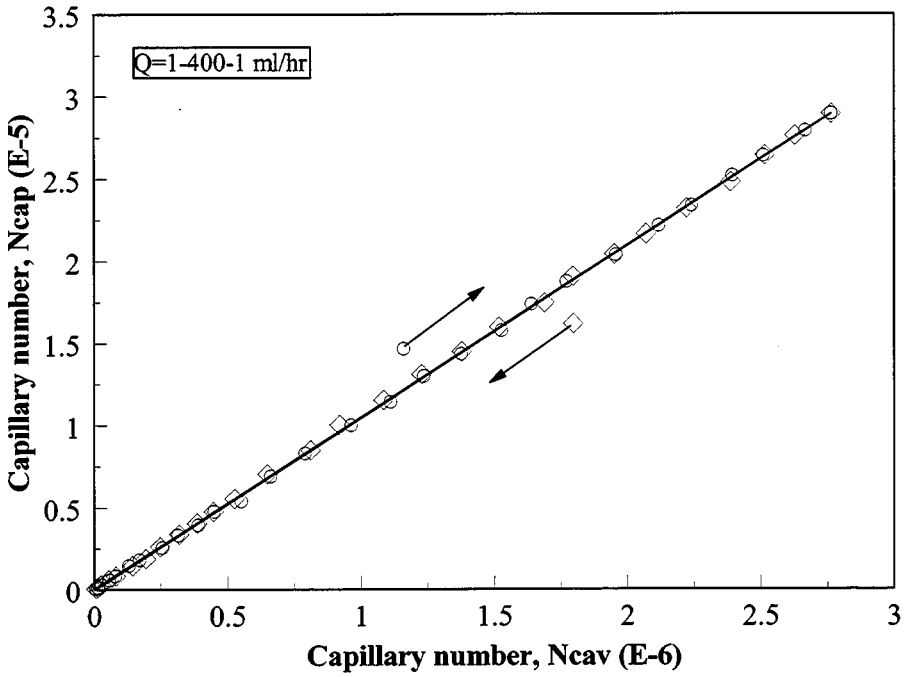

Figure 3.1-9. No rate dependence after high-rate (80 ml/hr) waterflood (strongly water-wet).

Fluids: Soltrol-130 & 2% $CaCl_2$ brine
B30: S_{wi}=19.8%, S_{or}=39.9%, $K_{rw}(S_{or})$=0.11

Case 2—Weakly water-wet:

Oil	*Brine*	*Cores*
Spraberry crude oil (SP)	Spraberry synthetic brine	Berea sandstone B22, B23, B24, B32

Four cores were utilized to study wettability and rate sensitivity using Spraberry crude oil and Spraberry synthetic brine. B23, B24 were used to study wettability only, while B22 and B32 were first used to conduct waterflooding and rate-sensitivity tests, followed by imbibition tests to investigate possible wetting alteration during waterflooding and rate tests. All core samples were pretreated by aging in crude oil for two weeks to establish initial wetting conditions. Table 3.1-6 lists the test sequences performed on each core sample.

Table 3.1-6. Experiments with SP oil/SP brine/Berea sandstone system

Core	Treatment	Test	S_{wi} (%)	S_{wf} (%)	R_{oil} (% OIP)	R_{water} (% WIP)	I_w	I_o
B22	age in oil for 2 weeks	1) WF, constant q=8 ml/hr	21.4	63.9	54.1			
		2) Rate test, q=1-200 ml/hr	63.9	67.3	4.3			
	age in brine for one month	3) Repeat rate test, q=1-400 ml/hr	67.3	67.3	0			
		4) OI	67.3	66.5		1.22		
		5) OF, 10 PV , to get end point	66.5	33.2		49.4		0.02
		6) WI	33.2	55.9	33.9			
		7) WF, 10 PV, to get end point	55.9	65.9	15.1		0.69	
B23	age in oil for 2 weeks	1) WF	20.1	65.4	56.7			
		2) OI	65.4	63.5		2.8		
		3) OF, 10 PV, to get end point	63.5	38.2		38.7		0.07
		4) WI	38.2	56.9	30.2			
		5) WF, 10 PV, to get end point	56.9	63.5	10.8		0.74	
B24	age in oil for 2 weeks	1) WI	20.8	49.0	35.5			
		2) WF, 10 PV, to get end point	49.0	61.6	15.9		0.69	
		3) OI	61.6	60.3		2.2		
		4) OF, 10 PV, to get end point	60.3	35.0		41.1		0.05
B32	age in oil for 2 weeks	1) WF, constant q= 80 ml/hr	20.3	67.4	59.1			
		2) Rate test, q=1-400 ml/hr	67.4	67.4	0			
		3) OI	67.4	66.8		0.84		
		4) OF, 10 PV, to get end point	66.8	25.6		61.2		0.01
		5) WI	25.6	53.8	38.0			
		6) WF, 10 PV, to get end point	53.8	56.1	3.0		0.93	

WI = spontaneous water imbibition
WF = waterflood
R_{oil} = oil recovery, % OIP
S_{wi} = initial water saturation, % PV
OI = spontaneous oil imbibition
OF = oilflood
R_{water} = water recovery, % WIP
S_{wf} = final water saturation, % PV

Imbibition tests: Figure 3.1-10 shows the results from all imbibition tests. Imbibition in B23 and B24 were conducted in opposite sequences. B24 imbibed brine first, then oil. B23 was waterflooded to residual oil, then imbibed first oil, then brine. After waterflooding and rate-sensitivity tests, wetting of cores B22 and B32 was checked by imbibing both oil and water in the same sequence as that of core B23.

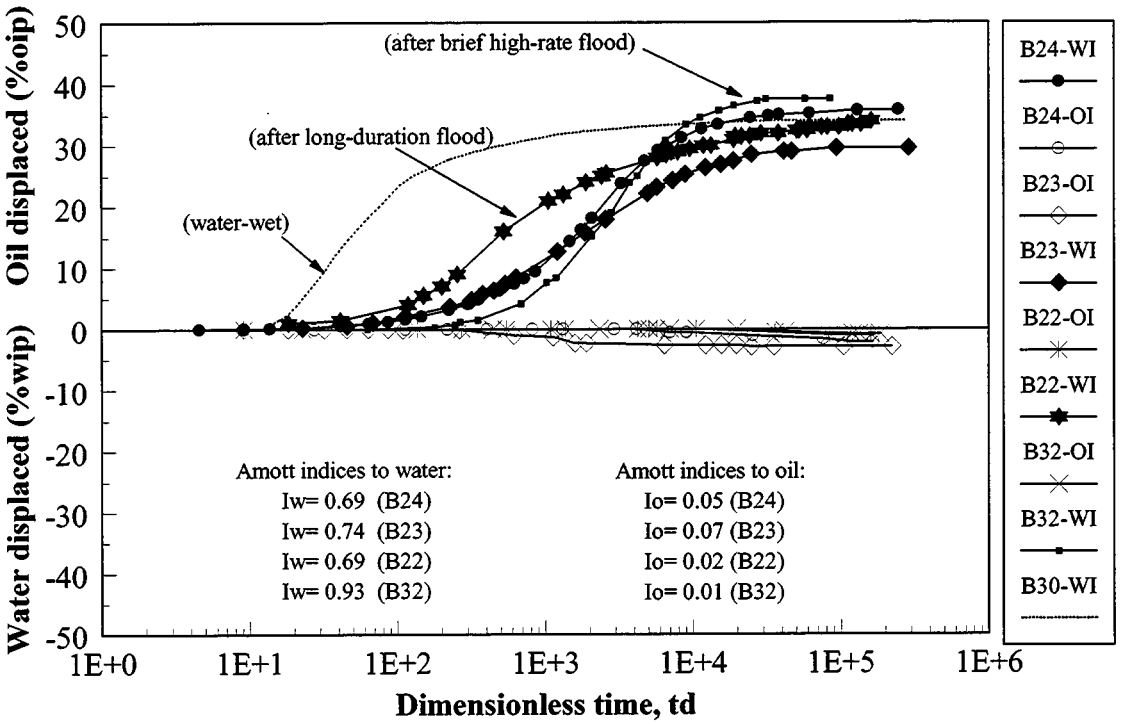

Figure 3.1-10. Displacement during spontaneous imbibition (weakly water-wet).

Fluids: SP crude oil and SP brine

All four cores imbibed water and a little oil, with Amott indices to water around 0.7 (except B32) and to oil less than 0.1, demonstrating **weakly water-wet** conditions. After prolonged aging in water, core B32 appeared to be more water-wet (I_w=0.93).

Waterflooding tests: With similar initial conditions, high flow-rate (80 ml/hr) waterflooding in B32 resulted in an early breakthrough, but with higher final oil recovery (59.1% OOIP) than from low flow-rate waterflooding in B22 (54.1% OOIP) (Fig.3.1-11). The waterflood of B22 was piston-like, with only a little oil produced after breakthrough. Both waterfloods produced more oil than the comparable water-wet cores (B29, B30).

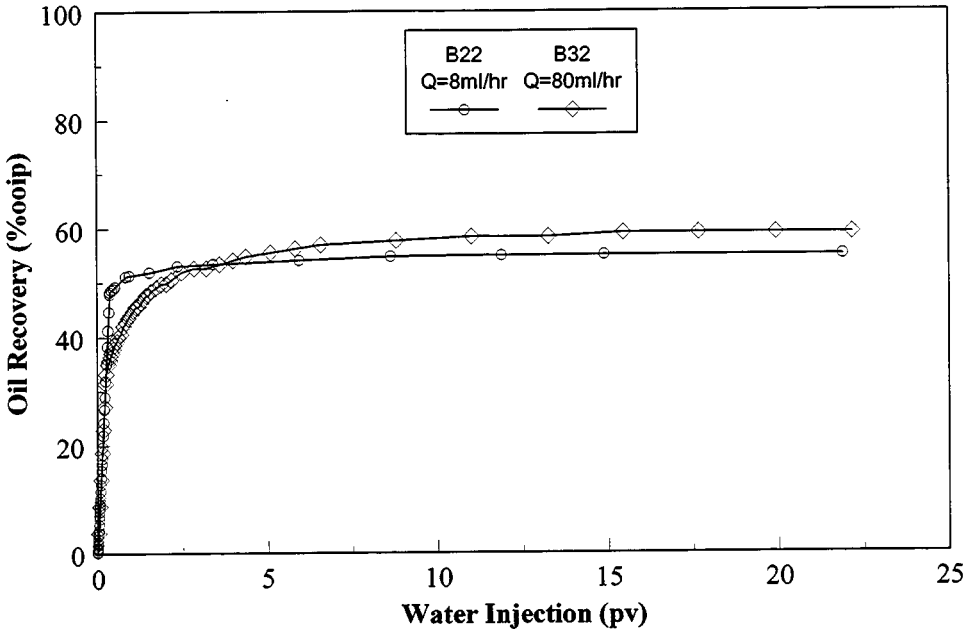

Figure 3.1-11. Displacement during waterflood (weakly water-wet).

Fluids: SP crude and SP brine
B22: S_{wi}=21.4%, S_{or}=36.1%, R=54.1% OOIP, $K_{rw}(S_{or})$=0.033
B32: S_{wi}=20.3%, S_{or}=32.6%, R=59.1% OOIP, $K_{rw}(S_{or})$=0.39

Rate dependence for k_{rw} at S_{or}: B22: After waterflooding, flow-rates were varied over several ranges. A total of about 4.3% OOIP additional oil was produced when the flow-rate was varied first from 1-40-1, then from 1-80-1, and finally from 1-200-1 ml/hr. Oil production ceased after the 1-200-1 ml/hr test loop. Hysteresis was observed between rate-increasing and rate-decreasing processes. An example is shown in Fig. 3.1-12 for the case with the greatest hysteresis during the 1-200-1 ml/hr test loop. N_{cap} increases nonlinearly with increasing N_{cav}, corresponding to an increasing k_{rw} with flow-rate. However, when flow-rates decrease steadily from 200 ml/hr to 1 ml/hr, N_{cap} decreases approximately linearly with N_{cav}, implying a constant k_{rw} during the rate-decreasing process. Similar nonlinear-increasing and linear-decreasing phenomena were observed in all the rate tests with non-water-wet cores.

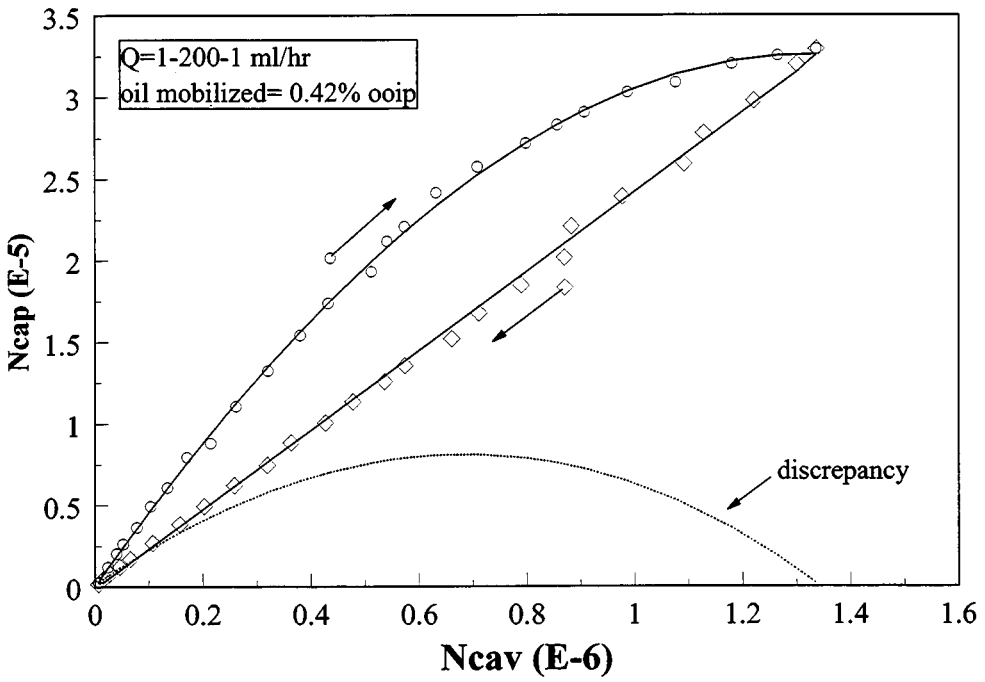

Figure 3.1-12. Rate dependence induced by residual oil mobilization (weakly water-wet).

Fluids: SP crude and SP brine
B22: S_{wi}=21.4%, original S_{or}=36.1%, oil mobilized in this test loop=0.42% OOIP
total oil mobilized=4.3% OOIP, new S_{or}=32.7%, max. $K_{rw}(S_{or})$=0.092

After oil production ceased, three additional test loops over the same flow-rate range 1-200-1 ml/hr were observed. Results plotted in Fig. 3.1-13 show that N_{cap} hysteresis between rate-increasing and rate-decreasing processes persists even without additional oil production, although the magnitude of the discrepancy is reduced. With repeated tests, a general increase in $k_{rw}(S_{or})$ is observed from loop to loop.

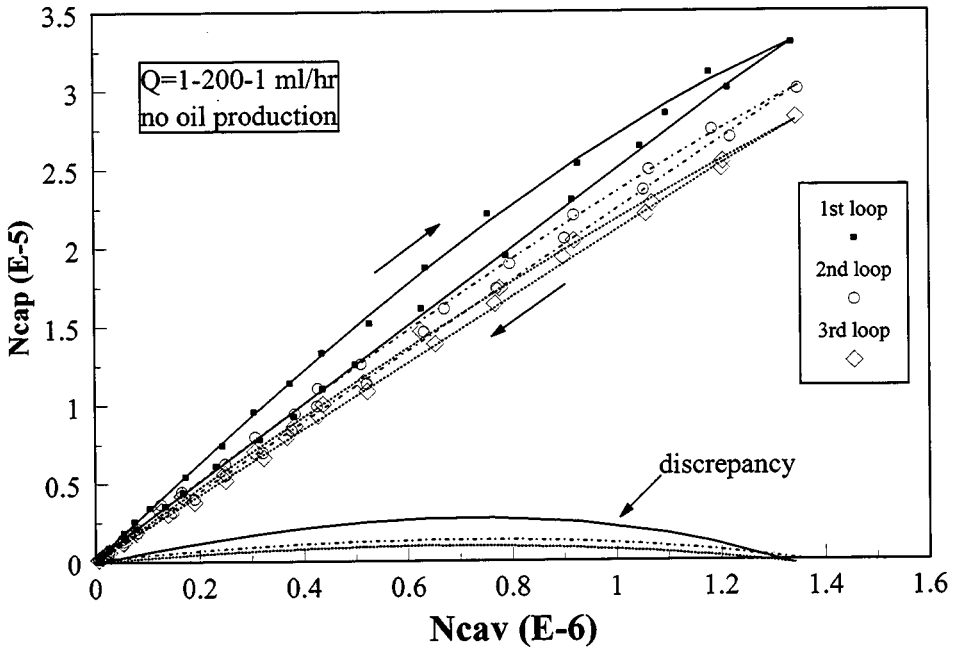

Figure 3.1-13. Rate dependence after oil mobilization (weakly water-wet).

Fluids: SP crude and SP brine

B22: S_{wi}=21.4%, S_{or}=32.7%, $K_{rw}(S_{or})$= 0.092 (1st loop), 0.100 (2nd loop), 0.107 (3rd loop)

Core sample B22 was then immersed in brine for about one month. No oil was displaced due to any further spontaneous water imbibition. After aging in brine, several additional rate tests were conducted on B22. It was observed that $k_{rw}(S_{or})$ had increased significantly from 0.107 before aging (see Fig.3.1-13) to 0.132 after aging. Rate dependence still existed but with much less hysteresis compared to that observed in tests using the same flow-rate range before aging. Further increasing flow-rate to 1-400-1 ml/hr increased $k_{rw}(S_{or})$ to an even higher value (0.150) and made hysteresis between rate-increasing and rate-decreasing processes significant again (Fig. 3.1-14).

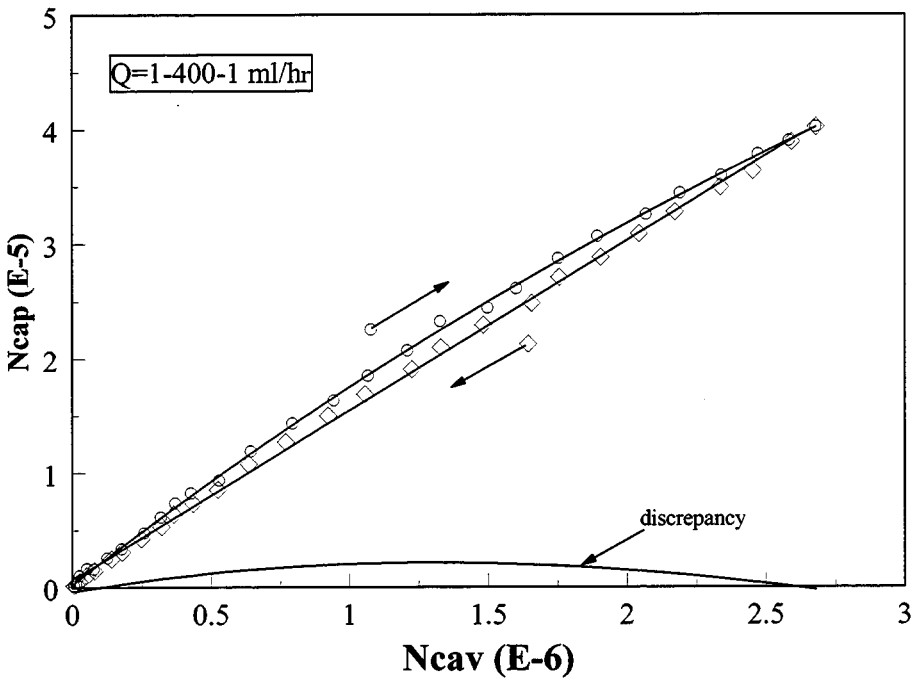

Figure 3.1-14. Rate dependence after immersing core in brine for one month (weakly water-wet).

Fluids: SP crude and SP brine
B22: S_{wi}=21.4%, S_{or}=32.7%, $K_{rw}(S_{or})$=0.15

B32: Core B32 was originally waterflooded at 80 ml/hr. At the end of the waterflood, rate sensitivity was tested. When the maximum flow rate in the test loop did not exceed the original flow rate (80 ml/hr) during the waterflood, no rate dependence was observed (Fig. 3.1-15). However, increasing flow rate to higher values (400 ml/hr) triggered a small but measurable rate dependence (Fig. 3.1-16). Unlike B22, no residual oil mobilization occurred for B32 during any of the rate test loops.

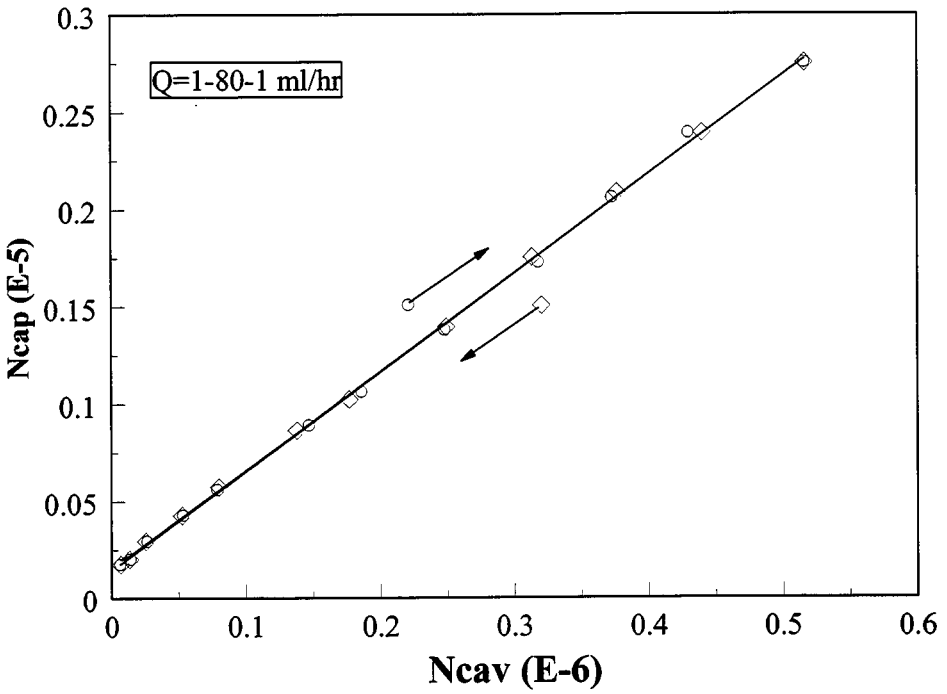

Figure 3.1-15. No rate dependence if the maximum flow rate (80 ml/hr) does not exceed the original waterflood rate (80 ml/hr) (weakly water-wet).

Fluids: SP crude and SP brine
B32: S_{wi}=20.3%, S_{or}=32.6%, $K_{rw}(S_{or})$=0.44

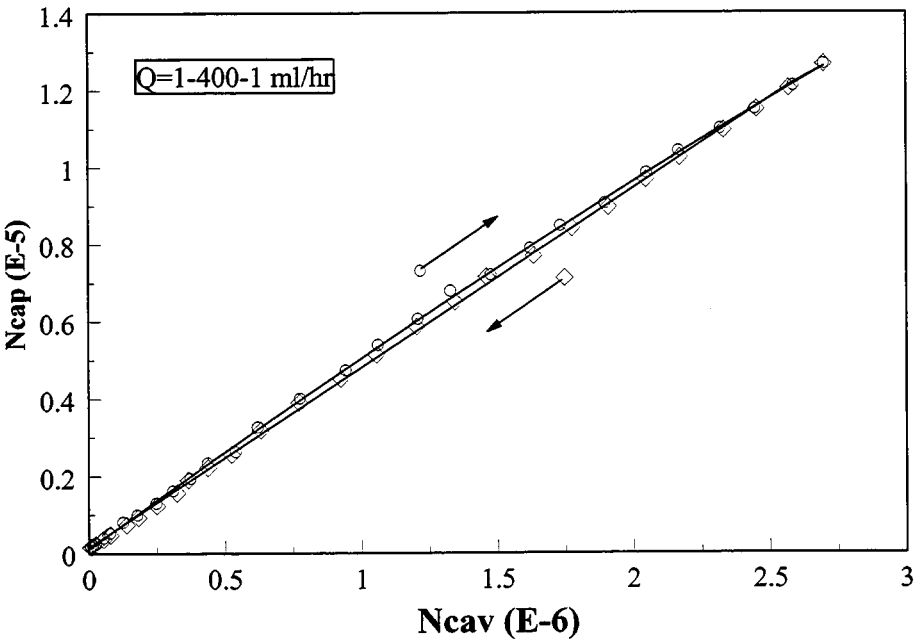

Figure 3.1-16. A little rate dependence still exists if the maximum flow rate (400 ml/hr) exceeds the original waterflood rate (80 ml/hr) (weakly water-wet).

Fluids: SP crude and SP brine
B32: S_{wi}=20.3%, S_{or}=32.6%, $K_{rw}(S_{or})$=0.48

Case 3—Mixed-wet:

Oil	*Brine*	*Cores*
Sulimar Queen crude oil (SQ)	Sulimar Queen synthetic brine	Berea sandstone B14, B15, B19, B35

Four cores were used for tests with the Sulimar Queen crude and brine system, with two (B14, B15) for wettability assessment only and another two (B19, B35) for waterfloods and rate tests followed by wetting verification. All cores were pretreated by aging in Sulimar Queen crude for two weeks. Table 3.1-7 lists the experiments performed on each core sample.

Table 3.1-7. Experiments with SQ oil/SQ brine/Berea sandstone system

Core	Treatment	Test	S_{wi} (%)	S_{wf} (%)	R_{oil} (% OIP)	R_{water} (% WIP)	I_w	I_o
B14	age in oil for 2 weeks	1) WI	19.6	39.2	24.4			
		2) WF, 10 PV, to get end point	39.2	64.8	31.9		0.43	
		3) OI	64.8	60.2		7.1		
		4) OF, 10 PV, to get end point	60.2	31.6		44.1		0.14
B15	age in oil for 2 weeks	1) WF	20.0	72.8	66.0			
		2) OI	72.8	66.7		8.5		
		3) OF, 10 PV, to get end point	66.7	30.2		50.1		0.14
		4) WI	30.2	41.2	15.8			
		5) WF, 10 PV, to get end point	41.2	65.6	35.0		0.31	
B19	age in oil for 2 weeks	1) WF, constant q= 8 ml/hr	20.2	75.8	69.7			
		2) Rate test, q=1-200 ml/hr	75.8	79.1	4.1			
	age in brine for one month	3)Repeat rate test, q=1-400 ml/hr	79.1	79.1	0			
		4) OI	79.1	77.4		2.1		
		5) OF, 10 PV, to get end point	77.4	35.5		53.1		0.04
		6) WI	35.5	57.0	33.4			
		7) WF, 10 PV, to get end point	57.0	69.2	19.0		0.64	
B35	age in oil for 2 weeks	1) WF, constant q= 80 ml/hr	20.9	74.3	67.5			
		2) Rate test, q=1-400 ml/hr	74.3	74.3	0			

WI = spontaneous water imbibition
OI = spontaneous oil imbibition
WF = waterflood
OF = oilflood
R_{oil} = oil recovery, % OIP
R_{water} = water recovery, % WIP
S_{wi} = initial water saturation, % PV
S_{wf} = final water saturation, % PV

Imbibition tests: All imbibition results are shown in Fig. 3.1-17. Opposite imbibing sequences in B14 (water imbibition first, followed by oil imbibition) and B15 (oil imbibition first, followed by water imbibition) gave similar trends to those in Case 2. Initial imbibing rates

were similar but the final oil displacement during water imbibition differed. Amott indices to both water and oil indicate that SQ crude and brine render B14 and B15 mixed-wet. After long-duration, high-rate waterflooding, B19 showed more water-wet imbibing behavior than either B14 or B15.

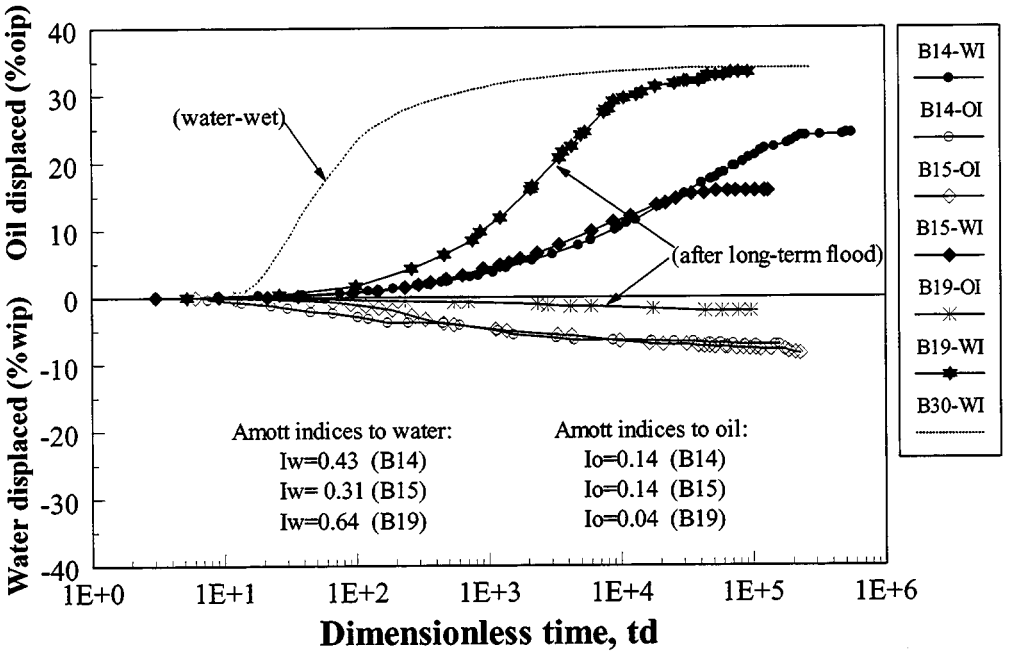

Figure 3.1-17. Displacement during spontaneous imbibition (mixed-wet).

Fluids: SQ crude oil and SQ brine

Waterflooding tests: As shown in Fig. 3.1-18, oil recovery from the low-rate (8 ml/hr) waterflooding nearly coincided with that from the high-rate flood (80 ml/hr). Extended production was observed even after 18 PV of water injection in the low-rate flood. Oil production from the high-rate flood cut off after about 10 PV injection. Both tests produced significantly more oil by waterflooding (69.7% OOIP at 8 ml/hr and 67.5 % OOIP at 80 ml/hr) than either the strongly water-wet (Case 1) or weakly water-wet (Case 2).

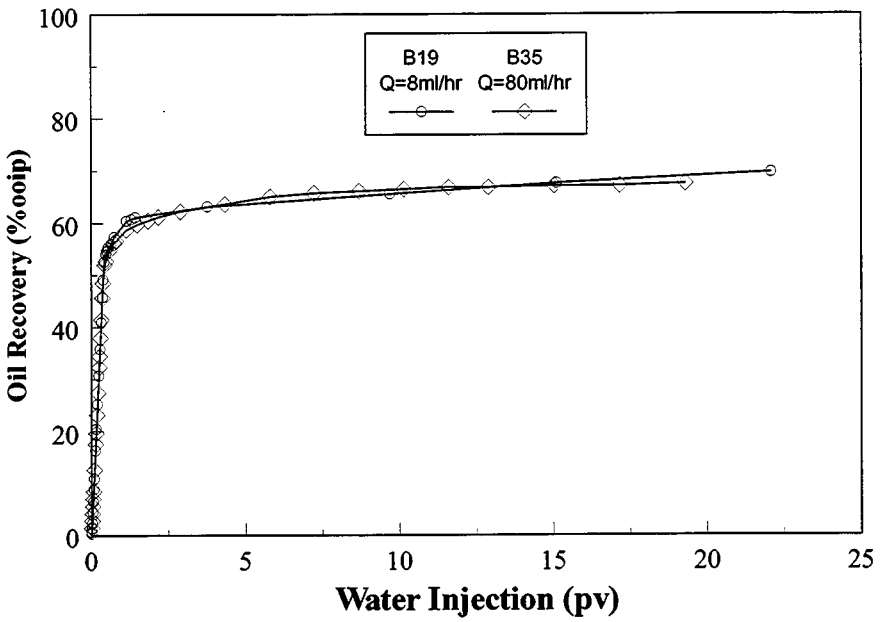

Figure 3.1-18. Displacement during waterflood (mixed-wet).

Fluids: SQ crude and SQ brine
B19: S_{wi}=20.2%, S_{or}=24.2%, R=69.7% OOIP, $K_{rw}(S_{or})$=0.131
B35: S_{wi}=20.9%, S_{or}=25.7%, R=67.5% OOIP, $K_{rw}(S_{or})$=0.279

Rate dependence for k_{rw} at S_{or}: B19: After the low-rate (8 ml/hr) original waterflood, water injection rates were increased steadily. In the first three test loops, flow-rates varied from 1-20-1, 1-40-1, and 1-80-1 ml/hr. Hysteresis was observed for N_{cap} between rate-increasing and rate-decreasing processes (see Fig. 3.1-19 for one example), accompanied by a small amount of oil production which totaled about 4.1% OOIP. Further test loops did not produce any more oil, while rate dependence is still shown by the N_{cap} versus N_{cav} curves. Figure 3.1-20 is one of these results (1-200-1 ml/hr test loop).

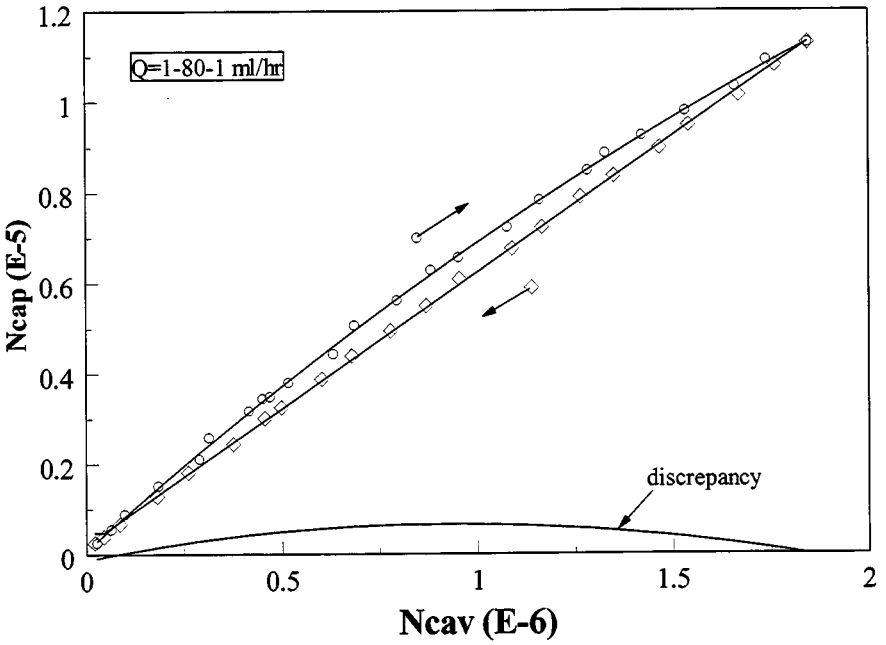

Figure 3.1-19. Rate dependence induced by residual oil mobilization (mixed-wet).

Fluids: SQ crude and SQ brine

B19: S_{wi}=20.2%, original S_{or}=24.2%, oil mobilized in this test loop=1.0% OOIP
total oil mobilized=4.1% OOIP, new S_{or}=20.9%, max. $K_{rw}(S_{or})$=0.266

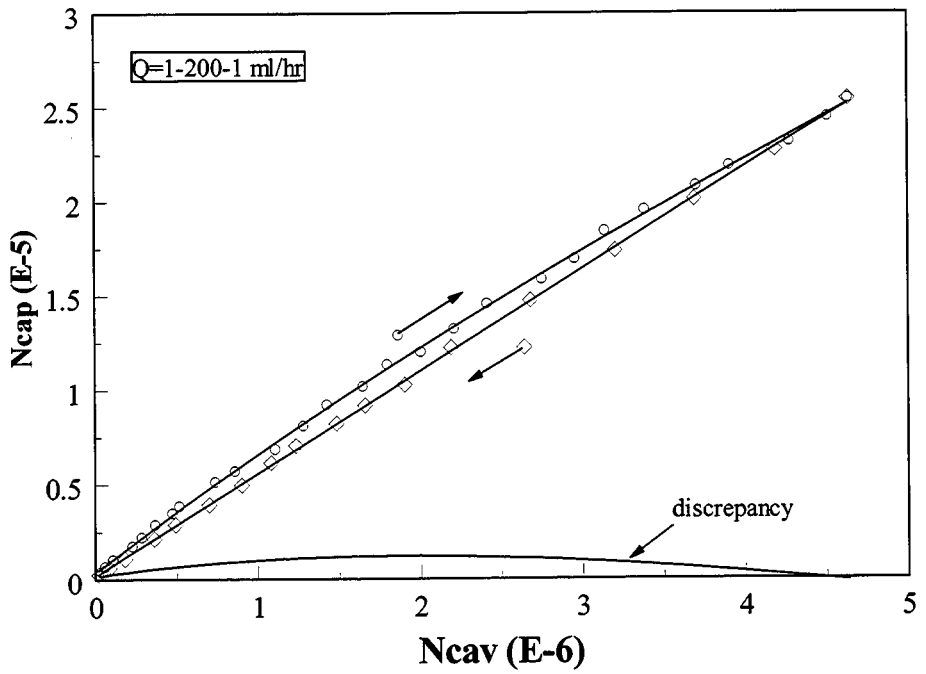

Figure 3.1-20. Rate dependence after oil mobilization (mixed-wet).

Fluids: SQ crude and SQ brine

B19: S_{wi}=20.2%, S_{or}=20.9%, max. $K_{rw}(S_{or})$=0.295

B19 was subsequently immersed in Sulimar Queen brine for one month. After aging in brine, repeated rate tests did not show any rate dependence when the maximum flow-rate did not exceed 200 ml/hr (Fig. 3.1-21). However, when maximum flow-rate was increased to 400 ml/hr, a slight rate dependence reappeared (Fig. 3.1-22).

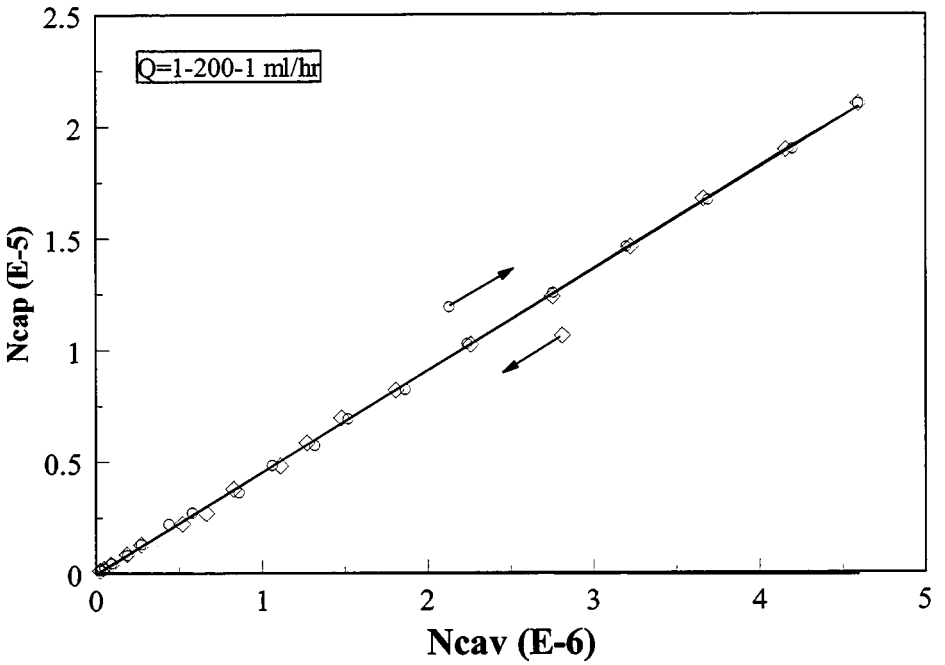

Figure 3.1-21. After immersing core in brine for one month, rate dependence disappears if the flow rate (200 ml/hr) does not exceed that before aging (mixed-wet).

Fluids: SQ crude and SQ brine
B19: S_{wi}=20.2%, S_{or}=20.9%, max. $K_{rw}(S_{or})$=0.351

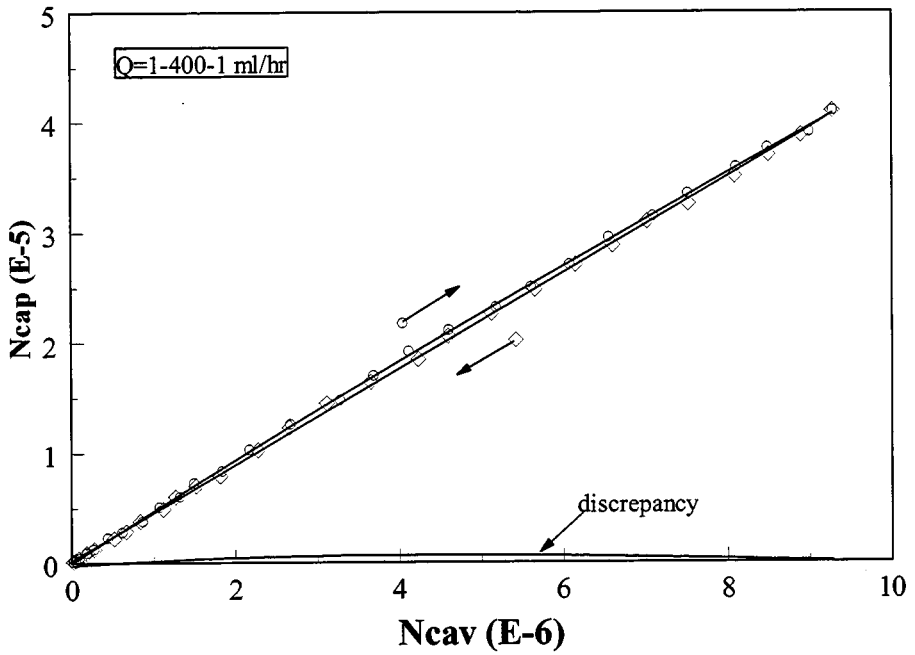

Figure 3.1-22. After immersing core in brine for one month, a little rate dependence still exists if the maximum flow rate is increased to 400 ml/hr (mixed-wet).

Fluids: SQ crude and SQ brine
B19: S_{wi}=20.2%, S_{or}=20.9%, max. $K_{rw}(S_{or})$=0.375

B35: Originally waterflooded at 80 ml/hr, B35 did not show any rate dependence up to a maximum rate of 200 ml/hr (Fig. 3.1-23), but increasing the flow rate to 400 ml/hr did result in rate dependence (Fig. 3.1-24). No additional oil was produced during all rate tests.

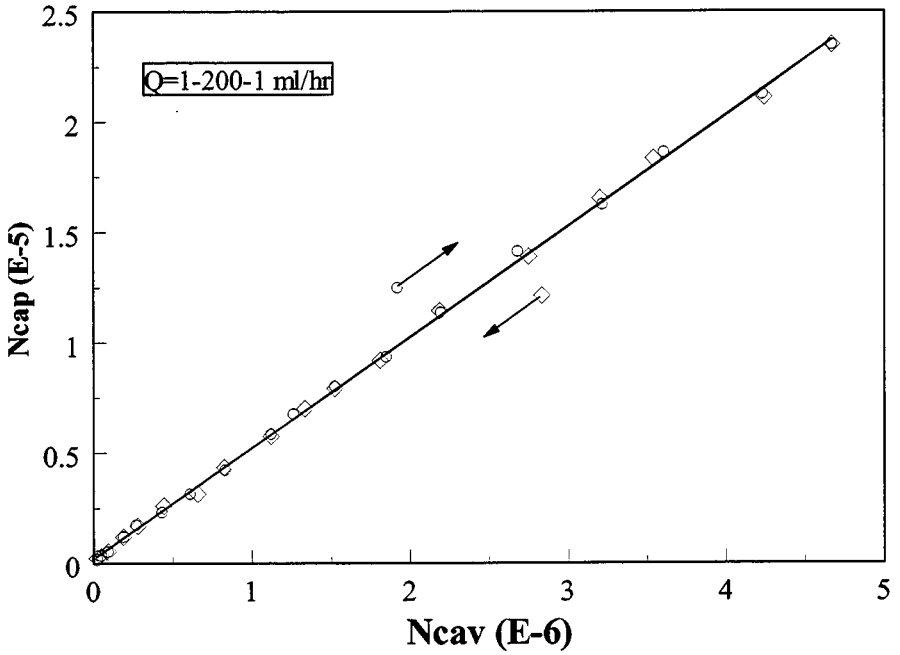

Figure 3.1-23. No rate dependence observed even though the maximum rate (200 ml/hr) is higher than the original waterflood rate (80 ml/hr).

Fluids: SQ crude and SQ brine
B35: S_{wi}=20.9%, S_{or}=25.7%, max. $K_{rw}(S_{or})$=0.319, no residual oil mobilization

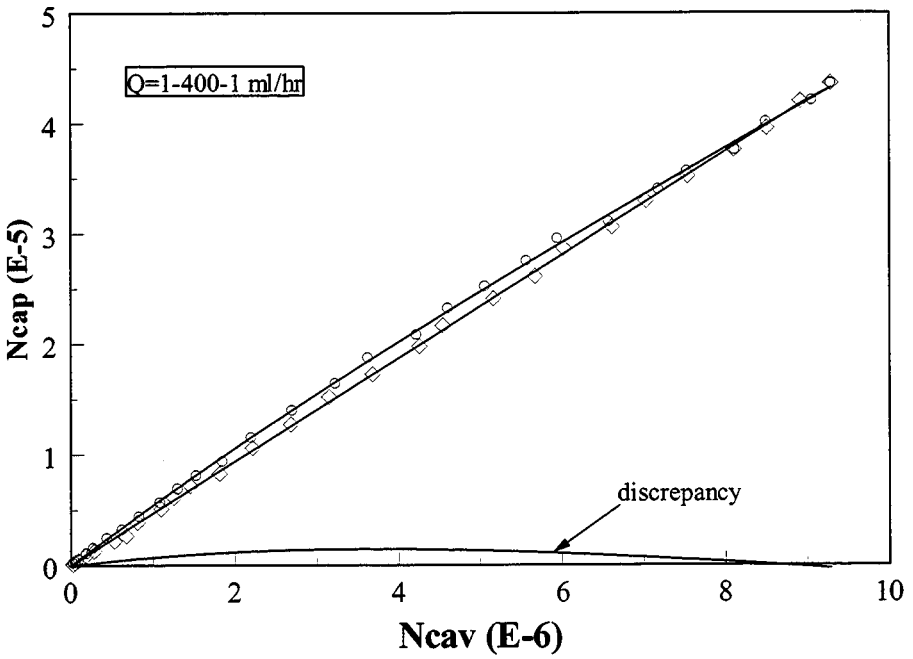

Figure 3.1-24. Much higher flow rate (400 ml/hr) will induce rate dependence again after the original high-rate (80 ml/hr) waterflood.

Fluids: SQ crude and SQ brine

B35: S_{wi}=20.9%, S_{or}=25.7%, max. $K_{rw}(S_{or})$=0.342, no residual oil mobilization

Case 4—Weakly water-wet:

Oil	*Brine*	*Cores*
Mixture of Sulimar Queen crude oil (80%) with Heptane (20%) (SQ-H)	Sulimar Queen synthetic brine	Berea sandstone B25, B26, B31

The effect of changing oil composition was tested using a mixture of 80% Sulimar Queen crude oil and 20% n-heptane. The effects of adding heptane to this crude oil are difficult to predict because it contains both waxes and asphaltenes. Addition of heptane increases the solubility of some waxes, but decreases stability of asphaltenes. These compositional changes which may affect wettability are potentially more important than the accompanying change in density, viscosity and interfacial tension. Test sequences for this case are listed in Table 3.1-8.

Table 3.1-8. Experiments with SQ-H oil/SQ brine/Berea sandstone system

Core	Treatment	Test	S_{wi} (%)	S_{wf} (%)	R_{oil} (% OIP)	R_{water} (% WIP)	I_w	I_o
B25	age in oil for 2 weeks	1) WI	20.5	53.0	40.9			
		2) WF, 10 PV, to get end point	53.0	62.7	12.2		0.77	
		3) OI	62.7	60.9		2.8		
		4) OF, 10 PV, to get end point	60.9	25.0		57.4		0.05
B26	age in oil for 2 weeks	1) WF	20.6	69.1	61.0			
		2) OI	69.1	68.4		0.97		
		3) OF, 10 PV, to get end point	68.4	33.4		50.6		0.02
		4) WI	33.4	57.0	35.4			
		5) WF, 10 PV, to get end point	57.0	61.0	6.1		0.85	
B31	age in oil for 2 weeks	1) WF, constant q=8 ml/hr	20.9	74.7	68.0			
		2) Rate test, q=1-200 ml/hr	74.7	74.7	0			
		4) OI	74.7	73.6		1.4		
		5) OF, 10 PV, to get end point	73.6	28.8		60.0		0.02
		6) WI	28.8	55.2	37.0			
		7) WF, 10 PV, to get end point	55.2	56.2	1.5		0.96	

WI = spontaneous water imbibition
OI = spontaneous oil imbibition
WF = waterflood
OF = oilflood
R_{oil} = oil recovery, % OIP
R_{water} = water recovery, % WIP
S_{wi} = initial water saturation, % PV
S_{wf} = final water saturation, % PV

Imbibition tests: Unlike those in Cases 2 and 3, effects of imbibing sequence on initial water imbibition rates were significant in this case (Fig. 3.1-25). Core B26 (oil imbibition first, followed by water imbibition) apparently showed a more water-wet imbibition character than B25 (water imbibition first, followed by oil imbibition). Amott indices to both water and oil indicate **weakly water-wet** conditions. After waterflooding and rate tests, core B31 was even more water-wet.

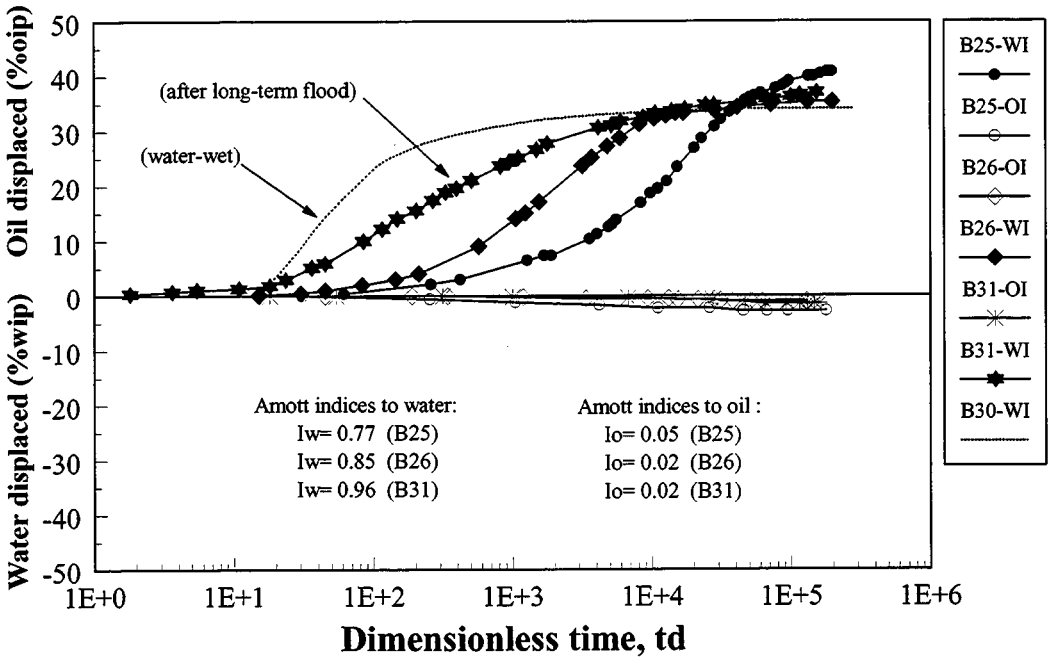

Figure 3.1-25. Oil displacement during spontaneous imbibition (weakly water-wet).

Fluids: SQ-H mixture oil and SQ brine

Waterflooding tests: A nearly clean breakthrough recovery was observed from waterflooding core B31 at 8 ml/hr (Fig. 3.1-26), similar to water-wet cores. However, the amount of oil produced (68.0% OOIP) was significantly higher than in the water-wet corefloods (see Fig.3.1-7).

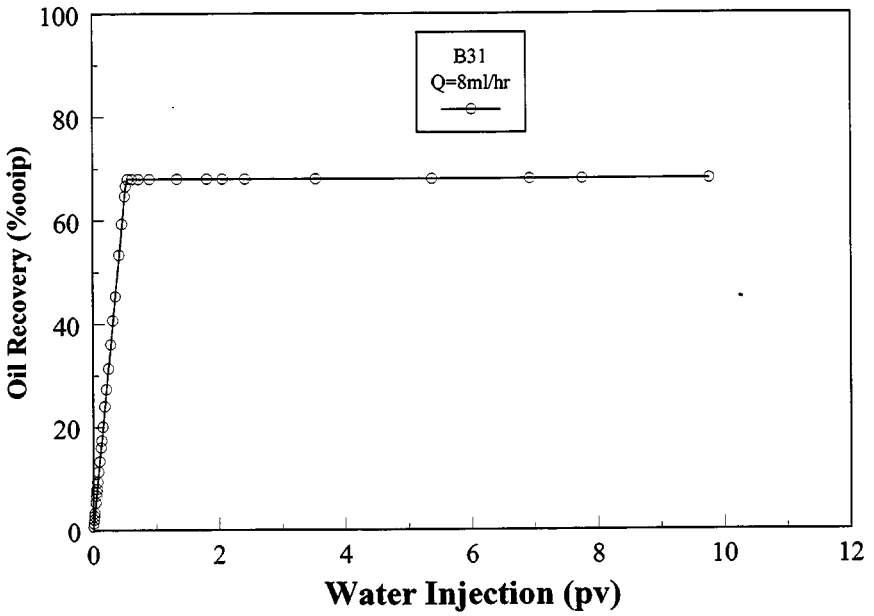

Figure 3.1-26. Oil displacement during waterflood (weakly water-wet).

Fluids: SQ-H mixture oil and SQ brine
B31: S_{wi}=20.9%, S_{or}=25.3%, R=68.0% OOIP, $K_{rw}(S_{or})$=0.144

Rate dependence for k_{rw} at S_{or}: After 8 ml/hr waterflooding, significant hysteresis between rate-increasing and rate-decreasing processes for 1-400-1 ml/hr test loop was observed, with no residual oil mobilized (Fig. 3.1-27).

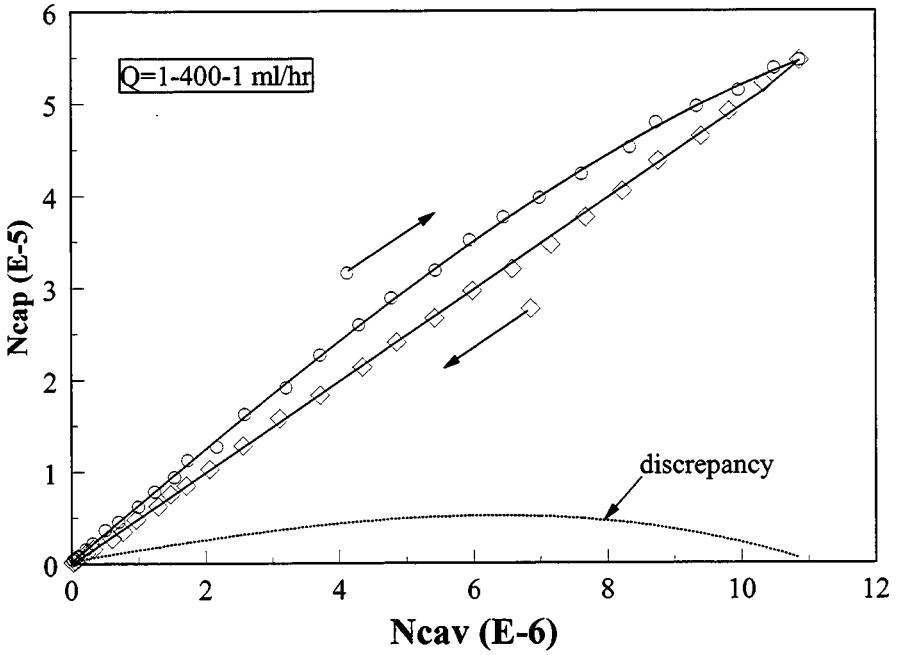

Figure 3.1-27. Rate dependence with no oil mobilized.

Fluids: SQ-H mixture oil and SQ brine
B31: S_{wi}=20.9%, S_{or}=25.3%, $K_{rw}(S_{or})$=0.260

From the experimental results presented above we can see that at the end of regular waterflooding, the pressure gradient ($\propto N_{cap}$) may vary with increasing flow rate ($\propto N_{cav}$), indicating a change of relative permeability to water at residual oil saturation. Rate-dependence phenomena are influenced by wetting conditions. Detail of this influence will be further discussed in next section.

Discussion

Results show that waterflood end-point relative permeabilities can be very sensitive to flow rate. The significance of rate dependence and the relationship between rate dependence and wetting conditions will be examined in this chapter. Possible mechanisms of rate sensitivity will be postulated to help explain the roles of flow rate and wettability in immiscible displacements.

Wettability determination:

Since wetting conditions are likely to contribute to the rate sensitivity of relative permeability measurements, it is important first to establish how to assess wettability and to show whether or not wettability can be altered during experiments of long duration.

Influence of initial water saturation S_{wi} on spontaneous water imbibition (strongly water-wet): For strongly water-wet conditions, only water spontaneously imbibes into a core. Figure 3.1-28 shows the evolution of both oil recovery and oil saturation during spontaneous water imbibition tests starting from different initial water saturations. Table 3.1-9 summarizes these results. Note that a second imbibition (WI2) was repeated for B30 from a different initial water saturation after the first imbibition (WI1).

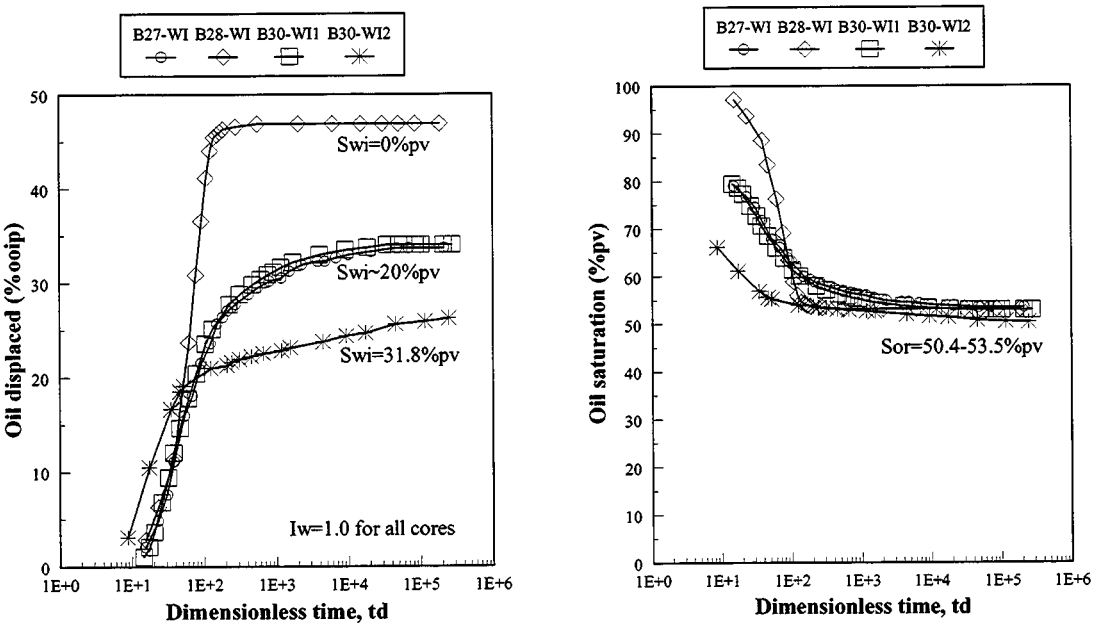

(a) oil recovery (b) oil saturation

Figure 3.1-28. Influence of initial water saturation on spontaneous imbibition (strongly water-wet).

Fluids: Soltrol-130 and 2% $CaCl_2$ brine

Table 3.1-9. Water imbibition from different initial water saturation (water-wet case)

Core	S_{wi} (% PV)	S_{or} (% PV)	ΔS_o (% PV)	R_{WI} (% OOIP)	I_w
B28	0	53.1	46.9	46.9	1.0
B27	19.3	53.8	26.9	33.7	1.0
B30	19.5	52.9	27.6	34.0	1.0
B30 (repeated)	31.8	50.4	17.8	26.1	1.0

R_{WI}—oil recovery from spontaneous water imbibition

With different initial water saturations, the initial rates of oil recovery by spontaneous imbibition were quite similar, but the final oil recoveries vary by as much as 20% OOIP. The lower the initial water saturation (higher oil saturation) is, the higher the final oil recovery will be.

Influence of measuring sequences on oil recovery and imbibition rate: Results of imbibition measurements with non-water-wet cores are re-plotted in Fig. 3.1-29 to Fig. 3.1-31. Major parameters from the water imbibition tests are listed in Table 3.1-10. For convenience, we will denote the process in which water imbibition was the first measurement followed by oil imbibition as SI-A; if oil imbibition preceded water imbibition the process is labeled SI-B.

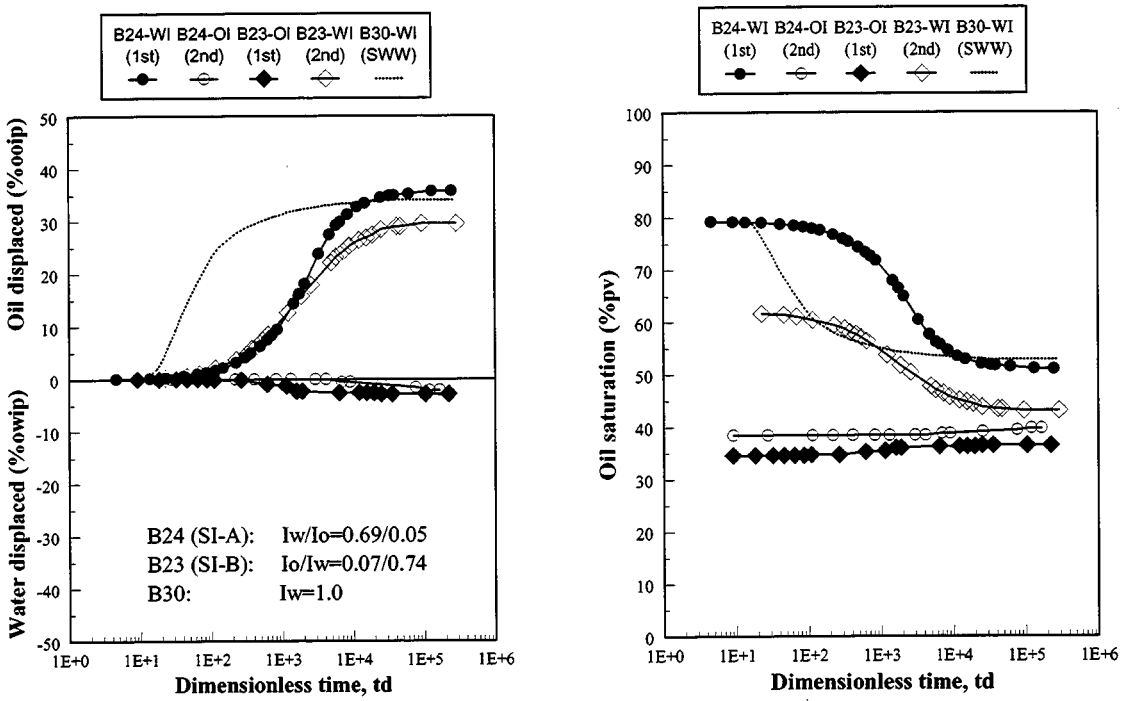

(a) oil recovery (b) oil saturation

Figure 3.1-29. Influence of measuring sequences on spontaneous imbibition (mixed-wet).

Fluids: SP crude and SP brine

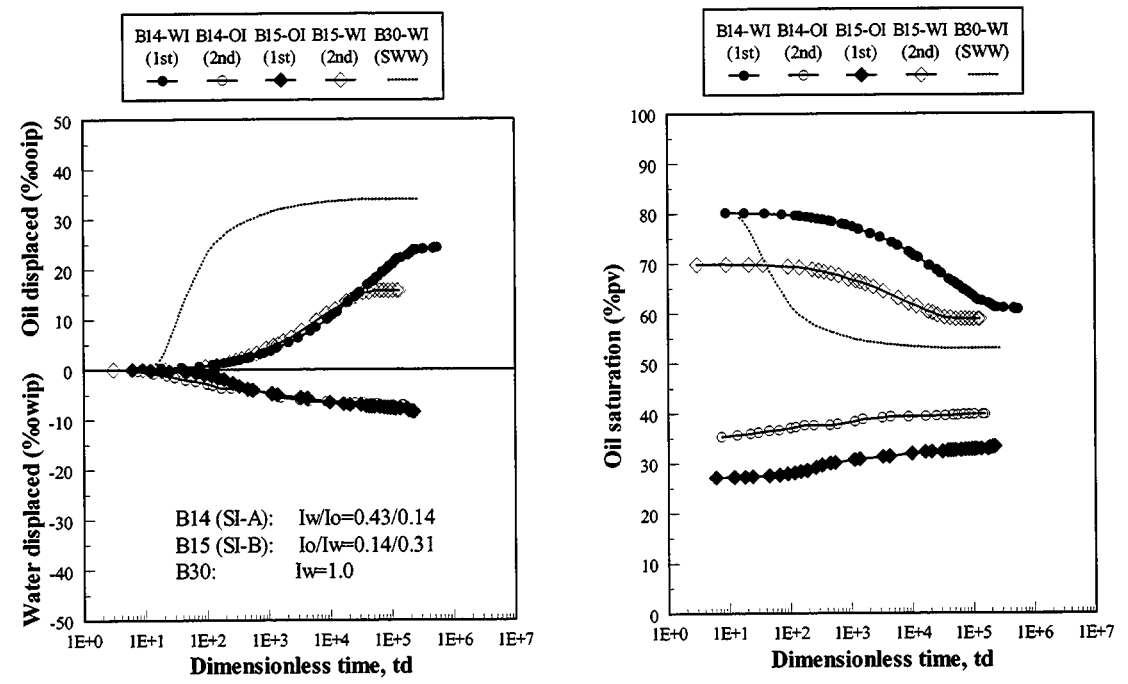

(a) oil recovery (b) oil saturation

Figure 3.1-30. Influence of measuring sequences on spontaneous imbibition (mixed-wet).

Fluids: SQ crude and SQ brine

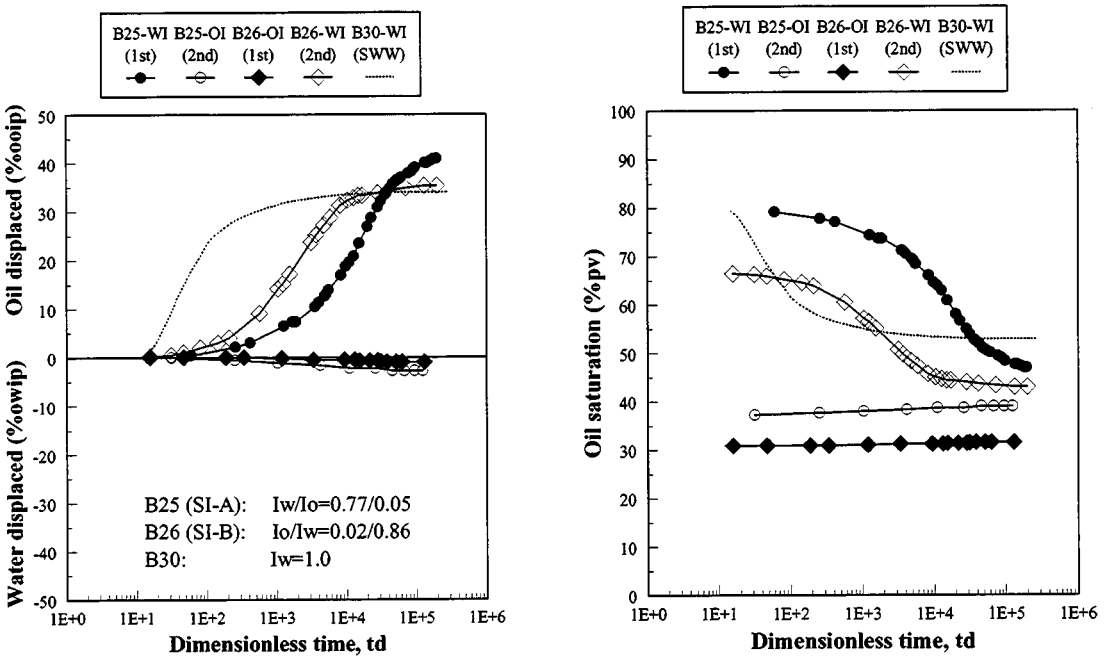

(a) oil recovery (b) oil saturation

Figure 3.1-31. Influence of measuring sequences on spontaneous imbibition (mixed wet).

Fluids: SQ-H oil and SQ brine

Table 3.1-10. Summary of water imbibition for non-water-wet cores

Core	Oil/water	Measuring Sequences	Imbibition Type	S_{wi} (% PV)	S_{or} (% PV)	ΔS_o (% PV)	R_{WI} (% OOIP)	I_w
B22	SP/SP	WF, OI, WI	SI-C	33.2	44.1	22.7	33.9	0.69
B23		OI, WI	SI-B	38.2	43.1	18.7	30.2	0.74
B24		WI, OI	SI-A	20.8	51.0	28.2	35.5	0.69
B32		WF, OI, WI	SI-C	25.6	46.2	28.2	38.0	0.93
B14	SQ/SQ	WI, OI	SI-A	19.6	60.8	19.6	24.4	0.43
B15		OI, WI	SI-B	30.2	58.8	11.0	15.8	0.31
B19		WF, OI, WI	SI-C	35.5	43.0	21.5	33.4	0.64
B25	SQ-H/SQ	WI, OI	SI-A	20.5	47.0	32.5	40.9	0.77
B26		OI, WI	SI-B	33.4	43.0	23.6	35.4	0.86
B31		WF, OI, WI	SI-C	28.8	44.8	26.4	37.0	0.96

SP Spraberry
SQ Sulimar Queen
SQ-H mixture of 80% SQ crude + 20% Heptane
WF Waterflooding
WI Spontaneous water imbibition
OI Spontaneous oil imbibition
R_{WI} Recovery from spontaneous water imbibition

Type:
SI-A WI first, followed by OI
SI-B OI first, followed by WI
SI-C SI-B imbibition after extensive waterflood and/or aging in brine

For water imbibition, ultimate displacement efficiencies are higher for SI-A tests than those for SI-B tests ((a) in Figs. 3.1-29 to 3.1-31). Residual oil saturations are also generally higher for SI-A tests than for SI-B tests ((b) in Figs. 3.1-29 to 3.1-31). Note that the oil saturation at the beginning of imbibition test was higher for SI-A than for SI-B. With more initial oil in place, both the final oil recovery and residual (trapped) oil by spontaneous water imbibition are increased.

In two cases (Fig. 3.1-29(a), Fig. 3.1-30(a)), SI-A and SI-B gave similar initial rates of change in oil recovery (% OOIP) during spontaneous water imbibition. In the third case (Fig.3.1-31(a)), initial rate of oil recovery from SI-B test was faster than in the SI-A test. Possibly the wetting condition established by aging core in SQ-H oil mixture (SQ crude with 20% heptane) changed slowly to more water-wet during the month-long duration of the first oil imbibition test.

Oil imbibition also gave a similar initial rate of water displaced (% OWIP) from cores B14 (SI-A) and B15 (SI-B) (see Fig. 3.1-30(a)). In other two cases, amounts of water displaced from oil imbibition for both SI-A and SI-B were too little to be comparable.

In general, the initial rates of change in oil recovery provide a convenient indicator of wetting.

Influence of extensive waterflooding on wetting evolution: Cores B19, B22, B31, B32 were used to investigate rate sensitivity of relative permeability at S_{or}. Conditions of these tests are summarized in Table 3.1-11. After rate testing, each core was subjected to both oil and water imbibition tests (SI-C) to determine whether or not the wettability had changed. Changes might result from exposure to (1) high flow rates, (2) many pore volumes of water injection, or (3) the long duration of these experiments.

Table 3.1-11. Summary of rate-sensitivity tests

Core	Oil/water	Initial WF (ml/hr)	Max. rate (ml/hr)	Injection (PV)	Duration (hr)	Rate sensitive?	Aging in brine	I_w^*
B22	SP/SP	8	400	~300	~100	serious	1 month	0.69
B32	SP/SP	80	400	~80	~30	slightly	no	0.93
B19	SQ/SQ	8	400	~300	~100	serious	1 month	0.64
B35	SQ/SQ	80	400	~60	~20	slightly	no	
B31	SQ-H/SQ	8	400	~200	~70	moderate	no	0.96

I_w^* = Amott index to water measured after rate-tests (and aging in brine)

Based on the initial oil imbibition rate (% OOIP), it can be seen from Fig. 3.1-32 to Fig. 3.1-33(a) that cores (B19, B31, B22) subjected to long-duration, high flow-rate waterflooding (B19 and B22 were also soaked in brine for one month after the first rate-test) all appear to be more water-wet than cores in which imbibition was tested immediately after aging (B15, B26, B23). However, results in Fig. 3.2-33(b) show that thewater imbibition rate (% OOIP) for core B32 after a high-rate, shorter duration waterflood has not become more water-wet.

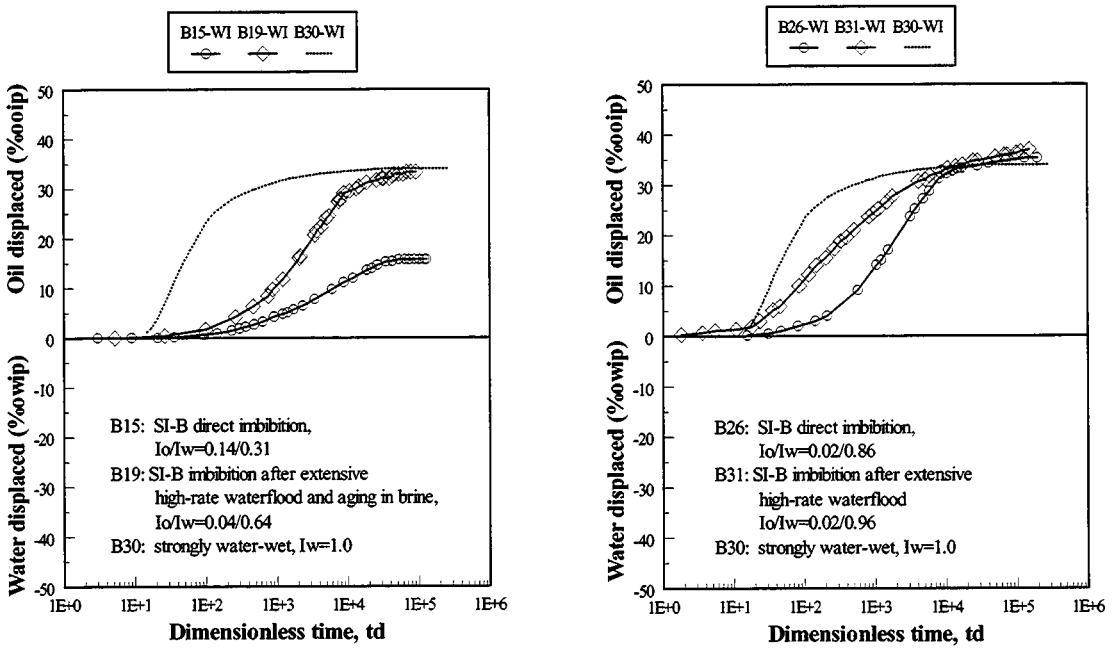

(a) waterflood and aging in brine
(SQ crude / SQ brine)

(b) waterflood
(SQ-H oil / SQ brine)

Figure 3.1-32. Extensive waterflood (and aging in brine) makes cores treated with SQ oil more water-wet.

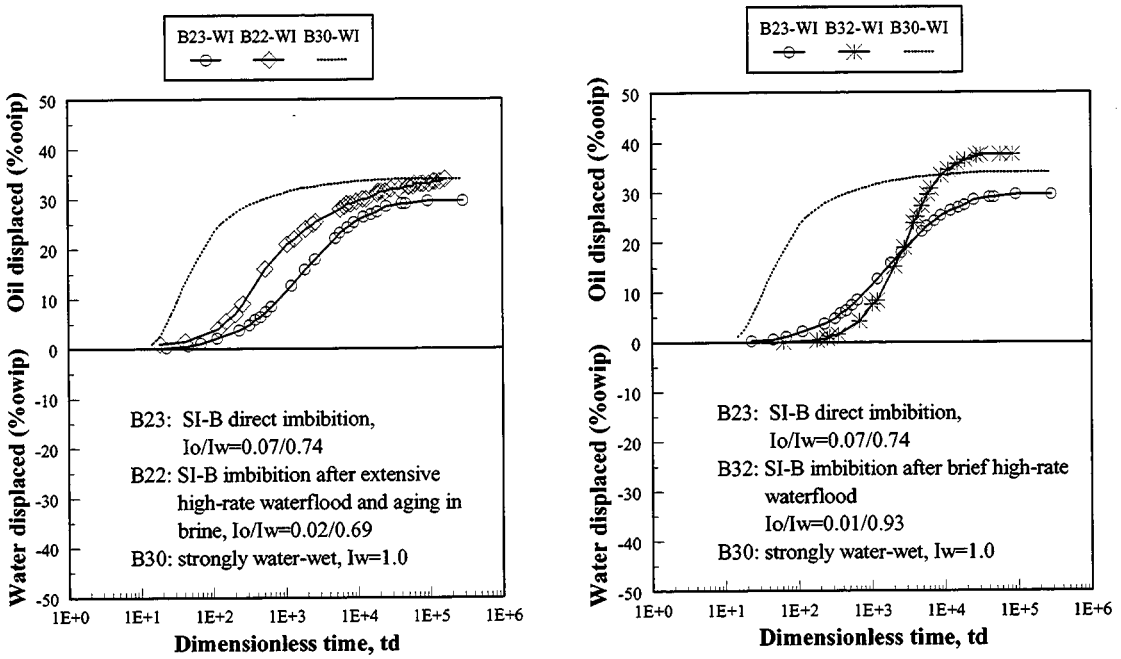

(a) long-duration waterflood (SP crude / SP brine)

(b) brief waterflood (SP crude / SP brine)

Figure 3.1-33. Long-duration, high-rate waterflood makes cores treated with SP oil more water-wet. A brief, high-rate waterflood does not.

As for the imbibition tests with different initial saturation and saturating history, the Amott index to water, I_w, widely used to assess wetting, is affected to some extent by the order of measurement (Fig. 3.1-34). However, all I_w values increase after prolonged waterfloods and/or aging in brine, indicating more water-wet conditions, which are consistent with observations of initial rate changes of oil recovery. The Amott index to oil, I_o, also shows a little decrease after waterfloods.

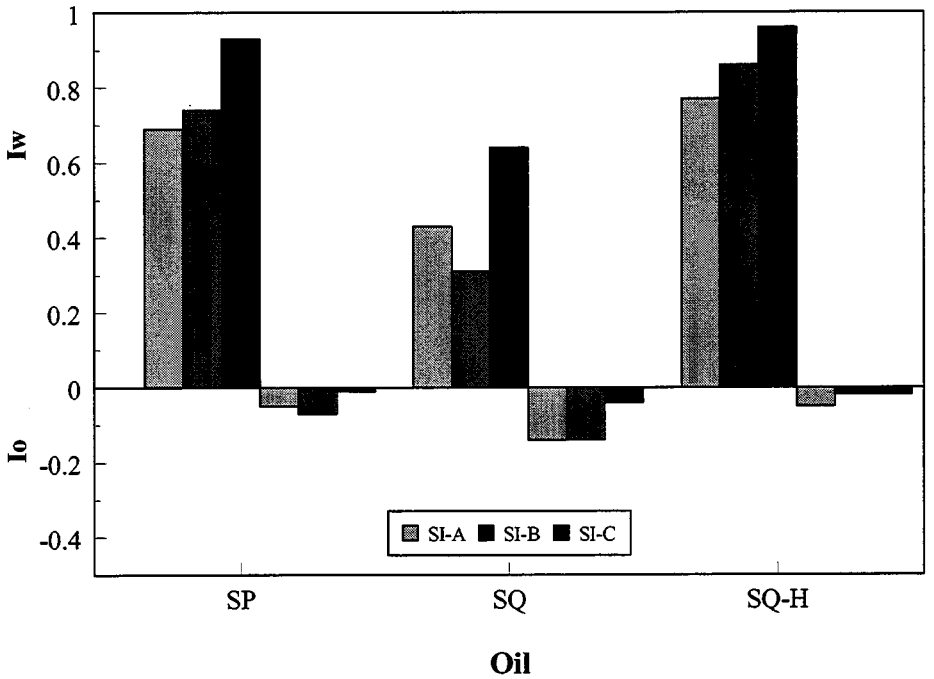

Figure 3.1-34. Amott index I_w is affected to some extent by the order of measurement (SI-A vs. SI-B); Prolonged waterfloods and/or aging in brine increase I_w and decrease I_o (SI-C).

While additional testing would be needed to separate the possible effects of flow rate, volume throughput, and time, comparisons here do suggest that changes in wetting require long times, not just a high throughput of water.

Rate dependence:

Two types of hysteresis of water relative permeability at residual oil saturation, $k_{rw}(S_{or})$, are referred to in this study:

- RD-A: changes of $k_{rw}(S_{or})$ observed during rate-increasing as compared to rate-decreasing processes;
- RD-B: changes of $k_{rw}(S_{or})$ from one test loop to another test loop.

All the $k_{rw}(S_{or})$ values in this section are treated as follows:

Measured data, N_{cap} versus N_{cav}, for rate-increasing are fit to a 3rd order polynomial function while rate-decreasing data are fit to a straight line, $N_{cap} = \kappa N_{cav} + N_{cap0}$, where κ is the

slope and N_{cap0} is the intercept. A small but non-zero value of N_{cap0} is probably due to capillary pressure in the tubing at the outflow end.

Values of $k_{rw}(S_{or})$ are calculated based on these fits using Equation (3.1-12).

Values of $k_{rw}(S_{or})$ are corrected by subtracting N_{cap0} from N_{cap}.

The **discrepancy** of $k_{rw}(S_{or})$ between rate-increasing and rate-decreasing processes is defined as

$$\varepsilon = \frac{k_{rwd} - k_{rwi}}{k_{rwi}} = \frac{N_{capi} - N_{capd}}{N_{capd}} \tag{3.1-21}$$

where subscript d represents rate-decreasing and i represents rate-increasing. A specific discrepancy ε_1, corresponding to $L\mu_w v = 1$, is used for purposes of comparison since

- $L\mu_w v = 1$ is commonly accepted as minimum value for eliminating end-effects;
- the error due to N_{cap} vs N_{cav} curve-fitting is much smaller when $L\mu_w v > 1$.

The **deviation** of $k_{rw}(S_{or})$ from one test loop to another test loop is given by:

$$\eta = \frac{k_{rw2} - k_{rw1}}{k_{rw1}} \times 100\% \tag{3.1-22}$$

where k_{rw1} and k_{rw2} represent the corrected $k_{rw}(S_{or})$ from the rate-decreasing process in each test loop. A specific deviation η_0 is defined as the deviation from $k_{rw}(S_{or})$ at the end of the low-rate waterflood to the maximum corrected $k_{rw}(S_{or})$ among all rate-tests.

$k_{rw}(S_{or})$ for the strongly water-wet case: No discrepancy exists between rate-increasing and rate-decreasing processes (RD-A) up to the maximum flow-rate of 400 ml/hr with strongly water-wet cores B29 and B30 (corresponding to maximum $L\mu v_w$ of 4.7 and 6.3 cm^2cp/min, respectively). Results from several rate-test cycles with different flow rate ranges indicated that there was also no RD-B type hysteresis. Figure 3.1-35 shows the maximum corrected $k_{rw}(S_{or})$ obtained from each rate test with core B30. A maximum deviation of only about 5% is well within the error range associated with measurement and curve fitting. Thus, for strongly water-

wet cores, both S_{or} and the relative permeability to water at residual oil saturation, $k_{rw}(S_{or})$, are independent of flow rate.

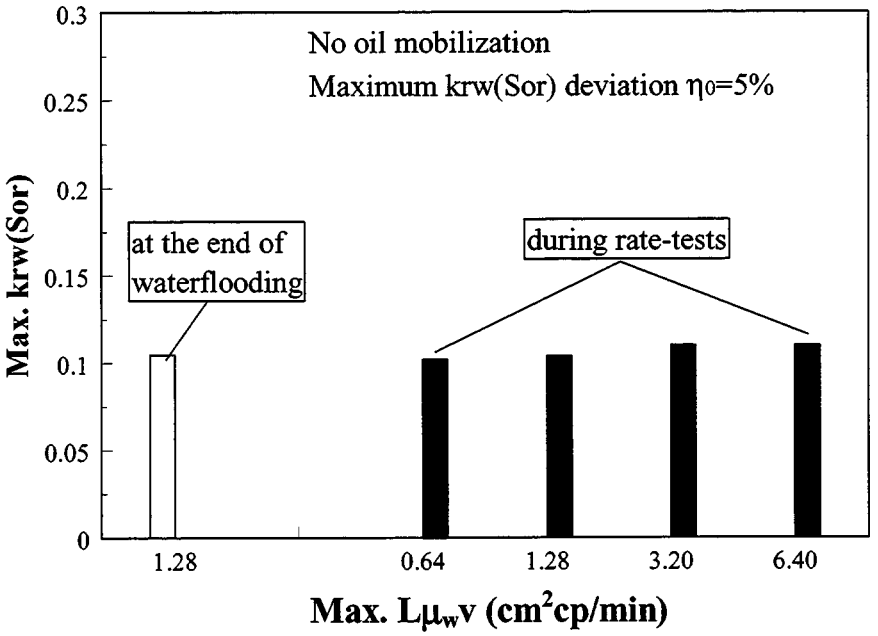

Figure 3.1-35. Deviations of $k_{rw}(S_{or})$ under strongly water-wet condition are negligible.

B30: S_{wi}=19.8%, S_{or}=39.9%, Fluids: Soltrol-130 & 2% $CaCl_2$ brine

Rate dependence associated with oil mobilization (mixed-wet and weakly water-wet cases): In two cases, elevating flow rates at the end of low-rate regular waterflooding (8 ml/hr) produced small amounts of crude oil. Both RD-A and RD-B types of hysteresis were observed during oil mobilization.

One of the test loops with maximum RD-A hysteresis obtained from core B22 is shown in Fig. 3.1-36. The discrepancy of $k_{rw}(S_{or})$, ε_1, is as high as 105%. In other words, increasing flow-rate to 200 ml/hr induced a doubling of water relative permeability, accompanied by production of a small amount of residual oil (0.42% OOIP).

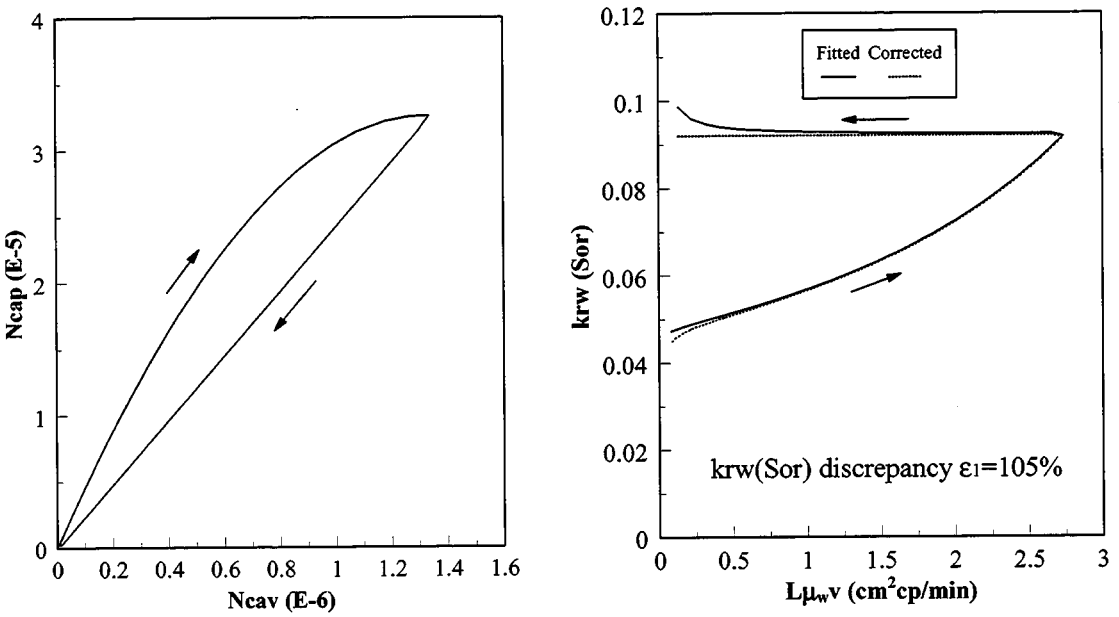

(a) Capillary number hysteresis (b) $k_{rw}(S_{or})$ hysteresis

Figure 3.1-36. Discrepancy of $k_{rw}(S_{or})$ associated with oil mobilization.

Fluids: SP oil and SP brine
B22: Q=1-200-1 ml/hr, oil mobilized= 0.42% OOIP

All RD-B hysteresis for core B22 during four rate-test cycles that produced oils are shown in Fig. 3.1-37. The maximum η_0 from the end of the low-rate waterflood (8 ml/hr) to the end of high-rate tests (200 ml/hr), associated with only 4.3% of total oil mobilization, is 165%.

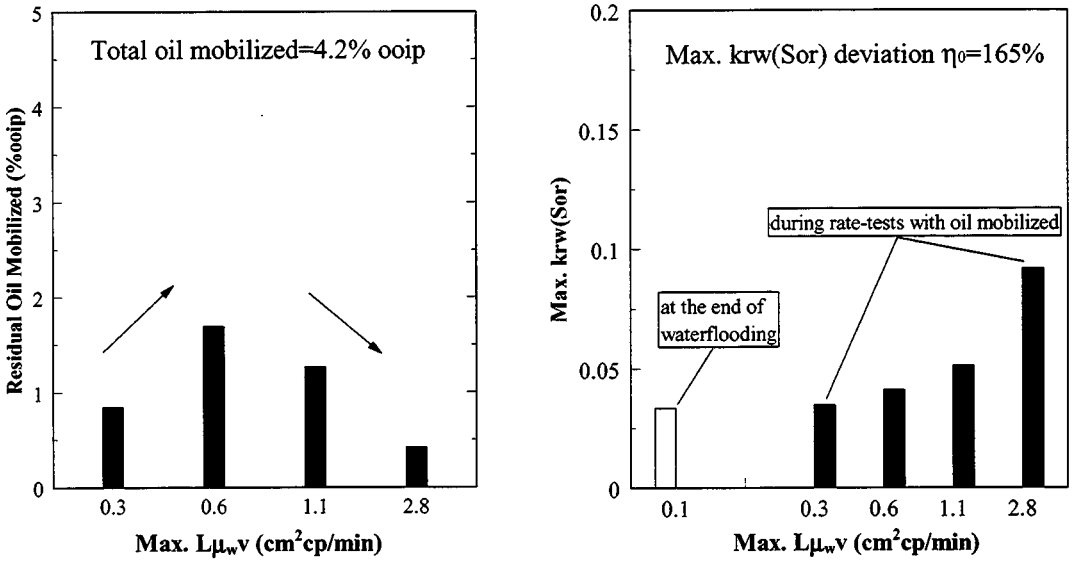

(a) oil mobilized from early test-loops (b) $k_{rw}(S_{or})$ deviation

Figure 3.1-37. Deviation of $k_{rw}(S_{or})$ associated with oil mobilization.

Fluids: SP oil and SP brine
B22: initial S_{or}=36.0%, final S_{or}=32.7%

Results from core B19 have similar trends, but are less severe. The maximum discrepancy ε_1 is about 15% for a test loop of 1-80-1 ml/hr. The maximum deviation η_0 from low-rate (8 ml/hr) waterflooding to the maximum flow rate (80 ml/hr) is about 103% with 4.1% OOIP of total oil mobilized (Fig. 3.1-38).

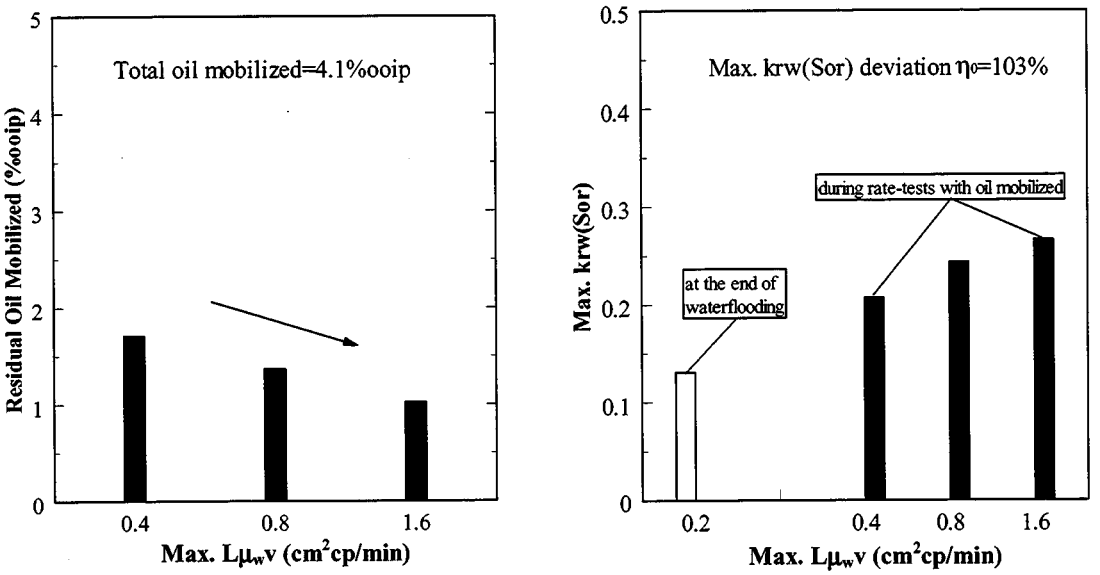

(a) oil mobilized from early test-loops (b) $k_{rw}(S_{or})$ deviation

Figure 3.1-38. Deviation of $k_{rw}(S_{or})$ associated with oil mobilization.

Fluids: SQ oil and SQ brine
B19: initial S_{or}=24.2%, final S_{or}=20.9%

The increases in relative permeability to water, $k_{rw}(S_{or})$, are at least partly due to mobilization of oil, but appear too large to be attributed only to changes in the residual oil saturation. Flow rate is obviously another important factor. To decouple rate and saturation dependent effects, the reminder of this discussion will focus on tests in which no oil was mobilized by varying flow rate.

Rate dependence after oil mobilization ceases (mixed-wet and weakly water-wet cases): A series of repeated increasing and decreasing rate tests were performed after oil production completely ceased, to demonstrate whether and under what conditions rate dependence was exhibited. Results from all three non-water-wet case studies (Case 2 to Case 4) demonstrated both RD-A and RD-B rate dependence. Rate dependence of $k_{rw}(S_{or})$ is affected by the highest flooding rate in each test cycle, the number of test cycles, and the flow rate during initial waterflooding.

Figures 3.1-39 to 3.1-41 show the RD-A hysteresis of $k_{rw}(S_{or})$ after oil production ceased. All three cores (B22, B19, B31) were initially waterflooded at low flow rate (8 ml/hr) before rate tests. The maximum flow-rate range applied for comparison is 1-200-1 ml/hr. It is seen that the magnitudes of discrepancy of $k_{rw}(S_{or})$ between rate-increasing and rate-decreasing steps increase with increasing the maximum flow rate in each test loop. Note that $k_{rw}(S_{or})$ during the rate-increasing step in a given cycle can be lower, the same as, or higher that during the rate-decreasing step in the previous loop. This indicates that the changes in $k_{rw}(S_{or})$ are partially reversible.

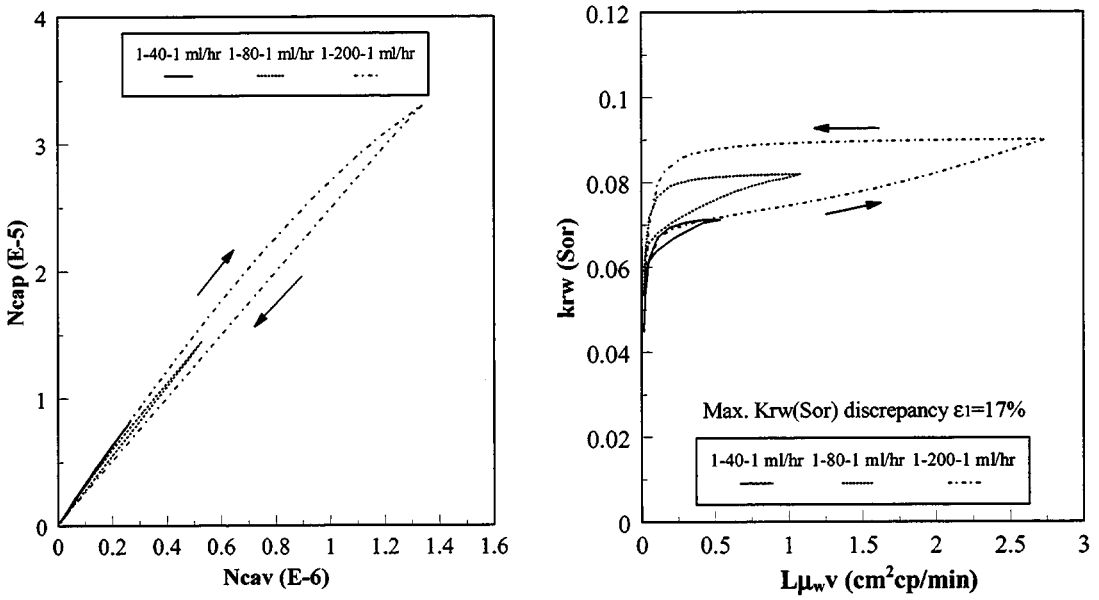

(a) Capillary number hysteresis (b) $k_{rw}(S_{or})$ hysteresis

Figure 3.1-39. Discrepancy of $k_{rw}(S_{or})$ under test cycles with different max. flow-rates.

Fluids: SP oil and SP brine
B22: S_{or}=32.7%, no oil production

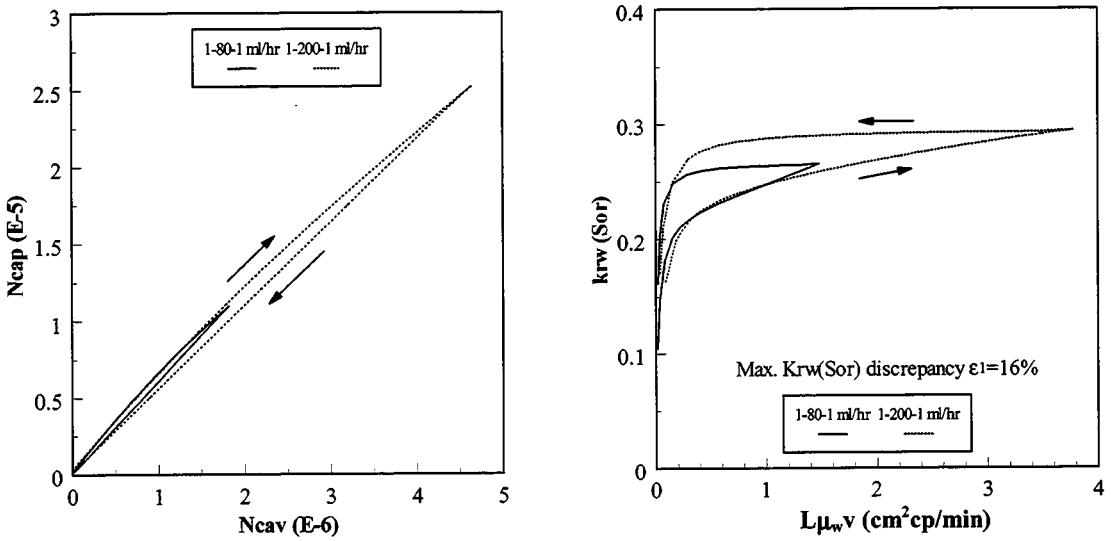

(a) Capillary number hysteresis (b) $k_{rw}(S_{or})$ hysteresis

Figure 3.1-40. Discrepancy of $k_{rw}(S_{or})$ under test cycles with different max. flow-rates.

Fluids: SQ oil and SQ brine
B19: S_{or}=20.9%, no oil production

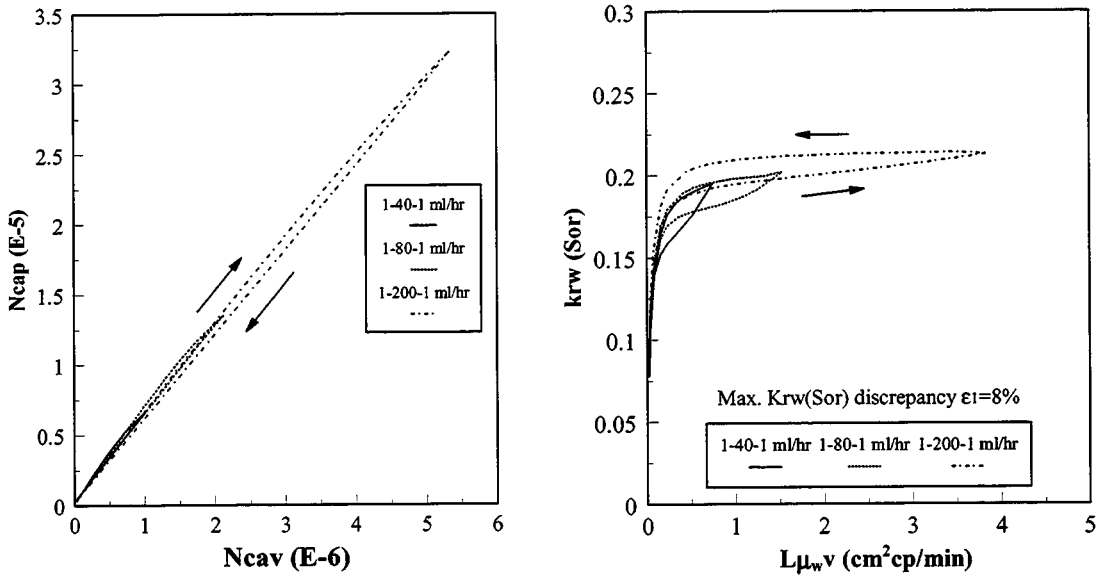

(a) Capillary number hysteresis (b) $k_{rw}(S_{or})$ hysteresis

Figure 3.1-41. Discrepancy of $k_{rw}(S_{or})$ under test cycles with different max. flow-rates.

Fluids: SQ-H oil and SQ brine
B31: S_{or}=25.3%, no oil production

In Fig. 3.1-42, three consecutive tests on core B22 with the same flow-rate range, 1-200-1 ml/hr, give different results: $k_{rw}(S_{or})$ increases steadily from cycle to cycle while the discrepancy between rate-increasing and rate-decreasing steps declines. Thus rate dependence of $k_{rw}(S_{or})$ is determined not only by the highest flow rate, but also by the number of test cycles.

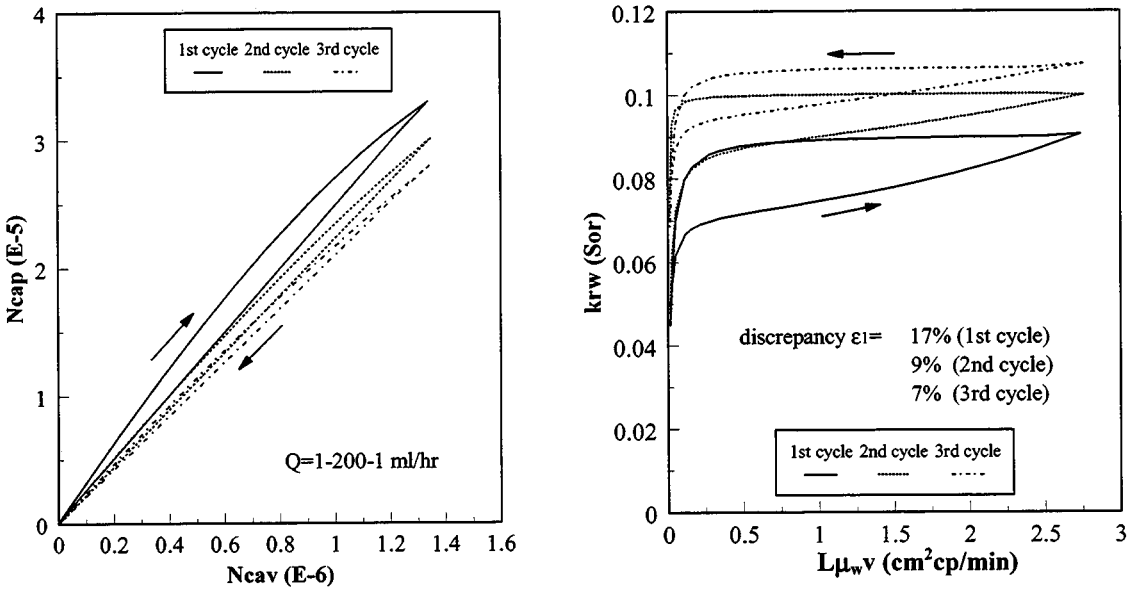

(a) Capillary number hysteresis (b) $k_{rw}(S_{or})$ hysteresis

Figure 3.1-42. Discrepancy of $k_{rw}(S_{or})$ under repeated cycles with the same max. flow rates.

Fluids: SP oil & SP brine
B22: S_{or}=32.7%, Q=1-200-1 ml/hr, no oil production

Figures 3.1-43 and 3.1-44 illustrate that type RD-A hysteresis of $k_{rw}(S_{or})$ is much smaller for cores (B32, B35) initially waterflooded at a high rate (80 ml/hr) than for those (B22, B19) initially waterflooded at a low rate (8 ml/hr). In fact, the discrepancy for cores B32 and B35 is almost negligible, even though the maximum flow rates (200 ml/hr) are much higher than initial waterflooding rate (80 ml/hr). Similar trends also exist for deviation of $k_{rw}(S_{or})$ in RD-B hysteresis (Figs. 3.1-45 and 3.1-46). Here we compare results between 80 ml/hr and 200 ml/hr (η').

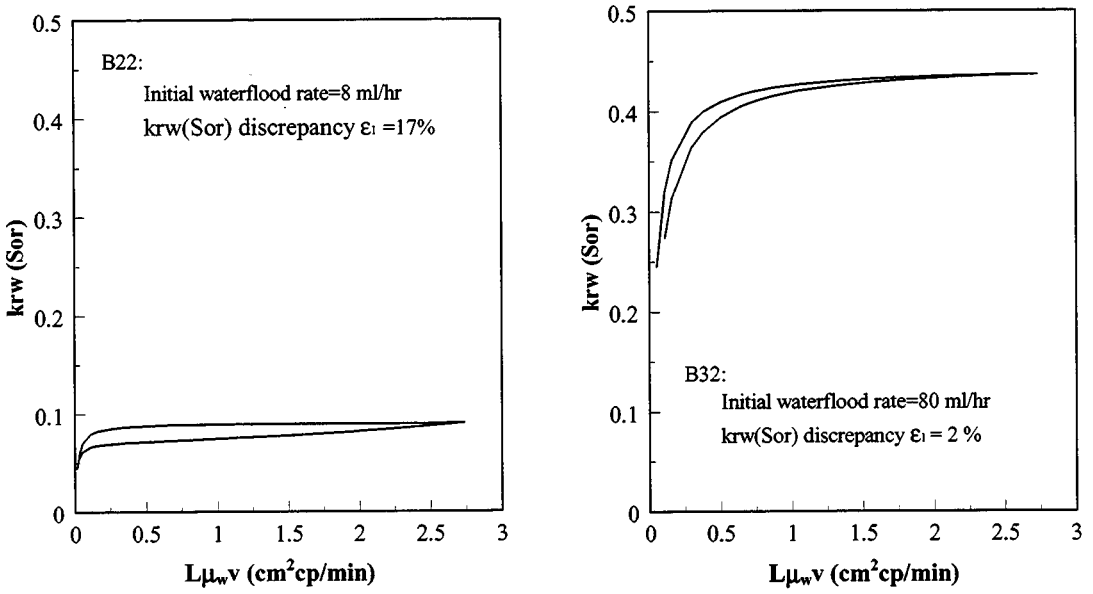

(a) after low-rate waterflood (b) after high-rate waterflood

Figure 3.1-43. Effect of initial waterflooding rate on RD-A type rate dependence.

Fluids: SP crude and SP brine
B22: S_{or}=32.7%, B32: S_{or}=32.6%, Q=1-200-1 ml/hr

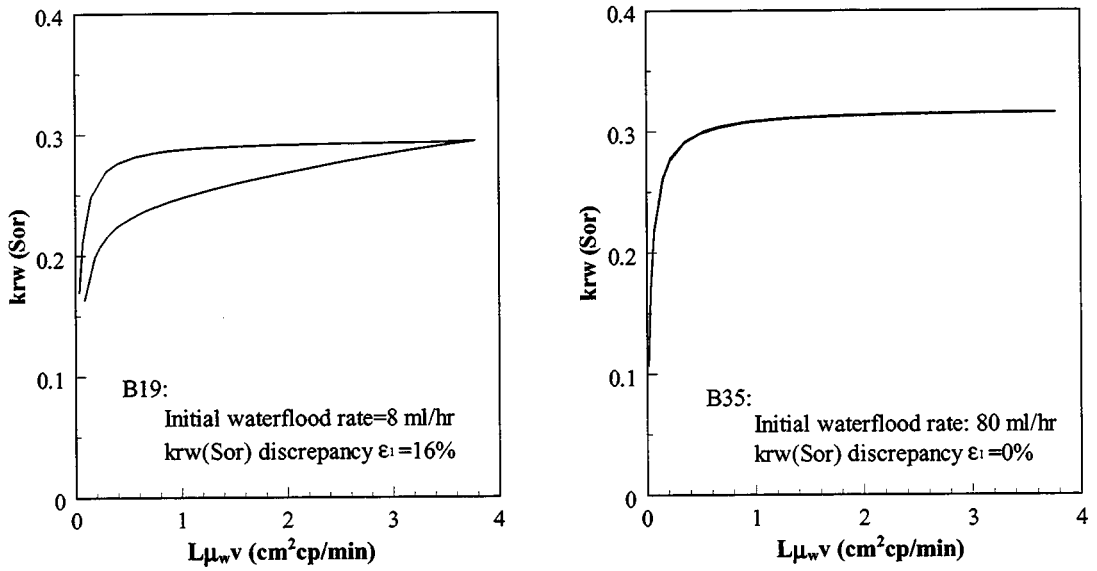

(a) after low-rate waterflood (b) after high-rate waterflood

Figure 3.1-44. Effect of initial waterflooding rate on RD-A type rate dependence.

Fluids: SQ crude and SQ brine
B19: S_{or}=20.9%, B35: S_{or}=25.7%, Q=1-200-1 ml/hr

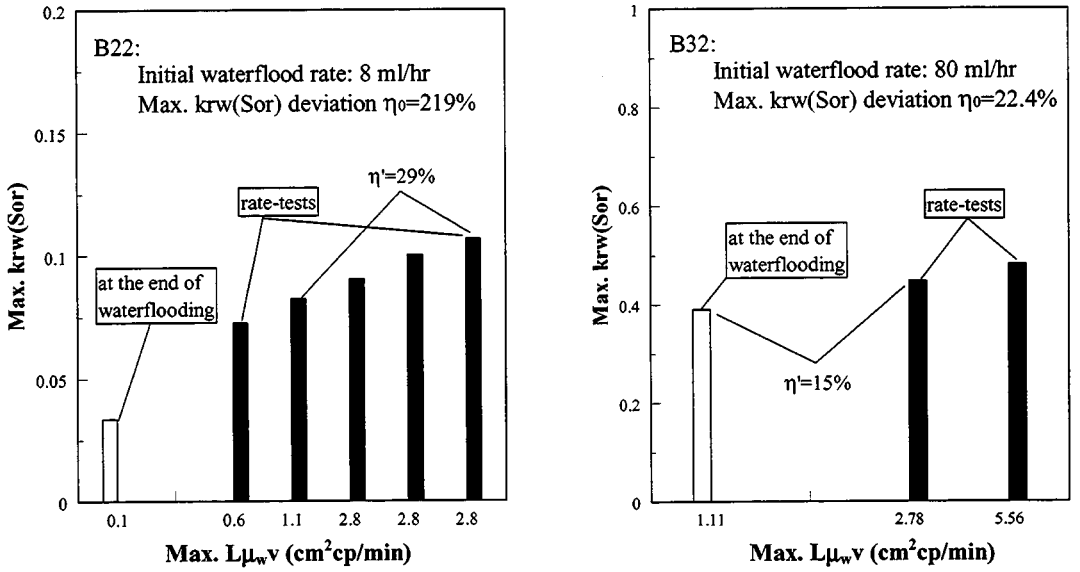

(a) after low-rate waterflood (b) after high-rate waterflood

Figure 3.1-45. Effect of initial waterflooding rate on RD-B type rate dependence.

Fluids: SP crude & SP brine
B22: S_{or}=32.7%, B32: S_{or}=32.6%

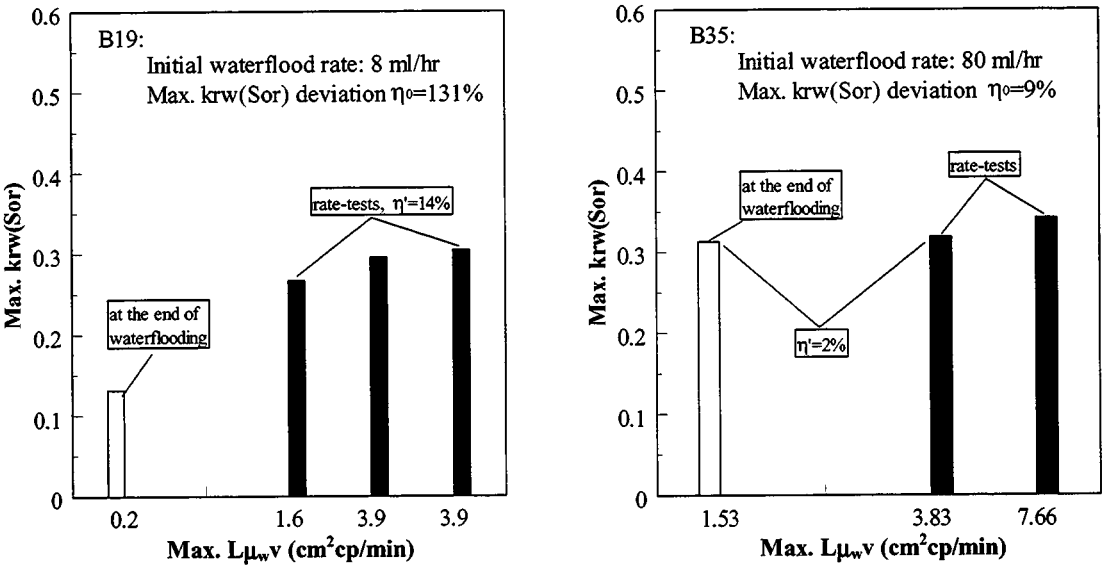

(a) after low-rate waterflood (b) after high-rate waterflood

Figure 3.1-46. Effect of initial waterflooding rate on RD-B type rate dependence.

Fluids: SQ crude and SQ brine
B19: S_{or}=20.9%, B35: S_{or}=25.7%

Cores B19 and B22 were immersed in brine for one month after a series of rate tests to 200 ml/hr. Subsequent rate tests up to 400 ml/hr after aging in brine showed a significant

increase of $k_{rw}(S_{or})$ even though there is no change to the residual oil saturation (Fig. 3.1-47). Note that before aging in brine, $k_{rw}(S_{or})$ for B22 increased from one test cycle to another at the same maximum flow rate, but became independent of the number of test loops after aging, suggesting the importance of slow changes that occur over long periods of time.

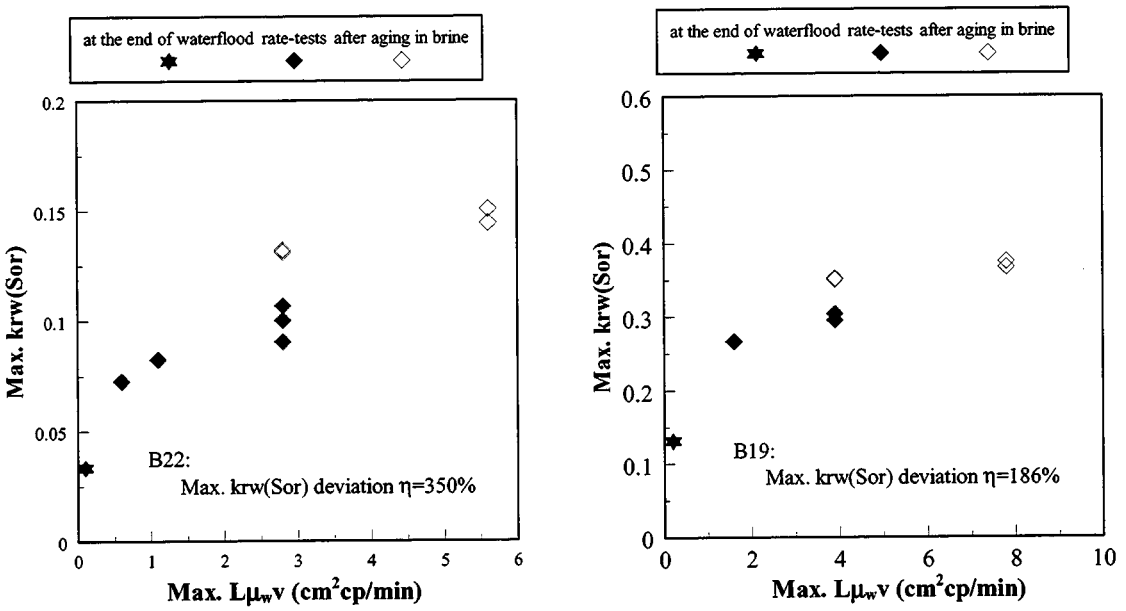

(a) core B22 (b) core B19

Figure 3.1-47. Effect of aging in brine on RD-B type rate dependence.

B22: SP crude & SP brine, initial waterflood rate=8 ml/hr, S_{or}=32.7%
B19: SQ crude & SQ brine, initial waterflood rate=8 ml/hr, S_{or}=20.9%

The $k_{rw}(S_{or})$ values presented thus far have been plotted versus $L\mu_w v$. In most of the rate tests, changes in $k_{rw}(S_{or})$ persist to $L\mu_w v$ values much higher than 1.0. This suggests that end effects should not have been a major factor contributing to the rate dependence of $k_{rw}(S_{or})$.

Experimental measurements also supported the assertion that end effects are not the main explanation for rate dependence. In some rate tests, flow direction was reversed at several flow rates (80 ml/hr, 200 ml/hr) but no obvious changes in pressure drop were observed, even after many PV of injection. If there were end effects, residual oil saturation would be unevenly distributed along the core axis. Reversing flowing direction would alter the oil distribution and

lead to a change of pressure drop. Since no change in pressure gradient was observed, we concluded that end effects are not significant.

Significance of rate dependence of $k_{rw}(S_{or})$:

Previous discussions reveal that, for non-water-wet conditions, the water relative permeability end point $k_{rw}(S_{or})$ can vary with the flow rate at which it is measured. The greatest deviation of $k_{rw}(S_{or})$ from the end of low-rate flooding (8 ml/hr) to maximum flow rate 400 ml/hr is about 350% for B22 (SP oil), 186% for B19 (SQ oil) and 81% for B31 (SQ-H oil), respectively. These deviations, of course, cannot be neglected. To demonstrate how significant rate dependence of $k_{rw}(S_{or})$ could be, all the values of $k_{rw}(S_{or})$ at various flow rates are plotted along with relative permeability curves obtained from history matching of constant low flow rate waterflooding data (Figs. 3.1-48 to 3.1-50). Only for core B22 do any of the new end point values appear to extend the original k_{rw} curve and then only if additional oil is produced.

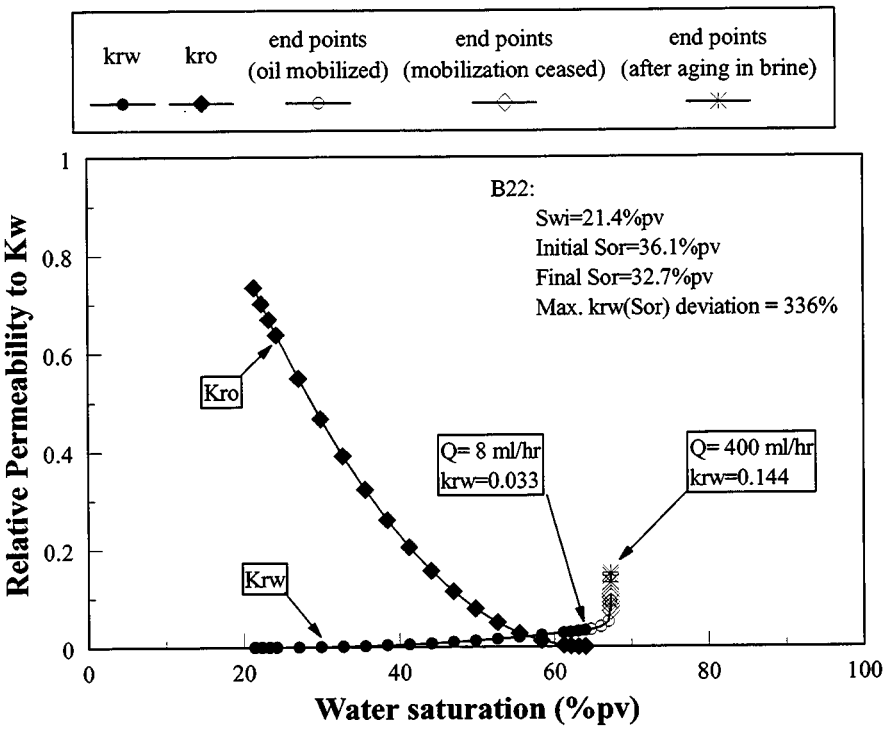

Figure 3.1-48. Relative permeability and end point $k_{rw}(S_{or})$.

B22: SP oil and SP brine

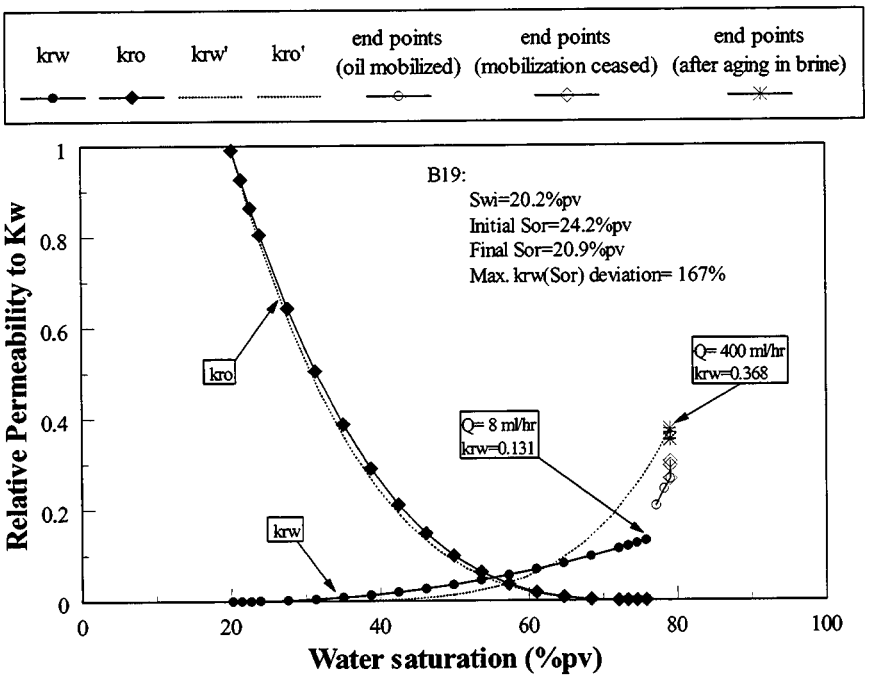

Figure 3.1-49. Relative permeability and end point $k_{rw}(S_{or})$.

B19: SQ oil & SQ brine

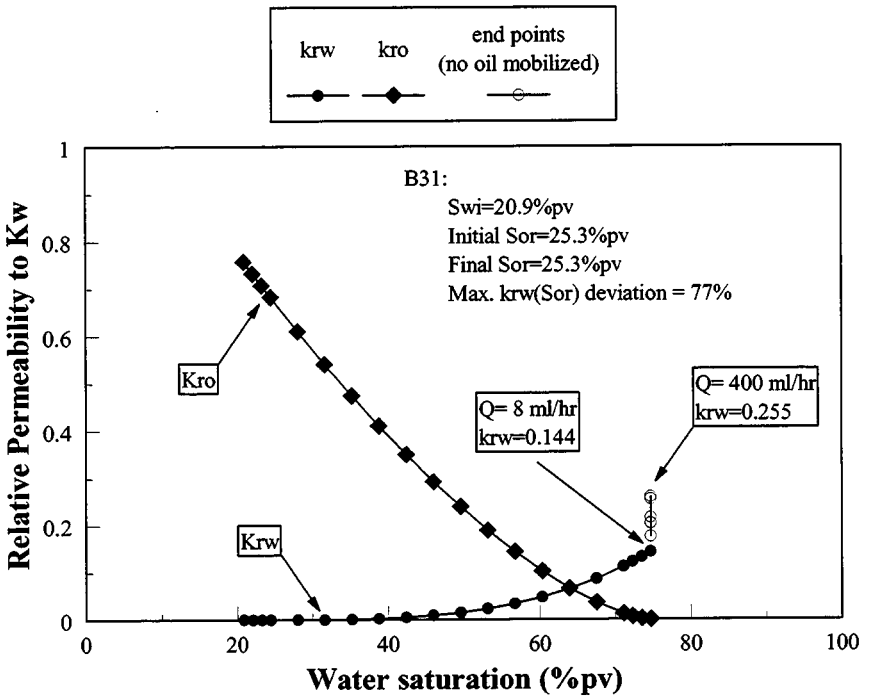

Figure 3.1-50. Relative permeability and end point $k_{rw}(S_{or})$.

B31: SQ-H oil & SQ brine

If the waterflooding data from B19 are re-interpreted using the maximum value of $k_{rw}(S_{or})$, the dashed line in Fig. 3.1-49 is obtained. The oil relative permeability curve is only affected slightly. The water relative permeability curve, however, is shifted significantly.

Oil-water distribution is less changeable at the end of waterflooding than during the displacement process. If $k_{rw}(S_{or})$ is rate sensitive, it is likely that the rest of the relative permeability curve may also depend on flow rate.

Probable mechanisms of rate dependence:

Is rate dependence of $k_{rw}(S_{or})$ a Forchheimer effect?: As discussed in section 3.1.4, for high-velocity flow in porous media the pressure gradient might be greater than that predicted by Darcy's law. In this study, however, pressure gradients are lower than expected and thus cannot be attributed to a Forchheimer effect.

Oil-water redistribution: A pore doublet model (Moore, *et al.*, 1956) will be employed here to illustrate how the residual oil distribution might vary with flow rate and the effect of this variation on water permeability. In this model, the complex pore structure is simplified into a repeated arrangement of pore doublets. Each doublet consists of two parallel pores, one narrower than the other, but with common inlet and outlet channels (Fig. 3.1-51).

Berea sandstone has a high pore-throat aspect ratio. In the case of **strongly water-wet** conditions, capillary forces trap a large amount of residual oil. Most of the residual oil is trapped in the center of large pore bodies, leaving the small pores, pore throats and the corners and surfaces of large pores occupied entirely by water. Since large pore bodies are almost completely filled with oil (Fig. 3.1-51(1)), small pores and pore throats account for most of the conductivity of water (Fig. 3.1-51(2), Fig. 3.1-51(3)). If the maximum flow rate does not exceed the critical value at which the trapped oil blobs can be mobilized, change of flow rate has little effect on permeability and no rate dependence of $k_{rw}(S_{or})$ can be detected.

For **mixed-wet** conditions, the most likely areas to have been altered from water-wet to intermediate or oil-wet during aging in crude oil are those surfaces that are not overlain by bulk water. Convex and protruding surfaces are most susceptible to wetting alteration since local capillary forces help to thin water films at those locations. None of the cores in this study were strongly oil-wet. Wetting was mixed with some pathways remaining water-wet and some surfaces becoming more oil-wet.

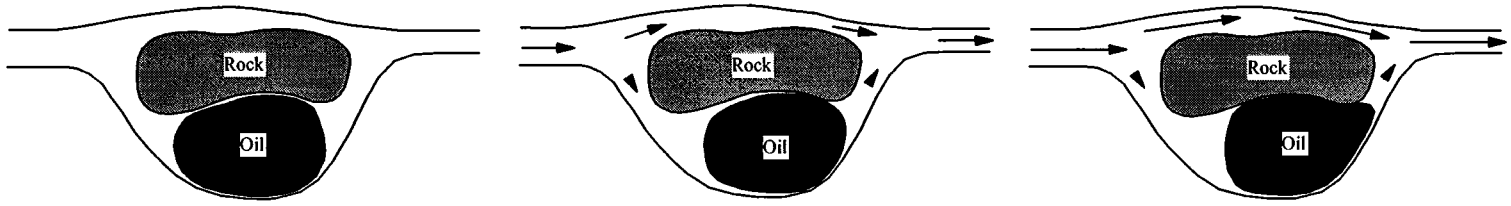

(1) no flow (2) low flow-rate (3) high flow-rate

Figure 3.1-51. Residual oil distribution in a pore doublet (strongly water-wet case).

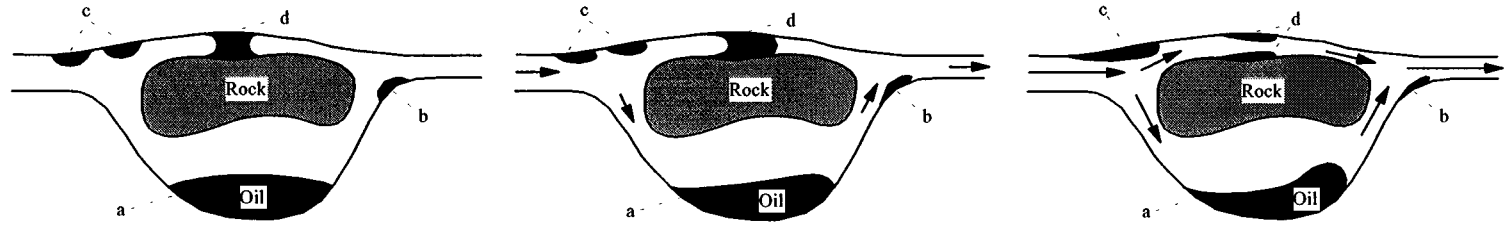

(1) no flow (2) low flow-rate (3) high flow-rate

Figure 3.1-52. Residual oil distribution in a pore doublet (mixed-wet). Letters refer to discussion in text.

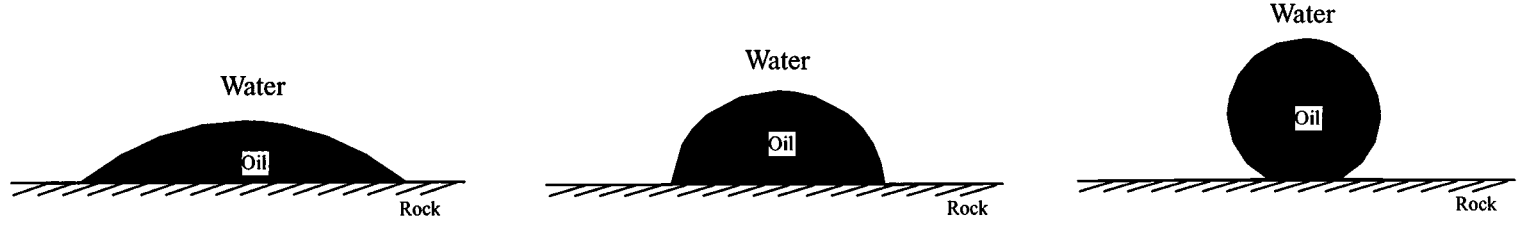

(1) oil-wet (2)neutral-wet (3)water-wet

Figure 3.1-53. Wetting evolution during large throughput waterflood or long-duration aging core in brine (mixed-wet).

Most of the residual oil may still reside in large pore bodies as oil blobs adhering to more oil-wet rock surfaces (a, in Fig. 3.1-52(1)). Some of the residual oil may adhere to those oil-wet surfaces in pore throats or near the entries from pore to throat (b and c, in Fig. 3.1-52(1)), while some may even block the flowing path by occupying the small pores as an oil plug under static conditions (d, in Fig. 3.1-52(1)).

The distribution of oil at the end of a low-rate waterflood represents an equilibrium between capillary and viscous forces (Fig. 3.1-52(2)). As the viscous force increases, the shape of a large oil blob may be altered slightly while still being pinned at the original oil-wet surface (a, in Fig. 3.1-52(3)), resulting in a little impact on the flowing resistance. Smaller oil drops may flatten (b, in Fig. 3.1-52(3)), or even commingle to form larger drops with lower curvature (c, in Fig. 3.1-52(3)). Oil plugs blocking the small pores may be broken through as the viscous force exceeds the capillary force (d, in Fig. 3.1-52(3)). All these deformations may enlarge the effective diameter for water flow channels and result in a reduced pressure gradient, or increase of $k_{rw}(S_{or})$ without any change in oil saturation.

A potential evolution of wettability may occur during large throughput of water, or during long-duration aging of a core in brine. Those oil-wet surfaces may experience a slow reversion to neutral-wet or even to water-wet (as illustrated in Fig. 3.1-53) if polar components originally adsorbed from crude oil onto rock surface during aging in crude oil desorb. The oil drops that originally adhered may become more movable. If they are subsequently displaced, the resistance to water flow would decrease. Under this scenario, $k_{rw}(S_{or})$ increases as the core become more water-wet.

Some oil might be moved downstream by increased viscous forces. Mobilized oil could be retrapped downstream, merging with and enlarging existing oil ganglia. These enlarged oil

ganglia might eventually be produced. Oil mobilization was observed within a relatively low flow-rate range in Cases 2 and 3. No mobilization was observed in Case 4.

As flow rate is decreased, the original distribution pattern of residual oil may be partially restored. This leads to a partial reversibility of $k_{rw}(S_{or})$ with flow rate.

Suggestions for Future Work

From this study we have observed that rate sensitivity of $k_{rw}(S_{or})$ can occur in non-water-wet cases. We have compared strongly water-wet conditions with weakly water-wet and mixed-wet conditions. The next step would be to widen this experimental investigation to neutral and oil-wet conditions. Since pore structure and lithology are some of the other factors that could influence the rate dependence of $k_{rw}(S_{or})$, similar rate tests should also be extended to other porous media before general conclusions can be achieved.

Conclusions

Wettability determination:

- For strongly water-wet conditions, spontaneous water imbibition tests starting from different initial water saturation result in a very similar initial rate of change in oil recovery (% OOIP) and similar residual oil saturation, but different amounts of final oil recovery. This illustrates that for strongly water-wet conditions, the initial rate of change of oil recovery (% OOIP) is a better indicator of wettability than final oil recovery (% OOIP).

- Cleaning with isopropanol did not make Berea sandstone less strongly water-wet.

- For mixed-wet conditions induced by aging in either Sulimar Queen crude oil or Spraberry crude oil, the initial rate of change in oil recovery (% OOIP) is independent of measuring sequence (water imbibition, followed by oil imbibition or oil imbibition, followed by water imbibition). However, both ultimate oil recoveries and residual oil saturations are

different. This indicates that the initial rate of change of oil recovery (% OOIP) is also a better indicator of wettability for mixed-wet conditions.

- A mixed-wet condition induced by aging a core in a mixture of Sulimar Queen crude oil with n-heptane (8:2) appears to be less stable and to have reverted to more water-wet conditions during the long-duration imbibition tests.

- Long-duration, high flow-rate waterfloods tend to alter Berea sandstone to more water-wet conditions. A brief high flow-rate waterflood did not change the wettability significantly, suggesting that the total throughput and total flooding duration have more effect on wetting than the magnitude of flow rate.

Rate dependence of $k_{rw}(S_{or})$:

- For strongly water-wet cores, water relative permeability at residual oil is independent of flow rate within the range of 1-400 ml/hr. No additional oil was produced at these rates.

- Two types of rate dependence have been demonstrated for mixed-wet cores: hysteresis of $k_{rw}(S_{or})$ between rate-increasing and rate-decreasing measurements and deviation in $k_{rw}(S_{or})$ from one test loop to another test loop. Change of flow rate from a low value (1 ml/hr) to a high value (maximum 400 ml/hr), with or without oil mobilization, can cause both types of rate dependence.

- In one case, a small amount of residual oil mobilized (0.42%) resulted in a doubling of water relative permeability $k_{rw}(S_{or})$. A total of 4.3% residual oil mobilized from the end of the low-rate waterflood (8 ml/hr) to the end of high-rate floods (400 ml/hr) in that same case gave a 165% deviation of $k_{rw}(S_{or})$. These increases in relative permeability to water, $k_{rw}(S_{or})$, appear too high to be attributed only to changes in the residual oil saturation.

- After oil recovery ceased, the deviation of $k_{rw}(S_{or})$ from the end of low-rate flooding (8 ml/hr) to a maximum flow rate of 400 ml/hr was as high as 350% (for the case with Spraberry oil/brine system). Lower, but still significant effects were recorded for Sulimar Queen oil/brine and for a mixture of Sulimar Queen oil with heptane/brine.

- Rate dependence of $k_{rw}(S_{or})$ is affected not only by the highest flow-rate, but also by the number of test cycles. Changes in wetting may occur slowly and appear to be related to total throughput and flooding duration.

- Cores initially flooded at high rate (80 ml/hr) appear to be less rate dependent than those initially flooded at low rate (8 ml/hr).

- Aging a core in brine at residual oil resulted in a significant increase of $k_{rw}(S_{or})$.

- End effects do not seem to be a major factor contributing to the rate dependence of $k_{rw}(S_{or})$.

- The rate dependence of $k_{rw}(S_{or})$ in this study cannot be explained by the Forchheimer effect. A nonlinear relationship is observed between flow rate and pressure gradient, but the trend is opposite to that expected.

- Rate dependence of $k_{rw}(S_{or})$ is large enough to influence significantly relative permeability curves based on waterflooding data. Application of high-rate waterflood core experiments to low-rate waterflood reservoir condition can be expected to lead to serious errors in prediction of waterflood results.

3.2 Wettability Changes during Production

In the lab we can vary asphaltene stability—and thereby affect an oil's tendency to alter wetting—by addition of *n*-heptane. Similar changes in asphaltene stability can occur in oil reservoirs in response to changes in reservoir pressure, temperature, and fluid compositions. Injection of gases and paraffinic liquids that are miscible with the reservoir oil can destabilize asphaltenes, raising the possibility that wetting is not constant, but may be changing during production. Two specific cases—pressure depletion and injection of CO_2—are considered to investigate the likelihood of asphaltene precipitation and associated wetting changes.

3.2.1 Pressure Depletion

Decreasing pressure decreases RI until the bubble-point is reached (Buckley *et al.*, 1998a). Figure 3.2-54 shows the relationship expected between pressure and refractive index. Depending on temperature and composition, some oils may experience asphaltene destabilization as a result of depressurization. As this point is approached at any given place in the reservoir, a change in the mechanism of wetting alteration might be expected for oils such as Mars-Pink, Tensleep, or A-93. If the pressure decreases below the bubble-point, the lightest components begin to separate into another phase, leaving the remaining oil phase a better solvent for its asphaltenes and returning rock/fluid interactions to the region of ionic mechanisms.

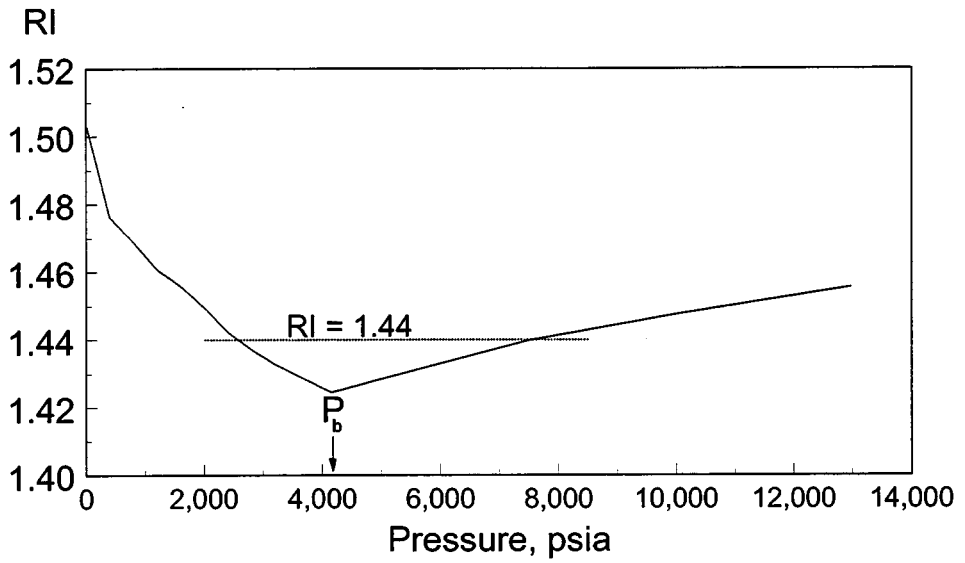

Figure 3.2-54. Refractive index as a function of pressure (after Buckley *et al.*, 1998a).

3.2.2 Gas Injection

Miscible or partially miscible gas injection processes can change oil composition and potentially destabilize asphaltenes. Consider the pseudo-ternary diagrams for CO_2 injection into the Wasson field (Gardner *et al.*, 1981) shown in Figure 3.2-55. Superimposed upon the pseudo-ternary diagram are hypothetical lines of constant RI, calculated from estimated values for CO_2 (RI=1.25), light ends (RI=1.35), and heavy ends (RI=1.56). RI of any mixture can be calculated by assuming that the contribution of each pseudo-component is proportional to its volume fraction in the mixture. Given these estimated values, the original live oil composition falls near the 1.5 iso-RI line, similar to most of the dead oil samples in this study. It should be emphasized that the RI values used in Figure 3.2-55 are estimates; they are not experimentally measured values.

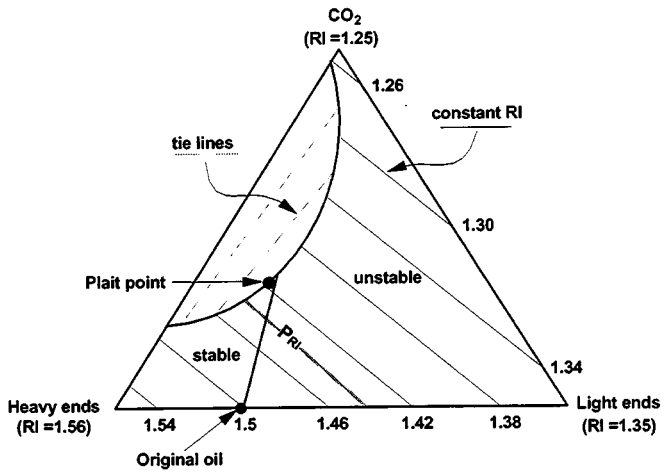

(a) Asphaltene precipitation begins in the single phase region.

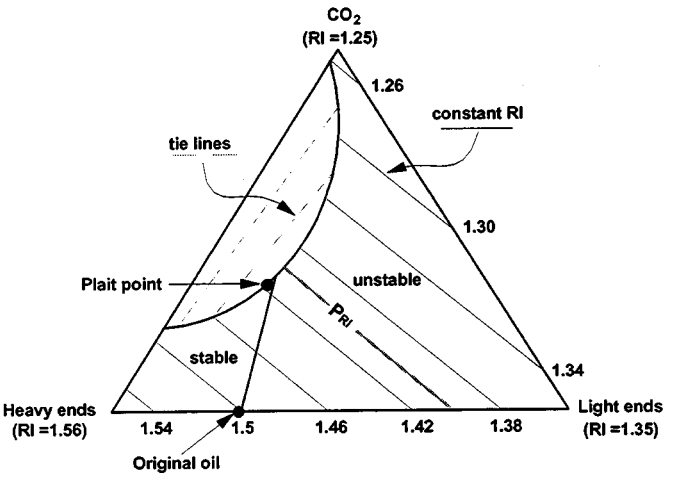

(b) Potential for asphaltene precipitation appears after the phase-split.

Figure 3.2-55. Pseudo-ternary phase diagrams based on CO_2/Wasson crude oil system at 2000 psi and 105°F (after Gardner *et al.*, 1981). Lines of constant RI have been calculated *assuming* RI values for CO_2, light ends and heavy ends of 1.25, 1.35 and 1.56, respectively. These assumed values give RI_{oil} = 1.5. (a) If P_{RI} = 1.44, the plait point composition is unstable with respect to asphaltenes. (b) If P_{RI} = 1.40, the plait point falls in the asphaltene-stable region.

Two possibilities can be considered for the onset conditions. If P_{RI} is equal to 1.44, the average value measured for the five crude oils in this study for the onset of precipitation with *n*-heptane, the plait point composition would fall within the region where asphaltenes are unstable. Precipitation would begin in the single-phase region. Within the two-phase envelope, asphaltenes would partition into the heavier, asphaltene-stable phase, but as the lighter phase contacts original oil, asphaltene precipitation would continue. Wettability alteration by the surface precipitation mechanism would occur over a narrow range of compositions, but asphaltenes would be removed from the oil mainly by bulk flocculation.

A more likely value for the onset conditions with CO_2 and the oil's light ends would be less than 1.44. In Figure 3.2-55b, a value of PRI=1.40 is selected, putting the plait point clearly in the asphaltene-stable region. No precipitation would occur until the overall composition reaches the two-phase envelope. Contact of original oil with the lighter phase would produce

mixtures in both the unstable and stable regions. Only if P_{RI} is less than 1.36 would asphaltene precipitation be avoided completely. Compositions that fall closest to the onset conditions have the greatest opportunity for wetting alteration.

A number of variables affect these pseudo-ternary representations. For example, shifting the original oil composition toward the lighter-components vertex would increase the likelihood of reaching the onset of asphaltene precipitation within the single-phase region. Changes in temperature and pressure would alter both the shape of the two-phase envelope and the RI values of the vertices. Generalizations about the effects of temperature and pressure on asphaltene stability are difficult to make in such a complex situation.

3.2.3 Discontinuous wetting

The steep variation in contact angles observed for three of the five oils tested raises the interesting possibility that, in some cases, wetting alteration by the surface precipitation mechanism might occur only over a very narrow range of mixture compositions and/or pressures. Spatially, this might translate into discontinuous oil-wet strips that occur only where these specific onset conditions are generated in the reservoir. Since both precipitation and wetting alteration can be slow processes, the zone of altered wetting might be widened at higher flow rates or sharpened if wells are shut in, which may occur when injection is switched from gas to water or water to gas.

The potential consequences of a sharp change in wetting, from strongly water-wet to strongly oil-wet, have been demonstrated in a high permeability bead pack (Vizika and Duouerroix, 1997). While changes in relative permeabilities are important, the effect of capillary pressure, often ignored, must also be considered. Both experiment and model calculations show that an oil-wet strip can act as a barrier to water flow. The implications of such wetting

discontinuities for injectivity and ultimate oil recovery in recovery processes where water and gas are injected alternately, have yet to be fully explored.

SUMMARY AND CONCLUSIONS

This five-year study of the evaluation of reservoir wettability and its effect on oil recovery has provided experience and insight into many facets of wettability alteration by crude oils. A database with information on hundreds of crude oil samples has been developed, which contains both crude oil properties and the results of wettability tests using those oils. There has been a great deal of interest in the crude oil evaluations performed under this project. Consequently the response of oil companies to requests for samples has far exceeded expectations. We expect that the data generated by this project will continue to serve as the basis for additional analysis and subsequent studies. A library of well-characterized crude oil samples is a valuable product of this project.

The volume of data obtained makes it possible to address questions such as whether there is a relationship between acid and base numbers. Contrary to the expectations of some geochemists, these two quantities appear to be uncorrelated. The need to quantify the condition of asphaltenes in their crude oil environment has led to development of measures of oil and onset mixture properties in terms of RI. RI is useful because differences in RI are related to the magnitude of van der Waals forces between non-polar species. Empirical observations with paraffinic precipitants of varying carbon chain length and molar volume have led to a correlation that can be used to predict the onset of asphaltene flocculation for a wide range of conditions from a minimal number of measurements at ambient conditions.

There are many variables involved in COBR interactions including oil composition, surface properties, and composition of the aqueous phase. Tests with quartz glass require extensive soaking of the substrate to develop a constant surface charge. Aging in oil at an elevated temperature is often needed to produce significant differences in wetting alteration for

different oils and different conditions, but oils contain components that can go through phase changes as a function of temperature. Waxes that are dissolved in oil at the aging temperature may be solid at the ambient conditions where the results of oil exposure are evaluated. Using mica as a model substrate for standard tests reduces uncertainty due to surface roughness or contamination that may be unavoidable if surfaces must be reused. Muscovite mica has a structural charge that is well characterized and reproducible. Using mica as a standard substrate in tests at a single temperature has been shown to help reduce the level of uncertainty in wettability alteration studies. Other improvements in surface wettability evaluation—such as centrifugal displacement of bulk water—have also been documented in this study.

Having succeeded in quantifying asphaltene stability, tests of the proposed surface precipitation mechanism could be designed, confirming that for 3 of 5 oils tested there is a significant increase in oil-wet character on mica surfaces aged in oil mixtures near the onset of asphaltene instability. In one case, contact angles were high for all mixtures tested. Only one oil failed to show significant wetting alteration from near-onset mixtures of oil and heptane. The qualitative effect of surface precipitation on displacement in a glass micromodel was demonstrated by comparing two tests with one oil diluted with toluene to produce weakly water-wet conditions and with heptane to near the onset of asphaltene flocculation, producing more oil-wet conditions.

Probes of oil-treated mica surfaces by FTIR revealed the presence of organic material, but interferences and small signal-to-noise ratio prevented differentiation between the material on the surface and that in bulk oil. The technique may be most useful in probing the amount of water that remains adsorbed on the surface after exposure to oil.

Inspection of literature data for the two most popular methods of quantifying wetting in porous media, the Amott and USBM methods, showed that if different samples were used, the results from the two techniques were almost uncorrelated. Better correspondence between the two indices was found for samples tested by the combined Amott-USBM technique in which both are measured for a single core in a sequence of displacements. Analytical and pore network models of mixed-wet media show that the two indices should be correlated and, except at the end points, should be numerically similar in value if the more water-wet and more oil-wet surfaces are randomly distributed (i.e., fractional wetting). Mixed-wet conditions in which either the larger or smaller pores are preferentially the more oil-wet should produce an offset between the two indices that is indicative of the wetting distribution.

Finally, the implications of wetting alteration for oil recovery have been considered. Unlike water-wet rocks, there appears to be a change in relative permeability as a function of flow velocity in the mixed-wet porous media in which wetting was altered by exposure to crude oil. Based on our understanding of wettability alteration mechanisms, changes in wetting that can occur during the producing life of a reservoir have also been considered.

REFERENCES

Abrams, A.: "The Influence of Fluid Viscosity, Interfacial Tension, and Flow Velocity on Residual Oil Saturation Left by Waterflood," SPEJ, 437, Oct., 1975.

Ahmed, N. and Sunada, D.K.: "Nonlinear Flow in Porous Media," J. Hydraul. Div. (1969) 95, 1847.

Al-Maamari, R.S.H.: "Effect of Asphaltene Destabilization on Wettability," PhD Thesis, New Mexico Institute of Mining and Technology, Socorro, New Mexico (May 2000).

Al-Maamari, R.S.H. and Buckley, J.S.: "Asphaltene Precipitation and Alteration of Wetting: Can Wettability Change During Oil Production?" paper SPE 59292 presented at the 2000 SPE/DOE IOR Symposium, Tulsa, April 3-5.

Akhlaq, M.S., Kessel, D., and Dornow, W.: "Separation and Chemical Characterization of Wetting Crude Oil Compounds," *J. Colloid Interface Sci.* (1996) **180**, 309-314.

Amott, E.: "Observations Relating to the Wettability of Porous Rock," *Trans.*, AIME (1959) **216**, 156-162.

Andersen, S.I.: "Flocculation Onset Titration of Petroleum Asphaltenes," *Energy & Fuels* (1999) **13**, 315-322.

Andersen, S.I., private communication, 2001.

Anderson, W.G.: "Wettability Literature Survey—Part 2: Wettability Measurement," *JPT* (Nov. 1986) **38**, No. 12, 1246-1262.

Anderson, W.G.: "Wettability Literature Survey-Part 5: The Effects of Wettability on Relative Permeability," 1453-1468, JPT, Nov., 1987.

ASTM Standard Test Method D 664-89: " Standard Test Method for Acid Number of Petroleum Products by Potentiometric Titration." Annual Book of ASTM Standards, Sect. 5, Am. Soc. Testing Materials, Philadelphia, (1989), p. 236-242.

ASTM D1744-83: "Standard Test Method for Water in Liquid Petroleum Products by Karl Fischer Reagent," *ASTM* (1983).

ASTM D2007-80: "Standard Test Method for Characteristic Groups in Rubber Extender and Processing Oils by the Clay-Gel Adsorption Chromatographic Method," *ASTM* (1980).

ASTM Standard Test Method D 2896-88: "Standard Test Method for Base Number of Petroleum Products by Potentiometric Perchloric Acid Titration." Annual Book of ASTM Standards, Sect. 5, Am. Soc. Testing Materials, Philadelphia, (1988), p. 542-547.

Barak, A.Z.: "Comments on 'High Velocity Flow in Porous Media' by Hassanizadeh and Gray," Transport in Porous Media, 2, 533, 1987.

Barton, Allan F. M.: *CRC Handbook of Solubility Parameters and Other Cohesion Parameters*, 2nd ed. CRC Press, Boca Raton (1991).

Basu. S. and Sharma, M.M.: "Measurement of Critical Disjoining Pressure for Dewetting of Solid Surfaces," *J. Colloid. Interface Sci.* (1996) **181**, 443-455.

Basu, S. and Sharma, M.M.: "Characterization of Mixed-Wettability States in Oil Reservoirs by Atomic Force Microscopy," *SPEJ* (Dec. 1997) **2**, 527-435.

Bichard, J.A.: "Oil Solubility," presented at the 19th Canadian Chem. Engr. Conf. and 3rd Symp. on Catalysts, Edmonton, Alberta, Oct. 19-22, 1969.

Blunt, M.J., "Effects of Heterogeneity and Wetting on Relative Permeability Using Pore Level Modelling", SPEJ, **2**(1), 70 (1997).

Boneau, D.F. and Clampitt, R.L., "A Surfactant System for the Oil-Wet Sandstone of the North Burbank Unit", JPT, May, 501 (1977).

Brady, P.V. and House, W.A.: "Surface-Controlled Dissolution and Growth of Minerals," in *Physics and Chemistry of Mineral Surfaces*, P.V. Brady, Ed. CRC Press (1996) 225-305.

Buckley, J.S.: "Multiphase Displacements in Micromodels," *Interfacial Phenomena in Oil Recovery*, N.R. Morrow, ed., Marcel Dekker, Inc., New York City (1991), 157-189.

Buckley, J.S.: "Microscopic Investigation of the Onset of Asphaltene Precipitation," *Fuel Sci. & Tech. Internat.*(1996a) **14**, 55-74.

Buckley, J.S.: "Mechanisms and Consequences of Wettability Alteration by Crude Oils," PhD Thesis, Heriot-Watt University, Edinburgh, Scotland (1996b).

Buckley, J.S.: "Wetting Alteration of Solid Surfaces by Crude Oils and Their Asphaltenes," Revue de l'Institut Français du Pétrole (1998) **53**, No. 3, 303-312.

Buckley, J.S. and Morrow, N.R.: "Characterization of Crude Oil Wetting Behavior by Adhesion Tests," paper SPE/DOE 20263 presented at the 1990 SPE/DOE EOR Symposium, Tulsa, April 23-25.

Buckley, J.S. and Morrow, N.R.: "An Overview of Crude Oil Adhesion Phenomena," in *Physical Chemistry of Colloids and Interfaces in Oil Production*, H. Toulhoat and J. Lecourtier, eds., Éditions Technip, Paris, 1992, 39-45.

Buckley, J.S., Bousseau, C., and Liu, Y.: "Wetting Alteration by Brine and Crude Oil: From Contact Angles to Cores," *SPEJ* (Sept. 1996) **1**, No. 3, 341-350.

Buckley, J.S., Hirasaki, G.J., Liu, Y., Von Drasek, S., Wang, J.X., and Gill, B.S.: "Asphaltene Precipitation and Solvent Properties of Crude Oils," *Petroleum Science and Technology* (1998a) **16**, No. 3&4, 251-285.

Buckley, J.S., Liu, Y., and Monsterleet, S.: "Mechanisms of Wetting Alteration by Crude Oils," *SPEJ* (Mar. 1998b) **3**, 54-61.

Buckley, J.S., Liu, Y., Xie, X., and Morrow, N.R.: "Asphaltenes and Crude Oil Wetting—The Effect of Oil Composition," *SPEJ* (June, 1997) 107-119.

Buckley, J.S., Takamura, K., and Morrow, N.R.: "Influence of Electrical Surface Charges on the Wetting Properties of Crude Oils," *SPEFE* (August 1989) 332-340.

Buckley, S.E., and Leverett, M.C.: "Mechanism of Fluid Displacement in Sands," Trans. AIME, 146, 107, 1942.

Burke, N.E., Hobbs, R.D., and Kashou, S.F.: "Measurement and Modeling of Asphaltene Precipitation," *JPT* (1990) 1440-1446.

Caudle, B.H., Slobod, R.L., and Brownscombe, E.R.: "Futher Developments in the Laboratory Determination of Relative Permeability," Trans. AIME, 192, 145, 1951.

Chatzis, I. and Morrow, N.R.: "Correlation of Capillary Number Relationships for Sandstone," SPEJ, 555-562, October, 1984.

Chavent, G., Cohen, G., Arlabosse, M., and Espy, M.: "Determination of Relative Permeabilities and Capillary Pressures by an Automatic Adjustment Method," paper SPE 9237, presented at SPE annual meeting hold in Dallas, Sept. 21-24, 1980.

Christenson, H.K. and Israelachvili, J.N.: "Direct Measurements of Interactions and Viscosity of Crude Oils in Thin Films between Model Clay Surfaces," *J. Colloid Interface Sci.* (1987) **119**, 194.

Cimino, R., Correra, S., Del Bianco, A., and Lockhart, T.P.: "Solubility and Phase Behavior of Asphaltenes in Hydrocarbon Media," *Asphaltenes: Fundamentals and Applications*, E.Y. Sheu and O.C. Mullins (eds.), NY: Plenum Press (1995) 97-130.

Clementz, D.M.: "Interaction of Petroleum Heavy Ends with Montmorillonite," *Clays and Clay Minerals* (1976) **24** 312-319.

Clementz, D.M.: "Alteration of Rock Properties by Adsorption of Petroleum Heavy Ends: Implications for Enhanced Oil Recovery," paper SPE/DOE 10683 presented at the 1982 SPE/DOE Joint Symp. on EOR, Tulsa, Apr 4-7.

Collins, R.E.: *Flow of Fluids Through Porous Materials*, 1st edition: Reinhold Publishing Corporation, New York, 1961, 2nd reprint: Research & Engineering Consultants, Inc., Englewood, Colorado, 1990, pp143-153.

Collins, S.H. and Melrose, J.C.: "Adsorption of Asphaltenes and Water on Reservoir Rock Minerals," paper SPE 11800 presented at the 1983 International Symposium on Oilfield and Geothermal Chemistry, Denver, June 1-3.

Cornell, D. and Katz, D.L.: "Flow of Gases Through Consolidated Porous Media," Ind. & Eng. Chem. (Oct., 1953) 45, 2145.

Craig, F.F.: *The Reservoir Engineering Aspects of Waterflooding*, Monograph Series, SPE, Richardson, TX (1971) 3.

Crocker, M.E.: "Wettability", Enhanced Oil Recovery, Progress Review for the Quarter Ending Sept. 30, DOE/BC-86/3, **47**, 100 (1986).

Cuiec, L.: "Restoration of the Natural State of Core Samples," paper SPE 5634 presented at the 1975 ATCE, Dallas, Sept. 28 - Oct. 1.

Cuiec, L.: "Wettability and Rock/Crude-Oil Component Interactions," paper presented at the 21st Intersociety Energy Conversion Engineering Conference, San Diego, Aug. 25-29, 1986.

Cuiec, L.: "Evaluation of Reservoir Wettability and Its Effects on Oil Recovery," in *Interfacial Phenomena in Oil Recovery*, N.R. Morrow, ed., Marcel Dekker, Inc., New York City (1991), 319-375.

Czarnecka, E. and Gillott, J.E.: "Formation and Characterization of Clay Complexes with Bitumen from Athabasca Oil Sand," *Clay and Clay Minerals* (1980) **28**, No. 3, 197-203.

Denekas, M.O., Mattax, C.C., and Davis, G.T.: "Effect of Crude Oil Components on Rock Wettability," *Trans.*, AIME (1959) **216**, 330-333.

Dixit, A.B., Buckley, J.S., McDougall, S.R., and Sorbie, K.S.: "Empirical Measures of Wettability in Porous Media and the Relationship between Them Derived From Pore-Scale Modelling," *Transport in Porous Media* (2000) **40**, 27-54.Donaldson, E.C., Thomas, R.D., and Lorenz, P.B.: "Wettability Determination and Its Effect on Recovery Efficiency", SPEJ, 13 (Mar., 1969) 13-20.

Dixit, A.B., McDougall, S.R. and Sorbie, K.S.: " A Pore Level Investigation of Relative Permeability Hysteresis in Water-wet Systems", paper SPE 37233 presented at SPE Oilfield Chemistry Symposium, Houston, Feb. 18-21 (1997).

Dixit, A.B., McDougall, S.R. and Sorbie, K.S.: " Analysis of Relative Permeability Hysteresis Trends in Mixed-wet Porous Media Using Network Models", SPE/DOE 39656, to appear at the SPE/DOE Eleventh Symposium on Improved Oil Recovery, Tulsa, April 19-22 (1998).

Dixit, A.B., McDougall, S.R., Sorbie, K.S. and Buckley, J.S. : "Pore Scale Modelling of Wettability Effects and Their Influence on Oil Recovery", paper SPE 35451 presented at SPE/DOE Tenth Symposium on Improved Oil Recovery, Tulsa, April 21-24 (1996).

Dong, M.: "A Study of Film Transport in Capillaries with an Angular Cross-Section," PhD Thesis, University of Waterloo, 1995.

Douglas, J., Jr., Blair, P.M., and Wagner, R.J.: "Calculation of Linear Waterflood Behavior Including the Effects of Capillary Pressure," Trans. AIME, 215, 96, 1958.

Dubey, S. T., Doe, P. H.: "Base Number and Wetting Properties of Crude Oils." SPE Reservoir Engineering (August, 1993), p. 195-200.

Dubey, S.T. and Waxman, M.H.: "Asphaltene Adsorption and Desorption from Mineral Surfaces," *SPERE* (Aug. 1991) 389-395.

Ducker, W.A., Xu, Z., and Issraelachvili, J.N.: "Measurements of Hydrophobic and DLVO Forces in Bubble-Surface Interactions in Aqueous Solutions," *Langmuir* (1994) **10**, 3279-3289.

Durand, C., and Beccat, P.: "Use Of XPS For Reservoir Sandstone Wettability Evaluation. Application To Kaolinite And Illite." *4th International Symposium on Wettability*, Montpellier, France, Sept.11-13, 1997.

Fancher, G.H. and Lewis, J.A.: "Flow of Simple Fluids Through Porous Materials," Ind. & Eng. Chem. (Oct., 1933) 25, No. 10, 1139.

Feynman, R.P., Leighton, R.B., and Sands, M.: *The Feynman Lectures on Physics*, Vol. II (1989) Addison-Wesley Publishing Co.

Firoozabadi, A., Thomas, L.K., and Todd, B.: "High-Velocity Flow in Porous Media," SPERE, pp.149-152, May, 1995.

Forchheimer, P.H.: "Wasserbewegung durch Boden," Zeitz. ver. Deutsch Ing. (1901) 45, 1781.

Funk, J.J., Dahlstrom, P.L., Haltmar, W.C., and Perdue, J.M.: "Techniques for observing oil-wetting of carbonate surfaces using FT-IR." SCA-9512, Proceedings of the 1995 SCA International Symposium, San Francisco, Sept. 12-14, 1995.

Gardner, J.W., Orr, F.M., and Patel, P.D.: "The Effect of Phase Behavior on CO_2-Flood Displacement Efficiency," *JPT* (1981) 2067-2081.

Gauchet, R.: "Waterfloodings on Intermediate Wet Porous Media: New Considerations on Two Phase Flow Proerties Determination," *Adv. in Core Evaluation, Reservoir Management*, Proc. Eurocas III, Gordon and Breach Science Publ. (1993) 251-273.

Gauchet, R., Chenevier, P., and Tricart, J.-P.: "Visualization of Rock Samples in Their Natural State Using Environmental Scanning Electron Microscope," paper SPE 26620 presented at the 1993 ATCE, Houston, October 3-6.

Green, L., and Duwez, P.: "Fluid Flow Through Porous Materials," J. Applied Mech., 18, 39, March, 1951.

Harrick, N. J. (1967). *Internal Reflection Spectroscopy*. New York: Interscience Publishers.

Hassanizadeh, S.M., and Gray, W.G.: "High Velocity Flow in Porous Media," Transport in Porous Media, 2, 521, 1987.

Hassler, G.L., Rice, R.R., and Leeman, E.H.: "Investigations of Recovery on the Oil from Sandstones by Gas-drive," Trans. AIME, 118, 116, 1936.

Heaviside, J., Brown, C.E., and Gamble, I.J.A.: "Relative Permeability for Intermediate Wettability Reservoirs," paper SPE 16968 presented at the SPE Annual Meeting, Dallas, Texas, Sept. 27-30, 1987.

Heithaus, J.J.: "Measurement and Significance of Asphaltene Peptization," *J. Institute of Petroleum* (Feb. 1962) **48** No. 458, 45.

Henderson, J.H. and Yuster, S.T.: "Relative Permeability Study," World Oil, 3, 139, 1948.

Herron, M.M., Matteson, A., and Gustavson, G.: "Dual-Range FT-IR Mineralogy and the Analysis of Sedimentary Formations," paper SCA 9730 presented at the 1997 Int. Symp., Calgary, 7-10 Sept.

Hildebrand, J.H. and Scott, R.L.: *The Solubility of Nonelectrolytes*, (1964) Dover Publications, Inc.

Hirasaki, G.J.: "Structural Interactions in the Wetting and Spreading of van der Waals Fluids," in *Contact Angle, Wettability and Adhesion*, Mittal, K.L. (ed.) VSP, Utrecht, 1993.

Hirasaki, G.J., Rohan, J.A., Dubey, S.T., and Niko, H.: "Wettability Evaluation during Restored State Core Analysis", paper SPE 20506 presented at the Annual Technical Conference and Exhibition of SPE, New Orleans, Sept. 23-26 (1990).

Hirschberg, A., deJong, L.N.J., Schipper, B.A., and Meijer, J.G.: "Influence of Temperature and Pressure on Asphaltene Flocculation," *SPEJ* (June 1984) 283-293.

Hotier, G. and Robin, M.: "Effects of Different Diluents on Heavy Oil Products: Measurement, Interpretation, and a Forecast of Asphaltene Flocculation," *Revue de l'IFP* (1983) **38**, 101.

Hough, D.B. and White, L.R.: "The Calculation of Hamaker Constants from Lifshitz Theory with Applications to Wetting Phenomena," *Advances in Colloid and Interface Science*, **14** (1980) 3-41.

Hurst, A.: "Problems of Reservoir Characterization in Some North Sea Sandstone Reservoirs Solved by the Application of Microscale Geological Data," *North Sea Oil & Gas Reservoirs*, Trondheim (Dec. 2-4, 1985), Graham & Trotman, Ltd., London (1987), 153-167.

Israelachvili, J.N.: *Intermolecular and Surface Forces*, 2nd Ed., Academic Press, San Diego (1991).

Jadhunandan, P.P.: "Effects of Brine Composition, Crude Oil, and Aging Conditions on Wettability and Oil Recovery," PhD dissertation, New Mexico Institute of Mining and Technology, Socorro, NM (1990).

Jadhunandan, P. and Morrow, N.R.: "Spontaneous Imbibition of Water by Crude Oil/Brine/Rock Systems," *In Situ* (1991) **15**, No. 4, 319-345.

Jadhunandan, P. and Morrow, N.R.: "Effect of Wettability on Waterflood Recovery for Crude Oil/Brine/Rock Systems," *SPERE* (1995) **10**, No. 1, 40-46.

Johnson, E.F., Bossler, D.P., and Naumann, V.O.: "Calculation of Relative Permeability from Displacement Experiments," Trans. AIME, 216, 370, 1959.

Jones, S.C. and Roszelle, W.O.: "Graphical Techniques for Determining Relative Permeability from Displacement Experiments," Trans. AIME, pp. 807-817, 265, 1978.

Kovscek, A.R., Wong, H., and Radke, C.J.: "A Pore-Level Scenario for the Development of Mixed Wettability in Oil Reservoirs," *AIChE J.* (June 1993) **39**, No. 6, 1072-1085.

Kyte, J.R., Rapoport, L.A.: "Linear Waterflood Behavior and End Effects in Water-wet Porous Media," Trans. AIME, 213, 423, 1958.

Labastie, A., Guy, M., Delclaud, J.P., and Iffly, R.: "Effect of Flow Rate and Wettability on Water-oil Relative Permeabilities and Capillary Pressure," paper SPE 9236 presented at the SPE Annual Meeting, Dallas, Texas, Sept. 21-24, 1980.

Lauridsen, R.: "Changes in Asphaltene Stability during Hydrotreating," MS thesis, Technical University of Denmark, 1999.

Leas, W.J., Jenks, L.H., and Russell, C.D.: "Relative Permeability to Gas," Trans. AIME, 189, 65, 1950.

Lefebvre du Prey, E.J.: "Factors Affecting Liquid-liquid Relative Permeabilities of a Consolidated Porous Medium," Soc. Pet. Eng. J., 2, 39, 1973.

Lenormand, R., Zarcone, C., and Sarr, A.: "Mechanisms of the Displacement of One Fluid by Another in a Network of Capillary Ducts," *J. Fluid Mech.* (1983) **135**, 337-353.

Leon, V., Toledo, P. G., and Araujo, Y. C.: "ISS Assessment of The Influence of Nonpore Surface in the XPS Analysis of Oil-Producing Reservoir Rocks." *Journal of Colloid and Interface Science* (1997) **192**, 281-285.

Leontaritis, K.J. and Mansoori, G.A.: "Asphaltene Flocculation During Oil Production and Processing: A Thermodynamic-Colloidal Model," paper SPE 16258 presented at the 1987 SPE International Symposium on Oilfield Chemistry, San Antonio, 4-6 Feb.

Leverett, M.C.: "Flow of Oil-water Mixtures through Unconsolidated Sands," Trans. AIME, 132, 149, 1939.

Leverett, M.C., and Lewis, W.B.: "Steady Flow of Gas-oil-water Mixtures through Unconsolidated Sands," Trans. AIME, 142, 107, 1941.

Liu, L. and Buckley, J.S.: "Alteration of Wetting of Mica Surfaces," *J. Pet. Sci. Eng.* (1999) **24**, 75-83.

Liu, Y.: "Wetting Alteration by Adsorption from Crude Oils," MS Thesis, New Mexico Institute of Mining and Technology, Socorro, NM (1993).

Liu, Y. and Buckley, J.S.: "Evolution of Wetting Alteration by Adsorption from Crude Oil," *SPEFE* (Mar. 1997) 5-11.

Liu, Y., Xie, X., Buckley, J.S., and Morrow, N.R.: "Static and Dynamic Measurements of Contact Angles on Crude Oil-Treated Surfaces," PRRC 96-04.

Longeron, D., Hammervold, W.L., and Skjaeveland, S.M. : "Water-Oil Capillary Pressure and Wettability Measurements Using Micropore Membrane Technique", paper SCA-9426, Proc. SCA International Symposium, Stavanger, Norway, Sept. 12-14, 285 (1994).

Ma, S.: *Effect of Firing on Petrophysical Properties of Berea Sandstone*, Master's Thesis, New Mexico Tect., Nov., 1988.

Ma, S., Mason, G., and Morrow, N.R.: "Effect of contact angle on drainage and imbibition in regular polygonal tubes," *Colloids and Surfaces A* (1996) **117**, 273-291.

Ma, S., Zhang, X., and Morrow, N.R.: "Influence of Fluid Viscosity on Mass Transfer between Fractures and Matrix," paper CIM 95-94, Petr. Soc. Of CIM Ann. Tech. Meeting, Banff, Alberta, May 14-17, 1995

MacMillan, D.J., Tackett, J.E., Jr., Jessee, M.A., and Monger-McClure, T.G.: "A Unified Approach to Asphaltene Precipitation: Laboratory Measurement and Modeling," paper SPE 28990 presented at the 1995 SPE International Symposium on Oilfield Chemistry, San Antonio, 14-17 Feb.

Martin F.D., Buckley, J.S., Weiss, W.W., and Ouenes, A.: *Integration of Advanced Geoscience and Engineering Techniques to Quantify Interwell Heterogeneity in Reservoir Models*, Second annual report, Oct., 1995, PRRC 95-35, New Mexico Tech.

Mason, G., Nguyen, M.D., and Morrow, N.: "Effect of Contact Angle on the Meniscus Between Two Equal Contacting Rods and a Plate," *J. Colloid Interface Sci.* (1983) **95**, No. 2, 494-501.

Mason, G. and Morrow, N.R.: "Effect of Contact Angle on Capillary Displacement Curvatures in Pore Throats Formed by Spheres," *J. Colloid Interface Sci.* (1984) **168**, No. 1, 130-141.

Mason, G. and Morrow, N.R.: "Capillary Behavior of a Perfectly Wetting Liquid in Irregular Triangular Tubes," *J. Colloid Interface Sci.* (1991) **141**, No. 1, 262-274.

Mayer, R.P. and Stowe, R.A.: "Mercury Porosimetry—Breakthrough Pressure for Penetration Between Packed Spheres," *J. Coll. Interface Sci.* (1965) **20**, 893-911.

McKay, J.F., Amend, P.J., Cogswell, T.E., Harnsberger, P.M., Erickson, R.B., and Latham, D.R.: "Petroleum Asphaltenes: Chemistry and Composition," in *Analytical Chemistry of Liquid Fuel Sources*, P.C. Uden, S. Siggia, and H.B. Jensen (eds.), Advances in Chemistry Series, ACS, Washington, D.C. (1978) **170**, 128-142.

McKellar, M. and Wardlaw, N.C.: "A Method of Making Two-Dimensional Glass Micromodels of Pore Systems," *J. Cdn. Pet. Tech.* (July-Aug 1982) 39-41.

McLean, J. D., and Kilpatrick, P. K.: "Comparison Of Precipitation and Extrography in the Fractionation of Crude Oil Residua," *Energy & Fuels*, (1997) **11**, 570-585.

Mennella, A., Morrow, N.R., and Xie, X.: "Application of the Dynamic Wilhelmy Plate to Identification of Slippage at a Liquid-Liquid-Solid Three-Phase Line of Contact," *J. Pet. Sci. Eng.* (1995) **13**, 179-192.

Mohanty, K.K. and Salter, S.J.: "Multiphase Flow in Porous Media: III. Oil Mobilization, Transverse Dispersion, and Wettability," SPE 12127, presented at the 58th Annual Technical Conference of the SPE, San Francisco, California, Oct. 5-8, 1983.

Morrow, N.R.: "Wettability and Its Effect on Oil Recovery," *JPT* (Dec. 1990) 1476-1484.

Morrow, N.R. and McCaffery, F.G.: "Fluid Displacement Studies in Uniformly Wetted Porous Media," in *Wetting, Spreading and Adhesion*, J.R. Padday, ed., New York: Academic Press (1978) 289-319.

Morrow, N.R., Chatzis, I., and Lim, H.T.: "Relative Permeabilities at Reduced Residual Saturations," paper 83-34-28 presented at the 1983 Annual Technical Meeting, Banff, Alta., Canada, May 10-13.

Morrow, N.R., Lim, H.T., and Ward, J.S.: "Effect of Crude-Oil-Induced Wettability Changes on Oil Recovery," *SPEFE* (Feb. 1986) 89-103.

Morrow, N.R., Ma, S., Zhou, X., and Zhang, X.: "Characterization of Wettability from Spontaneous Imbibition Measurements," paper CIM 94-47 presented at the 1994 Petr. Soc. of CIM Ann. Tech. Meeting and AOSTRA 1994 Ann. Tech. Conf., Calgary, June 12-15.

Morse, R.A., Terwilliger, P.K., and Yuster, S.T.: "Relative Permeability Measurements on Small Core Samples," Oil Gas J., 46, 109, 1947.

Moschopedis, D., and Speight, J. G.: "Oxygen Functions in Asphaltenes," *Fuel*, (1976) **55**, 187-192.

Odeh, A.S., and Dotson, B.J.: "A Method for Reducing the Rate Effect on Oil and Water Relative Permeabilities Calculated from Dynamic Displacement Data," paper SPE 14417, presented at the 1985 Annual Technical Meeting, Las Vegas, Sept. 22-25, 1985

Osoba, J.S., Richardson, J.G., Kerver, J.K., Hafford, J.A., and Blair, P.M.: "Laboratory Measurements of Relative Permeability," Trans. AIME, 192, 47, 1951.

Pan, H. and Firoozabadi, A.: "A Thermodynamic Micellization Model for Asphaltene Precipitation: Part I: Micellar Size and Growth," paper SPE 36741 presented at the 1996 ATCE, Denver, 6-9 Oct.

Parkash, S., Moschopedis, S., and Speight, J.: "Physical Properties and Surface Characteristics of Asphaltenes," *Fuel* (1979) **58**, 877-882.

Peck, A.S., Raby, L.H., and Wadsworth, M.E.: "An Infrared Study of the Flotation of Hematite with Oleic Acid and Sodium Oleate," Soc. Mining Eng. Trans. (Sept. 1966) 301-307.

Pirson, S.J.: *Oil Reservoir Engineering*, Ed., McGraw-Hill, New York, 1958, 68.

Princen, H.M.: "Capillary Phenomena in Assemblies of Parallel Cylinders. I. Capillary Rise between Two Cylinders," *J. Coll. Interface Sci.* (1969) **30**, 69-75.

Ransohoff, R.C. and Radke, C.J.: "Laminar Flow of a Wetting Liquid Along the Corners of a Predominantly Gas-Occupied Noncircular Pore," *J. Coll. Interface Sci.* (1988) **121**, 392-401.

Rapoport, L.A. and Leas, W.J.: "Properties of Linear Waterflood," Trans. AIME, 198, 1953, pp. 139-148.

Rassamdana, H., Dabir, B., Nematry, M., Farhani, M., and Sahimi, M.: "Asphalt Flocculation and Deposition: I. The Onset of Precipitation," *AIChE Journal* (Jan. 1996) **42**, 10.

Reichert, C., Fuhr, B.J., and Klein, L.L.: "Measurement of Asphaltene Flocculation in Bitumen Solutions," *J. Cnd. Pet. Tech.* (Sept.-Oct. 1986) 33-37.

Richardson, J.G., Kerver, J.K., Hafford, J.A., and Osoba, J.S.: "Laboratory Determinations of Relative Permeability," Trans. AIME, 195, 187, 1952.

Robin, M., Combes, R., and Rosenberg, E.: "Cryo-SEM and ESEM: New Techniques to Investigate Phase Interactions within Reservoir Rocks," paper SPE 56829 presented at the 1999 ATCE, Houston, Oct. 3-6.

Roof, J.G.: "Snap-Off of Oil Droplets in Water-Wet Pores," *SPEJ* (March 1970) 85-90, *Trans.*, AIME, 249.

Salathiel, R.A.: "Oil Recovery by Surface Film Drainage in Mixed-Wettability Rocks," *J. Pet. Tech.* (Oct. 1973) 1216-24; *Trans.*, AIME, **255**.

Sandberg, C.R., Gourney, L.S., Suppel, R.F.: "Effect of Fluid Flow Rate and Viscosity on Laboratory Determination of Oil-water Relative Permeabilities," Trans. AIME, 213, 36, 1958.

Sharma, M.M. and Wunderlich, R.W.: "The Alteration of Rock Properties Due to Interactions with Drilling Fluid Components", SPE 14302, presented at the Annual Technical Conference and Exhibition of SPE, Las Vegas, Sept. 22-25 (1985).

Sheth, S. R., and Leckband, D. E.: "Direct Force Measurements of Polymerization-Dependent Changes in the Properties of Diacetylene Films," *Langmuir,* (1997) **13**, 5652-5662.

STRAPP, version 1.0, distributed by NIST, Gaithersberg MD 20899 (1990).

Victorov, A.I. and Firoozabadi, A.: "Thermodynamics of Asphaltene Precipitation in Petroleum Fluids by a Micellization Model," *AIChE J.* (1996) **42**,1753.

Taber, J.J.: "Research on Enhanced Oil Recovery: Past, Present and Future," Pure & Appl. Chem., Vol.52, pp. 1323-1347, 1980.

Tang, G.Q. and Morrow, N.R.: "Effect of Temperature, Salinity and Oil Composition on Wetting Behavior and Oil Recovery by Waterflooding," paper SPE 36680 presented at the 1996 ATCE, Denver, 6-9 Oct.

Temeng, K.O.: *Effects of High Pressure Gradients on the Flow of Real Gases Through Porous Media*, PhD dissertation, Stanford U., Stanford, CA, 1989.

Torsæter, O. :"A Comparitive Study of Wettability Test Methods Based on Experimental Results from North Sea Reservoir Rocks", paper SPE 18281 presented at the 63rd Ann. Tech. Conf. and Exhib., Houston, Oct. 2-5 (1988).

Vedam, K. and Limsuwan, P.: "Piezo- and Elasto-optic Properties of Liquids under High Pressure. II Refractive Index vs. Density," *J. Chem. Phys.* (1978) **69** (11), 4772-4778.

Vizika, O. and Duouerroix, J.-P.: "Gas Injection and Heterogeneous Wettability: What Is the Relevant Information That Petrophysics Can Provide," paper SCA-9708 presented at the 1997 International Symposium, Calgary, Sept. 7-10.

Von Drasek, S.M.: "ATR-FTIR Analysis of Adsorption from Crude Oil onto Mineral Surfaces," MS Thesis, New Mexico Institute of Mining and Technology, Socorro, NM (1999).

Walsh, T.J.: "Capillary Properties of Model Pores," PhD Dissertation, Loughborough University of Technology, 1989.

Wang, J.X.: "Effect of Wettability on Rate-dependence of Relative Permeability End-points," MS Thesis, NMIMT, Socorro, April, 1998.

Wang, J.X.: "Prediction of Asphaltene Flocculation in Crude Oils," Ph.D. Thesis, New Mexico Institute of Mining & Technology, Socorro, New Mexico, USA, April 2000.

Wang, J.X. and Buckley, J.S.: "An Experimental Approach to Prediction of Asphaltene Flocculation," paper SPE 64994, to be presented at the 2001 SPE International Symposium on Oilfield Chemistry held in Houston, Texas, 13-16 Feb., 2001.

Wang, J.X., Brower, K.R., and Buckley, J.S.: "Observation of Asphaltene Destabilization at Elevated Temperature and Pressure," *SPEJ* **5**(4), December 2000.

Wardlaw, N.C.: "The effects of geometry, wettability, viscosity and interfacial tension on trapping in single pore-throat pairs," *J. Can. Pet. Tech.* (1982) 21-27.Washburn, E.W.: "The Dynamics of Capillary Flow," *Phys. Rev.* (1921) **17**, 274-5.

Weast, R.C.: *CRC Handbook of Chemistry and Physics*, 68th ed. (1987) CRC Press, Inc.

Welge, H.J.: "A Simplified Method for Computing Oil Recovery by Gas or Water Drive," Trans. AIME, 195, 91, 1952.

Wiehe, I.A.: "Two-Dimensional Solubility Parameter Mapping of Heavy Oils," *Fuel Sci. & Tech. Int.* (1996) **14**, 289-312.

Willard, H. H., Merritt, Jr., L. L., Dean, J. A., and Settle, Jr., F.A.: *Instrumental methods of analysis*. (7^{th} ed.). Belmont, CA,Wadsworth Publishing Company (1988).

Wu, Y.: "Crude Oil-Related Surface Wetting Study," Master's thesis, New Mexico Institute of Mining and Technology, Socorro, NM (1996).

Wyckoff, R.D., and Botset, H.G.: "Flow of Gas Liquid Mixtures through Sands," Physics, 7, 325, 1936.

Xie, X.: "Application of the Dynamic Wilhelmy Plate Technique to Investigation of Oil/Brine/Quartz Wetting Alteration by Adsorption from Crude Oil," PhD thesis, University of Wyoming, Laramie, WY (1996).

Xie, X., Morrow, N.R., and Buckley, J.S.: "Crude Oil/Brine Contact Angles on Quartz Glass," to be presented at the 1997 SCA Internat. Symp., Calgary, 11-13 Sept.

Yan, J., Menezes, J.L., and Sharma, M.M.: "Wettability Alteration Due to Interactions With Oil-Based Muds and Mud Components," *SPEDC* (Mar. 1993) 35.

Yan, J., Plancher, H., and Morrow, N.R.: "Wettability Changes Induced by Adsorption of Asphaltenes," *SPE PF* (Nov. 1997) 259-266.

Yang, S.-Y., Hirasaki, G.J., Basu, S., and Vaidya, R.: "Mechanisms for Contact Angle Hysteresis and Advancing Contact Angles," 5th International Symposium on Reservoir Wettability and Its Effect on Oil Recovery, Trondheim, 22-24 June, 1998.

Yildiz, H.Ö.: "Effect of Brine Composition on Oil Recovery by Waterflooding," Ph.D. Thesis, New Mexico Institute of Mining and Technolgy, Socorro, NM (1995).

Zhang, X., Morrow, N.R., and Ma, S.: "Experimental Verification of a Modified Scaling Group for Spontaneous Imbibition," paper SPE 30762 presented at the 1995 ATCE, Dallas, Oct. 22-25.

Zhou, X., Torsæter, O., Xie, X., and Morrow, N.R.: "The Effect of Crude-Oil Aging Time and Temperature on the Rate of Water Imbibition and Long-Term Recovery by Imbibition," *SPEFE* (Dec. 1995)259-265.

APPENDICES

Appendix I – Standard Asphaltene Onset Procedures at Ambient Conditions

Asphaltene stability is a function of composition, temperature and pressure. In the procedure outlined here, dead crude oil is titrated at ambient conditions with normal alkanes to find the first appearance of asphaltene aggregates. Microscopic aggregates are detected optically with transmitted light, setting an effective lower limit of about 0.5 μm on the size that can be reliably discerned. For some oils, the first appearance of aggregates is readily distinguished from clear solutions with only slightly less alkane precipitant. In other cases fine particles appear before aggregates are observed and it is more difficult to define an onset condition. In the latter case, two onset conditions can be defined: (1) the conditions where fine asphaltic particles first appear or *onset of fines*, and (2) the conditions where those particles first begin to aggregate or *onset of aggregates*. Between these conditions is a more or less continuous increase in the amount of particulate material.

The solubility conditions in the dead oil sample and at the onset are quantified by refractive index (RI) measured at 20°C at the wavelength of the sodium-D line (589 nm). Quantities of interest include RI of the dead oil sample (RI_{oil}) and RI of the mixture of oil and alkane at the onset of precipitation (P_{RI}). In effect, RI is a surrogate for the solubility parameter (δ), used because it can be readily measured whereas δ must be estimated for complex fluids like crude oils. For nonpolar liquids including crude oils, δ can be calculated from RI using an empirical correlation.

Interference is often encountered from asphaltene aggregates and other particulates and emulsified matter that are present in the dead oil samples, as received. Methods for dealing with samples that contain emulsions and/or particulates are included in this procedure.

Asphaltene flocculation can be a slow process, especially near the onset point. In most titration techniques the precipitant is added fairly quickly, which probably leads to an overestimate of the amount of precipitant at the onset point and a corresponding overestimate of asphaltene stability. Experience has shown that one day of aging is the minimum amount of time needed to make a reliable judgment about the onset; longer times would be better, but are seldom practical.

The overall asphaltene onset characterization scheme is outlined in Fig. AI-1 and discussed in detail in the sections that follow.

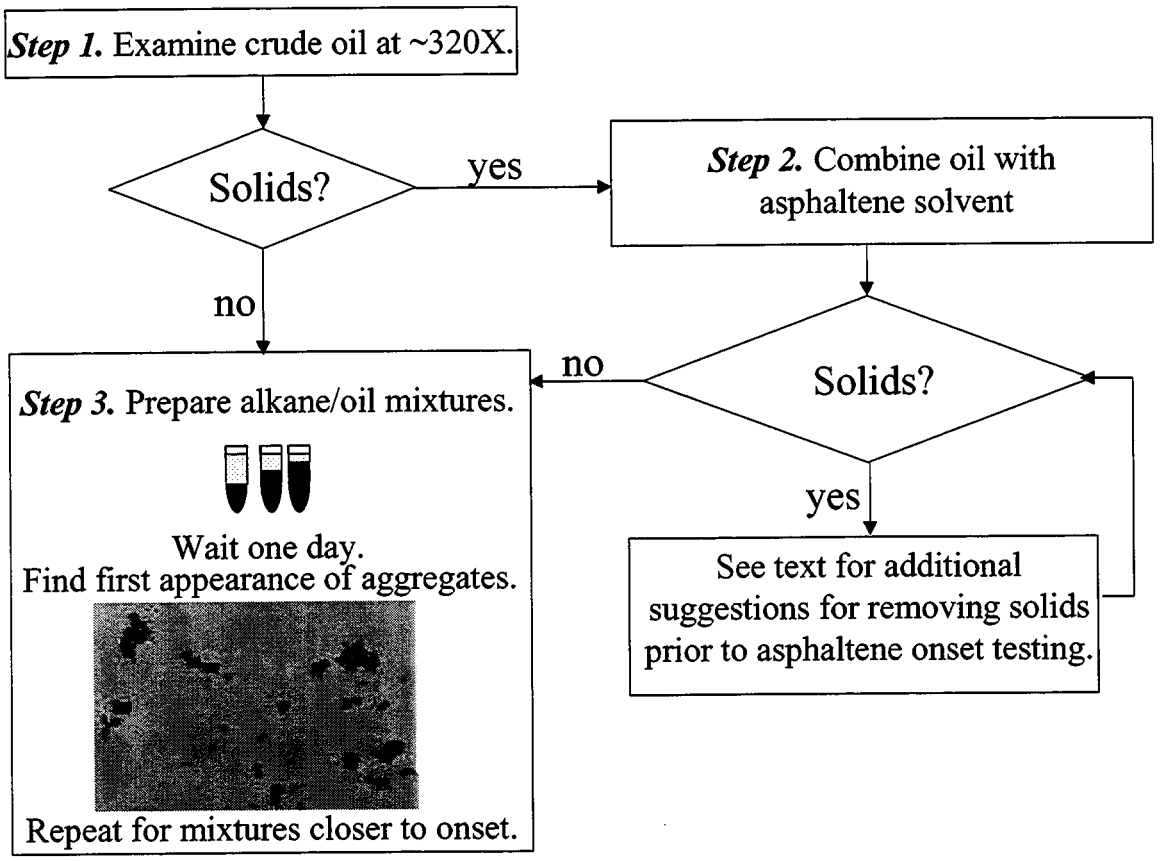

Figure AI-1. Outline of the asphaltene onset determination scheme.

Step 1. Microscopic examination

A drop of dead crude oil is placed on a microscope slide, covered with a cover slip, and observed microscopically at a magnification of about 320X. If the sample is clear and free from any particles, no special pretreatment is required. Skip Step 2 and proceed to Step 3.

Often crude oils contain aggregated asphaltenes, wax crystals, emulsified water, and other unidentified solid particles. The aggregated asphaltenes may appear as large aggregates, small aggregates, or individual fines or particles. Asphaltenes can often be observed adhering to one another. They can be distinguished from wax crystals by observing between polarizing filters oriented at 90° to one another. The crystalline waxes can pass polarized light and appear as bright spots whereas asphaltenes are amorphous and cannot be seen. Highly spherical objects are likely to be emulsified liquids. These oils cannot be used directly to find the onset point induced by adding n-alkanes since the existing aggregates or particles may obscure the onset observation. Strategies for removing sources of interference are outlined in Step 2.

Step 2. Redispersion of asphaltene aggregates

Asphaltene aggregates, waxes, and other particulates, could be removed mechanically by filtration or centrifugation. A better strategy, however, is to redisperse the asphaltene aggregates by addition of a good asphaltene solvent. This option is preferable because all the oil components are retained. Aromatic compounds, such as toluene or 1-MN (1-MN), are good asphaltene solvents. 1-MN is the stronger solvent, but it is also more viscous than toluene so the time required to disperse the asphaltenes is longer. The value of P_{RI} is shifted more by addition of toluene than by 1-MN. The value of P_{RI} obtained from a 50:50 mixture of oil mixed with 1-MN is normally only slightly different from the value of P_{RI} that would be measured for the crude oil without added solvent. If time and oil sample volume permit, however, a more

accurate value of P_{RI} can be obtained by testing two or more mixtures with different ratios of oil to 1-MN. P_{RI} can then be evaluated as a function of the amount of added solvent and extrapolated to the value of P_{RI} for oil with no added solvent.

For oil samples with asphaltene aggregates and/or other particulates or emulsions, the following steps are recommended:

2.1 Prepare a 1:1 mixture of oil with 1-MN. Stir the mixture for one to two days, checking for particles at ~320X. If no asphaltenes are visible proceed to Step 2.5.

2.2 If complete dispersion is not achieved, agitate the mixture in an ultrasonic water bath for several hours. If asphaltenes disappear, proceed to Step 2.5.

2.3 If asphaltene are still not completely dissolved, heat the mixtures to 60 to 70°C for several hours in sealed vials, taking care to prevent evaporation. If asphaltenes disappear, proceed to Step 2.5.

2.4 If none of these treatments redisperses the asphaltenes, add a known amount of 1-MN to the mixture to further reduce oil:1-MN volume ratio and repeat the sequence starting at 2.1 above.

2.5 If waxes remain after asphaltenes are completely redispersed, heat the solution as described at 2.3 above. Usually this will be sufficient to dissolve the waxes, which may reappear, but slowly so that they do not interfere with the onset tests. If there are no emulsions, proceed to Step 3.

2.6 Emulsified water may segregate from the oil and collect as a sediment on the bottom of the container during steps 2.1 to 2.5. If the sediment is gray or white in color, most asphaltenes that once may have collected at the oil/water interface have been redispersed. Proceed to Step 2.7. If the sediment is brown, some of the asphaltene fraction may

remain associated with the emulsion interfaces. Add a large volume of distilled water to the oil/1-MN mixture. Agitate in an ultrasonic water bath for about 30 minutes. This washing step should help to break the original emulsion, releasing the asphaltenes. The mixture can then be separated as described in Step 2.7.

2.7 If no emulsified droplets remain suspended, carefully separate the supernatant and proceed with Step 3. If emulsified droplets remain in suspension, centrifuge at 2000-3000 rpm for several hours in sealed centrifuge tubes. Separate the supernatant and proceed with Step 3. This step should also remove extraneous inorganic solids and extremely refractory organics (known as carbenes and carboids).

Step 3. Measure onset of asphaltene flocculation

The onset condition (or conditions—if both the *onset of fines* and *onset of aggregates* exist) can be determined to a reasonable tolerance by examination of mixtures of oil and precipitant that vary by 1% (by volume) in composition. If aggregates are observed in a mixture consisting of 50% oil (or oil/1-MN mixture) and 50% heptane, but a mixture with 51% oil and 49% heptane is clear, then the 50:50 mixture would be considered to be the onset mixture.

The onset search can be refined in a series of steps. If oil is the limiting factor, fewer mixtures would be included in each step and the number of steps would be increased. The extreme example would be a search by the bisection method beginning with a 50:50 mixture of oil and precipitant, followed by either a 25:75 or 75:25 mixture depending on whether asphaltenes were observed in the first mixture. If there is plenty of oil, time can be saved by making more mixtures in each step. In the extreme case, 99 separate mixtures would be prepared in the first step if the 1% tolerance level were the target. Clearly this is impractical and the most efficient search strategy lies between the two extremes.

As a compromise between conserving oil and minimizing time, begin with a coarse screening, consisting of a series of seven widely space mixtures (oil:precipitant = 20:80, 30:70, 40:60, 50:50, 60:40, 70:30, 80:20). Note that "oil" refers either to the original oil or the mixture of oil and solvent prepared in Step 2. Subsequent mixtures would be selected on the basis of the results of the coarse screening step. For precipitation with n-heptane, the onset is often found between 20:80 and 40:60, so oil might be conserved by beginning with mixtures in that range.

3.1 Prepare small glass vials. Clean glass vials (~6 ml is a convenient size), being careful to remove any traces of cleaning solution by flushing with plenty of distilled water. Contamination by trace amounts of surfactant can affect results. We soak vials in distilled water in an ultrasonic bath overnight. Dry thoroughly.

3.2 Add oil (or oil mixed with 1-MN) to vial. Accurately measure the amount of oil required into the sample vial. If the oil can be delivered by syringe, one strategy is to use a 1-ml glass syringe with 0.01 ml resolution. Parts of the syringe in contact with oil should be either glass or Teflon. If the oil cannot be delivered by syringe, the desired amount can be weighed into the vial and the volume calculated from the density. Larger volumes can be used to increase accuracy if sufficient oil is available.

3.3 Add precipitant to the oil. The required amount of n-heptane or other precipitant can be added to the vial using a similar syringe. Note: always add precipitant to oil (add slowly, with plenty of stirring to avoid high local concentrations of precipitant); **never add oil to precipitant**! Adding small volumes of oil to a large volume of precipitant will cause premature precipitation of the asphaltenes. While asphaltenes may, in theory, be stable in the final mixture, prematurely precipitated material may persist much more than the one-day period allotted for these tests.

3.4 Seal the vial immediately. A Teflon-lined aluminum cap works well. Precipitants and many of the components of the oil are volatile; evaporation will change the overall composition and invalidate the results of these tests. Shake the vial vigorously until the mixture appears homogeneous. Then allow the mixture to rest at ambient conditions for one day before observation.

3.5 Observe asphaltene flocculation. After aging for one day, a few drops of each mixture can be removed from the vial (disposable syringes are useful for this step), deposited on a glass microscope slide, covered with a cover slip, and observed immediately. It is helpful to prefocus the microscope using an old sample in which asphaltenes are obvious that is kept by the microscope for this purpose. Since evaporation begins when the sample is removed from the vial, it is important not to waste time during the actual observation. This is especially problematic with very light oils and highly volatile precipitants such as n-pentane and n-hexane; the accuracy of tests may be questionable if rapid evaporation is a problem. The flocculated asphaltenes usually appear as flowing particles and/or aggregates.

3.6 Measure refractive index. An additional sample can be removed from each vial and used to measure RI. An automatic refractometer (Index Instruments, model GPR 11-37) is convenient for this purpose. Temperature should be maintained at 20°C with a circulating water bath. Transfer mixture to the prism surface of refractometer as quickly as possible; seal immediately with the specially designed cap to prevent evaporation. Temperature equilibration requires a few seconds. Record the initial stabilized RI reading. With time, the RI may drift for these mixtures as asphaltenes adsorb and/or deposit on the prism surface, so it is important to take the initial reading.

3.7 Testing for the onset with additional precipitants. Once the onset has been found with n-heptane, that result can be used to predict the onset with other alkanes and used to streamline the search strategy for any additional tests. A maximum variation of between 5 and 15% in the amount of precipitant required at onset has been found for n-alkanes from pentane to pentadecane. For more information on the relationship between alkane molecular size and the onset conditions, refer to the references below.

Appendix II – HTHP Asphaltene Onset Equipment and Procedures

PVT and optical cell design and operation

A Ruska 2370 mercury-free system was used with minor modifications (Fig. AII-1). An optical cell with a very small spacing between two parallel glass plates was designed for viewing samples under controlled conditions of temperature and pressure. Details of the optical cell are shown in Fig. AII-2. The path length is controlled with shims and was estimated to be about 0.010 inches in these tests. The cell was tested to 10,000 psi.

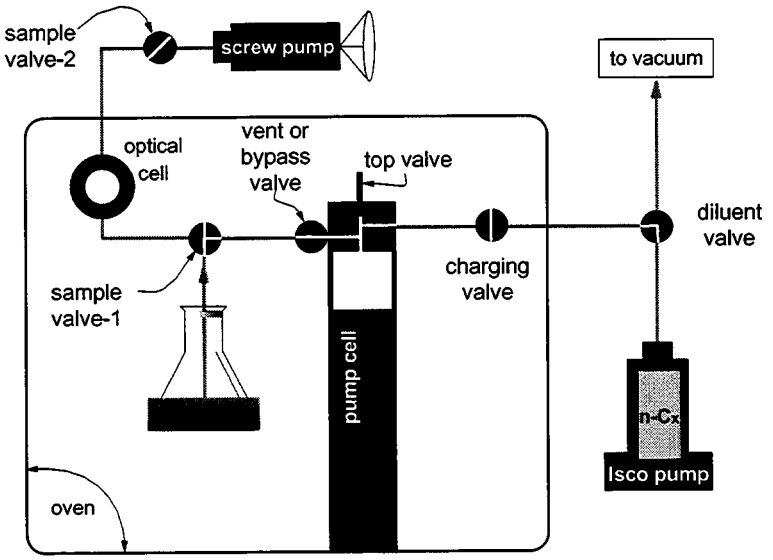

Figure AII-1. Adapted Ruska 2370 PVT apparatus configured for charging the pump cell with oil. Volume is controlled by movement of the pump cell piston.

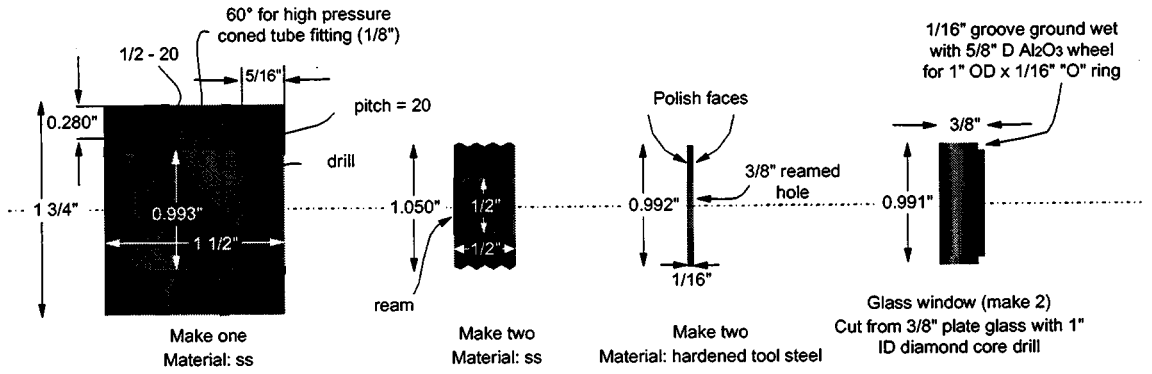

Figure AII-2. Optical cell designed for observation of oil samples for detection of onset of asphaltene precipitation.

With strong transmitted light, provided by the built-in optic fiber mounted behind the optical cell, adequate visibility was obtained with a 45X microscope (Edmund Scientific) with a 6.3 mm field of view and 65 mm working distance. The optical cell and fiber optic light were mounted on a removable frame just inside the oven door, while the microscope was mounted on a tripod, outside the oven door.

Dead volume calibration: With the pump cell cleaned and at its minimum volume and the top valve open, the cell was charged with nitrogen to an initial pressure P_o. The top valve was then closed. Using PRESET pump mode, the cell volume was increased in small increments. The volume at the top of the pump cell was found to be 2.23 ml.

Charging the pump cell with sample and precipitant: The cell was charged with crude oil (A-93) or with stable mixtures of oil and normal alkanes at ambient temperature and pressure. With the bypass valve and sample valve-1 open, the volume in the pump cell was increased by a predetermined amount. With about 50 ml of oil in the pump cell, the volume was decreased to expel air, the vent valve was closed, pressure was increased to about 100 psi, and the volume of oil recorded.

Precipitant was added through the charging valve using a metering pump. Pressure in the pump cell was reduced below that of the Isco pump (i.e. to about 20 to 40 psi) and the desired amount of precipitant delivered. With the pump cell isolated, the pressure was again increased to 100 psi and a second volume reading was taken. Pressure was then reduced to create a head space of about 5 to 10 ml. The contents of the pump cell were mixed for about 20 minutes using the magnetic stirrer included in the PVT apparatus. This mixing procedure was adopted after preliminary tests showed inadequate mixing near the top of the pump cell that resulted in premature appearance of asphaltene particles.

In preliminary tests with A-93 and *n*-pentane ($f_{V,oil} = 0.32$), a bubble point was reached at T=93°C and P=57 psi. Pressure was raised to about 100 psi after the initial mixing of oil and precipitant and before sampling.

Withdrawal of a sample for observation: The screw pump pressure was matched to the pump cell pressure with both at about 100 psi during the sampling process. This pressure is above the bubble point and compresses any precipitant in the line to the charging valve so that dilution does not occur at the point of sampling. The screw pump can be backed off very slowly. Each turn of the handle corresponds to about 0.4 ml of sample removed from the pump cell, through the optical cell. Four turns (1.6 ml) are required to replace fluids in the sampling lines completely. After sampling and observation, additional precipitant was added, as described above.

Recharging the pump cell: When a new crude oil sample was to be used, the pump cell and all the lines were completely cleaned. Since all the tests reported here were made with A-93 crude oil, rinsing the pump cell with fresh A-93 was sufficient to reduce the previously used alkane precipitant to trace levels. To accomplish this, the cell was rinsed before recharging by

filling and expelling three successive 20 ml aliquots of A-93 crude oil. The pump cell was then recharged with 50 ml of A-93 for the next series of tests.

Time and temperature dependence: The first samples of oil/precipitant mixtures contained no precipitated material. As the volume of precipitant increased, the point of onset was reached. The effect of increased temperature was explored near the onset of precipitation. Temperature was increased until the precipitate disappeared, then decreased and the volume fraction of precipitant was further increased. Appearance and disappearance of precipitated material required as much as several hours to reach a stationary state.

Estimation of RI and P_{RI}

RI measurements were not made at the elevated temperatures and pressures used in this study. Instead P_{RI} was estimated from the volume fraction of crude oil in the onset mixture, $f_{v,oil}$. For an ideal liquid mixture with m components

$$F_{RI} = \sum_{i=1}^{m} f_{v,i} \cdot F_{RI,i} \qquad \text{(AII-1)}$$

where F_{RI} is a function of refractive index, n, as defined by:

$$F_{RI} = \frac{n^2 - 1}{n^2 + 2} \qquad \text{(AII-2)}$$

$f_{v,i}$ and $F_{RI,i}$ are the volume fraction and F_{RI} value of I-th component, respectively. If the oil is considered to be a single pseudo-component, the RI of a mixture of crude oil with one precipitant is given by:

$$F_{RI} = f_{v,oil} \cdot F_{RI,oil} + (1 - f_{v,oil}) \cdot F_{RI,p} \qquad \text{(AII-3)}$$

where the subscript p refers to precipitant and oil refers to the crude oil.

F_{RI} is affected by temperature and pressure. At a given temperature and pressure, F_{RI} for a pure substance can be calculated by

$$F_{RI} = R\frac{\rho}{M} \qquad \text{(AII-4)}$$

where R is molar refraction, M is molecular weight, and ρ is density. Both R and M are independent of temperature and pressure; values are tabulated in handbooks (e.g., CRC). Only ρ varys with temperature and pressure. Thus F_{RI} and RI can be calculated if the relationship between density, temperature, and pressure is known.

In this study, STRAPP (1990) was used to estimate ρ as a function of temperature and pressure for alkanes (precipitant) and aromatics (solvent). RI was then estimated from equations (1.2-4) and (1.2-2). Results from some of the calculations are illustrated in Fig. AII-3. Note that for incompressible fluids, RI declines almost linearly with temperature. Pressure has little effect on RI up to 400 psi, the maximum pressure at which initial onset observations were made. The slopes d(RI)/dT are similar, with an average for pentane and higher molecular weights of

$$\frac{d(RI)}{dT} \approx -6.1\times10^{-4}\ /^{o}C \qquad \text{(AII-5)}$$

This average value was used to estimate RI for crude oils from RIs measured at ambient conditions.

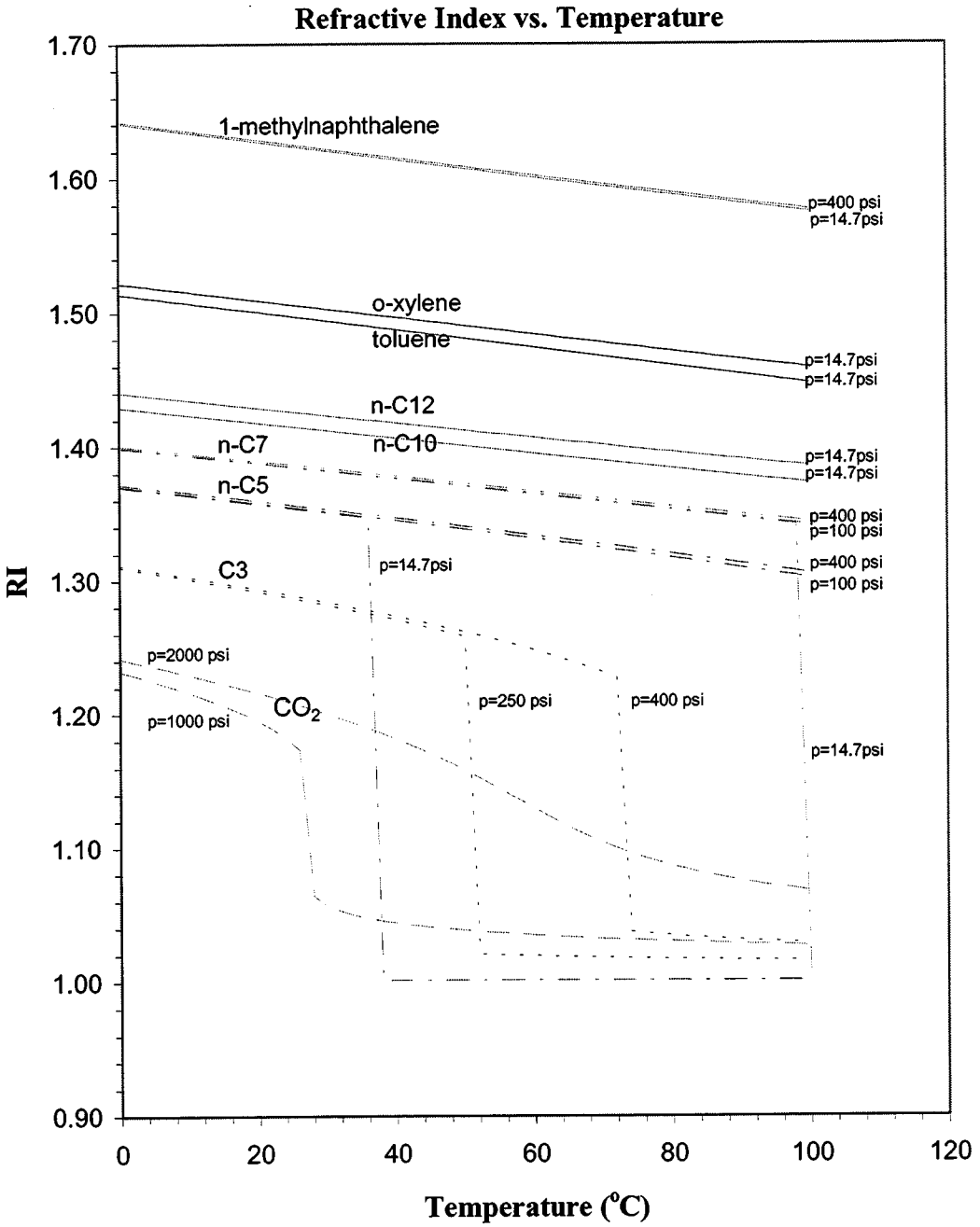

Figure AII-3. Refractive indices (RI) for pure substances decline with temperature.